

A Thesis Submitted for the Degree of PhD at the University of Warwick

Permanent WRAP URL:

<http://wrap.warwick.ac.uk/137236>

Copyright and reuse:

This thesis is made available online and is protected by original copyright.

Please scroll down to view the document itself.

Please refer to the repository record for this item for information to help you to cite it.

Our policy information is available from the repository home page.

For more information, please contact the WRAP Team at: wrap@warwick.ac.uk

The role of the N-glycolyl modification in Mycobacterial peptidoglycan synthesis and survival

Daniel Thomas McFeely

A thesis submitted in partial fulfillment
of the requirements for the degree of

Doctor of Philosophy



University of Warwick

School of Life Sciences

January 2019

Thesis Contents

Table of Contents.....	ii
List of Table.....	xv
List of Figures.....	xvi
Acknowledgements.....	xxii
Declaration.....	xxiii
Abstract.....	xxiv
Abbreviations.....	xxv

Chapter 1. Introduction

1.1 Tuberculosis.....	1
1.2 Mycobacteria.....	1
1.2.1 Mycobacterium tuberculosis complex (MTBC).....	2
1.2.1.1 <i>Mycobacterium tuberculosis</i>	2
1.2.2 Non-tuberculosis mycobacteria (NTM).....	2
1.2.2.1 <i>Mycobacterium smegmatis</i>	3
1.2.3 <i>Mycobacterium leprae</i>	3
1.3 Bacterial cell wall.....	4
1.3.1 Peptidoglycan.....	6
1.3.2 The structure of peptidoglycan.....	6
1.3.3 The cytoplasmic steps of peptidoglycan synthesis.....	7
1.3.4 Formation of Lipid II.....	10
1.3.5 Traversal of Lipid II to the extracellular face of the cytoplasmic membrane.....	10
1.3.6 Extracellular peptidoglycan integration.....	12
1.3.7 Recycling and maintenance of peptidoglycan.....	17
1.3.8 Modifications to peptidoglycan to facilitate resistance to hydrolytic enzymes.....	17
1.3.8.1 O-acetylation.....	18
1.3.8.2 N-deacetylation.....	19
1.3.8.3 Amidation.....	19
1.3.8.4 N-glycolylation.....	19
1.4 Tuberculosis infection.....	21
1.4.1 Innate immune response.....	21

1.4.1.1	Arresting phagosome maturation.....	24
1.4.1.2	Phagosome maturation.....	24
1.4.1.2.1	Lysozyme.....	25
1.4.1.2.1.1	Human lysozyme.....	26
1.4.1.2.2	β -hexosaminidase.....	27
1.5	Dormancy.....	29
1.5.1	<i>In vitro</i> dormancy models.....	33
1.5.2	<i>In vivo</i> dormancy models.....	34
1.5.3	Resuscitation.....	35
1.6	Diagnosis.....	36
1.7	Antimicrobial Discovery.....	36
1.7.1	Tuberculosis treatment.....	37
1.7.2	Antimicrobial resistance.....	38
1.7.3	Mechanisms of Antimicrobial resistance.....	39
1.7.4	Antimicrobial resistant Tuberculosis.....	40
1.8	Thesis aim.....	42

Chapter 2. Materials and Methods

2.1	Buffers and solutions.....	43
2.2	Growth media.....	43
2.2.1	7H9 media.....	43
2.2.2	Lysogeny broth (LB) broth.....	44
2.2.3	Super Optimal broth with Catabolite repression (SOC) media.....	44
2.2.4	Minimal growth media.....	44
2.2.5	Tryptic soy agar.....	45
2.2.6	LB-agar.....	45
2.2.7	Minimal media agar.....	45
2.3	Bacterial strains.....	46
2.4	Bacterial growth.....	47
2.4.1	Generation of glycerol stocks.....	47
2.4.2	Generation of competent cells.....	47
2.4.3	Aerobic growth of <i>M. smegmatis</i>	48

2.4.4	Determination of Minimal bactericidal concentration (MBC).....	48
2.4.5	Anaerobic growth of <i>M. smegmatis</i>	48
2.5	Assessment of hydrolytic enzyme activity against modified mycobacterial peptidoglycan.....	49
2.5.1	Mycobacterial agar colonisation against hydrolytic enzyme incubation.....	49
2.6	Cloning and editing of DNA.....	49
2.6.1	Polymerase Chain Reaction (PCR).....	50
2.6.2	DNA digestion by restriction enzymes.....	50
2.6.3	DNA purification.....	51
2.6.4	DNA ligation.....	51
2.6.5	Quantification of DNA concentration.....	51
2.6.6	Site directed mutagenesis.....	52
2.6.7	Agarose gel electrophoresis.....	52
2.6.8	DNA sequencing.....	53
2.6.9	Transformation.....	53
2.6.10	Isolation of plasmid DNA.....	54
2.7	Expression and purification of recombinant proteins.....	54
2.7.1	Recombinant protein over-expression with <i>E. coli</i> tuner (DE3) cells.....	55
2.7.1.1	SDS-Polyacrylamide Gel Electrophoresis.....	55
2.7.1.2	Development of SDS-PAGE.....	56
2.7.1.3	Western blotting.....	56
2.7.2	Fractionation of lysed <i>E. coli</i> cells.....	57
2.7.3	Recombinant protein purification.....	58
2.7.3.1	Affinity chromatography.....	58
2.7.3.2	Size exclusion chromatography.....	59
2.7.3.3	Ion exchange chromatography.....	60
2.7.4	Buffer exchange dialysis of recombinant protein.....	60
2.7.5	Concentration of recombinant protein.....	61
2.7.6	Quantification of recombinant protein.....	61
2.7.6.1	Bio-rad protein quantification.....	61
2.7.6.2	Bicinchoninic acid (BCA) protein quantification.....	62
2.8	Synthesis of Lipid II and intermediates.....	62
2.8.1	Biosynthesis of cytoplasmic peptidoglycan intermediates.....	62
2.8.1.1	Purification of cytoplasmic peptidoglycan intermediates.....	63

2.8.1.2	Quantification of cytoplasmic peptidoglycan intermediates.....	63
2.8.1.3	Biotinylation of UDP-MurNAc-pentapeptide.....	63
2.8.2	Lyophilisation of peptidoglycan intermediates.....	64
2.8.3	Preparation of bacterial cell membrane enzymes for Lipid II synthesis.....	64
2.8.4	Small-scale synthesis of Lipid II.....	65
2.8.4.1	Purification of Lipid II.....	65
2.8.4.2	Thin layer chromatography (TLC) of synthesized Lipid II.....	66
2.8.4.3	Quantification of Lipid II.....	66
2.9	Peptidoglycan intermediate accumulation.....	67
2.9.1	<i>B. subtilis</i> peptidoglycan intermediate accumulation.....	67
2.9.2	Trichloroacetic acid extraction of peptidoglycan intermediates.....	67
2.9.3	Di-ethyl ether extraction of TCA of peptidoglycan intermediate pool.....	68
2.10	Assessment of antimicrobials binding against biotinylated Lipid II variants..	68
2.10.1	Surface Plasma Resonance (SPR).....	68
2.10.2	Bio-Layer Interferometry (BLI).....	69
2.11	Spectrophotometric assays.....	70
2.11.1	Coupled NADH-linked pyruvate kinase/lactate dehydrogenase assay for amino acid Mur ligase activity.....	70
2.11.2	Amplex Red assay for transpeptidase activity.....	70
2.12	Mass spectrometry.....	71

Chapter 3. The role of the N-glycolylated muramic acid in protecting mycobacteria from host hydrolytic enzymes

3.1	Introduction.....	72
3.2	NamH deficient mutant.....	72
3.3	Experimental aims.....	73
3.4	Aerobic growth characterisation of <i>M. smegmatis</i> strains.....	73
3.5	Anaerobic growth characterisation of <i>M. smegmatis</i> strains.....	75
3.6	<i>M. smegmatis</i> sensitivity towards lysozyme.....	79
3.6.1	<i>M. smegmatis</i> sensitivity towards chicken egg white lysozyme.....	79
3.6.1.1	<i>M. smegmatis</i> sensitivity towards human lysozyme.....	85
3.6.1.2	Impact of pH on the sensitivity of <i>M. smegmatis</i> towards human lysozyme.....	90

3.6.1.3 Impact of extended incubation on the sensitivity of <i>M. smegmatis</i> towards human lysozyme.....	106
3.7 <i>M. smegmatis</i> sensitivity towards β-hexosaminidase.....	114
3.7.1 <i>M. smegmatis</i> sensitivity towards <i>S. plicatus</i> β -hexosaminidase.....	115
3.7.2 <i>M. smegmatis</i> sensitivity towards human β -hexosaminidase.....	119
3.7.2.1 The relationship between <i>M. smegmatis</i> sensitivity towards human β -hexosaminidase and pH.....	124
3.7.3 <i>M. smegmatis</i> sensitivity towards bovine β -hexosaminidase.....	130
3.8 Discussion.....	132
3.8.1 N-glycolyl modification during aerobic and anaerobic conditions.....	132
3.8.2 N-glycolyl modification against lysozyme.....	133
3.8.3 N-glycolyl modification against β -hexosaminidase.....	135
3.9 Further work.....	137
3.10 Conclusion.....	140

Chapter 4. The role of the N-glycolylated muramic acid in the protection of mycobacteria
from antimicrobial susceptibility

4.1 Introduction.....	141
4.2 Chapter Aim.....	142
4.3 DMSO tolerance of <i>M. smegmatis</i> strains.....	143
4.4 Antimicrobial MIC assessment of the <i>M. smegmatis</i> wild type and Δ<i>namH</i> strains.....	146
4.4.1 Ampicillin MIC assessment of <i>M. smegmatis</i> wild type and Δ NamH strains.....	147
4.4.2 Isoniazid MIC assessment of <i>M. smegmatis</i> wild type and Δ NamH strains.....	153
4.4.3 Ramoplanin MIC assessment of <i>M. smegmatis</i> wild type and Δ NamH strains.....	158
4.4.4 Tunicamycin MIC assessment of <i>M. smegmatis</i> wild type and Δ NamH strains.....	164
4.4.5 Mersacidin MIC assessment of <i>M. smegmatis</i> wild type and	

ΔNamH strains.....	169
4.4.6 Moenomycin MIC assessment of <i>M. smegmatis</i> wild type and ΔNamH strains.....	174
4.4.7 Vancomycin MIC assessment of <i>M. smegmatis</i> wild type and ΔNamH strains.....	179
4.4.8 Teixobactin MIC assessment of <i>M. smegmatis</i> wild type and ΔNamH strains.....	184
4.4.9 Arg-Teixobactin MIC assessment of <i>M. smegmatis</i> wild type and ΔNamH strains.....	189
4.5 Synthesis of Biotinylated Lipid II (MurNAc/NGlyc).....	194
4.6 Binding affinity of biotinylated Lipid II variants to antimicrobials.....	199
4.6.1 SPR analysis of binding of biotinylated Lipid II variants to antimicrobials.....	199
4.6.1.1 SPR analysis of binding of biotinylated Lipid II variants to ramoplanin.....	201
4.6.1.2 SPR analysis of binding of biotinylated Lipid II variants to mersacidin.....	204
4.6.1.3 SPR analysis of binding of biotinylated Lipid II variants to vancomycin.....	207
4.6.2 BLI of biotinylated Lipid II variants to antimicrobials.....	211
4.7 Discussion.....	215
4.7.1 Antimicrobial MIC assessment of ΔNamH <i>M. smegmatis</i>	215
4.7.1.1 The impact of non-peptidoglycan targeted antimicrobials on <i>M. smegmatis</i> growth.....	216
4.7.1.2 The impact of peptidoglycan targeted antimicrobials on <i>M. smegmatis</i> growth.....	216
4.8 Further work.....	220
4.9 Conclusion.....	221

Chapter 5. Variations in mycobacterial peptidoglycan
synthesis enzymes

5.1 Introduction.....	222
5.2 <i>M. leprae</i> peptidoglycan biosynthesis.....	222
5.3 Experimental aims.....	223
5.4 <i>M. leprae</i> MurA.....	223

5.4.1	Cloning of <i>M. leprae</i> MurA.....	225
5.4.2	Expression of <i>M. leprae</i> MurA.....	226
5.4.3	<i>M. leprae</i> MurA active site mutant.....	227
5.4.3.1	Site directed mutagenesis of <i>M. leprae</i> MurA active site.....	228
5.4.3.2	Expression of <i>M. leprae</i> MurA active site mutant.....	228
5.5	<i>M. leprae</i> MurC.....	229
5.5.1	Cloning of <i>M. leprae</i> MurC.....	230
5.5.2	Expression of <i>M. leprae</i> MurC.....	231
5.6	<i>M. smegmatis</i> Mur ligase.....	232
5.6.1	The kinetic profile of <i>M. smegmatis</i> MurC binding affinity towards muramic acid variants.....	233
5.6.2	The kinetic profile of <i>M. smegmatis</i> MurD binding affinity towards muramic acid variants.....	234
5.7	<i>M. tuberculosis</i> PonA1 and PonA2.....	236
5.7.1	Expression of <i>M. tuberculosis</i> PonA1 and PonA2.....	236
5.7.2	Purification of <i>M. tuberculosis</i> PonA1 and PonA2.....	236
5.7.3	Binding affinity of <i>M. tuberculosis</i> PonA1/PonA2 to Lipid II variants.....	238
5.8	Discussion.....	241
5.8.1	<i>M. leprae</i> Mur enzymes.....	241
5.8.2	<i>M. smegmatis</i> Mur enzymes.....	241
5.8.3	<i>M. tuberculosis</i> PBP enzymes.....	242
5.9	Further work.....	242
5.10	Conclusion.....	244

Chapter 6. Elucidating the role of known cell wall active compounds

6.1	Inhibition screening.....	245
6.1.1	Pywac compounds.....	245
6.1.2	Pywac compound structures and MIC concentrations.....	247
6.2	Experimental aims.....	249

6.3	DMSO tolerance of <i>B. subtilis</i>	249
6.4	<i>B. subtilis</i> MIC of pywac compounds	251
6.5	Analysis of <i>B. subtilis</i> peptidoglycan precursor intermediate standards	253
6.6	Normal cellular distribution of <i>B. subtilis</i> peptidoglycan intermediates	259
6.6.1	Intermediate accumulation of <i>B. subtilis</i> vancomycin control.....	263
6.6.2	Intermediate accumulation of <i>B. subtilis</i> against pywac compounds.....	266
6.6.2.1	Intermediate accumulation of <i>B. subtilis</i> against pywac compounds 1, 3, 5, 6 and 7.....	267
6.6.2.2	Intermediate accumulation of <i>B. subtilis</i> against pywac compound 2.....	270
6.6.2.3	Intermediate accumulation of <i>B. subtilis</i> against pywac compounds 4 and 9.....	271
6.6.2.4	Intermediate accumulation of <i>B. subtilis</i> against pywac 8.....	273
6.7	Purification of non-peptidoglycan intermediate standards	274
6.8	Inhibition of Lipid II synthesis	277
6.8.1	Lipid II synthesis utilising <i>B. subtilis</i> membranes.....	277
6.8.2	Lipid synthesis in the presence of pywac compounds.....	279
6.8.2.1	Purification of synthesised lipids co-incubated with pywac compounds.....	280
6.8.2.2	Identification of lipids co-incubated with pywac compounds.....	283
6.9	Intermediate accumulation of <i>S. aureus</i>	286
6.9.1	DMSO tolerance of <i>S. aureus</i>	287
6.9.2	Analysis of <i>S. aureus</i> peptidoglycan intermediate standards.....	289
6.9.3	Normal cellular distribution of <i>S. aureus</i> peptidoglycan intermediates.....	291
6.9.4	Intermediate accumulation of <i>S. aureus</i> vancomycin control.....	293
6.9.5	Intermediate accumulation of <i>S. aureus</i> against pywac compounds.....	296
6.9.5.1	Intermediate accumulation of <i>S. aureus</i> against pywac 1.....	296
6.9.5.2	Intermediate accumulation of <i>S. aureus</i> against pywac 2.....	297
6.9.5.3	Intermediate accumulation of <i>S. aureus</i> against pywac 6.....	299
6.9.5.4	Intermediate accumulation of <i>S. aureus</i> against pywac 8.....	300
6.9.5.5	Intermediate accumulation of <i>S. aureus</i> against pywac 9.....	301
6.10	Discussion	302
6.10.1	<i>B. subtilis</i> cytosolic phase intermediate accumulation assessment.....	302
6.10.2	Pywac inhibition of <i>B. subtilis</i> lipid synthesis.....	303
6.10.3	<i>S. aureus</i> cytosolic phase intermediate accumulation assessment.....	304
6.10.4	Potential isolation of incomplete gel filtration intermediate pools.....	306
6.11	Further work	306

6.12	Conclusion.....	308
-------------	------------------------	------------

Chapter 7. General discussion and final conclusions

7.1	Impact of N-glycolylation on standard mycobacterial growth.....	309
7.2	Impact of N-glycolylation on hydrolytic enzymes.....	310
7.3	Impact of N-glycolylation on antimicrobial therapy.....	311
7.4	Impact of N-glycolylation on peptidoglycan synthesis.....	313
7.5	Cell wall active drug discovery.....	315
7.6	Final conclusion.....	317
	Bibliography.....	318
	Appendix 1 Plasmids and mycobacterial genes utilised.....	345
	Appendix 2 Mass spectrometric analysis of synthesized biotinylated Lipid II variants.....	350
	Appendix 3 Mass spectrometric analysis of peptidoglycan intermediate accumulation attributed to cell wall active pywac compounds.....	359

List of Tables

Chapter 2. Materials and Methods

Table 2.1	Bacterial strains utilised within this thesis.....	46
Table 2.2	Primer sequence modifications to <i>M. leprae</i> MurA and MurC genes.....	50
Table 2.3	Restriction enzymes utilized for restriction digest of <i>M. leprae</i> Mur enzymes and the vector pCOLD.....	51
Table 2.4	Sequences of primers used for site directed mutagenesis of <i>M. leprae</i> MurA gene.....	52
Table 2.5	The nucleotide bases of upstream and downstream sequences encompassing the cloning/expression region within selected plasmids.....	53

Chapter 3. The role of the N-glycolylated muramic acid in protecting mycobacteria from host hydrolytic enzymes

Table 3.1	Statistical comparisons of <i>M. smegmatis</i> growth curves in the presence of increasing concentrations of chicken egg lysozyme	81
Table 3.2	Statistical comparisons of <i>M. smegmatis</i> growth curves in the presence of increasing concentrations of human lysozyme	87
Table 3.3	Average bacterial survival by <i>M. smegmatis</i> wild type and Δ NamH strains against human lysozyme at pH 7.....	94
Table 3.4	Average bacterial survival by <i>M. smegmatis</i> wild type and Δ NamH strains against human lysozyme at pH 6.5.....	101
Table 3.5	Average bacterial survival by <i>M. smegmatis</i> wild type and Δ NamH strains against human lysozyme at pH 6.0.....	102
Table 3.6	Average bacterial survival by <i>M. smegmatis</i> wild type and Δ NamH strains against human lysozyme at pH 5.5.....	103
Table 3.7	Average bacterial survival by <i>M. smegmatis</i> wild type and Δ NamH strains against human lysozyme at pH 5.0.....	105
Table 3.8	Average bacterial survival by <i>M. smegmatis</i> wild type and Δ NamH strains against human lysozyme at pH 5.0 incubated for 1.5 hours.....	108
Table 3.9	Average bacterial survival by <i>M. smegmatis</i> wild type and Δ NamH strains against human lysozyme at pH 5.0 incubated for 3 hours.....	109
Table 3.10	Average bacterial survival by <i>M. smegmatis</i> wild type and Δ NamH strains against human lysozyme at pH 5.0 incubated for 4.5 hours.....	110
Table 3.11	Student's t-test of <i>S. plicatus</i> β -hexosaminidase against <i>M. smegmatis</i> wild type and Δ NamH growth curves.....	117
Table 3.12	Student's t-test of human β -hexosaminidase against <i>M. smegmatis</i> wild type and Δ NamH growth curves.....	121
Table 3.13	Average bacterial survival by <i>M. smegmatis</i> wild type and Δ NamH strains against human β -hexosaminidase at pH 7.0 incubated for 1.5 hours.....	126

Table 3.14	Average bacterial survival by <i>M. smegmatis</i> wild type and Δ NamH strains against human β -hexosaminidase at pH 5.0 incubated for 1.5 hours.....	127
Table 3.15	Average bacterial survival by <i>M. smegmatis</i> wild type and Δ NamH strains against bovine β -hexosaminidase at pH 5.0 incubated for 1.5 hours.....	131

Chapter 4. The role of the N-glycolylated muramic acid in the protection of mycobacteria from antimicrobial susceptibility

Table 4.1	Statistical comparisons of <i>M. smegmatis</i> growth curves in the presence of increasing concentrations of DMSO.....	144
Table 4.2	Statistical comparisons of <i>M. smegmatis</i> growth curves in the presence of increasing concentrations of ampicillin.....	149
Table 4.3	Statistical comparisons of <i>M. smegmatis</i> growth curves in the presence of increasing concentrations of Isoniazid.....	155
Table 4.4	Statistical comparisons of <i>M. smegmatis</i> growth curves in the presence of increasing concentrations of Ramoplanin.....	160
Table 4.5	Statistical comparisons of <i>M. smegmatis</i> growth curves in the presence of increasing concentrations of tunicamycin.....	166
Table 4.6	Statistical comparisons of <i>M. smegmatis</i> growth curves in the presence of increasing concentrations of mersacidin.....	171
Table 4.7	Statistical comparisons of <i>M. smegmatis</i> growth curves in the presence of increasing concentrations of moenomycin.....	176
Table 4.8	Statistical comparisons of <i>M. smegmatis</i> growth curves in the presence of increasing concentrations of vancomycin.....	181
Table 4.9	Statistical comparisons of <i>M. smegmatis</i> growth curves in the presence of increasing concentrations of teixobactin.....	187
Table 4.10	Statistical comparisons of <i>M. smegmatis</i> growth curves in the presence of increasing concentrations of arg-teixobactin.....	192
Table 4.11	The mass/charge ratio for the peptidoglycan precursors UDP-MurNAc-pentapeptide (DAP) and UDP-MurNGlyc-	

	pentapeptide (DAP).....	195
Table 4.12	The equilibrium dissociation constants, K_D for biotinylated Lipid II variants to teixobactin and arg-teixobactin.....	214

Chapter 5. Variations in mycobacterial peptidoglycan synthesis enzymes

Table 5.1	<i>M. smegmatis</i> MurC kinetic activity constants comparison between binding affinity towards UDP-MurNAc and UDP-MurNGlyc substrates.....	234
Table 5.2	<i>M. smegmatis</i> MurD kinetic activity constants comparison between binding affinity towards UDP-MurNAc and UDP-MurNGlyc substrates	235
Table 5.3	The equilibrium dissociation constants, K_D for biotinylated Lipid II variants to <i>M. tuberculosis</i> PonA1 and PonA2.....	240

Chapter 6. Elucidating the role of known cell wall active compounds

Table 6.1	The cell wall active compounds identified by P_{ywaC} screening, designated pywac 1-9.....	248
Table 6.2	Statistical comparisons of <i>B. subtilis</i> growth curves in the presence of increasing concentrations of DMSO.....	250
Table 6.3	Conductivity of peptidoglycan precursor intermediate standards.....	257
Table 6.4	The mass/charge ratio for the peptidoglycan cytosolic DAP intermediates.....	258
Table 6.5	The mass/charge ratio for ATP, ADP and AMP.....	275
Table 6.6	The mass/charge ratio for N-acetylated Lipid I DAP and N-acetylated Lipid II DAP.....	283
Table 6.7	Concentrations of synthesised Lipid II co-incubated with 50 μ M of pywac compounds 1-9.....	285
Table 6.8	Statistical comparisons of <i>S. aureus</i> growth curves in the	

	presence of increasing concentrations of DMSO.....	288
Table 6.9	The mass/charge ratio for the peptidoglycan cytosolic Lysine Intermediates.....	290

List of Figures

Chapter 1 Introduction

Figure 1.1	Cross-section of the major components of the bacterial cell wall of (a) gram positive, (b) gram-negative and (c) Acid-Fast bacilli.....	5
Figure 1.2:	The structure of peptidoglycan in mycobacteria.....	6
Figure 1.3	The formation of UDP-MurNAc-pentapeptide from the peptidoglycan cytosolic biosynthesis pathway.....	9
Figure 1.4	The formation of Lipid II and the traversal of Lipid II across the plasma membrane.....	11
Figure 1.5	Transpeptidase activity of PBPs against parallel mycobacterial peptidoglycan strands forming a (4→3) cross-link between peptide stems.....	13
Figure 1.6	L,D-transpeptidase activity against parallel mycobacterial peptidoglycan strands forming a (3→3) cross-link between peptide stems.....	14
Figure 1.7	Nascent Lipid II incorporated into the overall peptidoglycan architecture by penicillin binding proteins.....	16
Figure 1.8	Modifications to the bacterial peptidoglycan monomer Lipid II to decrease susceptibility to host hydrolytic enzymes.....	18
Figure 1.9:	The hydroxylase activity of NamH.....	20
Figure 1.10	The antibacterial mechanisms of the phagosome to aid host microbial factors, or (b) against bacterial defense mechanisms.....	23
Figure 1.11	Hydrolysis of peptidoglycan by lysozyme.....	27

Figure 1.12	The cellular components and overall structure of a granuloma formed during tuberculosis infection.....	30
Figure 1.13	Activation of the <i>M. tuberculosis</i> DosR regulon by kinase sensors DosS (a) and DosT (b) to initiate mycobacterial dormancy.....	32

Chapter 3: The role of the N-glycolylated muramic acid in protecting mycobacteria from host hydrolytic enzymes

Figure 3.1	<i>M. smegmatis</i> Wild type and Δ NamH aerobic growth comparison.....	74
Figure 3.2	<i>M. smegmatis</i> colonization of selective nutrient agar during aerobic incubation.....	76
Figure 3.3	<i>M. smegmatis</i> colonization of selective nutrient agar during anaerobic incubation.....	77
Figure 3.4	<i>M. smegmatis</i> colonization of selective nutrient agar during aerobic incubation following prolonged anaerobic incubation.....	78
Figure 3.5	The hydrolytic activity of chicken egg white lysozyme against the mycobacterial modifications of peptidoglycan.....	80
Figure 3.6	Minimal bactericidal concentration of chicken egg white lysozyme against <i>M. smegmatis</i> strains.....	84
Figure 3.7	The hydrolytic activity of human lysozyme against the mycobacterial modifications of peptidoglycan.....	86
Figure 3.8	Minimal bactericidal concentration of human lysozyme against <i>M. smegmatis</i> strains.....	90
Figure 3.9	Colony count visibility of serially diluted <i>M. smegmatis</i> strains.....	91
Figure 3.10	Assessment of <i>M. smegmatis</i> strain serial dilution and HBSS incubation.....	92
Figure 3.11	<i>In vitro</i> human lysozyme assay for bactericidal activity against <i>M. smegmatis</i> at pH 7.....	93
Figure 3.12	<i>In vitro</i> human lysozyme bacterial survival percentage assay for bactericidal activity against <i>M. smegmatis</i> wild type at selected pH.....	96
Figure 3.13	<i>In vitro</i> human lysozyme bacterial survival percentage assay for bactericidal activity against <i>M. smegmatis</i> Δ NamH at selected pH.....	98

Figure 3.14	<i>In vitro</i> human lysozyme assay for bactericidal activity against <i>M. smegmatis</i> between pH 6.5 and 5.0.....	100
Figure 3.15	Effect of duration of exposure of <i>M. smegmatis</i> to human lysozyme at pH 5.0.....	107
Figure 3.16	Compilation of the effect of various durations of exposure to increasing lysozyme concentrations on the survival of <i>M. smegmatis</i> wild type at pH 5.0.....	112
Figure 3.17	Compilation of the effect of various durations of exposure to increasing lysozyme concentrations on the survival of <i>M. smegmatis</i> Δ NamH at pH 5.0.....	113
Figure 3.18	The hydrolytic activity of <i>S. plicatus</i> β -hexosaminidase against the mycobacterial modifications of peptidoglycan.....	116
Figure 3.19	The hydrolytic activity of human β -hexosaminidase against the mycobacterial modifications of peptidoglycan.....	120
Figure 3.20	Effect of exposure of <i>M. smegmatis</i> to increasing concentration of human β -hexosaminidase at pH 5.0 and 7.0.....	125
Figure 3.21	Impact of pH on wild type <i>M. smegmatis</i> survival of β -hexosaminidase treatment.....	128
Figure 3.22	Impact of pH on Δ NamH <i>M. smegmatis</i> survival of human β -hexosaminidase treatment.....	129
Figure 3.23	Impact of bovine β -hexosaminidase on the survival of <i>M. smegmatis</i> at pH 5.0.....	131

Chapter 4. The role of the N-glycolylated muramic acid in the protection of mycobacteria from antimicrobial susceptibility

Figure 4.1	DMSO tolerance of <i>M. smegmatis</i>	143
Figure 4.2:	The structure of the β -lactam antibiotic Ampicillin.....	147
Figure 4.3	The impact of N-glycolylation of peptidoglycan on sensitivity of <i>M. smegmatis</i> growth to ampicillin.....	148
Figure 4.4	Minimal bactericidal concentration of ampicillin against <i>M. smegmatis</i> strains.....	152

Figure 4.5:	The structure of the antibiotic Isoniazid.....	153
Figure 4.6	The impact of N-glycolylation of peptidoglycan on sensitivity of <i>M. smegmatis</i> growth of isoniazid.....	154
Figure 4.7	Minimal bactericidal concentration of isoniazid against <i>M. smegmatis</i> strains.....	157
Figure 4.8:	The structure of the glycolipodepsipeptide antibiotic Ramoplanin.....	158
Figure 4.9	The impact of N-glycolylation of peptidoglycan on sensitivity of <i>M. smegmatis</i> growth of ramoplanin.....	159
Figure 4.10	Minimal bactericidal concentration of ramoplanin against <i>M. smegmatis</i> strains.....	163
Figure 4.11:	The structure of the Tunicamycin.....	164
Figure 4.12	The impact of N-glycolylation of peptidoglycan of peptidoglycan on sensitivity of <i>M. smegmatis</i> growth to tunicamycin.....	165
Figure 4.13	Minimal bactericidal concentration of tunicamycin against <i>M. smegmatis</i> strains.....	168
Figure 4.14:	The structure of the lantibiotic Mersacidin.....	169
Figure 4.15	The impact of N-glycolylation of peptidoglycan on sensitivity of <i>M. smegmatis</i> growth on mersacidin.....	170
Figure 4.16	Minimal bactericidal concentration of mersacidin against <i>M. smegmatis</i> strains.....	173
Figure 4.17:	The structure of the glycosyltransferase antibiotic Moenomycin.....	174
Figure 4.18	The impact of N-glycolylation of peptidoglycan on sensitivity of <i>M. smegmatis</i> growth to moenomycin.....	175
Figure 4.19	Minimal bactericidal concentration of moenomycin against <i>M. smegmatis</i> strains.....	178
Figure 4.20:	The structure of the antibiotic Vancomycin.....	179
Figure 4.21	The impact of N-glycolylation of peptidoglycan on the sensitivity of <i>M. smegmatis</i> growth to vancomycin.....	180
Figure 4.22	Minimal bactericidal concentration of vancomycin against <i>M. smegmatis</i> strains.....	183
Figure 4.23:	The structure of the small molecule antibiotic Teixobactin.....	184
Figure 4.24	The impact of N-glycolylation of peptidoglycan on the sensitivity of <i>M. smegmatis</i> growth to teixobactin.....	186

Figure 4.25	Minimal bactericidal concentration of teixobactin against <i>M. smegmatis</i> strains.....	189
Figure 4.26	The structure of the modified small molecule antibiotic Teixobactin, designated Arginine-Teixobactin.....	190
Figure 4.27	The impact of N-glycolylation of peptidoglycan on the sensitivity of <i>M. smegmatis</i> growth to Arg-teixobactin.....	191
Figure 4.28	Minimal bactericidal concentration of arg-teixobactin against <i>M. smegmatis</i> strains.....	194
Figure 4.29	Ion exchange chromatography of biotinylated UDP-MurNAc-pentapeptide (DAP) from unlabelled UDP-MurNAc-pentapeptide (DAP).....	196
Figure 4.30	Ion exchange chromatography of biotinylated UDP-MurNGlyc-pentapeptide (DAP) from unlabelled UDP-MurNGlyc-pentapeptide (DAP).....	197
Figure 4.31	The structure of biotin labelled N-acetylated Lipid II DAP and N-glycolylated Lipid II DAP (L-Ala-D-Glu-m-DAP-D-Ala-D-Ala).....	198
Figure 4.32	Standard SPR sensorgram.....	200
Figure 4.33	SPR binding affinity of ramoplanin to streptavidin-immobilised biotinylated Lipid II (DAP) variants.....	202
Figure 4.34	SPR steady state response of immobilised biotinylated Lipid II (DAP) variants binding to ramoplanin.....	204
Figure 4.35	SPR binding affinity of mersacidin to streptavidin immobilised biotinylated Lipid II (DAP) variants.....	205
Figure 4.36	SPR steady state response of immobilised biotinylated Lipid II (DAP) variants binding to mersacidin.....	206
Figure 4.37	SPR binding affinity of vancomycin to streptavidin immobilised biotinylated Lipid II (DAP) variants.....	209
Figure 4.38	SPR steady state response of immobilised biotinylated Lipid II (DAP) variants binding to vancomycin.....	210
Figure 4.39	Basic BLI binding assessment.....	212
Figure 4.40.	Binding affinity of biotinylated Lipid II variants against newly identified antimicrobial teixobactin and the synthesised analogue arginine-teixobactin.....	213

Chapter 5. Variations in mycobacterial peptidoglycan synthesis enzymes

Figure 5.1	Protein sequence alignment of the peptidoglycan synthesis gene <i>murA</i> within selected mycobacteria.....	224
Figure 5.2	PCR amplification of <i>M. leprae murA</i>	225
Figure 5.3	SDS-PAGE and Western blot analysis of expressed <i>M. leprae</i> MurA.....	227
Figure 5.4	SDS-PAGE and Western blot analysis of expressed <i>M. leprae</i> MurA active site mutant	229
Figure 5.5	Protein sequence alignment of the peptidoglycan synthesis gene <i>murC</i> within selected mycobacteria.....	230
Figure 5.6	PCR amplification of <i>M. leprae murC</i>	231
Figure 5.7	SDS-PAGE and Western blot analysis of expressed <i>M. leprae</i> MurC.....	232
Figure 5.8	Initial rate of <i>M. smegmatis</i> MurC enzyme velocity against muramic acid variants.....	233
Figure 5.9	Initial rate of <i>M. smegmatis</i> MurD enzyme velocity against muramic acid variants	235
Figure 5.10	Purification of <i>M. tuberculosis</i> PonA1.....	237
Figure 5.11	Purification of <i>M. tuberculosis</i> PonA2.....	237
Figure 5.12	Binding affinity of biotinylated Lipid II variants against <i>M. tuberculosis</i> penicillin binding proteins PonA1 and PonA2.....	239

Chapter 6. Elucidating the role of known cell wall active compounds

Figure 6.1	The enzymatic luminescence reaction of reduced flavin mononucleotide and a long chain aldehyde.....	246
Figure 6.2	DMSO tolerance of <i>B. subtilis</i>	249
Figure 6.3	MIC of cell wall active pywac compounds against <i>B. subtilis</i>	251
Figure 6.4	MIC of vancomycin against <i>B. subtilis</i>	252
Figure 6.5:	The structures of the cytosolic peptidoglycan intermediates of <i>B. subtilis</i>	254

Figure 6.6:	Anion exchange chromatography of peptidoglycan intermediate standards.....	256
Figure 6.7:	Size exclusion chromatography of <i>B. subtilis</i> control cells TCA extracted cells.....	260
Figure 6.8:	Anion exchange chromatography of isolated peptidoglycan intermediate peak of <i>B. subtilis</i> control cells.....	261
Figure 6.9:	Size exclusion chromatography of <i>B. subtilis</i> TCA extracts of cells incubated with excess MIC vancomycin.....	264
Figure 6.10:	Anion exchange chromatography of gel filtration elutes (peak (i)) from <i>B. subtilis</i> treated with excess MIC vancomycin.....	265
Figure 6.11:	Size exclusion and ion exchange chromatography of <i>B. subtilis</i> TCA extracts of cells incubated with 2x MIC pywac 1, 3, 5, 6 and 7.....	268
Figure 6.12:	Size exclusion and ion exchange chromatography of <i>B. subtilis</i> TCA extracts of cells incubated with 2x MIC pywac 2.....	270
Figure 6.13:	Size exclusion and ion exchange chromatography of <i>B. subtilis</i> TCA extracts of cells incubated with 2x MIC pywac compounds 4 and 9.....	272
Figure 6.14:	Size exclusion and ion exchange chromatography of <i>B. subtilis</i> TCA extracts of cells incubated with 2x MIC pywac 8.....	273
Figure 6.15:	The structure of Adenosine mono-phosphate (AMP), Adenosine di-phosphate (ADP) and Adenosine tri-phosphate (ATP).....	274
Figure 6.16:	Anion exchange chromatography of AMP, ADP and ATP standards.....	275
Figure 6.17:	The structure of NADPH.....	276
Figure 6.18:	Anion exchange chromatography of NADPH standard.....	276
Figure 6.19:	TLC of fractions from lipid synthesis of Lipid II (DAP) to assess membrane activity in selected media.....	278
Figure 6.20:	TLC of unpurified fractions from lipid synthesis of Lipid II (DAP) co-incubated with 50µM of pywac compounds 1-9 and no compound control C.....	279
Figure 6.21:	Thin-layer chromatography of purified lipid fractions co-incubated with 50 µM pywac compounds 1, 2 3 and no compound control.....	281
Figure 6.22:	Thin-layer chromatography of purified lipid fractions co-incubated	

	with 50 μ M pywac compounds 4, 5, 6, 7, 8 and 9.....	282
Figure 6.23	DMSO tolerance of <i>S. aureus</i>	287
Figure 6.24:	The structures of cytosolic peptidoglycan intermediates of <i>S. aureus</i>	289
Figure 6.25:	Anion exchange chromatography of <i>S. aureus</i> peptidoglycan intermediate standards.....	290
Figure 6.26:	Size exclusion and ion exchange chromatography of <i>S. aureus</i> TCA extracted control cells.....	292
Figure 6.27	MIC of vancomycin against <i>S. aureus</i>	294
Figure 6.28:	Size exclusion and ion exchange chromatography of <i>S. aureus</i> TCA extracts of cells incubated with 2x MIC vancomycin.....	295
Figure 6.29:	Size exclusion and ion exchange chromatography of <i>S. aureus</i> TCA extracts of cells incubated with 4 μ M pywac 1.....	296
Figure 6.30:	Size exclusion and ion exchange chromatography of <i>S. aureus</i> TCA extracts of cells incubated with 2 μ M pywac 2.....	297
Figure 6.31:	Size exclusion and ion exchange chromatography of <i>S. aureus</i> TCA extracts of cells incubated with 8 μ M pywac 6.....	299
Figure 6.32:	Size exclusion and ion exchange chromatography of <i>S. aureus</i> TCA extracts of cells incubated with 8 μ M pywac 8.....	300
Figure 6.33:	Size exclusion and ion exchange chromatography of <i>S. aureus</i> TCA extracts of cells incubated with 4 μ M pywac 9.....	301

Acknowledgements

Primarily I would like to thank my supervisor Professor Chris Dowson, for giving me the opportunity to obtain the goal I have had since I discovered what a scientist was. For his advice, knowledge and direction throughout my thesis I am eternally grateful.

This thesis would not have been possible without Dr. Adrian Lloyd. His unending patience, ability to see the positive in my failures and willingness to go above and beyond to help me when I often seemed lost is never lost on me and I truly thank him for going above and beyond for me.

To Julie Tod and Anita Catherwood for their constant support and kindness, without whose presence everyday within the lab I would not be able to tie my shoes.

I would also like to thank all the members past and present of lab C10, particularly Greg Walkowiak, Amy O'Reilly and Nicola Galley. Even though it took me a little longer we got there in the end.

To all the doctors, GPs and surgeons who have figured out what's wrong with me better than I ever have and helped me maintain my health throughout my thesis.

And finally, to my family, we've gone through hard times recently but I know we'll be ok in the end. You've put up with my nonsense and kept me going.

Thank you to you all.

Declaration

I hereby declare that I personally have carried out the work submitted in this thesis under the supervision of Professor Christopher Dowson and Doctor David Roper at the School of Life Sciences, University of Warwick. Where work has been contributed to by other individuals it is specifically stated in the text.

No part of this work has previously been submitted to be considered for a degree or qualification. All sources of information are specifically acknowledged in the for of references.

Abstract

Mycobacteria are acid fast bacilli responsible for the wide spread global diseases tuberculosis and leprosy. The increased persistence of multidrug resistant (MDR) mycobacterial strains has led to the focus on discovery of new and under-utilised cellular targets such as the cell wall.

Peptidoglycan, the principle structural component of the bacterial cell wall is a heteropolymer comprised of alternating monosaccharides cross-linked by pentapeptide chains. The cell wall of mycobacteria are inherently resistant to antimicrobials and aid in evasion from host immune detection due to modifications to its composition. The hydroxylase enzyme NamH has been documented to play a role in the N-glycolylation of peptidoglycan monosaccharides, utilizing molecular oxygen during aerobic growth to convert N-acetyl- to N-glycolyl groups. This modification is found predominantly in Actinobacteria, except *Mycobacterium leprae* due to genomic reduction. The percentage incorporation of N-acetylated and N-glycolylated saccharides is dependent upon the environment and functional characterisation of the impact of each modification is vital to achieving a greater understanding into mycobacterial response to a range of factors including dormancy, resuscitation and intracellular propagation.

The investigations described in this thesis concern the susceptibility of a *M. smegmatis* $\Delta namH$ strain, the cell wall of which contains solely N-acetylated cell wall components towards: (a) selected hydrolytic enzymes, as a model of the survival of phagocytosed mycobacteria within the harsh conditions of the phagolysosome and; (b) new and existing antimicrobials commonly used as therapies against infection. The absence of the N-glycolylated sugar within the peptidoglycan cell wall led to consistently observed increases in susceptibility to a range of hydrolytic enzymes and antimicrobials, especially those which target the formation of peptidoglycan. Mycobacterial Mur ligases demonstrated increased catalytic bias towards N-glycolylated substrates to increase their inclusion into the wide peptidoglycan sacculus. Investigations were expanded to characterize the impact of newly discovered known cell wall active compounds against the peptidoglycan biosynthesis machinery.

Abbreviations

°C	Degrees Celsius
A _{xxx}	Absorbance
ADP	Adenosine 5'-diphosphate
AFB	Acid fact bacilli
AG	Arabinogalactan
Alr	Alanine racemase
AMR	Antimicrobial resistance
AMP	Adenosine 5'-monophosphate
ATP	Adenosine 5'-triphosphate
APS	Ammonium persulphate
AU	Absorbance Unit
<i>B. subtilis</i>	<i>Bacillus subtilis</i>
BaCWAN	Bacterial Cell Wall Assembly Network
BCA	Bicinchoninic acid
BCG	Bacillus Calmette Guérin
BSA	Bovine Serum Albumin
bp	Base pair
C-terminus	Carboxy-terminus
C-type	Chicken type
C ₅₅ -PP	Undecaprenyl pyrophosphate
CHAPS	3-[(3-Cholamidopropyl) dimethylammonio]-1-propanesulfonate
CO	Carbon monoxide
CT	Computed tomography
CV	Column volume
D-Ala	D-Alanine
D-Ala-D-Ala	D-Alanyl-D-Alanine
D-Glu	D-Glutamate
Da	Dalton
DAAO	D-amino acid oxidase
DAP	D-aminopimelic acid

DC-SIGN	Dendritic cell specific intracellular adhesion molecule-3-grabbing nonintegrin
Ddl	D-alanyl-D-alanine ligase
DMSO	Dimethyl Sulphoxide
DNA	Deoxyribonucleic acid
DNAase	Deoxyribonuclease enzyme
dNTPs	Deoxyribonucleotide triphosphate
DTT	Dithiothreitol
<i>E. coli</i>	<i>Escherichia coli</i>
EDTA	Ethylenediaminetetraacetic acid
EMB	Ethambutol
EPT	Efficient-plasmid-transformation
ESI-MS	Electrospray Ionisation Mass Spectrometry
<i>et al.</i>	<i>et alia</i> , and others
FAS-II	Fatty acid synthetase II
G	Gram
G-type	Goose type
GAF domain	cGMP, adenylyl cyclase, FhlA domain
GlcNAc	N-acetylglucosamine
GM2	Ganglioside monosialic 2
HCl	Hydrochloric acid
HEPES	4-(2-hydroxyethyl)-1-piperazineethanesulfonic acid
HIV	Human Immunodeficiency Virus
HPLC	High-Performance Liquid Chromatography
HRP	Horseradish peroxidase
I-type	Invertebrate
IC ₅₀	Inhibitory concentration
IFN- γ	Interferon- γ
IGRA	Interferon- γ release assays
IMAC	Immobilised Metal-Affinity Chromatography
INH	Isoniazid
IPTG	Isopropyl- β -D-thiogalactopyranoside
kb	Kilobase

K_{cat}	Michaelis-Menton Constant
K_D	Dissociation constant
K_m	Michaelis-Menton Constant
kpsi	kilopound per square inch
L	Litre
L-Lys	L-Lysine
LAM	Lipoarabinomannans
LB	Luria Broth
Lipid I	Undecaprenyl pyrophosphoryl-N-acetylmuramyl-L-Alanyl-D-Glutamyl-m-DAP-D-Alanyl-D-Alanine
Lipid I NGlyc	Undecaprenyl pyrophosphoryl-N-glycolymuramyl-L-Alanyl-D-Glutamyl-m-DAP-D-Alanyl-D-Alanine
Lipid II	Undecaprenyl pyrophosphoryl-N-acetylmuramyl (N-acetylglucoasminyl)-L-Alanyl-D-Glutamyl-m-DAP-D-Alanyl-D-Alanine
Lipid II NGlyc	Undecaprenyl pyrophosphoryl-N-glycolymuramyl-L-Alanyl-D-Glutamyl-m-DAP-D-Alanyl-D-Alanine
LprA	Lipoproteins
m	milli
M	Molar (grams per litre)
<i>M. leprae</i>	<i>Mycobacterium leprae</i>
<i>M. smegmatis</i>	<i>Mycobacterium smegmatis</i>
<i>M. tuberculosis</i>	<i>Mycobacterium tuberculosis</i>
mAGP	Mycolic acid, arabinogalactan, peptidoglycan
mAu	Milli-absorbance unit
MBC	Minimal Bactericidal Concentration
MDR	Multidrug-resistant
MESG	7-methyl-6-guanosine
MIC	Minimal Inhibitory Concentration
mol	Mole
M_r	Molecular weight
MTBC	Mycobacterium tuberculosis complex
MurNAc	N-acetylmuramic acid
MurNGlyc	N-glycolymuramic acid

m/z	Mass to charge ratio
n	nano
N-terminus	Amino-terminus
NAA	Nucleic acid amplification
NADH	Nicotinamide adenine dinucleotide
NF	Nuclear transcription factor
NO	Nitric oxide
NOD	Nucleotide-binding oligomerisation domain-containing protein
NRP	Non-replicating persistence
NTM	Non-tuberculosis mycobacteria
OatA	O-acetyltransferase
OD	Optical density
PAGE	Polyacrylamide gel electrophoresis
PAMPs	Pathogen-associated molecular patterns
PASTA domain	Penicillin binding protein and serine/threonine kinase associated domain
PBPs	Penicillin binding proteins
PCR	Polymerase chain reaction
PDB	Protein Data Bank
PEP	Phosphoenolpyruvate
PG	Peptidoglycan
pH	$-\log_{10}[\text{H}^+]$
pI	Isoelectric point
Pi	Inorganic phosphate
PI(3)P	Phosphatidylinositol 3-phosphate
PIM	Phosphatidylinositol mannoside
PLP	Pyridoxal 5'-phosphate
PMSF	Phenyl methyl sulphonyl fluoride
POA	Pyrazinoic acid
PPD	Purified protein derivative
PZA	Pyrazinamide
RIF	Rifampicin
RipA	Rpf-interacting protein A

RPFs	Resuscitation promoting factors
rpm	Rotations per minute
RpsA	Ribosomal protein S1
<i>S. aureus</i>	<i>Staphylococcus aureus</i>
SAP	Shrimp Alkaline phosphatase
SDM	Site-Directed Mutagenesis
SDS	Sodium dodecyl sulfate
SOC	Super Optimal Broth
TAE	Tris acetate ethylenediaminetetraacetic acid
TEMED	N,N,N'-tetramethylethylenediamine
TEV	Tobacco etch virus protease
TB	Tuberculosis
TG	Transglycosylase
TLC	Thin layer chromatography
TLR	Toll-like receptors
TM	Transmembrane domain
TNF- α	Tumour necrosis factor alpha
TP	Transpeptidase
Tris	Tris(hydroxymethyl)aminomethane
TX-100	Triton X-100
UDP	Uridine diphosphate
V	Volt
v/v	Volume to volume ratio
vH ⁺ -ATPase	Vacuolar proton transporting ATPase
V _{max}	Maximal velocity
w/v	Weight to volume ratio
WHO	World Health Organisation
XDR	Extensively drug-resistant
x g	centrifugal force
μ	micro

Standard three and one amino acid abbreviations are used throughout.

Amino acid code	Three Letter code	One letter
Alanine	Ala	A
Arginine	Arg	R
Asparagine	Asn	N
Aspartic acid	Asp	D
Cysteine	Cys	C
Glutamic acid	Glu	E
Glutamine	Gln	Q
Glycine	Gly	G
Histidine	His	H
Isoleucine	Ile	I
Leucine	Leu	L
Lysine	Lys	K
Methionine	Met	M
Phenylalanine	Phe	F
Proline	Pro	P
Serine	Ser	S
Threonine	Thr	T
Tryptophan	Trp	W
Tyrosine	Tyr	Y
Valine	Val	V

Chapter 1: Introduction

1.1 Tuberculosis

Tuberculosis (TB, tubercules bacillus) is a contagious disease affecting approximately a third of the human population (Houben and Dodd 2016). The World Health Organisation (WHO) categorises TB as the second most preeminent cause of death by an infectious disease (WHO, 2012). Worldwide occurrences of tuberculosis were diminishing towards the end of the 21st century, but the rise of widespread resistance to standard drug therapies and the number of human immunodeficiency virus (HIV) co-infections have led to the disease being categorised as a global health emergency (WHO, 2011). The rising global impact of tuberculosis coupled with the emergence of multiple therapy resistances leads to the requirement of new antimicrobial treatments as well as identifying new and re-examining pre-existing targets in mycobacteria such as the peptidoglycan (PG) cell wall.

1.2 Mycobacteria

Mycobacteria are aerobic unicellular rod organisms noted to include an increased C-G content of bases. Commonly aligned with Gram positive bacteria due to genetic similarity, the genus *Mycobacterium* is part of the family Actinobacteria, encompassing 170 species (Fedrizzi, *et al.* 2017). Mycobacteria are categorised as Acid-Fast bacilli (AFB) (Riello, *et al.* 2016), and include organisms such as *Mycobacterium tuberculosis* (*M. tuberculosis*), *Mycobacterium leprae* (*M. leprae*) and *Mycobacterium smegmatis* (*M. smegmatis*).

1.2.1 Mycobacterium tuberculosis complex (MTBC)

Mycobacterium tuberculosis is classified as part of the Mycobacterium tuberculosis complex (MTBC), a group of genetically similar mycobacteria (Chimara, *et al.* 2004), which infect numerous hosts with tuberculosis. *M. tuberculosis*, *M. africanum* and *M. canettii* are categorised as human pathogens (Somoskovi, *et al.* 2009, de Jong, *et al.* 2010), *M. bovis* infects both bovine and human subjects (Vayr, *et al.* 2018), and *M. microti* infects rodent species (Vayr, *et al.* 2018).

1.2.1.1 Mycobacterium tuberculosis

In 1882 Robert Koch first discovered the causative agent of tuberculosis in humans, *M. tuberculosis* (Koch, 1882). Koch demonstrated an *in vitro* method for reproducing the disease pathophysiology observed initially in humans by infecting animal cells with *M. tuberculosis*. The mycobacterium was visualised under a microscope utilising a newly conceived staining technique (Weigert, 1875), which led to Koch receiving the 1905 Nobel Prize in Medicine for his isolation and investigation of tuberculosis.

1.2.2 Non-tuberculosis mycobacteria (NTM)

Other members of the genus mycobacteria excluding the MTBC and *M. leprae* are classified as non-tuberculosis mycobacteria (NTM) (Fedrizzi, *et al.* 2017). NTM reside within a number of environments such as soil and water (Falkinham 2015), and though rarely pathogenic can cause infection notably in immunosuppressed hosts (Horsburgh, *et al.* 1993).

1.2.2.1 *Mycobacterium smegmatis*

Due to the laboratory containment procedures required to study *M. tuberculosis* and the inability to easily culture *M. leprae* (Bailey, *et al.* 2017), the weakly-pathogenic saprophyte *M. smegmatis* is commonly used as a model to investigate mycobacteria (He and De Buck 2010) due in part to the organism's fast growth and the ease of generating cultures in manufactured media. The original *M. smegmatis* wild type strain displayed a low transformation efficiency, and was resolved by the isolation of an efficient-plasmid-transformation (ept) mutant strain, defined as mc²155 (Snapper, *et al.* 1990).

1.2.3 *Mycobacterium leprae*

Leprosy, also known as Hansen's disease, was identified by Armauer G. Hansen in 1873 (Vera-Cabrera, *et al.* 2015). Leprosy is induced by the intracellular pathogen *M. leprae* and acknowledged to be a major public health issue in numerous developing countries (Sales, *et al.* 2011). Requiring an extended incubation period within host cells, infection predominantly occurs within the skin, the peripheral nervous system and the upper respiratory tract (Ooi and Srinivasan 2004). There are various methods of categorising leprosy. The World Health Organisation separates patients based upon the visible type and number of afflictions on the skin (Gaschignard, *et al.* 2016). Those who display less than five skin lesion with a negative bacterial skin sample are termed paucibacillary. Patients with either or both, a greater number of skin lesion than five and/or a positive skin test detection of bacteria are termed multibacillary. A second method of categorising leprosy is determined by the immune response of the host to the bacilli (Ochoa, *et al.* 1996). A robust immune system response contributes only to a smaller number of visible skin lesions and a thickening of peripheral nerves, culminating in the patient registering as moderately contagious, described as tuberculoid leprosy. An impaired immune system response leads to a more pronounced manifestation of skin lesions, a widespread impact on the nervous system and additional organs. This disease state is significantly more contagious and denoted as lepromatous leprosy. *M. leprae* is non-culturable long term *in vitro* on manufactured media and agar (Bailey, *et al.* 2017), requiring study through traditional *in vivo* animal models (Adams, *et al.* 2012).

The sequencing of the *M. leprae* genome (Cole, *et al.* 2001) has revealed extensive genomic reduction, with many of the equivalent genes found in *M. tuberculosis* described as pseudogenes displaying no function (Muro, *et al.* 2011), including of relevance to this thesis, NamH. With less than fifty percent functional genome, *M. leprae* lacks numerous metabolic systems justifying the required incubation period and the requirement of animal model culture systems. Leprosy is commonly diagnosed through a skin biopsy (Joshi 2011), and once confirmation of leprosy is attained, a lepromin skin test can also determine the form of leprosy (Krotoski, *et al.* 1993), evaluated by the capacity of the host to initiate a cell-mediated immune response to *M. leprae* bacilli. The presence of swelling and redness indicates the presence of tuberculoid leprosy while the absence of changes to the skin indicate lepromatous leprosy. Treatment for leprosy is generally a twelve-month multidrug therapy that is tailored to the type of leprosy observed (Malathi and Thappa 2013). Paucibacillary leprosy requires dapsone and rifampicin, whereas multibacillary leprosy requires both previously mentioned antibiotics plus clofazimine.

1.3 Bacterial cell wall

Classified upon the composition of the cell wall, bacteria are commonly identified based upon a technique known as Gram staining (Beveridge 2001). The stain was developed by Hans Christian Gram as a taxonomic tool based solely on the complexity of the bacterial cell wall and the total percentage of amassed peptidoglycan within the sacculus (Austrian 1960). The unique structural component is located in virtually all eubacteria, excluding *Mycoplasma*. The 20-80nm broad peptidoglycan layer of gram-positive organisms such as *Staphylococcus aureus* and *Streptococcus pneumoniae* consists of between 30-70% of the total structure of the cell wall (Schleifer and Kandler 1972). Gram-negative bacteria have a minimal 2-3nm peptidoglycan layer along with lipoproteins, phospholipids and lipopolysaccharides which are surrounded by an outer membrane (Beveridge 1999). Certain bacteria such as mycobacteria do not conform to identification through Gram-staining.

The cell wall of mycobacteria is impermeable to different commonly utilised identification techniques and the ability to resist decolourisation by acid alcohol is due in part to the inclusion of

mycolic acids, a structural component of the mycobacterial cell wall found predominantly in Actinobacteria (Kragelund, *et al.* 2007). Comprised of long chain, branched fatty acids, mycolic acids combine with arabinogalactan (AG) and peptidoglycan to form the mycolic acid, arabinogalactan and peptidoglycan (mAGP) complex, an integral part of mycobacterial cell wall architecture (Alderwick, *et al.* 2015). The varying components of the bacterial cell wall of Gram-positive, Gram-negative and acid-fast bacilli are depicted in Figure 1.1.

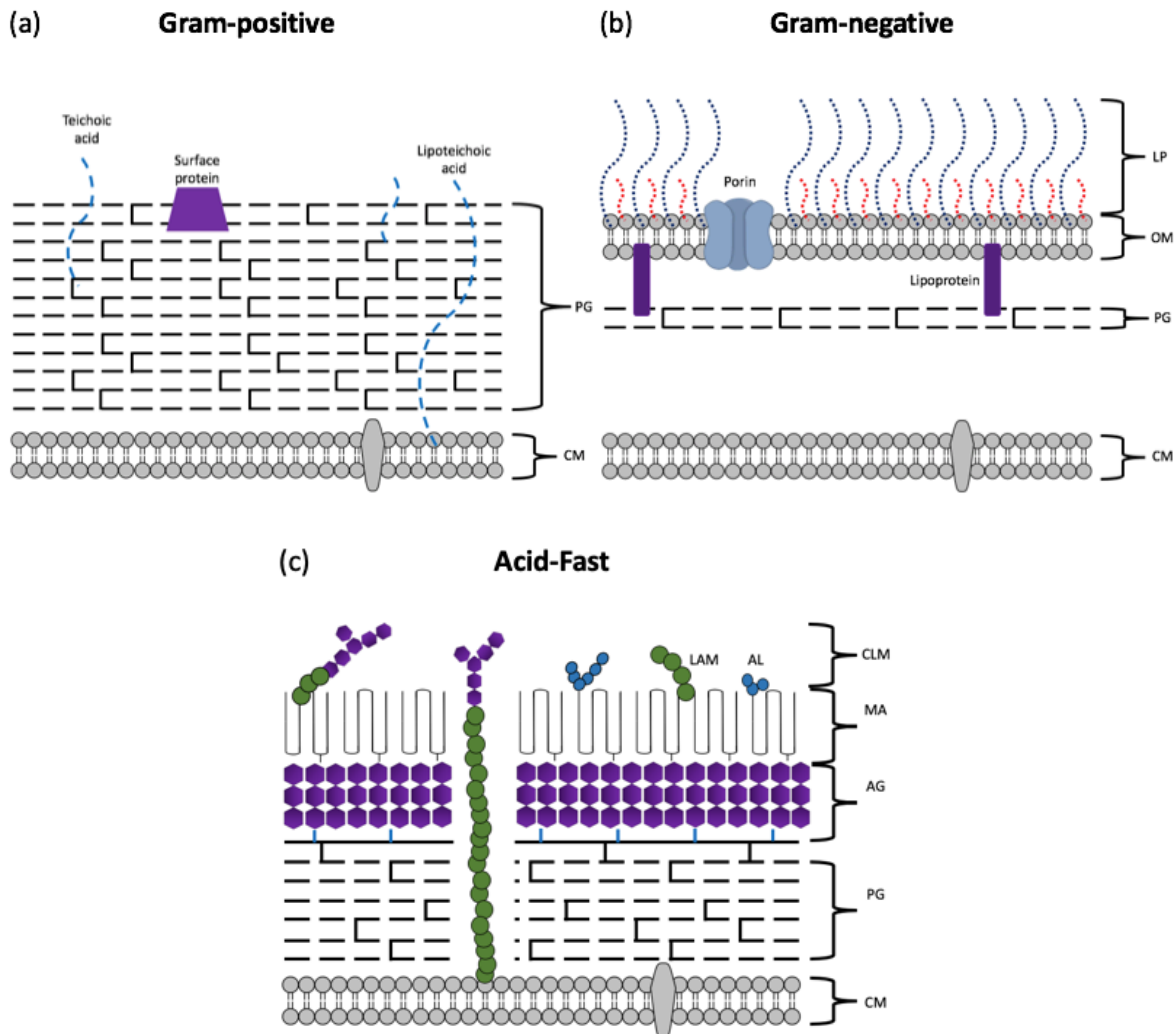


Figure 1.1 Cross-section of the major components of the bacterial cell wall of (a) gram-positive, (b) gram-negative and (c) Acid-Fast bacilli. Gram-positive bacteria contain a greater percentage of peptidoglycan. Gram-negative bacteria contain a smaller percentage of peptidoglycan and an outer membrane. Acid-Fast Bacilli contain the mycolic acid-arabinogalactan-peptidoglycan complex and an outer membrane comprised of glycopeptides and lipids. Abbreviations: CM – Cytoplasmic membrane, PG – Peptidoglycan, OM – Outer membrane, CLM – Capsule like material, AG – Arabinogalactan, MA – Mycolic acids, LP – Lipopolysaccharides. Adapted from Cabeen and Jacobs-Wagner (2005), Crick (2001) and Abrahams (2018).

1.3.1 Peptidoglycan

Peptidoglycan also known as murein (Vollmer and Holtje 2004) is present in virtually all known species of bacteria, excluding select examples such as *Mycoplasma* and archaeobacteria (Kim, *et al.* 2015). Peptidoglycan is not found in eukaryotic cells and is therefore a well-regarded site of antimicrobial investigation (Yount and Yeaman 2013). The purpose of the polymer is as a scaffold for the bacterial cell; preserving the overall shape, rigidity and stability of the cell membrane to protect from outside forces such as osmotic pressures, yet permitting steady bacterial growth, expansion and division (Vollmer, *et al.* 2008).

1.3.2 The structure of peptidoglycan

The fundamental structure of peptidoglycan, observed in the majority of bacteria consist of glycan strands interconnected by short cross-linked peptide side chains as depicted in Figure 1.2.

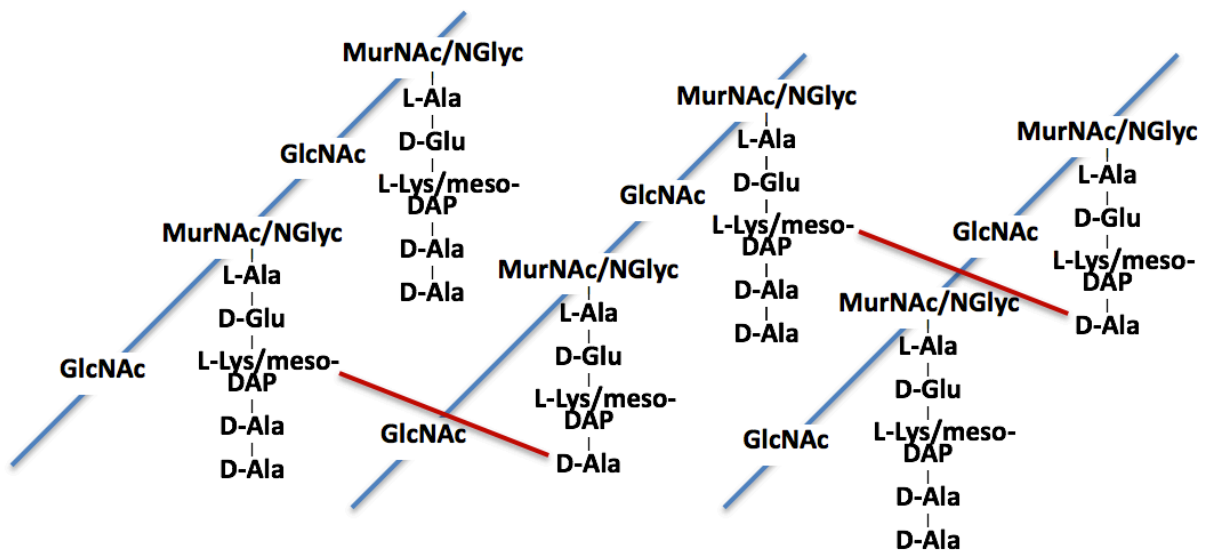


Figure 1.2: The structure of peptidoglycan in mycobacteria. Alternating N-acetylglucosamine (GlcNAc) and either N-acetylmuramic acid (MurNAc) or N-glycolylmuramic acid (MurNGlyc) sugars form glycan chains (blue lines) by β -1,4 glycosidic bonds. Chains are interconnected by cross-linking (red lines) amino acid 3 and 4 of parallel peptide stems. Position 3 is commonly L-Lysine for Gram-positive organisms and meso-DAP in Gram-negative and Acid-Fast bacilli. Abbreviations: MurNAc – N-acetylmuramic acid, GlcNAc – N-acetylglucosamine, L-Ala – L-Alanine, D-Glu – D-Glutamate, L-Lys – L-Lysine, m-DAP – meso-diaminopimelic acid. Adapted from Bugg, *et al.* (1999).

The mycobacterial peptidoglycan backbone is constructed from alternating N-acetylglucosaminyl (GlcNAc) and either N-acetylmuramyl (MurNAc) or N-glycolylmuramyl (MurNGlyc) sugar residues bound via $\beta(1\rightarrow4)$ linkages (Mihelic, *et al.* 2017). The cross linked bridges are formed initially from five bacterial specific amino acids. The formation of peptidoglycan involves the implementation of distinct phases to construct the overall sacculus. These are the cytosolic assembly of the UDP-MurNAc/NGlyc-pentapeptide subunits, the intracellular membrane-bound transport across the plasma membrane and integration into the interweaved sacculus architecture (Vollmer 2008).

1.3.3 The cytoplasmic steps of peptidoglycan synthesis

Uridine diphospho-N-acetylglucosamine (UDP-GlcNAc), the initial precursor of the cytosolic pathway is obtained from glucosamine biosynthesis, a product of carbohydrate metabolism (Spiro 1958). The first committed enzymatic step in the pathway involves MurA (Rv1315), an UDP-N-acetyl-glucosamine enolpyruvyl transferase catalyzing the transfer of an enolpyruvate group from phosphoenolpyruvate (PEP) to the C3 position of the glucosamine sugar ring of GlcNAc, culminating in UDP-GlcNAc-enolpyruvate (Babajan, *et al.* 2011). The subsequent enzyme in the pathway, MurB (Rv0482), an UDP-N-acetylenolpyruvylglucosamine reductase, permits the reduction of the enolpyruvate double bond utilising the transfer of electrons from NADPH via FAD to form the lactyl group of MurNAc, creating one of the two main subunits of peptidoglycan, linked to UDP (UDP-N-acetyl-muramic acid; UDP-MurNAc) (Eniyan, *et al.* 2018).

The remainder of the pathway appends selected amino acids to UDP-MurNAc to generate the pentapeptide stem. The residues appended to the subunit are specific to individual organisms. The four amino acid ligases MurC (Rv2151c), MurD (Rv2144c), MurE (Rv2158c) and MurF (Rv2157c) are ATP dependent enzymes (Munshi, *et al.* 2013) which employ an identical reaction mechanism involving a high-energy tetrahedral intermediate to react with the relevant amino acid to extend the peptidoglycan precursor by up to five amino acids. The standard pentapeptide stem is composed from L-Alanine, D-Glutamate, the third position for most Gram-positive organisms is L-Lysine or diaminopimelic acid (DAP) whereas most Gram-negative organisms and Acid-fast

bacilli incorporate DAP at this position (Consaul, *et al.* 2004). Variations to this sequence are observed in *M. leprae*. The mycobacterium incorporates L-Glycine into position one of the peptide stem as opposed to L-Alanine observed in other members of the mycobacterium genus (Mahapatra, *et al.* 2005). The final two residues are D-alanyl-D-alanine. D-amino acids are not natural cellular products, D-Alanine is generated from L-Alanine by a pyridoxal 5'-phosphate (PLP) cofactor dependent catalysis of alanine racemase (Alr), while D-Glutamate is isomerized from L-glutamate by glutamate racemase (MurI) which deprotonates the α -carbon of L-Glutamate with one active site thiol, and reprotonates the intermediate with a second thiol to bring about the L \rightarrow D conversion of glutamate (Glavas, *et al.* 2001). ATP dependent D-alanyl-D-alanine ligase (Ddl) combines two D-Alanine residues to incorporate them into the UDP-MurNAc peptide stem (Walsh 1989).

The cytosolic phase of peptidoglycan synthesis is tightly regulated to aid in mycobacterial pathogenesis and antibiotic survival. The activity of MurA is regulated by interaction with CwlM, an peptidoglycan amidase homologue which when phosphorylated by the Serine/Threonine protein kinase PknB increases MurA activity 30 fold (Boutte, *et al.* 2016). Direct phosphorylation of the cytosolic Mur ligases in mycobacteria (Thakur, *et al.* 2008) is also implemented by PknA and PknB to regulate the formation of the pentapeptide stem attached to UDP-MurNAc subunit against host stimuli (Munshi, *et al.* 2013). The cytosolic phase of peptidoglycan synthesis is depicted in Figure 1.3.

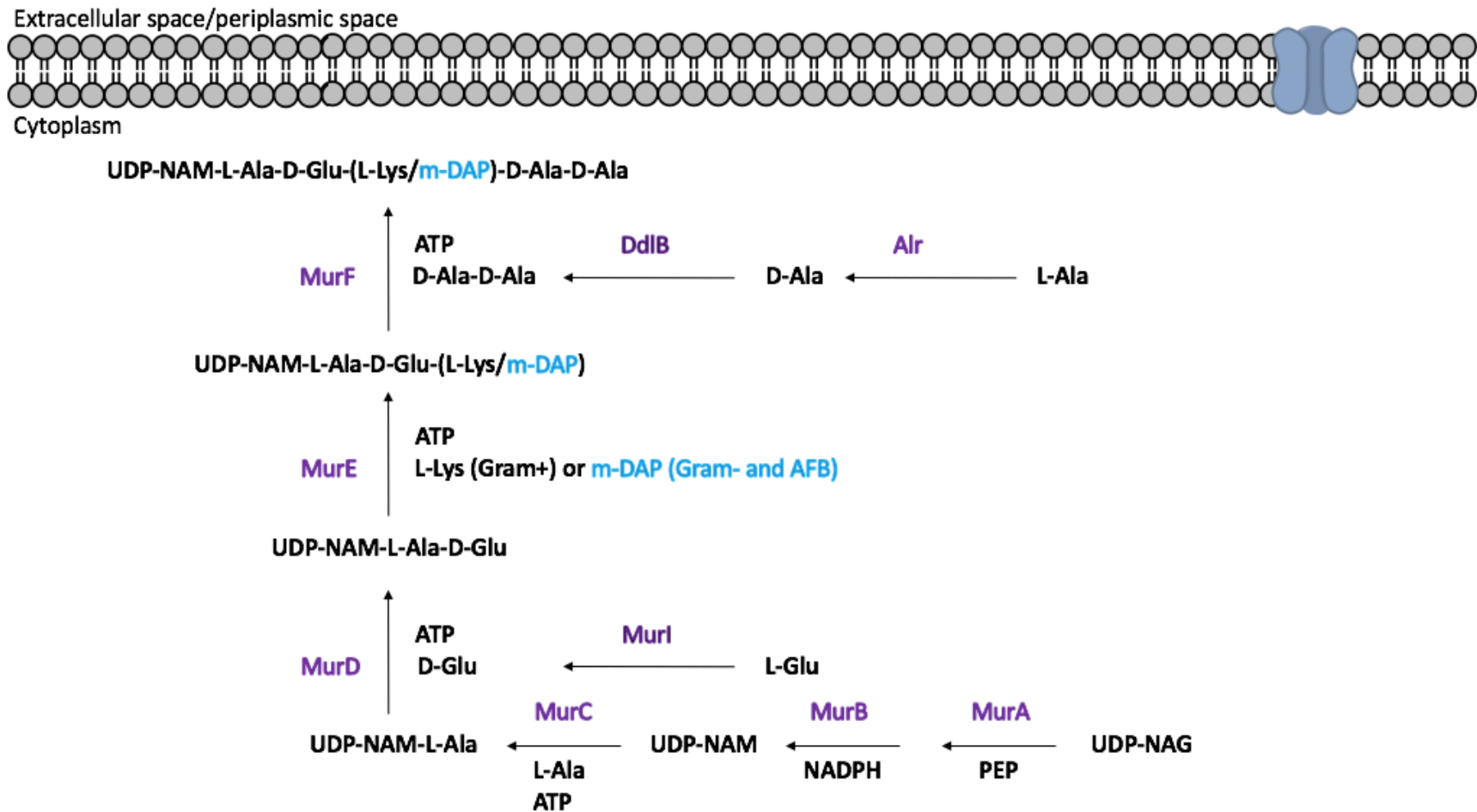


Figure 1.3 The formation of UDP-MurNAc-pentapeptide from the peptidoglycan cytosolic biosynthesis pathway. Cytosolic enzymes MurA and MurB transform UDP-GlcNAc into UDP-MurNAc. Four ATP dependent amino acid ligases MurC-F adhere bacterial specific residues (Black – Gram-positive, Blue – Gram-negative/Acid-Fast bacilli) to UDP-MurNAc creating UDP-MurNAc-pentapeptide. Abbreviations: NAM – N-acetylmuramic acid, NAG – N-acetylglucosamine, UDP – Uridine diphosphate, PEP – Phosphoenolpyruvate, ATP – Adenosine triphosphate, Alr – Alanine Racemase, DdlB – D-Ala-D-Ala ligase, AFB – Acid Fast Bacilli, L-Ala – L-Alanine, D-Glu – D-Glutamate, L-Lys – L-Lysine, m-DAP – meso-diaminopimelic acid. Adapted from Teo, *et al.* (2015).

1.3.4 Formation of Lipid II

Phospho-MurNAc-pentapeptide is translocated from UDP-MurNAc-pentapeptide to a prenyl phosphate which in most bacteria is the C₅₅ prenyl phosphate, undecaprenyl phosphate (Chen, *et al.* 2016). Mycobacteria are unique however in that they utilise the C₅₀ prenyl phosphate, decaprenyl phosphate for this purpose in a reaction catalysed by MurX (Rv2156c) to form Lipid I (decaprenyl diphospho-MurNAc-pentapeptide) (Mahapatra, *et al.* 2005). The enzyme MurG (Rv2153c), a glycosyltransferase is coupled to this reaction and transfers a GlcNAc subunit onto the C4 position of the muramyl sugar ring culminating in the formation of Lipid II (decaprenyl pyrophosphoryl-MurNAc-(GlcNAc)-pentapeptide) (Bouhss, *et al.* 2008). The decaprenyl phosphate carrier is acquired from two sources, the enzymatic phosphorylation of decaprenol or the dephosphorylation of decaprenyl pyrophosphate (Touz and Mengin-Lecreulx 2008).

1.3.5 Traversal of Lipid II to the extracellular face of the cytoplasmic membrane

Before incorporation into the peptidoglycan sacculus, Lipid II must be transported across the cytoplasmic membrane by a ‘flippase’. Currently the exact mechanism is unknown but two proteins have been reported to flip Lipid II. The first identified by Mohammadi *et al.* (2011) was *E. coli* FtsW corresponding to mycobacterial Rv2154c. This protein is important in cell division, and has the ability to move peptidoglycan subunits across proteoliposomes and membrane vesicles. The mechanism of transport involved a size-restricted pore-like structure with substrate specificity for Lipid II. The second protein (Sham *et al.* 2014) identified by *in vivo* experiments was MurJ, corresponding to mycobacterial Rv3910 as the unidentified flippase. Sham *et al.* (2004) also demonstrated that FtsW was unable to transport Lipid II *in vivo*. Coordination between a number of proteins is currently the suggested mechanism.

The formation of Lipid II and the traversal across the plasma membrane are depicted in Figure 1.4.

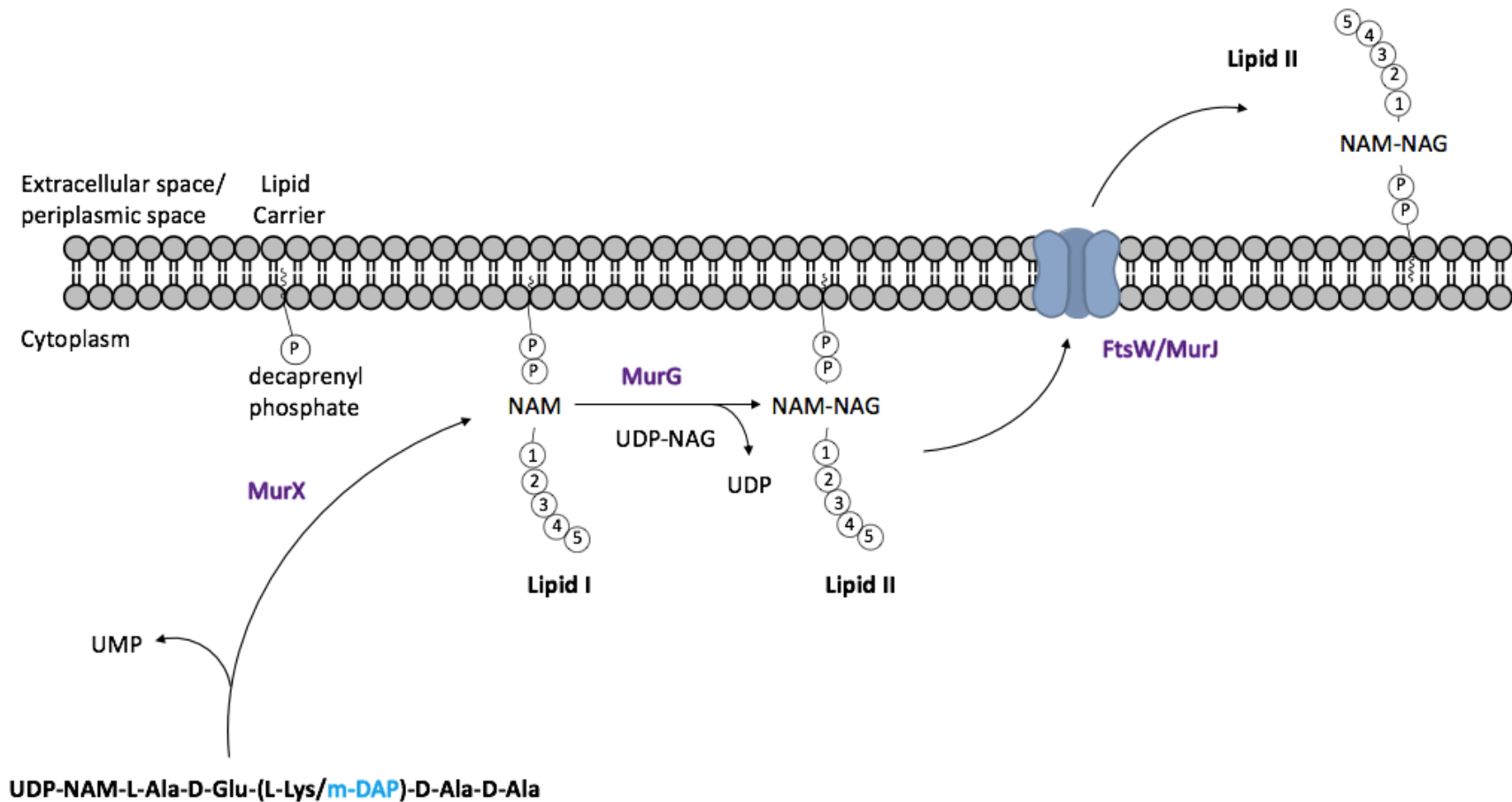


Figure 1.4 The formation of Lipid II and the traversal of Lipid II across the plasma membrane. UDP-MurNAc-pentapeptide synthesised within the cytoplasm is bound to a lipid carrier by MurX, generating Lipid I. MurG adheres GlcNAc to Lipid I forming Lipid II. Lipid II is transported between the cytoplasm and extracellular space/periplasmic space (Gram-positive/Gram-negative) by the plasma membrane bound ‘flippase’ FtsW or MurJ. Abbreviations: NAM – N-acetylmuramic acid, NAG – N-acetylglucosamine, UMP – Uridine monophosphate, UDP – Uridine diphosphate, L-Ala – L-Alanine, D-Glu – D-Glutamate, L-Lys – L-Lysine, m-DAP – meso-diaminopimelic acid. Adapted from Teo *et al.* (2015).

1.3.6 Extracellular peptidoglycan integration

Once Lipid II has been transferred across the plasma membrane it is integrated within the existing peptidoglycan chains. Penicillin binding proteins (PBPs) are extracellular enzymes, which are categorised by activity and molecular weight (Waxman and Strominger 1983). Select PBPs are unique in function whereas others display a redundancy (Sassine, *et al.* 2017). PBPs are divided into high molecular weight PBPs with either bifunctional transglycosylase and transpeptidase domains or monofunctional transpeptidases and low molecular weight PBPs, which are typically carboxypeptidases (Strobel, *et al.* 2014). Transglycosylation (TG) is the polymerisation of Lipid II to form the individual glycan chains that comprise peptidoglycan strands (Galley, *et al.* 2014). Transpeptidation (TP) is the cross-linking of the peptide stems to rigidify the glycan chain structures (Sauvage and Terrak 2016). Carboxypeptidation cleaves the terminal D-alanine residues from non-cross-linked peptide stems (Sauvage, *et al.* 2008).

In *M. tuberculosis* single strands of peptidoglycan are formed from Lipid II monomers along with the essential bifunctional PBPs PonA1/PBP1 (Rv0050) and PonA2/PBP2 (Rv3682) (Kieser, *et al.* 2015) which adhere the terminal 4'-OH of GlcNAc from one Lipid II onto a second Lipid II terminal MurNAc forming a β -1,4 glycosidic bond. The decaprenyl phosphate group is then displaced from Lipid II. Regulation of the mycobacterial PBP activity is modulated through phosphorylation of the cytoplasmic tail by the serine/threonine protein kinase PknB (Kieser, *et al.* 2015), a unique mechanism not observed currently in other organisms (Prisic, *et al.* 2010) and required to alter the rate of mycobacterial growth and cellular elongation (Kieser, *et al.* 2015).

The transpeptidation of parallel peptidoglycan strands occurs in two variations, either (4→3) or (3→3) cross-linking. Bifunctional PBPs contain TP domains that as far as have been observed, exclusively catalyse (4→3) cross-linking (Patru, *et al.* 2017). Transpeptidases that implement (3→3) cross-linking have not been found to possess TG activity (Hugonnet, *et al.* 2016). The most common form of cross-linking is (4→3) (Vollmer, *et al.* 2008), meaning the ϵ -amino group of the third position peptide of the stem, m-DAP in mycobacteria is connected to the α -carbonyl of the fourth position peptide, D-Alanine of a parallel glycan strand. Transpeptidation involves the formation of an acyl-enzyme intermediate (Sauvage, *et al.* 2008), a noncovalent complex between

the α -carbonyl carbon atom of the fourth position D-Alanine residue within the peptide stem of the donor peptidoglycan strand and the active site serine of the PBP transpeptidase domain. The TP active site utilises a lysine residue to abstract a proton to activate the nucleophilic activity of the active site serine (Kumarasiri, *et al.* 2014), causing the release of the terminal D-Alanine residue from the donor stem during acylation. Deacylation occurs through interaction of the acyl-enzyme intermediate with the ϵ -amino group of the third position amino acid of a secondary acceptor peptidoglycan strand displacing the PBP and forming a covalent bond with the donor strand resulting in transpeptidation (Macheboeuf, *et al.* 2007). The mechanism for (4 \rightarrow 3) peptide stem cross-linking is depicted in Figure 1.5.

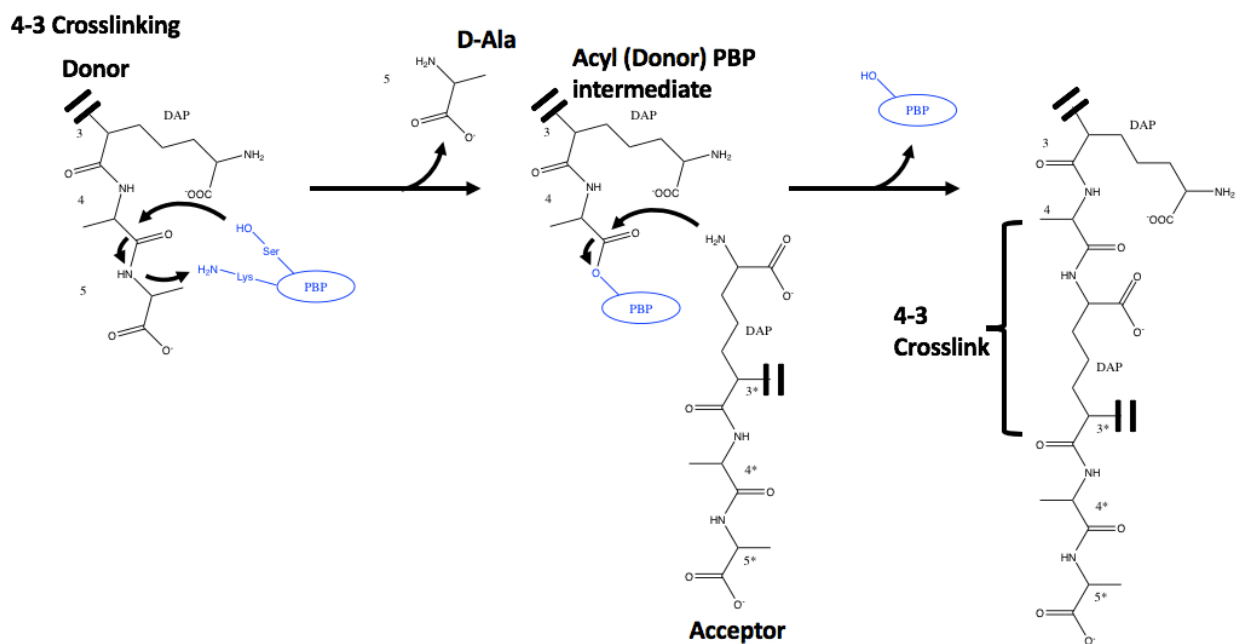


Figure 1.5 Transpeptidase activity of PBPs against parallel mycobacterial peptidoglycan strands forming a (4 \rightarrow 3) cross-link between peptide stems. The PBP active site lysine residue abstracts a proton to aid the formation of an acyl-enzyme intermediate implemented by the PBP active site serine residue against the α -carbonyl carbon atom of the fourth position D-Alanine of the donor stem. The terminal D-Alanine of the donor stem is released. Deacylation occurs through displacement of the PBP by the ϵ -amino acid group of the third position DAP of the acceptor peptide stem forming a covalent bond between the (4 \rightarrow 3) cross-link.

The second configuration of transpeptidation involves (3→3) cross-linking. The more rigid PG structure that results from (3→3) cross-linking is believed to aid against environmental stresses such as hypoxia and increase antimicrobial resistance (Peddireddy, *et al.* 2017). The peptide cross-links are constructed from transpeptidation by L,D-transpeptidases LdtMt1 (Rv0116c) and LdtMt2 (Rv2518c) (Correale, *et al.* 2013), containing an active site cysteine residue instead of the serine residue observed within the TP domain of PBPs (Magnet, *et al.* 2008). The tetrapeptide donor stem cleaved by carboxypeptidases interacts with the active site cysteine residue forming an acyl-intermediate with the third position DAP residue, and releasing the fourth position D-Alanine. Deacylation transpires when the enzyme is displaced by the ε-amino acid group of the third position DAP residue of the acceptor peptide stem forming a (3→3) cross-link covalent bond between the two DAP residues. The mechanism of (3→3) cross-linking of peptide stems is depicted in Figure 1.6.

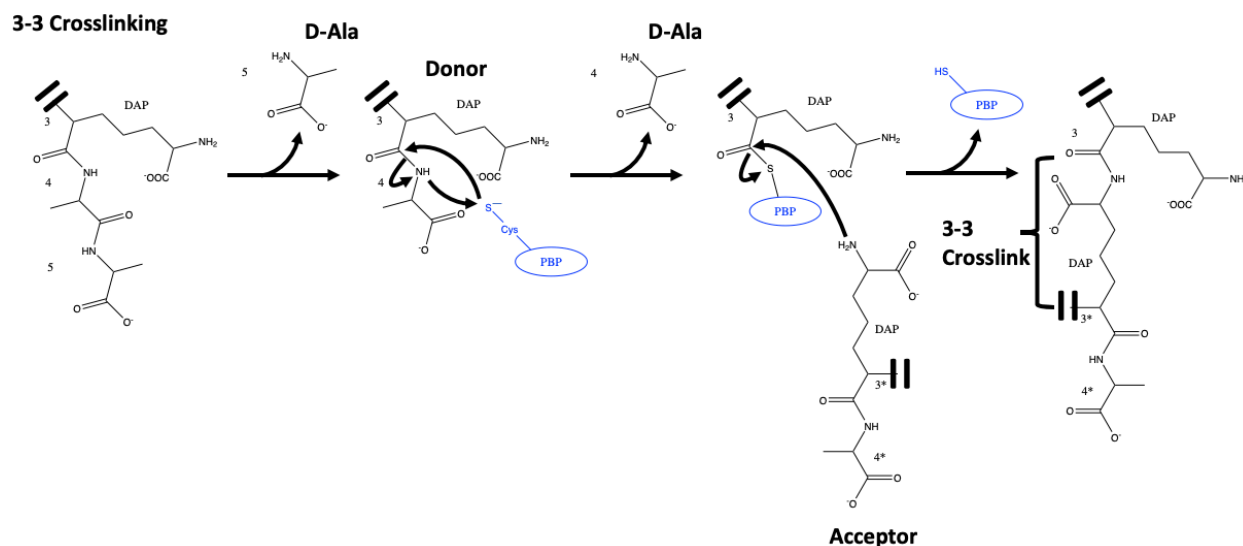


Figure 1.6 L,D-transpeptidase activity against parallel mycobacterial peptidoglycan strands forming a (3→3) cross-link between peptide stems. The L,D-transpeptidase active site cysteine residue forms an acyl-enzyme intermediate against the α -carbonyl carbon atom of the third position DAP residue of the donor stem. The terminal fourth position D-Alanine of the donor stem is released. Deacylation occurs through displacement of the transpeptidase by the ϵ -amino acid group of the third position DAP of the acceptor peptide stem forming a covalent bond between the (3→3) cross-link.

PBPs do not have a eukaryotic equivalent which makes them a key target of antibacterial investigations. As noted by the name penicillin binding proteins (Tipper and Strominger 1965), penicillins and other β -lactams such as cephalosporins interact with PBPs, specifically inhibiting the transpeptidase activity of the enzyme due to the structural similarity of these antibiotics to the donor substrate as well as the intrinsic reactivity of the β -lactam ring of penicillin, cephalosporin and related antibiotics. Lipid II integration into the polymerised peptidoglycan cell layer is depicted in Figure 1.7.

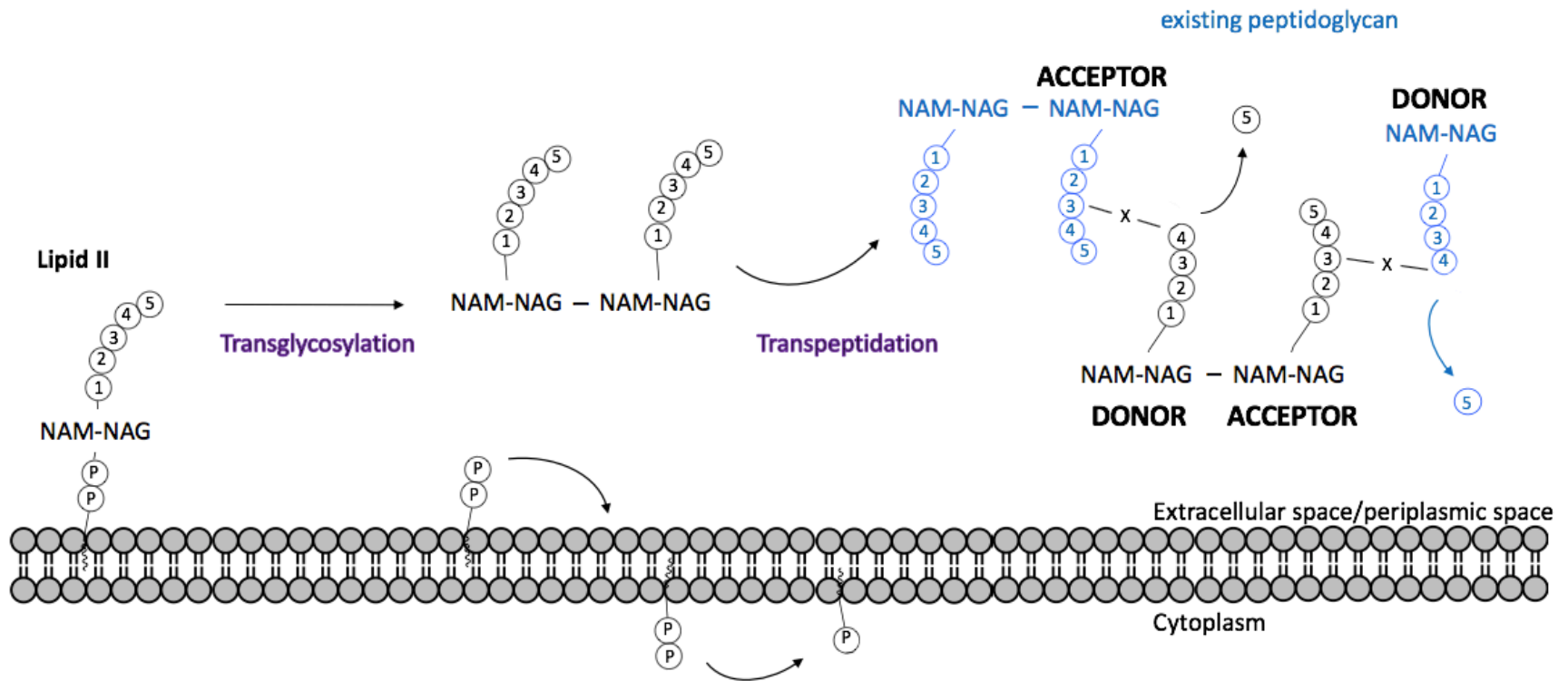


Figure 1.7 Nascent Lipid II incorporated into the overall peptidoglycan architecture by penicillin binding proteins. Translocated Lipid II synthesised within the cytoplasm is integrated by transglycosylation to extend the peptidoglycan glycan chain and parallel chains are cross-linked to improve structural stability by transpeptidation of the peptide stems. The lipid carrier is removed and recycled by traversing across the plasma membrane. Abbreviations: NAM – N-acetylmuramic acid, NAG – N-acetylglucosamine. Adapted from Teo *et al.* (2015).

1.3.7 Recycling and maintenance of peptidoglycan

The peptidoglycan sacculus is not a static structure. It is constantly being remodelled as new glycan monomers are incorporated and existing strands are cleaved to permit peptidoglycan turnover and cell division (Vollmer, *et al.* 2008). The localised removal of glycan strands is tightly regulated by peptidoglycan hydrolases. Those that cleave the β -1,4 glycosidic bonds of glycan strands are termed glycosidases and those who cleave the (4 \rightarrow 3) or (3 \rightarrow 3) peptide linkages are endopeptidases (Harty, *et al.* 2000). Once cleaved, the peptidoglycan disaccharides are recycled and redistributed as either a source of energy or reprocessed back into peptidoglycan biosynthesis (Park and Uehara 2008). Recycling of PG has traditionally been investigated in *E. coli*, as gram-positive bacteria lack an outer cell wall therefore it was initially assumed that PG was not recycled but instead lost (Park 1995), this is not a currently held belief (Borisova, *et al.* 2016), though the mechanisms for recycling in gram-positive organisms have not yet been identified. The membrane protein AmpG has been determined as the cytoplasmic transporter of PG monomers within *E. coli* (Lindquist, *et al.* 1993). A homologue of AmpG has yet to be classified in mycobacteria.

1.3.8 Modifications to peptidoglycan facilitating resistance to hydrolytic enzymes

The host's immune response to invading mycobacteria involves the release of hydrolytic enzymes such as lysozyme (Ragland, *et al.* 2017) to degrade the mycobacterial cell wall and aid immune signalling towards infected macrophages (Amaral, *et al.* 2016). Mycobacteria and other organisms attempt to mitigate these actions and evade recognition through specific peptidoglycan modifications to alter the composition of the bacterial cell (Ragland, *et al.* 2017) wall as depicted in Figure 1.8.

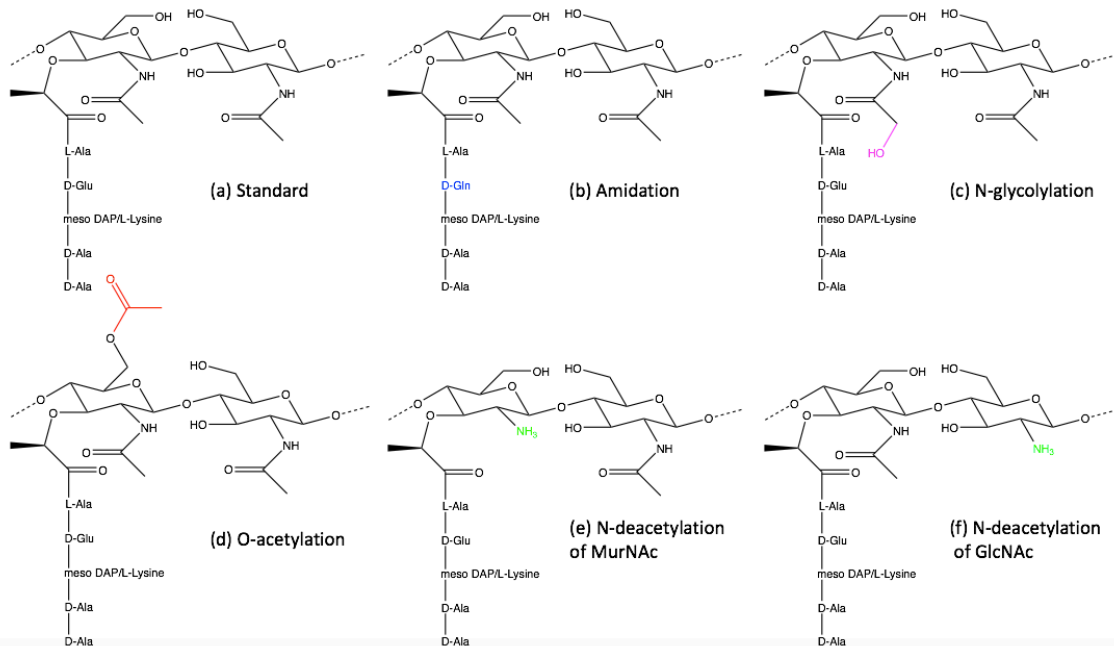


Figure 1.8 Modifications to the bacterial peptidoglycan monomer Lipid II to decrease susceptibility to host hydrolytic enzymes. Bacteria can utilise various alterations to the Lipid II structure to disrupt conventional enzyme binding. (a) The standard structure of Lipid II, (b) Amidation of D-glutamate to D-isoglutamine (Blue), (c) N-glycolylation of MurNAc to MurNGlyc (Pink), (d) O-acetylation of MurNAc (Red), (e) N-deacetylation of MurNAc to MurN (Green), (f) N-deacetylation of GlcNAc to GlcN (Green). Adapted from Ragland *et al.* (2017).

1.3.8.1 O-acetylation

O-acetylation is a ubiquitous peptidoglycan modification observed in numerous bacteria involving the appendage of an acetyl group to the C-6 hydroxyl of N-acetylmuramic acid sugars. The addition is administered by an O-acetyltransferase (OatA) within gram-positive bacteria (Moynihan and Clarke 2010) and coordinated through a transmembrane bound acetate transporter (PatA) and a periplasmic O-acetyltransferase (PatB) in Gram-negative bacteria (Bernard, *et al.* 2011). The modification is implemented on nascent peptidoglycan strands and perturbs lysozyme binding through steric hindrance without altering the host immune NOD (Nucleotide-binding oligomerisation domain-containing protein) recognition of peptidoglycan (Moynihan and Clarke 2010).

1.3.8.2 N-deacetylation

The removal of the C-2 acetyl group from either the GlcNAc or MurNAc moieties within the polymerised peptidoglycan, known as N-deacetylation is catalysed by the deacetylase PgdA (Rv1096), creating glucosamine, GlcN and muramic acid, MurN moieties (Vollmer and Tomasz 2000). This modification aids virulence by decreasing host immune NOD recognition of peptidoglycan (Boneca, *et al.* 2007) and reduces lysozyme activity by removing the proposed interaction between the acetyl groups and the lysozyme active site (Callewaert and Michiels 2010).

1.3.8.3 Amidation

Resistance towards hydrolytic enzymes can also be instigated through modification of the cross-linked peptide stem of peptidoglycan chains. The second and third residues of the peptidoglycan peptide stem D-Glutamate and m-DAP can be amidated (Ngadjeua, *et al.* 2018) with the D-Glutamate residue becoming D-Isoglutamine. This modification is predominantly found within gram-positive and acid-fast organisms and implemented by enzymes such as the mycobacterial amidotransferase GatCAB (Su, *et al.* 2016) to reduce the overall net negative charge of the cell envelope which attracts lysozymes (Figueiredo, *et al.* 2014).

1.3.8.4 N-glycolylation

N-glycolylation is a unique structural alteration of the muramic acid sugar predominantly found in all mycobacteria and members of the Actinobacteria family (Vollmer 2008), except *M. leprae* where the orthologue of MTB NamH in this organism (ML0085c) is a pseudogene (Mahapatra, *et al.* 2008). N-glycolylation differs from O-acetylation and N-deacetylation by the cellular region in which each modification takes place, occurring solely within the cytoplasm of the mycobacteria whereas the other two mentioned modifications occur in the extracellular region solely to polymerised PG. The methyl group of the N-acetyl moiety of UDP-MurNAc is oxidised to its

corresponding alcohol to form the N-glycolyl moiety by the hydroxylase, NamH (Rv3818) to form the N-glycolyl modification of peptidoglycan. (Raymond, *et al.* 2005), as depicted in Figure 1.9.

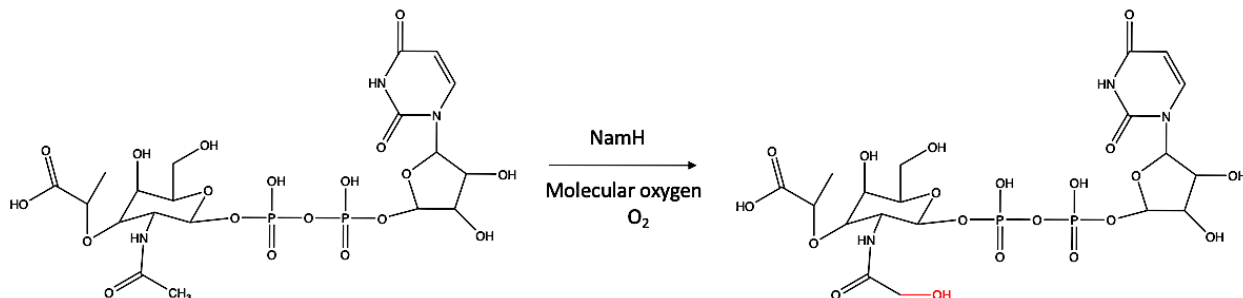


Figure 1.9: The hydroxylase activity of NamH. Molecular oxygen is fixed (highlighted in red) to the second position of the muramic acid ring of UDP-MurNAc due in part to the hydroxylase NamH oxidising the methyl group of the N-acetyl moiety into the N-glycolyl moiety generating UDP-MurNGlyc.

Categorised as a Rieske type monooxygenase enzyme (Rieske, *et al.* 1964), NamH catalyses the addition of a hydroxyl group to the muramic acid from oxygen molecules attained within an aerobic environment. NamH enzymes contain a 2Fe-2S centre to catalyse the reaction of oxygen with UDP-MurNAc substrates (Liu, *et al.* 2014). The active site is a flat rhombic cluster of two inorganic sulphide ions constructing a bridge with two Fe ions. One of the Fe ions interacts with two NamH cysteine residues while the other with two histidine residues. Utilising a reductase and cofactors such as NADPH permit the reduction of oxygen (D'Ordine, *et al.* 2009).

The mycobacterial cell wall incorporates both variants of muramic acid within the PG layer (Mahapatra, *et al.* 2005). The percentage incorporated can differ depending upon factors such as phase of cellular growth as well as location within host macrophages. The standard ratio of MurNGlyc:MurNAc sugars located within the peptidoglycan of exponentially growing *M. smegmatis* cells was observed by chromatographic and mass spectrometric analysis to be 7:3. (Raymond, *et al.* 2005). Though the addition of the N-glycolyl muramic acids within the peptidoglycan structure can mitigate against hydrolytic enzymes, the unique structural modifications permits increased immune recognition. The N-glycolylation of muramic acids was observed to significantly increase the stimulation of NOD2 receptor recognition during mycobacterial infection (Coulombe, *et al.* 2009). The innate host immune response to mycobacterial infection requires pattern recognition molecules such as Nod-like receptors and

Toll-like receptors coordinating to recognise the architecture relating to the invading bacilli and induce proinflammatory cytokine production (Bodar, *et al.* 2008). The findings reported by Coulombe *et al.* (2009) indicate that NOD2 pathway maybe precisely focused to recognise specific N-glycolylated mycobacterial cellular debris. The implementation of N-glycolylated peptidoglycan has however been demonstrated to not impact the pathogenicity of *M. tuberculosis* (Hansen, *et al.* 2014)

1.4 Tuberculosis infection

The obligate pathogen is transmitted from infectious patients in droplets of sputum, residing airborne for several hours (Singh, *et al.* 2016). Bacilli traverse the respiratory tract of hosts, invading the macrophages of lung alveoli (Guirado, *et al.* 2013).

1.4.1 Innate immune response

The first point of contact between the immune system of the host and invading bacilli, involves recognition of mycobacterial cell wall components such as lipoproteins (LprA) and lipoarabinomannans (LAM) (Welin, *et al.* 2008) by pattern recognition receptors (Toll-like receptors (TLR)) of the innate immune system (Takeda and Akira 2005). TLR-2 initiates a pro-inflammatory immune response, culminating in the activation of nuclear transcription factor (NF)- κ B within the macrophage and secretion of pro-inflammatory cytokines and chemokines to signal infection (Domingo-Gonzalez, *et al.* 2016).

The innate immune system identifies specific structures unique to bacteria such as the peptidoglycan cell wall, termed pathogen-associated molecular patterns (PAMPs) to activate pattern recognition receptors NOD1 and NOD2 (Fritz, *et al.* 2006). NOD1 is a receptor for muramyl peptides containing meso-diaminopimelic acid (DAP) within the peptide stem of released peptidoglycan fragments (Chamaillard, *et al.* 2003). NOD2 is a receptor for muramyl dipeptide ligands (Inohara, *et al.* 2003) (Mo, *et al.* 2012).

The bacilli are engulfed by phagocytes such as macrophages, neutrophils and dendritic cells forming a vacuole from the enclosed plasma membrane, known as a phagosome (Pauwels, *et al.* 2017). The internalised environment of the phagosome must undergo significant alterations to pH, hydrolytic enzyme content and nitric oxide concentration to successfully lyse the enclosed mycobacterial cell (Canton, *et al.* 2014). This maturation of the phagosome is a key component of the innate immune system. Once the bacilli has been phagocytosed two outcomes may transpire, favouring either the mycobacterium or the immune system as depicted in Figure 1.10.

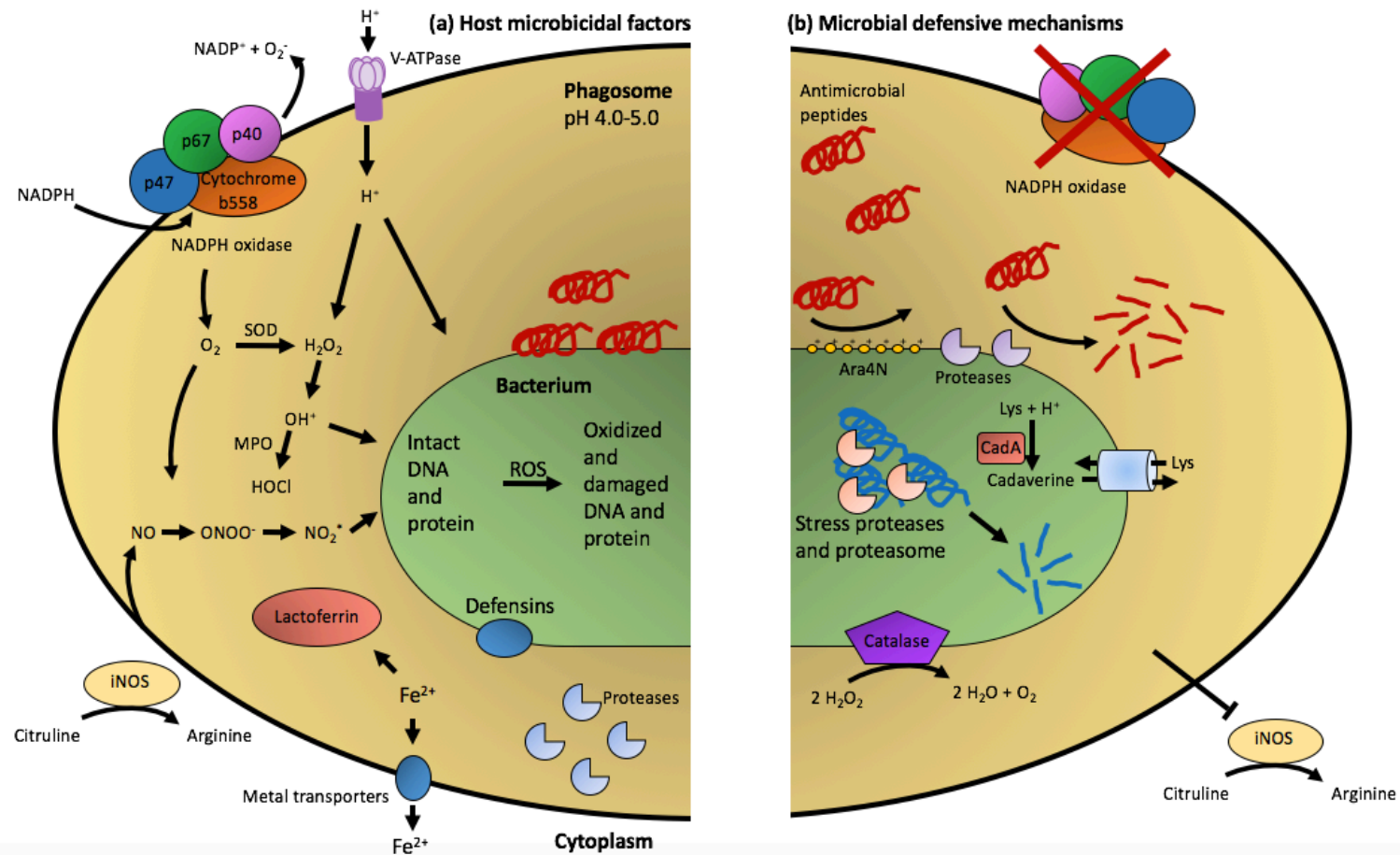


Figure 1.10 The antibacterial mechanisms of the phagosome to aid (a) host microbial factors, or (b) against bacterial defence mechanisms. Phagocytosed bacteria within the host macrophage phagosome attempt to prevent the activation of host antimicrobial activity such as the generation of reactive oxygen species (ROS), antimicrobial peptides, proteases and proton pumps. Bacteria utilise their own proteases to break down antimicrobial peptides, bacterial enzymes to alter harmful compounds, and inhibit recruitment of vital host protein complexes to synthesize ROS. Abbreviations: SOD - Superoxide dismutase, MPO - Myeloperoxidase, ROS - Reactive oxygen species, iNOS - inducible Nitric Oxide synthase, Ara4N - 4-amino-4-deoxy-arabinose, NADPH - Nicotinamide adenine dinucleotide phosphate. Adapted from Flannagan (2009).

1.4.1.1 Arresting phagosome maturation

The primary goal of the invading mycobacteria once phagocytosed is to prevent the maturation of the phagosome into the phagolysosome, forged by combining with lysosomes (Zimmerli, *et al.* 1996). Lipoarabinomannan (LAM), a glycolipid incorporated within the mycobacterial cell wall recognises and binds to both mannose and complement receptors (Kang, *et al.* 2005). The interaction aids mycobacterial virulence by preventing cytosolic increases in Ca^{2+} concentration, causing the incorporation of mannose capped with LAM onto the cell membrane of infected macrophages, impeding recognition. Mannose capped LAM ligands within dendritic cells bind to host mannose receptors and Dendritic cell specific intracellular adhesion molecule-3-grabbing nonintegrin (DC-SIGN) receptors suppress phagolysosome maturation, membrane antigen integration and macrophage apoptosis (Halder, *et al.* 2015). *M. tuberculosis* emits other targeted ligands to modulate macrophage response, for example phosphatidylinositol mannoside (PIM) binds Toll-like receptor-4 (TLR4) and inhibits the regulation the signalling pathways of infected macrophages (Doz, *et al.* 2009). Phagosome maturation suppression is essential to ensure mycobacterial reproduction and survival within host macrophages. Invading mycobacteria also diminish cytosolic phosphatidylinositol 3-phosphate (PI(3)P) concentration to delay phagosome maturation, by secreting the phosphatase SapM to hydrolyse PI(3)P (Vergne, *et al.* 2003). Unimpeded bacilli replicate and rupture the host cell macrophages to infect neighbouring cells (Simeone, *et al.* 2012). The halting of phagosome maturation is a key component for *M. tuberculosis* survival and proliferation within host macrophages (Welin, *et al.* 2008).

1.4.1.2 Phagosome maturation

If the innate immune system is unobstructed by the phagocytosed mycobacterium then phagolysosomal formation is established. The phagosome once formed is gradually integrated with other macrophage vesicles, firstly with an early endosome, then a late endosome and finally the lysosome (Desjardins, *et al.* 1994). The function of the phagolysosome is to provide a toxic environment to mycobacteria and ultimately lead to cell lysis. Mechanisms include the application of vacuolar proton transporting ATPase (vH^+ -ATPase) along with initiation of a Ca^{2+} signalling

cascade in order to reduce internal pH (Forster and Kane 2000), the generation of nitric oxide (von Bargen, *et al.* 2011) and ubiquitin derived autophagy (Bah, *et al.* 2016). The intrinsic pH of the phagolysosome measured at pH 5 (Flannagan, *et al.* 2009), optimises the lysosome derived acid hydrolysis of mycobacterium. The integrity of the mycobacterial cell membrane is destabilised by the generation of ubiquitin-derived peptides permitting generated nitric oxide to permeate the cell (Purdy, *et al.* 2009). Once cells are lysed within apoptotic vesicles, antigens derived from the mycobacterial architecture are integrated and distributed within the cell membrane of dendritic cells (Espinosa-Cueto, *et al.* 2017). Cytokine secretion initiated during recognition of bacteria attract a number of immune cells such as monocytes, neutrophils and lymphocytes to the site of infection (Lyadova 2017) and due to integration of mycobacterial antigens on the cell membrane, infected macrophages are recognised.

Macrophages release various cytokines and proteolytic enzymes as part of the innate immune response to *M. tuberculosis* invasion (Domingo-Gonzalez, *et al.* 2016). Over 50 distinct degradative enzymes such as proteases, glycosidases and phosphatases capable of impeding various cellular components are produced by the lysosome (Flannagan, *et al.* 2009), the majority of which are noted to display optimum enzymatic activity at acidic pH ranges (Odaka and Mizuochi 1999). These proteins vary in their roles from lactoferrin which prevents bacterial growth by sequestering iron within the phagosomal lumen (Masson, *et al.* 1969), to defensins which impact the integrity and permeability of the pathogen cell membrane (Lehrer, *et al.* 1993).

This thesis focusses on two specific hydrolytic enzymes secreted by the phagolysosome, lysozyme and β -hexosaminidase.

1.4.1.2.1 Lysozyme

Lysozymes are also known as either muramidases or N-acetylmuramide glycanhydrolases. They are characterised by their ability to hydrolyse the β -1,4 glycosidic bonds between either N-acetylmuramyl or N-glycolylmuramyl residues and N-acetylglucosaminyl residues of the carbohydrate components of the peptidoglycan of Gram-positive, Gram-negative or Acid-fast

organisms (Ragland and Criss 2017). Lysozyme was identified in numerous biological secretion and characterised as bacteriolytic (Fleming 1922). The structure of lysozyme was the first ever enzyme solved by x-ray diffraction (Blake, *et al.* 1967).

Found throughout bacterial, plant, animal species as well as in viruses, lysozymes are highly conserved anti-microbial enzymes and vital components of the innate immune response against microbial infection (Ragland and Criss 2017). The broad phylogenetic distribution of lysozymes is responsible for the evolution of bacterial mechanisms of resistance to these enzymes, either by modifying their peptidoglycan sacculus or through the utilisation of specific inhibitors (Ragland and Criss 2017). Lysozymes are sub divided into three main groups, c-type (Chicken), g-type (Goose) and i-type (Invertebrate), although other lysozyme variants from plants, bacteria and phages do occur (Jolles and Jolles 1984, Fastrez 1996). C-types include both the chicken and human lysozyme variants and are also noted to be standard models in the study of protein structure and function (Gourbatsi, *et al.* 2016). C-type lysozymes comprise two domains bridged by an alpha helix, where those enzymes have an optimal activity range of between pH 6-9, with an active site located in a deep cleft within the enzyme (Pincus, *et al.* 1977).

1.4.1.2.1.1 Human lysozyme

The human lysozyme consists of 130 residues with a molecular weight of 14.7 kDa. It shares around 58% amino acid sequence identity with the chicken homologue although the noted anti-bacterial activity is threefold greater (Wu, *et al.* 2015) as a result of variation in cationic residues and tri-dimensional structures. Human lysozyme, along with other C-type lysozymes are cationic (Callewaert and Michiels 2010), attracted to the negative charge of the targeted bacterial cell envelope, human lysozyme embeds itself within the cell membrane and forms pores to aid antibacterial activity (Zhang, *et al.* 2016). The two mechanisms of lysozyme activity are depicted in Figure 1.11.

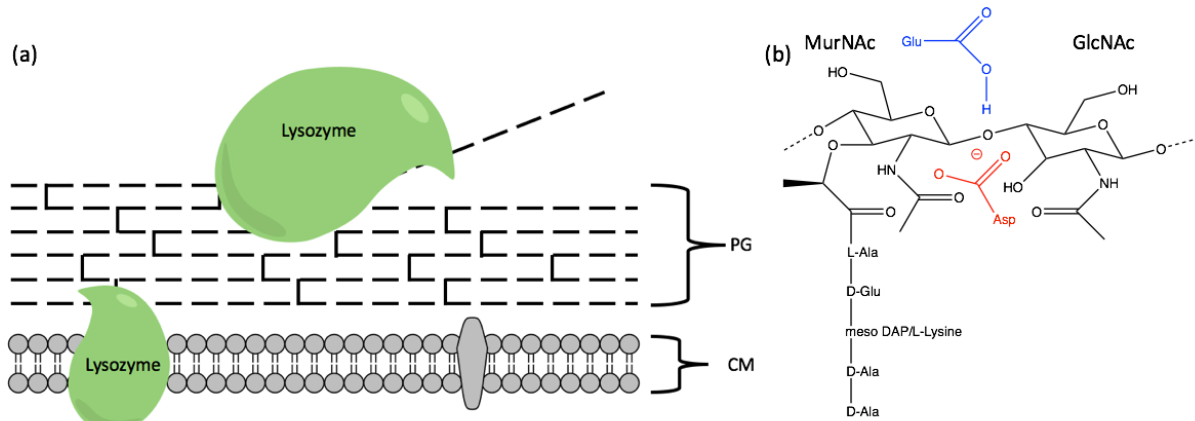


Figure 1.11 Hydrolysis of peptidoglycan by lysozyme. (a) The two proposed roles of lysozyme against microbial cells binding either to the peptidoglycan layer to hydrolyse PG monomers or embedded into the plasma membrane to disrupt integrity. (b) the hydrolysis reaction of lysozyme against the β -1,4-glycosidic bond between MurNAc and GlcNAc sugar monomers. The essential active site residues of the lysozyme active site, aspartic acid (red) and glutamic acid (blue) are depicted. Abbreviations: MurNAc – N-acetylmuramic acid, GlcNAc – N-acetylglucosamine, PG – Peptidoglycan, CM – Cytoplasmic membrane. Adapted from Ragland, *et al.* (2007).

Lysozyme plays a key role in the activation of the innate immune system. Macrophages secrete extracellular lysozyme during infection to produce PAMPs from the lysed bacterial peptidoglycan layer to initiate pattern recognition receptors (Davis, *et al.* 2011). The peptidoglycan of phagocytosed bacteria are hydrolysed by lysozyme within the phagolysosome and these peptidoglycan monomer ligands are transferred across the endosomal membrane of macrophages to NOD receptors to further increase immune recognition (Lee, *et al.* 2009). Occasionally viewed as an aid in disease diagnosis, raised concentrations of human lysozyme are observed in both the urine and serum of leukaemia patients (Osserman and Lawlor 1966). Lysozyme is a common antibacterial agent located within the blood and saliva as well as secreted by certain organs and cells such as the spleen, kidneys and white blood cells where specific missense mutation in the *lyz* gene can culminate as inheritable renal amyloidosis (Yazaki, *et al.* 2003).

1.4.1.2.2 β -hexosaminidase

β -hexosaminidase is the second enzyme produced by the lysosome (Koo, *et al.* 2008) to be investigated in this thesis. The enzyme has a similar mode of action to lysozyme although it cleaves

the β -1,4-linked glycosidic bond between MurNAc and GlcNAc subunits from the non-reducing end of oligosaccharide chains. The fully functional enzyme is comprised from one α and one β subunit transcribed from the genes *hexA* and *hexB* respectively. β -hexosaminidase is vital to regulating the central nervous system (Beutler 1979). It forms a complex with the cofactor GM2 activator protein within lysosomes, where it catalyses the decomposition of the ganglioside GM2 (Ganglioside monosialic 2). Mammalian β -hexosaminidases are organised into two functional isoforms composed of dimers from either α or β subunits (Dersh, *et al.* 2016). One isoform is β -hexosaminidase A, an α/β heterodimer which degrades GM2 gangliosides in neurons, whereas the other isoform, β -hexosaminidase B is a β/β homodimer secreted to degrade glycosphingolipids in the visceral organs. The role of the enzyme is vital as mutations in the genes of either the α or β subunits lead to accumulation of GM2 gangliosides within neurons concurrent with neurodegenerative disorders such as GM2 gangliosidosis. Gene mutation specific to the α subunit lead to Tay-Sachs disease (Myerowitz 1997), conversely β subunit gene mutations lead to Sandhoff disease (GM2-gangliosidosis type II) (Yamada, *et al.* 2013). Both disease states produce a debilitating ganglioside accumulation in lysosomes, especially those within neurons.

Recent investigations into β -hexosaminidase knockout mice indicate that the enzyme is an essential factor of innate immunity for the host, reducing mycobacterial infection and survival within macrophages (Koo, *et al.* 2008). *M. tuberculosis* infection has also been shown to impact regulation of specific hydrolytic enzyme expression within lysosomes. Infection leads to significant down-regulation of both α - and β -hexosaminidase subunits by a factor of 20- and 25-fold respectively (Hare, *et al.* 2017).

Patients who are carriers of the Tay-Sachs gene have been recognised as presenting an increased resistance to tuberculosis (Spyropoulos 1988). These patients, who are unable to form the functional α -chain and therefore have a deficiency of the α/β heterodimer form of β -hexosaminidase have significantly increased production of brain and fibroblast β -hexosaminidase B (β/β) by upwards of 200%. This has led to the understanding that the β/β homodimer is an important component of the host immune response to *M. tuberculosis* infection.

1.5 Dormancy

Dormancy is the process by which *M. tuberculosis* cells enter a reversible state of reduced metabolic activity to endure cellular stresses and the immune response of the host (Gengenbacher and Kaufmann 2012). This state known as non-replicating persistence (NRP) (Wayne 1994) is initiated by specific environmental factors such as immune response, pH and nutrient availability (Peddireddy, *et al.* 2017) in order for *M. tuberculosis* cells to persist without cellular division within the host for prolonged periods of time. Dormant *M. tuberculosis* bacilli were first identified within pulmonary lesions surgically excised from patients who tested negative to tuberculosis smear testing (Canetti 1955). Excised lesions were examined and found to contain both populations of viable and non-viable mycobacteria decades after initial infection, hence the term NRP. The bacilli contained within these persisting populations are profoundly heterogenic and can be divided into three separate categories based upon specific physiological states (Kaprelyants, *et al.* 1993). Bacilli can be described as viable, dormant or differentially culturable based upon their ability to propagate *in vitro*. Viable cells are able to grow readily within nutrient media; dormant cells depend upon resuscitation first before normal cellular growth can be obtained and differentially culturable cells are completely unable to be cultured *in vitro*. The immune response to mycobacterial invasion leads to the formation of granulomas, an aggregation of infected macrophages and activated T-cell lymphocytes encased in necrotic lesions to mitigate the pathogenesis of *M. tuberculosis* (Saunders and Britton 2007) as depicted in Figure 1.12.

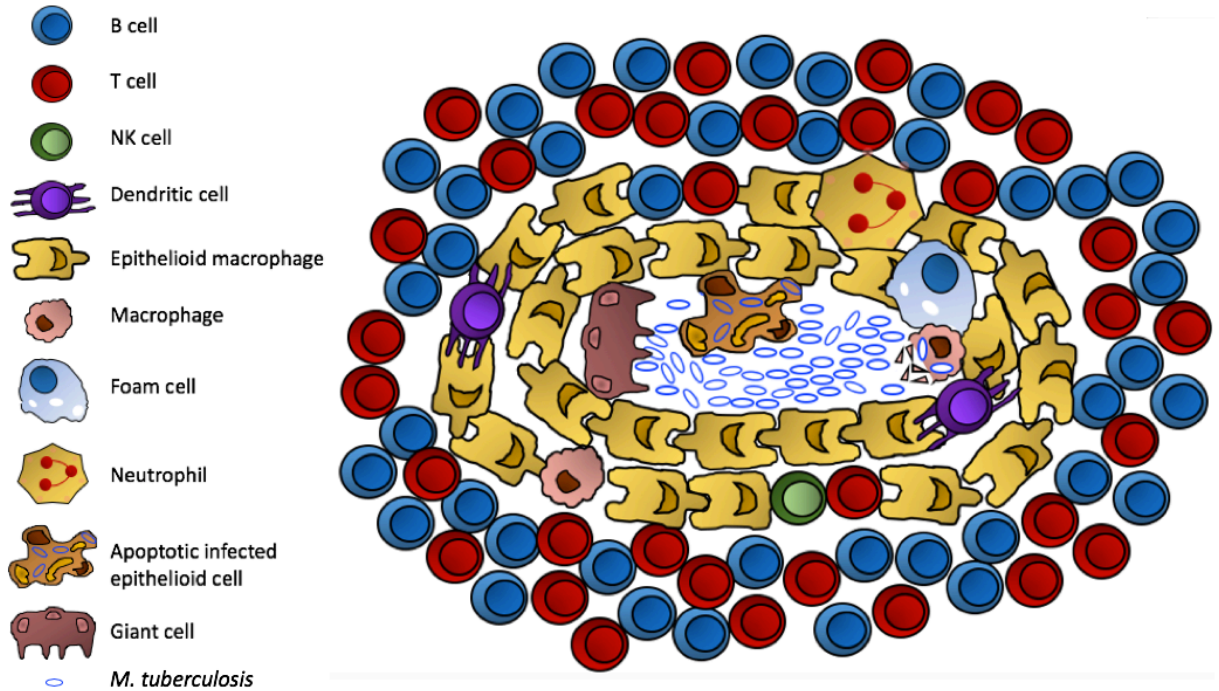


Figure 1.12 The cellular components and overall structure of a granuloma formed during tuberculosis infection. *M. tuberculosis* infected macrophages are encased with layers of interlinked epithelioid cells. Macrophages within the granuloma can combine to form multinucleated giant cells or differentiate into foam cells. Multiple other cell types aggregate to form a granuloma including T-cells, B-cells, NK cells, neutrophil cells and dendritic cells. The mycobacteria are localised within the necrotic core and are non-pathogenic to hosts. Adapted from Ramakrishnan (2012).

The granuloma microenvironment has a reduced pH and deprives the bacilli of oxygen and required nutrients for regular aerobic cellular growth. Mycobacteria persist within these necrotic granulomas by utilising a metabolic shift initiated by the two component regulatory system DosRS/T (Karakousis, *et al.* 2004). Genes related to this system were originally discovered within a virulent Dev strain of *M. tuberculosis*, leading to the genes for the DosR regulon being designated as *devR* (Rv3133c) and one of the two sensor histidine kinases, DosS being designated as *devS* (Rv3132c). The second kinase DosT, is expressed from the gene *dosT* (Rv2027c). The low oxygen, high nitric oxide (NO) and carbon monoxide (CO) environment of the granulomas stimulates the DosR regulon. *In vitro*, extended periods of stationary phase growth as well as static cultures can also lead to an activation of the DosR regulon (Honaker, *et al.* 2009).

Hypoxic conditions are a requirement for the regulon as even if activation is initiated by nitric oxide or carbon monoxide, the recognition of oxygen by the system is an inhibitor to dormancy

(Kumar, *et al.* 2007). The two sensor histidine kinases are activated by different environmental stimuli. DosS is a redox sensor, whereas DosT is a hypoxia sensor. The sensors exhibit comparable protein sequences although vary in their ability to autophosphorylate and phosphotransfer, with DosT more adept than DosS (Roberts, *et al.* 2004). As found in both eukaryotic and prokaryotic organisms, the sensors are known to contain the small-molecule binding, regulatory GAF domains (cGMP, adenylyl cyclase, FhlA) (Honaker, *et al.* 2009). These domains permit the sensors to bind heme, (Sivaramakrishnan and de Montellano 2013), which in turn binds the mentioned divalent gases, O₂, CO and NO and modulates the actions of the kinase response.

During aerobic conditions the redox sensor, DosS is in an inactive state attributed to the constant presence of oxygen. Its heme ligand is constantly oxidised to Fe³⁺, inhibiting kinase signalling. The DosT sensor in an aerobic environment is also inactive, bound to oxygen molecules, the kinase is able to resist oxidation (Sousa, *et al.* 2007), explaining the reason why it is able to respond to hypoxia, but unable to function as a redox sensor.

During immune response, macrophages produce nitric oxide. If concentrations of nitric oxide greatly exceed that of O₂, then nitric oxide will out compete the oxygen molecules for the heme binding sites of DosS (Voskuil, *et al.* 2003). Oxygen inhibits the DosS sensor fifty fold more than nitric oxide (Tuckerman, *et al.* 2002). In the absence of O₂ the heme bound to DosS is reduced to Fe²⁺, which in turn triggers autokinase activity of the sensor, signalling activation of the regulon. In the absence of O₂ the hypoxia sensor DosT is deoxygenated, initiating autokinase activity.

The redox/oxygenation state of the DosS/T sensors are used as a means of detecting the shifting environment and allowing the bacilli not only to adapt but persist. The induction of DosR is contingent upon the auto phosphorylation of either of the kinase sensors culminating in the phosphorylation of DosR (Roberts, Liao *et al.* 2004). DosR only regulates one of the two sensors, DosS in the two-hybrid system, due to the *dosS* gene residing within a region consisting of DosR regulon genes. *dosT* is situated close to one of these regions (Voskuil, *et al.* 2003) but does not act as though regulated by DosR. The expression of *dosT* is unaltered whether in aerobic or low oxygen environments (Saini, *et al.* 2004).

The DosT hypoxia sensor is important for initial recognition of environmental stresses and measuring the surrounding O₂ concentrations. Once O₂ decreases, DosT is induced and signals the DosR regulon and in turn increases the expression of *dosS*. The importance of DosT diminishes during hypoxic conditions and DosS is solely responsible for the induction of DosR regulated genes (Honaker, *et al.* 2009). The signalling of the DosR regulon by DosS and DosT is depicted in Figure 1.13.

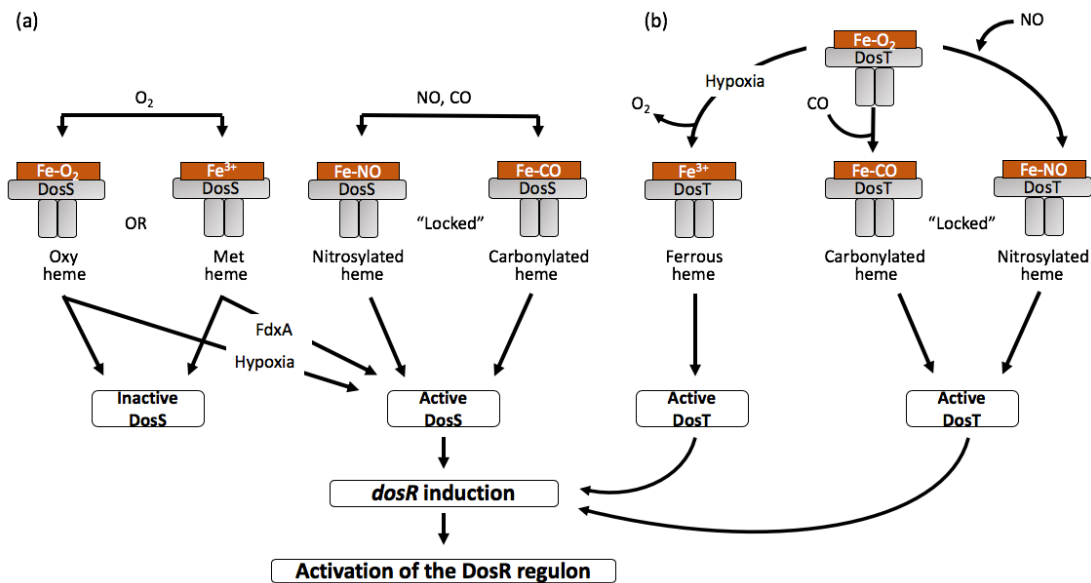


Figure 1.13 Activation of the *M. tuberculosis* DosR regulon by kinase sensors DosS (a) and DosT (b) to initiate mycobacterial dormancy. Interactions between the kinase sensors sensing divalent gases Oxygen (O₂), Nitric Oxide (NO) and Carbon Monoxide (CO) regulate the induction of the DosR regulon. (a) In the presence of O₂, the heme ligand of DosS is oxidised to Fe³⁺ inactivating signalling, in hypoxic conditions or with the aid of a cellular redox couple such as FdxA, DosS can be reduced implementing autokinase activity. DosS activity can also be initiated by interaction with NO and CO divalent molecules “locking” the sensor into an reduced active state initiating signalling. (b) In the presence of O₂, the heme ligand of DosT is oxygenated to Fe-O₂ impeding signalling. In hypoxic conditions or due to interactions with NO or CO divalent molecules, the sensor is “locked” into a deoxygenated active state initiating autokinase activity. The activation of the DosR regulon leads to the upregulation of highly conserved dormancy genes.

The DosR regulon consists of around 50 co-regulated genes vital for adapting and maintaining survival during dormancy (Leistikow, *et al.* 2010). Many of these genes transcribe hypothetical proteins with current unknown function, though specific genes aid in acquiring energy from alternative sources during dormancy such as nitrate reduction (Sohaskey 2005) and glyoxylate metabolism (Wayne and Lin 1982). The construction of a *M. tuberculosis dosR* deficient strain has

shown that genes upregulated by DosR in hypoxic conditions are contingent upon the regulon for induction (Park, Guinn *et al.* 2003). The majority of these DosR regulated genes have a DNA consensus motif preceding the sequence. Investigations have shown that DosR binds directly to this motif (Park, *et al.* 2003). Other environmental conditions known to induce the regulon include hydrogen peroxide (H₂O₂) and ethanol (C₂H₅OH) (Kendall, *et al.* 2004, Voskuil, *et al.* 2011). Dormant mycobacteria are not solely located within granulomas, and mycobacterial DNA have been identified from within adipose tissue (Neyrolles, *et al.* 2006). This type of tissue is also noted as a high nitric oxide/low oxygen environment. The physiological differences between aerobically cultured *M. tuberculosis* and dormant bacilli also impact treatment for patient. Those with latent tuberculosis require more tailored therapeutics as dormant cells are more resistant towards common antimicrobials (Aguilar-Ayala, *et al.* 2018). Dormant mycobacteria are non-infectious and can persist with the host several years until conditions within the granulomas change.

1.5.1 *In vitro* dormancy models

A number of models have been created to investigate dormancy *in vitro*, the most well-known being the Wayne model of non-replicating persistence characterises the impact of microaerophilic conditions on the growth and dormancy of *M. tuberculosis* (Wayne and Lin 1982). Previous methods noted that the sudden transfer of aerobically grown mycobacteria to an instantly anaerobic environment led solely to cell death but the gradual reduction of oxygen induced dormancy (Wayne 1994). The Wayne model identified two separate stages of non-replicating persistence (NRP) depending upon the oxygen concentration. NRP stage 1 was categorised once diminishing oxygen saturation had reached 1%. This stage involved a significant and constant formation of glycine dehydrogenase and a steady production and maintenance of ATP concentration. The turbidity of the culture slowly increased during this period though the cause was not attributed to an increase in CFU.

NRP stage 2 required 0.06% O₂ saturation. During this almost anaerobic stage the turbidity seen in stage 1 did not increase and the previously observed high production of glycine dehydrogenase was notably reduced. The survival of mycobacteria within NRP stage 2 was greatly increased by

acclimatising for an extended time period within NPR stage 1. The Wayne model also observed that NRP bacilli from either stage could be immediately resuscitated once introduced to optimal aerobic and nutrient conditions (Wayne 1994).

Other models of *in vitro* dormancy include nutrient starvation in PBS (Betts, *et al.* 2002), incubation in extended stationary phase (Smeulders, *et al.* 1999, Shleeva, *et al.* 2002) as well as the multiple stress model (Deb, *et al.* 2009).

1.5.2 *In vivo* dormancy models

Standard *in vivo* animal models of *M. tuberculosis* infection involve either rabbit, guinea pig or most commonly mouse hosts (Gupta and Katoch 2009) due to the similarity to the human immune response. Mouse models initially demonstrated the relationship between the immune response to infection and the triggering of mycobacterial dormancy, depicting the switch as not solely nutrient derived (Wayne and Sohaskey 2001).

Animals can be infected by aerosols to imitate the standard infection route in humans with low-dose bacterial loads or injected intravenously with high-dose bacterial loads such as the Cornell model (McCune and Tompsett 1956). Predominantly a study of chronic infection, the Cornell model in mice causes mycobacterial infection ($1-3 \times 10^6$ dose) led by an extended antimicrobial therapy of isoniazid and pyrazinamide to produce bacilli that are non-culturable. The disease state can be reactivated through suppression of the host immune system (McCune, *et al.* 1956). The mouse model displays a number of drawbacks to investigating latent tuberculosis infection. The granulomas created within mice lack the rigid formation and composition found in the human host, leading to a lack of necrosis at the core of the granuloma, vital for mycobacterial dormancy (Munoz-Elias, *et al.* 2005). To mimic human mycobacterial infection with greater accuracy, artificial granulomas are implanted within mice models subcutaneously to induce the latent mycobacterial disease state (Karakousis, *et al.* 2004).

1.5.3 Resuscitation

M. tuberculosis bacilli can remain in a state of dormancy for decades as long as the encased granuloma environment remains constant (Kapoor, *et al.* 2013). Maintaining the stability of granulomas requires tumour necrosis factor (TNF- α) activity (Keane, 2005) in signalling innate immunity. *In vivo* investigations in mouse models (Mohan, *et al.* 2001) have concluded that employing monoclonal anti-TNF antibodies to constrain the cytokine commences resuscitation. A compromised immune system constraining T-cells results during immunosuppression; common causes include advanced age (Montecino-Rodriguez, *et al.* 2013), treatment for autoimmune disease (Stenger, 2005) or HIV infection (Paige and Bishai 2010). Co-infection of TB and HIV leads to an active tuberculosis state as HIV infection diminishes the total number of CD4⁺ and/or CD8⁺ T-cells primed to respond to *M. tuberculosis* infection (Wells, *et al.* 2007).

Once the granuloma environment changes from an anaerobic to aerobic state, the mycobacteria must initiate resuscitation procedures in order to become a metabolically active infectious pathogen. Oxygen molecules once again outcompete other divalent gases and bind to the heme groups of DosS/T kinase sensors, terminating signalling to the dormancy regulon DosR (Tuckerman, *et al.* 2002).

Resuscitation is also instigated by lytic transglycosylases defined as resuscitation promoting factors (Rpfs) (Telkov, *et al.* 2006) and RipA (Rpf-interacting protein A), an endopeptidase (Hett, *et al.* 2007). Rpfs not only permit bacilli to revert back to an active state but also stimulate growth (Rosser, *et al.* 2017). Five *rpf* gene homologues, *rpfA-E* have been identified within the genome of *M. tuberculosis* (Mukamolova, *et al.* 2002), each possessing muralytic activity towards the β -1,4 glycosidic bonds of peptidoglycan in a similar method to c-type (chicken) lysozyme (Cohen-Gonsaud, *et al.* 2005). The homologues display a functional redundancy and are known to be non-essential for mycobacterial growth (Downing, *et al.* 2004). Non-culturable dormant *M. tuberculosis* *rpf*-deficient strains have been examined and determined to be significantly impaired during resuscitation (Downing, *et al.* 2005). Individual Rpfs form a two protein complex with RipA at the septa of cells undergoing cellular division (Hett, *et al.* 2007). The mechanism by which resuscitation is enacted is still undetermined.

1.6 Diagnosis

Basic laboratory identification of mycobacteria is obtained through Acid-fast Ziehl-Neelsen staining of acquired sputum samples (Riello, *et al.* 2016). A fuchsine based dye combined with the presence of phenol is used to penetrate the lipid layer, cells are decolourised by an acid-alcohol solution and counter stained for identification under microscopy. The relatively inexpensive diagnostic test has certain disadvantages including the inability to detect extrapulmonary TB (Purohit and Mustafa 2015). Frequently polymerase chain reaction (PCR) testing is coordinated with acid fast bacilli (AFB) staining to increase diagnostic precision and reduce false negative diagnoses (Ryu 2015). The oldest currently used technique is the tuberculin skin test, otherwise known as the Mantoux test (Nayak and Acharjya 2012), an intracutaneous tuberculin injection, instigating a delayed hypersensitivity reaction. The original hypothesis for the test was determined in 1890 by Robert Koch and the standard intradermal technique was pioneered by Charles Mantoux in 1907 (Yang, *et al.* 2012) utilising purified protein derivative (PPD) from *M. tuberculosis* cells. The methodology for amassing PPD was revised and standardised in 1934 by Seibert (Seibert 1934). PPD is no-longer acquired solely from MTB, instead less pathogenic alternatives have been developed, denoted by a suffix letter such as PPD-A for *M. avium*. Other common methods for evaluating pulmonary TB in patients include chest x-rays (Woodring, *et al.* 1986) and computed tomography (CT) scans to locate and define lesions (Lee, *et al.* 1993). Interferon- γ release assays (IGRAs) provide a twenty-four-hour outcome from initial testing (Banaei, *et al.* 2016). The assays measure the interferon- γ (IFN- γ) immune response of patients to specific *M. tuberculosis* antigens. The known drawback to IGRA testing is the inability to distinguish between active and dormant tuberculosis (Sharma, *et al.* 2017).

1.7 Antimicrobial Discovery

At the beginning of the 20th century the potential of antimicrobials was being hypothesised. A German physician, Paul Ehrlich ascertained that specific chemical dyes stained selective bacterial cells but not others, and extrapolated that certain compounds may kill selective cells (Bosch and Rosich 2008). The first antimicrobial, Arsphenamine was discovered in 1909 for the treatment of

sypilis (Williams 2009). In 1928, Alexander Fleming inadvertently discovered the antibiotic, Penicillin (Tan and Tatsumura 2015), secreted from the fungi *Penicillium notatum*. The mould prevented growth of Staphylococcus, creating a bacteria-free zone. The isolation and purification of the antibiotic by Florey and Chain (Gaynes 2017) led to penicillin being the first mass produced antimicrobial utilised to treat infection during the second world war. These discoveries led to the global effort during the 1900s to purify and distribute antimicrobial products to medicate against bacterial infection. Early antimicrobial discoveries include Sulphonamide (1935) (Jesman, *et al.* 2011), Cephalosporins (1945) (Nakajima 2003), Chloramphenicol (1947) (Wiest, *et al.* 2012), and Aminoglycosides (1943) (Vong and Auclair 2012). Predominant targets of antimicrobial therapies include DNA replication, protein synthesis and the bacterial cell wall (Kohanski, *et al.* 2010).

1.7.1 Tuberculosis treatment

The primary protection from *M. tuberculosis* infection in humans was the production of a vaccine (Luca and Mihaescu 2013). The Bacillus Calmette Guérin (BCG) vaccine containing a living attenuated strain of *M. bovis* is commonly administered to both infants and adults to present mycobacterial antigens to the immune system. Vaccination unfortunately impedes certain methods of tuberculosis detection in patients such as the tuberculin test (Buddle, *et al.* 1999). The standard antimicrobial treatment for tuberculosis is a six to nine-month multidrug combination (Kerantzas and Jacobs 2017), synergising the activities of four anti-tuberculosis therapies. Isoniazid (INH), a prodrug activated by the mycobacterial heme enzyme, KatG (Metcalf, *et al.* 2008) inhibits the formation of mycolic acids (Quemard, *et al.* 1991). Targeting the fatty acid synthetase II (FAS-II) system, Isoniazid inactivates InhA, a 2-trans-enoyl-acyl carrier protein reductase (Marrakchi, *et al.* 2000). Rifampicin (RIF) is primarily a derivative of rifamycin B, a product of the bacterium *Amycolatopsis mediterrani* (Nigam, *et al.* 2014). An inhibitor of bacterial DNA transcription to RNA, rifampicin binds to the β -subunits of the RNA polymerase RpoB. Pyrazinamide (PZA) is active as an anti-tuberculosis therapy once hydrolysed to pyrazinoic acid (POA) by a pyrazinamidase enzyme PncA expressed by *M. tuberculosis*. The mode of action of the prodrug once activated by PncA is currently unknown but was initially believed to obstruct metabolism and the mycobacterial plasma membrane (Zhang, *et al.* 2003). Currently it is thought that POA

impacts trans-translation and ribosomal protein S1 (RpsA) (Shi, *et al.* 2011), although this has been disputed (Dillon, *et al.* 2017). The efficacy of Pyrazinamide is elevated against slow and non-replicating bacilli (Pullan, *et al.* 2016). Ethambutol (EMB) is an antimicrobial targeting the mycobacterial cell wall (Alderwick, *et al.* 2015). A known inhibitor of several key components of the complex; ethambutol prevents the transport of mycolic acid into the cell wall, as well as the inhibition of arabinogalactan and lipoarabinomannan biosynthesis (Goude, *et al.* 2009).

The multidrug therapy administration can vary depending upon the stage of tuberculosis infection as certain treatments have greater efficacy against solely latent or active TB. Latent TB infection is commonly treated with a monotherapy of isoniazid, or rifampicin if isoniazid resistance is detected (Norton and Holland 2012). If resistance towards one or all of the first-line therapies occurs, then second-line therapies are implemented. Second-line treatments include fluoroquinolones and aminoglycosides (Falzon, *et al.* 2013) which inhibit DNA gyrase (Hooper 1999) and protein synthesis (Eustice and Wilhelm 1984) respectively.

Select antimicrobials utilised against standard drug resistant tuberculosis strains target the mycobacterial peptidoglycan biosynthesis pathway. D-cycloserine, another secondary TB therapy inhibits the enzymes Alr and Ddl responsible for the synthesis of D-Ala-D-alanyl, the fourth and fifth amino acids of the UDP-MurNAc/NGlyc-pentapeptide stem (Chen, *et al.* 2017). Vancomycin, a glycopeptide antibiotic enacts hydrogen bonding with the terminal D-Ala-D-Alanyl residues of UDP-MurNAc-pentapeptide, preventing incorporation of the precursor into the peptidoglycan layer (Soetaerta, *et al.* 2015).

1.7.2 Antimicrobial resistance

The prevalence of antimicrobial resistance (AMR) is impacting all aspects of antimicrobial therapy and research, rapidly becoming a global health threat (Gootz 2010). Current estimates predict AMR will supersede cancer as the leading global cause of death annually by the year 2050 (O'Neill 2015). Basic standard treatments to common infections are insufficient, with selected bacterial

strains becoming multidrug resistant (Zhang and Yew 2009). It is vital that new and existing targets be explored in order to develop contemporary antimicrobials to implement against AMR.

1.7.3 Mechanisms of Antimicrobial resistance

The acquisition and implementation of resistance to antimicrobial products is an evolutionary requirement and plays a key role in the survival of bacteria within a microenvironment (Miller, *et al.* 2016). The natural selection of resistance used to occur over an extended time period but recent advances in drug discovery and global application of therapies have produced a number of man-made selection pressures to pathogens, that have increased resistance acquisition (Kapil 2005). Resistance to antimicrobials can be gained, through acquiring genes such as methicillin resistance in *Staphylococcus aureus* (MRSA) (Lee, *et al.* 2018) the altering of genes such as pneumococcal penicillin resistance (Hakenbeck, *et al.* 2012), or inherently such as impermeable membranes (Gotoh 2001) and efflux pumps (Poole 2007).

The time frame for adaption of targets to therapies can vary. Resistance towards the antibiotic vancomycin, a peptidoglycan biosynthesis inhibitor, (Hammes and Neuhaus 1974) was identified 30 years after its original development (Launay, *et al.* 2006); whereas sulphonamide resistant streptococcal strains were identified within three years of the drug first being prescribed (Finland, *et al.* 1976).

The most basic instance of resistance is a mutation to the genetic sequence of an antimicrobial target. Examples include the simplest single point mutations, along with insertions, deletions and inversions of genes (Nollau and Wagener 1997). The alteration of a single nucleotide can significantly impact not only the amino acid sequence but also the 3-dimensional structure of the folded protein, altering the drug target.

A consequence of being unable to utilise the exchange of genetic material termed horizontal gene transfer, *M. tuberculosis* cultivates resistance to prevailing therapies such as rifampicin and streptomycin by genetic mutation (Ramaswamy and Musser 1998). Other methods of resistance

include impacting the efficacy of the antimicrobial through either hydrolysis (Tao, *et al.* 2012) or modification (Lambert 2005), inactivating the drug. β -lactamases hydrolyse the β -lactam ring, the functional group of β -lactam antibiotics such as penicillin (Heesemann 1993). Modifications of drug structure to impede activity are the focus of phosphoryltransferases and acetyltransferases which catalyse O-phosphorylation and N-acetylation respectively to impact aminoglycosides (Morita, *et al.* 2014) and chloramphenicol (Shaw 1983). The final noted bacterial mechanism to influence drug concentration are efflux pumps. Located ubiquitously within the membranes of all bacteria, efflux pumps diminish the intracellular concentration of administered antimicrobials (Poole 2007).

1.7.4 Antimicrobial resistant Tuberculosis

Aside from acquired resistance to selected antimicrobials, mycobacteria are inherently resistant to various therapies, that target the mycobacterial cell wall (Hett and Rubin 2008). The reduced rate of diffusion traversing the mAGP complex coupled with efflux pumps, antimicrobial degrading enzymes and response regulators impedes drug efficacy (Chambers, *et al.* 1995). Tolerance towards an antimicrobial is not equivalent to resistance. Tolerance is not a genetic predisposition (Murakami, *et al.* 2017), but avoidance of mycobacterial lysis instigated by dormant or non-replicating cells (Fattorini, *et al.* 2013) along with numerous drug resistance pumps (Poole 2007). Isoniazid, ethambutol and rifampicin tolerance has been established *in vitro* (Tudo, *et al.* 2010, de Keijzer, *et al.* 2016). Antimicrobial resistance to drug therapies can be separated into primary resistance, infection acquired through a resistant strain and acquired resistance, observed during drug treatment (Jenkins, *et al.* 2018). Acquired resistance to one of the standard multi-drug therapies to tuberculosis can be obtained through inadequate drug adherence, management or selection pressures (Kapil 2005).

Generally evoked due to genetic mutation, there are four classifications of mycobacterial resistance states (Chan, *et al.* 2009). The first state is when a strain is mono-resistant to a single first-line therapy. Poly-resistant when immune to two or more therapies excluding isoniazid and rifampicin. A strain identified as resistant to both isoniazid and rifampicin is termed multidrug-resistant

(MDR). The final classification encompasses both MDR, a fluoroquinolone and one other second-line therapy, deemed as extensively drug-resistant (XDR) (Zhang and Yew 2009).

Resistance towards Isoniazid treatment can be induced through a number of methods. A mutation in the peroxidase, KatG which activates isoniazid from the prodrug state. An increase in the expression of the target of inhibition, InhA or alterations to either NADH affinity or the NADH dehydrogenase enzyme (Miesel, *et al.* 1998, Tseng, *et al.* 2015). Rifampicin resistant *M. tuberculosis* is frequently the result of genetic mutations to the β -subunit of the mycobacterial RNA polymerase (Alifano, *et al.* 2015).

Antimicrobials resistance has also been observed towards therapies which target the peptidoglycan cell wall biosynthesis pathway. Fosfomycin is the sole administered antimicrobial which targets the cytoplasmic phase of peptidoglycan synthesis, inhibiting the first enzyme in the pathway MurA (Nasiri, *et al.* 2017). The active site of MurA commonly contains a cysteine residue which fosfomycin modifies to inhibit peptidoglycan synthesis in fosfomycin sensitive organisms. Mycobacteria are intrinsically resistant to a broad range of antimicrobials including fosfomycin due specifically to the active site cysteine being replaced with an aspartate residue (De Smet, *et al.* 1999). D-cycloserine resistance in mycobacteria is displayed either by overexpression of either of the targeted enzymes, Alr and Ddl (Feng, *et al.* 2003) or by mutations observed predominantly in the Alr enzyme (Chen, *et al.* 2017).

Synergy between existing antimicrobials has been shown to combat mycobacterial mechanisms of resistance. The genome of *M. tuberculosis* encodes the β -lactamase BlaC, expressed to hydrolyse standard β -lactam antimicrobials (Hugonnet, *et al.* 2009). Recent investigations have shown that co-administering clavulanate, an inhibitor of β -lactamases along-side common β -lactam classes such as penicillin, carbapenems and cephalosporin aid in therapy against previously resistant strains (Hugonnet and Blanchard 2007) (Kumar, *et al.* 2012).

The prevalence of drug resistance within strains of tuberculosis illustrate the *raison d'être* of an extended therapy period and underlines the requirement for additional anti-tuberculosis antimicrobials or modifications to existing treatments.

1.8 Thesis aim

The overall objective of this thesis is to evaluate the role of mycobacterial N-glycolylation on peptidoglycan and peptidoglycan precursors, in order to gain a better understanding of the observed resilience endowed by this modification towards a range of both hydrolytic enzymes and antimicrobial therapies. Furthermore this thesis will examine what variation the modification has on peptidoglycan synthesis flux, aiding mycobacteria against external pressures as well as investigating the role of newly discovered cell wall active treatments to combat the increasing spread of antimicrobial resistance towards standard therapies.

Chapter 2. Materials and Methods

2.1 Buffers and solutions

All buffers and solutions were prepared using Milli-Q purified water sterilised before use by autoclave or with a 0.2 µm filter. A WPA pH meter CD720 from Hanna instruments measured the pH of all solutions against pH buffer standards at pH 4, pH 7 and pH 10. Analytical grade chemicals were acquired from either Acros Organics (USA), Bachem (Germany), Calbiochem (USA), Chembridge (USA), Fisher Scientific (USA), Novabiochem (Germany) or Sigma-Aldrich (USA). Synthesised oligonucleotides were acquired from Integrated DNA Technologies (UK).

2.2 Growth media

The following growth media were utilized throughout this thesis.

2.2.1 7H9 media

7H9 medium was used for propagation of mycobacteria (Sigma Aldrich)

0.5% (w/v) $(\text{NH}_4)_2\text{SO}_4$, 0.5% (w/v) L-glutamic acid, 0.1% (w/v) Sodium citrate, 0.001% (w/v) Pyridoxine, 0.0005% (w/v) Biotin, 2.5% (w/v) Na_2HPO_4 , 1% (w/v) KH_2PO_4 , 0.001% (w/v) Ferric ammonium citrate and 0.001% (w/v) CuSO_4 , adjusted to pH 6.8. Media was sterilised by autoclave.

7H9 media was supplemented with 10% (v/v) ADC (comprising 5% (w/v) Bovine serum albumin, 2% (w/v) Dextrose, 0.8% (w/v) Sodium chloride, 0.003% (w/v) Catalase) and 0.05% (v/v) Tween 80, passed through at 0.2 µm filter. The complete medium was stored at 4°C.

2.2.2 Lysogeny broth (LB) broth

LB broth used for *E. coli* growth.

1% (w/v) Tryptone, 0.5% (w/v) NaCl and 0.5% (w/v) Yeast extract were combined and autoclaved. LB broth was stored at 4°C.

2.2.3 Super Optimal broth with Catabolite repression (SOC) media

SOC medium was used to promote growth of competent *E. coli* following transformation with a plasmid vector.

2% (w/v) Peptone, 0.5% (w/v) Yeast extract, 0.6% (w/v) NaCl, 1.9% (w/v) KCl, 1% (w/v) MgCl₂, 1.2% (w/v) MgSO₄, were combined and autoclaved. Media was supplemented with 3.6% (v/v) Glucose passed through at 0.2 µm filter. Combined medium was stored at 4°C.

2.2.4 Minimal growth media

Minimal growth media was used for *B. subtilis* growth.

1% (w/v) (NH₄)₂SO₄, 7% (w/v) K₂HPO₄, 3% (w/v) KH₂PO₄, and 1% (w/v) Sodium Citrate, were combined and autoclaved. Medium was combined with 0.2% (w/v) MgSO₄ 0.2% (w/v) Casein hydrolysate and 1% (w/v) Glucose passed through at 0.2 µm filter. Completed medium was stored at 4°C.

2.2.5 Tryptic soy agar

Tryptic soy agar was used for *M. smegmatis* growth.

1.5% (w/v) Casein peptone (pancreatic), 0.5% (w/v) Soya peptone (papain digest), 0.5% (w/v) NaCl was adjusted to pH 7.3, supplemented with 1.5% (w/v) Agar, and sterilized by autoclaving. Once cooled to 50°C, agar media was poured into sterile petri dishes and stored at 4°C.

2.2.6 LB-agar

LB-agar was used for *E. coli* growth.

1% (w/v) Tryptone, 0.5% (w/v) NaCl, 0.5% (w/v) Yeast extract, 1.5% (w/v) Bacto-agar was sterilized by autoclaving, selected antibiotics were incorporated into agar media once it had cooled to 50°C and poured into sterile petri dishes. It was stored at 4°C.

2.2.7 Minimal media agar

Minimal media agar was used for *M. smegmatis* growth.

1% (w/v) $(\text{NH}_4)_2\text{SO}_4$, 7% (w/v) K_2HPO_4 , 3% (w/v) KH_2PO_4 , 1% (w/v) Sodium Citrate, 0.2% (w/v) MgSO_4 were combined, adjusted to pH 7.4, supplemented with 1.5% (w/v) Agar and autoclaved. Once cooled to 50°C, medium was supplemented with 0.2% (w/v) Casein hydrolysate and 1% (w/v) Glucose passed through at 0.2 μm filter. Media was poured into sterile petri dishes and stored at 4°C.

2.3 Bacterial strains

Organism	Strain	Genotype	Reference
<i>M. smegmatis</i>	PM965 (Wild type)	ept-1 <i>rpsL4</i> Δ <i>blaS1</i>	Raymond, <i>et al.</i> (2005)
<i>M. smegmatis</i>	PM979 (Δ <i>namH</i>)	ept-1 <i>rpsL4</i> Δ <i>blaS1</i> Δ <i>namH1</i>	Raymond, <i>et al.</i> (2005)
<i>E. coli</i>	Top 10	F ⁻ <i>mcrA</i> Δ (<i>mrr</i> ⁻ <i>hsdRMS</i> ⁻ <i>mcrBC</i>) ϕ 80 <i>lacZ</i> Δ M15 Δ <i>lacX74</i> <i>deoR</i> <i>recA1</i> <i>araD139</i> Δ (<i>ara</i> ⁻ <i>leu</i>)7697 <i>galU</i> <i>galK</i> <i>rpsL</i> (Str ^R) <i>endA1</i> <i>nupG</i>	Grant, <i>et al.</i> (1990)
<i>E. coli</i>	BL21 (DE3)	F ⁻ <i>ompT</i> <i>gal</i> <i>dcm</i> <i>lon</i> <i>hsdSB</i> (<i>rB</i> ⁻ <i>mB</i> ⁻) λ (DE3 [<i>lacI</i> <i>lacUV5-T7p07</i> <i>ind1</i> <i>sam7</i> <i>nin5</i>]) [<i>malB</i> ⁺] _{K-12} (λ ^S)	Studier and Moffatt, (1986)
<i>E. coli</i>	BL21 (DE3) pRosetta	F ⁻ <i>ompT</i> <i>hsdSB</i> (<i>rB</i> ⁻ , <i>mB</i> ⁻) <i>gal</i> <i>dcm</i> (DE3) and pRosetta plasmid for rare codon overexpression	Studier and Moffatt, (1986)
<i>E. coli</i>	Tuner (DE3)	F ⁻ <i>ompT</i> <i>hsdSB</i> (<i>rB</i> ⁻ , <i>mB</i> ⁻) <i>gal</i> <i>dcm</i> <i>lacY1</i> (DE3)	Compaan and Ellington (2003)
<i>B. subtilis</i>	168	<i>trpC2</i>	Spizizen (1958)
<i>S. aureus</i>	ATCC 27664	<i>see, selq</i>	Bergdoll and Borja (1971)

Table 2.1 Bacterial strains utilised within this thesis

2.4 Bacterial growth

2.4.1 Generation of glycerol stocks

5 mL of LB media with antibiotic as required was inoculated with a single colony from solid media. Cultures were incubated with shaking at 180 rpm at 37°C. Exponentially grown cells were transferred to 1.8 mL Corning cyro-vials and aseptically mixed with growth media plus between 20-50% (v/v) glycerol, depending on the organism and frozen in liquid nitrogen. Purity of stocks were assessed through serial dilution and growth on nutrient agar. Stocks were stored at -80°C.

2.4.2 Generation of competent cells

E. coli expression strains of interest were inoculated from single isolated colonies in LB media with an antibiotic if required and incubated at 37°C with 180 rpm agitation overnight. Overnight cultures were then used as a 10% (v/v) inoculum of sterile LB, supplemented with 20 mM MgSO₄ and preferred antibiotic and grown as above until an optical density (OD_{600nm}) within the range of 0.4 to 0.6 was reached. Cells were pelleted by centrifugation at 4°C at 4500 x g for 10 minutes in a Beckman JA-14 rotor. Pellets were resuspended gradually in 100 mL of ice cold TFB1 (30 mM Potassium acetate, 10 mM Calcium chloride, 50 mM Manganese chloride, 100 mM Rubidium chloride, 15% (v/v) Glycerol pH 5.8). This suspension was incubated on ice for 5 minutes then pelleted by centrifugation at 4500 x g for 5 minutes at 4°C in a Beckman JA-14 rotor. Isolated pellets were resuspended in ice cold TFB2 buffer (10 mM MOPS, pH 6.5, 75 mM Calcium chloride, 10 mM Rubidium chloride, 15% (v/v) Glycerol) and incubated on ice for 1 hour. Competent cells were aliquoted, and frozen in liquid nitrogen. Stored at -80°C.

2.4.3 Aerobic growth of *M. smegmatis*

Frozen stocks of mycobacteria were cultured at 37°C with 180 rpm agitation in 250 mL baffled flasks to oxygenate the media for 30 hours. Once samples reached exponential phase, cultures were diluted to an OD_{600nm} of 0.1. Cells were passed through a 26-gauge needle to disrupt clumps and further diluted by a factor of 10⁴. 100 µL of diluted cultures were pipetted in triplicate into 96-well microtiter plates. As required concentrations of hydrolytic enzymes/antibiotics were added. Triplicate control wells containing media were used as negative and contamination controls. Microtiter plates were covered by gas permeable membrane barrier seals (4titude). Microtiter plates were incubated and analysed in a Varioskan flash multimode reader (Thermo Scientific) at 37°C with intermittent shaking, where growth was measured at OD_{600nm} at 3 hour intervals for 48-60 hours.

2.4.4 Determination of Minimal bactericidal concentration (MBC)

Cells which failed to produce observable growth in the presence of hydrolytic enzymes/antibiotics were pipetted in 10 µL volumes onto segmented nutrient agar plates. Plates were incubated at 37°C in aerobic conditions for 72 hours. Presence of growth used to inform MBC values.

2.4.5 Anaerobic growth of *M. smegmatis*

Cultures were grown as in Section 2.4.3 and then diluted to an OD_{600nm} of 0.1. Cultures were serially diluted ten-fold in media until an OD_{600nm} of 10⁻⁸ was reached. 20 µL from each dilution was pipetted onto tryptic soy agar (Section 2.2.5) and minimal agar (Section 2.2.7) plates. Plates were initially incubated in an anaerobic cabinet for 21 days at 30°C. The agar plates were then transferred to an aerobic 37°C incubator for six days. Control plates were incubated in aerobic conditions for six days.

2.5 Assessment of hydrolytic enzyme activity against modified mycobacterial peptidoglycan

2.5.1 Mycobacterial agar colonisation against hydrolytic enzyme incubation

M. smegmatis was cultured to exponential phase and centrifuged at 3,200 x g for 10 minutes. The supernatant was removed and pellets were resuspended twice in incomplete Hank's balanced salt solution (HBSS) buffer (8% (w/v) NaCl, 0.4% (w/v) KCl, 0.05% (w/v) Na₂HPO₄, 1% (w/v) Glucose, 0.06% (w/v) KH₂PO₄ and 0.035% (w/v) NaHCO₃) minus Mg²⁺ and Ca²⁺. Cells were passed through a 26-gauge needle (Sigma Aldrich) to break down aggregates. Samples were diluted to 10⁵ Colony forming units (CFU).mL⁻¹ using complete HBSS buffer composed of chemicals mentioned above in addition to MgSO₄ (0.12% (w/v)) and CaCl₂ (0.14% (w/v)). 90 µL of diluted cells were pipetted into 96-well microtiter plates in triplicate and incubated with 10 µL of increasing concentrations (128-0.03 µg.mL⁻¹) of hydrolytic enzymes. Microtiter plates were coated with a gas permeable membrane barrier seal and incubated for 1.5 hours unless stated otherwise at 37°C. Aliquots of wells were pipetted onto TSB agar plates in triplicate. Plates were incubated for 72 hours at 37°C and the percentage of viable colonies were counted, averaged, imaged and analysed. Standard concentrations of lysozyme were dissolved in media. Standard concentrations of β-hexosaminidase were prepared in media, based upon units of activity per milligram specified by the acquired sample.

2.6 Cloning and editing of DNA

DNA plasmids and gene constructs utilised during this thesis are outlined in Appendix 1.

Primer sequences to introduce cleavable TEV and poly-Histidine tag sequences are stated in Table 2.2. Denaturing temperature was 98°C, annealing temperature was 48°C and extension temperature was 72°C unless otherwise stated.

Primer	Sequence
MurA Forward	GCGCGCCATATGGTGGCTGAACGCTTT GTTGTTACGGGCGGCAATCG
MurA Reverse C-term + TEV	GCGCGCGGATTGAAAGTACAGGTTCTC CAGACACACAGTTC
MurA Reverse C-term + TEV + His	GCGCGCCTCGAGCTAGTGGTGGTGGTGG TGGTGGGATTGAAAGTACAGG
MurC Forward	GCGCGCCATATGAACGCTGGTCAACTGCC
MurC Reverse + TEV	GCGCGCGGATTGGAAATACAGGTTCTC TTGCAGGACACCGCTACAGCC
MurC Reverse + TEV + His	GCGCGCCTCGAGCTAGTGGTGGTGGTGG TGGTGGGATTGAAATACAGG

Table 2.2 Primer sequence modifications to *M. leprae* MurA and MurC genes. Forward and reverse primers to include a C-terminal cleavable TEV sequence, a poly-histidine tag and enzyme restriction sites to pCOLD-*M. leprae* MurA and pCOLD-*M. leprae* MurC plasmids.

2.6.1 Polymerase Chain Reaction (PCR)

Reagents and primer concentrations specified by the manufacturer were combined in accordance with the requirements of the Phusion[®] polymerase at a scale depending upon the number of PCR samples required. Samples were transferred into the Mastercycler Gradient thermocycler and pre-programmed temperature cycles for primer denaturation, annealing and extension were selected. Annealing temperatures were dependent upon length and GC content of synthesized oligonucleotides.

2.6.2 DNA digestion by restriction enzymes

Based upon the plasmid utilised and the available restriction sites contained within the cloning/expression region, vectors were digested by specific New England Biolabs (NEB) restriction enzymes. Digestion of plasmid DNA or PCR products were optimised by incubation of 500 ng of DNA with the desired restriction enzyme in a suitable NEB buffer (provided by manufacturer) at 37°C for a minimum of 3 hours. Restriction enzymes utilised in this project are noted in Table 2.3.

Restriction enzyme	Sequence
NdeI	CA [^] TATG GTAT [^] AC
XhoI	C [^] TCGAG GAGCT [^] C

Table 2.3 Restriction enzymes utilized for restriction digest of *M. leprae* Mur enzymes and the vector pCOLD. Genetic sequences targeted for enzyme digestion are indicated. Enzymes were incubated for 4 hours at 37°C in manufacturer's recommended NEB buffer 4.

2.6.3 DNA purification

PCR, digestion and ligation products were purified using a Qiagen QIAquick[®] PCR Purification kit. Purification was conducted to manufacturer's specifications.

2.6.4 DNA ligation

Digested plasmid DNA were incubated at 37°C for 1 hour with Shrimp alkaline phosphatase to dephosphorylate. The enzyme was denatured following incubation at 65°C for 30 minutes and the digested plasmid was purified. Digested PCR products and plasmid DNA with reciprocal sticky nucleotide ends were ligated together in a final volume of 10 µL by T4 DNA ligase from NEB according to the manufacturer's instructions. A negative control without enzyme was also produced. Ligations were incubated at 37°C for 1 hour and resulting ligated plasmids were transformed in *E. coli* TOP10 cells and grown on LB agar at 37°C overnight.

2.6.5 Quantification of DNA concentration

A NanoDrop ND-1000 spectrophotometer (Thermo Scientific) was used to quantify 1 µL DNA samples at $A_{260/280}$.

2.6.6 Site directed mutagenesis

Complementary oligonucleotides between 25-45 base pairs in length with a greater than 78°C melting temperature were synthesized. The point mutation was located within the centre of the synthesised oligonucleotides. Whole PCR amplification to generate the newly mutated plasmid was conducted with an Aligent QuikChange II Site-Directed Mutagenesis Kit in accordance with the manufacturer's instructions.

Primer	Sequence (5'-3')
MurA Forward D-C active site	CGCGTGGCACTGCCGGGCGGTT GCGCAATCGGCTCTCGTCCG
MurA Reverse D-C active site	CGGACGAGAGCCGATTGCGCAA CCGCCCGGCAGTGCCACGCG

Table 2.4 Sequences of primers used for site directed mutagenesis of *M. leprae* MurA gene. Forward and reverse genetic overlapping primers to substitute a cysteine residue (Highlighted in **bold**) for the aspartate residue within the active site of MurA.

2.6.7 Agarose gel electrophoresis

The size and purity of plasmids, digests and PCR products were determined with a 1% (w/v) agarose gel. 1 g of agarose (Sigma) was combined with 100 mL of 1 x Tris-acetate EDTA buffer (TAE, 40 mM Tris acetate, 1 mM EDTA, pH 8.3), the agarose was melted using microwave heating. A gel cast was constructed containing an inserted comb indicating the required number and size of sample wells. Proceeding only once the solution was cooled enough to be held, Ethidium bromide was carefully added, 3 µL per 100 mL solution to a final concentration of 0.5 µg.mL⁻¹. The final solution was then thoroughly mixed and poured into the pre-made cast to set. The agarose gel was excised from the cast and placed within a geneflow gel tank and immersed completely in 1 x TAE buffer. DNA samples were combined in eppendorfs with 1 x DNA loading dye (Fermentas 6 x stock: 0.25% (w/v) bromophenol blue, 0.25% (w/v) xylene cyanol FF and 15% (v/v) Ficoll 400). Samples were loaded into individual wells alongside a DNA ladder (Fermentas) comprising DNA fragments of lengths appropriate for estimation of the presumed size of samples and a negative control absent of DNA. The voltage and duration of electrophoresis was dependent

upon the size of gel. Standard agarose gels (100mm by 100mm) were electrophoresed at 90 volts (V) for 45 minutes. Gels were analysed under ultraviolet light with a Syngene GeneSnap G:Box gel illuminator.

2.6.8 DNA sequencing

Isolated DNA plasmids were sequenced by submission to GATC Biotech (Germany). Samples were submitted as 10 μL aliquots containing 80-100 $\text{ng}\cdot\mu\text{L}^{-1}$ of plasmid DNA and 5 $\text{pmol}\cdot\mu\text{L}^{-1}$ of DNA primer, usually the vector promoter or terminator sequence. Plasmid primer sequences used during this project are recorded in Table 2.5.

Primer	Sequence (5'-3')
pUC57 forward	GTAAAACGACGGCCAGTG
pUC57 reverse	GGAAACAGCTATGACCATG
T7 promoter	TAATACGACTCACTATAGGG
T7 Terminator	GCTAGTTATTGCTCAGCGG
pCOLD forward	GCACGCCATATCGCCGAAAGGC
pCOLD reverse	GGCAGGGATCTTAGATTCTGTGC

Table 2.5. The nucleotide bases of upstream and downstream sequences encompassing the cloning/expression region within selected plasmids. These sequences were used to amplify plasmid genes during PCR for DNA sequencing/cloning techniques.

The DNA sequences obtained from submitted samples were analysed and aligned against the known complete nucleotide sequence of the relevant genes using the plasmid editor software ApE (<http://jorgensen.biology.utah.edu/wayned/ap/>).

2.6.9 Transformation

2 μL of plasmid DNA (50-100 ng) was added to a 30 μL suspension of competent *E. coli* cells and incubated on ice for 30 minutes. Incubations were then heat-shocked at 42°C for 45 seconds and

cooled on ice for 2.5 minutes. Cells were then supplemented with 200 μ L of SOC medium (Section 2.2 Growth media) and incubated for 1 hour at 37°C at 180 rpm. Successfully transformed cells were identified by aseptic plating onto LB-agar containing the appropriate antibiotic selection and incubated at 37°C overnight.

2.6.10 Isolation of plasmid DNA

Plasmids propagated in *E. coli* TOP10 cells cultured in LB media plus plasmid specific antibiotic overnight were purified by the manufacturer's instructions outlined within a Fermentas GeneJet™ miniprep extraction kit.

2.7 Expression and purification of recombinant proteins

Any deviation from the methods described are stated in the relevant chapter.

Plasmids containing genes of interest were transformed into competent *E. coli* cells grown on antibiotic selective agar. Individual colonies were inoculated and incubated overnight at 37°C and 180 rpm agitation and grown in a 5 mL volume of LB media with any required antibiotics. Overnight cultures were then used to inoculate 1 litre volumes of LB media plus the required antibiotic at 37°C until culture optical density achieved OD_{600nm} 0.5-0.7. Recombinant protein expression was induced by addition of 1 mM Isopropyl- β -D-thiogalactopyranoside (IPTG) at which point incubation was continued unless otherwise stated at 37°C for 4 hours. Small volume expression trials were conducted with newly constructed plasmids to identify optimal induction temperatures to elicit the greatest quantity of recombinant protein. IPTG-induction conditions that were investigated included 37°C and 25°C for 4 hours and 16°C overnight. Cells were pelleted by centrifugation in a Beckman JLA-8.1000 rotor at 10,000 x g, and resulting cell pellets were transferred to containers and stored at -20°C.

2.7.1 Recombinant protein over-expression with *E. coli* tuner (DE3) cells

Expression of recombinant proteins transformed within *E. coli* tuner (DE3) cell lines aid in protein folding leading to increasing soluble protein concentrations by induction of protein chaperones and the ability to titrate target protein expression with IPTG concentration. Cells were cultured at 37°C as described in Section 2.7, with one exception. Cells were grown in the presence of two antibiotics, one determined by the resistance of the transformation plasmid and chloramphenicol to retain an intrinsic pLacI plasmid until optical density reached OD_{600nm} 0.5-0.7. Tetracycline and arabinose at final concentrations 6 ng.mL⁻¹ and 2 mg.mL⁻¹ respectively were added to express different sets of chaperones. Tetracycline induced GroES/GroEL chaperones and arabinose induced DnaJ, DnaK and GrpE chaperones. Culture flasks were then incubated at 16°C for 1 hour, at which point, cultures were induced by 1 mM IPTG overnight at 16°C. Cells were pelleted at 4°C by 10,000 x g centrifugation in a Beckman JLA-8.1000 rotor, and the resulting cell pellets were transferred to suitable containers and stored at -20°C.

Small volume expression trials were conducted with newly constructed plasmids to identify optimal concentration of IPTG to elicit the greatest concentration of recombinant protein.

2.7.1.1 SDS-Polyacrylamide Gel Electrophoresis

A polyacrylamide resolving gel was cast in a Hoeffer Mighty Small gel kit, comprising 12% acrylamide:bis-acrylamide (37.5:1), 375 mM Tris pH8.8 and 0.4% (w/v) SDS. Once the resolving gel had set, a stacking gel (4% acrylamide:bis-acrylamide (37.5:1), 125 mM Tris pH 6.8, 0.4% (w/v) SDS) was cast above the resolving gel. Both gels were polymerised by 10% (w/v) Ammonium persulphate (APS) and *N,N,N',N'*-Tetramethylethylenediamine (TEMED). To enable a straight interface between both gels, 96% (v/v) ethanol was overlain on the resolving gel while it set. The ethanol was then removed and the stacking gel was poured. A well-shaped comb was inserted into the unpolymerised stacking gel to create wells of selected size and number within the gel. Protein samples were mixed 5:1 with a 6 x sample buffer (6 x; 2.5% (w/v) bromophenol blue, 5% (v/v) β-mercaptoethanol, 20% (v/v) glycerol, 63.5 mM Tris pH 6.8, 0.4% (w/v) SDS). 5-10 µg protein

samples and molecular weight standards were heat-denatured by 10-minute incubation using an Eppendorf Mastercycler Gradient thermocycler at 95°C. 20 µL maximum sample volume was pipetted into SDS-PAGE wells. SDS-Polyacrylamide Gel Electrophoresis (SDS-PAGE) utilised a Tris-glycine buffer system (Laemmli 1970). Gels were run at 180 volts (V) once submerged in SDS-PAGE running buffer (25 mM Tris pH 8.3, 190 mM glycine, 0.1% (w/v) SDS). The procedure was concluded once the dye front has migrated to the bottom of the gel.

2.7.1.2 Development of SDS-PAGE

Detection of separated protein were visualized by staining overnight with Instant Blue (Sigma-Aldrich). Stained gels were rinsed in H₂O and analysed using the Syngene GeneSnap G:Box Gel Documentation and analysis system.

2.7.1.3 Western blotting

Poly-histidine tagged recombinant proteins were initially separated by SDS-PAGE (Section 2.7.1.1) along with histidine tagged protein markers (Invitrogen). The resolving gel was incubated in transfer buffer (25 mM Tris pH 8.3, 192 mM Glycine, 20% methanol (v/v) and 0.05% SDS) and layered on a PVDF membrane (Hybond-P, GE Healthcare) which was pre-soaked in methanol followed by a subsequent wash in deionising water followed by submersion in transfer buffer. The membrane and gel were placed within an electroblotting kit (BioRad) for one hour and thirty minutes at 120 V. To prevent non-specific binding, membranes were incubated at room temperature for 1 hour in 10% milk powder TBS solution plus 0.1% (w/v) Tween-20 (TBS-T). Membrane were then placed overnight still within the milk TBS-T solution at 4°C.

Membranes were washed on three occasions with TBS-T for 10 minutes each followed by incubation in 5% milk TBS-T solution plus 20 µL of primary antibody (Anti-His IgG mouse monoclonal) (Roche) for one hour. Performed three 10 minutes TBS-T washed followed by incubation in 5% milk TBS-T solution plus 10 µL of secondary antibody (Anti-mouse IgG) and

horseradish peroxidase (Sigma) for 2 hours. Concluded with three final 15 minutes washes within TBS-T.

The ECL solutions A and B (GE Healthcare) were mixed together within a darkroom and applied to the membrane for two minutes. Remove Excess solution was removed from the membrane and inserted within an cassette. The membrane was exposed to x-ray film for 5 minutes and then developed.

2.7.2 Fractionation of lysed *E. coli* cells

Weighted frozen cell pellets containing cells that over-expressed proteins of interest were thawed on ice and were resuspended per gram at 4°C with 3 mL of phosphate buffer saline (PBS) containing 20 $\mu\text{g}\cdot\text{mL}^{-1}$ DNase, 1 μM of protease inhibitors leupeptin and pepstatin and 2.5 $\text{mg}\cdot\text{mL}^{-1}$ chicken egg white lysozyme.

Dependent upon the total volume of the resuspended cell solution, cells were lysed by two methods. Small volumes less than 10 mL such as those used in expression trials were sonicated using a Bandelin Sonoplus sonicator at 30% power on ice in three sets of 10 second periods interspaced by 20 seconds of cooling on ice. An aliquot of lysed cells was retained from each sample, and the remaining cell lysate was pelleted by centrifugation at 3,200 x g in an Eppendorf centrifuge 5810R for 10 minutes at 4°C. A consistent volume aliquot of the soluble phase of the eppendorf sample was isolated and run on an SDS-PAGE gel (Section 2.7.1.1 SDS-Page Gel Electrophoresis) along with the isolated whole cell lysate aliquot to determine percentage of soluble protein expressed.

Large volume cell suspensions greater than 100 mL were lysed by gradual passage through a 4°C 30 kpsi continuous cell disruptor (Constant Cell Disruption Systems) three times on ice. The resultant lysate was then pelleted by centrifuged at 4°C for 40 minutes at 25,000 x g. The suspension from this step contained solubly expressed proteins and membranes. The membrane fraction was further purified if required by further centrifugation in a Beckman Ti45 rotor at 4°C,

at 100,000 x g for 1 hour. The resulting pellet was isolated and resuspended using a glass homogenizer in a membrane resuspension buffer (25 mM Tris pH 7.5, 10 mM MgCl₂, 1 M NaCl, 20 mM (v/v) Glycerol). Proteins were extracted from the membrane fractions with 2% (v/v) Triton X-100 with gentle agitation gently at 4°C for 2 hours. The samples were then ultracentrifuged at 150,000 x g at 4°C for 1.5 hours.

2.7.3 Recombinant protein purification

Any deviation from the methods described are stated in the relevant chapter.

2.7.3.1 Affinity chromatography

Immobilised metal affinity chromatography (IMAC) was utilised to purify poly-histidine tagged proteins. Two IMAC methods were implemented within this thesis using either a pre-packed 5 mL Nickel or Cobalt HisTrap column (GE healthcare) or a 5 mL column TALON Cobalt Metal Affinity Resin (Clontech) packed within an Econo-Pac[®] Chromatography column (BioRad). In the former case, equilibration, sample loading, column washing and final elution of the target protein was performed with the column as poured. In the latter case, the TALON resin was equilibrated, mixed with the protein sample with gentle agitation and then poured as a column, subsequent to which it was washed and then eluted to obtain the desired protein.

For both IMAC methods, the metal resin was washed with 10 column volumes (CV) of sterile water, followed with 10 CV of purification buffer A (25 mM Tris pH 7.5, 10 mM MgCl₂, 1 M NaCl, 20% (v/v) glycerol, 0.25 (v/v) TritonX-100) supplemented with 15 mM Imidazole. Pre-packed columns were loaded with sample. Alternatively sample was mixed with 5 mL TALON Cobalt beads and incubated at 4°C for 1 hour, at which point the resin was poured as a column. Both IMAC methods then followed the same protocol.

Flow through sample loading for both column types was collected and columns were washed with a further 10 CV of purification buffer A plus 15 mM Imidazole before purified proteins were eluted in convenient volume fractions by a purification buffer A plus 1 M Imidazole gradient at 1 mL.min⁻¹ over 10 CV unless otherwise stated. Protein elutions were monitored by absorbance at 280 nm by the AKTA 10/100 system. Identification of protein fractions of interest and assessment of sample purity was achieved using SDS-PAGE.

Pre-packed columns were cleaned with 10 CV of purification buffer A followed by 10 CV of 20% (v/v) Ethanol and stored at 4°C.

2.7.3.2 Size exclusion chromatograph

Samples were separated at room temperature by size either through the use of a Bio-gel[®] P200 column (Bio-Rad) for peptidoglycan precursors or a Superdex 200 (GE Healthcare) for protein purification.

A Bio-gel[®] P200 column (dimensions: diameter 2.5 cm/height 80 cm/volume 393 mL) was attached to the AKTA 10/100 system (GE healthcare) and equilibrate overnight in 2 CV of sterile water at a flow rate of 1 mL.min⁻¹. Samples were resuspended after freeze-drying in 2 mL of sterile water and loaded onto the column with a 5 mL injection loop. The column was then eluted at a flow rate of 1 mL.min⁻¹ where 5 mL fractions were collected. Elutions of species of interest were monitored by absorbance measured at 254 and 280 nm.

The Superdex 200 column was attached to the AKTA 10/100 system (GE healthcare) and equilibrated in 2 CV of Gel filtration buffer (20 mM Tris pH 8.0, 100 mM NaCl and 10% (v/v) Glycerol). Samples were concentrated (Section 2.7.5) to 2 mL and loaded onto the column with a 5 mL injection loop. The column was eluted at a flow rate of 1 mL.min⁻¹ where 0.5 mL fractions were collected. Elutions were monitored by absorbance measured at 254 and 280 nm.

2.7.3.3 Ion exchange chromatography

Purified protein samples were further purified by anion exchange chromatography. A MonoQ 5/50 column (Sigma Aldrich), packed with the beads of the strong anion exchanger MonoQ, containing quaternary amine groups, mounted on an AKTA 10/100 system was washed with 10 CV of sterile water. The column was equilibrated with 10 CV of MonoQ buffer A (20 mM HEPES pH 7.6, 10 mM NaCl, 10% (v/v) Glycerol), 10 CV of MonoQ buffer B (20 mM HEPES pH 7.6, 1 M NaCl, 10% (v/v) Glycerol) and finally 10 CV of MonoQ buffer A. Samples were either concentrated or resuspended in MonoQ buffer A to a 2 mL final volume. Samples were injected onto the column followed by 10 CV of MonoQ buffer A. All flow through volumes were collected. Bound samples were eluted by a gradual NaCl concentration increase due to the percentage of MonoQ buffer B present. Small volume fractions were collected and samples identified by absorbance measured at 218/254/280 nm or by SDS-PAGE.

Peptidoglycan precursor samples resulting from fractionation by Bio-Gel P200 by size exclusion chromatography (Section 2.7.3.2) were further purified using the same method with alternate buffer compositions. Buffer A consisted of 10 mM Ammonium acetate pH 7.6 and buffer B consisted of 1 M Ammonium acetate pH 7.6. Small volume fractions were collected and samples identified by absorbance measured at 218/254/280 nm.

2.7.4 Buffer exchange dialysis of recombinant protein

Proteins purified in one buffer were often required to be transferred to another buffer. Specific buffers are stated within the relevant chapters. Generally, a 1 litre dialysis buffer was assembled and stored at 4°C. Dialysis tubing sufficient in length to contain the protein sample was washed in H₂O and tied at one end and clipped to prevent leakage. The protein sample was added to the tubing and the other end was tied and clipped. The dialysis tubing was submerged in the required dialysis buffer and placed overnight at 4°C with a magnetic stirring bar on a magnetic stirrer. The buffer was gently and continually stirred overnight, to facilitate buffer exchange by dialysis.

2.7.5 Concentration of recombinant protein

Dilute proteins were concentrated through a Satorius Vivaspin® centrifugal concentrator. Concentrator selection was dependent upon the molecular weight of the protein, being concentrated. Concentrators with molecular weight cut offs of 10, 30 or 100 kDa were used as appropriate. Large volumes were concentrated in stages within a 4°C centrifuge (Eppendorf Centrifuge 5810R) at 1,800 x g until the requisite protein volumes and concentrations were obtained.

2.7.6 Quantification of recombinant protein

There were two methods used to quantify protein concentration, the choice of either depending upon the presence of detergents.

2.7.6.1 Bio-rad protein quantification

Purified proteins in the absence of detergents were quantified using a Bio-rad colorimetric assay to determine concentration. 1 mL of diluted Bio-rad reagent (1:5; Bio-rad:H₂O) plus 2 µL of the protein sample buffer was used as a blank control in plastic semi-micro cuvettes where absorbance was measured with a Jenway 6306 UV-visible spectrophotometer at 595 nm. 2 µL of purified protein sample was mixed with the reagent and absorbance measured. Samples exceeding the measureable range were diluted and multiple readings were taken to acquire an average. The formula for calculating protein concentration of a known sample is noted below;

$$[\text{Protein}] (\mu\text{g.mL}^{-1}) = (A_{595\text{nm}}/0.1) \times 1.95 \times \text{dilution factor} \times (1000/2).$$

Formula based on a linear response of the assay between 0-20 µg bovine serum albumin (BSA) where an A_{595} of 0.1 was generated by 1.95 µg protein in the assay.

2.7.6.2 Bicinchoninic acid (BCA) protein quantification

Purified protein in the presence of detergents were quantified using a Thermo Scientific Pierce BCA protein assay kit to determine concentration. Manufacturer's instructions were followed. 25 μ L serial dilutions of a known BSA protein standard were combined with 1000 μ L working BCA reagent (reagent A and B mixed at a 50:1 ratio) such that 10, 20, 30, 40 and 50 μ g BSA were added to each assay. Solutions were incubated at 37°C for 30 minutes and absorbance was measured at 562 nm using a Jenway 6306 UV-visible spectrophotometer. Standard values obtained were plotted against known standard concentrations and the concentration of the unknown sample treated identically to the BSA samples was interpreted from the resulting calibration curve.

2.8 Synthesis of Lipid II and intermediates

2.8.1 Biosynthesis of cytoplasmic peptidoglycan intermediates

The protocol for production of individual cytoplasmic peptidoglycan precursors employed here was developed from the method described by Lloyd *et al.* (2008). Dependent upon the precursor required specific components of the cytosolic peptidoglycan pathway were incubated for 18 hours at 37°C within a final 2 mL reaction volume. The production of N-glycolylated variants of any described precursor was obtained by the exchanging of UDP-MurNAc from the reaction mixture with UDP-MurNGlyc (GVK biosciences).

For the production of UDP-MurNAc-L-Ala, synthesis contained: 50 mM HEPES pH 7.5, 10 mM MgCl₂, 50 mM KCl, 1 mM dithiothreitol (DTT), 200 μ M NADPH, 6 mM ATP, 25 mM isocitrate, 40 units isocitrate dehydrogenase (Sigma Aldrich), 500 units pyruvate kinase (Sigma Aldrich), 200 mM PEP, 10 mM UDP-GlcNAc, 30 mM L-Ala, 300 μ g MurA, 2000 μ g MurB and 750 μ g MurC.

For the production of UDP-MurNAc-L-Ala-D-Glu, synthesis contained the previously mentioned components plus 30 mM D-Glu and 1000 µg MurD. For the production of UDP-MurNAc-L-Ala-D-Glu-L-Lys/m-DAP, synthesis contained the previously mentioned components plus 30 mM L-Lys/m-DAP and 1250 µg MurE. For the production of UDP-MurNAc-L-Ala-D-Glu-L-Lys/m-DAP-D-Ala-D-Ala, synthesis contained the previously mentioned components plus 30 mM D-Alanyl-D-Ala and 1500 µg MurF.

After incubation, synthesis were diluted with 5 mL of sterile water and the protein components were filtered out using a 10 kDa Vivaspin[®] centrifugal concentrator.

2.8.1.1 Purification of cytoplasmic peptidoglycan intermediates

Purification of the synthesised intermediates were performed by anion exchange chromatography as described in Section 2.7.3.3. Removal of acquired ammonium acetate was by size exclusion chromatography as described in Section 2.7.3.2 or more usually by three rounds of lyophilisation from water (Section 2.8.2).

2.8.1.2 Quantification of cytoplasmic peptidoglycan intermediates

The peptidoglycan precursors were quantified using the absorbance of the uracil ring (extinction coefficient at 260 nm = 10,000 M⁻¹cm⁻¹) permitting the measurement of produced precursor concentration within a quartz cuvettes using a Jenway 6303 UV-visible spectrophotometer.

2.8.1.3 Biotinylation of UDP-MurNAc-pentapeptide

UDP-MurNAc-pentapeptide and UDP-MurNGlyc-pentapeptide were synthesised as described in Section 2.8.1. Synthesised precursors were biotinylated using the EZ-linkTM Sulfo-NHS-LC-

Biotinylation Kit (Sigma Aldrich) following the manufacturer's instructions. Samples were freeze dried, resuspended in 50 mL sterile water and freeze dried again. Labelled and unlabelled monosaccharides were isolated by ion exchange chromatography. Lipid synthesis was conducted as described in Section 2.8.4.

2.8.2 Lyophilisation of peptidoglycan intermediates

Excess liquid was removed from dissolved peptidoglycan/lipid/protein solutions by freeze-drying. Solutions were transferred to round bottomed flask able to sufficiently accommodate the volume contained. Flasks were placed within liquid nitrogen and rotated constantly to evenly distribute the frozen solution throughout the inside of the flask. Flasks were placed onto the freeze-dryer and the vacuum pressure applied.

2.8.3 Preparation of bacterial cell membrane enzymes for Lipid II synthesis

Single colonies of *M. flavus*/ *B. subtilis* were inoculated in either LB or minimal media 100 mL overnight at 37°C with 180 rpm agitation. 800 mL of either fresh media was re-inoculated with 4 mL 20% (w/v) glucose and 15 mL of overnight bacterial culture in 2 litre flasks. Flasks were subsequently incubated at 37°C and 180 rpm. The optical density at 600 nm of the cell culture was evaluated every hour and cells were harvested at 10,000 x g for 20 minutes at 4°C once cells entered log phase. The supernatant was discarded and pellets were resuspended in cold resuspension buffer (20 mM Tris pH 7.5, 1 mM MgCl₂, 2 mM β-mercaptoethanol).

Samples were centrifuged at 15,000 x g for 20 minutes at 4°C, the supernatant was removed and the pellet was resuspended in buffer at a ratio of 3 mL per gram of cells. 2.5 mg per mL of chicken egg lysozyme was added to the resuspended cells. The cells were incubated at 4°C with steady agitation for 20 minutes. Bacterial cells were lysed by repeated processing through a continuous cell disruptor (Constant Cell Disruption Systems) at 4°C and a constant pressure of 30 kpsi. Lysed

samples were transferred to centrifuge tubes and centrifuged at 10,000 x g for 1 hour at 4°C. The resulting supernatant was centrifuged again at 75,000 x g for 1 hour at 4°C. The pellet containing the cell membranes was retained and resuspended in a small volume (2.5 mL) of resuspension buffer. Protein concentration was determined with the Bio-rad protein assay (Section 2.7.6.1). Resuspended membranes were stored at -80°C.

2.8.4 Small-scale synthesis of Lipid II

Based upon published work by Breukink *et al.* (2003). 0.654 µg of extracted cellular membranes, 0.57 mg.mL⁻¹ MurG, 6 mM UDP-GlcNAc (Sigma-Aldrich), 4 mM UDP-MurNAc-pentapeptide or UDPMurNGlyc-pentapeptide, 4.8 µmol undecaprenyl phosphate and 40 µL buffer (100 mM Tris.HCl pH 8, 5 mM MgCl₂, 1% (v/v) Triton X-100) were combined in a final volume of 200 µL and were incubated for 4 hours at 37°C. To isolate synthesized lipids, an equal volume of 6 M pyridine-acetate pH 4.2 and two volumes of N-butanol were added to the incubated synthesis. Reactions were transferred to glass tubes and centrifuged at 3,000 x g for 10 minutes. The upper phase (N-butanol) was retained, and washed with an equal volume of H₂O. The upper lipid phase was subjected to rotary evaporation and frozen at -80°C.

2.8.4.1 Purification of Lipid II

Purification of synthesized lipids was conducted by anion exchange chromatography. 15 mL glass pipettes were clamped upright, glass wool was placed inside the base and 4 mL DEAE-Sephacel resin was poured into each. Columns were then washed with 40 mL of 1 M ammonium acetate, followed by 60 mL of H₂O and finally 38 mL of solvent A (chloroform:methanol:water; 2:3:1). The flow-through for each wash was disposed of. Dried down synthesized lipids were resuspended completely in 6 mL of solvent A and loaded onto a DEAE-Sephacel column. The subsequent column flow through was collected for TLC analysis. Unbound contaminants were eluted from the column with 3 column volumes of solvent A. Separation of Lipid II from unreacted undecaprenyl

phosphate was achieved by eluting the column isocratically with increasing concentrations of ammonium bicarbonate (AB) between 50 mM to 1 M in solvent A. Aliquots from each elution were rotary evaporated and stored at -80°C for TLC analysis.

2.8.4.2 Thin layer chromatography (TLC) of synthesized Lipid II

A TLC tank was pre-warmed at 37°C. TLC plates were marked in pencil to evenly separate out pipetted samples. Marks were drawn 2.5 cm from the bottom of the plate and 1.5 cm from the side. The TLC plates were pre-heated at 60°C for 20 minutes prior to use. Purified dried lipid fractions were resuspended in a small volume (15 µL) of solvent A, and pipetted onto marked spots on the TLC plates in 2 µL aliquots and permitted to air dry. TLC mobile phase (chloroform:methanol:water:ammonia (88:48:10:1)) was poured into the TLC tank to a depth of 1 cm. The loaded TLC plates were placed into the TLC tank which was then covered. Thin layer chromatography was allowed to run at 25°C for around 3 hours until the mobile phase was within 1 cm of the top of the TLC plate. To visualize the separated species, plates were stained in a sealed container with iodine vapours. Results were scanned immediately as the stain faded rapidly.

2.8.4.3 Quantification of Lipid II

Two small 50 µL aliquots of Lipid II were dried down using nitrogen to remove the chloroform/methanol/water (2:3:1). A control aliquot of chloroform/methanol/ water (2:3:1) was also dried down. The contents of each vial were resuspended in a total of 50 µL volume of 50 mM HEPES, 10 mM MgCl₂, 30 mM KCl, 1.5% (w/v) CHAPS pH 7.6 and supplemented with 50 µL 1 M HCl. Vials were then boiled for 20 minutes, followed by a 5 minute 3,000 x g centrifugation. The pH of each vial was adjusted by addition of 1 M NaOH to pH 7.6.

Quantification of Lipid II was measured as a function of phosphate released in the above acid hydrolysis. The structure of Lipid II contains two equivalents of P_i which were released from the

lipid in the form of inorganic pyrophosphate and probably also phosphate during acid hydrolysis. Therefore samples were treated with inorganic pyrophosphatase (IPP) to convert all remaining pyrophosphate to free P_i which was then measured using purine nucleoside phosphorylase (PNP) to catalyse the phosphorolysis of 7-methyl-6-guanosine (MESG) (Berry and Associates, USA) to ribose 1-phosphate and 7-methyl-6-thioguanine with the concomitant increase in absorbance at 360 nm ($A_{360} = 10000 \text{ M}^{-1} \text{ cm}^{-1}$ per Molar phosphate).

The assay consists of 50 mM HEPES pH 7.6, 10 mM MgCl_2 , 1 units of Inorganic Pyrophosphatase, 0.2 mM MESG and 1 unit of Purine Nucleoside Phosphorylase.

2.9 Peptidoglycan intermediate accumulation

2.9.1 *B. subtilis* peptidoglycan intermediate accumulation

Single *B. subtilis* colonies were inoculated in minimal media (Section 2.2 Growth media) and grown overnight at 37°C. Subsequent cultures were then used to inoculate 1 L of minimal media, grown at 37°C and 180 rpm. $\text{OD}_{600\text{nm}}$ readings were taken until cells reached $\text{OD}_{600\text{nm}}$ 1.0. Pywac reporter screened cell wall active compounds and the positive control antibiotic vancomycin, were added at twice their MIC values and cultures were incubated for a further three hours. Cells were harvested by centrifugation at 3,200 x g for 10 minutes, the supernatant was then removed and the cell pellets were stored at 4°C.

2.9.2 Trichloroacetic acid extraction of peptidoglycan intermediates

Harvested pellets were cooled on ice and resuspended in ice cold 10% (w/v) Trichloroacetic acid (TCA), at a ratio of five mLs TCA per gram of pellet wet weight and incubated at 4°C with agitation for 30 minutes. Concurrent with the incubation, a Beckman JA 25.5 centrifuge rotor was also cooled at 4°C. After incubation, samples were centrifuged at 48,000 x g for 10 minutes at

4°C. The resulting supernatant was retained on ice. The TCA precipitation protocol was repeated twice more on the pellet of the first extraction, with the volume of TCA half of the first extraction. The three supernatants were then combined.

2.9.3 Di-ethyl ether extraction of TCA of peptidoglycan intermediate pool

The total TCA supernatant was poured into a separating funnel and equal volume of ice cold di-ethyl ether was added. The combined volume was mixed gently to extract the TCA. The ethanol and aqueous phases were separated. The aqueous phase was retained while the ether phase containing the TCA was discarded. The aqueous phase was reextracted twice more with equal volumes of ether. The pH of the aqueous phase was then adjusted to pH 7.2. The sample was rotary evaporated to remove residual solvents and freeze dried. Cell wall intermediates were isolated by size exclusion chromatography (Section 2.7.3.2) and ion exchange chromatography (Section 2.7.3.3) and identified by Mass spectrometry (Section 2.12).

2.10 Assessment of antimicrobial binding against biotinylated Lipid II variants

2.10.1 Surface Plasma Resonance (SPR)

Streptavidin coated SPR chips (GE healthcare) were analysed at 25°C using a Biacore T200 (GE healthcare). Individual labelled vials were inserted into the system containing 20 $\mu\text{g}\cdot\text{mL}^{-1}$ biotinylated N-acetylated Lipid II DAP, biotinylated N-glycolylated Lipid II DAP, and biocytin to act as a control. The four flow cells of the SPR chip were washed three times with degassed and filtered HBS-EP buffer (0.01 M HEPES pH 7.4, 0.15 M NaCl, 3 mM EDTA and 0.005% (v/v) Surfactant P20). Each flow cell was prepared by immobilizing the specific biotinylated lipid or biocytin control onto the surface and washed once more with HBS-EP buffer. Investigated antimicrobials were prepared by serial dilution from concentrated stocks, with the DMSO

concentration, if required for antimicrobial solubility maintained across the concentration range. The antimicrobial dilutions were aliquoted into individual vials, labelled and randomized within the Biacore T200. The sensorgram was performed by injection of antimicrobials at $20 \mu\text{L}\cdot\text{min}^{-1}$ across all concentrations. Increasing concentrations of NaCl (0.5-5 M) were present to remove bound ligands if required to completely regenerate the SPR chip.

2.10.2 Bio-Layer Interferometry (BLI)

Biosensors coated in streptavidin or nickel-charged tris-nitriloacetic acid (Ni-NTA) were submerged in selected assay buffers for 10 minutes. The streptavidin assay buffer for Lipid II variants consisted of 25 mM Tris pH 8.0 and 0.1% (v/v) Triton X-100. The Ni-NTA assay buffer for PBP enzymes PonA1/A2 consisted of 50 mM Bis-Tris pH 8.0, 20 mM NaCl and 0.1% (v/v) Triton X-100. Within a 96 well black opaque microtiter plates known concentrations of biotinylated Lipid II variants and antimicrobials of interest were aliquoted into columns. Biosensors and the microtiter plate were inserted and integrated into the Octet RED96 biolayer interferometer system (FortéBio, Pall Inc.). The sensors were sequentially programmed to be submerged first into the wells containing the $2 \mu\text{g}\cdot\text{mL}^{-1}$ biotinylated lipid II or $2 \mu\text{M}$ poly-histidine tagged PonA1/A2, to reversibly immobilise the ligands to the sensor. The bound sensors were washed three times in assay buffer. The BLI assay was performed at 30°C and consisted of a 60 second baseline measurement in assay buffer, a 120 second association step against a range of selected antimicrobial concentrations and a 120 second disassociation step in assay buffer.

2.11 Spectrophotometric assays

2.11.1 Coupled NADH-linked pyruvate kinase/lactate dehydrogenase assay for amino acid Mur ligase activity

Amino acid ligase activity was measured at an absorbance of 360 nm in a Varian Cary 100 spectrophotometer by coupling the ligase catalysis generation of ADP to pyruvate kinase which rephosphorylated the ADP to ATP with the concomitant generation of pyruvate. Lactate dehydrogenase reduced the pyruvate to lactate oxidising one equivalent of NADH to NAD⁺ with the consequent drop in NADH absorbance at 340 nm. The addition of a single amino acid to the UDP-MurNAc/MurNGlyc intermediate consumes ATP releasing ADP and P_i from the reaction. ADP was then monitored over time as described above.

The reaction mixture within a quartz cuvette contained 50 mM HEPES pH 7.6, 10 mM MgCl₂, 1 mM DTT, 50 mM KCl, 1 mM ATP, 2 mM PEP, 0.2 mM NADH, 5.8 Units/200 μL of Pyruvate kinase/Lactate dehydrogenase mix, 0.4 mM UDP-MurNAc/MurNGlyc intermediate and 40 μg.mL⁻¹ Mur enzyme. Once a level baseline was established 5 mM of the required amino acid was added. Absorbance was read over time at 37°C.

2.11.2 Amplex Red assay for transpeptidase activity

Transpeptidase activity was measured at 30°C with a Varian Cary 100 spectrophotometer by following the release of the terminal D-Alanine residue from the peptide stem of Lipid II variants. Here, D-alanine was oxidatively deaminated to pyruvate and hydrogen peroxide, where the latter was consumed by horseradish peroxidase (HRP) with the concomitant conversion of amplex red to the chromophore resorufin with an intense absorbance of 555 nm ($\epsilon_{1\text{cm}, 555} = 55,000 \text{ M}^{-1}.\text{cm}^{-1}$). Amplex Red assay measured absorbance at A_{555nm}. The assays were performed in quartz cuvettes and were comprised of 50 mM HEPES pH 7.6, 10 mM MgCl₂, 50 μM Amplex Red, 33.51 mM.min⁻¹ d-amino acid oxidase (DAAO), 14.82 mM.min⁻¹ HRP. A level baseline was achieved

before individual additions of Lipid II and PBP were inserted into the reaction mixture. Reactions were measured at 555 nm, if no activity was observed *E. coli* PBP 1b was added in excess as a positive control to the mixture to prove the reaction mixture was correct. The concentrations necessary for the assay for both DAAO and HRP catalytic activity were calculated independently.

DAAO activity was measured by Dr. Adrian Lloyd at an absorbance of $A_{340\text{nm}}$, the variation between the absence or addition of the D-amino acid, D-alanine ($\epsilon_{1\text{cm}, 340\text{ nm}} = 6,220\text{ M}^{-1}\cdot\text{cm}^{-1}$) within the reaction volume. DAAO was prepared by dilution of the enzyme stock with 50 mM Tris pH 7.5, 50 mM lactitol, 10% (v/v) Glycerol, 5 mM EDTA, to a starting concentration of 54.13 nM. The DAAO assay consisted of 50 mM Bis-Tris propane pH 8.5, 0.1% (v/v) Triton X-100, 20 mM MgCl_2 , 5.8 units pyruvate kinase/lactate dehydrogenase mix, 0.3 mM NADH, 1.35 nM DAAO. The absorbance at 340 nm and 37°C was followed in a Cary UV/Vis spectrophotometer and after a control rate was determined, DAAO activity was initiated with 0.1 mM D-alanine.

Horse radish peroxidase catalytic activity was measured at $A_{555\text{nm}}$. The reaction volume consisted of 50 mM Bis-Tris propane pH 8.5, 20 mM MgCl_2 , 50 mM Amplex Red and 18.5 pM HRP. The enzyme was initially prepared in 50 mM Bis-Tris propane pH 8.5. Once a level baseline was achieved, hydrogen peroxide was added to a final concentration of 20 μM to initiate HRP activity. The resorufin extinction coefficient ($\epsilon_{1\text{cm}, 555} = 55,000\text{ M}^{-1}\cdot\text{cm}^{-1}$) was used to calculate HRP activity.

2.12 Mass spectrometry

Purified intermediates and lipids were resuspended in 50% acetonitrile using a Waters Synapt G2 Q-TOF Mass Spectrometer and analysed by negative or positive ion nanospray ionization mass spectrometry (ESI-MS) by Dr Adrian Lloyd and Mrs. Anita Catherwood, conducted within the Proteomic Facility RTP (School of Life Sciences, University of Warwick). Data analysis of the products were verified using MassLynx (Waters, USA). The instrument was calibrated in either ion mode with sodium iodide capillary voltage was 1.5 kV.

Chapter 3. The role of the N-glycolylated muramic acid in the protection of mycobacteria from host hydrolytic enzymes

3.1 Introduction

The core focus of this thesis is the role of the N-glycolylation of mycobacterial peptidoglycan against the host immune response of various organisms through utilization of hydrolytic enzymes. The unique structural modification identified in the Actinobacteria family (Raymond, *et al.* 2005) by which MurNAc subunits within the peptidoglycan sacculus are modified with oxygen is dependent upon the enzyme NamH (Rv3808) (Section 1.3.8.4), which converts UDP-MurNAc to UDP-MurNGlyc to form the MurNGlyc residues in the actinobacterial peptidoglycan.

3.2 NamH deficient mutant

The *namH* gene is comprised of 1551 base pairs encoding a 516 amino acid 57 kDa enzyme (Reddy, *et al.* 2009). To establish the function of the protein encoded by the *namH* gene, the construction of a *namH* mutant from the saprophyte *M. smegmatis* (Raymond, *et al.* 2005) was achieved. In this instance, excision of the known dominant β -lactamase gene *blaS*, (Flores, *et al.* 2005) led to the formation of the strain PM965 followed by allelic exchange of the *namH* gene, leading to the creation of the *blaS*⁻; *namH* double mutant PM979. Mass spectrometric analysis of the mycobacterial cell wall composition of the two newly created strains indicated that PM979 produced solely MurNAc sugars throughout the peptidoglycan cell wall layer whereas the PM965 *blaS*⁻ strain incorporated both MurNGlyc and MurNAc moieties in a ratio of 7:3 during standard aerobic growth conditions (Raymond, *et al.* 2005). Previous investigations into PM979 concluded that *namH* deficient strains were 2-fold more susceptible to human lysozyme in minimal media such as 7H9 and 8-fold more susceptible in rich media such as LB (Raymond, *et al.* 2005). It was therefore proposed that NamH was important in hydrolytic enzyme resistance due in part to the

increase in hydrogen bonding along peptidoglycan chains (Raymond, *et al.* 2005) and interference caused by the N-glycolyl modification on recognition by peptidoglycan hydrolases.

3.3 Experimental aims

The acquisition of the two strains, PM965 and PM979 permitted the expansion of the investigation into the role of the N-glycolyl modification towards the mycobacterial response to various lytic hydrolases. Therefore, an investigation into the impact of N-glycolylation of peptidoglycan muramyl residues have on the sensitivity of *M. smegmatis* towards the hydrolytic enzymes, lysozyme and β -hexosaminidase was pursued. Further, exploration of peptidoglycan lytic properties of these enzymes at pH ranges physiologically similar to those found in and around the phagolysosome and plasma membrane was also undertaken.

From this point onwards, *M. smegmatis* strain PM965 is referred to as wild type and PM979 as $\Delta namH$. The strains obtained from the Pavelka group were sequenced before delivery.

3.4 Aerobic growth characterisation of *M. smegmatis* strains

In order to characterize the growth kinetics of wild type and *namH* *M. smegmatis* to determine any strain-specific variation in aerobic growth, the two *M. smegmatis* strains were inoculated from frozen stocks in nutrient 7H9 media supplemented with ADC and Tween80 (Section 2.2) in baffled flasks to maximise aeration during the normal phenotypical mycobacterial growth in aerobic and nutrient rich conditions. Results are depicted in Figure 3.1.

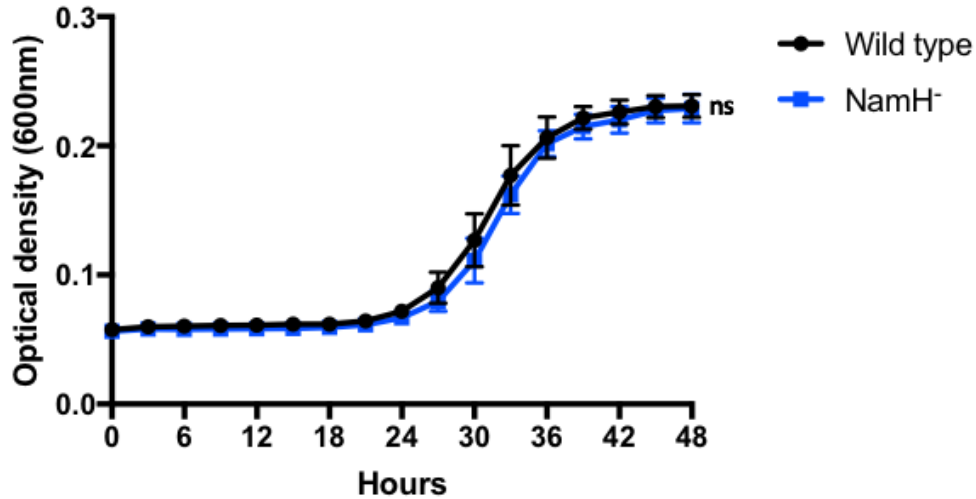


Figure 3.1 *M. smegmatis* Wild type and Δ NamH aerobic growth comparison. Cells were grown in 96 well microtiter plates in triplicate at 37°C with intermittent shaking every 20 minutes, absorbance was measured at OD_{600nm} at 3 hour intervals for 48 hours. Each well contained 100 μ L culture media (7H9, ADC, 0.05% (w/v) Tween 80). The cultured *M. smegmatis* wild type (Black) and Δ NamH (Blue) strains were standardized to an OD_{600nm} of 1 and diluted further by a factor of 10³ prior to incubation. Error bars represent standard deviation of triplicate measurements. Results show no observable variation between strains under standard growth conditions as defined by a student's t-test with a p-value >0.05. Ns = not statistically significant.

In the previous investigation by the Pavelka group it was noted that the *namH* gene was not an essential requirement for the cell. The data shown in Figure 3.1 reports the same findings in aerobic and nutrient rich conditions. Both strains achieved a normal cellular growth pattern, exiting apparent lag phase after 24 hours and reaching stationary phase after 46 hours. The doubling time (Td) calculated from the exponential growth phase between hours 24 and 33 for the wild type strain (Figure 3.1: Black line) was 6.81 hours and for the Δ NamH strain (Figure 3.1: Blue line) was 6.96 hours. The Td variation between the two strains during exponential phase led to a measurable difference when comparing the area under the curve (AUC) for each strain. The Δ NamH produced an area under the curve value 8% less than the wild type. The growth curves of the wild type and NamH deficient strains were statistically analysed using an unpaired t-test to observe if there was a significant statistical difference between the two strains. A p-value less than 0.05 permits the rejection of the null hypothesis that there is no statistically significant difference between two sets of data. The p-value was > 0.5 and so it was accepted that there was no observed difference between the two strains during normal cellular growth in nutrient media.

3.5 Anaerobic growth characterisation of *M. smegmatis* strains

The N-glycolyl modification of MurNAc is only possible in the presence of molecular oxygen (Mahapatra, *et al.* 2005) and therefore the function of NamH is only significant in oxygen rich environments such as during normal cellular growth or during cellular resuscitation from a dormancy-like state amongst degraded granulomas. In a low oxygen environment or one that contains the absence of oxygen, the bacterial peptidoglycan sacculus can solely be formed from N-acetylated muramic acids. To ascertain the impact of an anaerobic environment on the phenotypic growth of the wild type and NamH⁻ strains, the protocol adapted from Cordone, *et al.* (2011) was implemented. Cultures of 7H9 media supplemented with ADC and Tween80 containing wild type and Δ NamH *M. smegmatis* strains were inoculated in baffled flasks in order to aerate the media and facilitate the incorporation of a higher percentage of MurNGlyc residues into the peptidoglycan of the wild type strain. Once cultures reached exponential phase, both strains were diluted to an OD_{600nm} of 1 and 10-fold serial dilutions were pipetted onto both minimal media agar and tryptic soy broth (TSB) agar plates. These were incubated in anaerobic conditions for an extended period of 21 days to replicate the dormancy-like environment experienced by granuloma encased *M. tuberculosis* in infected macrophages. The strains were selected to be cultured on minimal media agar to mimic the nutrient and oxygen deprivation found within granulomas, whilst the TSB agar cultures were selected to mimic the absence of oxygen solely. Subsequently after 21 days the agar plates were transferred to aerobic conditions and incubated for a further 6 days to simulate the resuscitation of cells from the dormancy. The control for this experiment involved both media agar plates containing serial dilutions of both strains grown only in aerobic conditions for 6 days. The colony propagation controls before and after 6 day 37°C aerobic incubation are shown in Figure 3.2.

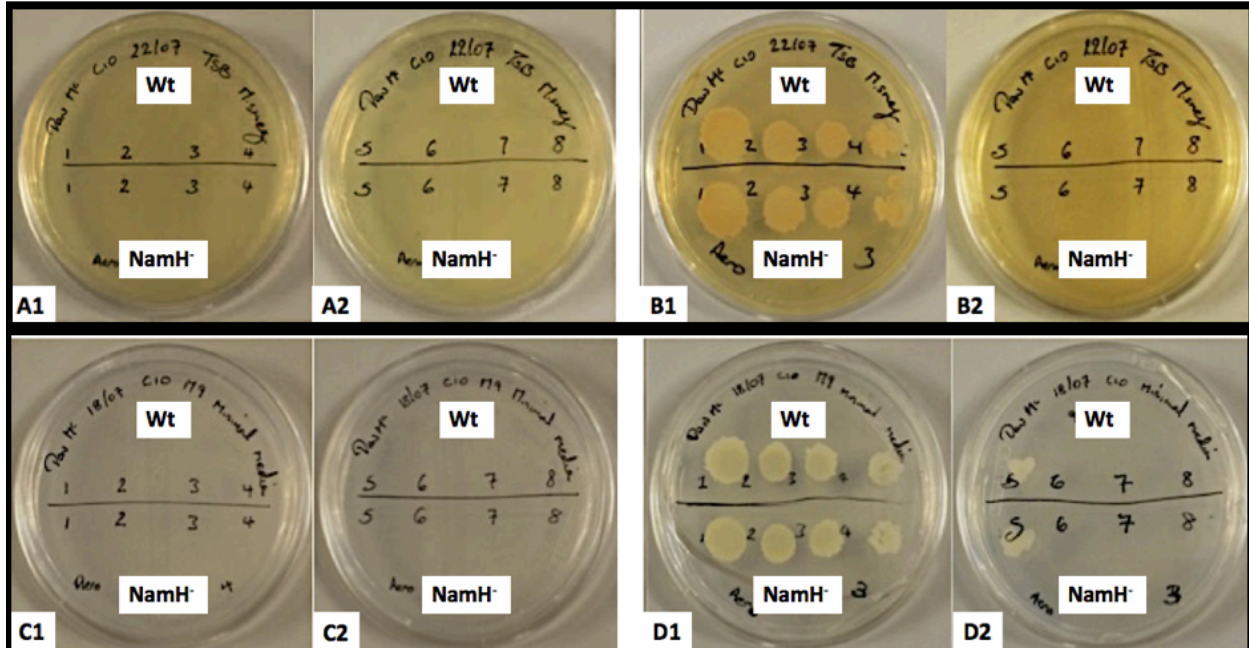


Figure 3.2 *M. smegmatis* colonization of selective nutrient agar during aerobic incubation. Serial dilutions of *M. smegmatis* strains wild type (top half of each plate) and Δ NamH (bottom half of each plate) grown on tryptic soy broth agar (top row) and minimal media (bottom row) plates for 0-6 days at 37°C in an aerobic environment. Serial dilutions labelled 1 (Dilution 10^1) to 8 (Dilution 10^8). A1-A2 Serially diluted *M. smegmatis* strains on TSB agar before 6 day aerobic incubation. B1-B2 Serially diluted *M. smegmatis* strains on TSB agar after 6 day aerobic incubation. C1-C2 Serially diluted *M. smegmatis* strains on minimal media agar before 6 day aerobic incubation. D1-D2 Serially diluted *M. smegmatis* strains on minimal media agar after 6 day aerobic incubation.

Results from Figure 3.2 indicate that both strains were culturable on both nutrient diverse agar plates within similar growth across the six days of aerobic incubation and were similarly able to colonise at a 10,000-fold dilution (10^{-4}) from the initial starting OD_{600nm} of 1. The minimal media (Figure 3.2: D1-D2) was observed to further permit culturable growth at a 100,000-fold dilution (10^{-5}) for both strains. This slight disparity between the nutrient agar is likely due to an increased glucose concentration in the minimal media recipe compared to the tryptic soy broth (Section 2.2).

The next stage of this investigation involved repeating the serial dilution of both strains on both sets of selected agar plates followed by incubation within an anaerobic environment for 21 days at 37°C. Images of the serially diluted agar plated were taken before and after anaerobic incubation and are displayed in Figure 3.3.

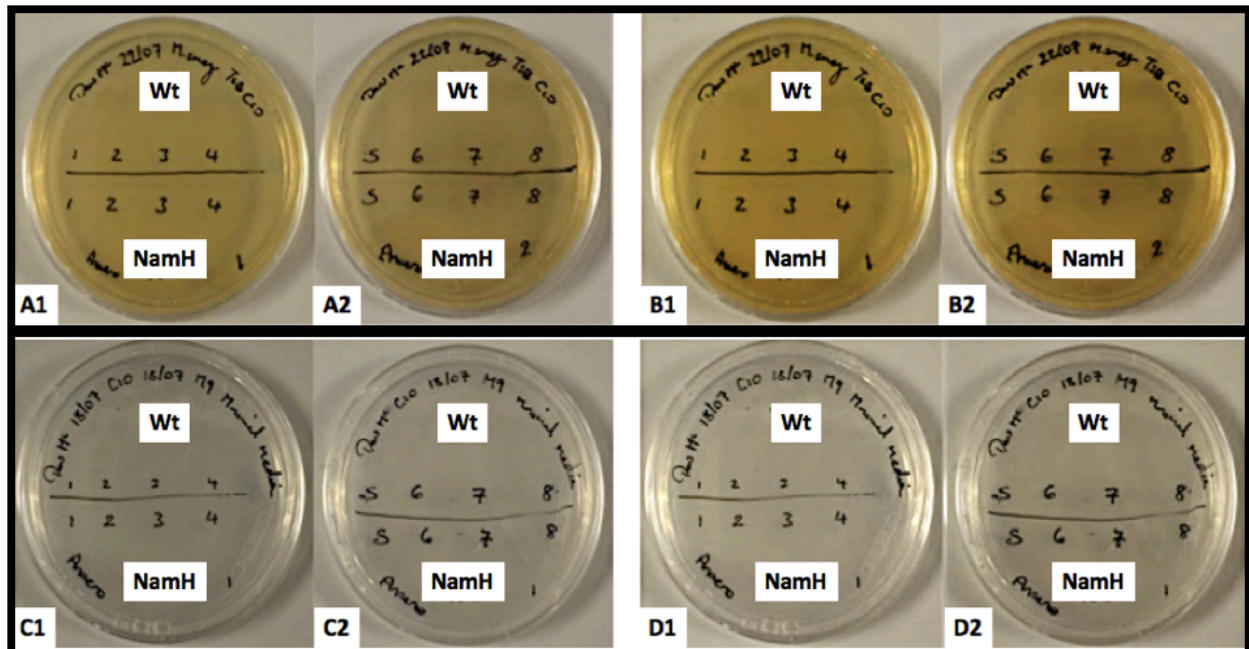


Figure 3.3 *M. smegmatis* colonization of selective nutrient agar during anaerobic incubation. Serial dilutions of *M. smegmatis* strains wild type (top half of each plate) and Δ NamH (bottom half of each plate) grown on tryptic soy broth agar (top row) and minimal media (bottom row) plates for 0-21 days at 37°C in an anaerobic environment. Serial dilutions labelled 1 (Dilution 10^1) to 8 (Dilution 10^8). A1-A2 Serially diluted *M. smegmatis* strains on TSB agar before 21 days anaerobic incubation. B1-B2 Serially diluted *M. smegmatis* strains on TSB agar after 21 days anaerobic incubation. C1-C2 Serially diluted *M. smegmatis* strains on minimal media agar before 21 days anaerobic incubation. D1-D2 Serially diluted *M. smegmatis* strains on minimal media agar after 21 days anaerobic incubation.

The extended incubation period within a solely anaerobic environment led to the both strains being unable to visibly colonise the nutrient agar of either selective media at any investigated dilution (Figure 3.3). The anaerobically incubated agar plates were then placed within an aerobic incubator for six days, the equal time period as the solely aerobic controls at 37°C in Figure 3.2. Once completed, images of each plate were taken. The results of this experiment are presented in Figure 3.4.

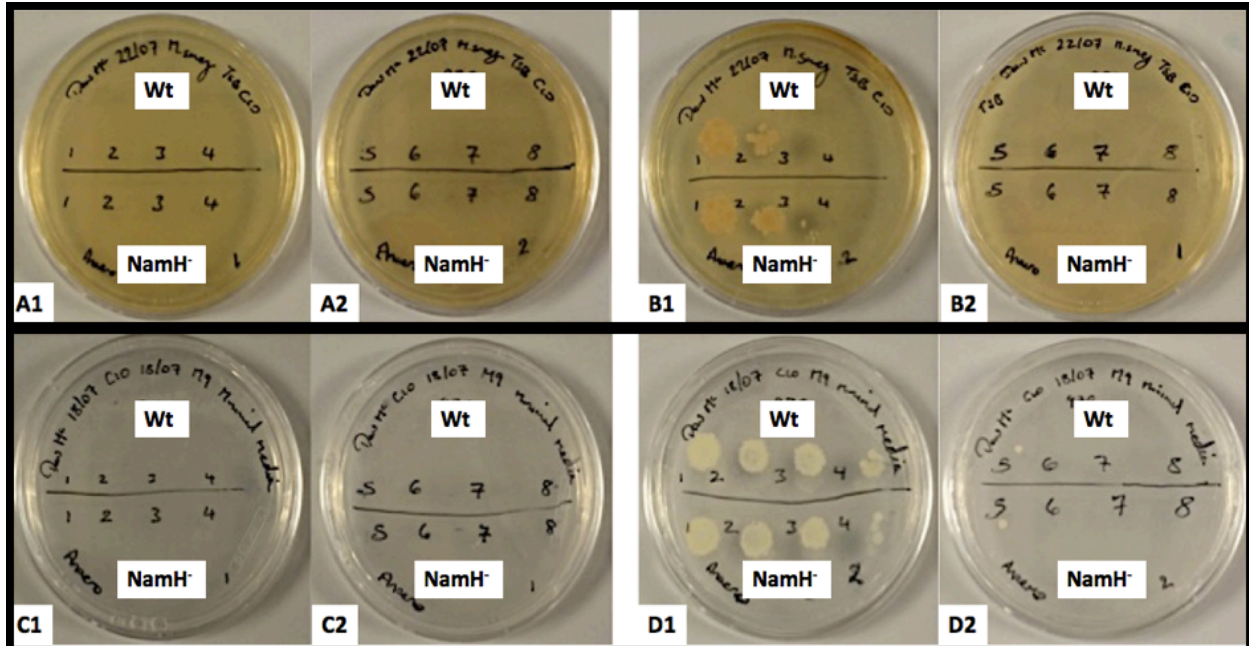


Figure 3.4 *M. smegmatis* colonization of selective nutrient agar during aerobic incubation following prolonged anaerobic incubation. Serial dilutions of *M. smegmatis* strains wild type (top half of each plate) and Δ NamH (bottom half of each plate) grown on tryptic soy broth agar (top row) and minimal media (bottom row) plates were incubated for 21 days at 37°C in an anaerobic environment. Plates were subsequently incubated aerobically at 37°C for 6 days. Serial dilutions labelled 1 (Dilution 10^1) to 8 (Dilution 10^8). A1-A2 Serially diluted *M. smegmatis* strains on TSB agar after 21 day anaerobic incubation. B1-B2 Serially diluted *M. smegmatis* strains on TSB agar after 21 days anaerobic incubation followed by 6 days aerobic incubation. C1-C2 Serially diluted *M. smegmatis* strains on minimal media agar after 21 days anaerobic incubation. D1-D2 Serially diluted *M. smegmatis* strains on minimal media agar after 21 days anaerobic incubation followed by 6 days aerobic incubation.

The results shown in Figure 3.4 show that once the nutrient agar plates incubated initially in anaerobic conditions were permitted to be incubated aerobic then the serially diluted aliquots of *M. smegmatis* strains on the surface of each media were able to colonise. Colony growth was noticeably reduced in both strains from the aerobic control experiment on the nutrient rich TSB agar plates. (Figure 3.4: B1-B2). Both strains demonstrated about a 100-fold decrease in bacterial survival from 10^4 dilution (Figure 3.2: B1) 10^2 dilution (Figure 3.4: B1) on the TSB nutrient agar plates. The ability to colonize at higher dilutions was less pronounced on minimal media agar (Figure 3.4: D2). Both strains once again equal displayed the capacity to form a single colony once diluted by 10^5 . This was the exact maximum dilution observed in the aerobic control experiment (Figure 3.2: D2) for both strains, though the number of colonies was significantly more pronounced on the minimal media control plates. The variation in bacterial survival between the two selected agar plates after anaerobic incubation is likely due in part to oxygen deprivation being

a greater factor in *M. smegmatis* colonization than nutrient deprivation, as well as the slightly increased glucose concentration aiding colonization.

Based on these results it could be concluded that *namH* is not essential to the viability of the cell, as reported by Raymond *et al.* (2005), not required to assist the resuscitation of dormant cells or support normal cellular growth whether during aerobic or anaerobic conditions. With time permitting further work could determine whether there had not been any reversion of the *namH* gene to the wild type sequence during colonization.

3.6 *M. smegmatis* sensitivity towards lysozyme

3.6.1 *M. smegmatis* sensitivity towards chicken egg white lysozyme

The peptidoglycan of both wild type and *namH* deficient *M. smegmatis* strains have been shown to be substrates for lysozymes. To characterise the response of both strains to specific lytic enzymes, the minimal inhibitory concentration (MIC) of both strains challenged with chicken egg lysozyme in nutrient 7H9 media was assessed (Section 2.4.3). In short, cells were cultured from glycerol stocks in 7H9 nutrient media supplemented with ADC and Tween80 in baffled flasks to mid exponential phase to maximise oxygen distribution within the culture. Cells were diluted to an OD_{600nm} of 0.1 and passed with a syringe through a 21-gauge needle to disrupt clumps of cells. Cells were diluted further by a factor of 10³ and incubated in 96-well microtiter plates with increasing concentrations of chicken egg lysozyme in triplicate. Plates were incubated at 37°C with agitation for 60 hours under a gas permeable seal and OD_{600nm} values were measured routinely every 3 hours. The MIC growth curves for both strains is presented in Figure 3.5.

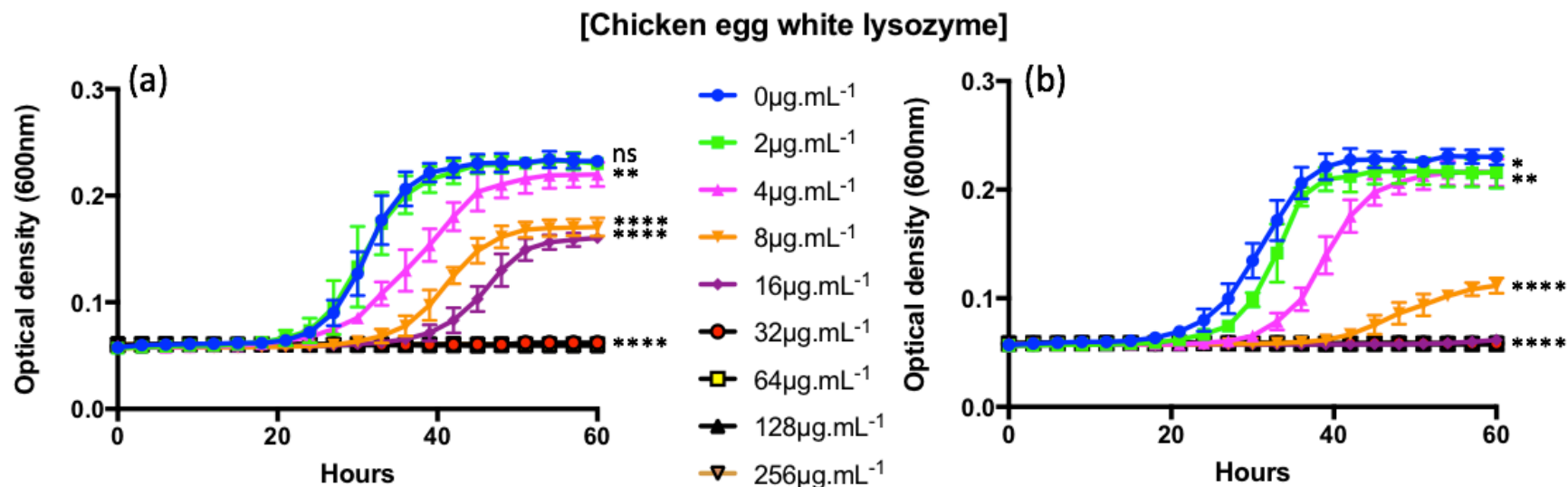


Figure 3.5 The hydrolytic activity of chicken egg white lysozyme against the mycobacterial modifications of peptidoglycan. Wild type (a) and (b) Δ NamH *M. smegmatis* MIC growth curves against chicken egg white lysozyme. Cells were grown in 96-well microtiter plates in triplicate at 37°C with intermittent shaking every 20 minutes, where the absorbance was measured at 600nm at 3 hour intervals for 60 hours. Each well contained 100 μ L culture media (7H9, ADC, 0.05% (w/v) Tween 80) with increasing concentrations of chicken egg white lysozyme. The cultured *M. smegmatis* wild type (a) and (b) Δ NamH strains were standardized to an OD_{600nm} of 1 and diluted further by a factor of 10⁴ prior to addition of enzyme and incubation. Error bars represent standard deviation of triplicate measurements. Chicken egg white lysozyme concentrations: 0 μ g.mL⁻¹ (Blue), 2 μ g.mL⁻¹ (Green), 4 μ g.mL⁻¹ (Pink), 8 μ g.mL⁻¹ (Orange), 16 μ g.mL⁻¹ (Purple), 32 μ g.mL⁻¹ (Red), 64 μ g.mL⁻¹ (Yellow), 128 μ g.mL⁻¹ (Black), 256 μ g.mL⁻¹ (Brown). Statistically significant results are indicated with * = p-value <0.05, ** = <0.01, *** = <0.001 and **** = <0.0001. Results: Δ NamH displayed greater susceptibility to chicken egg white lysozyme than wild type. MIC results: Wild type (a) 32 μ g.mL⁻¹, Δ NamH (b) 16 μ g.mL⁻¹.

Chicken egg lysozyme ($\mu\text{g.mL}^{-1}$)	Wild type <i>M. smegmatis</i>					ΔNamH <i>M. smegmatis</i>					(b) vs (a) p-values
	Apparent Lag phase (h)	Td (h^{-1})	AUC (%)	Stationary Phase $\text{OD}_{600\text{nm}}$	Wild type p-values (a)	Apparent Lag phase (h)	Td (h^{-1})	AUC (%)	Stationary Phase $\text{OD}_{600\text{nm}}$	ΔNamH p-values (b)	
0	21	8.01	-	0.23	-	21	7.9	-	0.23	-	>0.05
2	21	7.96	99.21	0.23	>0.05	24	6.42	86.59	0.21	>0.05	>0.05
4	21	12.05	74.48	0.22	<0.01	30	8.28	65.34	0.21	<0.01	>0.05
8	30	10.23	42.58	0.17	<0.0001	42	16.82	12.03	0.11	<0.0001	<0.001
16	45	12.34	29.66	0.16	<0.0001	60	0.00	0.00	0.00	<0.0001	<0.001
32	60	0.00	0.00	0.05	<0.0001	60	0.00	0.00	0.00	<0.0001	-
64	60	0.00	0.00	0.05	<0.0001	60	0.00	0.00	0.00	<0.0001	-
128	60	0.00	0.00	0.05	<0.0001	60	0.00	0.00	0.00	<0.0001	-
256	60	0.00	0.00	0.05	<0.0001	60	0.00	0.00	0.00	<0.0001	-

Table 3.1 Statistical comparisons of *M. smegmatis* growth curves in the presence of increasing concentrations of chicken egg lysozyme. Wild type and ΔNamH strains incubated for 60 hours at 37°C with selected concentrations of chicken egg lysozyme produced growth curves measured at $\text{OD}_{600\text{nm}}$ in Figure 3.5. Variations between growth curves were measured by time taken to exit apparent lag phase (hours), the doubling time (Td) of cells during exponential phase (hours^{-1}), the area under the curve (AUC) percentage compared to the 0 $\mu\text{g.mL}^{-1}$ control (%), the $\text{OD}_{600\text{nm}}$ value achieved during stationary phase and whether the growth curve variations were statistically significant compared to each 0 $\mu\text{g.mL}^{-1}$ control with p-values <0.05 deemed significant. The statistical significance of ΔNamH (b) growth curves compared to wild type (a) at equivalent chicken egg lysozyme concentrations were determined by p-values <0.05.

The standard control growth curve of the *M. smegmatis* wild type strain under aerobic and nutrient conditions displayed in Figure 3.5 (a) (Blue), showed a normal growth progression between phases and based on the initial dilution and media acclimatisation achieved observable growth above the background of the microtiter plate after 21 hours. The doubling time (Td) of the strain was 8.01 hours with growth plateauing at OD_{600nm} 0.23 after 45 hours. The statistical significance of the results in Figure 3.5 were analysed with a paired Student t-test comparing the standard growth phenotype OD values of the wild type control to those in the presence of increasing concentrations chicken egg lysozyme. Analysis of the wild type strain (Table 3.1) noted that all growth phenotypes except for cells grown in the presence of 2 µg.mL⁻¹ were statistically significant compared to the 0 µg.mL⁻¹ control. P-values for each concentration were 2 µg.mL⁻¹ (>0.05), 4 µg.mL⁻¹ (<0.01) and 8-256 µg.mL⁻¹ (<0.0001).

The addition of 4 µg.mL⁻¹ of chicken egg lysozyme (Figure 3.5 (a): Pink) to the wild type strain culminated in the first observable indication of cellular growth inhibition caused by the lysozyme. Although the initial apparent lag phase in the presence of 4 µg.mL⁻¹ lysozyme matched the time frame of the 0 µg.mL⁻¹ control at 21 hours, the gradient of growth during exponential phase was reduced leading to a 50% increase in doubling time to 12.05 hours. Growth plateaued at a similar optical density to the control OD_{600nm} 0.22 though the area under the curve (AUC) for the 4 µg.mL⁻¹ data set was reduced by 25% compared to the control.

Subsequent concentrations of lysozyme: 8 µg.mL⁻¹ (Figure 3.5 (a): Orange) and 16 µg.mL⁻¹ (Figure 3.5 (a): Purple) differed from the lower concentrations due to the noted extended time period with apparent lag phase of 10 and 15 hours respectively. Both concentrations displayed a similar Td to 4 µg.mL⁻¹, attaining 10.23 and 12.34 hours respectively. These two concentrations plateaued at a similar OD_{600nm} entering stationary phase after 51 hours. The final optical density reached by 8 µg.mL⁻¹ and 16 µg.mL⁻¹ data sets was 74% and 69% the value obtained by the control. The AUC for both 8 µg.mL⁻¹ and 16 µg.mL⁻¹ concentrations were 57% and 69% relative to the control data set. The sixty-hour time frame of the experiment was insufficient to observe growth present in those wells containing 32 µg.mL⁻¹ lysozyme, (Figure 3.5 (a): Red) leading to the MIC of the wild type strain being recorded as 32 µg.mL⁻¹.

As noted in Figure 3.1 the Δ NamH strain demonstrated a comparable growth curve to the wild type under normal conditions. In Figure 3.5 the Δ NamH control experiment (Figure 3.5 (b): Blue), presented a similar growth phenotype to the wild type control (Figure 3.5 (a)). Exponential growth was observed after 21 hours and the cell cultures within the triplicate wells reached stationary phase after 45 hours. The Td during exponential phase was also equivalent to the wild type strain at 7.9 hours. A student's t-test analysis of the Δ NamH strain (Table 3.1) against chicken lysozyme indicated that all measured growth curves were statistically significant compared to the 0 $\mu\text{g.mL}^{-1}$ lysozyme absent control. P-values for each concentration were 2 $\mu\text{g.mL}^{-1}$ (>0.05), 4 $\mu\text{g.mL}^{-1}$ (<0.01) and 8-256 $\mu\text{g.mL}^{-1}$ (<0.0001).

The addition of 2 $\mu\text{g.mL}^{-1}$ chicken egg white lysozyme (Figure 3.5 (b): Green) led to an almost 20% decrease in Td to 6.42 hours. A reason for this variation from the control data may be due in part to very low concentrations of lysozyme disrupting remaining mycobacterial cell clumps, not separated sufficiently by growth within media containing Tween80 or by not adequately passing through a narrow syringe before incubation. Other observed differences from the wild type strain in the 2 $\mu\text{g.mL}^{-1}$ data set were more in keeping with previous incubation with lysozyme. The apparent lag phase was extended to 24 hours and the AUC data showed a reduction by 14% compared to the control.

Doubling the enzyme concentration to 4 $\mu\text{g.mL}^{-1}$ (Figure 3.5 (b): Pink) increased the Td to 8.28 hours and extended the apparent lag phase to 30 hours but did not impact the maximum optical density reached during the stationary phase compared to 2 $\mu\text{g.mL}^{-1}$. The AUC of the curve was reduced to 65% of the control which was 10% greater than the equivalent concentration against the wild type (Figure 3.5 (a): Pink). The final lysozyme concentration for which a measurable growth phenotype for the Δ NamH *M. smegmatis* strain could be measured was 8 $\mu\text{g.mL}^{-1}$ (Figure 3.5 (b): Orange), where the growth curve plateaued at 47.8% of the maximum optical density reached by the control. The Td of 8 $\mu\text{g.mL}^{-1}$ lysozyme doubled from the control data set to 16.82 hours and achieved an AUC of 14% relative to the control. All other lysozyme concentrations were sufficient to completely inhibit growth, leading to the conclusion that the MIC for chicken egg

white lysozyme against *M. smegmatis* Δ NamH cells was 16 $\mu\text{g.mL}^{-1}$ (Figure 3.5 (b): Purple), which is half the MIC of the wild type (Figure 3.5 (a): Red).

Student's t-test analysis comparing the inhibition of growth curves for both *M. smegmatis* strains at equivalent chicken lysozyme concentrations (Table 3.1) indicated that concentrations below 4 $\mu\text{g.mL}^{-1}$ were not significant with p-values >0.05 . Contrasting the two strains at equivalent chicken lysozyme concentrations at 8 $\mu\text{g.mL}^{-1}$ and 16 $\mu\text{g.mL}^{-1}$ which permitted observable growth in the wild type did demonstrate statistically significant data producing p-values for both concentrations of <0.001 .

Wells containing MIC or greater for both wild type and Δ NamH strains were pipetted onto TSB agar plates and incubated for 72 hours to determine the minimal bactericidal concentration (MBC). The findings are presented in Figure 3.6.

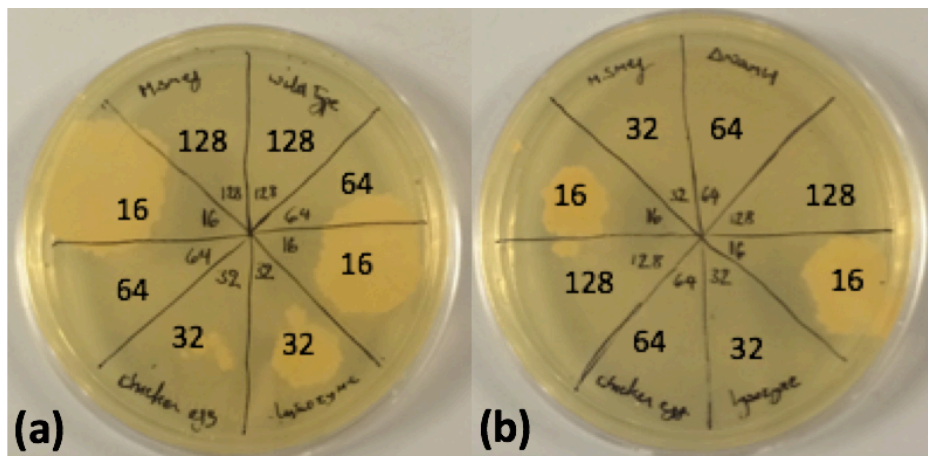


Figure 3.6 Minimal bactericidal concentration of chicken egg white lysozyme against *M. smegmatis* strains. *M. smegmatis* wild type (a) and Δ NamH (b) cells incubated in liquid media with increasing concentrations of lysozyme that did not produce growth (Figure 3.5) were pipetted in duplicate onto TSB agar to determine MBC. Each quadrant denotes the enzyme concentration in $\mu\text{g.mL}^{-1}$. Results: Wild type MBC 64 $\mu\text{g.mL}^{-1}$, Δ NamH MBC 32 $\mu\text{g.mL}^{-1}$.

Although no growth was observed at these concentrations in the microtiter plates (Figure 3.5), once transferred to nutrient agar both strains incubated with 16 $\mu\text{g.mL}^{-1}$ of chicken egg white lysozyme were able to colonise the agar plate (Figure 3.6). The wild type strain (Figure 3.6 (a)) also achieved colonisation after incubation with 32 $\mu\text{g.mL}^{-1}$ of lysozyme, although the ΔNamH did not. The two remaining highest concentrations, 64 $\mu\text{g.mL}^{-1}$ and 128 $\mu\text{g.mL}^{-1}$ were sufficient to prevent any observable measurement of growth either within the microtiter plate or subsequently on agar. These results lead to the conclusion that the MBC values for both strains, 64 $\mu\text{g.mL}^{-1}$ for the wild type and 32 $\mu\text{g.mL}^{-1}$ for the ΔNamH are double the MIC concentrations for each strain.

3.6.1.1 *M. smegmatis* sensitivity towards human lysozyme

The human lysozyme variant has been shown to be significantly more potent than the chicken egg equivalent in cleaving sugar residues (Wu, *et al.* 2015). Previous investigations by the Pavelka group (Raymond, *et al.* 2005) noted the MIC for the newly constructed wild type (PM965) and the ΔNamH (PM979) *M. smegmatis* strains against human lysozyme were 16 $\mu\text{g.mL}^{-1}$ and 8 $\mu\text{g.mL}^{-1}$ respectively. The MIC activity for both strains against human lysozyme was re-evaluated here (Figure 3.7). As the MIC assessment of chicken egg lysozyme showed that the lysozyme MIC was 32 $\mu\text{g.mL}^{-1}$, the decision was taken to change the investigated concentration range from 2-256 $\mu\text{g.mL}^{-1}$ to 1-128 $\mu\text{g.mL}^{-1}$.

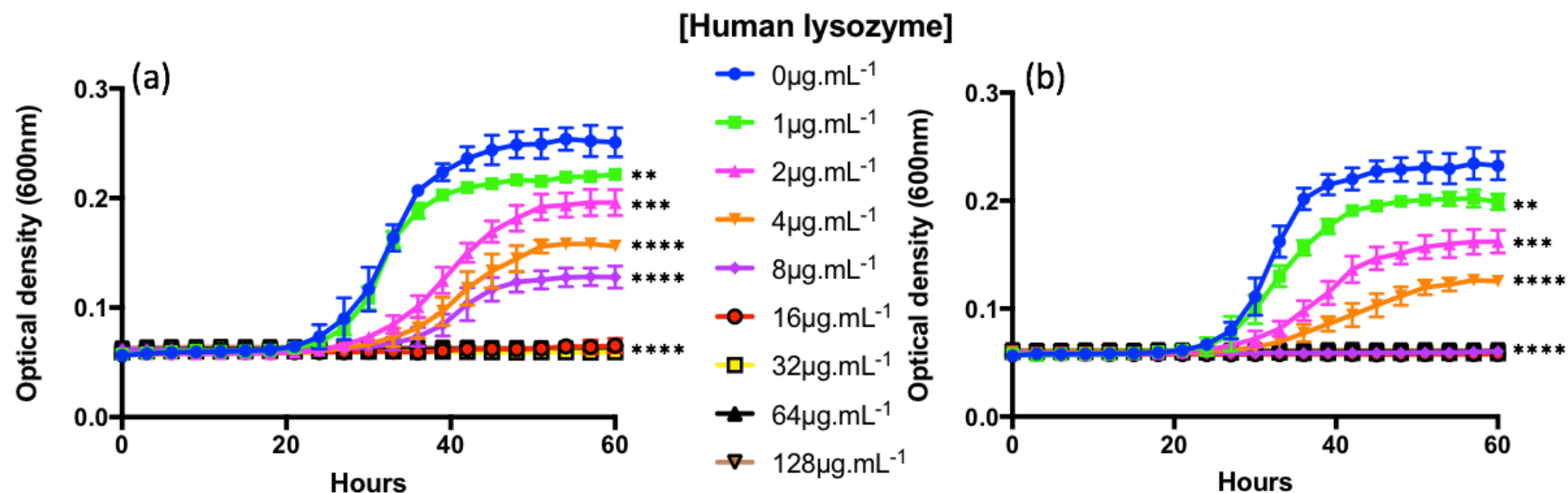


Figure 3.7 The hydrolytic activity of human lysozyme against the mycobacterial modifications of peptidoglycan. Wild type (a) and ΔNamH (b) *M. smegmatis* MIC growth curves against human lysozyme. Cells were grown in 96-well microtiter plates in triplicate at 37°C with intermittent shaking every 20 minutes, where the absorbance was measured at 600nm at 3 hour intervals for 60 hours. Each well contained 100 μL culture media (7H9, ADC, 0.05% (w/v) Tween 80) with increasing concentrations of human lysozyme. The cultured *M. smegmatis* wild type (a) and ΔNamH (b) strains were standardized to an $\text{OD}_{600\text{nm}}$ of 1 and diluted further by a factor of 10^4 prior to addition of enzyme and incubation. Error bars represent standard deviation of triplicate measurements. Human lysozyme concentrations: 0 $\mu\text{g.mL}^{-1}$ (Blue), 1 $\mu\text{g.mL}^{-1}$ (Green), 2 $\mu\text{g.mL}^{-1}$ (Pink), 4 $\mu\text{g.mL}^{-1}$ (Orange), 8 $\mu\text{g.mL}^{-1}$ (Purple), 16 $\mu\text{g.mL}^{-1}$ (Red), 32 $\mu\text{g.mL}^{-1}$ (Yellow), 64 $\mu\text{g.mL}^{-1}$ (Black), 128 $\mu\text{g.mL}^{-1}$ (Brown). Statistically significant results are indicated with * = p-value <0.05, ** = <0.01, *** = <0.001 and **** = <0.0001. Results: ΔNamH displayed greater susceptibility to human lysozyme than wild type. MIC results: Wild type 16 $\mu\text{g.mL}^{-1}$, ΔNamH 8 $\mu\text{g.mL}^{-1}$.

Human lysozyme ($\mu\text{g.mL}^{-1}$)	Wild type <i>M. smegmatis</i>					ΔNamH <i>M. smegmatis</i>					(b) vs (a) p-values
	Apparent Lag phase (h)	Td (h^{-1})	AUC (%)	Stationary Phase $\text{OD}_{600\text{nm}}$	Wild type p-values (a)	Apparent Lag phase (h)	Td (h^{-1})	AUC (%)	Stationary Phase $\text{OD}_{600\text{nm}}$	ΔNamH p-values (b)	
0	21	6.95	-	0.25	-	21	6.95	-	0.23	-	>0.05
1	21	7.16	84.58	0.22	<0.01	21	8.88	79.04	0.20	<0.01	<0.01
2	27	11.71	54.09	0.19	<0.001	27	13.2	46.85	0.16	<0.001	<0.01
4	33	12.42	36.60	0.15	<0.0001	33	19.2	25.92	0.12	<0.0001	<0.001
8	36	15.40	26.29	0.13	<0.0001	60	0.00	0.00	0.05	<0.0001	<0.001
16	60	0.00	0.00	0.05	<0.0001	60	0.00	0.00	0.05	<0.0001	-
32	60	0.00	0.00	0.05	<0.0001	60	0.00	0.00	0.05	<0.0001	-
64	60	0.00	0.00	0.05	<0.0001	60	0.00	0.00	0.05	<0.0001	-
128	60	0.00	0.00	0.05	<0.0001	60	0.00	0.00	0.05	<0.0001	-

Table 3.2 Statistical comparisons of *M. smegmatis* growth curves in the presence of increasing concentrations of human lysozyme. Wild type and ΔNamH strains incubated for 60 hours at 37°C with selected concentrations of human lysozyme produced growth curves measured at $\text{OD}_{600\text{nm}}$ in Figure 3.7. Variations between growth curves were measured by time taken to exit apparent lag phase (hours), the doubling time (Td) of cells during exponential phase (hours^{-1}), the area under the curve (AUC) percentage compared to the 0 $\mu\text{g.mL}^{-1}$ control (%), the $\text{OD}_{600\text{nm}}$ value achieved during stationary phase and whether the growth curve variations were statistically significant compared to each 0 $\mu\text{g.mL}^{-1}$ control with p-values <0.05 deemed significant. The statistical significance of ΔNamH (b) growth curves compared to wild type (a) at equivalent human lysozyme concentrations were determined by p-values <0.05.

The growth kinetics of the wild type control correlated with the data obtained from the previous experiment involving chicken egg lysozyme (Figure 3.5 (a)). Growth was measurable after 21 hours, the Td during exponential phase was 6.95 hours and the control reached a maximum optical density of 0.25 during stationary phase after 45 hours (Figure 3.7 (a): Blue). A student's t-test analysis of the growth of wild type strain (Table 3.2) against human lysozyme demonstrated that all concentrations were statistically significant compared to the 0 $\mu\text{g.mL}^{-1}$ lysozyme absent control. P-values for the wild type strain were 1 $\mu\text{g.mL}^{-1}$ (<0.01), 2 $\mu\text{g.mL}^{-1}$ (<0.001) and 4-128 $\mu\text{g.mL}^{-1}$ (<0.0001).

The presence of 1 $\mu\text{g.mL}^{-1}$ human lysozyme (Figure 3.7 (a) Green) did not impact the length of apparent lag phase or the time taken to reach stationary phase, which remained 45 hours, but did slightly increase the Td to 7.16 hours. The final optical density achieved by the 1 $\mu\text{g.mL}^{-1}$ data set during stationary phase was reduced by 12% of the control and also impacted the AUC, calculated as 85% of the area obtained by the wild type control.

The variation in the impact on growth of the wild type *M. smegmatis* strain between the human and chicken egg white lysozymes was most clearly evident with 2 $\mu\text{g.mL}^{-1}$ of the enzyme (Figure 3.7 (a): Pink). Whereas the chicken egg lysozyme did not impact upon the growth of *M. smegmatis* at this concentration, the human enzyme extended the apparent lag phase of *M. smegmatis* by 6 hours, increased the Td to 11.71 hours and reduced the stationary phase OD by 22% and the AUC to 55% of the control value. Treatment of *M. smegmatis* with 4 $\mu\text{g.mL}^{-1}$ human lysozyme (Figure 3.7 (a): Orange) significantly extended the apparent lag phase of the organism to 33 hours, increased the Td to 12.42 hours where the corresponding AUC was reduced by 62% compared to the control. The final concentration of human lysozyme permitting an observable growth phenotype was 8 $\mu\text{g.mL}^{-1}$ (Figure 3.7 (a): Purple), exiting apparent lag phase after 36 hours with a two-fold increase in the doubling time to 15.40 hours and a reduction by 72% of the AUC compared to the control. The 60-hour time frame was just insufficient to register growth from the 16 $\mu\text{g.mL}^{-1}$ (Figure 3.7 (a): Red) triplicate, leading the MIC to be observed to be 16 $\mu\text{g.mL}^{-1}$. This concentration was half of the MIC result from chicken egg lysozyme against the wild type strain (Figure 3.5 (a)).

The human lysozyme MIC results for the Δ NamH strain (Figure 3.7 (b)) as with the wild type fell similarly in line with the results obtained against the chicken egg lysozyme variant (Figure 3.5 (b)), although the potency of enzyme activity had notably increased. The Δ NamH control data was identical to the wild type *M. smegmatis* growth phenotype, producing observable growth after 21 hours, with a Td of 6.95 hours and an entrance into stationary phase with an OD_{600nm} of 0.24 after 45 hours. Similarly, to the wild type strain, all concentrations of human lysozyme impacted the growth phenotype of the Δ NamH strain in a statistically significant manner (Table 3.2). P-values for each concentration were 1 $\mu\text{g.mL}^{-1}$ (<0.01), 2 $\mu\text{g.mL}^{-1}$ (<0.001) and 4-128 $\mu\text{g.mL}^{-1}$ (<0.0001).

The addition of 1 $\mu\text{g.mL}^{-1}$ human lysozyme (Figure 3.7 (b): Green) did not extend the apparent lag phase but impacted the doubling time, increasing it to 8.88 hours. The AUC decreased by 11% and maximum stationary OD was 85% of the control data value.

2 $\mu\text{g.mL}^{-1}$ of human lysozyme (Figure 3.7 (b): Pink) was adequate enough to almost double the Td to 13.2 hours, reduce measurable growth such that the AUC total was 48%, extended the apparent lag phase by 6 hours and diminished the maximum OD reached during stationary phase to 69% of the control. The final concentration of human lysozyme to permit cellular growth was 4 $\mu\text{g.mL}^{-1}$ (Figure 3.7 (b): Orange). The growth curve AUC represented 30% of the control, the apparent lag phase and Td were increased to 32 hours and 19.2 hours respectively and culminated in a 53% maximum OD during stationary phases compared to the control. The MIC of the Δ NamH strain was 8 $\mu\text{g.mL}^{-1}$ (Figure 3.7 (b): Purple).

Student's t-test analysis comparing the two *M. smegmatis* strains at equivalent human lysozyme concentrations indicated statistical significance variation between growth curves at each investigated concentration (Table 3.2). The significance increased as the concentration of human lysozyme increased. P-values produced at each concentration were <0.01 (1 and 2 $\mu\text{g.mL}^{-1}$) and <0.001 (4 and 8 $\mu\text{g.mL}^{-1}$).

These values were consistent with the initial experiments reported by Raymond, *et al.* (2005), where the human lysozyme MIC of the wild type (PM965) strain was 16 $\mu\text{g.mL}^{-1}$ and that of the

Δ NamH (PM979) was $8 \mu\text{g.mL}^{-1}$. Those human lysozyme concentrations from both strains (Figure 3.7) which did not produce any visible sign of growth were transferred to nutrient agar to determine the MBC values for each strain. The results are shown in Figure 3.8.

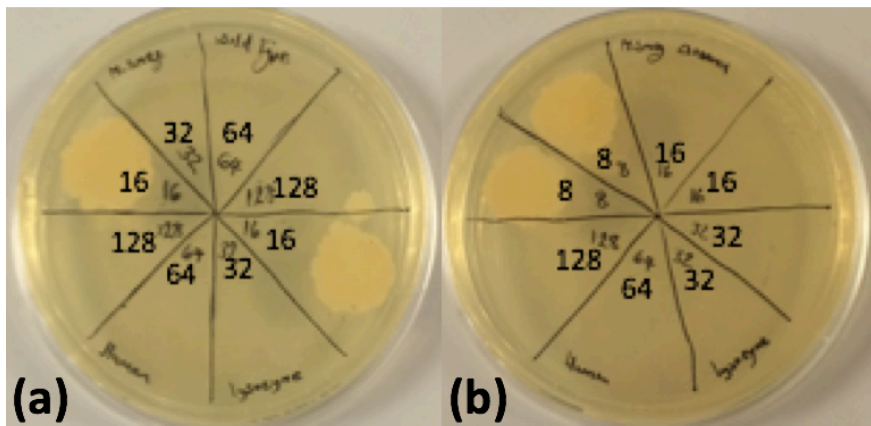


Figure 3.8 Minimal bactericidal concentration of human lysozyme against *M. smegmatis* strains. *M. smegmatis* wild type (a) and Δ NamH (b) cells were incubated in liquid media with increasing concentrations of lysozyme that did not produce growth (Figure 3.7) were pipetted in duplicate onto TSB agar to determine MBC values. Each quadrant denotes the enzyme concentration in $\mu\text{g.mL}^{-1}$. Results: Wild type MBC $32 \mu\text{g.mL}^{-1}$, Δ NamH MBC $16 \mu\text{g.mL}^{-1}$.

Plating onto agar those wells that did not produce any visible signs of growth (Figure 3.7), led to an MBC values of $32 \mu\text{g.mL}^{-1}$ for the wild type and $16 \mu\text{g.mL}^{-1}$ for the Δ NamH (Figure 3.8). These values are double the minimal inhibitory concentrations observed in Figure 3.7, and once again show that the Δ NamH strain is more susceptible to lysozyme than the wild type strain.

3.6.1.2 Impact of pH on the sensitivity of *M. smegmatis* towards human lysozyme

The standard pH for *in vitro* growth of mycobacteria is pH 6.8, commonly cultured within 7H9 media. The pH range over which hydrolytic enzymes released from the phagolysosome are active can range between low acidic to slightly basic conditions. Since the phagolysosome is a low pH environment, pH 5 (Levitz, *et al.* 1999) the effects of enzyme activity during these extremes is important to analyse. *M. smegmatis* cells are unable to grow at a low pH as observed by their switch into a state of dormancy once encased within granulomas (Section 1.5). The protocol to

investigate mycobacterial survival at lower pH values with viable cells was described by Eric Brown's group (Koo, *et al.* 2008). In short, incubated cells that had grown to exponential phase were diluted and passed through a syringe to break up any aggregated clumps. Cells were incubated in Hank's Balanced Salt Solution (HBSS) buffer at specific pH ranges in the absence of specific nutrients to prevent growth along with the varying concentrations of hydrolytic enzymes. (Section 2.5.1) After a selected time period of 1.5 hours the wells were pipetted onto agar plates in triplicate, incubated at 37°C for 72 hours and the resulting colonies counted and averaged.

Before assessment of the hydrolytic enzymes was undertaken, serial dilutions of cell cultures were investigated to determine the range of visible colony separation necessary to accurately distinguish and count viable single colonies. As previously described, cells from both wild type and Δ NamH strains were cultured and once growth entered exponential phase, cultures were isolated from the nutrient growth by centrifugation and resuspended in HBSS buffer pH7. The optical density of each strain was diluted to OD_{600nm} 0.1, from which serial 10-fold dilutions were prepared in HBSS, ranging from OD_{600nm} 10⁻² to 10⁻⁷. A 100 μ L aliquots from each dilution were pipetted onto TSB agar plates and incubated at 37°C for 72 hours. Once incubation was complete the plates were examined and assessed for ease of visualising individual colonies. The serial dilutions of *M. smegmatis* cells are depicted in Figure 3.9.

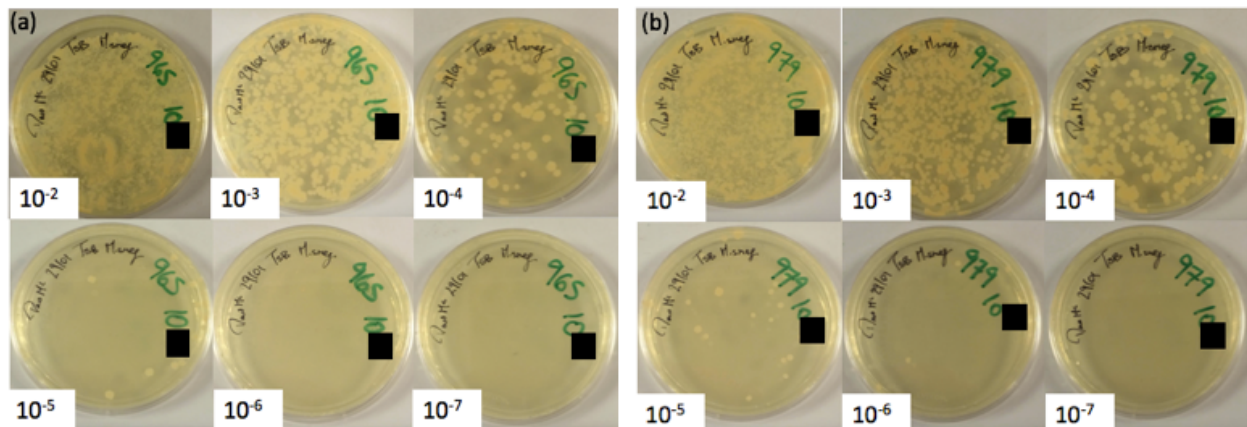


Figure 3.9 Colony count visibility of serially diluted *M. smegmatis* strains. Wild type (a) and Δ NamH (b) cells cultured to exponential phase in nutrient media, centrifuged and resuspended in HBSS buffer pH 7. Cells from both strains were diluted to OD_{600nm} 0.1 and subsequently serially diluted 10-fold from OD_{600nm} 10⁻² to 10⁻⁷ to assess colony count viability. Result: OD_{600nm} 10⁻⁵ dilution for both strain produced the most visible colony separation.

The results of Figure 3.9 depict that utilising a final dilution below $OD_{600nm} 10^{-5}$ for both strains leads to an insufficient number of colonies forming on the agar plates as a control in the absence of hydrolytic enzymes. Utilising a dilution above $OD_{600nm} 10^{-5}$ inversely leads to significant colonisation of the agar plate preventing the ability to distinguish between individual colonies. Based upon the results depicted in Figure 3.9 the standard final dilution utilised during the chapter for both strains was $OD_{600nm} 10^{-5}$ (0.00001).

The controls for each experiment involved the wild type and $\Delta NamH$ strains incubated for the equivalent time period in HBSS buffer in the absence of enzyme as cells incubated in the presence of enzyme. To assess the difficulty of accurately counting single colonies in untreated controls on triplicate agar plates, both strains were diluted to $OD_{600nm} 10^{-5}$ and 100 μL pipetted onto individual agar plates. Plates were incubated for 72 hours and the resulting colonies were counted by hand. The results are displayed in Figure 3.10.

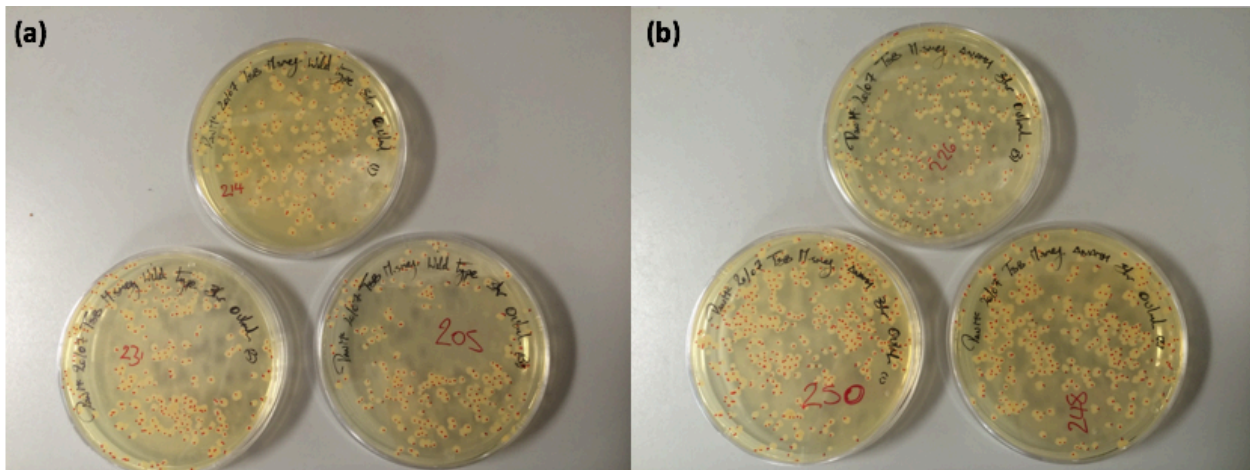


Figure 3.10 Assessment of *M. smegmatis* strain serial dilution and HBSS incubation. *M. smegmatis* (a) wild type and (b) $\Delta NamH$ cells were incubated in 100 μL HBSS in a 96 well microtiter plate. After 1.5 hour incubation at 37°C bacterial survival was determined. Wells were pipetted on TSB agar plates and incubated at 37°C for 72 hours. Colony forming units were counted and averaged from triplicate plates.

The $OD_{600nm} 10^{-5}$ dilutions for both strains in Figure 3.10 were sufficient to permit an abundant number of viable colonies during control conditions. Each plate produced over 200 visible colonies with no signs of contamination.

The previously mentioned Brown (2008) protocol was applied to investigate the impact of varying concentrations of human lysozyme on *M. smegmatis* cells buffered to different pH values. The pH of the buffer was measured before and after the experiment to maintain accuracy. The initial experiment determined the effect of lysozyme at pH 7 at selected concentrations for both strains. The colony forming units (CFU) were counted and averaged and the percentage survival of each strain during incubation with each concentration of lysozyme was compared to the 0 $\mu\text{g.mL}^{-1}$ control. This data is demonstrated in Figure 3.11.

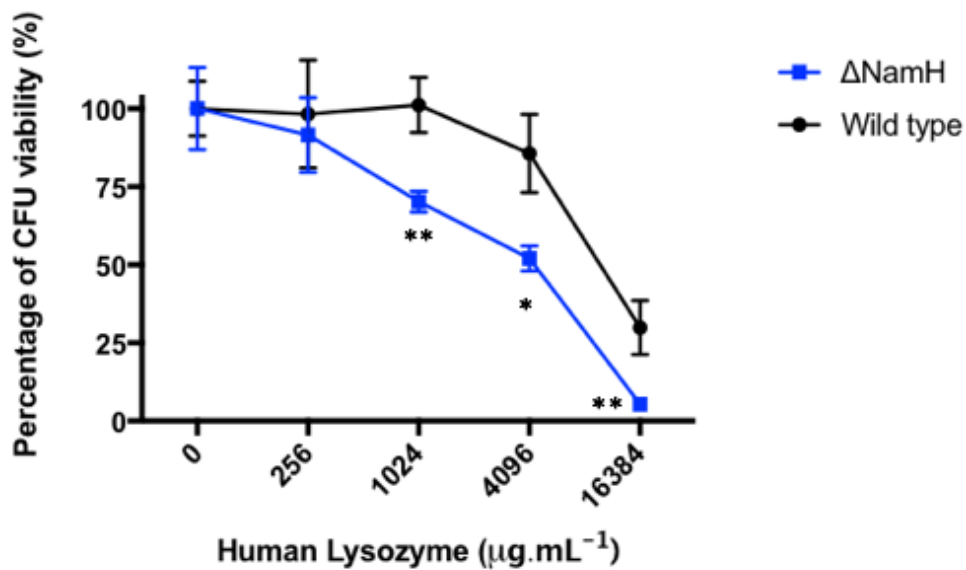


Figure 3.11 *In vitro* human lysozyme assay for bactericidal activity against *M. smegmatis* at pH 7. *M. smegmatis* wild type (Black) and ΔNamH (Blue) cells were incubated with 0, 256, 1024, 4096 and 16384 $\mu\text{g.mL}^{-1}$ of human lysozyme in 100 μL HBSS in a 96 well microtiter plate. After 1.5 hour incubation at 37°C bacterial survival was determined. Wells were pipetted on TSB agar plates and incubated at 37°C for 72 hours. Colony forming units were counted and averaged from triplicate plates. Error bars represent standard deviation of these data. Statistically significant results are indicated with * = p-value <0.05, ** = <0.01, *** = <0.001 and **** = <0.0001. Result: The ΔNamH strain was more susceptible at each human lysozyme concentration, producing fewer colonies than the wild type strain.

Lysozyme concentration ($\mu\text{g.mL}^{-1}$)	Wild type % (1) Survival (mean \pm SD, n=3)	Δ NamH % (2) Survival (mean \pm SD, n=3)	Significance student's t-test (2) v (1)
0.0	100.00 \pm 8.74	100.00 \pm 13.13	N/A
256	98.27 \pm 17.24	91.55 \pm 11.95	p >0.05
1024	101.14 \pm 8.84	70.22 \pm 3.35	p <0.005
4096	85.63 \pm 12.47	52.00 \pm 4.00	p <0.05
16384	29.88 \pm 8.67	5.33 \pm 1.33	p <0.01

Table 3.3 Average bacterial survival by *M. smegmatis* wild type and Δ NamH strains against human lysozyme at pH 7. Results depicted in a graph in Figure 3.11. Standard deviation is of triplicate measurements. Statistically significant results were indicated by p-values <0.05.

The initial CFU averages for the wild type strain in the absence of enzyme (0 $\mu\text{g.mL}^{-1}$) was 77 ± 6.76 (n=3) colonies per plate, 23% less than the equivalent result, 100 ± 13.13 (n=3) colonies for the Δ NamH strain. The percentage obtained from the initial experiment demonstrated that at pH 7 (Figure 3.11) the difference between the two strains in terms of lysozyme susceptibility was visible from the lowest incubated concentration (Table 3.3). At 256 $\mu\text{g.mL}^{-1}$ human lysozyme, the wild type showed a 1.7% decrease in bacterial survival count compared to the wild type control whereas the Δ NamH survival decreased by 8.5% compared to its control. 1024 $\mu\text{g.mL}^{-1}$ human lysozyme failed to significantly impact upon the survival of wild type *M. smegmatis* strain, the bacterial survival was identical compared to the control within the margin of error. The Δ NamH strain incubated with 1024 $\mu\text{g.mL}^{-1}$ suffered a notable drop in survival to 70% of the total colonies present in the control. 4096 $\mu\text{g.mL}^{-1}$ was the lowest concentration of human lysozyme that altered bacterial survival of wild type cells, where the total number of colonies present decreased by 15% at this concentration. The Δ NamH strain on the other hand continued to display greater susceptibility with a 48% decrease in cell survival at this lysozyme concentration. The highest concentration of 16,384 $\mu\text{g.mL}^{-1}$ human lysozyme tested reduced the survival of wild type *M. smegmatis* to below 30% total survival, whereas the NamH deficient strain to only 5% total bacterial survival.

A student's t-test comparative analysis of the percentage survival of both strains against human lysozyme at pH 7.0 (Table 3.3) demonstrated that that initial survival variation at 256 $\mu\text{g.mL}^{-1}$ was not deemed statistically significant with a p-value >0.05 . Subsequent comparisons between strains at concentration greater than 256 $\mu\text{g.mL}^{-1}$ were deemed statistically significant with p-values of <0.005 (1024 $\mu\text{g.mL}^{-1}$), <0.05 (4096 $\mu\text{g.mL}^{-1}$) and <0.01 (16384 $\mu\text{g.mL}^{-1}$). This experiment successfully underlines the difference between the two stains first described by the Pavelka group as well as to indicate that the protocol published by the Brown group is applicable for this investigation.

The standard protocol outlined in Figure 3.11 was subsequently repeated, except that the pH of the HBSS buffer was altered to pH 6.5, 6.0, 5.5 and 5.0. Due to the stark difference in survival of the ΔNamH strain observed between human lysozyme concentrations 4096 $\mu\text{g.mL}^{-1}$ and 16384 $\mu\text{g.mL}^{-1}$ at pH 7.0 (Figure 3.11), a mid-point concentration of 8192 $\mu\text{g.mL}^{-1}$ was selected to collect more data related to decline in bacterial survival to enzyme concentration. The following data sets were formed from triplicate colony counts on agar plates. The data was analysed and average colony counts obtained were equated against the 0 $\mu\text{g.mL}^{-1}$ control of each data set as percentages, as depicted in Figure 3.12.

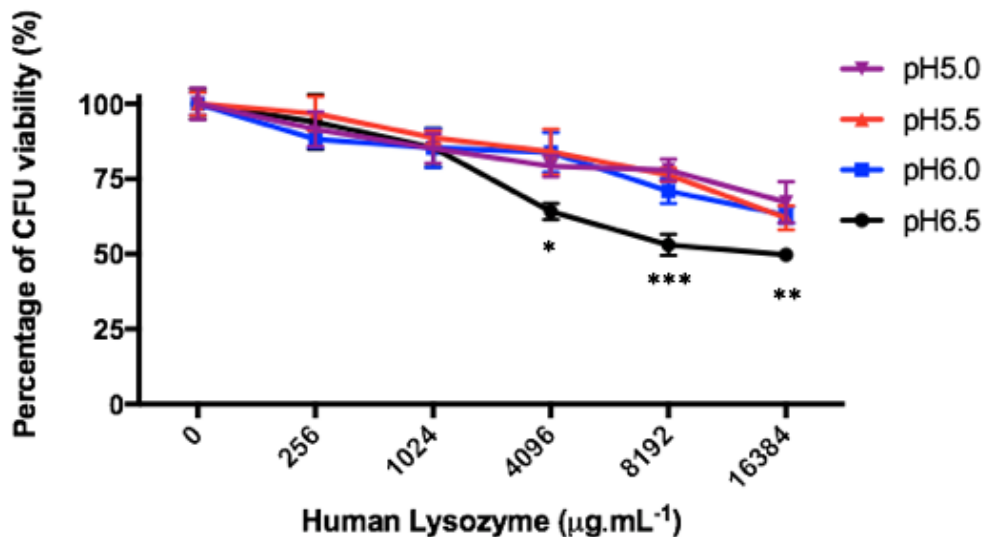


Figure 3.12 *In vitro* human lysozyme bacterial survival percentage assay for bactericidal activity against *M. smegmatis* wild type at selected pH. *M. smegmatis* wild type cells were incubated with 0, 256, 1024, 4096, 8192 and 16384 $\mu\text{g.mL}^{-1}$ of human lysozyme in 100 μL HBSS at pH 5.0 (Purple), 5.5 (Red), 6.0 (Blue) and 6.5 (Black) in a 96 well microtiter plate. After 1.5 hrs incubation at 37°C bacterial survival was determined. Wells were pipetted onto TSB agar plates and incubated at 37°C for 72 hours. Colony forming units were counted and averaged from triplicate plates. Error bars represent standard deviation of triplicate measurements. Averages at each concentration were compared to the control 0 $\mu\text{g.mL}^{-1}$ as a percentage. Statistically significant results are indicated with * = p-value <0.05, ** = <0.01, *** = <0.001 and **** = <0.0001. Result: Percentage survival at each pH was consistent as human lysozyme concentration increased except pH 6.5 at higher concentrations which were significantly reduced.

The initial data obtained from the colony counts of CFU from the wild type produce three similar sets of data and one outlier. The total colony count for the wild type in the absence of human lysozyme at pH 6.5 was reduced by 13% compared to the other conditions with an average of 238 ± 12.12 ($n=3$) colonies across the triplicate plates. The reason for this reduction is not due to the pH as 6.5 is the highest and nearest to neutral pH of the four investigated conditions. The nutrient media commonly used to culture *M. smegmatis in vitro* is stated as pH 6.8 (Section 2.2.1). A likely reason for this discrepancy is an initial pipetting error during the serial dilution of cells to achieve $\text{OD}_{600\text{nm}} 10^{-4}$. Each additional pH condition began similarly with an initial total near 280 single colonies per plate and concluded with 100 fewer colonies after 16384 $\mu\text{g.mL}^{-1}$ human lysozyme incubation. The initial CFU average for the remaining pH conditions were 274.66 ± 10.26 ($n=3$) for pH 6.0, 275.00 ± 10.53 ($n=3$) for pH 5.5 and 289 ± 15.13 ($n=3$) for pH 5.0.

The percentage bacterial survival of the wild type strain at each selected pH condition (Figure 3.12) displayed a similar decline in bacterial survival against the two lowest investigated

concentrations, 256 $\mu\text{g.mL}^{-1}$ and 1024 $\mu\text{g.mL}^{-1}$. Each average bacterial survival percentage regardless of pH decreased by 15% compared to the 0 $\mu\text{g.mL}^{-1}$ control once incubated with 1024 $\mu\text{g.mL}^{-1}$, indicating that although the colony count average was reduced for cells incubated at pH 6.5 the effect of lysozyme activity was equivalent at all pH conditions. As observed in Figure 3.12 increasing the concentration of human lysozyme above 4096 $\mu\text{g.mL}^{-1}$ at pH 6.5 aided lysozyme activity (Figure 3.12: Black), decreasing the percentage survival compared to the corresponding results at pH 6.0 (Figure 3.12: Blue), by 19% at 4096 $\mu\text{g.mL}^{-1}$, 17% at 8192 $\mu\text{g.mL}^{-1}$ and 13% at 16384 $\mu\text{g.mL}^{-1}$. The final total survival for the wild type strain at 16384 $\mu\text{g.mL}^{-1}$ was 50% at pH 6.5, these results coupled with Figure 3.11 shows that reduction of the pH from pH 7 to pH 6.5 decrease lysozyme activity and increased survival of the strain by 50% (Table 3.3). The activity of the enzyme is believed to be at its optimum at pH 7 (Yang, *et al.* 2011). The percentages obtained at pH 6.5 were statistically compared to those obtained at the lower pH conditions to determine their significance. The bacterial survival at the initial two lysozyme concentrations, 256 and 1024 $\mu\text{g.mL}^{-1}$ were deemed insignificant (p-value >0.05) where-as the three highest concentrations generating statistically significant results compared to the other conditions, with p-values of <0.05 (4096 $\mu\text{g.mL}^{-1}$), <0.001 (8192 $\mu\text{g.mL}^{-1}$) and <0.01 (16384 $\mu\text{g.mL}^{-1}$).

The three remaining pH conditions, 6.0 (Figure 3.12: Blue), 5.5 (Figure 3.12: Red) and 5.0 (Figure 3.12: Purple) mirror each other's survival at each concentration with only slight deviation around the standard error. The gradual decline for each condition was not impacted significantly by pH or lysozyme concentration, where each condition permitted around 65% bacterial survival at the highest concentration 16384 $\mu\text{g.mL}^{-1}$. The data from Figure 3.12 indicated that lysozyme activity towards the wild type strain did not alter between pH 6.0 and 5.0.

The ΔNamH CFU survival frequency averages were plotted as % CFU viability relative to the 0 $\mu\text{g.mL}^{-1}$ lysozyme control for each pH against increasing lysozyme concentration as depicted in Figure 3.13.

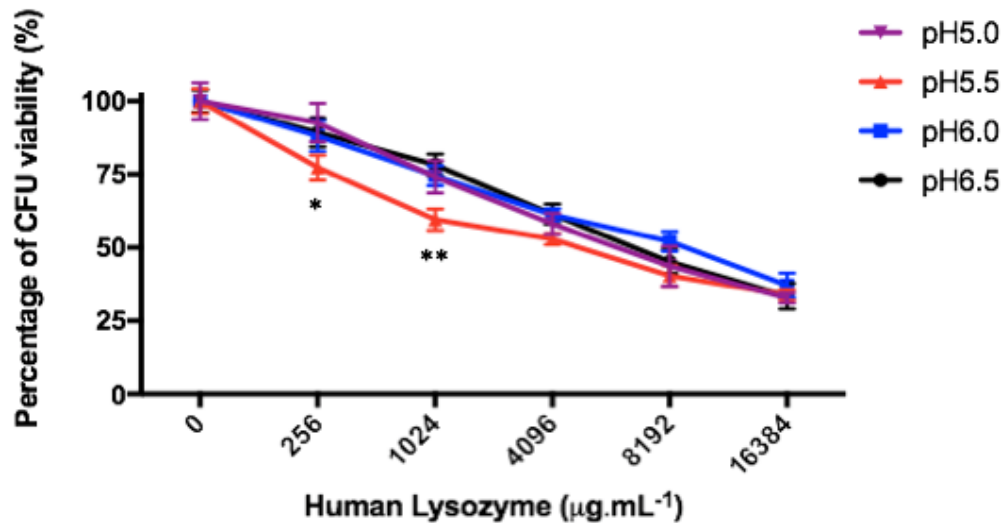


Figure 3.13 *In vitro* human lysozyme bacterial survival percentage assay for bactericidal activity against *M. smegmatis* Δ NamH at selected pH. *M. smegmatis* Δ NamH cells were incubated with 0, 256, 1024, 4096, 8192 and 16384 $\mu\text{g.mL}^{-1}$ of human lysozyme in 100 μL HBSS at pH 5.0 (Purple), 5.5 (Red), 6.0 (Blue) and 6.5 (Black) in a 96 well microtiter plate. After 1.5 hrs incubation at 37°C bacterial survival was determined. Wells were pipetted onto TSB agar plates and incubated at 37°C for 72 hours. Colony forming units were counted and averaged from triplicate plates. Error bars represent standard deviation of triplicate measurements. At each pH averages at each lysozyme concentration were compared to the 0 $\mu\text{g.mL}^{-1}$ control as a percentage. Statistically significant results are indicated with * = p-value <0.05, ** = <0.01, *** = <0.001 and **** = <0.0001. Result: Percentage survival at each pH was unchanged as human lysozyme concentration increased except pH 5.5 at lower concentrations.

The average colony counts for the Δ NamH strain demonstrated greater deviation between pH conditions than the wild type strain. The initial 0 $\mu\text{g.mL}^{-1}$ control averages for pH 6.5 and pH 5.5 produced the greatest number of colonies per plate with an average of 381.33 ± 14.57 (n=3) and 380.33 ± 15.63 (n=3) respectively. pH 6.0 supported growth of 339.66 ± 5.13 (n=3) colonies per plate, an 11% decrease from the other two pH values. The final pH test was 5.0, which produced the fewest number of Δ NamH strain colonies with an average count of 237 ± 14.73 (n=3). The reduction in the average of colonies at pH 5.0 compared to either pH 6.5 or pH 5.5 was 38%. The Δ NamH mutation of the knockout strain may have led to a decrease in cell tolerance to pH and increased lysis. This reduction at pH 5.0 was not observed in the wild type CFU which produced a similar CFU average to cells incubated at pH 6.0 and 5.5.

Combining the percentage survival of the Δ NamH strain at each incubated pH value (Figure 3.13) demonstrated the similar effect incubation with increasing concentrations of human lysozyme had on cells exposed to each pH value. The two extremes of the pH values investigated, pH 6.5 (Figure 3.13: Black) and pH 5.0 (Figure 3.13: Purple) displayed the same propensity towards lysozyme susceptibility regardless of concentration, maintaining only a 3% difference in average bacterial survival. Each of the four pH values resulted in a final total bacterial survival percentage of close to 33% at 16384 $\mu\text{g.mL}^{-1}$ human lysozyme, demonstrating that the alteration in pH conditions from pH 6.5 to pH 5.0 did not impact the activity of human lysozyme, similarly to the equivalent result obtained in the wild type in Figure 3.12. pH 5.5 (Figure 3.13: Red) was the only condition which demonstrated initial increased susceptibility towards 256 $\mu\text{g.mL}^{-1}$ and 1024 $\mu\text{g.mL}^{-1}$ to a greater degree with reductions of 10% and 15% respectively than other conditions, although once lysozyme concentration increased above 4096 $\mu\text{g.mL}^{-1}$ the percentage bacterial survival at pH 5.5 matched that observed at the other pH. The greater susceptibility was not visible during incubation with pH 5.0 (Figure 3.13: Purple), and is not believed to be caused by altering lysozyme activity. The percentage survival at pH 5.5 at 256 and 1024 $\mu\text{g.mL}^{-1}$ lysozyme was compared to their equivalent results at other pH conditions and deemed statistically significant with p-values of <0.05 (256 $\mu\text{g.mL}^{-1}$) and <0.005 (1024 $\mu\text{g.mL}^{-1}$) respectively.

The percentage bacterial survival results for human lysozyme incubation against both *M. smegmatis* strains at the four selected pH values were combined as detailed in Figure 3.14.

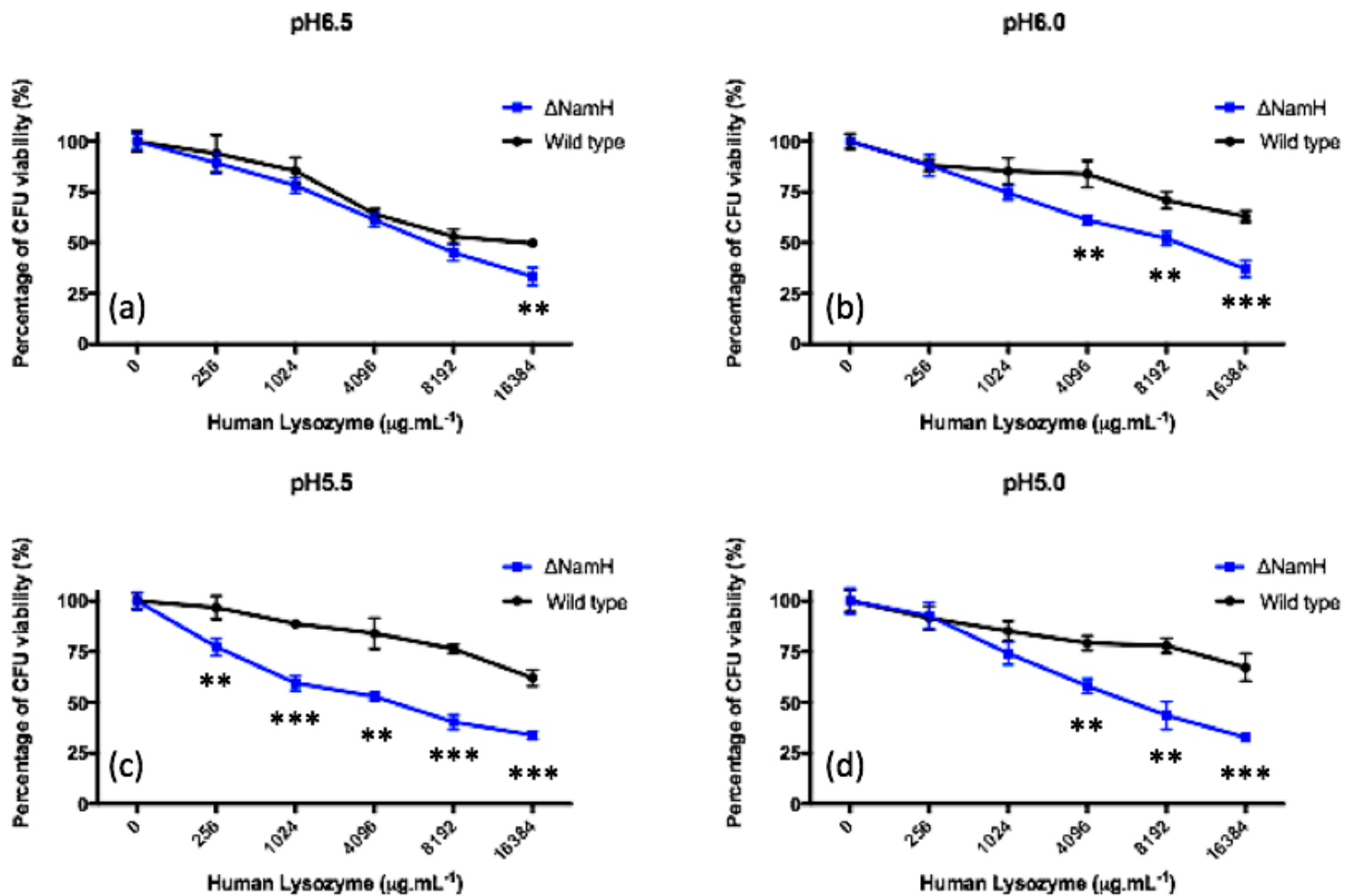


Figure 3.14 *In vitro* human lysozyme assay for bactericidal activity against *M. smegmatis* between pH 6.5 and 5.0. *M. smegmatis* wild type (Black) and Δ NamH (Blue) cells were incubated with 0, 256, 1024, 4096, 8192 and 16384 $\mu\text{g.mL}^{-1}$ of human lysozyme in 100 μL HBSS at four specific pH values; (a) pH 6.5, (b) pH 6.0, (c) pH 5.5 and (d) pH 5.0 in a 96 well microtiter plate. After 1.5 hour incubation at 37°C bacterial survival was determined. Wells were pipetted on TSB agar plates and incubated at 37°C for 72 hours. Colony forming units were counted and averaged from triplicate plates. Error bars represent standard deviation of triplicate measurements. Statistically significant results are indicated with * = p-value <0.05, ** = <0.01, *** = <0.001 and **** = <0.0001. Result: The Δ NamH strain was more susceptible at each human lysozyme concentration and each selected pH to varying degrees.

Lysozyme concentration ($\mu\text{g.mL}^{-1}$)	Wild type % (1) Survival (mean \pm SD, n=3)	ΔNamH % (2) Survival (mean \pm SD, n=3)	Significance student's t-test (2) v (1)
0.00	100.00 \pm 5.09	100.00 \pm 3.82	N/A
256	93.97 \pm 9.13	89.33 \pm 4.84	p >0.05
1024	85.43 \pm 6.52	78.23 \pm 3.73	p >0.05
4096	64.14 \pm 2.70	61.36 \pm 3.43	p >0.05
8192	53.08 \pm 3.49	45.19 \pm 4.03	p >0.05
16384	49.71 \pm 0.64	33.39 \pm 4.36	p <0.005

Table 3.4 Average bacterial survival by *M. smegmatis* wild type and ΔNamH strains against human lysozyme at pH 6.5. Results depicted in a graph in Figure 3.14 (a). Standard deviation is of triplicate measurements. Statistically significant results were indicated by p-values <0.05.

The highest pH condition investigated pH 6.5 (Figure 3.14 (a)) was still in the range of normal cellular growth for *M. smegmatis* (Piddington, *et al.* 2000). The decrease in pH from the initial investigation at pH 7 (Figure 3.11) eliminated the noted variation between the two strains towards human lysozyme. The decrease in survival for each strain at each selected lysozyme concentration were relatively equal to each other, as opposed to the observed survival deviation at pH 7. Incubation with the selected lysozyme concentrations at pH 6.5 lead to a gradual decline in bacterial survival by both strains (Table 3.4) as the lysozyme concentration increased, leading to 49.71% and 33.39% total bacterial survival of the wild type and ΔNamH strains respectively at the highest investigated concentration, 16384 $\mu\text{g.mL}^{-1}$. The decrease in wild type survival at pH 6.5 between 256 and 4096 $\mu\text{g.mL}^{-1}$ could be due to an increased activity of the enzyme compared to pH 7.0, although this was considered unlikely as this increased lysozyme activity was not also viewed in the ΔNamH strain data at pH 6.5 (Figure 3.14 (a)). The ΔNamH strain has previously been shown to be more susceptible to lysozyme than the wild type at pH 7.0 (Figure 3.11). The comparative survival between the two strains at the highest lysozyme concentration 16384 $\mu\text{g.mL}^{-1}$, increased by 20% in the wild type strain (49.71%) and 28% in the ΔNamH strain (33.39%) respectively at pH 6.5 compared to the equivalent results at pH 7 (Figure 3.11). This indicated that the lysozyme had reduced hydrolytic activity at pH 6.5 compared to pH 7.0. The standard deviation for the wild type was greatest against incubation with the two lowest enzyme

concentrations at pH 6.5. It is therefore possible that greater than normal variation between data points from these averages is the cause of discrepancy between the pH 7 and pH 6.5 data.

A student's t-test analysis (Table 3.4) of the human lysozyme concentrations against both strains at pH 6.5 indicate that bacterial survival variation between the two strains below 16384 $\mu\text{g.mL}^{-1}$ was statistically insignificant with p-values > 0.05. The p-value of 16384 $\mu\text{g.mL}^{-1}$ was <0.005, which was deemed statistically relevant.

Lysozyme concentration ($\mu\text{g.mL}^{-1}$)	Wild type % (1) Survival (mean \pm SD, n=3)	ΔNamH % (2) Survival (mean \pm SD, n=3)	Significance student's t-test (2) v (1)
0.00	100.00 \pm 3.73	100.00 \pm 1.51	N/A
256	88.23 \pm 2.92	88.12 \pm 5.23	p >0.05
1024	85.31 \pm 6.47	74.58 \pm 3.38	p >0.05
4096	83.85 \pm 6.61	61.13 \pm 2.08	p <0.005
8192	70.99 \pm 4.13	52.11 \pm 3.31	p <0.005
16384	62.98 \pm 2.74	37.09 \pm 4.12	p <0.001

Table 3.5 Average bacterial survival by *M. smegmatis* wild type and Δ NamH strains against human lysozyme at pH 6.0. Results depicted in a graph in Figure 3.14 (b). Standard deviation is of triplicate measurements. Statistically significant results were indicated by p-values <0.05.

Further reducing the pH to 6.0 led to a clear distinction between wild type and Δ NamH *M. smegmatis* strains as the lysozyme concentration increased (Figure 3.14 (b)). Initial colony counts at the lowest concentration, 256 $\mu\text{g.mL}^{-1}$ for both strains culminated in an identical percentage survival (88%) (Table 3.5), however, the two strains deviated in their sensitivity to lysozyme from this point onwards. The Δ NamH strain demonstrated a gradual decline in bacterial survival as lysozyme concentration increased similar to the Δ NamH data obtained at pH 6.5 (Figure 3.14 (a)), culminating in a final 37% total bacterial survival at pH 6.0 at 16384 $\mu\text{g.mL}^{-1}$ human lysozyme. The wild type displayed a slight increase in susceptibility towards the lysozyme at 256 $\mu\text{g.mL}^{-1}$ compared to the equivalent result at pH 6.5, reducing the percentage CFU to 88% of the control compared to 93% at pH 6.5. The wild type strain was unaffected as shown in Table 3.5 by the

subsequent increases in enzyme concentration, 85.31% survival at 1024 $\mu\text{g.mL}^{-1}$ and 83.85% survival at 4096 $\mu\text{g.mL}^{-1}$. The wild type strain resisted the activity of the lysozyme to a greater degree than previously demonstrated at pH 6.5, producing data more equivalent during incubation at pH 7 (Figure 3.11) terminating in a final bacterial survival at the highest lysozyme concentration 13% greater than pH 6.5.

The statistical significance between the two *M. smegmatis* strains at pH 6.0 were analysed (Table 3.5). P-values determined that bacterial survival at concentrations 256 $\mu\text{g.mL}^{-1}$ (>0.05) and 1024 $\mu\text{g.mL}^{-1}$ (>0.05) were not statistically significant whereas bacterial survival variations between concentrations 4096 $\mu\text{g.mL}^{-1}$ (<0.005), 8192 $\mu\text{g.mL}^{-1}$ (<0.005) and 16384 $\mu\text{g.mL}^{-1}$ (<0.001) were statistically significant.

Lysozyme concentration ($\mu\text{g.mL}^{-1}$)	Wild type % (1) Survival (mean \pm SD, n=3)	Δ NamH % (2) Survival (mean \pm SD, n=3)	Significance student's t-test (2) v (1)
0.00	100.00 \pm 3.83	100.00 \pm 4.10	N/A
256	96.72 \pm 5.71	77.30 \pm 4.23	p <0.01
1024	88.72 \pm 2.27	59.51 \pm 3.62	p <0.0005
4096	84.00 \pm 7.51	52.93 \pm 1.84	p <0.005
8192	76.36 \pm 2.18	40.31 \pm 3.68	p <0.0005
16384	62.06 \pm 4.00	33.82 \pm 1.84	p <0.0005

Table 3.6 Average bacterial survival by *M. smegmatis* wild type and Δ NamH strains against human lysozyme at pH 5.5. Results depicted in a graph in Figure 3.14 (c). Standard deviation is of triplicate measurements. Statistically significant results were indicated by p-values <0.05 .

The bacterial survival shown in Table 3.6 of both *M. smegmatis* strains was the most divergent at pH 5.5 (Figure 3.14 (c)). From the lowest concentration of human lysozyme, 256 $\mu\text{g.mL}^{-1}$ the bacterial survival of the two strains immediately diverged. This result differed from the other investigated pH conditions, with wild type and Δ NamH diminishing by equivalent percentages at pH 6.5 (Figure 3.14 (a)), 6.0 (Figure 3.14 (b)) and 5.0 (Figure 3.14 (d)) at the lowest investigated concentration 256 $\mu\text{g.mL}^{-1}$. The wild type strain demonstrated almost the exact same relationship

between bacterial survival and human lysozyme concentration as the strain did at pH 6.0 (Figure 3.14 (b)) except with an initial 6% increase in survival at the lowest enzyme concentration of 96.7%. The Δ NamH strain was more sensitive to initial lysozyme concentrations demonstrating 77% total survival at 256 $\mu\text{g.mL}^{-1}$. This percentage survival was 10% reduced from equivalent values at pH 6.5 and 6.0. The knockout strain exhibited 59% total bacterial survival at 1024 $\mu\text{g.mL}^{-1}$ compared to 78% and 74% from the previous pH 6.5 (Figure 3.14 (a)) and pH 6.0 (Figure 3.14 (b)) conditions.

The more pronounced deviation between the bacterial survival percentages of two strains at pH 5.5 than was observed during the two previously investigated pH conditions, did not continue with the final investigated concentration 16384 $\mu\text{g.mL}^{-1}$. The variation between growth inhibition of each strain at pH 5.5 at the highest lysozyme concentration was equivalent to totals shown at pH 6.0 (Figure 3.14 (b)), with 62% survival for wild type and 34% for Δ NamH. The equivalent total survival at 16384 $\mu\text{g.mL}^{-1}$ for both strains at pH 6.0 (Figure 3.14 (b)) and pH 5.5 (Figure 3.14 (c)) indicate that enzyme activity may not alter between these two conditions and cell tolerance towards pH may be the reason for the greater variation observed at lower concentrations.

All bacterial survival percentages for *M. smegmatis* Δ NamH compared to the wild type were measured to be statistically significant (Table 3.6). P-values for each concentration were 256 $\mu\text{g.mL}^{-1}$ (<0.01), 1024 $\mu\text{g.mL}^{-1}$ (<0.0005), 4096 $\mu\text{g.mL}^{-1}$ (<0.005), 8192 $\mu\text{g.mL}^{-1}$ (<0.0005) and 16384 $\mu\text{g.mL}^{-1}$ (<0.0005).

Lysozyme concentration ($\mu\text{g.mL}^{-1}$)	Wild type % (1) Survival (mean \pm SD, n=3)	Δ NamH % (2) Survival (mean \pm SD, n=3)	Significance student's t-test (2) v (1)
0.00	100.00 \pm 5.23	100.00 \pm 6.21	N/A
256	91.58 \pm 5.73	92.68 \pm 6.54	p >0.05
1024	85.12 \pm 4.90	74.12 \pm 5.50	p >0.05
4096	79.23 \pm 3.61	58.08 \pm 3.51	p <0.005
8192	77.97 \pm 3.63	43.60 \pm 6.83	p <0.005
16384	67.24 \pm 6.83	32.77 \pm 1.70	p <0.001

Table 3.7 Average bacterial survival by *M. smegmatis* wild type and Δ NamH strains against human lysozyme at pH 5.0. Results depicted in a graph in Figure 3.14 (d). Standard deviation is of triplicate measurements. Statistically significant results were indicated by p-values <0.05.

The results obtained in Table 3.7 of the final and lowest pH condition, pH 5.0 (Figure 3.14 (d)) correlated strongly with the findings of human lysozyme activity at pH 6.0 (Figure 3.14 (b)). Both wild type and NamH deficient strains were equally susceptible to the lowest initial lysozyme concentration of 256 $\mu\text{g.mL}^{-1}$, where CFU survival was 91.5% and 92.6% respectively compared to the lysozyme absent controls. Subsequent increases in lysozyme concentration led to an observable divergence between the two strains. As noted previously the wild type strain was more resilient to lysozyme with measurable bacterial survival diminishing gradually, to a final count 32% less than the control at the highest concentration 16384 $\mu\text{g.mL}^{-1}$. The Δ NamH strain survival decreased steadily by almost 15% with each increasing concentration, concluding with a final colony total 67% less than the control at 16384 $\mu\text{g.mL}^{-1}$.

The statistical significance of the pH 5.0 data (Table 3.7) also matched results obtained at pH 6.0. Concentrations 256 $\mu\text{g.mL}^{-1}$ and 1024 $\mu\text{g.mL}^{-1}$ were deemed statistically insignificant with p-values >0.05. The three highest concentrations were deemed statistically significant with p-values <0.005 (4096 $\mu\text{g.mL}^{-1}$), <0.005 (8192 $\mu\text{g.mL}^{-1}$) and <0.005 (16384 $\mu\text{g.mL}^{-1}$).

3.6.1.3 Impact of extended incubation on the sensitivity of *M. smegmatis* towards human lysozyme

The other aspect of the protocol published by Eric Brown's group, detailing methods to investigate mycobacterial susceptibility towards lytic enzymes is the effect of incubation time at a set pH (Koo, *et al.* 2008). To evaluate the impact of prolonged exposure to lysozyme, pH 5.0 was selected as this resembled the intra-phagolysosomal within infected macrophages (Flannagan, *et al.* 2009). The three separate incubation periods chosen were, 1.5 hours (Figure 3.15 (a)), 3 hours (Figure 3.15 (b)) and 4.5 hours (Figure 3.15 (c)) using the same human lysozyme concentrations as mentioned previously.

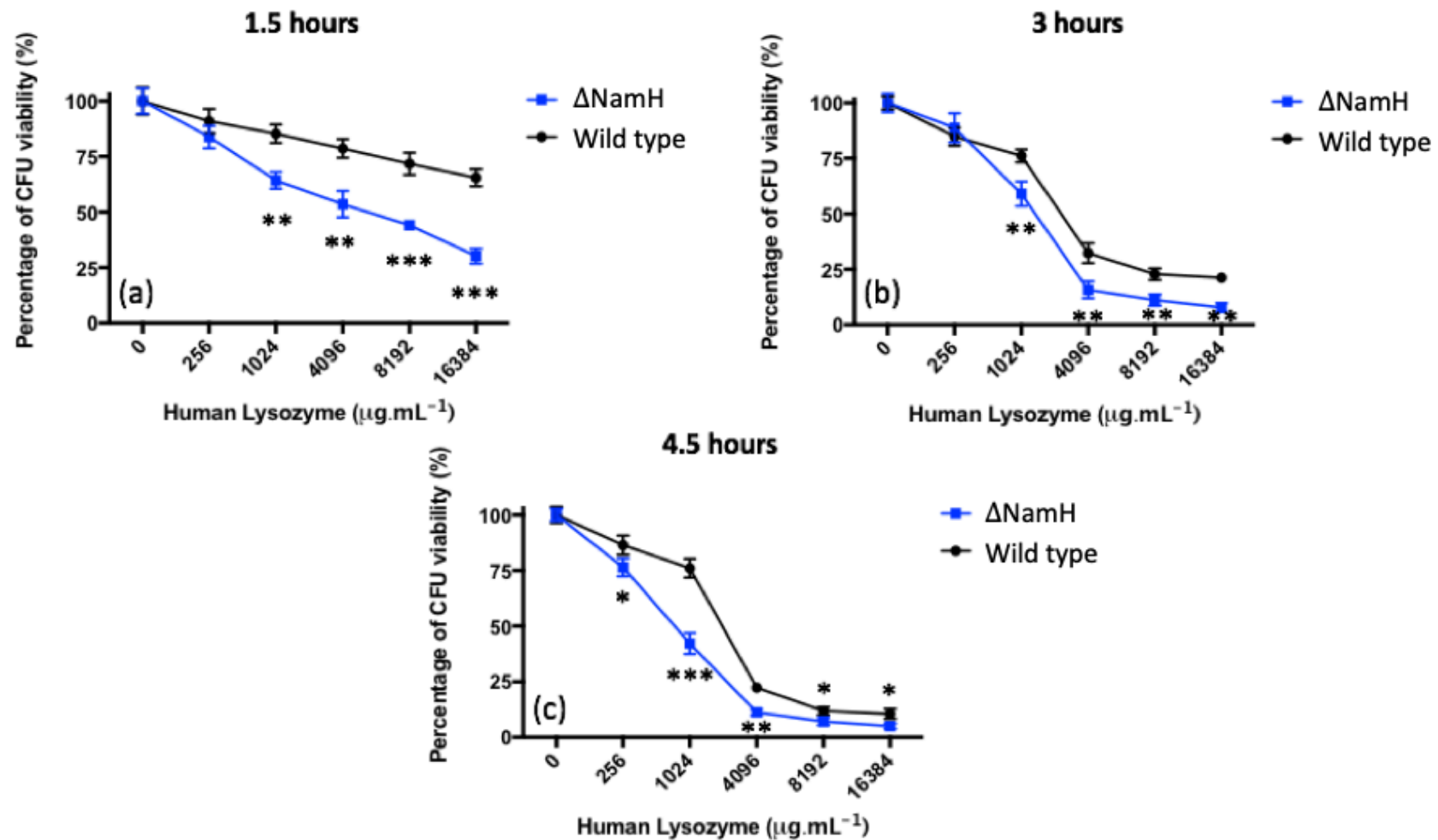


Figure 3.15 Effect of duration of exposure of *M. smegmatis* to human lysozyme at pH 5.0. *M. smegmatis* wild type (Black) and ΔNamH (Blue) cells were incubated with 0, 256, 1024, 4096, 8192 and 16384 $\mu\text{g.mL}^{-1}$ of human lysozyme in 100 μL HBSS at pH 5.0 in a 96 well microtiter plate. Microtiter plates were incubated for (a) 1.5 hours, (b) 3 hours and (c) 4.5 hours. After incubation at 37°C bacterial survival was determined. Wells were pipetted on TSB agar plates and incubated at 37°C for 72 hours. Colony forming units were counted and averaged from triplicate plates. Error bars represent standard deviation of triplicate measurements. Statistically significant results are indicated with * = p-value <0.05, ** = <0.01, *** = <0.001 and **** = <0.0001. Result: Extended incubation led to decreased bacterial survival above 4096 $\mu\text{g.mL}^{-1}$, variation between strains was not exacerbated.

Lysozyme concentration ($\mu\text{g.mL}^{-1}$)	Wild type % (1) Survival (mean \pm SD, n=3)	Δ NamH % (2) Survival (mean \pm SD, n=3)	Significance student's t-test (2) v (1)
0.00	100.00 \pm 6.11	100.00 \pm 5.75	N/A
256	90.96 \pm 5.48	83.80 \pm 5.07	p >0.05
1024	85.28 \pm 4.16	64.27 \pm 3.75	p <0.005
4096	78.65 \pm 4.19	53.58 \pm 5.97	p <0.005
8192	71.73 \pm 5.02	44.16 \pm 1.55	p <0.001
16384	65.48 \pm 3.87	30.22 \pm 3.34	p <0.0005

Table 3.8 Average bacterial survival by *M. smegmatis* wild type and Δ NamH strains against human lysozyme at pH 5.0 incubated for 1.5 hours. Results depicted in a graph in Figure 3.15 (a). Standard deviation of triplicate measurements. Statistically significant results were indicated by p-values <0.05.

The standard incubation time of 1.5 hours (Figure 3.15 (a)) showed similar results to previous incubation data at pH 5.0 in Figure 3.14 (d) with a steady decline in survival as reported by CFU as the lysozyme concentration increased across both strains. As previously seen, the wild type survival percentages were higher than those seen in the NamH deficient strain (Table 3.8). The reduction in survival of *M. smegmatis* was steady with each concentration of human lysozyme leading to a drop of between 10-15% for both strains as concentration increased, culminating in final bacterial survival percentages of 65% for the wild type and 30% for Δ NamH strains.

A student's t-test comparison (Table 3.8) between wild type and Δ NamH indicated that all data points except for 256 were statistically significant with p-values for the Δ NamH data set >0.05 (256 $\mu\text{g.mL}^{-1}$), <0.005 (1024 $\mu\text{g.mL}^{-1}$), <0.005 (4096 $\mu\text{g.mL}^{-1}$), <0.001 (8192 $\mu\text{g.mL}^{-1}$) and <0.0005 (16384 $\mu\text{g.mL}^{-1}$) compared to the wild type strain.

Lysozyme concentration ($\mu\text{g.mL}^{-1}$)	Wild type % (1) Survival (mean \pm SD, n=3)	ΔNamH % (2) Survival (mean \pm SD, n=3)	Significance student's t-test (2) v (1)
0.00	100.00 \pm 2.98	100.00 \pm 4.13	N/A
256	84.82 \pm 4.06	88.78 \pm 6.50	p >0.1
1024	76.15 \pm 2.86	59.03 \pm 5.52	p <0.01
4096	32.33 \pm 4.48	15.84 \pm 3.78	p <0.01
8192	22.85 \pm 2.57	11.20 \pm 2.58	p <0.01
16384	21.22 \pm 2.25	7.87 \pm 1.98	p <0.005

Table 3.9 Average bacterial survival by *M. smegmatis* wild type and ΔNamH strains against human lysozyme at pH 5.0 incubated for 3 hours. Results depicted in a graph in Figure 3.15 (b). Standard deviation of triplicate measurements. Statistically significant results were indicated by p-values <0.05.

Doubling the incubation period to 3 hours (Figure 3.15 (b)) in the presence of human lysozyme was observed to have smallest effect on survival of either strain at the lowest concentration of lysozyme, 256 $\mu\text{g.mL}^{-1}$ with both wild type and ΔNamH strains of *M. smegmatis* being within 5% (Table 3.9) of the previous percentage survival after lysozyme exposure for 1.5 hours (Figure 3.15 (a)). The wild type strain after 3 hour incubation with 256 $\mu\text{g.mL}^{-1}$ produced 5% fewer colonies and the ΔNamH strain produced 5% more colonies than the equivalent result after 1.5 hours (Figure 3.15 (a)). At 1024 $\mu\text{g.mL}^{-1}$ human lysozyme, the ΔNamH strain colony percentage decreased by 29%, though this result is 5% less than the equivalent result at 1.5 hours. The wild type survival after 3 hours decreased by 8% at the same concentration, 9% less than the equivalent result after 1.5 hours. In the presence of 4096 $\mu\text{g.mL}^{-1}$ lysozyme, the survival of the wild type and the knockout were 32% and 15% respectively after 3 hours of incubation (Figure 3.15 (b)), compared to 78% and 53% respectively after 1.5 hours of incubation (Figure 3.15 (a)).

The dramatic decrease in survival did not continue as the concentrations of lysozyme doubled. Exposure to 8192 $\mu\text{g.mL}^{-1}$ lysozyme led to the survival of wild type strain further decreasing in survival percentage by 10%, leading to a 22% total survival compared to the 0 $\mu\text{g.mL}^{-1}$ control. Survival of the ΔNamH strain diminished only by a further 4% after treatment with 8192 $\mu\text{g.mL}^{-1}$ lysozyme to a total of 11% CFU present relative to that in the absence of lysozyme. Doubling the concentration of human lysozyme to 16384 $\mu\text{g.mL}^{-1}$ did not significantly alter the survival

percentage of either strain compared to that observed at 8192 $\mu\text{g.mL}^{-1}$ lysozyme, where wild type and NamH strain survival percentage decreased only by a further 1%, to 21% final CFU and 4% final CFU respectively. The final percentage results for both strains are both less than a third of the equivalent results after a 1.5 hour incubation (Figure 3.15 (a)).

The ΔNamH 3-hour incubation data set mirrors the statistical significance of the 1.5-hour incubation with all except the initial 256 $\mu\text{g.mL}^{-1}$ human lysozyme concentration achieving statistical significance (Table 3.9) compared to the wild type. P-values for the data set include >0.05 (256 $\mu\text{g.mL}^{-1}$), <0.01 (1024 $\mu\text{g.mL}^{-1}$), <0.01 (4096 $\mu\text{g.mL}^{-1}$), <0.01 (8192 $\mu\text{g.mL}^{-1}$) and <0.005 (16384 $\mu\text{g.mL}^{-1}$).

Lysozyme concentration ($\mu\text{g.mL}^{-1}$)	Wild type % (1) Survival (mean \pm SD, n=3)	ΔNamH % (2) Survival (mean \pm SD, n=3)	Significance student's t-test (2) v (1)
0.00	100.00 \pm 3.62	100.00 \pm 2.78	N/A
256	86.44 \pm 4.33	76.46 \pm 4.00	p <0.05
1024	76.03 \pm 4.21	42.12 \pm 4.67	p <0.001
4096	22.31 \pm 1.54	11.23 \pm 1.46	p <0.005
8192	11.90 \pm 1.78	7.16 \pm 1.74	p <0.05
16384	10.57 \pm 2.23	5.04 \pm 1.15	p <0.05

Table 3.10 Average bacterial survival by *M. smegmatis* wild type and ΔNamH strains against human lysozyme at pH 5.0 incubated for 4.5 hours. Results depicted in a graph in Figure 3.15 (c). Standard deviation of triplicate measurements. Statistically significant results were indicated by p-values <0.05 .

The final duration of exposure for wild type and ΔNamH strains of *M. smegmatis* to increasing human lysozyme concentration was extended to 4.5 hours (Figure 3.15 (c)). The survival of the wild type strain was identical to the 3 hour exposure to 256 and 1024 $\mu\text{g.mL}^{-1}$ lysozyme (86% at 256 $\mu\text{g.mL}^{-1}$ and 76% at 1024 $\mu\text{g.mL}^{-1}$ lysozyme respectively) (Figure 3.15 (b)). The data depicted in table 3.10 indicates that at the two lowest concentrations evaluated there was little effect on increasing the incubation time from 3 to 4.5 hours for the wild type strain. Reminiscent of the data obtained on three hour exposure to human lysozyme, exposure of wild type *M. smegmatis* to 4096

$\mu\text{g.mL}^{-1}$ lysozyme lead to a significant drop in survival to 22 % of the original control colony population. Matching the data obtained after 3 hour incubation, doubling the concentration of lysozyme to $8192 \mu\text{g.mL}^{-1}$ reduced the survival of the wild type strain by 10%, and doubling the concentration again to $16384 \mu\text{g.mL}^{-1}$ lysozyme reduced its survival by only 1%, culminating in a final percentage survival of 10%. The final three highest concentrations $4096 \mu\text{g.mL}^{-1}$, $8192 \mu\text{g.mL}^{-1}$ and $16384 \mu\text{g.mL}^{-1}$ lysozyme impacted the wild type in a similar manner after 3 hour and 4.5 hours with the only notable difference being the halving in percentage survival of these lysozyme concentrations obtained after 4.5 hours.

The ΔNamH strain on the other hand showed greater initial susceptibility at 4.5 hours (Figure 3.15 (c)) than during the three hour exposure to lysozyme (Figure 3.15 (b)). At $256 \mu\text{g.mL}^{-1}$ lysozyme reduced survival of the ΔNamH strain by 24% compared to the control, which was 12 % greater than the survival after a 3 hour incubation. Increasing the lysozyme concentration to $1024 \mu\text{g.mL}^{-1}$ reduced survival by 57.88% indicating that while the wild type strain was more resilient even over longer periods such as 3 and 4.5 hours exposed to lower lysozyme concentrations, 256 and $1024 \mu\text{g.mL}^{-1}$ the knockout was more susceptible after an extended period. The 50% increase in incubation time to 4.5 hours did not impact ΔNamH survival at the highest three concentrations. As seen previously a significant drop in colonies occurred during incubation with $4096 \mu\text{g.mL}^{-1}$ lysozyme by 84%, relative to the survival percentages plateauing at $8192 \mu\text{g.mL}^{-1}$ (7%) and $16384 \mu\text{g.mL}^{-1}$ lysozyme (5%). The percentage survival at the three highest lysozyme concentrations only deviated by 2-4% at 4.5 hours compared to their corresponding 3 hour values.

The 4.5 hours data sets from both *M. smegmatis* strains were deemed to be entirely statistically significant from one another in the presence of human lysozyme (Table 3.10). P-values for the ΔNamH data set were <0.05 ($256 \mu\text{g.mL}^{-1}$), <0.001 ($1024 \mu\text{g.mL}^{-1}$), <0.005 ($4096 \mu\text{g.mL}^{-1}$), <0.05 ($8192 \mu\text{g.mL}^{-1}$) and <0.05 ($16384 \mu\text{g.mL}^{-1}$).

The data sets from Figure 3.15 for each individual strain were compiled and analysed, to compare the wild type (Figure 3.16) and ΔNamH (Figure 3.17) strains resilience with respect to increasing lysozyme concentrations at pH 5.0 at 1.5, 3 and 4.5 hour exposure to the enzyme.

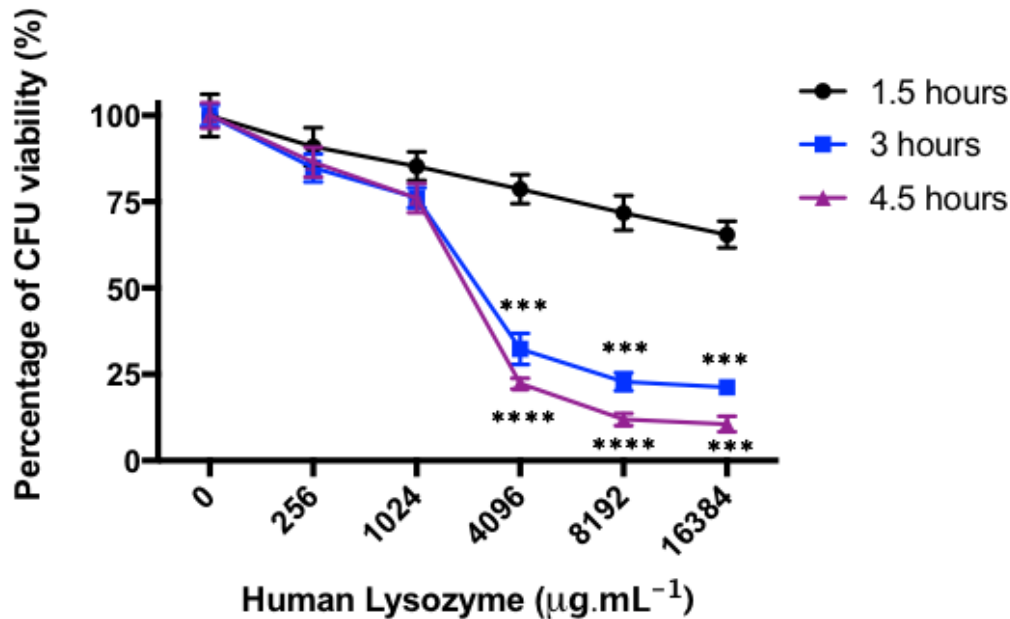


Figure 3.16 Compilation of the effect of various durations of exposure to increasing lysozyme concentrations on the survival of *M. smegmatis* wild type at pH 5.0. *M. smegmatis* wild type cells were incubated with 0, 256, 1024, 4096, 8192 and 16384 µg.mL⁻¹ of human lysozyme in 100 µL HBSS at pH 5.0 in a 96 well microtiter plate. After 1.5 (Black), 3 (Blue) and 4.5 (Purple) hours incubation at 37°C bacterial survival was determined. Wells were pipetted on TSB agar plates and incubated at 37°C for 72 hours. Colony forming units were counted and averaged from triplicate plates. Error bars represent standard deviation of triplicate measurements. Averages at each concentration were compared to the relevant 1.5, 3 or 4.5 hour control at 0 µg.mL⁻¹ lysozyme as a percentage. Statistically significant results are indicated with * = p-value <0.05, ** = <0.01, *** = <0.001 and **** = <0.0001. Result: Increasing incubation period for wild type strain does not greatly impact at lysozyme concentrations below 1024 µg.mL⁻¹ but greatly impact at higher concentrations. Little difference between 3 hour and 4.5 hour incubations.

Wild type *M. smegmatis* was resilient to lysozyme treatment regardless of the incubation time at the lowest two enzyme concentrations tested (Figure 3.16: 256 µg.mL⁻¹ and 1024 µg.mL⁻¹), indicating tolerance to the activity of lysozyme for extended periods under these conditions. Only once the lysozyme concentration exceeded 1024 µg.mL⁻¹ did the period for which the organism was exposed to lysozyme become significant. At 1.5 hours (Figure 3.16: Black) the relationship between lysozyme concentration and survival was essentially a linear gradual decline. However, during incubations extended to 3 (Figure 3.16: Blue) and 4.5 (Figure 3.16: Purple) hours, where the concentrations of human lysozyme the wild type strain was exposed to exceeded 1024 µg.mL⁻¹, there was a dramatic reduction in bacterial survival. As previously mentioned after both 3 and 4.5 hour incubations with 4096 µg.mL⁻¹ the colony count for both strains significantly reduced by over 65% and 78% respectively. The lysozyme activity plateaued after 4096 µg.mL⁻¹, but survival was never fully prevented even at the highest lysozyme concentration of 16384 µg.mL⁻¹ survival

remained at 21% after 3 hours and 10% after 4.5 hours. Little variation was obtained by increasing incubation from 3 to 4.5 hours for the wild type strain.

The statistical significance of the three incubation periods on wild type survival against human lysozyme concentrations was investigated. The 3 and 4.5 hour survival percentages were compared against those obtained during a 1.5-hour incubation. The survival measured during 3 and 4.5 hour incubations against 256 and 1024 $\mu\text{g.mL}^{-1}$ were deemed non statistically significant with p-values >0.05 . All three subsequent human lysozyme concentrations for both extended incubations were deemed statistically significant. P-values for the 3-hour incubation were <0.001 (4096 $\mu\text{g.mL}^{-1}$), <0.001 (8192 $\mu\text{g.mL}^{-1}$) and <0.001 (16384 $\mu\text{g.mL}^{-1}$). The 4.5-hour incubation produced p-values of <0.0001 (4096 $\mu\text{g.mL}^{-1}$), <0.0001 (8192 $\mu\text{g.mL}^{-1}$) <0.0005 (16384 $\mu\text{g.mL}^{-1}$).

The combined incubation results for the ΔNamH strain are shown in Figure 3.17.

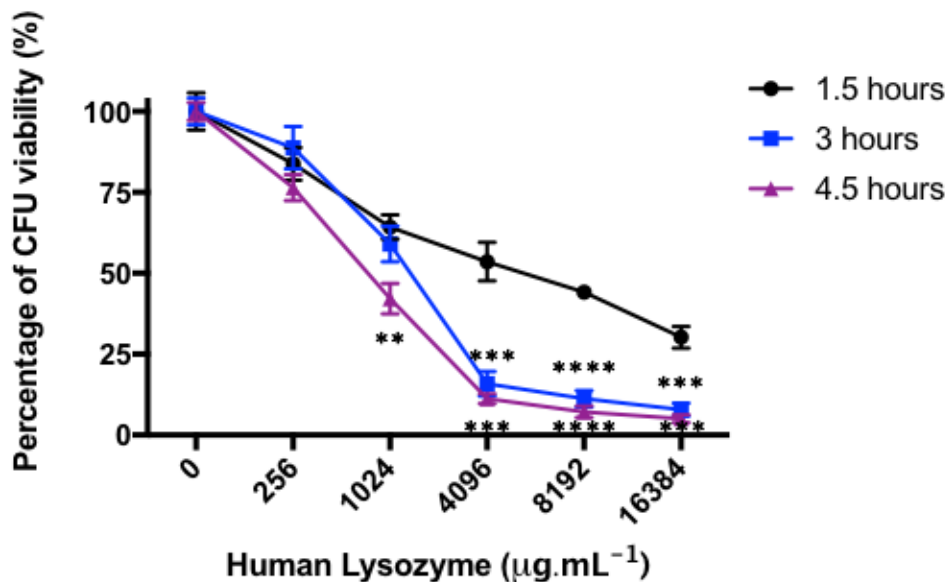


Figure 3.17 Compilation of the effect of various durations of exposure to increasing lysozyme concentrations on the survival of *M. smegmatis* ΔNamH at pH 5.0. *M. smegmatis* ΔNamH cells were incubated with 0, 256, 1024, 4096, 8192 and 16384 $\mu\text{g.mL}^{-1}$ of human lysozyme in 100 μL HBSS at pH 5.0 in a 96 well microtiter plate. After 1.5 (Black), 3 (Blue) and 4.5 (Purple) hours incubation at 37°C bacterial survival was determined. Wells were pipetted on TSB agar plates and incubated at 37°C for 72 hours. Colony forming units were counted and averaged from triplicate plates. Error bars represent standard deviation of triplicate measurements. Averages at each concentration were compared to the relevant 1.5, 3 or 4.5 hour control at 0 $\mu\text{g.mL}^{-1}$ lysozyme as a percentage. Statistically significant results are indicated with * = p-value <0.05 , ** = <0.01 , *** = <0.001 and **** = <0.0001 . Result: Increasing incubation period for wild type strain does not greatly impact low concentrations but greatly impact high concentrations. Little difference between 3 hour and 4.5 hour incubations.

Comparing the data sets from only the Δ NamH strain (Figure 3.17), shows that the percentage survival of the strain is equal after both 1.5 (Figure 3.17: Black) and 3 hour (Figure 3.17: Blue) incubations against 256 $\mu\text{g.mL}^{-1}$ and 1024 $\mu\text{g.mL}^{-1}$ lysozyme, whereas extending the incubation to 4.5 hours (Figure 3.17: Purple) reduces the initial survival by 12% and 17% at these lysozyme concentrations respectively. Similarly, as with the wild type (Figure 3.16) after a 1.5 hour incubation the increase in lysozyme concentration lead to a gradual decrease in survival, whereas 3 and 4.5 hour incubations decrease rapidly once exposed to greater than 4096 $\mu\text{g.mL}^{-1}$. The variation between the two longest incubation periods is minimal after 4096 $\mu\text{g.mL}^{-1}$, with each plateauing in a similar manner to the wild type.

The statistical significance of the Δ NamH strain survival at various incubation time frames were analysed with a student's t-test. The 3 and 4.5 hour incubation periods were compared to those obtained during the 1.5 hour incubation in a similar manner to the wild type strain. Each of the two lowest human lysozyme concentrations 256 and 1024 $\mu\text{g.mL}^{-1}$ were deemed statistically insignificant (p -value >0.05) after extending the incubation to 3 hours and the three highest lysozyme concentrations were deemed statistically significant with p -values <0.001 (4096 $\mu\text{g.mL}^{-1}$), <0.0001 (8192 $\mu\text{g.mL}^{-1}$) <0.001 (16384 $\mu\text{g.mL}^{-1}$). Incubation for 4.5-hours produced a greater initial divergence in survival, relative to survival of Δ NamH cells incubated for 1.5 hours at all lysozyme concentrations except 256 $\mu\text{g.mL}^{-1}$. P -values for the 4.5-hour incubation were <0.05 (256 $\mu\text{g.mL}^{-1}$), <0.005 (1024 $\mu\text{g.mL}^{-1}$), <0.0005 (4096 $\mu\text{g.mL}^{-1}$), <0.0001 (8192 $\mu\text{g.mL}^{-1}$) and <0.0005 (16384 $\mu\text{g.mL}^{-1}$).

3.7 *M. smegmatis* sensitivity towards β -hexosaminidase

The second hydrolytic enzyme released by the phagolysosome to be investigated in this chapter was β -hexosaminidase (Section 1.4.1.2.2). This enzyme is produced by both prokaryotes and eukaryotes (Hossain and Roslan 2014) and the impact of hexosaminidases from both kingdoms was investigated on *M. smegmatis*.

3.7.1 *M. smegmatis* sensitivity towards *Streptomyces plicatus* β -hexosaminidase

Initial experiments were conducted with *S. plicatus* β -hexosaminidase recombinantly expressed in *E. coli*. (Source NEB). The stock concentration of the enzyme was related to its activity in Units.mL⁻¹, where one unit was defined as the amount sufficient to cleave 95% of the terminal β -D-*N*-acetyl-galactosamine from 1 nmol of GalNAc β 1-4Gal β 1-4Glc-7-amino-4-methyl-coumarin in 1 hour at 37°C in a total reaction volume of 10 μ L. Knowledge of the activity of the *S. plicatus* β -hexosaminidase allowed the impact of known amounts of enzyme activity on *M. smegmatis* growth. Both *M. smegmatis* wild type and Δ NamH strains growth under standard aerobic conditions at pH 6.8 were measured in the presence of increasing concentrations of *S. plicatus* β -hexosaminidase activity to observe enzymatic impact on cellular growth (Figure 3.18).

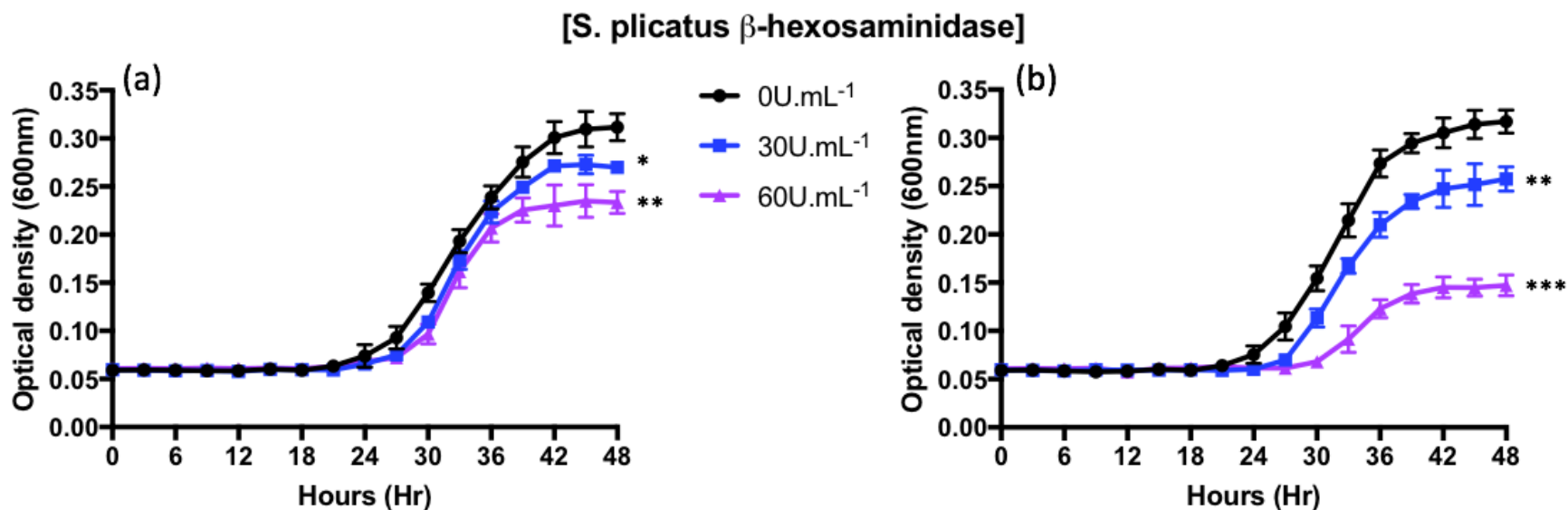


Figure 3.18 The hydrolytic activity of *S. plicatus* β -hexosaminidase against the mycobacterial modifications of peptidoglycan. Wild type (a) and Δ NamH (b) *M. smegmatis* MIC growth curves against *S. plicatus* β -hexosaminidase. Cells were grown in 96-well microtiter plates in triplicate at 37°C with intermittent shaking. Absorbance was measured at OD_{600nm} at 3 hour intervals for 45 hours. Each well contained 100 μ L culture media (7H9, ADC, 0.05% (w/v) Tween 80) with increasing concentrations of *S. plicatus* β -hexosaminidase. The cultured *M. smegmatis* wild type (a) and Δ NamH (b) strain was standardized to an OD_{600nm} of 1 and diluted further by a factor of 10⁴ prior to addition of enzyme and incubation. Error bars represent standard deviation of triplicate measurements. *Streptomyces plicatus* β -hexosaminidase concentrations: 0 Units.mL⁻¹ (Blue), 30 Units.mL⁻¹ (Black), 60 Units.mL⁻¹ (Red). Statistically significant results are indicated with * = p-value <0.05, ** = <0.01, *** = <0.001 and **** = <0.0001. Results: Δ NamH strain displays greater susceptibility to *S. plicatus* β -hexosaminidase than Wild type.

<i>S. plicatus</i> β-hexosaminidase (Units.mL ⁻¹)	Wild type <i>M. smegmatis</i>					ΔNamH <i>M. smegmatis</i>					(b) vs (a) p-values
	Apparent Lag phase (h)	Td (h ⁻¹)	AUC (%)	Stationary Phase OD _{600nm}	Wild type p- values (a)	Apparent Lag phase (h)	Td (h ⁻¹)	AUC (%)	Stationary Phase OD _{600nm}	ΔNamH p- values (b)	
0.00	21	5.88	-	0.31	-	21	6.19	-	0.31	-	>0.05
30	24	5.60	83.66	0.27	<0.05	24	5.88	70.01	0.25	<0.01	<0.05
60	27	5.58	71.74	0.23	<0.01	27	7.60	28.97	0.15	<0.001	<0.01

Table 3.11 Statistical comparisons of *M. smegmatis* growth curves in the presence of increasing concentrations of *S. plicatus* β-hexosaminidase. Wild type and ΔNamH strains incubated for 60 hours at 37°C with selected concentrations of *S. plicatus* β-hexosaminidase produced growth curves measured at OD_{600nm} in Figure 3.18. Variations between growth curves were measured by time taken to exit apparent lag phase (hours), the doubling time (Td) of cells during exponential phase (hours⁻¹), the area under the curve (AUC) percentage compared to the 0 μg.mL⁻¹ control (%), the OD_{600nm} value achieved during stationary phase and whether the growth curve variations were statistically significant compared to each 0 μg.mL⁻¹ control with p-values <0.05 deemed significant. The statistical significance of ΔNamH (b) growth curves compared to wild type (a) at equivalent *S. plicatus* β-hexosaminidase concentrations were determined by p-values <0.05.

The growth phenotypes produced by *M. smegmatis* wild type (Figure 3.18 (a): Black) and Δ NamH (Figure 3.18 (b): Black) strains in the absence of *S. plicatus* β -hexosaminidase match those observed previously in the rest of the chapter. Both strains produced visible signs of growth, exiting apparent lag phase after 21 hours, the Td measured during exponential phase was 5.88 hours for the wild type and 6.19 hours for the Δ NamH. Stationary phase was reached after 42 hours at an OD_{600nm} of 0.3.

The 30 and 60 Units.mL⁻¹ concentrations of Streptomyces β -hexosaminidase employed in this experiment equated to addition of 3 μ g.mL⁻¹ and 6 μ g.mL⁻¹ β -hexosaminidase protein respectively. The addition of 30 Units.mL⁻¹ of Streptomyces β -hexosaminidase to the wild type strain (Figure 3.18 (a): Blue) altered apparent lag phase relative to the 0 Units.mL⁻¹ control by 3 hours to 24 hours. The 30 Units.mL⁻¹ result produced a slight decrease in Td between 27 and 36 hours to 5.60 hours with the addition of β -hexosaminidase. The AUC of *M. smegmatis* wild type growth curves in the presence of 30 Units.mL⁻¹ β -hexosaminidase was reduced to 83.66% and although the curve similarly plateaued after 42 hours, the OD_{600nm} reached by stationary phase was 90% of the control. Increasing the β -hexosaminidase concentration to 60 Units.mL⁻¹ (Figure 3.18 (a): Purple) extended the apparent lag phase by 6 hours to 27 hours. This data set was characterized by a similar Td to the control of 5.58 hours at 60 Units.mL⁻¹ treated, though its AUC total was 71.74% of the 0 Units.mL⁻¹ control. The wild type strain entered stationary phase at a 22% lower optical density relative to when incubated in the absence of β -hexosaminidase. Both of the two β -hexosaminidase concentration data sets were identified as statistically significant (Table 3.11) when compared against the 0 Units.mL⁻¹ wild type control with p-values of <0.05 (30 Units.mL⁻¹) and <0.01 (60 Units.mL⁻¹) respectively.

The *M. smegmatis* Δ NamH strain displayed an increase in susceptibility towards β -hexosaminidase (Figure 3.18 (b)). The addition of β -hexosaminidase altered the apparent lag phase of the knockout strain at 30 Units.mL⁻¹ by 3 hours to 24 hours (Figure 3.18 (b): Blue), and at 60 Units.mL⁻¹ (Figure 3.18 (b): Purple) by 6 hours to 27 hours. The Td of this strain in the presence of 30 Units.mL⁻¹ β -hexosaminidase was 5.88 hours, equivalent to the Td of the 0 Units.mL⁻¹ control (Figure 3.18 (b): Black). The Td of the strain incubated with 60 Units.mL⁻¹ β -

hexosaminidase was increased to 7.60 hours. The stationary phase maximum optical density obtained by the Δ NamH control after 42 hours was decreased by 17% with the addition of 30 Units.mL⁻¹ β -hexosaminidase and by 52% with 60 Units.mL⁻¹ relative to the 0 Units.mL⁻¹ control. The AUC for the Δ NamH strain in the presence of 30 Units.mL⁻¹ β -hexosaminidase was 70.01% of that of the 0 Units.mL⁻¹ control. The Δ NamH strain incubated with 60 Units.mL⁻¹ β -hexosaminidase produced an AUC of 28.97% of the 0 Units.mL⁻¹ control. These AUC values were reduced by 13.65% and 42.77% respectively, compared to the wild type strain. The growth curves produced by the Δ NamH strain in the presence of *S. plicatus* β -hexosaminidase were analysed by a student's t-test (Table 3.11) to determine statistical significance compared to the 0 Units.mL⁻¹ control. Both concentrations produced statistically significant inhibition to Δ NamH growth curves with p-values of <0.01 (30 Units.mL⁻¹) and <0.001 (60 Units.mL⁻¹) respectively.

Comparisons between the two *M. smegmatis* strains at equivalent β -hexosaminidase concentrations were also analysed and both of the variations depicted from growth curves at 30 (<0.05) and 60 (<0.01) Units.mL⁻¹ were deemed statistically significant between each strain.

3.7.2 *M. smegmatis* sensitivity towards human β -hexosaminidase

The human equivalent of β -hexosaminidase shares only 25% sequence similarity to the *S. plicatus* version (www.ncbi.nih.gov/BLAST). According to Koo *et al.* (2008) the minimum concentration of human β -hexosaminidase required to achieve a significant decrease in survival was only 4 Units.mL⁻¹. The impact of between 0.5 to 4 Units.mL⁻¹ of human β -hexosaminidase on the growth of *M. smegmatis* wild type and Δ NamH strains was evaluated (Figure 3.19).

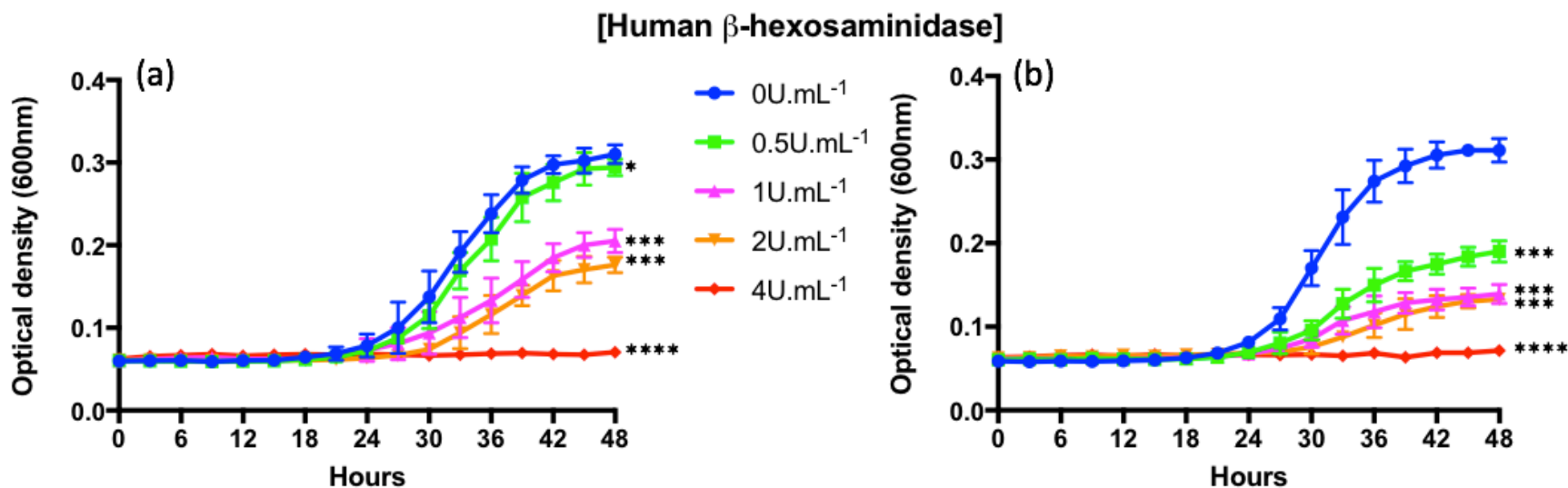


Figure 3.19 The hydrolytic activity of human β -hexosaminidase against the mycobacterial modifications of peptidoglycan. Wild type (a) and Δ NamH (b) *M. smegmatis* MIC growth curves against human β -hexosaminidase. Cells were grown in 96-well microtiter plates in triplicate at 37°C with intermittent shaking, absorbance was measured at OD_{600nm} at 3 hour intervals for 48 hours. Each well contained 100 μ L culture media (7H9, ADC, 0.05% (w/v) Tween 80) with increasing concentrations of human β -hexosaminidase. The cultured *M. smegmatis* wild type (a) and Δ NamH (b) strains were standardized to an OD_{600nm} of 1 and diluted further by a factor of 10⁴ prior to addition of enzyme and incubation. Error bars represent standard deviation of triplicate measurements. Human β -hexosaminidase concentrations: 0 Units.mL⁻¹ (Blue), 0.5 Units.mL⁻¹ (Green), 1 Units.mL⁻¹ (Pink), 2 Units.mL⁻¹ (Orange), 4 Units.mL⁻¹ (Red). Statistically significant results are indicated with * = p-value <0.05, ** = <0.01, *** = <0.001 and **** = <0.0001. Results: Δ NamH displays greater susceptibility to human β -hexosaminidase than wild type at each concentration. MIC results: Wild type 4 Units.mL⁻¹, Δ NamH 4 Units.mL⁻¹.

Human β -hexosaminidase (Units.mL ⁻¹)	Wild type <i>M. smegmatis</i>					Δ NamH <i>M. smegmatis</i>					(b) vs (a) p-values
	Apparent Lag phase (h)	Td (h ⁻¹)	AUC (%)	Stationary Phase OD _{600nm}	Wild type p-values (a)	Apparent Lag phase (h)	Td (h ⁻¹)	AUC (%)	Stationary Phase OD _{600nm}	Δ NamH p-values (b)	
0	21	6.93	-	0.31	-	21	6.41	-	0.31	-	>0.05
0.5	24	7.35	87.21	0.30	<0.05	24	10.37	45.02	0.19	<0.001	<0.001
1	24	11.90	50.92	0.20	<0.001	24	13.45	29.59	0.14	<0.001	<0.05
2	27	11.36	36.73	0.17	<0.001	27	14.96	25.73	0.13	<0.001	<0.05
4	60	0.00	0.00	0.05	<0.0001	60	0.00	0.00	0.05	<0.0001	-

Table 3.12 Statistical comparisons of *M. smegmatis* growth curves in the presence of increasing concentrations of human β -hexosaminidase. Wild type and Δ NamH strains incubated for 60 hours at 37°C with selected concentrations of human β -hexosaminidase produced growth curves measured at OD_{600nm} in Figure 3.19. Variations between growth curves were measured by time taken to exit apparent lag phase (hours), the doubling time (Td) of cells during exponential phase (hours⁻¹), the area under the curve (AUC) percentage compared to the 0 μ g.mL⁻¹ control (%), the OD_{600nm} value achieved during stationary phase and whether the growth curve variations were statistically significant compared to each 0 μ g.mL⁻¹ control with p-values <0.05 deemed significant. The statistical significance of Δ NamH (b) growth curves compared to wild type (a) at equivalent human β -hexosaminidase concentrations were determined by p-values <0.05.

The human β -hexosaminidase concentration range identified by Koo, *et al.* (2008) was appropriate for evaluation of the MIC of human β -hexosaminidase. Based upon the specific activity of the enzyme, 20 Units.mg⁻¹ amount of enzyme activity used in Figure 3.19 equated to additions in $\mu\text{g.mL}^{-1}$ was 25 $\mu\text{g.mL}^{-1}$, 50 $\mu\text{g.mL}^{-1}$, 100 $\mu\text{g.mL}^{-1}$ and 200 $\mu\text{g.mL}^{-1}$ human β -hexosaminidase respectively. The human β -hexosaminidase MIC for the wild type *M. smegmatis* was 4 Units.mL⁻¹ (Figure 3.19 (a) Red). The control data, wild type growth in the presence of 0 Units.mL⁻¹ β -hexosaminidase (Figure 3.19 (a): Blue) was characterised by a apparent lag phase of 21 hours, a Td of 6.93 hours and an entrance into stationary phase at OD_{600nm} 0.31 after 45 hours. Significance student's t-test of the wild type strain against human β -hexosaminidase (Table 3.12) demonstrated that the results depicted by the addition of all investigated concentrations were statistically significant compared to the 0 Units.mL⁻¹ control. P-values for each concentration were <0.05 (0.5 Units.mL⁻¹), <0.001 (1 and 2 Units.mL⁻¹) and <0.0001 (4 Units.mL⁻¹) respectively.

The addition of 0.5 Units.mL⁻¹ of enzyme (Figure 3.19 (a) Green) had a slight impact on the growth phenotype of the strain, compared to the growth of wild type *M. smegmatis* in the absence of β -hexosaminidase. The lowest investigated concentration led to an apparent lag phase duration of 24 hours, an increase in Td to 7.35 hours and the reduction of the AUC percentage to 87.21%. The incubation of wild type cells with either 1 (Figure 3.19 (a) Pink) or 2 (Figure 3.19 (a) Orange) Units.mL⁻¹ of human β -hexosaminidase had similar effects on reducing growth. Both data sets demonstrated observable growth after 24 and 27 hours respectively, 3 and 6 hours longer than the control. The Td for both data sets was 11.90 hours and 11.36 hours respectively, and the AUC of each growth curve in the presence of 1 or 2 Units.mL⁻¹ β -hexosaminidase were respectively 50.92% and 36.73% that of the control.

The *M. smegmatis* ΔNamH strain 0 Units.mL⁻¹ control (Figure 3.19 (b) Blue) demonstrated a similar growth curve to the wild type control (Figure 3.19 (a) Blue) with a 21 hour apparent lag phase a Td of 6.41 hours and a final stationary phase OD_{600nm} value of 0.31. All of the investigated concentrations of human β -hexosaminidase inhibited growth to a statistically significant degree with p-values of <0.001 (0.5, 1 and 2 Units.mL⁻¹) and <0.0001 (4 Units.mL⁻¹) respectively.

The *M. smegmatis* NamH strain was more sensitive to growth inhibition by β -hexosaminidase at every concentration of the enzyme investigated (Figure 3.19 (b)) compared to the wild type (Figure 3.19 (a)). This was exemplified most clearly by the impact of $0.5 \text{ Units.mL}^{-1}$ of β -hexosaminidase on growth of the Δ NamH. Whereas this concentration of β -hexosaminidase minimally impaired growth of the wild type strain (Figure 3.19 (a) Green), the growth of the Δ NamH strain (Figure 3.19 (b) Green) was significantly attenuated with respect to all currently used measures of growth. Δ NamH cells did not display visible signs of growth in the presence of $0.5 \text{ Units.mL}^{-1}$ β -hexosaminidase until 3 hours after the control, the AUC was 45.02% of the value obtained by the 0 Units.mL^{-1} control absence of the enzyme, and the cells achieved an $\text{OD}_{600\text{nm}}$ of 0.19. The Td was also almost two-fold greater, requiring 10.37 hours compared to 6.41 hours for the control.

Raising the β -hexosaminidase concentration to $1.0 \text{ Units.mL}^{-1}$ β -hexosaminidase (Figure 3.19 (b) Pink) further impaired growth, the cells exited apparent lag phase after 24 hours the AUC was measured at 29.59% relative to the untreated control, and the Td was raised to 13.45 hours culminating in a final $\text{OD}_{600\text{nm}}$ value during stationary phase of 0.14. The addition of 2 Units.mL^{-1} β -hexosaminidase (Figure 3.19 (b) Orange) as seen in the wild type did not significantly increase the inhibition of growth over that caused by 1 Units.mL^{-1} of β -hexosaminidase producing only a 5% difference in AUC (25.73%) and a Td only 1.5 hours greater (14.96 hours) compared to 1 Units.mL^{-1} . The MIC for the Δ NamH strain was 4 Units.mL^{-1} (Figure 3.19 (b) Red), identical to that of the wild type, sufficient to inhibit observable growth. The true difference between the two strains was most evident from a comparative student's t-test. Each of the investigated concentrations of human β -hexosaminidase which permitted cell growth were deemed statistically significant (Table 3.12) between each *M. smegmatis* strain. P-values for each concentration were <0.001 ($0.5 \text{ Units.mL}^{-1}$), <0.05 (1 Units.mL^{-1}) and <0.05 (2 Units.mL^{-1}).

3.7.2.1 The relationship between *M. smegmatis* sensitivity towards human β -hexosaminidase and pH

As with previous experiments, the activity of the human β -hexosaminidase enzyme was studied according to Koo, *et al.* (2008) at pH conditions representative of the of the enzyme within the phagolysosome at pH 5.0 and throughout the cytoplasm of the macrophage at pH 7.0 (Koo, *et al.* (2008). The concentrations of human β -hexosaminidase that *M. smegmatis* was exposed to were between 0.5-4 Units.mL⁻¹. The average colony counts for each strain were converted into percentage survival at each concentration of human β -hexosaminidase compared to the 0 Units.mL⁻¹ control. The results are shown in Figure 3.20.

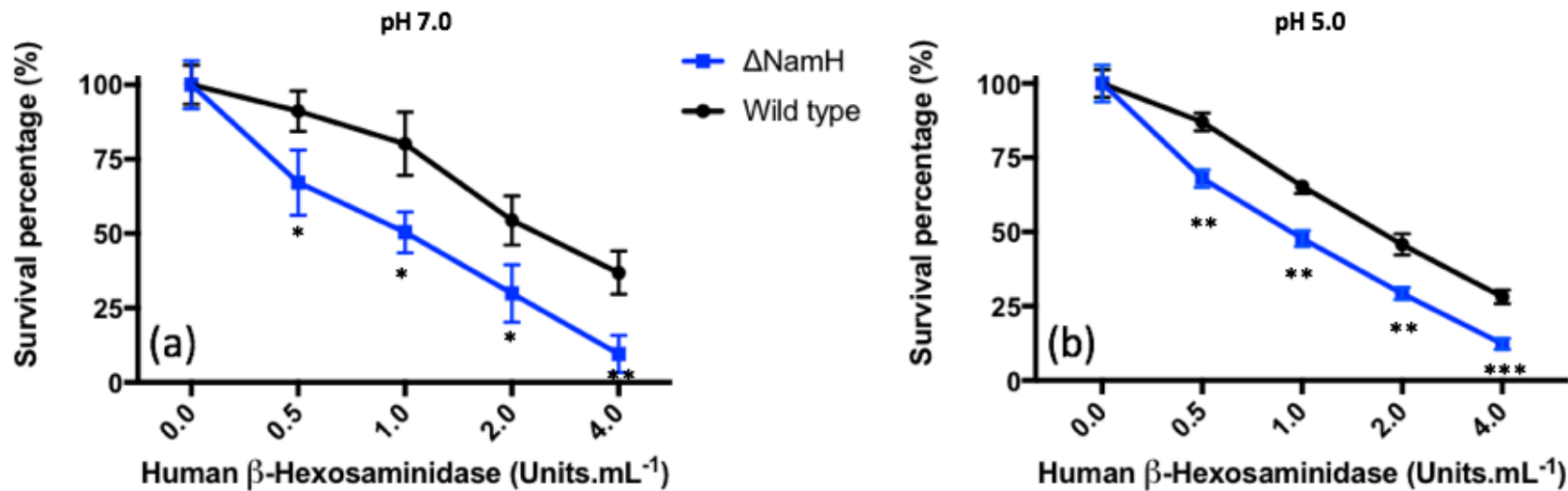


Figure 3.20. Effect of exposure of *M. smegmatis* to increasing concentration of human β -hexosaminidase at pH 5.0 and 7.0. *M. smegmatis* wild type (Black) and Δ NamH (Blue) cells were incubated with 0, 0.5, 1, 2 and 4 Units.mL⁻¹ of human β -hexosaminidase in 100 μ L HBSS at (a) pH 7.0 and (b) pH 5.0 in a 96 well microtiter plate. Microtiter plates were incubated for 1.5 hours. After incubation at 37°C bacterial survival was determined. Wells were pipetted on TSB agar plates and incubated at 37°C for 72 hours. Colony forming units were counted and averaged from triplicate plates. Error bars represent standard deviation of triplicate measurements. Statistically significant results are indicated with * = p-value <0.05, ** = <0.01, *** = <0.001 and **** = <0.0001. Result: Δ NamH was more susceptible to β -hexosaminidase at each pH but variation between strains was less pronounced at pH 5.0.

β-hexosaminidase concentration (Units.mL⁻¹)	Wild type % (1) Survival (mean \pm SD, n=3)	ΔNamH % (2) Survival (mean \pm SD, n=3)	Significance student's t-test (2) v (1)
0.0	100.00 \pm 6.55	100.00 \pm 8.03	N/A
0.5	91.15 \pm 6.78	67.10 \pm 10.91	p <0.05
1.0	80.16 \pm 10.65	50.41 \pm 6.84	p <0.05
2.0	54.42 \pm 8.26	29.91 \pm 9.67	p <0.05
4.0	36.86 \pm 7.24	9.58 \pm 6.23	p <0.01

Table 3.13 Average bacterial survival by *M. smegmatis* wild type and Δ NamH strains against human β -hexosaminidase at pH 7.0 incubated for 1.5 hours. Results depicted in a graph in Figure 3.20 (a). Standard deviation of triplicate measurements. Statistically significant concentrations indicated with p-values <0.05.

The colony count for both strains at pH 7.0 was above 200 CFU, with the wild type producing a triplicate average of 248 ± 16.28 (n=3) colonies per plate and the Δ NamH strain an average of 202 ± 16.19 (n=3). At pH 7.0, the survival of the Δ NamH strain was consistently 25-30% less than that of the wild type strain (Figure 3.20 (a)). The decline in survival of wild type *M. smegmatis* with increasing β -hexosaminidase concentration was gradual, decreasing between 10-15% over every incremental increase in β -hexosaminidase concentration (Table 3.13). The wild type strain survival was diminished by 4 Units.mL⁻¹ human β -hexosaminidase to 36% of the average CFU obtained in the 0 Units.mL⁻¹ control.

The most significant reduction in survival of the Δ NamH knockout was achieved by incubation with the lowest concentration of 0.5 Units.mL⁻¹ β -hexosaminidase (Figure 3.20 (a)). Once incubated with the enzyme survival of the Δ NamH strain decreased by 33%, three times greater than the impact of this concentration of β -hexosaminidase on the wild type. The survival decreased in a dose dependant manner decreasing by almost 20% with each increasing enzyme concentration, culminating in 9.58% survival of Δ NamH cells relative to that of untreated Δ NamH cells at 4 Units.mL⁻¹ β -hexosaminidase. Each of the human β -hexosaminidase concentrations produced statistically significant variation between the two strains at pH 7.0 (Table 3.13), with p-values of <0.05 (0.5, 1 and 2 Units.mL⁻¹) and <0.01 (4 Units.mL⁻¹).

β-hexosaminidase concentration (Units.mL⁻¹)	Wild type % (1) Survival (mean \pm SD, n=3)	ΔNamH % (2) Survival (mean \pm SD, n=3)	Significance student's t-test (2) v (1)
0.0	100.00 \pm 4.68	100.00 \pm 6.13	N/A
0.5	87.02 \pm 2.99	68.00 \pm 2.95	p <0.005
1.0	65.34 \pm 2.35	47.76 \pm 2.72	p <0.005
2.0	45.78 \pm 3.58	29.25 \pm 2.05	p <0.005
4.0	28.12 \pm 2.27	12.31 \pm 1.84	p <0.001

Table 3.14 Average bacterial survival by *M. smegmatis* wild type and Δ NamH strains against human β -hexosaminidase at pH 5.0 incubated for 1.5 hours. Results depicted in a graph in Figure 3.20 (b). Standard deviation of triplicate measurements. Statistically significant concentrations indicated with p-values <0.05.

Both strains produced triplicate average CFU counts above 300 at pH 5.0, with the wild type cultivating an average CFU of 303 ± 14.17 (n=3) and the Δ NamH a CFU average of 365 ± 22.36 (n=3). When the growth response of wild type and Δ NamH *M. smegmatis* to β -hexosaminidase was evaluated at pH 5.0 (Figure 3.20 (b)), the more observable variation between strains at pH 7.0 (Figure 3.20 (a)) was less apparent at pH 5.0 with both strain producing similar declines in total averages at each selected concentration. Previously the wild type strain maintained a difference in survival of 25-30% in excess of that displayed by the Δ NamH strain regardless of the β -hexosaminidase concentration. This discrepancy was reduced to 18-16% between the two strains at pH 5.0 (Table 3.14).

The greatest change between the two pH conditions was the effect on the survival of the wild type strain, not the Δ NamH, as has previously been observed in this chapter. Although the bacterial survival percentages remained higher for the wild type compared to the Δ NamH, the wild type strain displayed more pronounced susceptibility to β -hexosaminidase at all measured concentrations at pH 5.0 than the previously investigated pH 7.0 (Table 3.13). The difference was most pronounced at 1 Units.mL⁻¹ with a 15% drop in bacterial survival for the wild type at pH 5.0 relative to that seen at pH 7.0. The change of pH from pH 7.0 to 5.0 once again diminished the Δ NamH survival, most notably during incubation with the lowest enzyme concentrations, however subsequently the Δ NamH strain produced only slight variations in survival

percentages when comparing the strain's survival at both pH 7.0 and pH 5.0 conditions. Though the variation between the two strains was narrower at pH 5.0 than at pH 7.0, the standard deviation between triplicate results was also narrower leading to the percentage bacterial survival of both strain at all investigated concentrations being statistically more significant than at pH 7.0. P-values for each concentration were <0.005 (0.5, 1 and 2 Units.mL⁻¹) and <0.001 (4 Units.mL⁻¹).

The data sets from the wild type and Δ NamH strains were considered separately and comparisons were made on enzyme activity and bacterial survival between each selected pH condition. The wild type strain survival percentage is shown in Figure 3.21.

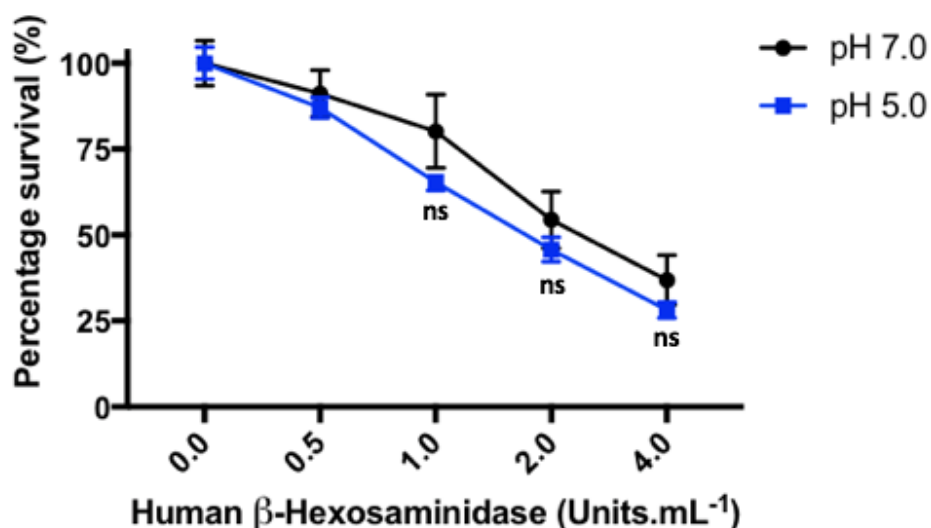


Figure 3.21. Impact of pH on wild type *M. smegmatis* survival of β -hexosaminidase treatment. *M. smegmatis* wild type cells were incubated with 0, 0.5, 1, 2 and 4 Units.mL⁻¹ of human β -hexosaminidase in 100 μ L HBSS at pH 7.0 (Black) and pH 5.0 (Blue) in a 96 well microtiter plate for 1.5 hours at 37°C. Bacterial survival was then determined. Wells were pipetted on TSB agar plates and incubated at 37°C for 72 hours. Colony forming units were counted and averaged from triplicate plates. Error bars represent standard deviation of triplicate measurements. Averages at each concentration were compared to the control 0 μ g.mL⁻¹ as a percentage. Statistically significant results are indicated with * = p-value <0.05, ** = <0.01, *** = <0.001 and **** = <0.0001. Ns = not statistically significant. Result: The wild type strain showed increased susceptibility for each concentration at pH 5.0. Any impact of pH on survival was most noticeable at 1 Units.mL⁻¹.

The wild type strain in Figure 3.21 showed a greater resilience to β -hexosaminidase at pH 7.0 (Figure 3.21: Black) than pH 5.0 (Figure 3.21: Blue). At pH 7.0 the percentage of bacterial survival, indicated that cells resisted lysis to a greater extent especially at 1.0 Units.mL⁻¹ than at pH5.0. The strain was observed to be more susceptible to the human β -hexosaminidase after incubation at pH 5.0 with each concentration indicating that the enzyme is more active towards the wild type at the lower pH condition, equivalent to the known pH of the phagolysosome than at neutral conditions. At pH 5.0 the survival percentage of the wild type strain is most similar to pH 7.0 at 0.5 Units.mL⁻¹ with survival deviating by only 3%. This percentage reduction increased to 14% at 1.0 Units.mL⁻¹ compared to pH 7.0. The final two investigated concentrations 2.0 and 4.0 Units.mL⁻¹ reduced percentage survival each equally by a further 9% as the concentration doubled. A student's t-test determined that the variation between percentage bacterial survival of the wild type strain at pH 7.0 and 5.0 at each human β -hexosaminidase concentration was not statistically significant with p-values >0.05.

The Δ NamH strain pH comparison data is depicted in Figure 3.22.

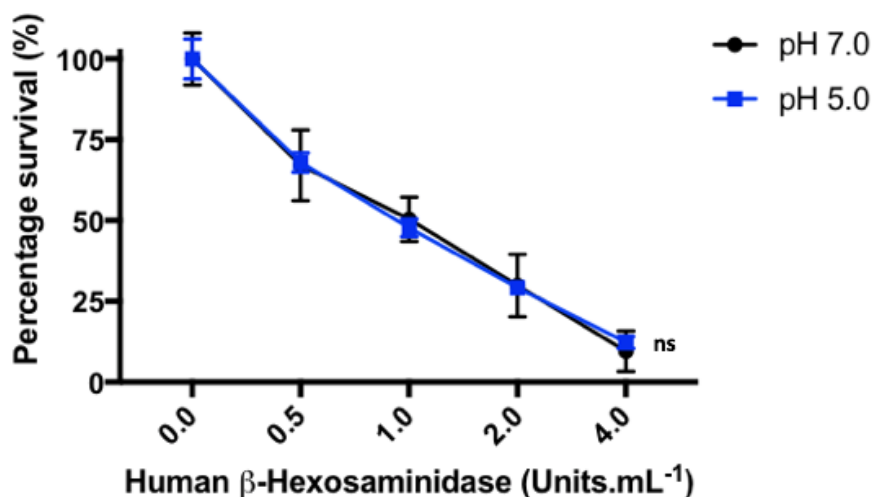


Figure 3.22. Impact of pH on Δ NamH *M. smegmatis* survival of human β -hexosaminidase treatment. *M. smegmatis* Δ NamH cells were incubated with 0, 0.5, 1, 2 and 4 Units.mL⁻¹ of human β -hexosaminidase in 100 μ L HBSS at pH 7.0 (Black) and pH 5.0 (Blue) in a 96 well microtiter plate for 1.5 hours at 37°C. Bacterial survival was then determined. Wells were pipetted on TSB agar plates and incubated at 37°C for 72 hours. Colony forming units were counted and averaged from triplicate plates. Error bars represent standard deviation of triplicate measurements. Averages at each concentration were compared to the control 0 μ g.mL⁻¹ as a percentage. Statistically significant results are indicated with * = p-value <0.05, ** = <0.01, *** = <0.001 and **** = <0.0001. Ns = not statistically significant. Result: Δ NamH strain was equally susceptible to β -hexosaminidase at each pH.

Figure 3.22 shows an equivalency between data sets at each investigated pH condition. The impact of β -hexosaminidase activity on the survival of the Δ NamH *M. smegmatis* strain did not alter between the two pH values, maintaining the same measured reduction in percentage bacterial survival as hexosaminidase concentration increased. Percentage survival for each data point was within 3% and the standard error, therefore none of the human β -hexosaminidase concentrations against the Δ NamH strain at the two investigated pH conditions were deemed statistically significant (p-values >0.05).

The human variant of β -hexosaminidase was difficult to reliably acquire and available only from a single source (Sigma-Aldrich). The low quantity provided and the infrequent availability meant that further investigations with human β -hexosaminidase were not possible within the time available. An alternative variant was procured to attempt to extend this line of investigation.

3.7.3 *M. smegmatis* sensitivity towards bovine β -hexosaminidase

The final version of β -hexosaminidase tested for its impact on *M. smegmatis* growth was the bovine variant, as mycobacterial infection in cattle is caused by *M. bovis* and is a significant issue in agriculture (Mathews, *et al.* 2006). The sequence similarity between the human and bovine alpha and beta β -hexosaminidase subunits are 84% and 70% respectively (www.ncbi.nih.gov/BLAST). The bovine β -hexosaminidase had an enzymatic activity of around 50 Units.mg⁻¹. Based on this information, mycobacterial strains were incubated with bovine β -hexosaminidase concentrations of 2.5, 5 and 10 Units.mL⁻¹ at pH 5.0. The specific enzyme activity equates these concentrations to 50, 100 and 200 μ g.mL⁻¹.

The percentage bacterial survival data for both strains against bovine β -hexosaminidase was analysed and depicted in Figure 3.23.

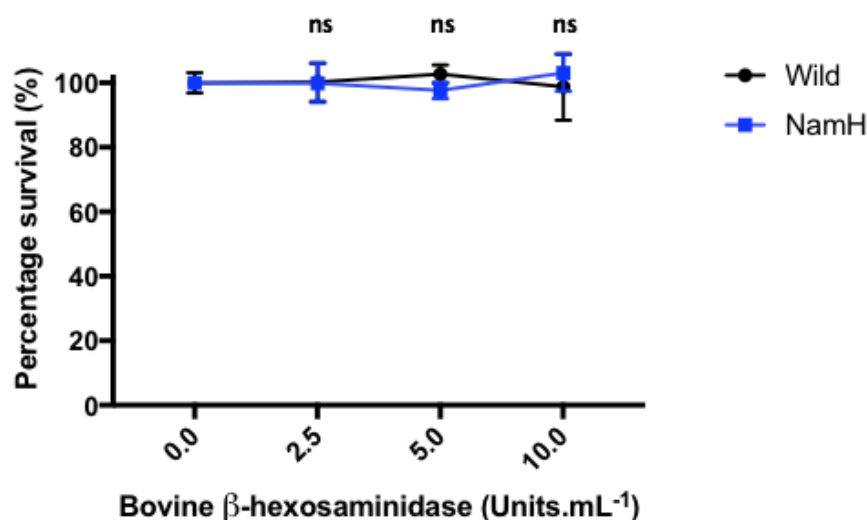


Figure 3.23. Impact of bovine β-hexosaminidase on the survival of *M. smegmatis* at pH 5.0. *M. smegmatis* wild type (Black) and ΔNamH (Blue) cells were incubated with 0, 2.5, 5 and 10 Units.mL⁻¹ of bovine β-hexosaminidase in 100 μL HBSS at pH 5.0 in a 96 well microtiter plate. for 1.5 hours at 37°C. Bacterial survival was then determined. Wells were pipetted on TSB agar plates and incubated at 37°C for 72 hours. Colony forming units were counted and averaged from triplicate plates. Error bars represent standard deviation of triplicate measurements. Averages at each concentration were compared to the control 0 μg.mL⁻¹ as a percentage. Statistically significant results are indicated with * = p-value <0.05, ** = <0.01, *** = <0.001 and **** = <0.0001. Ns = not statistically significant. Result: Concentrations of bovine β-hexosaminidase investigated were insufficient to impact bacterial survival of either strain.

β-hexosaminidase concentration (Units.mL ⁻¹)	Wild type % (1) Survival (mean ± SD, n=3)	ΔNamH % (2) Survival (mean ± SD, n=3)	Significance student's t-test (2) v (1)
0.0	100.00 ± 3.16	100.00 ± 2.03	N/A
2.5	100.24 ± 5.96	99.89 ± 5.98	p > 0.05
5.0	102.73 ± 2.84	97.65 ± 2.50	p > 0.05
10.0	98.72 ± 10.32	103.10 ± 5.67	p > 0.05

Table 3.15 Average bacterial survival by *M. smegmatis* wild type and ΔNamH strains against bovine β-hexosaminidase at pH 5.0 incubated for 1.5 hours. Results depicted in a graph in Figure 3.23. Standard deviation of triplicate measurements. Statistically significant concentrations indicated with p-values <0.05.

The control colony count totals for both strains were robust enough to compare colony count survival with increasing concentrations of bovine β-hexosaminidase. Total averages achieved by the wild type and ΔNamH strain were 270 ± 8.50 (n=3) and 325 ± 6.65 (n=3) CFU respectively. The addition of bovine β-hexosaminidase at the

concentrations investigated (Figure 3.23) were unable to reduce the colony count in either strain.

The percentage survival for both strains remained steady regardless of enzyme concentration. The exposure of wild type *M. smegmatis* to bovine β -hexosaminidase concentrations (Figure 3.23 (a)) more than double the Units.mL⁻¹ MIC of the human counterpart reduced survival by only 1.28% (Table 3.15) after incubation with 10 Units.mL⁻¹ equivalent to 200 μ g.mL⁻¹. The Δ NamH strain (Figure 3.23 (b)) increased in the number of viable colonies present during 10 Units.mL⁻¹ incubation to 103% of the total achieved by the strain in the absence of enzyme although this was not statistically significant (Table 3.15). The concentrations of hydrolytic enzymes may have been too low to significantly impact survival of *M. smegmatis* but may have disrupted remaining clumps of cells not homogenised sufficiently during cell preparation. None of the investigated concentration produced statistically significant data. It is impossible to determine if whether the inactivity of the hexosaminidase was due to substrate specificity, low enzyme activity or an inactive batch of enzyme.

The human and bovine variants of β -hexosaminidase was difficult to procure compared to the variants of lysozyme investigated, therefore avenues of the investigation undertaken were narrower than expected. Outstanding experiments will be outlined in further work (Section 3.9).

3.8 Discussion

3.8.1 N-glycolyl modification during aerobic and anaerobic growth

The absence of the *namH* gene prevents the incorporation during mostly aerobic incorporation of N-glycolylated sugars into the wider peptidoglycan layer. This deficiency does not significantly impact upon the aerobic phenotypic growth profile of the Δ NamH mutant compared to the wild type strain (Figure 3.1), suggesting that the presence of the modification does not positively or negatively impact growth alone

(Raymond, *et al.* 2005). The NamH enzyme utilises molecular oxygen but was shown to not be essential for cellular propagation on nutrient rich or deficient agar during resuscitation from an anaerobic environment (Figure 3.2). The incorporation of N-glycolylated Lipid II which occurs solely during aerobic conditions, does not lead to the conclusion that the expression of *namH* is vital in aiding cell reanimation from dormancy within newly ruptured granulomas initiating a more active disease state in the previously latent mycobacteria (Cordone, *et al.* 2008). Based upon these results, the purpose of NamH does not appear to accelerate growth when oxygen concentrations are the only limiting factor.

3.8.2 N-glycolyl modification against lysozyme

Based upon the previous investigated documented by Raymond, *et al.* (2005) the absence of N-glycolylated saccharides within the peptidoglycan structure of *M. smegmatis* led to a greater susceptibility towards lysozyme. The previously observed *M. smegmatis* MIC for human lysozyme (Raymond, *et al.* 2005) was successfully repeated for both strains (Figure 3.7), with the Δ namH deficient variant susceptible at half the concentration of the wild type. MIC experiments were conducted at pH 6.8 for optimal growth of the mycobacteria, which is also within the optimal range of human lysozyme activity (Pincus, *et al.* 1977). Interactions between mycobacteria and lysozyme at this pH would take place surrounding the plasma membrane of host's macrophages (Koo, *et al.* 2008) and based upon results the absence of N-glycolylated peptidoglycan in the Δ NamH strain would impede mycobacterial growth two-fold compared to wild type due in part to the steric hindrance of N-glycolylation preventing lysozyme binding. MIC assessment of hen egg white lysozyme (Figure 3.5) demonstrated a requirement for a two-fold greater required concentration of this protein compared to that of the human lysozyme for inhibition of phenotypic growth in both strains. Chicken lysozyme MIC variation matched the findings of human lysozyme with the *namH* deficient mutant displaying a lack of growth at half the MIC of the wild type. MBC values for both investigated lysozymes were consistently double the MIC result for each strain (Figure 3.6 and Figure 3.8).

Assessment of mycobacterial bacterial survival on nutrient agar after human lysozyme incubation at optimal activity pH 7 (Figure 3.11), demonstrated similar findings to the MIC investigation (Figure 3.7). The percentage bacterial survival was more pronounced in the Δ namH strain than the wild type although the percentage difference between each strain at increasing concentrations remained equivalent. Increasing the human lysozyme concentration greater than 256 $\mu\text{g.mL}^{-1}$ equally impacted the survival of both strains, indicating that the absence of N-glycosylation does not lead to more susceptible organism in excess lysozyme concentrations.

The reduction of the pH of the incubation to 6.5 reduced the efficacy of the lysozyme and increased the survival of both strains, a characteristic most pronounced in the Δ NamH strain, narrowing the previously observed disparity between wild type and Δ NamH strain susceptibility to lysozyme (Figure 3.14). The effectiveness of human lysozyme did not measurably diminish as pH was reduced from pH 6.0 to pH 5.0 (Figure 3.14) more in keeping with the acidic environment generated within the phagolysosome (Flannagan, *et al.* 2009). These results imply that human lysosome activity would not be greatly impacted by the gradual decrease in pH within the phagolysosome to around pH 5.0 caused by H^+ ion pumps (Forster and Kane 2000), although as shown the lysozyme would have the greatest activity within a more neutral environment such as near the cell membrane. Variations observed to bacterial survival in the NamH deficient mutant at pH 5.5 demonstrated decreased survival at the lowest investigated human lysozyme concentrations, indicating increased enzyme activity, although this effect was not observed at either pH 6.0 or pH 5.0 and was likely caused by a discrepancy during the generation of diluted enzyme stocks.

Extending the incubation time frame above 1.5 hours (Figure 3.15) was not deemed necessary to increase the variation in survival between the two strains and based upon the findings of this investigation increasing the incubation above 3 hours was not necessary unless required to measure low human lysozyme concentrations. The lack of variation in human lysozyme activity at decreasing pH conditions appears to be due in part to the length of incubation. Wild type survival was especially greatly impacted by extending the incubation phase decreasing at a more pronounced degree at high concentrations, though the gulf in susceptibility between strain remains constant.

Prolonged exposure to hydrolytic enzymes at acidic pH conditions mimics the purpose of the phagolysosome. If mycobacteria are unable to escape through the rupture of the phagosomal membrane by type VII secretion systems (van der Wel, *et al.* 2007), the combination of synergistic conditions aid in cell lysis by hydrolytic activity.

3.8.3 N-glycolyl modification against β -hexosaminidase

Initial β -hexosaminidase investigations were conducted with *S. plicatus* β -hexosaminidase. The organism is commonly identified within soil (Hasani *et al.* 2014) which is also the habitat for non-tubercular mycobacteria such as *M. smegmatis* (Tsukamura, *et al.* 1976). Though focus of this thesis was primarily towards host macrophage invasion of mycobacteria, the β -hexosaminidase from *S. plicatus* permitted *in vitro* assessment of Streptomyces-secreted enzymes on mycobacteria. Due to similarity of targeting by both β -hexosaminidase and lysozyme, the presence of solely N-acetylated peptidoglycan of the Δ NamH strain once again correlated with growth impairment compared to the wild type (Figure 3.18). The MIC for both strains was not established due to insufficient concentrations of available stocks of *S. plicatus* β -hexosaminidase.

Human β -hexosaminidase was ten-fold more active than the *S. plicatus* variant, and impeded the growth phenotype of both strains to produce an MIC (Figure 3.19). In the first instance, during the MIC assessment of hydrolytic enzymes against wild type and Δ NamH *M. smegmatis* mycobacterial strains the MIC was equal. Both strains displayed growth at 2 Units.mL⁻¹ but not at 4 Units.mL⁻¹. These results do not indicate equivalency, however. Comparisons between both strains at each investigated human β -hexosaminidase concentration demonstrated statistically significant variation in their enzyme susceptibility. Further investigation at 3 Units.mL⁻¹ would likely lead to MIC variation between strains.

Measuring the strain survival of treatment by human β -hexosaminidase at the two extreme host pH conditions, pH 7.0 and pH 5.0 showed that the wild type maintained its resilience to inactivation by β -hexosaminidase inhibition over Δ NamH regardless of pH condition (Figure 3.20). Though comparisons between each strain at pH 5.0

appeared to show a narrower gulf between strain survival (Figure 3.20), analysis of each strain at both pH conditions (Figure 3.21 and Figure 3.22) presented no statistically significant alteration in bacterial survival at pH 7.0 compared to 5.0. This indicated that the alteration of pH does not impact the enzyme. Other factors therefore must be important to increase mycobacterial lysis within the phagolysosome. Both the human β -hexosaminidase MIC assessment (Figure 3.19) and the bacterial survival utilised the equivalent enzyme concentration range. The 60 hour time frame of the MIC data led to complete growth inhibition at 4 Units.mL⁻¹ compared to the 1.5 hour incubation for bacterial survival leading to 10% survival in both strains. The requirement for extended enzyme incubation periods requires further study to ascertain significance.

The data reported here indicated that human β -hexosaminidase activity was stable between both pH 7 and 5, which would be advantageous *in vivo* to the enzyme once located with a newly formed phagolysosome as the pH of the compartment is gradually reduced to aid mycobacterial cell lysis.

Human β -hexosaminidase is also known to be located at both the more pH neutral cell membrane (Koo, *et al.* 2008) therefore, the ability to maintain a stable activity regardless of its cellular location would be important to aid in the immune response whether during initial contact with the mycobacteria or during phagolysosome degradation.

The initial investigations into bovine β -hexosaminidase at equivalent concentrations to the human variant failed to produce an impact on growth of wild type or Δ NamH *M. smegmatis* at pH 5.0. The optimal conditions for enzyme activity needs to be identified before further investigations can be conducted.

3.9 Further work

- Equivalent enzyme comparison

The investigations made against bovine β -hexosaminidase were insufficient to reduce survival of either *M. smegmatis* strains (Figure 3.23). These concentrations were equivalent to active concentrations of human β -hexosaminidase (Figure 3.20) and acquiring increased quantities of the enzyme are required to determine the optimum active concentration of bovine β -hexosaminidase. Initial investigations have been made into a selection of both lysozymes and β -hexosaminidases from a range of hosts to make broad comparisons between enzymatic activity towards mycobacterial interactions. It would be useful to standardise the activity of all investigated enzymes to ensure equivalent activities of enzymes were being used to draw important comparisons such as between the two mammalian host's immune responses during extended incubation or at selected pH conditions resembling the conditions within the phagolysosome of host's macrophages. One possible method to determine equivalency could be adapted from Koo *et al.* (2008) measuring alterations in the optical density of set *M. smegmatis* cultures at selected time points with various enzyme concentrations.

- Enzyme stability

Aerobic growth phenotypes of *M. smegmatis* strains were assessed against hydrolytic enzymes at 37°C for up to 60 hours due to the slow growth rate of mycobacteria. During the experiment sub MIC concentrations led to cells remaining within apparent lag phase for extended periods before demonstrating exponential growth. To ascertain whether measurement of growth is due to each strain overcoming a stable enzyme concentration or whether extended incubation periods lead to a denaturing and reduced efficacy of the enzyme which in turn permits cellular growth, control experiments utilising each investigated enzyme will be incubated at 37°C in the absence of mycobacteria prior to repeating the hydrolytic enzyme susceptibility of mycobacteria and contrast the results with non-preincubated enzymes to determine overall stability.

- Synergy between lysozyme and β -hexosaminidase

Release of enzymes by the phagolysosome impacts the cell wall of invading mycobacteria. Synergy between β -hexosaminidase and lysozyme would aid in increasing mycobacterial cell lysis thereby priming the innate immune system (Weiss and Schaible 2015). Lysozyme and β -hexosaminidase both cleave the β -1,4 glycosidic bonds between MurNAc/MurNGlyc and GlcNAc within the peptidoglycan, although it has been suggested that β -hexosaminidase targets terminal sugar rings (Fernandes, *et al.* 1997). Based on this differential specificity, the possibility of synergy between β -hexosaminidase and lysozyme should be investigated to complement the investigations made for each isolated enzyme, with respect to their antimycobacterial activity.

- Other lytic enzymes

Expanding upon the initial work involving the organism *S. plicatus* β -hexosaminidase (Figure 3.18), examining the role of other secreted hydrolytic enzymes from organisms and phages is an important area of investigation. Lytic bacteriophages release endolysins (Schmelcher, *et al.* 2012) which has a similar hydrolytic mode of action against peptidoglycan as other investigated enzymes to bypass the bacterial cell wall to invade and utilise the replication mechanisms of the host to propagate. There has been interest in the exploitation of mycobacteriophage endolysins in the regard (Catalão and Pimentel 2018). Resuscitation promoting factors (RPFs) are secretory protein encoded by MTB (Kana, *et al.* 2008) which cleave peptidoglycan monomers to signal the presence of an aerobic environment to previously dormant cells. Studies involving RFP knockout, in a wild type and Δ NamH background might reveal relationship between N-glycolylation and RPF function and any possible relationship with emergence from dormancy.

- *M. tuberculosis* Δ NamH

Collaborators in the Mukamolova lab at the University of Leicester have generated an MTB Δ NamH strain. Once obtained, the investigations made in *M. smegmatis* against variants of lysozyme and β -hexosaminidase will be repeated, to evaluate the difference between the low pathogenic *M. smegmatis* and the more highly pathogenic MTB as it relates to incorporation of the N-glycolyl modification into tubercular PG. Similar to the work done with *M. smegmatis* Δ NamH the percentage of N-glycolyl PG incorporation will be measured by methods outlined by Raymond, *et al.* (2005) isolating the peptidoglycan layer of aerobically grown cells and analysing the components by mass spectrometry. These experiments could be complemented by anaerobic studies to analysis more closely the relationship between dormancy, NamH activity and environmental oxygen tension.

- Survival within amoeba

The ability to probe intracellular survival of mycobacteria within various hosts is important. Non-tuberculosis mycobacteria are commonly isolated from water and soil environments containing free-living amoeba (Hu, *et al.* 2017). Many of the intracellular survival mechanisms adopted by mycobacteria within macrophages were likely honed against amoeba, as the *Mycobacterium tuberculosis* complex organisms have been identified as amoeba-resistant. Collaborators in the Wellington lab at the University of Warwick are investigating the relationship between amoeba and intracellular bacteria. Experiments would include measuring at a range of environmental conditions the survival difference within the amoeba between the wild type and NamH strains, as MTB has been demonstrated to survive for 14 days (Medie, *et al.* 2011).

3.10 Conclusion

The mycobacterial incorporation of MurNGlyc into the peptidoglycan sacculus has been demonstrated in this chapter to enable resistance to the activities of lytic enzymes such as lysozyme and β -hexosaminidase from a range of potential hosts and competing organisms. The absence of *namH* is not essential to cell propagation in aerobic conditions but dramatically impacts upon the resilience of the organism to hydrolytic enzymes at low pH environments and during extended incubation periods. Initial assessment of enzyme activity ranges were established in all expect bovine β -hexosaminidase, with comparisons between equivalent activities yet to be determined.

Chapter 4. The role of the N-glycolylated muramic acid in the protection of mycobacteria from antimicrobial susceptibility

4.1 Introduction

As previously stated (Section 1.2) mycobacteria are attributed to a number of global diseases such as tuberculosis and leprosy. The standard antimicrobial therapies against mycobacterial infection are becoming increasingly less potent as the percentage of antimicrobial resistance rises (Section 1.7.4). A number of key antimicrobials target specific synthetic steps or structures of the bacterial cell wall which have no eukaryotic equivalents (Yount and Yeaman 2013).

Mycobacteria are inherently resilient to cell wall targeting antimicrobials due to the composition of the cell wall structure containing the mycolyl-arabinogalactan-peptidoglycan (mAGP) complex (Hett and Rubin 2008) and due to the expression of antimicrobial degrading enzymes like β -lactamases such as BlaS (Flores, *et al.* 2005). The standard treatment for tuberculosis infection (Section 1.7.1) is a combination therapy of four antimicrobials, isoniazid, rifampicin, ethambutol and pyrazinamide. The increase in widespread resistance to standard treatments had led to utilization of second-line antimicrobials like vancomycin (Soetaerta, *et al.* 2015).

The N-glycolylation of mycobacterial peptidoglycan monosaccharides has been shown in the previous chapter to be important in aiding mycobacterial tolerance towards hydrolytic enzymes such as lysozyme.

4.2 Chapter Aim

The importance of the N-glycolyl modification in determining the activity of cell wall targeted antimicrobials was evaluated utilizing clinically well-established antibiotics as well as the newly discovered antimicrobial teixobactin (Ling, *et al.* 2015) and its derivative Arg-teixobactin (Jad, *et al.* 2015).

4.3 DMSO tolerance of *M. smegmatis* strains

Standard investigations into the antimicrobial activity of compounds against bacterial strains are commonly performed in nutrient media (EUCAST 2000). Many antimicrobials utilised within this chapter were insufficiently soluble in aqueous solution and required dissolution initially in dimethyl sulfoxide (DMSO), a dipolar aprotic solvent (Alastruey-Izquierdo, *et al.* 2012). To ascertain mycobacterial tolerance for DMSO increasing percentages of the latter were incubated with growing *M. smegmatis* wild type and NamH deficient cells. The impact of DMSO on mycobacterial proliferation is shown in Figure 4.1.

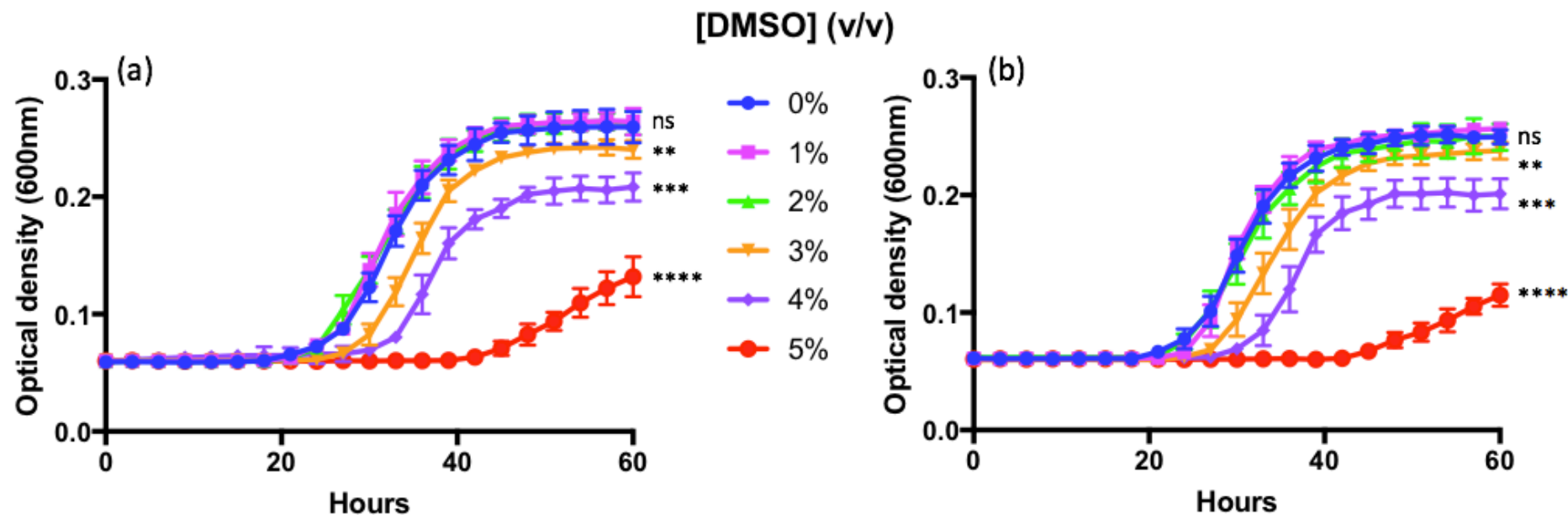


Figure 4.1 DMSO tolerance of *M. smegmatis*. Wild type (a) and NamH deficient (b) cells were grown in the presence of increasing concentrations of DMSO to identify optimal tolerance for the solvent, in 96 well microtiter plates in triplicate at 37°C with intermittent shaking. Absorbance was measured at OD_{600nm} at 3 hour intervals for 60 hours. Each well contained 100 μL 7H9 media supplemented with ADC + Tween80. The cultured *M. smegmatis* cells were standardized to an OD_{600nm} of 1 and diluted further by a factor of 10⁴ prior to incubation. Error bars represent standard deviation of triplicate measurements. DMSO concentration (v/v): 0% (Blue), 1% (Pink), 2% (Green), 3% (Orange), 4% (Purple), 5% (Red). Statistically significant results of comparisons of growth at increasing DMSO concentrations compared to 0% (v/v) DMSO for each strain are indicated with * = p-value < 0.05, ** = < 0.01, *** = < 0.001 and **** = < 0.0001. Ns = not statistically significant. Result: DMSO concentrations below 2% (v/v) did not alter growth whereas DMSO concentration above 2% (v/v) significantly reduced growth.

DMSO Conc (v/v) (%)	Wild type <i>M. smegmatis</i>					Δ NamH <i>M. smegmatis</i>					(b) vs (a) p- values
	Apparent Lag phase (h)	Td (h ⁻¹)	AUC (%)	Stationary Phase OD _{600nm}	Wild type p-values (a)	Apparent Lag phase (h)	Td (h ⁻¹)	AUC (%)	Stationary Phase OD _{600nm}	Δ NamH p- values (b)	
0	21	7.03	-	0.26	-	21	6.76	-	0.25	-	>0.05
1	21	6.91	104.31	0.26	>0.05	21	6.73	101.50	0.25	>0.05	>0.05
2	21	6.84	103.67	0.25	>0.05	21	6.69	101.50	0.24	>0.05	>0.05
3	27	6.81	82.26	0.24	<0.01	27	6.71	80.66	0.24	<0.01	>0.05
4	30	7.19	62.23	0.21	<0.001	30	6.96	60.29	0.20	<0.001	>0.05
5	45	15.61	12.12	0.13	<0.0001	45	19.25	8.76	0.11	<0.0001	>0.05

Table 4.1 Statistical comparisons of *M. smegmatis* growth curves in the presence of increasing concentrations of DMSO. Wild type and Δ NamH strains incubated for 60 hours at 37°C with selected concentrations of DMSO (v/v) produced growth curves measured at OD_{600nm} in Figure 4.1. Variations between growth curves were measured by time taken to exit apparent lag phase (hours), the doubling time (Td) of cells during exponential phase (hours⁻¹), the area under the curve (AUC) percentage compared to the 0 % control (%), the OD_{600nm} value achieved during stationary phase and whether the growth curve variations were statistically significant compared to each 0 % control with p-values <0.05 deemed significant. The statistical significance of Δ NamH (b) growth curves compared to wild type (a) at equivalent DMSO concentrations were determined by p-values <0.05.

The impact of DMSO concentration was investigated in order to ascertain the maximum percentage of DMSO compatible with normal cellular growth of *M. smegmatis*. Both wild type and NamH deficient strains responded to DMSO equally, with no significant variation noted between the strains (Table 4.1). The standard growth phenotype of the wild type (Figure 4.1 (a) Blue) and Δ NamH (Figure 4.1 (b) Blue) strains both exited apparent lag phase after 21 hours, achieved a Td of 7.03 and 6.76 hours respectively and reached stationary phase at OD_{600nm} 0.26 and 0.25 respectively after 45 hours.

The growth curves produced for each strain were analysed separately by a Student's t-test (Table 4.1) to compare the growth inhibition observed with increasing concentrations of DMSO against the 0% (v/v) DMSO control. Results indicated that growth variation by DMSO concentrations below 3% (v/v) in both strains were not deemed statistically significant with p-values >0.05 (Table 4.1). The growth inhibition measured by addition of 3% (v/v) DMSO or greater were equally statistically significant against both *M. smegmatis* strains with p-values of <0.01 (3% (v/v)), <0.001 (4% (v/v)) and <0.0001 (5% (v/v)) respectively. T-test comparisons of *M. smegmatis* strains at equivalent DMSO concentrations determined that any variation between wild type and Δ NamH growth curves was not statistically significant with p-values >0.05.

The first deviation from the growth phenotype was observed with the addition of 3% (v/v) DMSO (Figure 4.1 Orange) equally in both *M. smegmatis* strains. The *M. smegmatis* cells incubated with 3% (v/v) DMSO differed most notably from the 0% (v/v) control during apparent lag phase, which with the presence of the solvent increased by a further 6 hours resulting in a 27 hour duration before growth was observed. 3% (v/v) DMSO did not impact the Td or final OD_{600nm} value reached during stationary phase in both strains, but due to the extended apparent lag phase reduced the AUC to around 80% (Table 4.1) of the 0% (v/v) control.

The addition of 4% (v/v) DMSO (Figure 4.1 Purple), extended apparent lag phase of both wild type and Δ NamH *M. smegmatis* strains to 30 hours, increased the Td marginally to 7.19 hours in the wild type and 6.96 hours in the Δ NamH strain and decreased the AUC to 62.23% and 60.29% respectively. At 5% (v/v) DMSO (Figure 4.1 Red) the most noted impact on phenotypic growth was observed. The apparent lag

phase for both strains was extended to 45 hours, the Td during exponential phase doubled to 15.61 hours in the wild type and 19.25 hours in the Δ NamH strain. The AUC of both *M. smegmatis* strains was significantly impacted with values of 12.12% (wild type) and 8.76% (Δ NamH) respectively.

Based upon the findings shown in Figure 4.1 The decision was taken to utilize 2% (v/v) DMSO for all required investigations. Therefore 2% (v/v) DMSO was also added to control wells in the absence of antibiotic.

4.4 Antimicrobial MIC assessment of the *M. smegmatis* wild type and Δ NamH strains

The two *M. smegmatis* strains acquired from the Pavelka group (Raymond, *et al.* 2005) were generated initially by removal of the dominant β -lactamase gene *blaS*, (Flores, *et al.* 2005) creating the strain PM965 denoted as “wild type” in this chapter. Strain PM979 deemed “ Δ NamH” was subsequently formed by allelic exchange of the *namH* gene from PM965 creating the double mutant *blaS⁻ namH*. Mass spectrometric analysis of the composition of the mycobacterial cell wall structures constructed by the wild type strain detailed a 7:3 ratio of N-glycolylated monosaccharides to N-acetylated monosaccharides (Raymond, *et al.* 2005) within the peptidoglycan chains. The Δ NamH mutant strain produced peptidoglycan chains containing solely N-acetylated monosaccharides. Raymond, *et al.* (2005) assessed antimicrobial susceptibility of both strains against single concentrations of amoxicillin (20 μ g), ampicillin (10 μ g), isoniazid (5 μ g) and ethambutol (50 μ g). The average zones of inhibition for both strains were equal against isoniazid and ethambutol, with the Δ NamH strain more susceptible to both amoxicillin and ampicillin. This effect on the Δ NamH strain was caused by the deletion of the *blaS⁻* gene. This permitted assessment of β -lactam antimicrobials as *M. smegmatis* *blaS⁺* strains exposed to the ampicillin disk diffusion assay exhibited no zone of inhibition (Flores, *et al.* (2005)). Additionally, here the absence of *blaS⁺* in the PM965 strain permitted comparison of the impact of the NamH knockout and therefore N-glycolylation on β -lactam sensitivity of *M. smegmatis*.

Known antibiotics with distinct cellular targets were evaluated with respect to their MIC and MBC values against both *M. smegmatis* strains.

4.4.1 Ampicillin MIC assessment of *M. smegmatis* wild type and Δ NamH strains

Ampicillin is a β -lactam antibiotic due to its structure containing a β -lactam ring (Kong, *et al.* 2010) as demonstrated in Figure 4.2.

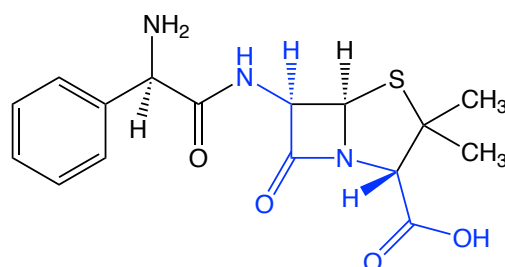


Figure 4.2: The structure of the β -lactam antibiotic Ampicillin. Molecular weight: 349.41; Chemical formula: $C_{16}H_{19}N_3O_4S$. The above schematic was created using ChemBioDraw. The coloured substructure (Blue) is the portion of the β -lactam that mimics the D-alanyl-D-alanine terminus of the PBP substrate.

The targets of ampicillin are the transpeptidase domains of penicillin binding proteins (PBPs) due to the structural similarity of the D-alanyl-D-alanine dipeptide terminus of the pentapeptide stem of peptidoglycan saccharides to the β -lactam (Figure 4.2 highlighted blue) (Hujer, *et al.* 2005). The PBP active site serine forms a covalent bond with the antibiotic impeding the construction of the overall peptidoglycan sacculus. Both *M. smegmatis* strains have had the *blaS* gene excised, removing the dominant *M. smegmatis* β -lactamase, BlaS. The enzyme is targeted specifically to degrade and inactivate β -lactam antibiotics such as ampicillin by hydrolysing the β -lactam ring (Abraham, *et al.* 1988). The *M. smegmatis blaS*⁺ strain had an ampicillin MIC of 128 $\mu\text{g.mL}^{-1}$ whereas removal of the *blaS* gene reduced the MIC to 2 $\mu\text{g.mL}^{-1}$ (Flores, *et al.* 2005). Antimicrobial analysis of the two *M. smegmatis* PM965 and PM979 strains revealed that the double knockout Δ NamH mutant was more susceptible towards ampicillin (Raymond, *et al.* 2005). Both *blaS*⁻ *M. smegmatis* strains were reassessed in Figure 4.3 against increasing concentrations of ampicillin to evaluate the MIC of the antibiotic.

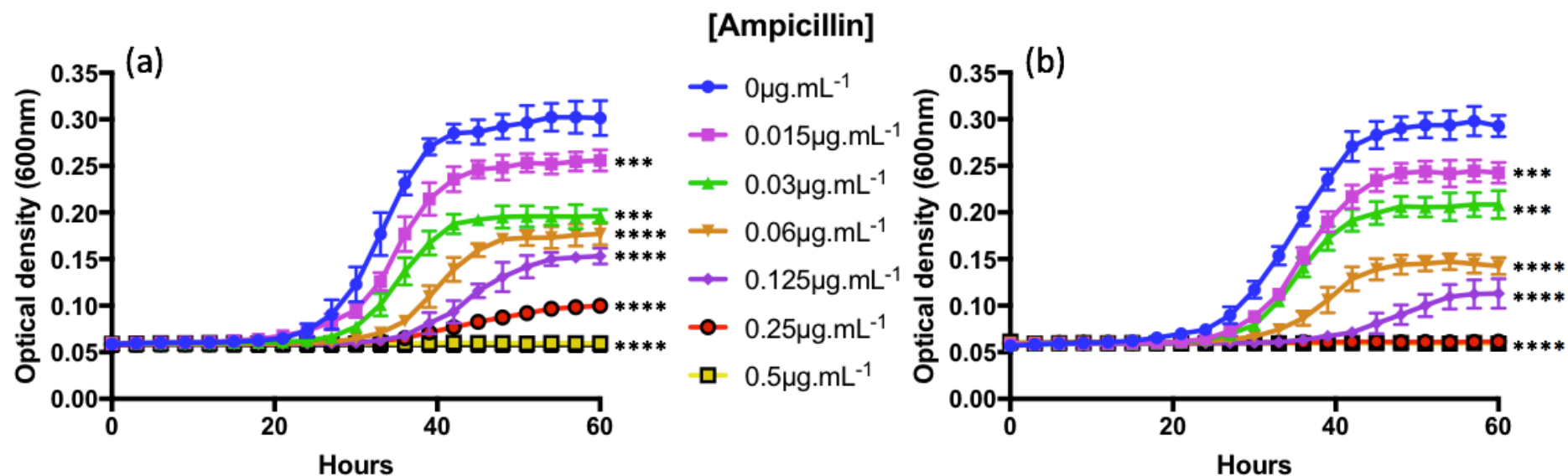


Figure 4.3 The impact of N-glycolylation of peptidoglycan on sensitivity of *M. smegmatis* growth to ampicillin. Wild type (a) and (b) Δ NamH *M. smegmatis* MIC growth curves against ampicillin. Cells were grown in 96-well microtiter plates in triplicate at 37°C with intermittent shaking, OD_{600nm} was measured at 3 hour intervals for 60 hours. Each well contained 100 μ L culture media (7H9, ADC, 0.05% (w/v) Tween 80) with increasing concentrations of ampicillin at a total DMSO concentration of 2% (v/v). *M. smegmatis* wild type (a) and (b) \square NamH strains were standardized to an OD_{600nm} of 1 and diluted further by a factor of 10⁴ prior to addition to wells and incubation. Error bars represent standard deviation of triplicate measurements. Ampicillin concentrations: 0 μ g.mL⁻¹ (Blue), 0.015 μ g.mL⁻¹ (Green), 0.03 μ g.mL⁻¹ (Pink), 0.06 μ g.mL⁻¹ (Orange), 0.125 μ g.mL⁻¹ (Purple), 0.25 μ g.mL⁻¹ (Red), 0.5 μ g.mL⁻¹ (Yellow), 1 μ g.mL⁻¹ (Black) and 2 μ g.mL⁻¹ (Brown). Statistically significant results of comparisons of growth of increasing ampicillin concentrations compared to growth at 0 μ g.mL⁻¹ ampicillin for each strain are indicated with * = p-value <0.05, ** = <0.01, *** = <0.001 and **** = <0.0001. Ns = not statistically significant. Results: Δ NamH displayed greater susceptibility to ampicillin than wild type. MIC results: Wild type (a) 0.5 μ g.mL⁻¹, Δ NamH (b) 0.25 μ g.mL⁻¹.

Ampicillin ($\mu\text{g.mL}^{-1}$)	Wild type <i>M. smegmatis</i>					ΔNamH <i>M. smegmatis</i>					(b) vs (a) p-values
	Apparent Lag phase (h)	Td (h^{-1})	AUC (%)	Stationary Phase OD _{600nm}	Wild type p-values (a)	Apparent Lag phase (h)	Td (h^{-1})	AUC (%)	Stationary Phase OD _{600nm}	ΔNamH p- values (b)	
0	21	6.54	-	0.30	-	21	7.35	-	0.30	-	>0.05
0.015	21	8.13	77.15	0.25	<0.001	24	8.35	73.53	0.24	<0.001	>0.05
0.03	24	7.95	52.45	0.19	<0.001	24	8.63	59.89	0.20	<0.001	>0.05
0.06	27	9.04	36.38	0.17	<0.0001	30	11.25	31.42	0.14	<0.0001	<0.01
0.125	36	11.90	23.46	0.15	<0.0001	42	18.43	12.08	0.11	<0.0001	<0.01
0.25	36	26.45	9.95	0.10	<0.0001	60	0.00	0.00	0.05	<0.0001	<0.01
0.5	60	0.00	0.00	0.05	<0.0001	60	0.00	0.00	0.05	<0.0001	-
1	60	0.00	0.00	0.05	<0.0001	60	0.00	0.00	0.05	<0.0001	-
2	60	0.00	0.00	0.05	<0.0001	60	0.00	0.00	0.05	<0.0001	-

Table 4.2 Statistical comparisons of *M. smegmatis* growth curves in the presence of increasing concentrations of ampicillin. Wild type and ΔNamH strains incubated for 60 hours at 37°C with selected concentrations of ampicillin produced growth curves measured at OD_{600nm} in Figure 4.3. Variations between growth curves were measured by time taken to exit apparent lag phase (hours), the doubling time (Td) of cells during exponential phase (hours⁻¹), the area under the curve (AUC) percentage compared to the 0 $\mu\text{g.mL}^{-1}$ control (%), the OD_{600nm} value achieved during stationary phase and whether the growth curve variations were statistically significant compared to each 0 $\mu\text{g.mL}^{-1}$ control with p-values <0.05 deemed significant. The statistical significance of ΔNamH (b) growth curves compared to wild type (a) at equivalent ampicillin concentrations were determined by p-values <0.05.

The MIC assessment of the wild type (Figure 4.3 (a)) and Δ NamH (Figure 4.3 (b)) demonstrated that the absence of N-glycolylated peptidoglycan moderately sensitised *M. smegmatis* to ampicillin. This results reinforced the findings of Raymond, *et al.* (2005), emphasising the increased resilience of the wild type strain.

The normal growth phenotype of the wild type (Figure 4.3 (a) Blue) and Δ NamH (Figure 4.3 (b) Blue) strains were used as controls to compare against growth in the presence of ampicillin. The normal cell growth of both strains exited apparent lag phase after 21 hours, during exponential phase demonstrated a doubling time (Td) of 6.54 (wild type) and 7.35 (Δ NamH) hours respectively and plateaued during stationary phase at a maximum optical density of OD_{600nm} 0.3 after 45 hours.

The presence of increasing concentrations of ampicillin led to a gradual increase in the duration of apparent lag phase and the Td within exponential phase as well as a reduction in the final stationary phase OD_{600nm} and the AUC compared to the 0 $\mu\text{g.mL}^{-1}$ strain control. The four lowest ampicillin concentrations 0.015 $\mu\text{g.mL}^{-1}$ (Figure 4.3 Pink), 0.03 $\mu\text{g.mL}^{-1}$ (Figure 4.3 Green), 0.06 $\mu\text{g.mL}^{-1}$ (Figure 4.3 Orange) and 0.125 $\mu\text{g.mL}^{-1}$ (Figure 4.3 Purple) permitted *M. smegmatis* growth of both strains, but displayed a more pronounced effect on the growth of the Δ NamH strain. Variation between the two strains was most evident after the incubation of cells with 0.25 $\mu\text{g.mL}^{-1}$ (Figure 4.3 Red) ampicillin. The wild type strain demonstrated observable growth after 36 hours (Table 4.2) whereas the Δ NamH strain did not show any measurable growth in nutrient media during the 60 hour experiment. The ampicillin MIC for the Δ NamH strain was therefore concluded as 0.25 $\mu\text{g.mL}^{-1}$, half the 0.5 $\mu\text{g.mL}^{-1}$ MIC (Figure 4.3 (a) Yellow) of the wild type.

The growth curves in Figure 4.3 were analysed with a Student's t-test against the normal cellular phenotype expressed in the 0 $\mu\text{g.mL}^{-1}$ control (Table 4.2) of each strain. This showed that the inhibition towards wild type growth attributed to ampicillin at each investigated concentration was deemed statistically significant with p-values <0.001 (0.015 and 0.03 $\mu\text{g.mL}^{-1}$) and <0.0001 (0.06-2 $\mu\text{g.mL}^{-1}$) respectively. Δ NamH strain inhibition attributed to all ampicillin concentrations were also deemed

statistically significant with p-values of <0.001 for ampicillin concentrations 0.015 and $0.03 \mu\text{g.mL}^{-1}$ and <0.0001 for all remaining concentrations between 0.06 to $2 \mu\text{g.mL}^{-1}$.

The significance of the observed variation in the responses of the wild type (Figure 4.3 (a)) and ΔNamH (Figure 4.3 (b)) *M. smegmatis* strains to equivalent ampicillin concentrations showed that variation in antimicrobial inhibition caused by addition of less than $0.03 \mu\text{g.mL}^{-1}$ ampicillin to both strains was not statistically significant with a p-value >0.05 . The variation observed at concentrations greater than $0.03 \mu\text{g.mL}^{-1}$ were deemed statistically significant from one another with p-values at each concentration (0.06 , 0.125 and $0.25 \mu\text{g.mL}^{-1}$) of <0.01 .

To determine if no growth equates to bacterial killing, microtiter plate well contents at the 60 hour time point were pipetted onto TSB agar plates to evaluate ampicillin MBC for both *M. smegmatis* strains. Results are shown in Figure 4.4.

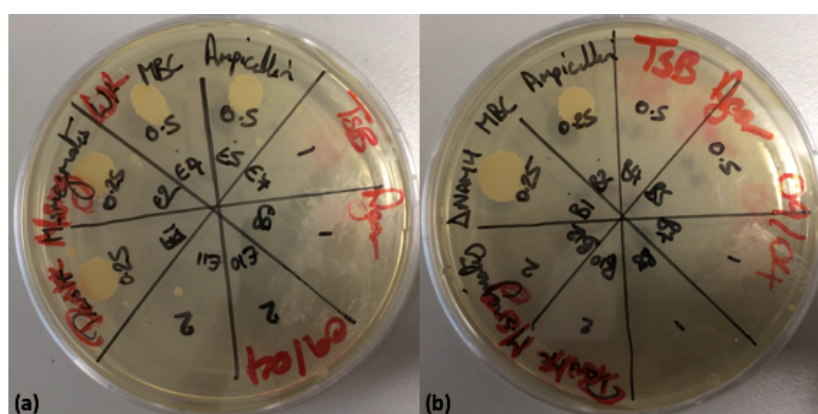


Figure 4.4 Minimal bactericidal concentration of ampicillin against *M. smegmatis* strains. *M. smegmatis* wild type (a) and ΔNamH (b) cells incubated in liquid media with increasing concentrations of ampicillin that did not produce growth (Figure 4.3) were pipetted in duplicate onto TSB agar to determine the MBC. Each quadrant denotes the ampicillin concentration in $\mu\text{g.mL}^{-1}$. Results: Wild type MBC $1 \mu\text{g.mL}^{-1}$, ΔNamH MBC $0.5 \mu\text{g.mL}^{-1}$.

The MBC assessment of wild type (Figure 4.4 (a)) and ΔNamH (Figure 4.4 (b)) cells after incubation with MIC or greater concentrations of ampicillin showed that the ΔNamH strain remained more susceptible to the antimicrobial, with an MBC half the value obtained in the wild type. The MBC values were $1 \mu\text{g.mL}^{-1}$ (wild type) and $0.5 \mu\text{g.mL}^{-1}$ (ΔNamH), which were double the corresponding MIC values for each strain.

4.4.2 Isoniazid MIC assessment of *M. smegmatis* wild type and Δ NamH strains

Isoniazid is one of the four standard first-line antimicrobials against tuberculosis infection (Metcalf, *et al.* 2008). A prodrug activated within mycobacteria by the heme enzyme KatG (Metcalf, *et al.* 2008). Once active, the drug targets mycolic acid synthesis, a major component of the mycobacterial cell wall which forms the mAGP complex (Quemard, *et al.* 1991). The structure of isoniazid is shown in Figure 4.5.

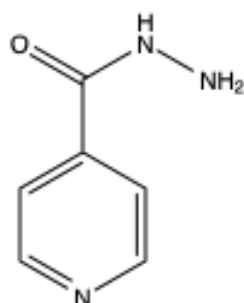


Figure 4.5: The structure of the antibiotic Isoniazid. Molecular weight: 137.14; Chemical formula: C₆H₇N₃O. The above schematic was created using ChemBioDraw.

Raymond, *et al.* (2005) assessed isoniazid activity against the *M. smegmatis* PM965 and PM979 strains and concluded that no variation in susceptibility was observed in the Δ NamH strain compared to the wild type. These findings were reassessed to determine the isoniazid MIC for both strains in Figure 4.6.

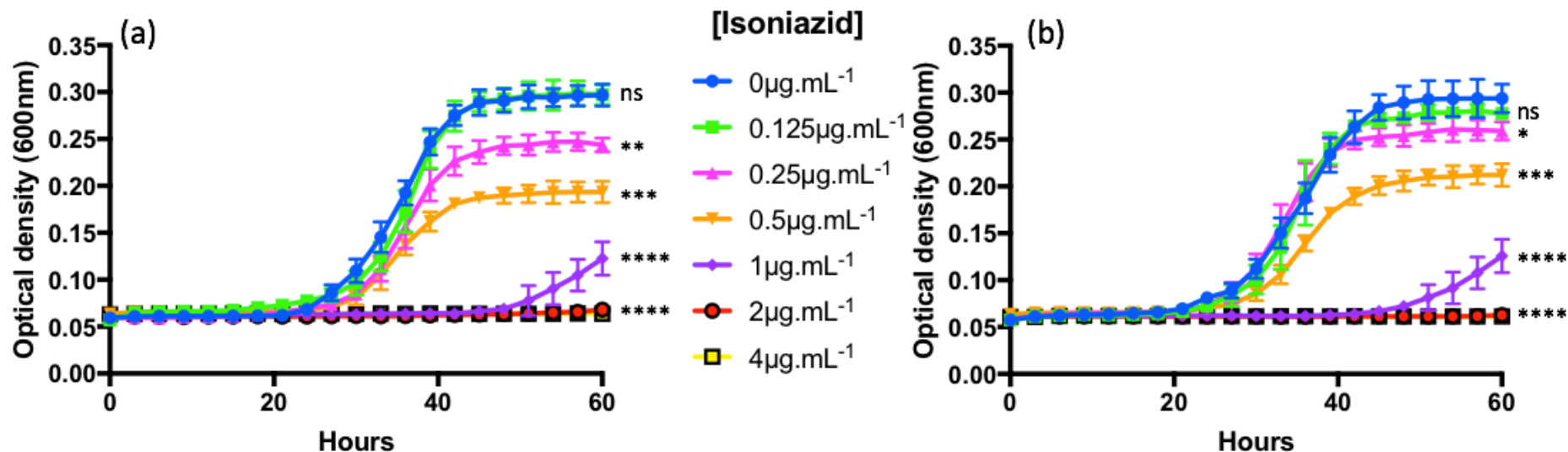


Figure 4.6 The impact of N-glycolylation of peptidoglycan on sensitivity of *M. smegmatis* growth of isoniazid. Wild type (a) and (b) Δ NamH *M. smegmatis* MIC growth curves against isoniazid. Cells were grown in 96-well microtiter plates in triplicate at 37°C with intermittent shaking, OD_{600nm} was measured at 3 hour intervals for 60 hours. Each well contained 100 μ L culture media (7H9, ADC, 0.05% (w/v) Tween 80) with increasing concentrations of isoniazid at a total DMSO concentration of 2% (v/v). *M. smegmatis* wild type (a) and (b) Δ NamH strains were standardized to an OD_{600nm} of 1 and diluted further by a factor of 10⁴ prior to addition to wells and incubation. Error bars represent standard deviation of triplicate measurements. Isoniazid concentrations: 0 μ g.mL⁻¹ (Blue), 0.125 μ g.mL⁻¹ (Green), 0.25 μ g.mL⁻¹ (Pink), 0.5 μ g.mL⁻¹ (Orange), 1 μ g.mL⁻¹ (Purple), 2 μ g.mL⁻¹ (Red), 4 μ g.mL⁻¹ (Yellow). Statistically significant results of comparisons of growth at increasing isoniazid concentrations compared to growth at 0 μ g.mL⁻¹ isoniazid for each strain are indicated with * = p-value <0.05, ** = <0.01, *** = <0.001 and **** = <0.0001. Ns = not statistically significant. Results: Both strains display equal susceptibility to isoniazid. MIC results: Wild type (a) 2 μ g.mL⁻¹, Δ NamH (b) 2 μ g.mL⁻¹.

Isoniazid ($\mu\text{g.mL}^{-1}$)	Wild type <i>M. smegmatis</i>					ΔNamH <i>M. smegmatis</i>					(b) vs (a) p-values
	Apparent Lag phase (h)	Td (h ⁻¹)	AUC (%)	Stationary Phase OD _{600nm}	Wild type p-values (a)	Apparent Lag phase (h)	Td (h ⁻¹)	AUC (%)	Stationary Phase OD _{600nm}	ΔNamH p- values (b)	
0	21	7.14	-	0.30	-	21	7.19	-	0.29	-	>0.05
0.125	21	7.10	99.89	0.30	>0.05	21	7.02	94.28	0.28	>0.05	>0.05
0.25	21	7.10	76.28	0.24	<0.01	21	7.18	91.01	0.26	<0.05	<0.05
0.5	24	7.80	57.68	0.19	<0.001	24	8.85	63.69	0.21	<0.001	>0.05
1	45	13.75	9.48	0.12	<0.0001	45	14.29	9.28	0.12	<0.0001	>0.05
2	60	0.00	0.00	0.05	<0.0001	60	0.00	0.00	0.05	<0.0001	-
4	60	0.00	0.00	0.05	<0.0001	60	0.00	0.00	0.05	<0.0001	-

Table 4.3 Statistical comparisons of *M. smegmatis* growth curves in the presence of increasing concentrations of Isoniazid. Wild type and ΔNamH strains incubated for 60 hours at 37°C with selected concentrations of isoniazid produced growth curves measured at OD_{600nm} in Figure 4.6. Variations between growth curves were measured by time taken to exit apparent lag phase (hours), the doubling time (Td) of cells during exponential phase (hours⁻¹), the area under the curve (AUC) percentage compared to the 0 $\mu\text{g.mL}^{-1}$ control (%), the OD_{600nm} value achieved during stationary phase and whether the growth curve variations were statistically significant compared to each 0 $\mu\text{g.mL}^{-1}$ control with p-values <0.05 deemed significant. The statistical significance of ΔNamH (b) growth curves compared to wild type (a) at equivalent isoniazid concentrations were determined by p-values <0.05.

The absence of the N-glycolyl modification did not appear to impact the isoniazid MIC, with both wild type and Δ NamH strains producing equivalent growth curves at equal concentrations of isoniazid (Table 4.3). In this data set, the growth curves for the wild type (Figure 4.6 (a) Blue) and Δ NamH (Figure 4.6 (b) Blue) strains in the absence of isoniazid were virtually identical to the equivalent data in the ampicillin experiment (Figure 4.3) whereby strains demonstrated an apparent lag phase of 21 hours, produced Td of 7.14 and 7.19 hours respectively and entered stationary phase around OD_{600nm} 0.3 after 45 hours.

The addition of the lowest investigated isoniazid concentration 0.125 $\mu\text{g.mL}^{-1}$ (Figure 4.6 Green) to both strains did not alter the normal distribution of growth compared to the equivalent 0 $\mu\text{g.mL}^{-1}$ control. The duration of apparent lag phase, the Td and the final OD_{600nm} during stationary phase demonstrated no observable inhibition towards cellular growth at 0.125 $\mu\text{g.mL}^{-1}$ isoniazid (Table 4.3). Doubling the concentration of isoniazid to 0.25 $\mu\text{g.mL}^{-1}$ (Figure 4.6 Pink) in both strains only impacted the final OD_{600nm} value during stationary phase. Both the duration of apparent lag phase and Td remained constant to their respective 0 $\mu\text{g.mL}^{-1}$ controls. This variation caused by 0.25 $\mu\text{g.mL}^{-1}$ isoniazid reduced the AUC of both strains to 76.28% (wild type) and 91.01% (Δ NamH) respectively (Table 4.3).

The subsequent isoniazid concentrations 0.5 $\mu\text{g.mL}^{-1}$ (Figure 4.6 Orange) and 1 $\mu\text{g.mL}^{-1}$ (Figure 4.6 Purple) were insufficient to prevent growth during the 60 hour experiment and equally effected both *M. smegmatis* strains increasing apparent lag phase, Td and reducing stationary phase OD (Table 4.3). The AUC values during 0.5 $\mu\text{g.mL}^{-1}$ isoniazid incubation were 57.68% (wild type) and 63.69% (Δ NamH) respectively, whilst during 1 $\mu\text{g.mL}^{-1}$ isoniazid incubation were reduced significantly to 9.48% (wild type) and 9.28% (Δ NamH) (Table 4.3) respectively. The isoniazid MIC for both *M. smegmatis* strains was 2 $\mu\text{g.mL}^{-1}$. Both the wild type (Figure 4.6 (a): Red) and Δ NamH (Figure 4.6 (b): Red) were completely inhibited at this concentration.

A Student's t-test analysis of both strains comparing the inhibition observed in the presence of increasing concentrations of the antimicrobial isoniazid to the 0 $\mu\text{g.mL}^{-1}$ control for each strain produced matching results at almost all investigated

concentrations (Table 4.3). The addition of $0.125 \mu\text{g.mL}^{-1}$ to either strain inhibited growth in a manner that was not deemed statistically significant with p-values >0.05 . The presence of $0.25 \mu\text{g.mL}^{-1}$ isoniazid produced statistically significant results in both strains compared to their $0 \mu\text{g.mL}^{-1}$ controls with p values of <0.01 (Wild type) and <0.05 (ΔNamH) respectively. Isoniazid concentrations greater than $0.25 \mu\text{g.mL}^{-1}$ resulted in equally statistically significant inhibition in both strains culminating in p-values of <0.01 ($0.5 \mu\text{g.mL}^{-1}$) and <0.001 ($1-4 \mu\text{g.mL}^{-1}$) respectively.

T-test comparisons made between strains during incubation with equivalent isoniazid concentrations determined that any strain specific variation in growth curves was deemed not be statistically significant with p-values >0.05 in all concentrations except at $0.25 \mu\text{g.mL}^{-1}$ isoniazid due to the difference noted in measured AUC (Table 4.3), which led to growth curve variation between strains at this sole concentration deemed significant with a p-value of <0.05 .

Wells containing the MIC and higher isoniazid concentrations incubated with both *M. smegmatis* strains were transferred onto TSB agar plates and incubated for 72 hours to determine the MBC values. The results are shown in Figure 4.7.

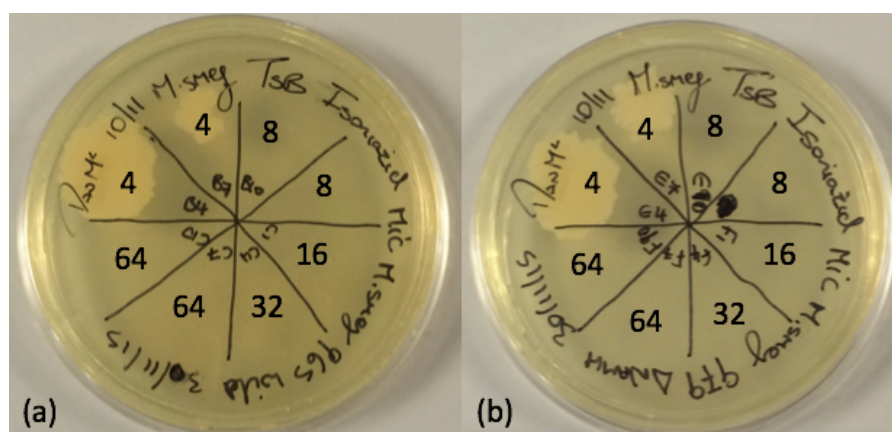


Figure 4.7 Minimal bactericidal concentration of isoniazid against *M. smegmatis* strains. *M. smegmatis* wild type (a) and ΔNamH (b) cells incubated in liquid media with increasing concentrations of isoniazid that did not produce growth (Figure 4.6) were pipetted in duplicate onto TSB agar to determine MBC. Each quadrant denotes the isoniazid concentration in $\mu\text{g.mL}^{-1}$. Results: Wild type MBC $8 \mu\text{g.mL}^{-1}$, ΔNamH MBC $8 \mu\text{g.mL}^{-1}$.

As observed in the MIC growth curve analysis (Figure 4.6) the isoniazid MBC for both strains was $8 \mu\text{g}\cdot\text{mL}^{-1}$. Therefore, the presence of the N-glycolyl modification present in the wild type *M. smegmatis* peptidoglycan did not alter MBC relative to the ΔNamH strain which possessed exclusively MurNAc based peptidoglycan. The isoniazid MBC was 4 times greater than the isoniazid MIC values of $2 \mu\text{g}\cdot\text{mL}^{-1}$.

4.4.3 Ramoplanin MIC assessment of *M. smegmatis* wild type and ΔNamH strains

Ramoplanin is a gram-positive-directed, broad spectrum antimicrobial which inhibits transglycosylase activity of PBPs by binding specifically to Lipid II and preventing the extension of peptidoglycan chains (Fang, *et al.* 2006). Ramoplanin was initially proposed to inhibit MurG through binding of Lipid I (Reynolds, *et al.* 1990), although due to its size and high solubility is unlikely that ramoplanin would easily traverse the cell membrane (Fang, *et al.* 2006). The structure of ramoplanin is detailed in Figure 4.8.

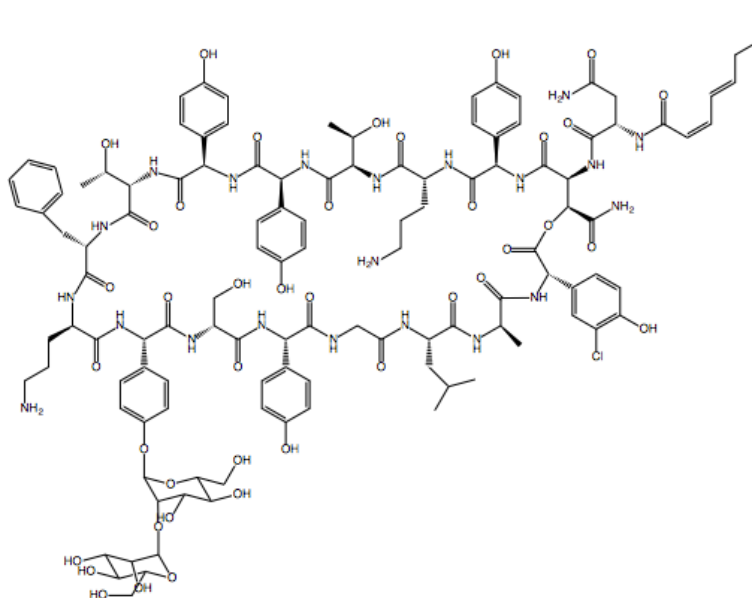


Figure 4.8: The structure of the glycolipodepsipeptide antibiotic Ramoplanin. Molecular weight: 2524.04; Chemical formula: $\text{C}_{117}\text{H}_{150}\text{ClN}_{21}\text{O}_{40}$. The above schematic was created using ChemBioDraw.

The MIC of ramoplanin with respect to inhibition of growth of both *M. smegmatis* strains was assessed in Figure 4.9.

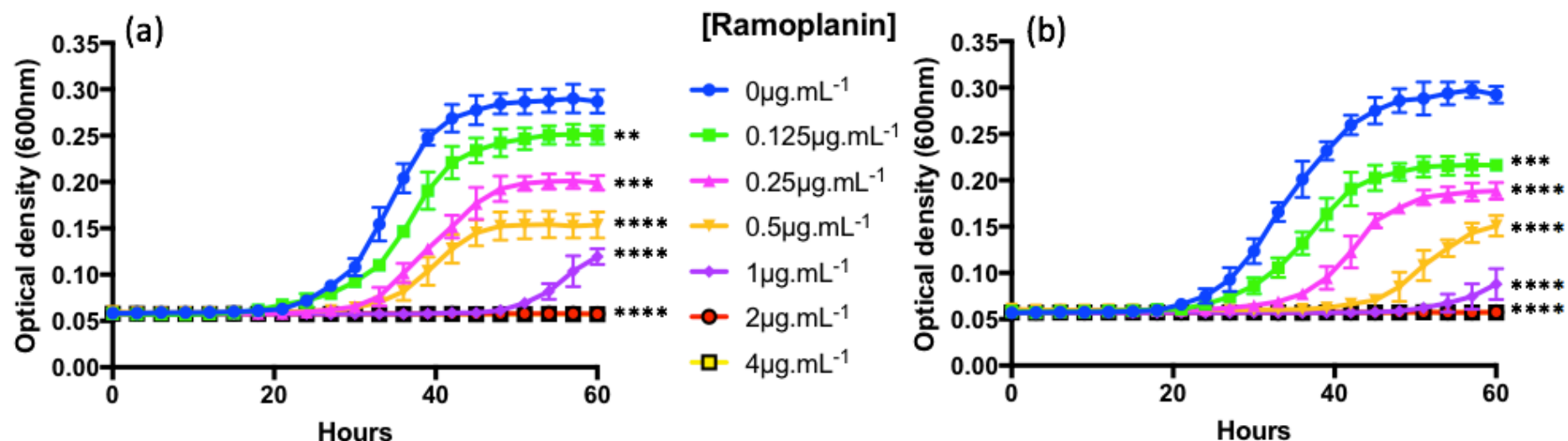


Figure 4.9 The impact of N-glycosylation of peptidoglycan on sensitivity of *M. smegmatis* growth of ramoplanin. Wild type (a) and (b) Δ NamH *M. smegmatis* MIC growth curves against ramoplanin. Cells were grown in 96-well microtiter plates in triplicate at 37°C with intermittent shaking, OD_{600nm} was measured at 3 hour intervals for 60 hours. Each well contained 100 μ L culture media (7H9, ADC, 0.05% (w/v) Tween 80) with increasing concentrations of ramoplanin with a total DMSO concentration of 2% (v/v). The cultured *M. smegmatis* wild type (a) and (b) Δ NamH strains were standardized to an OD_{600nm} of 1 and diluted further by a factor of 10⁴ prior to addition to wells and incubation. Error bars represent standard deviation of triplicate measurements. Ramoplanin concentrations: 0 μ g.mL⁻¹ (Blue), 0.125 μ g.mL⁻¹ (Green), 0.25 μ g.mL⁻¹ (Pink), 0.5 μ g.mL⁻¹ (Orange), 1 μ g.mL⁻¹ (Purple), 2 μ g.mL⁻¹ (Red), 4 μ g.mL⁻¹ (Yellow), 8 μ g.mL⁻¹ (Black) and 16 μ g.mL⁻¹ (Brown). Statistically significant results of comparisons of growth at increasing ramoplanin concentrations compared to growth at 0 μ g.mL⁻¹ ramoplanin for each strain are indicated with * = p-value <0.05, ** = <0.01, *** = <0.001 and **** = <0.0001. Ns = not statistically significant. Results: Both strains display equal susceptibility to ramoplanin. MIC results: Wild type (a) 2 μ g.mL⁻¹, Δ NamH (b) 2 μ g.mL⁻¹.

Ramoplanin ($\mu\text{g.mL}^{-1}$)	Wild type <i>M. smegmatis</i>					ΔNamH <i>M. smegmatis</i>					(b) vs (a) p- values
	Apparent Lag phase (h)	Td (h^{-1})	AUC (%)	Stationary Phase $\text{OD}_{600\text{nm}}$	Wild type p-values (a)	Apparent Lag phase (h)	Td (h^{-1})	AUC (%)	Stationary Phase $\text{OD}_{600\text{nm}}$	ΔNamH p- values (b)	
0	21	7.22	-	0.29	-	21	7.81	-	0.29	-	>0.05
0.125	21	8.43	77.34	0.25	<0.01	24	9.53	62.07	0.21	<0.001	<0.01
0.25	30	9.04	48.99	0.20	<0.0001	33	8.80	38.96	0.19	<0.0001	<0.01
0.5	30	10.20	33.26	0.15	<0.0001	42	10.40	14.59	0.15	<0.0001	<0.001
1	54	11.32	5.36	0.12	<0.0001	54	11.12	1.89	0.09	<0.0001	<0.05
2	60	0.00	0.00	0.05	<0.0001	60	0.00	0.00	0.05	<0.0001	-
4	60	0.00	0.00	0.05	<0.0001	60	0.00	0.00	0.05	<0.0001	-
8	60	0.00	0.00	0.05	<0.0001	60	0.00	0.00	0.05	<0.0001	-
16	60	0.00	0.00	0.05	<0.0001	60	0.00	0.00	0.05	<0.0001	-

Table 4.4 Statistical comparisons of *M. smegmatis* growth curves in the presence of increasing concentrations of Ramoplanin. Wild type and ΔNamH strains incubated for 60 hours at 37°C with selected concentrations of Ramoplanin produced growth curves measured at $\text{OD}_{600\text{nm}}$ in Figure 4.9. Variations between growth curves were measured by time taken to exit apparent lag phase (hours), the doubling time (Td) of cells during exponential phase (hours^{-1}), the area under the curve (AUC) percentage compared to the 0 $\mu\text{g.mL}^{-1}$ control (%), the $\text{OD}_{600\text{nm}}$ value achieved during stationary phase and whether the growth curve variations were statistically significant compared to each 0 $\mu\text{g.mL}^{-1}$ control with p-values <0.05 deemed significant. The statistical significance of ΔNamH (b) growth curves compared to wild type (a) at equivalent Ramoplanin concentrations were determined by p-values <0.05.

The control growth curves demonstrated by the wild type (Figure 4.9 (a) Blue) and Δ NamH (Figure 4.9 (b) Blue) strains in the absence of the ramoplanin during this 60 hour incubation was used as a marker to compared the incubation of increasing antimicrobial concentrations. In this set of experiments, cells exited apparent lag phase after 21 hours, produced a Td of 7.22 (wild type) and 7.81 (Δ NamH) hours respectively and both reached an OD_{600nm} of 0.29 after 45 hours during stationary phase (Table 4.4).

The addition of increasing concentrations of ramoplanin resulted in an equivalent MIC of 2 $\mu\text{g.mL}^{-1}$ (Figure 4.9 Red) for both strains during the 60 hour experiment. The lower preceding ramoplanin concentrations 0.125 $\mu\text{g.mL}^{-1}$ (Figure 4.9 Green), 0.25 $\mu\text{g.mL}^{-1}$ (Figure 4.9 Pink), 0.5 $\mu\text{g.mL}^{-1}$ (Figure 4.9 Orange) and 1 $\mu\text{g.mL}^{-1}$ (Figure 4.9 Purple) demonstrated a gradual decline in growth measured by the reduction in the AUC of both strains compared to their respective 0 $\mu\text{g.mL}^{-1}$ controls (Table 4.4), although inhibition was observed to a greater degree in the Δ NamH strain.

The growth curves of both wild type and Δ NamH strains in the presence of increasing concentrations of ramoplanin were analysed with a Student's t-test against the equivalent growth curve of each strain in the absence of the antimicrobial to determine where observed inhibition was statistically significant (Table 4.4). Results show that all investigated concentrations of ramoplanin produced statistically significant inhibition compared to the strain's respective 0 $\mu\text{g.mL}^{-1}$ control. The addition of the lowest investigated concentration 0.125 $\mu\text{g.mL}^{-1}$ led to significant inhibition in both strains with p-values of <0.01 (Wild type) and <0.001 (Δ NamH) respectively. Subsequent concentrations (0.25-16 $\mu\text{g.mL}^{-1}$) of ramoplanin produced equivalent statistical significance in both strains with p-values of <0.0001 for each investigated concentration.

Comparative Student's t-tests between the wild type and Δ NamH strains at equivalent concentrations of ramoplanin were assessed to determine if inter-strain growth curve variation was statistically significant (Table 4.4). Results demonstrated that all observed differences between strains at matching concentrations were found to be statistically significant with p-values of <0.01 (0.125 and 0.25 $\mu\text{g.mL}^{-1}$), <0.001 (0.5 $\mu\text{g.mL}^{-1}$) and <0.05 (1 $\mu\text{g.mL}^{-1}$) respectively.

After the 60 hours incubation period, wells which did not produce observable *M. smegmatis* growth for either strain were pipetted in 10 μL volumes onto TSB agar and incubated at 37°C for 72 hours for MBC assessment. Results are shown in Figure 4.10.

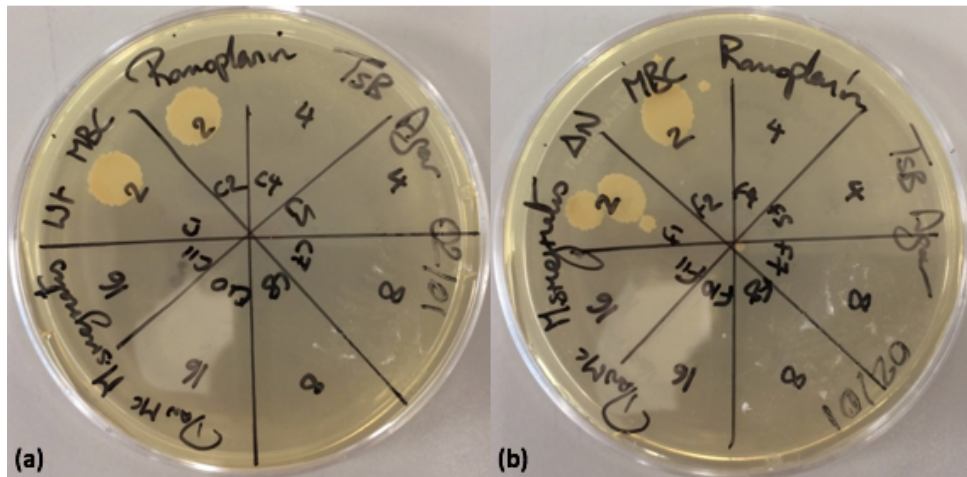


Figure 4.10 Minimal bactericidal concentration of ramoplanin against *M. smegmatis* strains. *M. smegmatis* wild type (a) and ΔNamH (b) cells incubated in liquid media with increasing concentrations of ramoplanin that did not produce growth (Figure 4.9) were pipetted in duplicate onto TSB agar to determine MBC. Each quadrant denotes the ramoplanin concentration the *M. smegmatis* strains were exposed to in $\mu\text{g.mL}^{-1}$. Results: Wild type MBC 4 $\mu\text{g.mL}^{-1}$, ΔNamH MBC 4 $\mu\text{g.mL}^{-1}$.

The ramoplanin MBC assessment in Figure 4.10 showed that both *M. smegmatis* strains had the equivalent MBC value of 4 $\mu\text{g.mL}^{-1}$. Cells incubated at ramoplanin concentrations 4 $\mu\text{g.mL}^{-1}$, 8 $\mu\text{g.mL}^{-1}$ or 16 $\mu\text{g.mL}^{-1}$ were unable to propagate on TSB agar. This concentration was double the MIC value (Figure 4.9) for each *M. smegmatis* strain.

4.4.4 Tunicamycin MIC assessment of *M. smegmatis* wild type and Δ NamH strains

Tunicamycin is an antimicrobial that targets numerous cellular processes. The inhibitor prevents protein N-glycosylation and impacts not only peptidoglycan biosynthesis but also the bridging of teichoic acids to peptidoglycan (Price, *et al.* 2005). The peptidoglycan biosynthesis target of tunicamycin is the active site of MraY which it irreversibly binds to preventing the conversion of undecaprenyl phosphate and UDP-MurNAc-pentapeptide to Lipid I (Al-Dabbagh, *et al.* 2008). The structure of tunicamycin is shown in Figure 4.11.

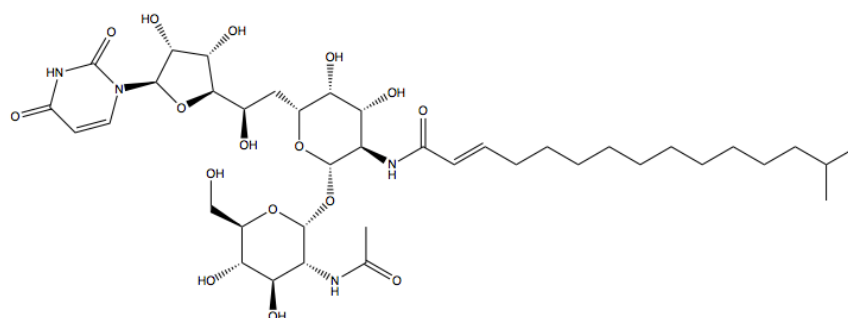


Figure 4.11: The structure of the Tunicamycin. Molecular weight: 844.95; Chemical formula: $C_{39}H_{64}N_4O_{16}$. The above schematic was created using ChemBioDraw.

To determine the impact of N-glycosylation of peptidoglycan on mycobacterial sensitivity to this antibiotic, the tunicamycin MIC for *M. smegmatis* wild type and Δ NamH strains were determined (Figure 4.12).

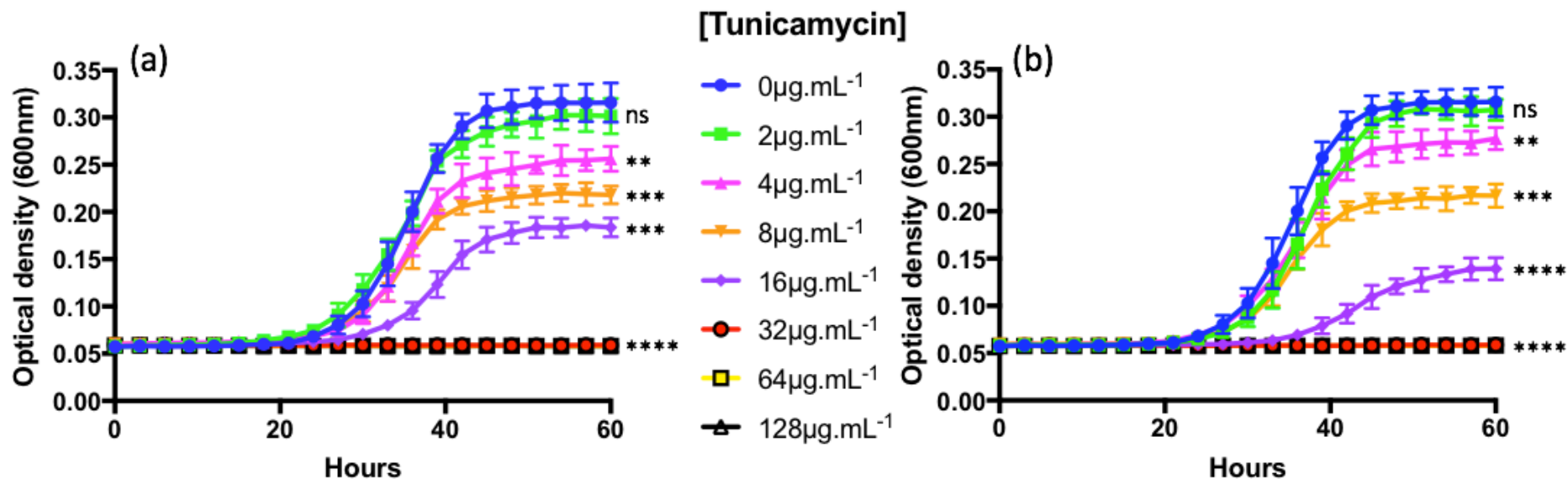


Figure 4.12 The impact of N-glycosylation of peptidoglycan on sensitivity of *M. smegmatis* growth to tunicamycin. Wild type (a) and (b) ΔNamH *M. smegmatis* MIC growth curves against tunicamycin. Cells were grown in 96-well microtiter plates in triplicate at 37°C with intermittent shaking, $\text{OD}_{600\text{nm}}$ was measured at 3 hour intervals for 60 hours. Each well contained 100 μL culture media (7H9, ADC, 0.05% (w/v) Tween 80) with increasing concentrations of tunicamycin at a total DMSO concentration of 2% (v/v). *M. smegmatis* wild type (a) and (b) ΔNamH strains were standardized to an $\text{OD}_{600\text{nm}}$ of 1 and diluted further by a factor of 10^4 prior to addition to wells and incubation. Error bars represent standard deviation of triplicate measurements. Tunicamycin concentrations: 0 $\mu\text{g.mL}^{-1}$ (Blue), 2 $\mu\text{g.mL}^{-1}$ (Green), 4 $\mu\text{g.mL}^{-1}$ (Pink), 8 $\mu\text{g.mL}^{-1}$ (Orange), 16 $\mu\text{g.mL}^{-1}$ (Purple), 32 $\mu\text{g.mL}^{-1}$ (Red) and 64 $\mu\text{g.mL}^{-1}$ (Yellow). Statistically significant results of comparison of growth at increasing tunicamycin concentrations compared to growth at 0 $\mu\text{g.mL}^{-1}$ tunicamycin for this strain are indicated with * = p-value <0.05, ** = <0.01, *** = <0.001 and **** = <0.0001. Ns = not statistically significant. Results: Both strains display equal susceptibility to tunicamycin. MIC results: Wild type (a) 32 $\mu\text{g.mL}^{-1}$, ΔNamH (b) 32 $\mu\text{g.mL}^{-1}$.

Tunicamycin ($\mu\text{g.mL}^{-1}$)	Wild type <i>M. smegmatis</i>					ΔNamH <i>M. smegmatis</i>					(b) vs (a) p- values
	Apparent Lag phase (h)	Td (h^{-1})	AUC (%)	Stationary Phase $\text{OD}_{600\text{nm}}$	Wild type p-values (a)	Apparent Lag phase (h)	Td (h^{-1})	AUC (%)	Stationary Phase $\text{OD}_{600\text{nm}}$	ΔNamH p- values (b)	
0	21	6.82	-	0.31	-	21	6.73	-	0.31	-	>0.05
2	21	7.93	97.02	0.30	>0.05	21	7.44	90.34	0.30	>0.05	>0.05
4	21	7.62	76.78	0.25	<0.01	21	8.19	82.83	0.27	<0.01	>0.05
8	21	8.69	64.68	0.22	<0.001	21	8.56	60.93	0.21	<0.001	>0.05
16	30	11.30	42.37	0.18	<0.001	36	13.56	20.50	0.14	<0.0001	<0.001
32	60	0.00	0.00	0.05	<0.0001	60	0.00	0.00	0.05	<0.0001	-
64	60	0.00	0.00	0.05	<0.0001	60	0.00	0.00	0.05	<0.0001	-
128	60	0.00	0.00	0.05	<0.0001	60	0.00	0.00	0.05	<0.0001	-

Table 4.5 Statistical comparisons of *M. smegmatis* growth curves in the presence of increasing concentrations of tunicamycin. Wild type and ΔNamH strains incubated for 60 hours at 37°C with selected concentrations of tunicamycin produced growth curves measured at $\text{OD}_{600\text{nm}}$ in Figure 4.12. Variations between growth curves were measured by time taken to exit apparent lag phase (hours), the doubling time (Td) of cells during exponential phase (hours^{-1}), the area under the curve (AUC) percentage compared to the 0 $\mu\text{g.mL}^{-1}$ control (%), the $\text{OD}_{600\text{nm}}$ value achieved during stationary phase and whether the growth curve variations were statistically significant compared to each 0 $\mu\text{g.mL}^{-1}$ control with p-values <0.05 deemed significant. The statistical significance of ΔNamH (b) growth curves compared to wild type (a) at equivalent tunicamycin concentrations were determined by p-values <0.05.

In this set of experiments, the *M. smegmatis* wild type (Figure 4.12 (a) Blue) and Δ NamH (Figure 4.12 (b) Blue) control growth curves both exited apparent lag phase after 21 hours, with a log phase Td of 6.82 and 6.73 hours respectively and both plateaued after 45 hours at an OD_{600nm} of 0.31 (Table 4.5). The addition of the lowest concentration to both *M. smegmatis* strains 2 $\mu\text{g.mL}^{-1}$ (Figure 4.12 Green), led to similar growth curves to the 0 $\mu\text{g.mL}^{-1}$ controls in terms of apparent lag phase duration and final stationary phase OD but differed when measuring exponential phase. The Td of each growth curve increased by around an hour to 7.93 (wild type) and 7.44 (Δ NamH) hours respectively. The subsequent tunicamycin concentrations 4 $\mu\text{g.mL}^{-1}$ (Figure 4.12 Pink) and 8 $\mu\text{g.mL}^{-1}$ (Figure 4.12 Orange) did not impact apparent lag phase which remained constant at 21 hours (Table 4.5) but reduced the AUC of both strains by further increasing Td and reducing stationary phase.

The final sub MIC of tunicamycin investigated for both strains was 16 $\mu\text{g.mL}^{-1}$ (Figure 4.12 Purple). At this concentration deviation was observed between the two strains for the first time. The previous concentrations of tunicamycin produced a maximum of 7% variation between AUC values of each strain at equivalent concentrations compared to their respective control (Table 4.5). The addition of 16 $\mu\text{g.mL}^{-1}$ extended apparent lag phase by 6 hours in the NamH strain compared to the wild type resulting in a 21.87% difference in AUC values. The tunicamycin MIC for both strains was equivalent at 32 $\mu\text{g.mL}^{-1}$ (Figure 4.12 Red).

A Student's t-test analysis of both the wild type and Δ NamH strains against increasing concentrations of tunicamycin compared to their respective 0 $\mu\text{g.mL}^{-1}$ control (Table 4.5), demonstrated that the addition of the antimicrobial at 2 $\mu\text{g.mL}^{-1}$ produced no statistically significant inhibition (p-value >0.05). Investigated concentrations above this 2 $\mu\text{g.mL}^{-1}$ threshold for both strains were each deemed statistically significant. The inhibition observed at 4 and 8 $\mu\text{g.mL}^{-1}$ tunicamycin produced p-values of <0.01 and <0.001 respectively. The statistical significance of the inhibition attributed to 16 $\mu\text{g.mL}^{-1}$ tunicamycin against the Δ NamH (p-value <0.0001) strain was more pronounced than the wild type (<0.001). This result was the only observed difference between the two strains with all subsequent tunicamycin concentrations (32-128 $\mu\text{g.mL}^{-1}$) generating p-values of <0.0001.

Comparisons made between the two strains at each concentration of tunicamycin indicated that all variations observed between strains at equivalent concentrations was not statistically significant (p-values >0.05), except the variation noted between the two strains at 16 $\mu\text{g.mL}^{-1}$ which was deemed statistically significant with a p-value of <0.001.

Concentrations of tunicamycin which did not produce observable growth, 32 $\mu\text{g.mL}^{-1}$ or greater were transferred onto TSB agar plates to measure the MBC. Results are shown in Figure 4.13.

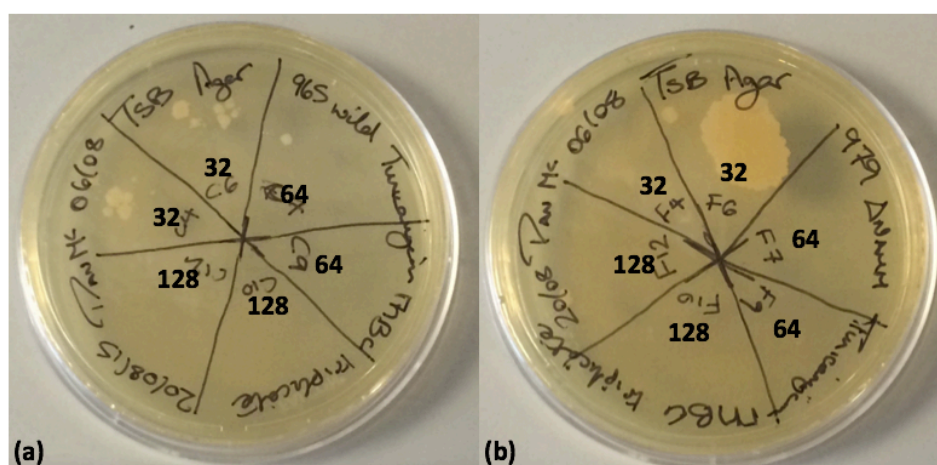


Figure 4.13 Minimal bactericidal concentration of tunicamycin against *M. smegmatis* strains. *M. smegmatis* wild type (a) and ΔNamH (b) cells incubated in liquid media with increasing concentrations of tunicamycin that did not produce growth (Figure 4.12) were pipetted in duplicate onto TSB agar to determine MBC. Each quadrant denotes the tunicamycin concentration in $\mu\text{g.mL}^{-1}$. Results: Wild type MBC 64 $\mu\text{g.mL}^{-1}$, ΔNamH MBC 64 $\mu\text{g.mL}^{-1}$.

Tunicamycin MBC assessment (Figure 4.13) showed that although 32 $\mu\text{g.mL}^{-1}$ tunicamycin (Figure 4.12 Red) was the MIC sufficient to inhibit growth during antimicrobial incubation, this concentration was not completely bactericidal towards *M. smegmatis* cells. Increasing the tunicamycin concentration to 64 $\mu\text{g.mL}^{-1}$ led to a lack of observable growth for both strains and was therefore defined as the MBC.

4.4.5 Mersacidin MIC assessment of *M. smegmatis* wild type and Δ NamH strains

Mersacidin is an antimicrobial peptide made from 20 amino acids including uncommon residues such as lanthionine and is therefore termed as a lantibiotic (Schmitz, *et al.* 2006). The structure of mersacidin is shown in Figure 4.14.

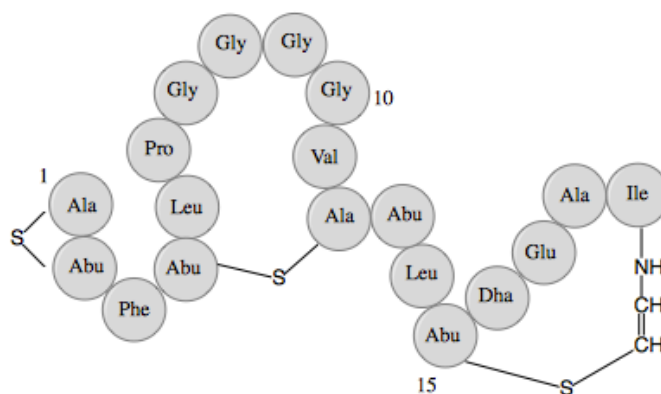


Figure 4.14: The structure of the lantibiotic Mersacidin. The above schematic was created using ChemBioDraw. Unusual amino acid abbreviations: Abu aminobutyric acid; Dha: dehydroalanine.

Mersacidin is targeted towards Lipid II, binding to which inhibits transglycosylase activity and the formation of elongated peptidoglycan chains (Appleyard, *et al.* 2009). Mersacidin activity is most pronounced towards Gram-positive organisms due to the increased cellular percentage of peptidoglycan (Schleifer and Kandler 1972). Assessment of the mersacidin MIC against the two *M. smegmatis* strains at a concentration range of 2 $\mu\text{g.mL}^{-1}$ to 128 $\mu\text{g.mL}^{-1}$ is shown in Figure 4.15.

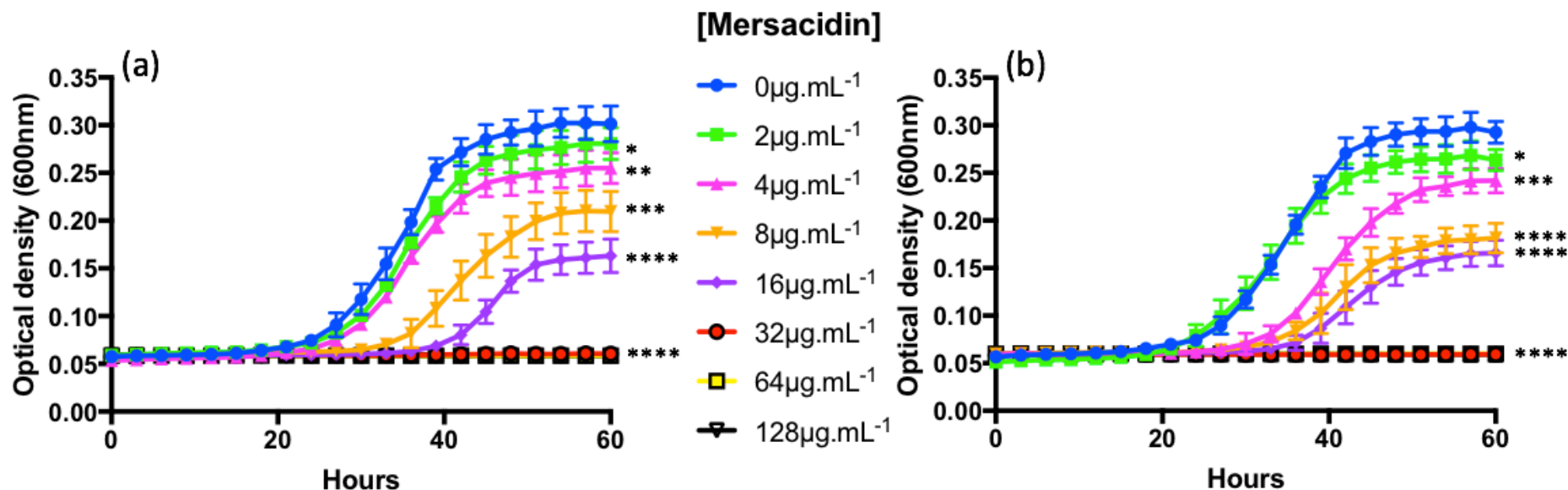


Figure 4.15 The impact of N-glycolylation of peptidoglycan on sensitivity of *M. smegmatis* growth on mersacidin. Wild type (a) and (b) ΔNamH *M. smegmatis* MIC growth curves against mersacidin. Cells were grown in 96-well microtiter plates in triplicate at 37°C with intermittent shaking, $\text{OD}_{600\text{nm}}$ was measured at 3 hour intervals for 60 hours. Each well contained 100 μL culture media (7H9, ADC, 0.05% (w/v) Tween 80) with increasing concentrations of mersacidin with a total DMSO concentration of 2% (v/v). *M. smegmatis* wild type (a) and (b) ΔNamH strains were standardized to an $\text{OD}_{600\text{nm}}$ of 1 and diluted further by a factor of 10^4 prior to addition to wells and incubation. Error bars represent standard deviation of triplicate measurements. Mersacidin concentrations: 0 $\mu\text{g.mL}^{-1}$ (Blue), 2 $\mu\text{g.mL}^{-1}$ (Green), 4 $\mu\text{g.mL}^{-1}$ (Pink), 8 $\mu\text{g.mL}^{-1}$ (Orange), 16 $\mu\text{g.mL}^{-1}$ (Purple), 32 $\mu\text{g.mL}^{-1}$ (Red), 64 $\mu\text{g.mL}^{-1}$ (Yellow) and 128 $\mu\text{g.mL}^{-1}$ (Black). Statistically significant results of comparison of growth at increasing mersacidin concentrations compared to growth at 0 $\mu\text{g.mL}^{-1}$ mersacidin for each strain are indicated with * = p-value <0.05, ** = <0.01, *** = <0.001 and **** = <0.0001. Ns = not statistically significant. Results: Both strains were equally susceptible to mersacidin. MIC results: Wild type (a) 32 $\mu\text{g.mL}^{-1}$, ΔNamH (b) 32 $\mu\text{g.mL}^{-1}$.

Mersacidin ($\mu\text{g.mL}^{-1}$)	Wild type <i>M. smegmatis</i>					ΔNamH <i>M. smegmatis</i>					(b) vs (a) p- values
	Apparent Lag phase (h)	Td (h^{-1})	AUC (%)	Stationary Phase OD _{600nm}	Wild type p-values (a)	Apparent Lag phase (h)	Td (h^{-1})	AUC (%)	Stationary Phase OD _{600nm}	ΔNamH p- values (b)	
0	21	7.78	-	0.30	-	21	7.72	-	0.29	-	>0.05
2	21	7.99	87.58	0.28	<0.05	21	9.17	92.11	0.26	<0.05	>0.05
4	24	7.99	76.68	0.25	<0.01	30	9.48	58.99	0.24	<0.001	<0.001
8	33	9.00	44.44	0.21	<0.001	33	10.69	38.73	0.18	<0.0001	<0.01
16	42	8.94	24.54	0.16	<0.0001	36	10.31	30.32	0.16	<0.0001	<0.01
32	60	0.00	0.00	0.05	<0.0001	60	0.00	0.00	0.05	<0.0001	-
64	60	0.00	0.00	0.05	<0.0001	60	0.00	0.00	0.05	<0.0001	-
128	60	0.00	0.00	0.05	<0.0001	60	0.00	0.00	0.05	<0.0001	-

Table 4.6 Statistical comparisons of *M. smegmatis* growth curves in the presence of increasing concentrations of mersacidin. Wild type and ΔNamH strains incubated for 60 hours at 37°C with selected concentrations of mersacidin produced growth curves measured at OD_{600nm} in Figure 4.15. Variations between growth curves were measured by time taken to exit apparent lag phase (hours), the doubling time (Td) of cells during exponential phase (hours^{-1}), the area under the curve (AUC) percentage compared to the 0 $\mu\text{g.mL}^{-1}$ control (%), the OD_{600nm} value achieved during stationary phase and whether the growth curve variations were statistically significant compared to each 0 $\mu\text{g.mL}^{-1}$ control with p-values <0.05 deemed significant. The statistical significance of ΔNamH (b) growth curves compared to wild type (a) at equivalent mersacidin concentrations were determined by p-values <0.05.

In this set of experiments the standard 0 $\mu\text{g.mL}^{-1}$ mersacidin wild type (Figure 4.15 (a): Blue) and ΔNamH (Figure 4.15 (b): Blue) control growth curves were characterised by identical 21 hour apparent lag phases before entering exponential phase with Td values of 7.78 (wild type) and 7.72 (ΔNamH) hours respectively. Growth of both strains plateaued after 45 hours at OD_{600nm} of 0.3 (wild type) and 0.29 (ΔNamH) respectively (Table 4.6).

The addition of mersacidin at the lowest investigated concentration, 2 $\mu\text{g.mL}^{-1}$ (Figure 4.15 Green) demonstrated equivalent inhibition towards each strain. The antimicrobial at this concentration did not impact the duration of the apparent lag phase, although it did marginally increase the Td and reduce the final stationary phase OD. This resulted in an AUC reduction to around 90% of their respective 0 $\mu\text{g.mL}^{-1}$ controls (Table 4.6). Doubling the concentration of mersacidin to 4 $\mu\text{g.mL}^{-1}$ (Figure 4.15 Pink) led to the most notable variation between the two strains, demonstrating an increased potency towards the ΔNamH strain not observed during incubation at 2 $\mu\text{g.mL}^{-1}$. The two strains produced a 6 hour difference in duration of the apparent lag phase with 24 hours for the wild type and 30 hours for the ΔNamH strain. This result combined with the wild type Td of 7.99 hours compared to ΔNamH 9.48 hours led to an AUC difference of 17.69% (Table 4.6).

The subsequent mersacidin concentrations 8 $\mu\text{g.mL}^{-1}$ (Figure 4.15 Orange) and 16 $\mu\text{g.mL}^{-1}$ (Figure 4.15 Purple) permitted growth of both *M. smegmatis* strains. Both concentrations led to similar Td values in the wild type (9 hours) and ΔNamH (10 hours) strains, although the apparent lag phase was more pronounced in both strains at the highest concentration (Table 4.6). 32 $\mu\text{g.mL}^{-1}$ (Figure 4.15 Red) mersacidin was sufficient to present no observation of *M. smegmatis* growth of either strain and was therefore identified as the MIC value.

Statistical significance of the impact of mersacidin on *M. smegmatis* wild type was determined relative to growth in the absence of the drug by a Student's t-test (Table 4.6). The wild type inhibition observed during incubation with all investigated concentrations of mersacidin were measured as statistically significant with p-values of <0.05 (2 $\mu\text{g.mL}^{-1}$), <0.01 (4 $\mu\text{g.mL}^{-1}$), <0.001 (8 $\mu\text{g.mL}^{-1}$) and <0.0001 (16-128 $\mu\text{g.mL}^{-1}$).

¹⁾ respectively. Inhibition attributed to all mersacidin concentrations against *M. smegmatis* Δ NamH cells were statistically significant (Table 4.6) with p-values <0.05 ($2 \mu\text{g.mL}^{-1}$), <0.001 ($4 \mu\text{g.mL}^{-1}$) and <0.0001 ($8-128 \mu\text{g.mL}^{-1}$).

Comparative t-test analysis comparing wild type and Δ NamH growth curves at the same concentrations of mersacidin (Table 4.6) demonstrated that growth curve variation at $2 \mu\text{g.mL}^{-1}$ was not statistically significant (p-value >0.05). All subsequent mersacidin concentrations demonstrating increased potency towards the Δ NamH strain were statistically significant with p-values of <0.001 ($4 \mu\text{g.mL}^{-1}$) and <0.01 (8 and $16 \mu\text{g.mL}^{-1}$) respectively.

Wells containing both *M. smegmatis* strains incubated with mersacidin concentrations 32 , 64 and $128 \mu\text{g.mL}^{-1}$ were pipetted onto TSB agar to determine the mersacidin MBC. Results are shown in Figure 4.16.

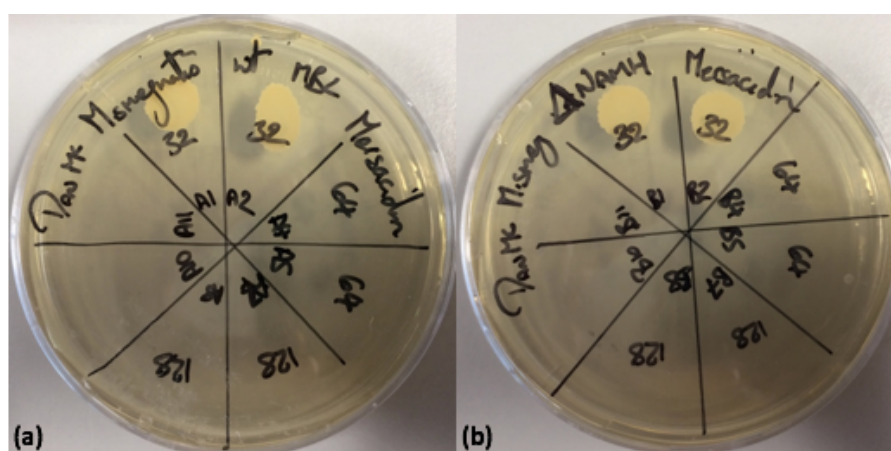


Figure 4.16 Minimal bactericidal concentration of mersacidin against *M. smegmatis* strains. *M. smegmatis* wild type (a) and Δ NamH (b) cells incubated in liquid media with increasing concentrations of mersacidin that did not produce growth (Figure 4.15) were pipetted in duplicate onto TSB agar to determine MBC. Each quadrant denotes the mersacidin concentration in $\mu\text{g.mL}^{-1}$. Results: Wild type MBC $64 \mu\text{g.mL}^{-1}$, Δ NamH MBC $64 \mu\text{g.mL}^{-1}$.

Mersacidin at $64 \mu\text{g.mL}^{-1}$ or greater (Figure 4.16) was bactericidal to both strains equally and so $64 \mu\text{g.mL}^{-1}$ was determined to be the MBC.

4.4.6 Moenomycin MIC assessment of *M. smegmatis* wild type and Δ NamH strains

Moenomycin is an antimicrobial which reversibly binds directly to the active site of peptidoglycan glycosyltransferases (PGTs), preventing the extension of peptidoglycan chains by addition of Lipid II (Ostash, *et al.* 2009). The structure of the phosphoglycolipid antibiotic moenomycin shown in Figure 4.17 strongly resembles the known structure of Lipid IV, comprised of two Lipid II subunits.

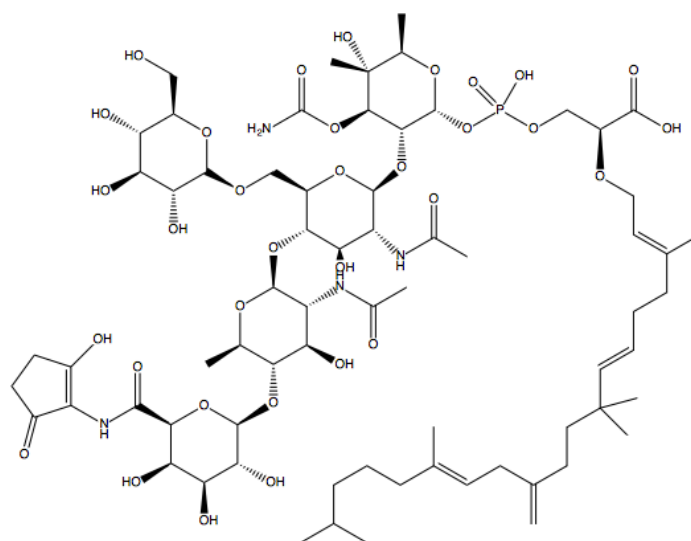


Figure 4.17: The structure of the glycosyltransferase antibiotic Moenomycin. Molecular weight: 1554.62; Chemical formula: $C_{69}H_{111}N_4O_{33}P$. The above schematic was created using ChemBioDraw.

Moenomycin was original identified as a product of *Streptomyces ghanaensis* (Ostash, *et al.* 2009) and demonstrated potent activity towards gram-positive organisms, but due to unsuitable pharmacokinetics more commonly administered in agriculture (Galley, *et al.* 2014). The MIC of moenomycin against both *M. smegmatis* PM965 and PM979 strains was assessed in Figure 4.18.

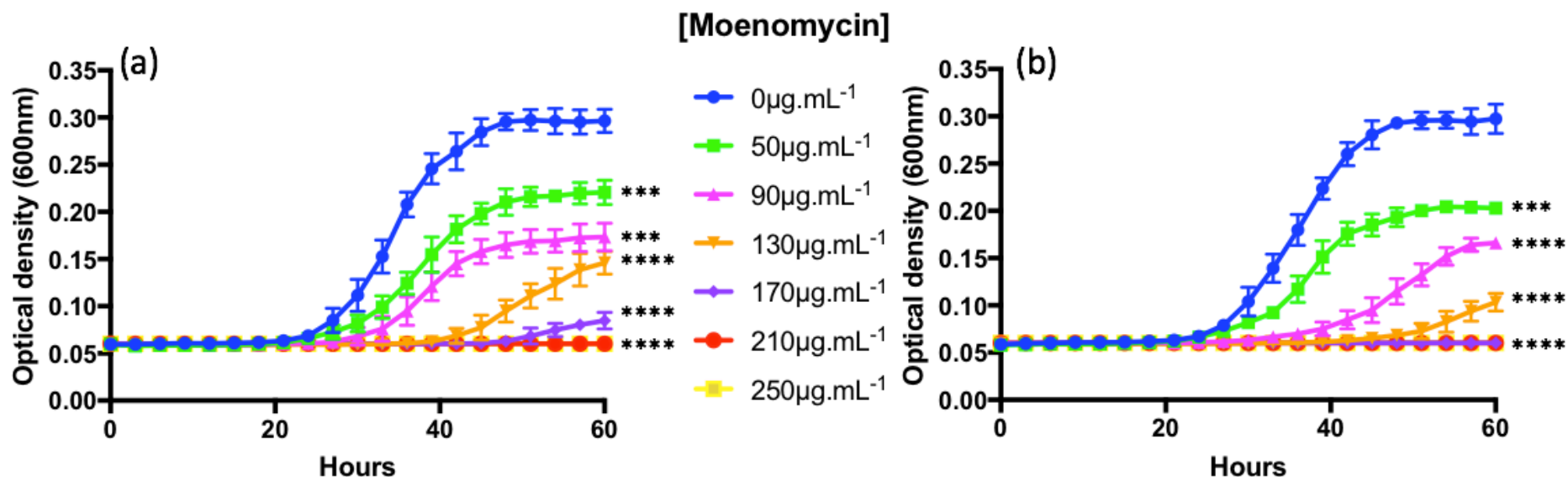


Figure 4.18 The impact of N-glycosylation of peptidoglycan on sensitivity of *M. smegmatis* growth to moenomycin. Wild type (a) and (b) Δ NamH *M. smegmatis* MIC growth curves against moenomycin. Cells were grown in 96-well microtiter plates in triplicate at 37°C with intermittent shaking, OD_{600nm} was measured at 3 hour intervals for 60 hours. Each well contained 100 μ L culture media (7H9, ADC, 0.05% (w/v) Tween 80) with increasing concentrations of moenomycin at a total DMSO concentration of 2% (v/v). *M. smegmatis* wild type (a) and (b) Δ NamH strains were standardized to an OD_{600nm} of 1 and diluted further by a factor of 10⁴ prior to addition to wells and incubation. Error bars represent standard deviation of triplicate measurements. Moenomycin concentrations: 0 μ g.mL⁻¹ (Blue), 50 μ g.mL⁻¹ (Green), 90 μ g.mL⁻¹ (Pink), 130 μ g.mL⁻¹ (Orange), 170 μ g.mL⁻¹ (Purple), 210 μ g.mL⁻¹ (Red), 250 μ g.mL⁻¹ (Yellow). Statistically significant results of comparison of growth at increasing moenomycin concentrations compared to growth at 0 μ g.mL⁻¹ moenomycin for each strain are indicated with * = p-value <0.05, ** = <0.01, *** = <0.001 and **** = <0.0001. Ns = not statistically significant. Results: Δ NamH was more susceptible to moenomycin than wild type. MIC results: Wild type (a) 210 μ g.mL⁻¹, Δ NamH (b) 170 μ g.mL⁻¹.

Moenomycin ($\mu\text{g.mL}^{-1}$)	Wild type <i>M. smegmatis</i>					ΔNamH <i>M. smegmatis</i>					(b) vs (a) p- values
	Apparent Lag phase (h)	Td (h ⁻¹)	AUC (%)	Stationary Phase OD _{600nm}	Wild type p-values (a)	Apparent Lag phase (h)	Td (h ⁻¹)	AUC (%)	Stationary Phase OD _{600nm}	ΔNamH p- values (b)	
0	21	6.95	-	0.30	-	21	7.59	-	0.30	-	>0.05
50	24	9.73	59.84	0.22	<0.001	21	9.97	57.22	0.20	<0.001	>0.05
90	30	10.67	39.67	0.17	<0.001	33	13.40	24.65	0.16	<0.0001	<0.01
130	42	13.32	14.92	0.14	<0.0001	42	17.63	5.70	0.10	<0.0001	<0.05
170	54	28.99	3.17	0.08	<0.0001	60	0.00	0.00	0.05	<0.0001	<0.05
210	60	0.00	0.00	0.05	<0.0001	60	0.00	0.00	0.05	<0.0001	-
250	60	0.00	0.00	0.05	<0.0001	60	0.00	0.00	0.05	<0.0001	-

Table 4.7 Statistical comparisons of *M. smegmatis* growth curves in the presence of increasing concentrations of moenomycin. Wild type and ΔNamH strains incubated for 60 hours at 37°C with selected concentrations of moenomycin produced growth curves measured at OD_{600nm} in Figure 4.18. Variations between growth curves were measured by time taken to exit apparent lag phase (hours), the doubling time (Td) of cells during exponential phase (hours⁻¹), the area under the curve (AUC) percentage compared to the 0 $\mu\text{g.mL}^{-1}$ control (%), the OD_{600nm} value achieved during stationary phase and whether the growth curve variations were statistically significant compared to each 0 $\mu\text{g.mL}^{-1}$ control with p-values <0.05 deemed significant. The statistical significance of ΔNamH (b) growth curves compared to wild type (a) at equivalent moenomycin concentrations were determined by p-values <0.05.

In this set of experiments, the 0 $\mu\text{g.mL}^{-1}$ control included to compared against wild type (Figure 4.18 (a) Blue) and ΔNamH (Figure 4.18 (b) Blue) growth curves inhibited by addition of increasing concentration of moenomycin, both exited apparent lag phase after 21 hours, generated a Td within exponential phase of 6.95 and 7.59 hours respectively and plateaued during stationary phase at $\text{OD}_{600\text{nm}}$ 0.3 (Table 4.7).

The addition of the lowest investigated concentration of moenomycin 50 $\mu\text{g.mL}^{-1}$ (Figure 4.18 Green) to both strains similarly altered growth, increasing the Td to 9.73 (Wild type) and 9.97 (ΔNamH) hours respectively and significantly reduced the AUC to 59.84% (Wild type) and 57.22% (ΔNamH) compared to their respective controls (Table 4.7). Subsequent moenomycin concentrations, 90 $\mu\text{g.mL}^{-1}$ (Figure 4.18 Pink) and 130 $\mu\text{g.mL}^{-1}$ (Figure 4.18 Orange) permitted measurable growth from both strains but demonstrated greater potency towards the ΔNamH strain. The most noted variation between the two *M. smegmatis* strains was most evident in cells incubated for 60 hours with 170 $\mu\text{g.mL}^{-1}$ (Figure 4.18 Purple) moenomycin. This time frame was sufficient for the wild type (Figure 4.18 (a) Purple) to demonstrate measurable growth after a 54 hour duration within apparent lag phase. The ΔNamH strain on the other hand was unable to display observable growth (Figure 4.18 (b) Purple), therefore the MIC for *namH* deficient strain was 170 $\mu\text{g.mL}^{-1}$. Increasing the moenomycin concentration to 210 $\mu\text{g.mL}^{-1}$ (Figure 4.18 (a) Red) prevent the wild type from propagating within the nutrient microtiter wells and was therefore determined to be the MIC.

A Student's t-test was done for the growth curves produced from each individual *M. smegmatis* strain with increasing concentrations of moenomycin against the corresponding 0 $\mu\text{g.mL}^{-1}$ control. All moenomycin concentrations for both strains were deemed statistically significant. For the wild type strain moenomycin concentrations 50 and 90 $\mu\text{g.mL}^{-1}$ produced growth curves with p-values of <0.001. For each subsequent concentration the wild type growth curve inhibition resulted in p-values of <0.0001 (130-250 $\mu\text{g.mL}^{-1}$). For the ΔNamH strain the inhibition attributed to 50 $\mu\text{g.mL}^{-1}$ led to a statistically significant growth curve with a p-value of <0.001. All subsequent moenomycin concentrations possessed p-values of <0.0001 (90- 250 $\mu\text{g.mL}^{-1}$).

Moenomycin impacted the Δ NamH strain to a greater degree than the wild type at equivalent concentrations based upon the AUC values generated. A Student's t-test analysis of the variation between the two strains at equal concentrations was conducted and determined that the disparity between growth curves from each strain was statistically significant above $50 \mu\text{g}\cdot\text{mL}^{-1}$ (p-value >0.05). All subsequent moenomycin concentrations produced p-values of <0.01 ($90 \mu\text{g}\cdot\text{mL}^{-1}$) and <0.05 (130 and $170 \mu\text{g}\cdot\text{mL}^{-1}$) respectively.

Wells containing cells incubated with moenomycin concentrations at the MIC or greater were pipetted onto TSB agar plates to determine the MBC in Figure 4.19.

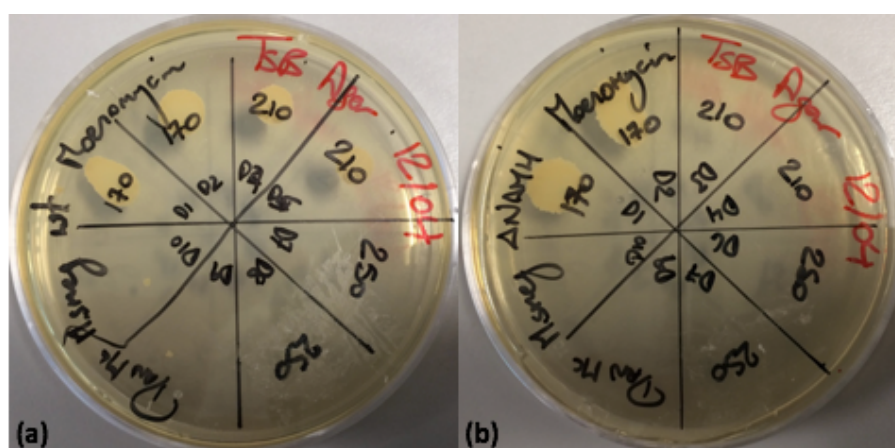


Figure 4.19 Minimal bactericidal concentration of moenomycin against *M. smegmatis* strains. *M. smegmatis* wild type (a) and Δ NamH (b) cells incubated in liquid media with increasing concentrations of moenomycin that did not produce growth (Figure 4.18) were pipetted in duplicate onto TSB agar to determine MBC. Each quadrant denotes the moenomycin concentration in $\mu\text{g}\cdot\text{mL}^{-1}$. Results: Wild type MBC $250 \mu\text{g}\cdot\text{mL}^{-1}$, Δ NamH MBC $210 \mu\text{g}\cdot\text{mL}^{-1}$.

The variation between the two *M. smegmatis* strains observed during moenomycin MIC determination (Figure 4.18) continued into MBC assessment in Figure 4.19. Both strains were able to propagate on TSB agar after incubation with $170 \mu\text{g}\cdot\text{mL}^{-1}$ moenomycin. Increasing the concentration to $210 \mu\text{g}\cdot\text{mL}^{-1}$ did not impact the wild type which still grew but the Δ NamH strain was unable to colonize the agar plate therefore indicating that the MBC for the Δ NamH strain was $210 \mu\text{g}\cdot\text{mL}^{-1}$. The highest concentration of moenomycin, $250 \mu\text{g}\cdot\text{mL}^{-1}$ was sufficient to prevent mycobacterial growth in both strains and was therefore the MBC value for the wild type strain.

4.4.7 Vancomycin MIC assessment of *M. smegmatis* wild type and Δ NamH strains

Vancomycin is a first generation glycopeptide antibiotic and common therapy against gram-positive organisms (Chua, *et al.* 2009) and a secondary therapy to numerous drug resistant *M. tuberculosis* infections (Soetaerta, *et al.* 2015)). The mode of action of vancomycin is to form hydrogen bonds towards D-alanyl-D-alanine (Wang, *et al.* 2018), the terminal dipeptide residues of the peptide stem of extracellular disaccharide pentapeptides, preventing their incorporation into the wider peptidoglycan architecture (Ge, *et al.* 1999). The structure of vancomycin is depicted in Figure 4.20.

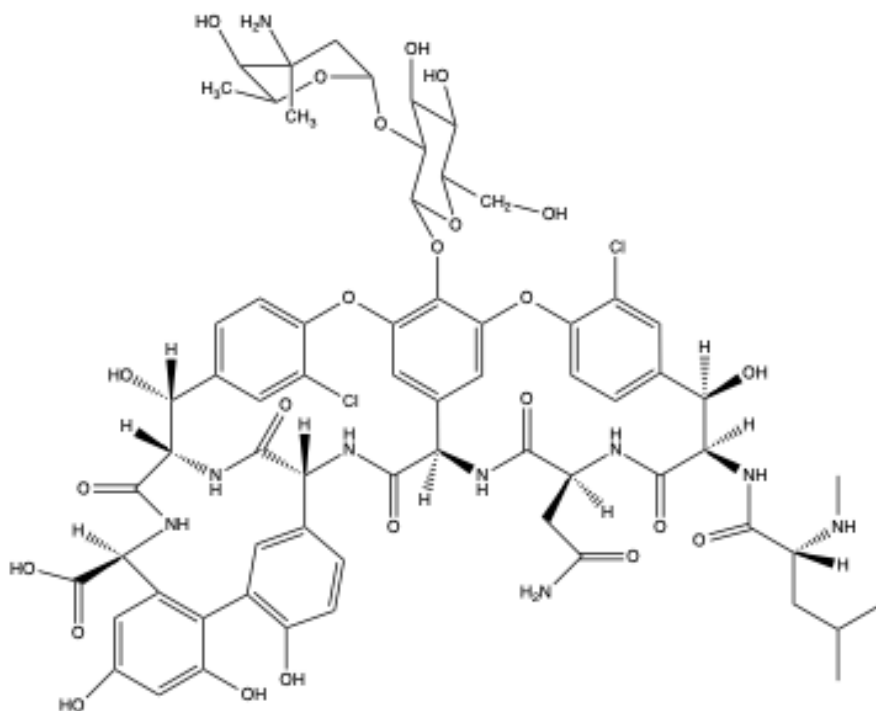


Figure 4.20: The structure of the antibiotic Vancomycin. Molecular weight: 1447.27; Chemical formula: $C_{66}H_{75}Cl_2N_9O_{24}$. The above schematic was created using ChemBioDraw.

The MIC of vancomycin was determined for each of the two *M. smegmatis* strains in Figure 4.21.

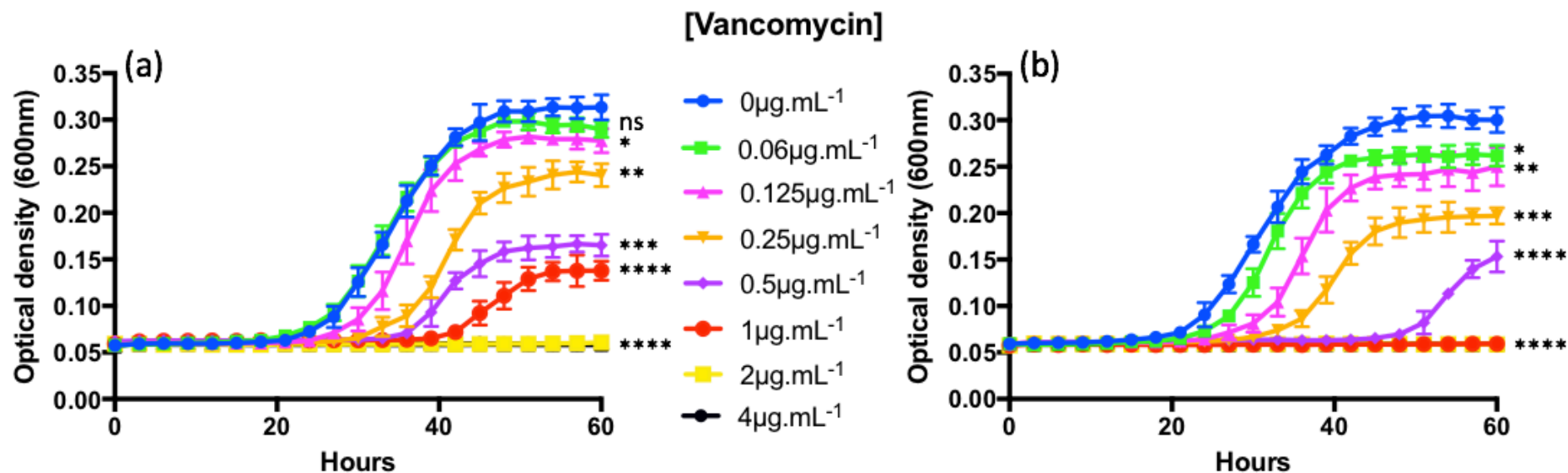


Figure 4.21 The impact of N-glycosylation of peptidoglycan on the sensitivity of *M. smegmatis* growth to vancomycin. Wild type (a) and (b) Δ NamH *M. smegmatis* MIC growth curves against vancomycin. Cells were grown in 96-well microtiter plates in triplicate at 37°C with intermittent shaking, OD_{600nm} was measured at 3 hour intervals for 60 hours. Each well contained 100 μL culture media (7H9, ADC, 0.05% (w/v) Tween 80) with increasing concentrations of vancomycin to a total DMSO concentration of 2% (v/v). *M. smegmatis* wild type (a) and (b) Δ NamH strains were standardized to an OD_{600nm} of 1 and diluted further by a factor of 10^4 prior to addition to wells and incubation. Error bars represent standard deviation of triplicate measurements. Vancomycin concentrations: 0 $\mu\text{g.mL}^{-1}$ (Blue), 0.06 $\mu\text{g.mL}^{-1}$ (Green), 0.125 $\mu\text{g.mL}^{-1}$ (Pink), 0.25 $\mu\text{g.mL}^{-1}$ (Orange), 0.5 $\mu\text{g.mL}^{-1}$ (Purple), 1 $\mu\text{g.mL}^{-1}$ (Red), 2 $\mu\text{g.mL}^{-1}$ (Yellow) and 4 $\mu\text{g.mL}^{-1}$ (Black). Statistically significant results are indicated with * = p-value <0.05, ** = <0.01, *** = <0.001 and **** = <0.0001. Ns = not statistically significant. Results: Δ NamH displays greater susceptibility to vancomycin than wild type. MIC results: Wild type (a) 2 $\mu\text{g.mL}^{-1}$, Δ NamH (b) 1 $\mu\text{g.mL}^{-1}$.

Vancomycin ($\mu\text{g.mL}^{-1}$)	Wild type <i>M. smegmatis</i>					ΔNamH <i>M. smegmatis</i>					(b) vs (a) p- values
	Apparent Lag phase (h)	Td (h^{-1})	AUC (%)	Stationary Phase $\text{OD}_{600\text{nm}}$	Wild type p-values (a)	Apparent Lag phase (h)	Td (h^{-1})	AUC (%)	Stationary Phase $\text{OD}_{600\text{nm}}$	ΔNamH p- values (b)	
0	21	7.12	-	0.31	-	21	6.81	-	0.30	-	>0.05
0.06	21	7.33	97.30	0.29	>0.05	24	7.30	81.92	0.26	<0.05	<0.01
0.125	24	7.10	81.86	0.28	<0.05	27	7.94	65.15	0.25	<0.01	<0.01
0.25	30	7.79	54.61	0.24	<0.01	33	8.32	40.60	0.19	<0.001	<0.01
0.5	36	9.10	32.38	0.16	<0.001	48	9.98	10.78	0.15	<0.0001	<0.001
1	42	10.72	18.50	0.14	<0.0001	60	0.00	0.00	0.05	<0.0001	<0.001
2	60	0.00	0.00	0.05	<0.0001	60	0.00	0.00	0.05	<0.0001	-
4	60	0.00	0.00	0.05	<0.0001	60	0.00	0.00	0.05	<0.0001	-

Table 4.8 Statistical comparisons of *M. smegmatis* growth curves in the presence of increasing concentrations of vancomycin. Wild type and ΔNamH strains incubated for 60 hours at 37°C with selected concentrations of vancomycin produced growth curves measured at $\text{OD}_{600\text{nm}}$ in Figure 4.21. Variations between growth curves were measured by time taken to exit apparent lag phase (hours), the doubling time (Td) of cells during exponential phase (hours^{-1}), the area under the curve (AUC) percentage compared to the 0 $\mu\text{g.mL}^{-1}$ control (%), the $\text{OD}_{600\text{nm}}$ value achieved during stationary phase and whether the growth curve variations were statistically significant compared to each 0 $\mu\text{g.mL}^{-1}$ control with p-values <0.05 deemed significant. The statistical significance of ΔNamH (b) growth curves compared to wild type (a) at equivalent vancomycin concentrations were determined by p-values <0.05.

The wild type (Figure 4.21 (a) Blue) and Δ NamH (Figure 4.21 (b) Blue) $0 \mu\text{g.mL}^{-1}$ controls were utilised during this experiment to compare against vancomycin inhibition of growth curves. Both strains exited apparent lag phase after 21 hours, produced a Td of 7.12 (Wild type) and 6.81 (Δ NamH) hours respectively and reached stationary phase after 45 hours achieving a final $\text{OD}_{600\text{nm}}$ during stationary phase of 0.30 (Table 4.8).

Vancomycin at each investigated concentration impacted the growth of Δ NamH *M. smegmatis* cells to a greater degree than the wild type at each equivalent concentration (Figure 4.21). The addition of the lowest investigated concentration $0.06 \mu\text{g.mL}^{-1}$ (Figure 4.21 (a) Green) did not alter the duration of apparent lag phase or the Td compared to the $0 \mu\text{g.mL}^{-1}$ control (Figure 4.21 (a) Blue) in the wild type but did impact both measurements in Δ NamH cells (Figure 4.21 (b) Green) compared to the $0 \mu\text{g.mL}^{-1}$ control (Figure 4.21 (b) Blue). Subsequent vancomycin concentrations $0.125 \mu\text{g.mL}^{-1}$ vancomycin (Figure 4.21 Pink), $0.25 \mu\text{g.mL}^{-1}$ vancomycin (Figure 4.21 Orange) and $0.5 \mu\text{g.mL}^{-1}$ vancomycin (Figure 4.21 Purple) each gradually decreased the growth of both strains but still permitted observable growth to be measured. The presence of $1 \mu\text{g.mL}^{-1}$ vancomycin (Figure 4.21 Red) completely inhibited growth of the Δ NamH *M. smegmatis* cells (Figure 4.21 (b) Red) during the 60 hour experiment time frame. The wild type cells (Figure 4.21 (a) Red) demonstrated growth after 42 hours (Table 4.8). Doubling the vancomycin concentration to $2 \mu\text{g.mL}^{-1}$ (Figure 4.21 (a): Yellow) was sufficient to completely inhibit growth in the wild type. The MIC of the *M. smegmatis* strains based upon the findings in Figure 4.21 was $2 \mu\text{g.mL}^{-1}$ for the wild type and $1 \mu\text{g.mL}^{-1}$ vancomycin for the Δ NamH strain, half the MIC of the wild type.

The statistical significance (Table 4.8) of the inhibition of wild type growth caused by increasing concentrations of vancomycin compared to the $0 \mu\text{g.mL}^{-1}$ control was analysed with a Student's t-test. The inhibition attributed to the lowest concentration, $0.06 \mu\text{g.mL}^{-1}$ was deemed not statistically significant with a p-value >0.05 . Subsequent concentrations of vancomycin were increasingly statistically significant with p-values of <0.05 ($0.125 \mu\text{g.mL}^{-1}$), <0.01 ($0.25 \mu\text{g.mL}^{-1}$), <0.001 ($0.5 \mu\text{g.mL}^{-1}$) and <0.0001 ($1-4 \mu\text{g.mL}^{-1}$) respectively. The statistical significance (Table 4.8) of the Δ NamH strain to each of the vancomycin concentrations was deemed statistically significant and to a

greater degree than their wild type counterparts. The p-values for each concentration were <0.05 ($0.06 \mu\text{g.mL}^{-1}$), <0.01 ($0.125 \mu\text{g.mL}^{-1}$), <0.001 ($0.25 \mu\text{g.mL}^{-1}$) and <0.0001 ($0.5\text{-}4 \mu\text{g.mL}^{-1}$) respectively.

A Student's t-test analysis comparison (Table 4.8) between the wild type and ΔNamH strains at comparative concentrations of vancomycin determined that all investigated concentrations of the glycopeptide produced variable inhibition to ΔNamH *M. smegmatis* growth curves that was deemed statistically significant with p-values <0.01 ($0.06\text{-}0.25 \mu\text{g.mL}^{-1}$) and <0.001 ($0.5\text{-}1 \mu\text{g.mL}^{-1}$). Both strains were completely inhibited by 2 and $4 \mu\text{g.mL}^{-1}$ vancomycin therefore variations were not statistically significant (p-value >0.05).

MIC and greater concentrations of vancomycin were pipetted onto TSB agar plates to assess MBC values for both strains against the antimicrobial. Results are shown in Figure 4.22.

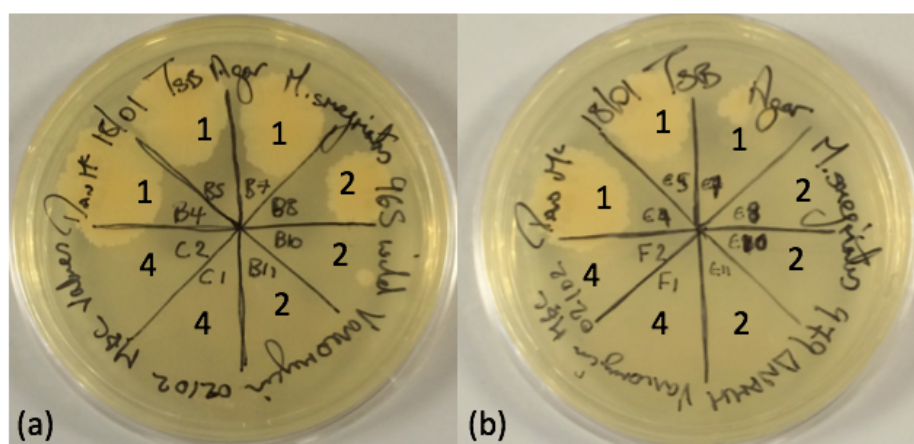


Figure 4.22 Minimal bactericidal concentration of vancomycin against *M. smegmatis* strains. *M. smegmatis* wild type (a) and ΔNamH (b) cells incubated in liquid media with increasing concentrations of vancomycin that did not produce growth (Figure 4.21) were pipetted in duplicate onto TSB agar to determine MBC. Each quadrant denotes the vancomycin concentration in $\mu\text{g.mL}^{-1}$. Results: Wild type MBC $4 \mu\text{g.mL}^{-1}$, ΔNamH MBC $2 \mu\text{g.mL}^{-1}$.

The variation in susceptibility towards vancomycin noted during antimicrobial incubation was also observed during MBC assessment. The wild type strain (Figure 4.22 (a)) was not able to grow in the presence of $2 \mu\text{g.mL}^{-1}$ vancomycin in nutrient media, but once cells were isolated and grown in TSB agar growth was observed.

The MBC for the wild type was 4 $\mu\text{g}\cdot\text{mL}^{-1}$. Similarly ΔNamH cells were unable to grow in the presence of 1 $\mu\text{g}\cdot\text{mL}^{-1}$ during MIC assessment but were able to propagate on TSB agar. The MBC for the ΔNamH strain was 2 $\mu\text{g}\cdot\text{mL}^{-1}$, half the value observed for the wild type.

4.4.8 Teixobactin MIC assessment of *M. smegmatis* wild type and ΔNamH strains

Due to the expanding resistance of micro-organisms towards front-line drug treatments, the requirement for alternative candidates have led to antimicrobial peptides as a valid source of potential antibiotics (Toke, *et al.* 2005). Possessing low toxicity and potent specific biological activities, the natural product teixobactin and its discovery are championed as a unique method of antimicrobial exploration. The structure of teixobactin is depicted in Figure 4.23.

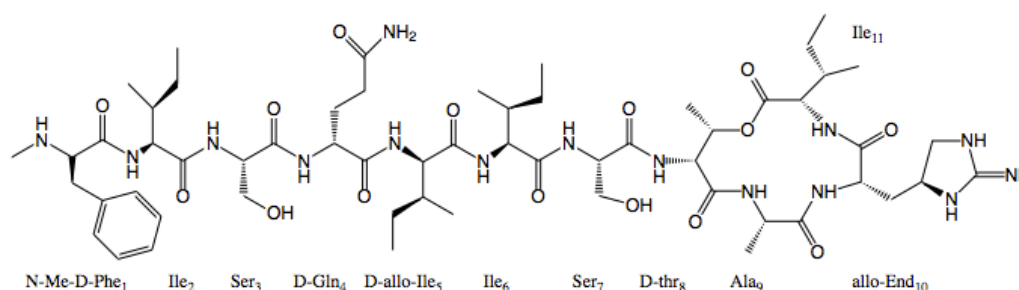


Figure 4.23: The structure of the small molecule antibiotic Teixobactin. Molecular weight: 1242.49; Chemical formula: $\text{C}_{58}\text{H}_{95}\text{N}_{15}\text{O}_{15}$. The above schematic was created using ChemBioDraw.

An unconventional depsipeptide, teixobactin contains both methylphenylalanine and enduracidine as well as four D-amino acids critical for antimicrobial activity (Ling, *et al.* 2015). The 1242 Dalton peptide elicits a mode of action which differs from common therapeutics of bacterial infection (Piddock, *et al.* 2015), binding the prenyl-pyrophosphate-GlcNAc region of Lipid II, a highly conserved motif in bacteria. The antimicrobial peptide elucidated potent activity ($< 1 \mu\text{g}\cdot\text{mL}^{-1}$) towards both mycobacteria and Gram-positive bacteria, in addition to drug resistant strains, although it did not exhibit activity towards Gram-negative bacteria (Ling, *et al.* 2015).

Teixobactin is synthesized from a newly identified β -proteobacterium, *Eleftheria terrae*. The natural product was described through a new technique of isolating and growing previously unculturable organisms termed iChip (Sherpa, *et al.* 2015). In short, soil samples were diluted to contain approximately a single bacterial cell and transferred to a set channel. Two semi-permeable membranes enclosed each channel and the whole device was positioned within soil. Dissemination of both nutrients and important growth factors across the membranes permitted the secretion of potential antibiotics as well as the growth of unculturable bacteria in a natural environment.

The teixobactin compound was acquired from Ling *et al.* (2015) and the stated MIC against *M. tuberculosis* of $0.125 \mu\text{g.mL}^{-1}$ was investigated in *M. smegmatis* wild type and ΔNamH strains in Figure 4.24.

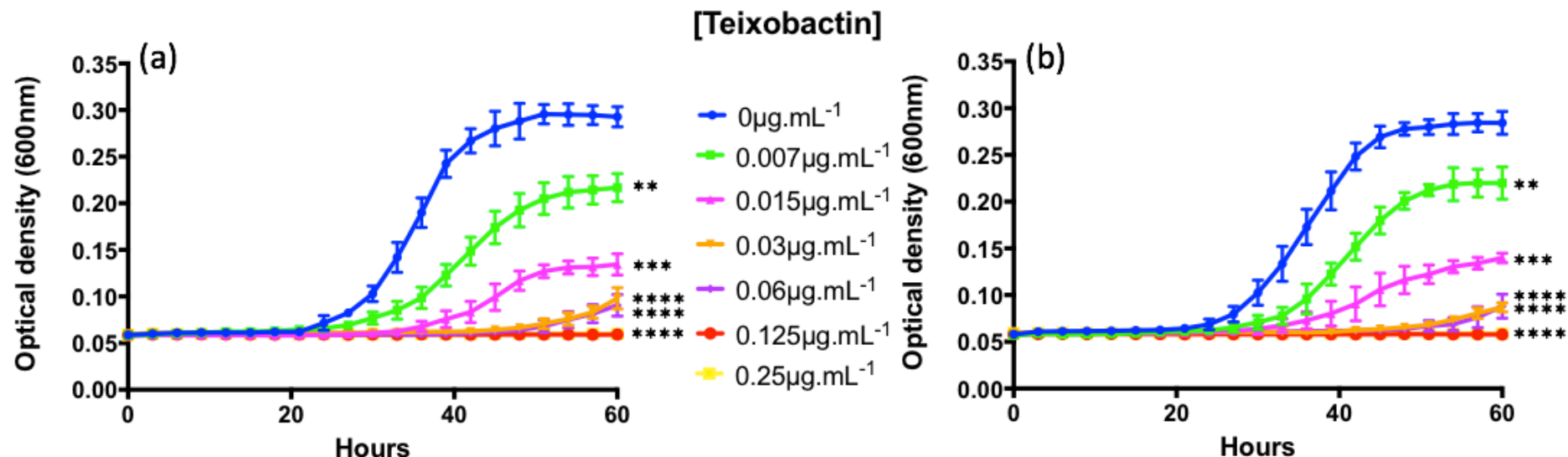


Figure 4.24 The impact of N-glycolylation of peptidoglycan on the sensitivity of *M. smegmatis* growth to teixobactin. Wild type (a) and (b) Δ NamH *M. smegmatis* MIC growth curves against teixobactin. Cells were grown in 96-well microtiter plates in triplicate at 37°C with intermittent shaking, OD_{600nm} was measured at 3 hour intervals for 60 hours. Each well contained 100 μL culture media (7H9, ADC, 0.05% (w/v) Tween 80) with increasing concentrations of teixobactin at a total DMSO concentration of 2% (v/v). *M. smegmatis* wild type (a) and (b) \square NamH strains were standardized to an OD_{600nm} of 1 and diluted further by a factor of 10^4 prior to addition to wells and incubation. Error bars represent standard deviation of triplicate measurements. Teixobactin concentrations: 0 $\mu\text{g.mL}^{-1}$ (Blue), 0.007 $\mu\text{g.mL}^{-1}$ (Green), 0.015 $\mu\text{g.mL}^{-1}$ (Pink), 0.03 $\mu\text{g.mL}^{-1}$ (Orange), 0.06 $\mu\text{g.mL}^{-1}$ (Purple), 0.125 $\mu\text{g.mL}^{-1}$ (Red) and 0.25 $\mu\text{g.mL}^{-1}$ (Yellow). Statistically significant results of comparison of growth at increasing concentrations of teixobactin compared to growth at 0 $\mu\text{g.mL}^{-1}$ teixobactin for each strain are indicated with * = <math><0.05</math>, ** = <math><0.01</math>, *** = <math><0.001</math> and **** = <math><0.0001</math>. Ns = not statistically significant. Results: Both strains were equally susceptible to teixobactin. MIC results: Wild type (a) 0.125 $\mu\text{g.mL}^{-1}$, Δ NamH (b) 0.125 $\mu\text{g.mL}^{-1}$.

Teixobactin ($\mu\text{g.mL}^{-1}$)	Wild type <i>M. smegmatis</i>					ΔNamH <i>M. smegmatis</i>					(b) vs (a) p- values
	Apparent Lag phase (h)	Td (h^{-1})	AUC (%)	Stationary Phase OD _{600nm}	Wild type p-values (a)	Apparent Lag phase (h)	Td (h^{-1})	AUC (%)	Stationary Phase OD _{600nm}	ΔNamH p- values (b)	
0	21	7.36	-	0.29	-	21	7.95	-	0.29	-	>0.05
0.007	24	11.03	53.00	0.22	<0.01	24	10.25	57.16	0.22	<0.01	>0.05
0.015	36	16.69	20.11	0.13	<0.001	33	16.61	23.41	0.14	<0.001	>0.05
0.03	48	19.41	4.97	0.1	<0.0001	48	21.47	3.80	0.09	<0.0001	>0.05
0.06	48	22.42	3.40	0.09	<0.0001	48	19.86	3.32	0.09	<0.0001	>0.05
0.125	60	0.00	0.00	0.05	<0.0001	60	0.00	0.00	0.05	<0.0001	-
0.25	60	0.00	0.00	0.05	<0.0001	60	0.00	0.00	0.05	<0.0001	-

Table 4.9 Statistical comparisons of *M. smegmatis* growth curves in the presence of increasing concentrations of teixobactin. Wild type and ΔNamH strains incubated for 60 hours at 37°C with selected concentrations of teixobactin produced growth curves measured at OD_{600nm} in Figure 4.24. Variations between growth curves were measured by time taken to exit apparent lag phase (hours), the doubling time (Td) of cells during exponential phase (hours^{-1}), the area under the curve (AUC) percentage compared to the 0 $\mu\text{g.mL}^{-1}$ control (%), the OD_{600nm} value achieved during stationary phase and whether the growth curve variations were statistically significant compared to each 0 $\mu\text{g.mL}^{-1}$ control with p-values <0.05 deemed significant. The statistical significance of ΔNamH (b) growth curves compared to wild type (a) at equivalent teixobactin concentrations were determined by p-values <0.05.

In this set of experiments the control ($0 \mu\text{g.mL}^{-1}$ teixobactin) growth curves of the wild type (Figure 4.24 (a) Blue) and ΔNamH (Figure 4.24 (b) Blue) strains, both produced observable growth after 21 hours, with a Td during exponential phase of 7.36 (Wild type) and 7.97 (ΔNamH) hours respectively and both strains plateaued at an $\text{OD}_{600\text{nm}}$ of 0.29 during stationary phase after 45 hours.

The introduction of teixobactin at the concentrations investigated impacted both *M. smegmatis* strains equally, producing similar levels of inhibition at equivalent concentrations (Table 4.9). The lowest two investigated concentrations of teixobactin $0.007 \mu\text{g.mL}^{-1}$ (Figure 4.24 Green) and $0.0015 \mu\text{g.mL}^{-1}$ (Figure 4.24 Pink) significantly impacted growth reducing the AUC of both strains to around 55% and 22% of the growth obtained by their respective $0 \mu\text{g.mL}^{-1}$ controls (Table 4.9).

The final two concentrations that permitted growth were $0.03 \mu\text{g.mL}^{-1}$ (Figure 4.24 Orange) and $0.06 \mu\text{g.mL}^{-1}$ (Figure 4.24 Purple). Both teixobactin concentrations once incubated with each *M. smegmatis* strain demonstrated equal growth over the measured 60 hours. All cells exited apparent lag phase after 48 hours, produced a Td of 20 hours and measured greatly reduced AUC values between 3% and 4% total compared to their respective $0 \mu\text{g.mL}^{-1}$ control (Table 4.9). It is likely these AUC values are underestimated because the experiment was terminated before growth under these conditions reached stationary phase. The addition of $0.125 \mu\text{g.mL}^{-1}$ teixobactin (Figure 4.24 Red) was sufficient to completely inhibit growth in both strains and therefore was established as the MIC for both the wild type and ΔNamH strains. This value was the same MIC as published by Ling, *et al.* (2015) against MTB.

Each of the investigated teixobactin concentrations produced *M. smegmatis* wild type and ΔNamH growth curves which were equally statistically significant compared to the $0 \mu\text{g.mL}^{-1}$ control (Table 4.9). P-values for each teixobactin concentration were <0.01 ($0.007 \mu\text{g.mL}^{-1}$), <0.001 ($0.015 \mu\text{g.mL}^{-1}$) and <0.0001 ($0.03\text{-}0.25 \mu\text{g.mL}^{-1}$) respectively. A Student's t-test (Table 4.9) comparing variations between both strains at equivalent concentrations of teixobactin indicated that there was no statistical significance at any investigated concentration with all investigated growth curves producing p-values >0.05 .

Wells containing the teixobactin MIC or greater for both strains were transferred onto TSB agar plates and incubated for 72 hours to establish MBC values. The results are displayed in Figure 4.25.

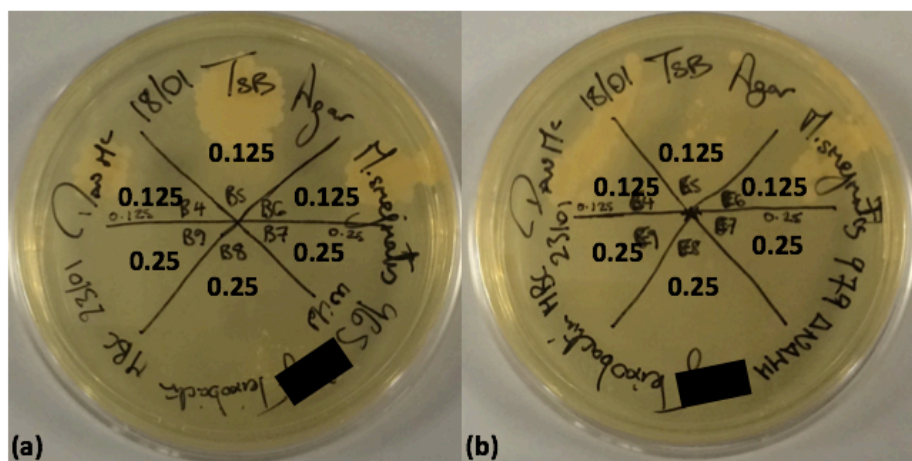


Figure 4.25 Minimal bactericidal concentration of teixobactin against *M. smegmatis* strains. *M. smegmatis* wild type (a) and Δ NamH (b) cells incubated in liquid media with increasing concentrations of teixobactin that did not produce growth (Figure 4.24) were pipetted in duplicate onto TSB agar to determine MBC. Each quadrant denotes the teixobactin concentration in $\mu\text{g.mL}^{-1}$. Results: Wild type MBC $0.25 \mu\text{g.mL}^{-1}$, Δ NamH MBC $0.25 \mu\text{g.mL}^{-1}$.

As with the equivalent MIC values (Figure 4.24) for both strains the MBC values were also equivalent. Growth was observed for both strains from wells containing the teixobactin MIC of $0.125 \mu\text{g.mL}^{-1}$ in each of the triplicate results but no growth was observed in any quadrant containing cells incubated with $0.25 \mu\text{g.mL}^{-1}$ teixobactin. Therefore, the teixobactin MBC for both *M. smegmatis* strains was $0.25 \mu\text{g.mL}^{-1}$.

4.4.9 Arg-Teixobactin MIC assessment of *M. smegmatis* wild type and Δ NamH strains

Building upon the identification of the newly discovered teixobactin structure as a potent antimicrobial, analogues of the structure were synthesized *in vitro* by Jad, *et al.* (2015). Arginine-teixobactin (Arg-Teixobactin) substitutes the unique cyclic guanidine-based amino acid L-allo-enduracididine residue for the linear L-Arginine (Figure 4.26 highlighted in red). The analogue displayed similar but reduced potency relative to unmodified teixobactin towards Gram-positive organisms and equivalent

inactivity towards Gram-negative organisms. The structure of arg-teixobactin is shown in Figure 4.26 highlighting the structural variation between the analogue and teixobactin.

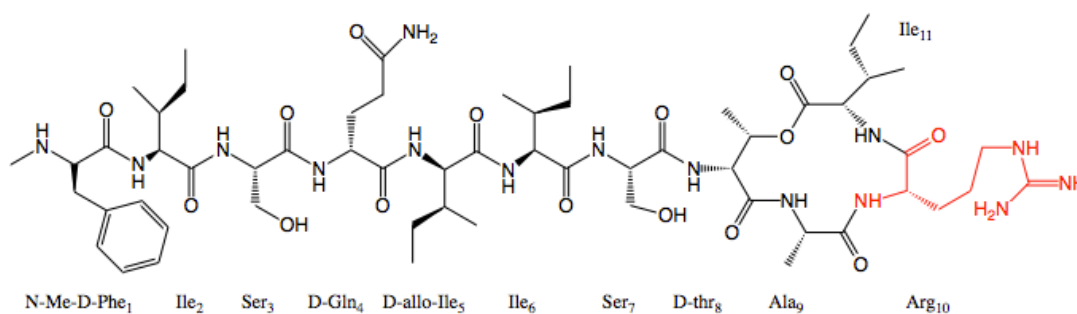


Figure 4.26 The structure of the modified small molecule antibiotic Teixobactin, designated Arginine-Teixobactin (Arg-Teixobactin). Molecular weight: 1229.47; Chemical formula: C₅₈H₉₄N₁₅O₁₅. The variation in chemical structure from Teixobactin is highlighted (red). The above schematic was created using ChemBioDraw.

The teixobactin analogue, although less active than the original towards Gram-positive organisms was not tested against mycobacteria. Therefore, the compound was acquired from Jad, *et al.* (2015) and similarly tested to determine MIC values against both *M. smegmatis* strains. These results are shown in Figure 4.27.

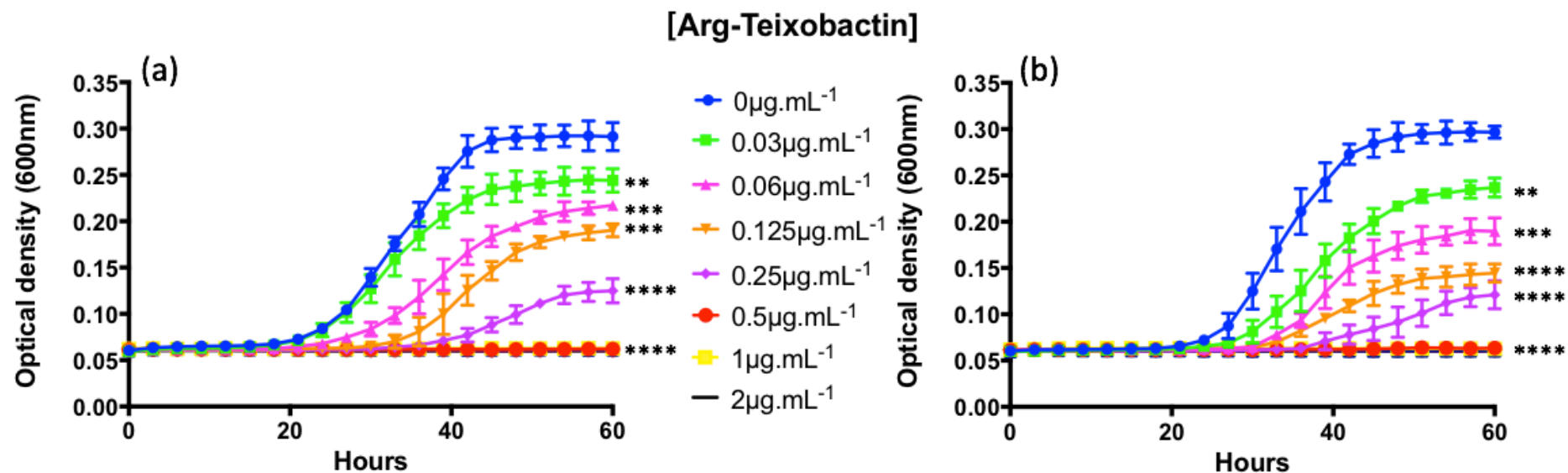


Figure 4.27 The impact of N-glycosylation of peptidoglycan on the sensitivity of *M. smegmatis* growth to Arg-teixobactin. Wild type (a) and (b) ΔNamH *M. smegmatis* MIC growth curves against Arg-teixobactin. Cells were grown in 96-well microtiter plates in triplicate at 37°C with intermittent shaking, OD_{600nm} was measured at 3 hour intervals for 60 hours. Each well contained 100 μL culture media (7H9, ADC, 0.05% (w/v) Tween 80) with increasing concentrations of Arg-teixobactin at a total DMSO concentration of 2% (v/v). *M. smegmatis* wild type (a) and (b) ΔNamH strains were standardized to an OD_{600nm} of 1 and diluted further by a factor of 10^4 prior to addition to wells and incubation. Error bars represent standard deviation of triplicate measurements. Arg-teixobactin concentrations: 0 $\mu\text{g.mL}^{-1}$ (Blue), 0.03 $\mu\text{g.mL}^{-1}$ (Green), 0.06 $\mu\text{g.mL}^{-1}$ (Pink), 0.125 $\mu\text{g.mL}^{-1}$ (Orange), 0.25 $\mu\text{g.mL}^{-1}$ (Purple), 0.5 $\mu\text{g.mL}^{-1}$ (Red), 1 $\mu\text{g.mL}^{-1}$ (Yellow) and 2 $\mu\text{g.mL}^{-1}$ (Black). Statistically significant results of comparison of growth at increasing arg-teixobactin concentrations compared to growth at 0 $\mu\text{g.mL}^{-1}$ arg-teixobactin for each strain are indicated with * = p-value < 0.05, ** = < 0.01, *** = < 0.001 and **** = < 0.0001. Ns = not statistically significant. Results: Both strains were equally susceptible to Arg-teixobactin. MIC results: Wild type (a) 0.5 $\mu\text{g.mL}^{-1}$, ΔNamH (b) 0.5 $\mu\text{g.mL}^{-1}$.

Arg-Teixobactin ($\mu\text{g.mL}^{-1}$)	Wild type <i>M. smegmatis</i>					ΔNamH <i>M. smegmatis</i>					(b) vs (a) p-values
	Apparent Lag phase (h)	Td (h^{-1})	AUC (%)	Stationary Phase $\text{OD}_{600\text{nm}}$	Wild type p-values (a)	Apparent Lag phase (h)	Td (h^{-1})	AUC (%)	Stationary Phase $\text{OD}_{600\text{nm}}$	ΔNamH p-values (b)	
0	21	7.56	-	0.29	-	21	7.14	-	0.30	-	>0.05
0.03	21	9.46	79.44	0.24	<0.01	24	9.48	61.71	0.24	<0.01	<0.05
0.06	27	10.64	53.20	0.22	<0.001	33	9.83	42.89	0.19	<0.001	<0.05
0.125	33	12.61	37.11	0.19	<0.001	36	15.67	26.94	0.14	<0.0001	<0.01
0.25	36	17.02	15.42	0.12	<0.0001	39	20.32	13.62	0.12	<0.0001	>0.05
0.5	60	0.00	0.00	0.05	<0.0001	60	0.00	0.00	0.05	<0.0001	-
1	60	0.00	0.00	0.05	<0.0001	60	0.00	0.00	0.05	<0.0001	-
2	60	0.00	0.00	0.05	<0.0001	60	0.00	0.00	0.05	<0.0001	-

Table 4.10 Statistical comparisons of *M. smegmatis* growth curves in the presence of increasing concentrations of arg-teixobactin. Wild type and ΔNamH strains incubated for 60 hours at 37°C with selected concentrations of arg-teixobactin produced growth curves measured at $\text{OD}_{600\text{nm}}$ in Figure 4.27. Variations between growth curves were measured by time taken to exit apparent lag phase (hours), the doubling time (Td) of cells during exponential phase (hours^{-1}), the area under the curve (AUC) percentage compared to the 0 $\mu\text{g.mL}^{-1}$ control (%), the $\text{OD}_{600\text{nm}}$ value achieved during stationary phase and whether the growth curve variations were statistically significant compared to each 0 $\mu\text{g.mL}^{-1}$ control with p-values <0.05 deemed significant. The statistical significance of ΔNamH (b) growth curves compared to wild type (a) at equivalent arg-teixobactin concentrations were determined by p-values <0.05.

The growth of *M. smegmatis* in the presence of increasing arg-teixobactin concentrations was compared to the wild type (Figure 4.27 (a) Blue) and Δ NamH (Figure 4.27 (b) Blue) strain control growth curves in the absence of the antimicrobial. Both controls exited apparent lag phase after 21 hours, established a Td of 7.56 and 7.14 hours and reached a final stationary phase OD_{600nm} of 0.29 and 0.3 respectively after 45 hours (Table 4.10).

The addition of each investigated concentration of arg-teixobactin 0.03 $\mu\text{g.mL}^{-1}$ (Figure 4.27 Green), 0.06 $\mu\text{g.mL}^{-1}$ (Figure 4.27 Pink), 0.125 $\mu\text{g.mL}^{-1}$ (Figure 4.27 Orange) and 0.25 $\mu\text{g.mL}^{-1}$ (Figure 4.27 Purple) gradually increased the duration of the apparent lag phase, the Td during exponential phase as well as reduced the AUC of both strains (Table 4.10). The potency of the antimicrobial analogue was slightly more pronounced against the Δ NamH strain at each arg-teixobactin concentration except 0.25 $\mu\text{g.mL}^{-1}$. The presence of 0.5 $\mu\text{g.mL}^{-1}$ arg-teixobactin (Figure 4.27 Red) or greater was sufficient to prevent any observation of cell growth in both investigated strains over the 60 hours. Therefore, the wild type and Δ NamH *M. smegmatis* arg-teixobactin MIC was determined to be 0.5 $\mu\text{g.mL}^{-1}$.

A Student's t-test analysis to determine the statistical significance of the impact of arg-teixobactin on *M. smegmatis* wild type growth curves compared to the 0 $\mu\text{g.mL}^{-1}$ control (Table 4.10) was conducted. Each of the arg-teixobactin concentrations were deemed statistically significant from the 0 $\mu\text{g.mL}^{-1}$ wild type control, with p-values of <0.01 (0.03 $\mu\text{g.mL}^{-1}$), <0.001 (0.06 and 0.125 $\mu\text{g.mL}^{-1}$) and <0.0001 (0.25-2 $\mu\text{g.mL}^{-1}$) respectively. A Student's t-test of Δ NamH growth curves comparing the addition of arg-teixobactin to the 0 $\mu\text{g.mL}^{-1}$ control (Table 4.10) showed that as with the wild type the inhibition observed by the presence of each concentration was deemed statistically significant with p-values <0.01 (0.03 $\mu\text{g.mL}^{-1}$), <0.001 (0.06 $\mu\text{g.mL}^{-1}$) and <0.0001 (0.125-2 $\mu\text{g.mL}^{-1}$) respectively.

Though the addition of teixobactin did not differentially impact the two *M. smegmatis* strains, the analogue did display a slight increased activity towards the Δ NamH with all but one of the p-values comparing both strains at equivalent arg-teixobactin

concentrations statistically significant with p-values of <0.05 (0.03 and $0.06 \mu\text{g}\cdot\text{mL}^{-1}$) and <0.01 ($0.125 \mu\text{g}\cdot\text{mL}^{-1}$) respectively.

Wells containing MIC or greater concentrations of arg-teixobactin were pipetted onto TSB agar plates and incubated for 72 hours. MBC values were determined in Figure 4.28.

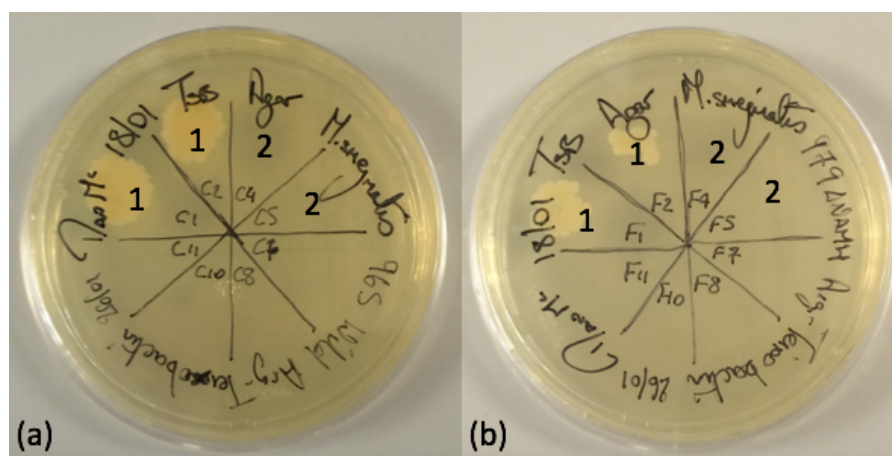


Figure 4.28 Minimal bactericidal concentration of arg-teixobactin against *M. smegmatis* strains. *M. smegmatis* wild type (a) and ΔNamH (b) cells incubated in liquid media with increasing concentrations of arg-teixobactin that did not produce growth (Figure 4.27) were pipetted in duplicate onto TSB agar to determine MBC. Each quadrant denotes the arg-teixobactin concentration in $\mu\text{g}\cdot\text{mL}^{-1}$. Results: Wild type MBC $2 \mu\text{g}\cdot\text{mL}^{-1}$, ΔNamH MBC $2 \mu\text{g}\cdot\text{mL}^{-1}$.

The MBC values for arg-teixobactin in Figure 4.28 were once again equivalent for both strains at $2 \mu\text{g}\cdot\text{mL}^{-1}$. This concentration was 8 times the MBC value of $0.25 \mu\text{g}\cdot\text{mL}^{-1}$ for teixobactin (Figure 4.25). The MBC was also 4 times the arg-teixobactin MIC value of $0.5 \mu\text{g}\cdot\text{mL}^{-1}$, unlike the 2 fold increase in MBC over MIC seen in investigation of the antimicrobial properties of teixobactin.

4.5 Synthesis of Biotinylated Lipid II (MurNAc/NGlyc)

To further probe the role of the N-glycolyl modification in peptidoglycan *in vitro* synthesis of UDP-MurNAc-pentapeptide (DAP) and UDP-MurNGlyc-pentapeptide (DAP) were synthesized according to Lloyd *et al.* (2008) (Section 2.8). In short UDP-MurNAc and UDP-MurNGlyc were incubated for 18 hours at 37°C within a final 2 mL

reaction volume with the L-alanine, D-glutamate, m-DAP and the D-alanyl-D-alanine dipeptide and the corresponding MurC-F ligases. Synthesized UDP-MurNAc/NGlyc-pentapeptides (DAP) were isolated by centrifugal concentrator filtration and purified by anion exchange chromatography.

Both UDP muramyl pentapeptide were analysed by mass spectrometry to determine if synthesis was successful. The mass spectra for UDP-MurNAc-pentapeptide is found in Figure A2.1 (Appendix 2) and for UDP-MurNGlyc-pentapeptide in Figure A2.2 (Appendix 2). The observed and expected m/z values for each variant are recorded in Table 4.11.

UDP Species	Observed (m-1)/1	Expected (m-1)/1	Observed (m-2)/2	Expected (m-2)/2	Observed (m-3)/3	Expected (m-3)/3
UDP-MurNAc-pentapeptide (DAP)	1192.34	1192.33	595.67	595.66	396.77	396.77
UDP-MurNGlyc-pentapeptide (DAP)	1208.33	1208.32	603.66	603.66	402.10	402.10

Table 4.11 The mass/charge ratio for the peptidoglycan precursors UDP-MurNAc-pentapeptide (DAP) and UDP-MurNGlyc-pentapeptide (DAP). The observed and expected singly (m-1)/1, doubly (m-2)/2 and triply (m-3)/3 charged species of each monosaccharide.

Results determined the sole presence of each correct monosaccharide variant. The singly (Observed 1192.34, expected 1192.33), doubly (Observed 595.67, expected 595.66) and triply (Observed 396.77, expected 396.77) charged species for UDP-MurNAc-pentapeptide as well as the singly (Observed 1208.33, expected 1208.33), doubly (Observed 603.66, expected 603.66) and triply (Observed 402.10, expected 402.10) charged species for UDP-MurNGlyc-pentapeptide were detected.

Both UDP muramyl pentapeptides were then labelled on the amino group of their m-DAP residues with biotin (Section 2.8.1.3). The biotinylated UDP muramyl pentapeptides were then purified by ion exchange chromatography with a monoQ 5/50 resin column to isolate biotin-labelled from unlabelled UDP muramyl pentapeptides.

The purification of biotinylated UDP-MurNAc-pentapeptide (DAP) is shown in Figure 4.29.

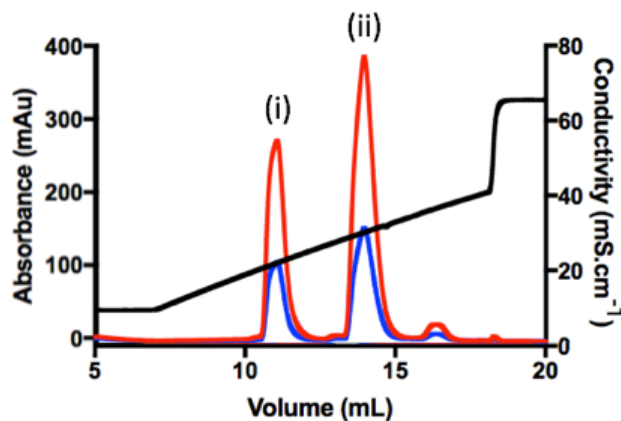


Figure 4.29 Ion exchange chromatography of biotinylated UDP-MurNAc-pentapeptide (DAP) from unlabelled UDP-MurNAc-pentapeptide (DAP). (i) Unlabelled UDP-MurNAc-pentapeptide (DAP) (conductivity 21.98 mS.cm^{-1}) and (ii) Biotinylated UDP-MurNAc-pentapeptide (DAP) (conductivity 30.12 mS.cm^{-1}) were isolated by MonoQ 5/50 GL resin. Red trace is absorbance at 254nm, blue trace: absorbance at 280nm and black trace; conductivity. Peak identities were confirmed by mass spectrometric analysis.

The ion exchange chromatogram (Figure 4.29) of the biotinylated UDP-MurNAc-pentapeptide sample resolved two distinct peaks from the initial sample. Peak (i) (Figure 4.29: (i)) eluted at a conductivity of 21.98 mS.cm^{-1} . The second noted peak (ii) (Figure 4.29: (ii)) eluted once conductivity achieved 30.12 mS.cm^{-1} . Based on the loss of the amino group positive charge on the m-DAP moiety on modification with biotin increasing the net negative charge, strengthening its binding to an anion exchanger relative to the unbiotinylated species it was believed that the biotinylated monosaccharide eluted second. To confirm the identity of each isolated species, samples were analysed by mass spectrometry. The mass spectra of the first peak is evaluated in Figure A2.3 (Appendix 2) and the second peak in Figure A2.4 (Appendix 2).

Results of mass spectra analysis determined that the initial eluted peak (Figure 4.29: (i)) contained UDP-MurNAc-pentapeptide (DAP) singly (Observed 1192.34, expected 1192.33), doubly (Observed 599.67, expected 595.66) and triply (Observed 396.77, expected 396.77) charged species. The second eluted peak (Figure 4.29: (ii)) was evaluated to contain biotinylated UDP-MurNAc-pentapeptide (DAP) singly (Observed

1418.41, expected 1418.41) and doubly (Observed 708.70, expected 708.70) charged species.

The biotinylated UDP-MurNGlyc-pentapeptide (DAP) was purified from unlabelled UDP-MurNGlyc-pentapeptide (DAP) by ion exchange chromatography as shown in Figure 4.30.

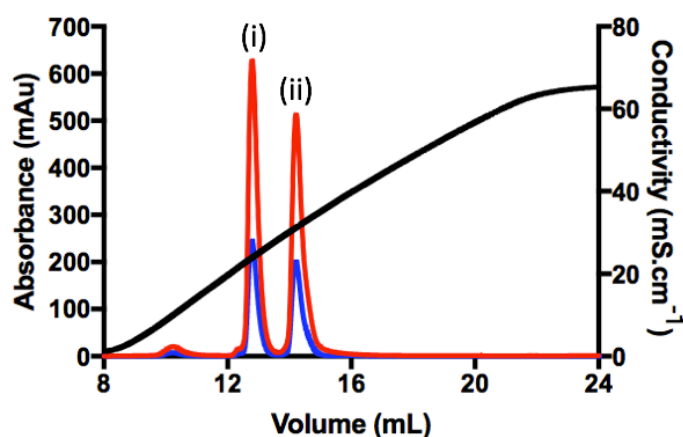


Figure 4.30 Ion exchange chromatography of biotinylated UDP-MurNGlyc-pentapeptide (DAP) from unlabelled UDP-MurNGlyc-pentapeptide (DAP). Noted peaks (i) Unlabelled UDP-MurNGlyc-pentapeptide (DAP) (conductivity 22.71 mS.cm⁻¹) and (ii) Biotinylated UDP-MurNGlyc-pentapeptide (DAP) (conductivity 30.28 mS.cm⁻¹) were isolated by MonoQ 5/50 GL resin. Red trace is absorbance at 254nm, blue trace: absorbance at 280nm and black trace; conductivity. Peak identities were confirmed by mass spectrometric analysis.

The ion exchange purification of the biotin-labelled and unlabelled UDP-MurNGlyc-pentapeptide (DAP) shown in Figure 4.30 indicates the separation of two nucleotide species peaks. The first peak (Figure 4.30: (i)) eluted with a conductivity of 22.71 mS.cm⁻¹. The second isolated peak (Figure 4.30: (ii)) eluted with a conductivity of 30.28 mS.cm⁻¹. Based upon the previous UDP-MurNAc-pentapeptide (DAP) ion exchange purification in Figure 4.29 the secondary peak is likely to contain the labelled monosaccharide and the first peak contains unlabelled UDP-MurNGlyc-pentapeptide (DAP). The two isolated peaks were analysed by mass spectrometry to distinguish between biotinylated and unbiotinylated UDP N-glycolyl muramyl pentapeptide. The mass spectrum of the first isolated peak is shown in Figure A2.5 (Appendix 2) and the second peak in Figure A2.6 (Appendix 2).

Results demonstrated that the first eluted peak (Figure 4.30: (i)) contained the unlabelled UDP-MurNGlyc-pentapeptide (DAP) with singly (Observed 1208.33, expected 1208.32) and doubly (Observed 603.66, expected 603.66) charged species identified. The mass spectrum analysis of the second isolated elution (Figure 4.30: (ii)) confirmed the presence of biotinylated UDP-MurNGlyc-pentapeptide (DAP) with singly (Observed 1434.40, expected 1434.40) and doubly (Observed 716.69, expected 716.69) charged species detected.

Both biotinylated UDP muramyl pentapeptides were utilized to generate biotinylated versions of N-acetylated Lipid II (DAP) and N-glycolylated Lipid II (DAP) (Section 2.8.1.3). The anticipated structure of biotinylated N-acetylated Lipid II (DAP) and biotinylated N-glycolylated Lipid II (DAP) is shown in Figure 4.31.

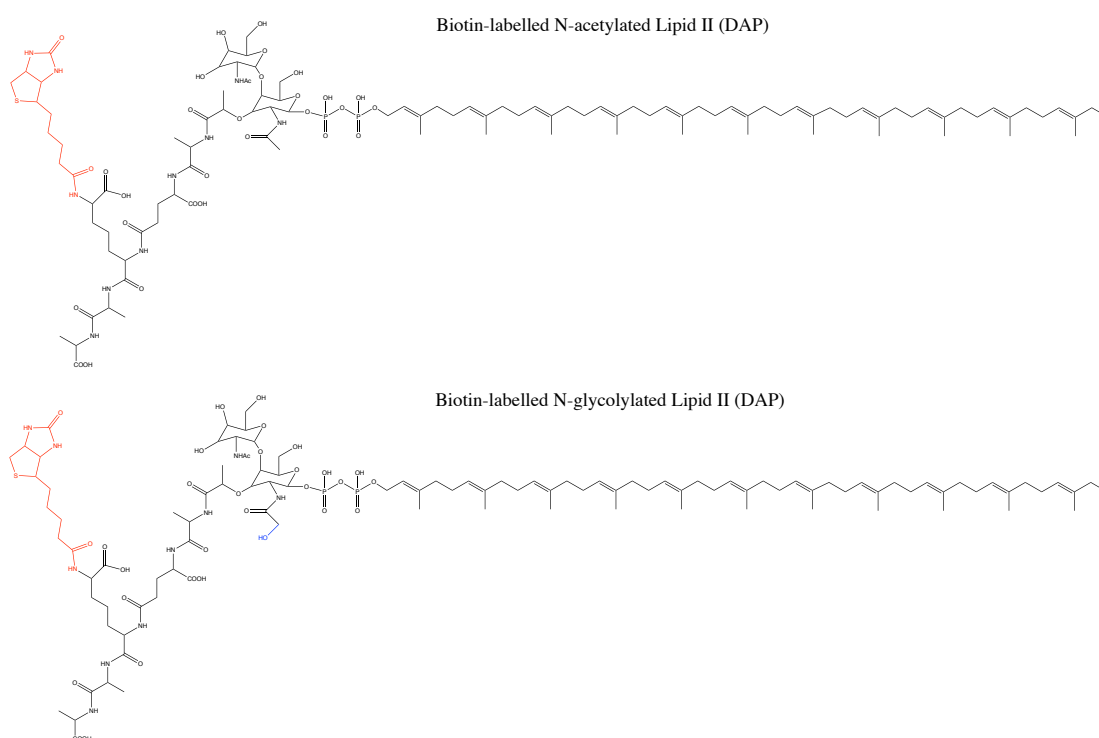


Figure 4.31 The structure of biotin labelled N-acetylated Lipid II DAP and N-glycolylated Lipid II DAP (L-Ala-D-Glu-m-DAP-D-Ala-D-Ala). Biotinylation (labelled red) occurs at the third amino acid (m-DAP) position. The N-glycolylation of muramic acid (labelled blue) The above schematic was created using ChemBioDraw.

Once Lipid II synthesis was complete and lipid products were extracted with by pyridine-acetate and N-butanol separation followed by anion exchange chromatography (Section 2.7.3.3) samples were analysed by mass spectrometry to

confirm the synthesis of the desired biotinylated Lipid II variants. The results of biotinylated N-acetylated Lipid II (DAP) as shown in Figure A2.7 (Appendix 2) and biotinylated N-glycolylated Lipid II (DAP) as shown in Figure A2.8 (Appendix 2).

Synthesis of biotinylated N-acetylated Lipid II was successful, as singly (Observed 2144.13, expected 2144.12), doubly (Observed 1071.56, expected 1071.55) and triply (Observed 714.04, expected 714.03) charged species were measured (Figure A1.7). The mass spectral analysis of the biotinylated N-glycolylated Lipid II (DAP) in Figure A2.8 also correctly identified the singly (Observed 2160.11, expected 2160.11), doubly (Observed 1079.55, expected 1079.55) and triply (Observed 719.36, expected 719.36) charged species of the labelled N-glycolylated lipid (Figure A1.8).

4.6 Binding affinity of biotinylated Lipid II variants to antimicrobials

To determine whether N-glycolylation impacted on the binding of antibiotics that act through binding to Lipid II, the binding affinity of biotin labelled Lipid II variants were measured by interactions with streptavidin coated sensors through surface plasma resonance (SPR) and Bio-layer interferometry (BLI) analysis of N-acetylated and N-glycolylated Lipid II DAP species to ramoplanin, mersacidin and vancomycin.

4.6.1 SPR analysis of binding of biotinylated Lipid II variants to antimicrobials

Biotin labelled Lipid II (DAP) variants were first assessed by SPR. The technique immobilises the biotinylated lipids via binding to streptavidin coated chips. SPR measured light refraction between a gold layer within the glass slide and the overflowing solution which have two unique refractive indexes (Roper 2007). Excitation of the plasmons on the surface by light leads to an electric field intensity throughout the gold surface and a subsequent reduction in the reflected light intensity at a given incident angle (Tang, *et al.* 2011). The streptavidin-biotin bound lipid molecules produce a measurable baseline SPR angle. The addition of potential binding

partners such as antimicrobials can lead to alterations in this SPR angle as interactions occur and the mass on the gold surface increases. These interactions result in a measurable binding curve (Lund-Katz, *et al.* 2010). A basic example of this binding profile is depicted in Figure 4.32.

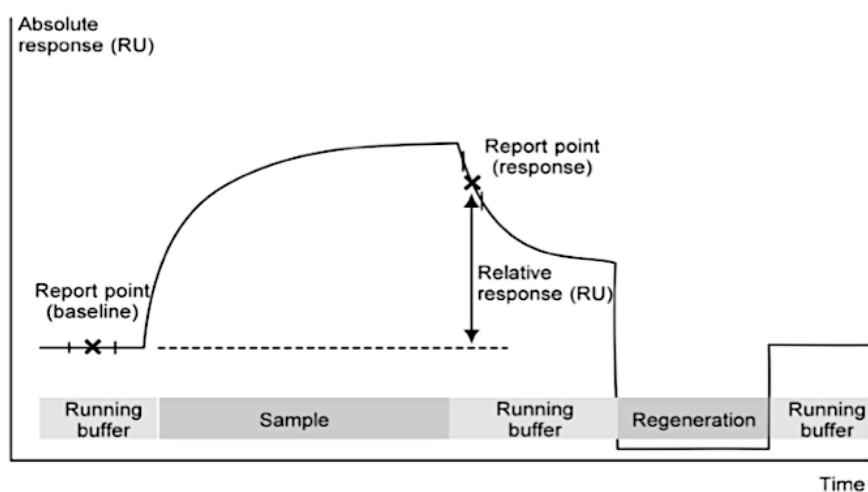


Figure 4.32 Standard SPR sensorgram. An immobilised ligand interaction with a complementary binding partner within a flowing solution across the sensor surface alters the SPR angle and forms a binding curve. Once partner is remove from flow response is altered and sensor is regenerated. Figure source from Biacore – Sensor Surface Handbook (GE Healthcare).

The binding of in this case antimicrobials to immobilised lipids occurs through distinct phases within a sensorgram (Figure 4.32). Pre-binding measures the baseline of bound biotinylated lipids. The addition of the binding partner to the flow solution leads to a measured binding curve from which an association rate (k_{on}) can be measured as binding saturation is achieved. Dissociation is then subsequently measured in the absence of the binding partner to the flow solution, from which a dissociation rate can be obtained (k_{off}). The final step if necessary is then regeneration of the chip to re-establish the initial baseline. The entire reaction is measured in response units (RU) and by comparing the k_{on} and k_{off} rates an equilibrium dissociation constant (K_d) can be deciphered for the binding interaction, as a ratio k_{off}/k_{on} .

Biotinylated Lipid II variants were fixed to a streptavidin coated chip as outlined in Section 2.10.1. A control run is performed for each antimicrobial tested with a flow solution absent of the investigated antimicrobial. The sensorgram produced by this

result is subtracted from each sensorgram run at varying antibiotics concentrations to remove background alterations to signalling.

4.6.1.1 SPR analysis of binding of biotinylated Lipid II variants to ramoplanin

MIC assessment of ramoplanin with respect to *M. smegmatis* indicated that there was no statistical significance in terms of sensitivity to the drug between cells which were comprised of solely N-acetylated peptidoglycan (Δ NamH) or both N-acetylated and N-glycolylated peptidoglycan (wild type) (Figure 4.9).

Immobilised biotin-labelled N-acetylated Lipid II (DAP) and N-glycolylated Lipid II (DAP) were exposed to two fold serial dilutions of ramoplanin from 500 μ M to 3.90 μ M to measure binding affinity. Flow cells were initially exposed to buffer only for 60 seconds, ramoplanin was added to the flow solution for 180 seconds followed by solely buffer again for a further 240 seconds. The SPR ramoplanin binding curves are shown in Figure 4.33.

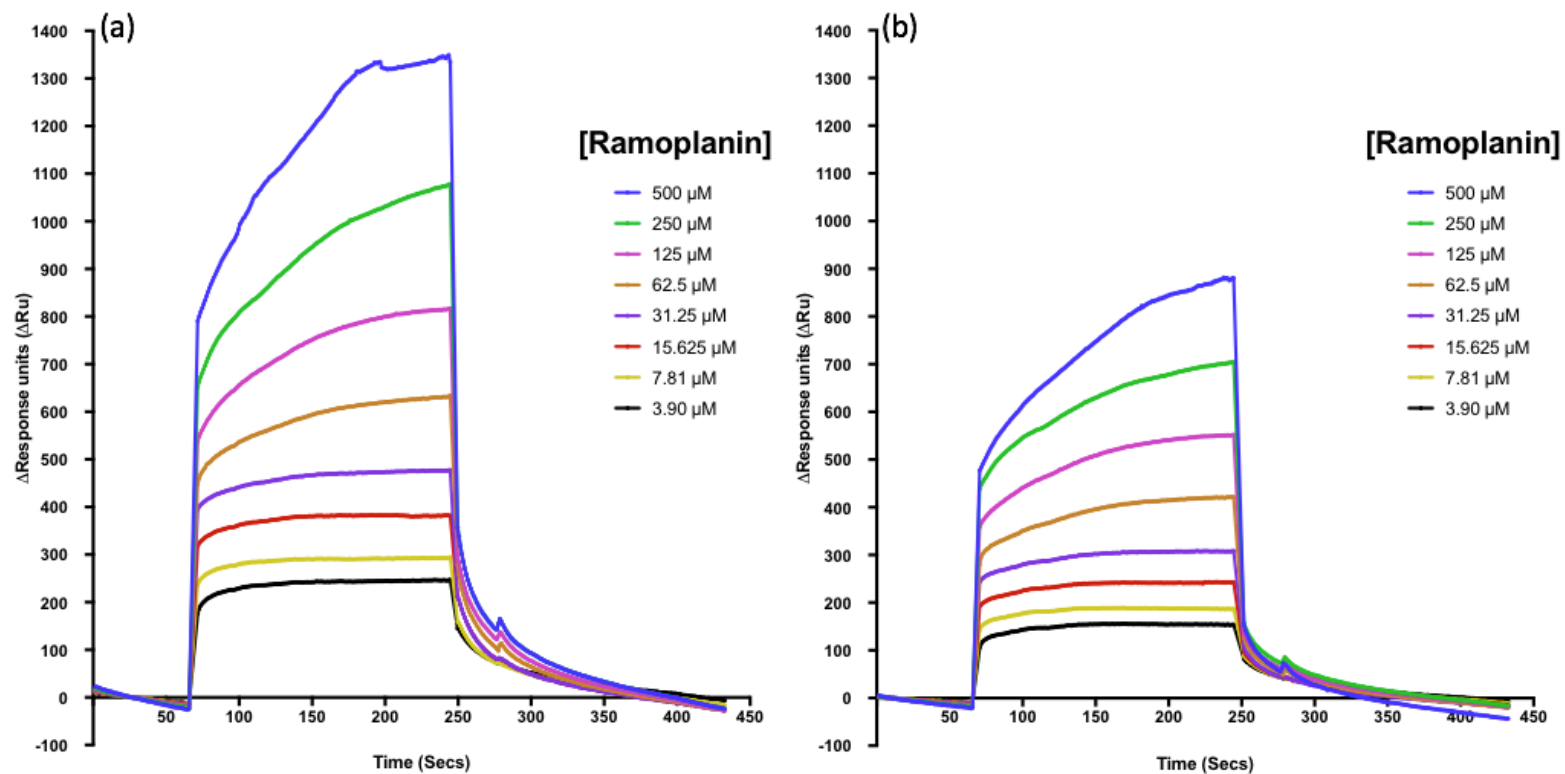


Figure 4.33 SPR binding affinity of ramoplanin to streptavidin-immobilised biotinylated Lipid II (DAP) variants. Sensorgram of (a) biotin labelled muramyl N-acetylated Lipid II (DAP) and (b) biotin labelled muramyl N-glycolylated Lipid II (DAP) binding to increasing concentrations of ramoplanin. Binding affinity measured in response units (RU) for 180 seconds. Ramoplanin concentrations: 500 μM (Blue), 250 μM (Green), 125 μM (Pink), 62.5 μM (Orange), 31.25 μM (Purple), 15.625 μM (Red), 7.81 μM (Yellow) and 3.90 μM (Black).

The initial binding response to ramoplanin at all investigated concentrations was immediate for both N-acetylated (Figure 4.33: (a)) and N-glycosylated (Figure 4.33: (b)) variants of Lipid II (DAP). The addition of ramoplanin to the flow solution at 60 seconds instantly registered significant alterations in the binding response at each concentration. The increase was most notable at 500 μM ramoplanin (Figure 4.33 Blue) which instantly measured 800 RU (N-acetylated) and 500 RU (N-glycosylated) increases in signal.

Ramoplanin concentrations 500 μM and 250 μM (Figure 4.33 Green) did not appear to plateau during the 180 second flow solution in with ramoplanin was present, with both reaching their maximum RU value at the conclusion of the run. Ramoplanin concentrations 125 μM (Figure 4.33 Pink) and 62.50 μM (Figure 4.33 Orange) achieved steady state after 140 seconds for both Lipid II variants, whereas concentrations between 32.25 μM (Figure 4.33 Purple) and 3.90 μM (Figure 4.33 Black) plateaued immediately once ramoplanin was added to the flow solution. Once the ramoplanin was removed from the flow solution the binding response for each concentration immediately reduced, and returned to near baseline after 400 seconds.

Based upon the apparently concentration-independent immediacy of both ramoplanin association and dissociation, the kinetics of association and dissociation of ramoplanin from the immobilised Lipid II variants could not be compared. Instead, the maximum measured response during ramoplanin binding at equivalent concentrations for each Lipid II variant were compared as shown in Figure 4.34.

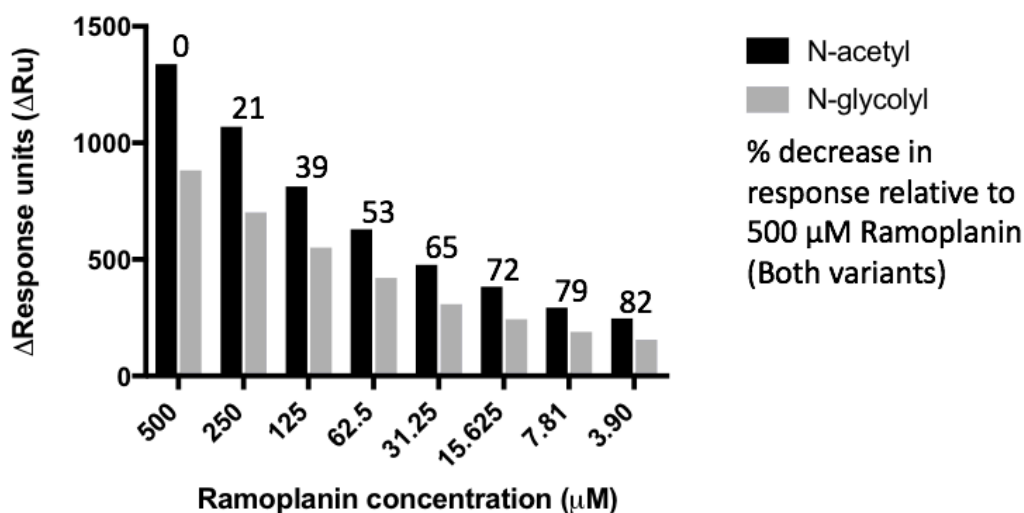


Figure 4.34 SPR steady state response of immobilised biotinylated Lipid II (DAP) variants binding to ramoplanin. Comparison of streptavidin bound biotin labelled N-acetylated Lipid II (DAP) (Black) and N-glycolylated Lipid II (DAP) (Grey) maximum response units (RU) value to interactions with increasing concentrations of ramoplanin. The percentage decrease in relative response compared to the 500 μM highest concentration for both Lipid II variants is labelled.

The steady state comparisons made in Figure 4.34 demonstrate the clear binding preference of ramoplanin binding to the N-acetylated Lipid II over the N-glycolylated molecule over the entire ramoplanin concentration range. The percentage difference between each biotinylated Lipid II variant remained constant at all ramoplanin concentrations, where the N-glycolylated Lipid II (DAP) RU value was consistently observed to be 63-65% of the N-acetylated variant. The constant percentage difference indicated that even at low concentrations ramoplanin binds more readily to the N-acetylated Lipid II (DAP).

4.6.1.2 SPR analysis of binding of biotinylated Lipid II variants to mersacidin

The second investigated antimicrobial whose binding affinity for Lipid II variants were determined by SPR was mersacidin. Mersacidin MIC assessment of wild type and ΔNamH strains (Figure 4.15) demonstrated no observable variation in susceptibility to the antimicrobial in wild type cells expressing either both N-acetylated and N-glycolylated peptidoglycan or the ΔNamH *M. smegmatis* whose peptidoglycan is solely N-acetylated (Raymond, *et al.* 2005). The binding affinity as revealed by two fold serial dilutions of mersacidin from 500 μM to 3.90 μM was assessed in Figure 4.35.

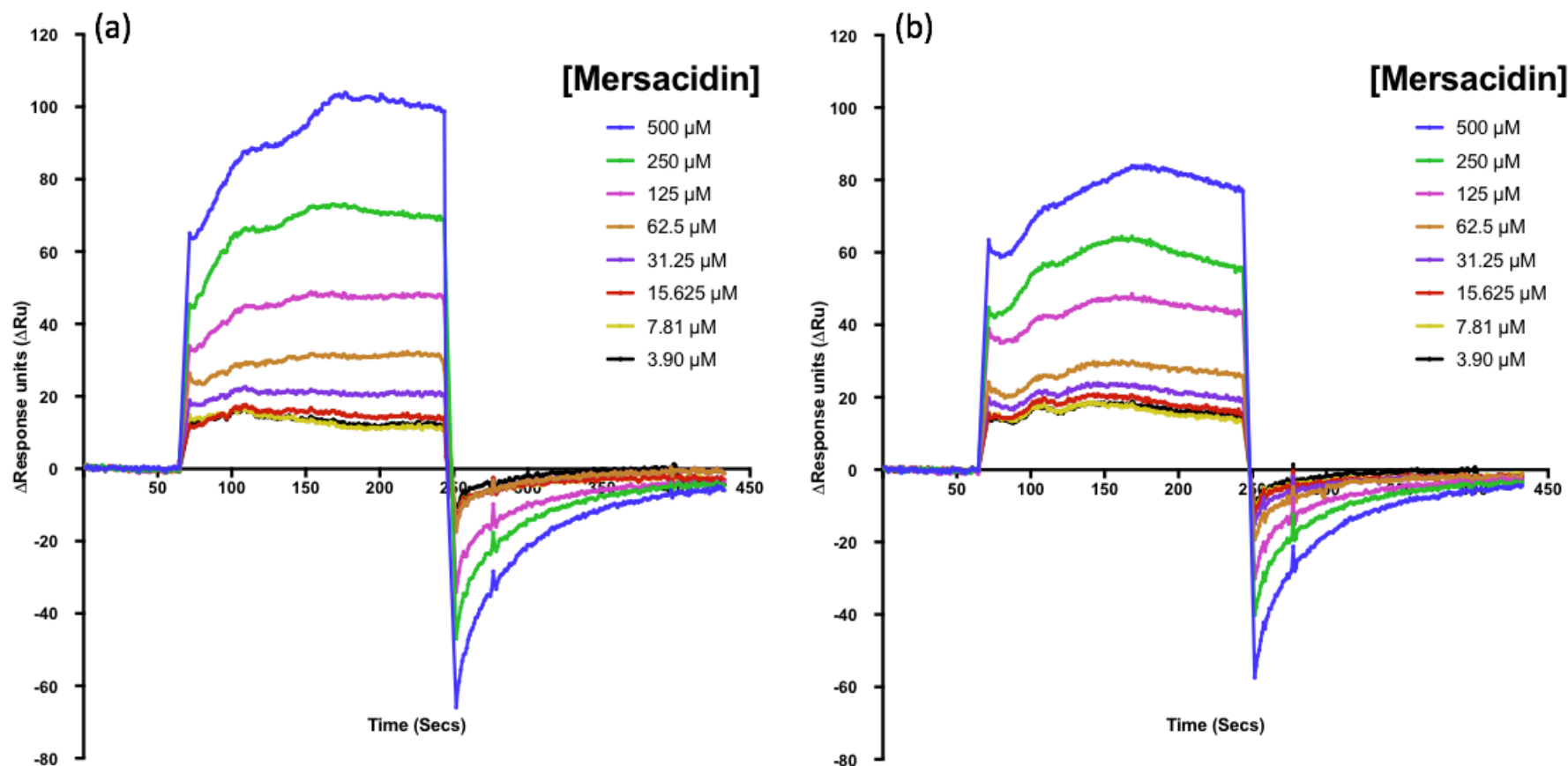


Figure 4.35 SPR binding affinity of mersacidin to streptavidin immobilised biotinylated Lipid II (DAP) variants. Sensorgram of (a) biotin labelled muramyl N-acetylated Lipid II (DAP) and (b) biotin labelled muramyl N-glycolylated Lipid II (DAP) binding to increasing concentrations of mersacidin. Binding affinity measured in response units (RU) for 180 seconds. Mersacidin concentrations: 500 μM (Blue), 250 μM (Green), 125 μM (Pink), 62.50 μM (Orange), 31.25 μM (Purple), 15.625 μM (Red), 7.81 μM (Yellow) and 3.90 μM (Black).

The observation of an immediate increase in RU once the antimicrobial was added to the flowing solution seen in Figure 4.33 was reminiscent of the behaviour of ramoplanin although the increase was less pronounced. However the association/dissociation kinetics were still too rapid to analyse and therefore estimates of k_{on} , k_{off} and k_d could not be made. The increase for 500 μM (Figure 4.35 Blue) was 65 RU (N-acetylated) and 60 RU (N-glycolylated) respectively. Binding of mersacidin to both lipid II variants was not characterised by a steady increase or maintained plateau, at each antibiotic concentration (Figure 4.35) with peaks and valleys caused by periods of binding association and dissociation during the addition of the antimicrobial to the flowing solution. Steady state was achieved for each concentration below 250 μM .

The dissociation of mersacidin after 240 seconds was also immediate at each concentration and altered the binding curve, causing it to drop below the baseline of the sensorgram due to the analyte absent buffer altering the refractive index of the sensor as it is being regenerated to baseline. The maximum RU for each mersacidin concentration was plotted versus mersacidin concentration to compare the binding affinity of the antibiotic to each immobilised lipid as shown in Figure 4.36.

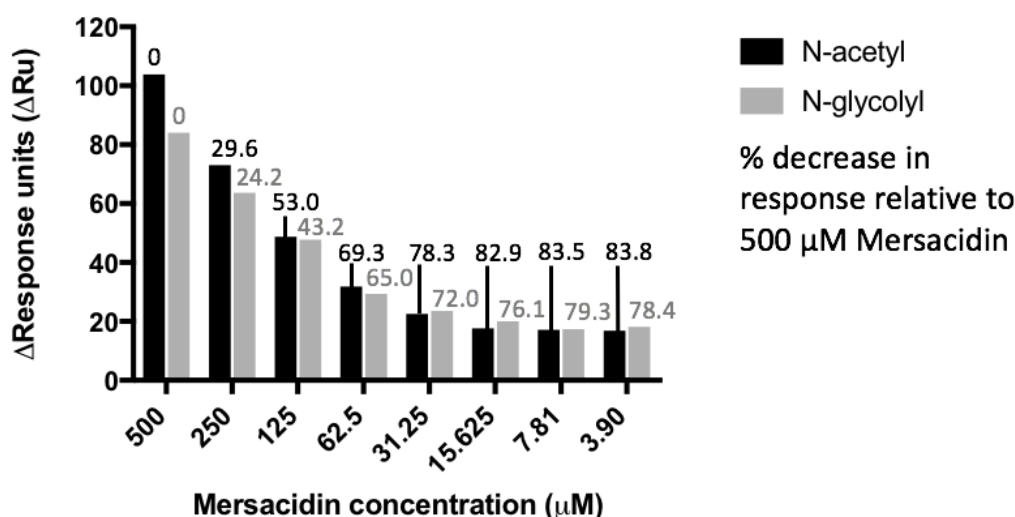


Figure 4.36 SPR steady state response of immobilised biotinylated Lipid II (DAP) variants binding to mersacidin. Comparison of streptavidin bound biotin labelled N-acetylated Lipid II (DAP) (Black) and N-glycolylated Lipid II (DAP) (Grey) maximum response units (RU) value to interactions with increasing concentrations of mersacidin. The percentage decrease in relative response compared to the 500 μM highest concentration for both Lipid II variants is labelled.

The steady state comparison of mersacidin binding in Figure 4.36 demonstrated an at best, marginal preference of the antimicrobial in binding to the N-acetylated Lipid II

(DAP) (Figure 4.36 Black) than the N-glycolylated Lipid II (DAP) Figure 4.36 Grey) at concentrations less than 31.25 μM . At 500 μM the maximum RU achieved by each lipid was 103.87 RU (N-acetylated) and 84.07 RU (N-glycolylated). The percentage difference in RU between binding of N-glycolyl and N-acetyl Lipid II species at these higher concentrations was 19.07% (500 μM) 12.92% (250 μM), 2.2% (125 μM) and 7.74% (62.5 μM) although the significance of these differences was too small to rule out simple experimental errors as a source of the RU differences. Concentrations below 62.5 μM demonstrated a greater equivalency between the two lipids with N-glycolylated lipid producing slight increases in percentage difference at lower RU values. Variations between the two lipids were 4.44% (31.25 μM), 13.76% (15.625 μM), 1.22% (7.81 μM) and 7.79% (3.90 μM). However again, these differences were too small to be considered indicative of a genuine influence of N-glycolylation on mersacidin binding to Lipid II.

The binding affinity of N-acetylated lipid towards mersacidin decreased gradually at the highest concentrations followed by a plateau as the antimicrobial concentration was serially diluted. The percentage decreases in RU for the N-acetylated lipid relative to the 500 μM value were 29.64% (250 μM), 53.04% (125 μM), 69.35% (62.5 μM), 78.31% (31.25 μM), 82.99% (15.625 μM), 83.51% (7.81 μM) and 83.82% (3.9 μM)

The binding affinity of the N-glycolylated lipid towards mersacidin also decreased gradually at high concentrations and remained constant at low concentrations. The percentage decreases in RU for the N-glycolylated lipid were 24.27% (250 μM), 43.24% (125 μM), 65.06% (62.5 μM), 72.01% (31.25 μM), 76.10% (15.625 μM) and 79.38% (7.81 μM) and 78.44% (3.9 μM).

4.6.1.3 SPR analysis of binding of biotinylated Lipid II variants to vancomycin

The MIC assessment of vancomycin showed that cells absent of N-glycolylated peptidoglycan were more susceptible to the actions of the antimicrobial, reducing both the MIC (Figure 4.21) and MBC (Figure 4.22) by half. The SPR binding analysis of

both N-acetylated and N-glycolylated biotinylated Lipid II (DAP) was therefore undertaken to determine if N-glycolylation directly affected the binding of this antibiotic to Lipid II. SPR results are shown in Figure 4.37.

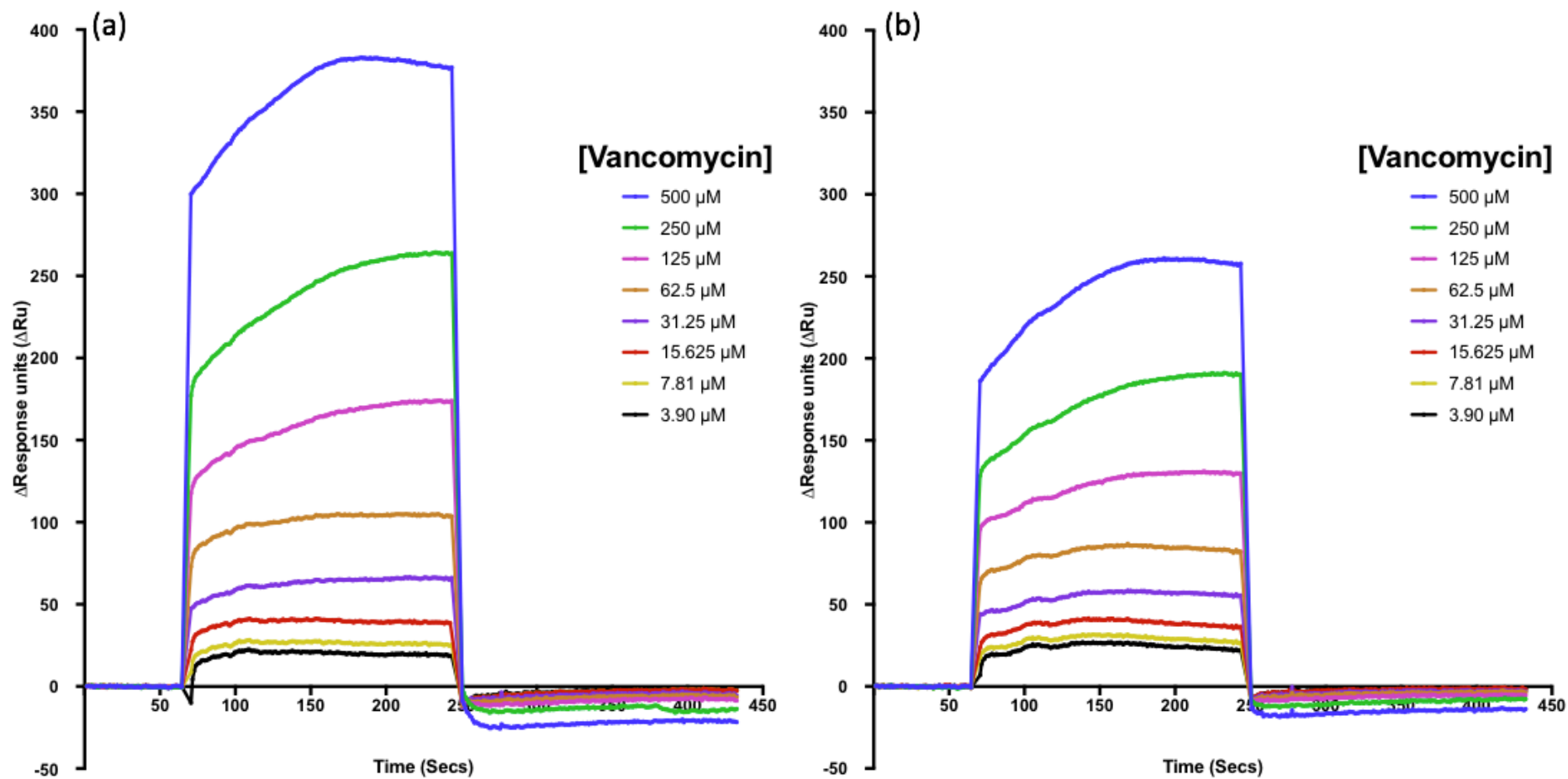


Figure 4.37 SPR binding affinity of vancomycin to streptavidin immobilised biotinylated Lipid II (DAP) variants. Sensorgram of (a) biotin labelled muramyl N-acetylated Lipid II (DAP) and (b) biotin labelled muramyl N-glycolylated Lipid II (DAP) binding to increasing concentrations of vancomycin. Binding affinity measured in response units (RU) for 180 seconds. Vancomycin concentrations: 500 μM (Blue), 250 μM (Green), 125 μM (Pink), 62.50 μM (Orange), 31.25 μM (Purple), 15.625 μM (Red), 7.81 μM (Yellow) and 3.90 μM (Black).

Like mersacidin, vancomycin also demonstrated an initial increase in the binding curve with the addition of the antimicrobial to either lipids. At 500 μM the response of each lipid achieved during steady state was 383.17 RU for the N-acetylated lipid (Figure 4.37 (a)) and 261.10 RU for the N-glycolylated lipid (Figure 4.37 (b)). Once vancomycin was removed from the flowing solution the binding curve at each concentration immediately reverted to the baseline, therefore preventing accurate K_D assessment. The RU values obtained during steady state for each concentration of vancomycin bound to each variant of Lipid II (DAP) was compared to assess binding affinity (Figure 4.38).

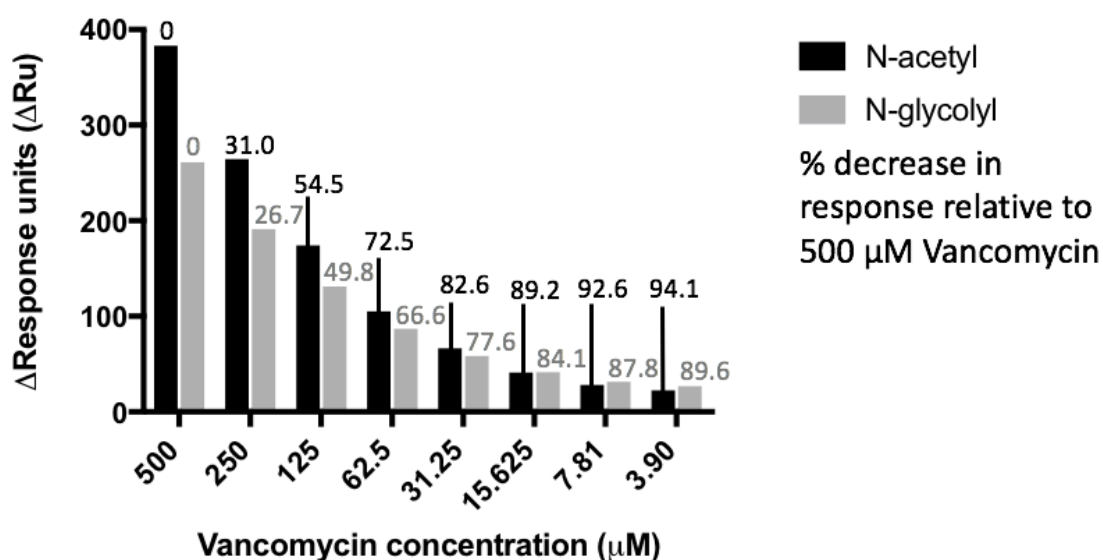


Figure 4.38 SPR steady state response of immobilised biotinylated Lipid II (DAP) variants binding to vancomycin. Comparison of streptavidin bound biotin labelled N-acetylated Lipid II (DAP) (Black) and N-glycolylated Lipid II (DAP) (Grey) maximum response units (RU) value to interactions with increasing concentrations of vancomycin. The percentage decrease in relative response compared to the 500 μM highest concentration for both Lipid II variants is labelled.

Similar to the results obtained for mersacidin in Figure 4.36, the greater the concentration of the antimicrobial the more pronounced the preference for the N-acetylated variant of Lipid II (DAP). The difference reduced with the decrease in vancomycin concentration, where below 15.625 μM vancomycin, both N-glycolylation and N-acetylation lipids behaved identically, although the reduced RU values for each diluted vancomycin concentration, made estimates of response ratios unreliable. The percentage variation between the N-glycolylated and N-acetylated lipids were 31.% (500 μM), 27.95% (250 μM), 24.75% (125 μM), 17.20% (62.5 μM), 12.26% (31.25

μM), 0.65% (15.625 μM), 11.88% (7.81 μM) and 19.86% (3.90 μM). The greater variation observed at 7.81 μM and 3.90 μM was due to the low RU obtained with 11.88% difference between 28.28 RU (N-acetylated) and 31.64 RU (N-glycolylated).

The binding affinity of N-acetylated lipid towards vancomycin decreased gradually at the highest concentrations followed by a plateau as the antimicrobial concentration was serially diluted. The percentage decrease in RU for the N-acetylated lipid relative to the response at 500 μM vancomycin (0%) were 31.00% (250 μM), 54.55% (125 μM), 72.58% (62.5 μM), 82.60% (31.25 μM), 89.23% (15.625 μM) 92.61% (7.81 μM) and 94.12% (3.90 μM).

The binding affinity of the N-glycolylated lipid towards vancomycin also decreased gradually at high concentrations and remained constant at low concentrations. The percentage decrease in RU for the N-glycolylated lipid were 26.76% (250 μM), 49.81% (125 μM), 66.68% (62.5 μM), 77.60% (31.25 μM), 84.09% (15.625 μM), 87.87% (7.81 μM) and 89.66% (3.90 μM).

4.6.2 BLI of biotinylated Lipid II variants to antimicrobials

Biotin labelled Lipid II (DAP) variants were also bound on streptavidin sensors to assess antimicrobial binding affinity by bio-layer interferometry. In short, the binding of antimicrobials in solution to immobilised lipids on biosensor tips alters the measured wavelength ($\Delta\lambda$) shifting the interference pattern caused by an increase in the thickness of the biological layer (Sultana, *et al.* 2015). These variations can be detected and analysed to assess binding affinity. The major difference between SPR and BLI is the formers use of a constantly flowing solution over the coated surface as opposed to the BLI transfer of coated sensors between various solutions (Shah, *et al.* 2015). The stages of an example BLI as demonstrated in Figure 4.39.

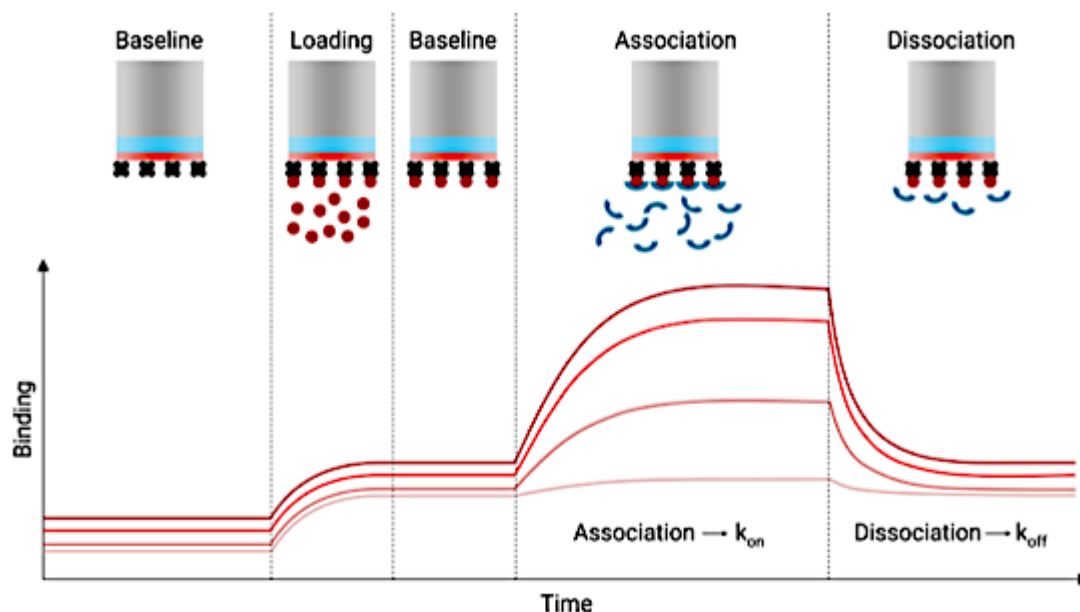


Figure 4.39 Basic BLI binding assessment. Biotin labelled lipids are bound to streptavidin coated sensors and exposed to antimicrobials to assess binding association and dissociation by variations to the measured wavelength. Figure source 2bind molecular solutions.

BLI binding assessment was measured as described by Figure 4.39 by streptavidin coated sensors immobilising biotin labelled lipids and the binding association/dissociation of antimicrobials measured by alterations in the measured wavelength. The BLI protocol outlined in 2.10.2 was utilised against teixobactin, the newly synthesised cell wall active antimicrobial and the analogue arg-teixobactin. Each compound was assessed at two fold diluted concentrations between 500 μM and 15.62 μM . The pre-binding baseline assessment was 30 seconds, antimicrobial association was for 60 seconds and antimicrobial dissociation was for 60 seconds. The results are shown in Figure 4.40.

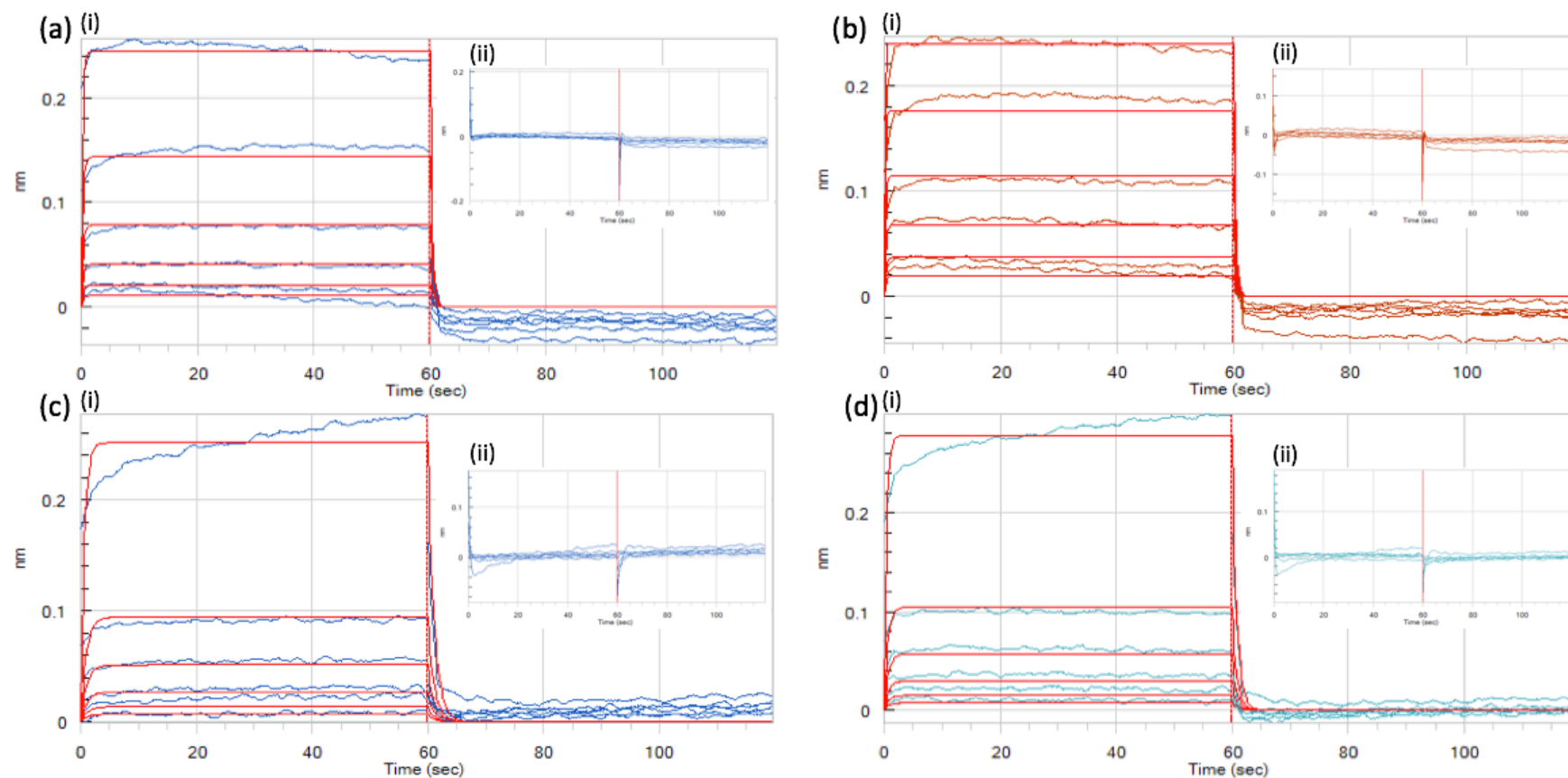


Figure 4.40. Binding affinity of biotinylated Lipid II variants against newly identified antimicrobial teixobactin and the synthesised analogue arginine-teixobactin. Sensorgrams of streptavidin coated sensors bound to N-acetylated Lipid II and N-glycolylated Lipid II were assessed by their affinity towards two-fold serial dilutions from 500 μM to 15.6 μM of teixobactin and arg-teixobactin (i). Reference sensors were used to remove any non-specific binding (ii). (a) N-acetylated Lipid II (DAP) and teixobactin, (b) N-glycolylated Lipid II (DAP) and teixobactin, (c) N-acetylated Lipid II (DAP) and arg-teixobactin and (d) N-glycolylated Lipid II (DAP) and arg-teixobactin. Binding constants were measured with the Octet Data Analysis software on an Octet Red, by global fitting the data with the 1:1 heterogenous ligand model.

The equilibrium dissociation constants (K_D) for both Lipid II (DAP) variants against both teixobactin and arg-teixobactin determined from Figure 4.40 are shown in table 4.12.

Lipid II	Antimicrobial	K_D (M)	K_D Error	K_a (1/Ms)	K_a Error	K_d (1/s)	K_d Error
NAc	Teixobactin	1.55 10^{-3}	8.14 10^{-4}	1.04 10^{+2}	5.38 10^{+2}	1.61 10^{+0}	1.44 10^{-1}
NGlyc	Teixobactin	3.30 10^{-4}	5.46 10^{-5}	5.92 10^{+2}	7.02 10^{+2}	1.95 10^{+0}	2.25 10^{-1}
NAc	Arg- Texiobactin	1.25 10^{-3}	1.27 10^{-4}	7.40 10^{+2}	5.70 10^{+1}	9.21 10^{-1}	6.10 10^{-2}
NGlyc	Arg- Texiobactin	1.21 10^{-3}	1.02 10^{-4}	1.08 10^{+3}	6.77 10^{+1}	1.30 10^{+0}	7.42 10^{-2}

Table 4.12. The equilibrium dissociation constants, K_D for biotinylated Lipid II variants to teixobactin and arg-teixobactin. N-acetylated and N-glycolylated Lipid II (DAP) attached to streptavidin biosensors binding measured against concentrations of Teixobactin and Arg-teixobactin between 1000 μ M and 15.62 μ M.

Teixobactin results from table 4.12 indicated that the antimicrobial demonstrated a greater binding affinity with the N-glycolylated Lipid II (DAP) with a K_D of 0.33 mM, five times greater compared to the K_D with the N-acetylated Lipid II (DAP) of 1.55 mM. The K_D is based upon the relationship between the association (k_a) and dissociation (k_d) of teixobactin towards each lipid. The rate of dissociation for each lipid was similar with k_d values of 1.61 s^{-1} (N-acetylated) and 1.95 s^{-1} (N-glycolylated). The variation was noted during association with k_a values of 104 Ms^{-1} (N-acetylated) and 592 Ms^{-1} (N-glycolylated) respectively.

The arginine analogue of teixobactin displayed a similar binding affinity towards each of the lipids compared to texiobactin with a lower K_D of 1.25 mM for the N-acetylated lipid than the 1.22 mM for the N-glycolylated lipid. The association constant of each lipid was 74 Ms^{-1} (N-acetylated) and 108 Ms^{-1} (N-glycolylated) respectively, which led to the K_D variation observed. The dissociation constant for each lipid was 0.9 s^{-1} (N-acetylated) and 1.30 s^{-1} (N-glycolylated) respectively.

4.7 Discussion

4.7.1 Antimicrobial MIC assessment of Δ NamH *M. smegmatis*

Mycobacteria are inherently resistant to antimicrobials (Hett and Rubin 2008) due in part to the expression of β -lactamases, efflux pumps and the composition of the mycobacterial cell wall. The incorporation of N-glycolylated Lipid II within the mycobacterial peptidoglycan layer was previously demonstrated to increase resistance towards hydrolytic enzymes as well as antimicrobial therapies. These treatments commonly target unique structural architecture displayed solely by bacteria, without a eukaryotic equivalent such as peptidoglycan.

Generation of *blaS⁻*, and *blaS⁻ namH⁻* strains by Flores, *et al.* (2005), permitted the probing of antimicrobial susceptibility of mycobacteria against standard treatments and measured average zones of clearing at set concentrations of antibiotics. Previously published results by Raymond, *et al.* (2005) demonstrated that antimicrobials such as isoniazid and ethambutol which targeted non peptidoglycan synthesis components, were equally active towards both mycobacterial strains whereas, the β -lactam antibiotics ampicillin and amoxicillin produced greater zones of inhibition against *namH* deficient organisms. Further assessment of antimicrobial efficacy towards these strains was required as well as an expansion of investigated targets.

The low aqueous solubility of the antimicrobials considered in this chapter required the determination of mycobacterial solvent tolerance. Growth of both *blaS⁻*, and *blaS⁻ namH⁻* strains was equally sensitive to increasing percentages of DMSO. Nevertheless, a solvent concentration of 2% (v/v) DMSO (Figure 4.1) effectively solubilised the investigated antimicrobials without impacting mycobacterial growth.

4.7.1.1 The impact of non-peptidoglycan targeted antimicrobials on *M. smegmatis* growth

Acquisition of the Δ NamH *M. smegmatis* knockout mutants led to initial reassessment of standard isoniazid antimicrobial treatment. Both wild type and knockout *M. smegmatis* were equally sensitive to this antibiotic to which they responded with the same MIC and MBC values (Figure 4.6). Mycolic acids form a complex with both peptidoglycan and arabinogalactan (mAGP) (Alderwick, *et al.* 2015) Isoniazid targets mycolic acid synthesis particularly the 2-trans-enoyl-acyl carrier protein reductase, InhA (Marrakchi, *et al.* 2000). Consistent with this therefore, is the observation made here that the potency of isoniazid is unaffected by the nature of the N-acyl group appended to the muramyl component of the peptidoglycan.

4.7.1.2 The impact of peptidoglycan targeted antimicrobials on *M. smegmatis* growth

Raymond, *et al.* (2005), observed that growth of Δ NamH *M. smegmatis* with a peptidoglycan containing entirely N-acetylated muramyl residues was more sensitive to ampicillin, the corresponding wild type strain which contained both N-acetylated and N-glycolylated sugars. Ampicillin differentially impacted the growth of wild type and Δ NamH *M. smegmatis* strains, reducing the MIC and MBC of the Δ NamH strain to half that of the wild type (Figure 4.3 and Figure 4.4). Both the wild type and Δ NamH cells are *bla*S⁻ mutants which also increase β -lactam susceptibility due to the absence of the β -lactamase BlaS.

Previously studied *bla*S⁻ *M. smegmatis* displayed an ampicillin MIC of 2 $\mu\text{g.mL}^{-1}$ (Flores, *et al.* 2005), greater than the corresponding 0.5 $\mu\text{g.mL}^{-1}$ and 0.25 $\mu\text{g.mL}^{-1}$ values observed here for the wild type and Δ NamH strains respectively (Figure 4.3). The discrepancy between the two sets of findings is unknown though the results obtained by Flores, *et al.* (2005) was from a separate *M. smegmatis* strain not related to the one used here that was acquired from Raymond, *et al.* (2005). However, there was no indication that ampicillin MIC assessment was measured below 2 $\mu\text{g.mL}^{-1}$

¹ in Flores, *et al.* (2005), suggesting that differences in ampicillin sensitivity could be artifactual.. The functional impact of N-glycolylation modification of monosaccharides may involve changes in recognition by PBPs of their peptidoglycan precursor substrates or the rapidity with which the transglycosylase polymerises the substrate, where this activity is greater with N-glycolylated precursors which therefore compete better against β -lactam challenge, resulting in sooth wild type was more resistant than Δ NamH to ampicillin.

The pool of investigated antimicrobials was expanded to include a number of inhibitors which specifically target either transglycosylase activity of PBPs or MraY. Ramoplanin prevents transglycosylation by binding to the head group of Lipid II (Fang, *et al.* 2006). Its inclusion permitted an assessment of whether N-glycolylation impacted the binding affinity of the antimicrobial, in part explaining the abundance of MurNGlyc:MurNAc saccharides within the peptidoglycan layer (Raymond, *et al.* 2005). Growth of NamH deficient *M. smegmatis* was more significantly attenuated than wild type by ramoplanin, although, the final MIC was the same ($1 \mu\text{g.mL}^{-1}$) for both strains (Figure 4.9).

Generation of biotin labelled N-acetylated (Figure 4.29) and N-glycolylated (Figure 4.30) Lipid II allowed for a more detailed SPR investigation into the binding of ramoplanin to the individual variants of Lipid II. Here, ramoplanin bound more strongly to N-acetylated lipids than N-glycolylated lipids (Figure 4.34), maintaining a stable 35% measured response across all investigated ramoplanin concentrations. Combining the findings of the MIC assessment and the SPR binding affinity show that the decreased susceptibility of the wild type strain could be attributed to the increased percentage of N-glycolylated lipids within the peptidoglycan layer, resulting in reduced interactions with the antimicrobial.

The transglycosylase inhibitor mersacidin functions by chelation of Lipid II preventing the binding to the TG domain of PBPs (Appleyard, *et al.* 2009). Mersacidin MIC assessment revealed that as with ramoplanin, solely N-acetylated peptidoglycan of the Δ NamH strain was more susceptible than the wild type at equivalent mersacidin concentrations (Figure 4.15), though the MIC for both strains was the same. Both antimicrobials bind directly to Lipid II. Data therefore indicates that the interactions between both ramoplanin and mersacidin and Lipid II are impeded by the presence

of the N-glycolyl group, however, this detriment was not able to solely increase cell antimicrobial tolerance at MIC concentrations. The binding affinity of mersacidin to biotin labelled N-acetylated Lipid II were greater than N-glycolylated Lipid II at high concentrations of mersacidin (Figure 4.36). The N-acetylated binding preference was diminished as investigated antimicrobial concentrations were reduced with binding affinity of the two lipid variants remaining equivalent. Conclusions drawn from this data were that in high concentrations of mersacidin binding to the N-acetylated lipid was increased compared to the N-glycolylated lipid leading to the NamH strain demonstrating increased susceptibility to this antibiotic..

Tunicamycin targets the active site of MraY located on the cytosolic face of the cytoplasmic membrane. The drug and binds irreversibly to MraY to prevent the formation of Lipid I (Al-Dabbagh, *et al.* 2008). As previously stated, N-glycolylation occurs within the cytosol of the mycobacteria unlike other common peptidoglycan modifications (Moynihan and Clarke 2010). MIC assessment (Figure 4.12) concluded that relative to wild type, the Δ NamH strain was equally impacted by each tunicamycin concentration with no noted statistically significant variation between strains, yielding identical with tunicamycin MIC values. Competitive inhibition by tunicamycin of the MraY active site was therefore unaffected by the N-glycolylation of its UDP-MurNGlyc-pentapeptide substrate.

The MIC assessment of moenomycin showed that the Δ NamH strain is more susceptible than the wild type and displayed notable variation in comparing the growth phenotype of wild type and Δ NamH *M. smegmatis* strains. Moenomycin mimics Lipid IV and inhibits peptidoglycan glycosyltransferases (Galley, *et al.* 2014). It is possible that the N-glycolyl modified Lipid II bound more tightly than the N-acetylated lipid to these enzymes and so competed better against moenomycin for TG active sites. Therefore, removal of the N-glycolyl moiety from the mycobacterial peptidoglycan would, as observed, increase the sensitivity to moenomycin inhibition, rendering the Δ NamH strain more sensitive to the drug than the wild type.

The prevalence of antimicrobial resistance in tuberculosis has led to the utilisation of vancomycin as a secondary antibiotic therapy (Chua, *et al.* 2009), targeting the extracellular D-alanyl-D-alanine of the amino acid stem of disaccharide pentapeptides (Wang, *et al.* 2018). The importance of the

N-glycolyl group to antimicrobial resistance was clearest during vancomycin MIC assessment (Figure 4.21). The Δ NamH strain demonstrated increased susceptibility at each evaluated vancomycin concentration and was entirely inhibited from growth at half the vancomycin concentration of the wild type.

These results complemented the findings of the SPR binding affinities towards the antimicrobial by each modified Lipid II (Figure 4.38). Mersacidin as observed with other antimicrobial preferentially binds to the N-acetylated more readily than the N-glycolylated lipid II equivalent. This preference was shown across all but the lowest of concentrations. Vancomycin interacts with the terminal residues of the peptide stem, so therefore interactions impeded by the hydroxyl group attached to the muramic acid saccharide must depend upon the three dimension structure of the intermediate (Figure 1.8). Alternatively, the rate of synthesis of the N-glycolylated lipid II and/or its incorporation into the cell wall might be such that N-glycolylated precursors are better able to out-compete the impact of vancomycin (and for that matter other cell wall antibiotics) than N-acetylated species, accounting for the greater sensitivity of NamH *M. smegmatis* to vancomycin and other peptidoglycan directed antimicrobials.

Antimicrobial resistance towards standard therapies also is leading to the need for new discoveries and treatments. The newly isolated teixobactin is being hailed as a major breakthrough with a unique target of the prenyl-pyrophosphate-GlcNAc region of Lipid II (Ling, *et al.* 2015). MIC assessment determined that N-glycolylated substrates did not the activity of teixobactin with the MIC and MBC values for both the wild type and Δ NamH strains being equivalent. Teixobactin binding affinities towards each variant of lipid were evaluated by BLI (Figure 4.40) which demonstrated that the antimicrobial had a five times lower K_D for the N-acetylated lipid relative to its the N-glycolylated homologue. The observed preferential binding although, did not impede the MIC of the Δ NamH. Interactions between the antimicrobial and the N-glycolyl may reduce binding efficiency but not to a significant enough degree to impede the mycobacterial growth phenotype of the Δ NamH. Again, the impact of the binding affinity of teixobactin may well be offset by differential rates of peptidoglycan synthesis driven by N-glycolylated relative to N-acetylated precursors.

The teixobactin analogue, arginine-teixobactin has been previously described as possessing more modest antimicrobial activity than teixobactin (Jad, *et al.* 2015), which was demonstrated with an MIC four times greater (Figure 4.27) and an MBC eight times greater (Figure 4.28) in the analogue compared to the original. Both wild type and Δ NamH *M. smegmatis* strains demonstrated the same MIC and MBC values against arg-teixobactin, although sub MIC concentrations impacted the Δ NamH to a more significant degree than the wild type. Binding affinities of the two lipid variants were evaluated against the analogue by BLI and findings concluded that arg-teixobactin interacts with an equal K_D value to both lipids. The analogue is formed by the utilisation of L-arginine substituted in place of the original residue, L-allo-endurcididine. This substitution reduces both the activity of the antimicrobial and the interactions with the N-glycolyl group of the wild type compared to teixobactin.

4.8 Further work

- Assess *namH* susceptibility with a *blaS*⁺ strain

The *M. smegmatis* strains investigated were both *blaS*⁻, removing the dominant β -lactamase (Raymond, *et al.* 2005), reducing the resistance of the strains to common β -lactam antibiotics such as ampicillin (Flores, *et al.* 2005). This chapter demonstrated that the *blaS*⁻ *namH* *M. smegmatis* strain demonstrated greater susceptibility than the solely *blaS* strain to ampicillin. Generation of both *blaS*⁺ and *blaS*⁺ *namH* strains and implementation of antimicrobial assessment would determine the relationship between the β -lactamase enzyme and the N-glycolylation of Lipid II in providing increased resistance during antimicrobial therapy.

- Explore methods of peptidoglycan intermediate labelling

Biotinylation occurs at the third amino acid of the pentapeptide stem. The close proximity to the stem terminal may affect the interactions with antimicrobials such as vancomycin. Therefore,

investigation of other methods of labelling peptidoglycan intermediates that are either smaller in size or located elsewhere on the intermediate may be warranted. One alternative is dansylation (Bouhss *et al.* 2008) the modification of the third position amino acid of the pentapeptide stem by dansyl chloride to fluorescently label Lipid II.

- Improve SPR coating

Issues arose with the SPR analysis and measuring association and dissociation binding, due to over saturation during the coating of the SPR streptavidin coated flow cells. Application of a lower set of concentrations of each biotinylated lipid loaded onto each flow cell to achieve a set response unit value would increase the time period from initial antimicrobial interaction to complete saturation permitting binding analysis to be determined.

- Assess further antimicrobials by BLI and SPR

An avenue of investigation highlighted by the results reported here would be to expand the investigation into variants of Lipid II and their associated binding affinities towards a broader range of antimicrobials.

4.9 Conclusion

The absence of N-glycolylated peptidoglycan monosaccharides impacted the susceptibility of *M. smegmatis* cells depending on the mode of action of the antimicrobial. Compounds which targeted the pentapeptide stem or enzymes which interact with it will be more susceptible than those that targeted other structures. The binding affinity of these compounds was greater towards the N-acetylated lipids in most cases providing an explanation for the role of the N-glycolyl modification in antimicrobial resistance.

Chapter 5. Variations in mycobacterial peptidoglycan synthesis enzymes

5.1 Introduction

The N-glycolylation of peptidoglycan investigated in previous chapters are modified during aerobic conditions (Raymond, *et al.* 2005) throughout the cytoplasmic formation of the peptidoglycan subunit Lipid II (Vollmer 2008). This alteration differs from other common peptidoglycan modifications such as O-acetylation (Section 1.3.8.1) and N-deacetylation (Section 1.3.8.2) due to cellular localization of enzymes which enact these modifications (Moynihan and Clarke 2010). The ability of mycobacterial organisms to synthesize N-glycolylated Lipid II solely during aerobic conditions has led to investigations into the role of NamH on the cellular flux of peptidoglycan biosynthesis, with particular focus on the Mur ligases.

5.2 *M. leprae* peptidoglycan biosynthesis

Due to the effects of significant genomic degradation, the mycobacterial pathogen *M. leprae* does not possess a functional gene equivalent to NamH, and instead contains only a pseudogene (ML0085c) (Mahapatra, *et al.* 2008). Therefore *M. leprae* is unable to create N-glycolylated peptidoglycan, expressing only the N-acetylated variant. The implementation of N-glycolylated lipids within the peptidoglycan layer confers resistance to both hydrolytic enzymes and antimicrobials (Raymond, *et al.* 2005) as has been described previously in this thesis.

The Mur ligases within *M. leprae* also possesses specific characteristics. As with other mycobacteria, the first enzyme in the peptidoglycan biosynthesis pathway MurA (Nasiri, *et al.* 2017) demonstrates inherent resistance towards the antimicrobial fosfomycin (De Smet, *et al.* 1999). The antimicrobial's mode of action is to modify the MurA active site cysteine residue to inhibit activity. The mycobacterial *murA* gene sequence translates an aspartate residue at this

position to counteract inhibition. The standard amino acid sequence for a broad range of organisms affix the pentapeptide stem with an L-alanine residue at position one by the enzyme MurC (Vollmer 2008). *M. leprae* MurC adheres an L-lysine at the muramic acid saccharide instead (Mahapatra, *et al.* 2000).

5.3 Experimental aims

To probe the mycobacterial variations in peptidoglycan synthesis, through cloning, expression and characterization of a range of mycobacterial peptidoglycan enzymes within the pathway. To investigate the effect of N-glycolylated substrates on mycobacterial Mur ligases and PBPs to measure the variation on cell flux and binding affinity compared to the N-acetylated substrate.

5.4 *M. leprae* MurA

The *murA* gene of the organism *Mycobacteria leprae* is 1254 bp long with a comparative protein sequence similarity to other mycobacteria of 95.9% (*M. tuberculosis*) and 90.67% (*M. smegmatis*) respectively as shown in Figure 5.1 (www.ncbi.nih.gov/BLAST).

```

M. leprae      MAERFVVTGGNRLSGEVAVGGAKNSVLKLMMAATLLAEGTSTITNCPDILDVPLMAEVLRG 60
M. tuberculosis MAERFVVTGGNRLSGEVTVGGAKNSVLKLMMAATLLAEGTSTITNCPDILDVPLMAEVLRG 60
M. smegmatis   MSERFVVTGGNRLSGEVAVGGAKNSVLKLMMAAALLAEGTSTITNCPDILDVPLMAEVLRG 60
*:*:*:*:*:*:*:*:*:*:*:*:*:*:*:*:*:*:*:*:*:*:*:*:*:*:*:*:*:*:*:*:*:*

M. leprae      LGATVELDGDVARITAPDEPKYDADFAAVRQFRASVCLGPLVGRCKRARVALPGGDAIG 120
M. tuberculosis LGATVELYGDVARITSPDEPKYDADFAAVRQFRASVCLGPLVGRCKQARVALPGGDAIG 120
M. smegmatis   LGATVELDGATVRITSPDEPKYDADFAAVRQFRASVCLGPLVGRCKKARVALPGGDAIG 120
***** * . :*:*:*:*:*:*:*:*:*:*:*:*:*:*:*:*:*:*:*:*:*:*

M. leprae      SRPLDMHQAGLRQLGAHCNIEHGCVVARAETLRGAEIQLEFPSSVGATENILMAAVVAEGV 180
M. tuberculosis SRPLDMHQAGLRQLGARCNIHGCVVAESAETLRGAEIQLEFPSSVGATENILMAAVVAEGV 180
M. smegmatis   SRPLDMHQAGLRQLGATCNIHGCVVAEADHLHGAEIQLEFPSSVGATENILMAAVVAEGV 180
***** * . :*:*:*:*:*:*:*:*:*:*:*:*:*:*:*:*:*:*:*:*:*

M. leprae      TTIHNAAREPDVVDLCTMLNQMGAGQVEGAGSPTMTITGVPRLPTEHRVIGDRIVAATWG 240
M. tuberculosis TTIHNAAREPDVVDLCTMLNQMGAGQVEGAGSPTMTITGVPRLYPTEHRVIGDRIVAATWG 240
M. smegmatis   TTIHNAAREPDVVDLCAMLNEMGAQISGAGTSTLTITGVDRLYPTEHRVIGDRIVAATWG 240
*****:*:*:*:*:*:*:*:*:*:*:*:*:*:*:*:*:*:*:*:*:*

M. leprae      IAAAMTRGDISVAGVDPAPHLQLVLHKLHDAGATVTQTDASFRVTQYERP KAVNVATLFFP 300
M. tuberculosis IAAAMTRGDI AVTVGDPAPHLQLVLHKLHDAGATVTQDD SFRVAQYERP KAVNVATLFFP 300
M. smegmatis   IAAAMTRGDI TVTVGDPQHLQLVLHKLHDAGATVTQNDNGFRV VQYERP KAVNVATLFFP 300
*****:*:*:*:*:*:*:*:*:*:*:*:*:*:*:*:*:*:*:*:*

M. leprae      GFPTDLQPMIALAS IADGTSMITENVFEARFRFVEEMIRLGADARTDGHHA VVRGLPQL 360
M. tuberculosis GFPTDLQPMIALTS IADGTSMITENVFEARFRFVEEMIRLGADARTDGHHA VVRGLPQL 360
M. smegmatis   GFPTDLQPMIAGLAAIADGTSMITENVFEARFRFVEEMIRLGADARTDGHHA VVRGIPQL 360
*****.*:*:*:*:*:*:*:*:*:*:*:*:*:*:*:*:*:*:*:*

M. leprae      SSAPVWCSDIRAGAGLVLAGLVADGDTEVHDVPHIDRGYPLFVENLVSLGAEIERVCC 418
M. tuberculosis SSAPVWCSDIRAGAGLVLAGLVADGDTEVYDVPHIDRGYPLFVENLANLGAEIERVCC 418
M. smegmatis   SSAPVWSSDIRAGAGLVLAGLVADGETEVHDVPHIDRGYPLFVENLVSLGAEIERVSS 418
*****.*:*:*:*:*:*:*:*:*:*:*:*:*:*:*:*:*:*:*:*

```

Figure 5.1 Protein sequence alignment of the peptidoglycan synthesis gene *murA* within selected mycobacteria. *M. tuberculosis*, *M. leprae*, and *M. smegmatis* demonstrate a significant amount of amino acid homology between organisms. (*) indicate conserved residues, (:) indicate strongly similar residues and (.) indicate weakly similar residues. (www.ncbi.nih.gov/BLAST). The active site aspartate at position 118 for each enzyme is highlighted in red.

The *murA* gene was acquired from GenScript, and was synthesized to present a NdeI restriction site at the 5' end and a XhoI restriction site at the 3' end. The restriction sites are shown in Table 2.3. The gene was selected to be optimized for expression within *E. coli* and inserted within a standard pUC57 vector (Section A1.1). The *murA* gene was amplified by PCR (Section 2.6.1) to determine its presence within the plasmid using pUC57 forward and reverse primers (Section 2.6.8) corresponding to genetic sequences upstream and downstream of the *murA* gene sequence within the multiple cloning region of the pUC57 plasmid. The annealing temperature during PCR was 48°C. Results of this PCR are shown in Figure 5.2.

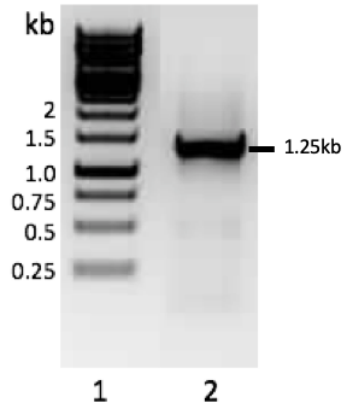


Figure 5.2 PCR amplification of *M. leprae murA*. 1% Agarose gel electrophoresis of *M. leprae murA* gene utilizing forward and reverse primers targeting the up- and downstream regions of the multiple cloning site with the vector pUC57. Lane 1. DNA marker, Lane 2. *M. leprae murA*. Result: observation of single amplified 1.25 kb DNA band corresponding to the known size of *M. leprae murA*

DNA amplified by PCR showed a single bold band with an estimated size, based upon the DNA markers (Figure 5.2) of 1.25 kb corresponding to *M. leprae murA*. The gene contained within the sample plasmid was sent for sequencing analysis with the same primers and returned a positive and accurate genetic match for *murA*.

5.4.1 Cloning of *M. leprae MurA*

M. leprae murA gene was amplified by PCR, using the pUC57 forward and reverse primers. The gene and the expression plasmid pCOLD (Section A1.2) were digested by NdeI and XhoI restriction enzymes (Section 2.6.2). Following restriction, digested products were purified (Section 2.6.3) to isolate the genetic material and quantified to determine the DNA concentration. Digested plasmid concentration was 220 ng/μL and the *murA* gene insert was 344 ng/μL. To prevent the pCOLD plasmid reannealing, 30 minutes incubation with shrimp alkaline phosphatase (SAP) was performed before ligation (Section 2.6.4). The ratio of *murA* to vector was 3:1 for ligation to maximize potential annealing. Samples were incubated for 1 hour and transformed into *E. coli* TOP10 cells. Successful ligations were identified through *E. coli* TOP10 propagation on ampicillin imbedded agar due to the pCOLD vector containing an ampicillin resistance cassette. Newly formed pCOLD-*murA* plasmids were evaluated for in-frame matching of the original *M. leprae murA* gene utilizing pCOLD forward and reverse primers. pCOLD plasmids lack a poly-histidine

tag sequence to aid purification of recombinant proteins. Primers were created, complementing the *murA* gene to adhere a C-terminal poly-histidine tag sequence and a cleavable TEV region, to remove the expressed tag following protein purification. Due to the size of these regions, the TEV and histidine tag sequences were added in stages to improve cloning efficiency. The genetic sequences of the TEV and histidine tag are described in Table 2.2. Once completed *M. leprae murA* genes were once again digested and ligated into pCOLD vectors as described previously, generating two versions of *murA*, one labelled and one unlabeled for further investigations. The resulting genes were sequenced to confirm the presence of the implemented modifications and also the retained *murA* sequence.

5.4.2 Expression of *M. leprae* MurA

pCOLD-*M. leprae murA* plasmids containing the poly-histidine tag sequence were transformed (Section 2.6.9) into competent (Section 2.4.2) *E. coli* tuner (DE3) expression cells, cultured in liquid media and initiated recombinant protein expression through IPTG induction (Section 2.7.1). Once incubation was completed cells were pelleted by centrifugation and fractionated (Section 2.7.2). Cell debris and the insoluble fraction was isolated by centrifugation, and the soluble fractions were analysed by both SDS-PAGE and Western blotting. Results are demonstrated in Figure 5.3.

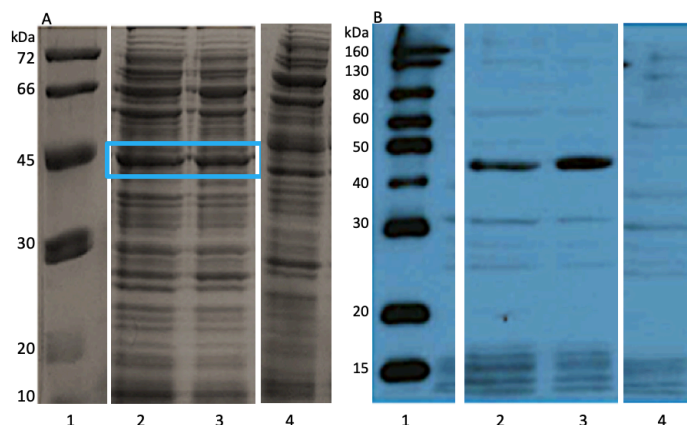


Figure 5.3 SDS-PAGE and Western blot analysis of expressed *M. leprae* MurA. Recombinant MurA protein was expressed in *E. coli* tuner (DE3) cells by the addition of 1 mM IPTG and reduction of incubation temperature from 37°C to 16°C to induced the TEE element. Cells were pelleted, resuspended and lysed by sonication and soluble fractions isolated for electrophoresis separation. Proteins were run on two SDS-PAGE gels, one (A) was Coomassie-stained and another (B) was Western blotted onto a PVDF membrane with anti-His antibodies. Lanes A1: Protein marker, A2: Expression of *M. leprae* MurA (1), A3: Expression of *M. leprae* MurA (2), A4: Expression of empty plasmid, B1: Western blot maker, B2: Expression of *M. leprae* MurA (1), B3: Expression of *M. leprae* MurA (2), B4: Expression of empty plasmid. Results: Presence of histidine tagged *M. leprae* MurA detected in each sample.

The findings of Figure 5.3 displayed that *M. leprae* MurA was successfully expressed in the *E. coli* tuner (DE3) cell line (Figure 5.3: A2-A3 Blue rectangle). Both the SDS-PAGE gel and the Western blotting x-ray produced a noticeable band correlating in size to the protein markers at around 46 kDa, the correct weight for the enzyme. The Western blotting x-ray shows that this protein bound with the anti-His antibodies due to the expression of the C-terminal poly-histidine tag. The expression of the empty plasmid (Figure 5.3: A4) did not lead to expression of MurA as expected.

5.4.3 *M. leprae* MurA active site mutant

To complement the investigation into *M. leprae* MurA, the decision was taken to create an active site mutant to probe the interactions between the enzyme and the antimicrobial fosfomycin (De Smet, *et al.* 1999). The active site of *M. leprae* MurA is resistant towards perturbation by the antimicrobial due to an aspartate residue at position 118 in the amino acid sequence (Figure 5.1 Highlighted red). Fosfomycin susceptibility has been previously described in MurA enzyme which utilize an active site cysteine residue.

5.4.3.1 Site directed mutagenesis of *M. leprae* MurA active site

The *M. leprae* MurA gene was optimized for *E. coli*, which led to the amino acid sequence remaining equivalent, although selected codons were altered to aid expression in *E. coli*. The original aspartate residue was transcribed from the genetic sequence GAT, to transcribe a cysteine residue in its place the codon substitution must be altered to either TGT or TGC. The latter was selected and overlapping extended primers containing this substitution were synthesized. Site directed mutagenesis primers were used on pCOLD-*M. leprae murA* (C-terminal poly-histidine tag) plasmids to amplify the substituted gene through PCR (Section 2.6.6). The genetic sequences for each primer are illustrated in Table 2.4. Resulting genetic material was sequenced to confirm the implementation of the mutation before digestion by NdeI and XhoI and the resulting *murA* (D118C) mutant gene was ligated into pCOLD vectors as described previously.

5.4.3.2 Expression of *M. leprae* MurA active site mutant

pCOLD-*M. leprae murA* (D118C) active site mutant plasmid was transformed into *E. coli* tuner (DE3) and cultured till cells reached OD_{600nm} 0.5-0.7. Exponentially grown cells were then induced with 1 mM IPTG at 16°C overnight. Cells were isolated, fractionated and centrifuged to separate the soluble phase, which was then analysed by SDS-PAGE and Western blotting as displayed in Figure 5.4.

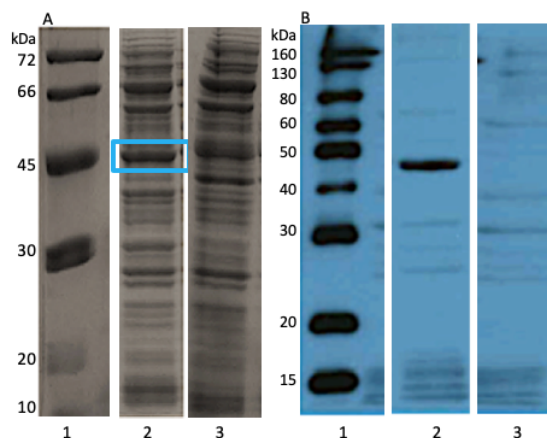


Figure 5.4 SDS-PAGE and Western blot analysis of expressed *M. leprae* MurA active site mutant. Recombinant MurA active site mutant protein was expressed in *E. coli* tuner (DE3) cells by the addition of 1 mM IPTG and reduction of incubation temperature from 37°C to 16°C to induced the TEE element. Cells were pelleted, resuspended and lysed by sonication and soluble fractions isolated for electrophoresis separation. Proteins were run on two SDS-PAGE gels, one (A) was Coomassie-stained and another (B) was Western blotted onto a PVDF membrane with anti-His antibodies. Lanes A1: Protein marker, A2: Expression of *M. leprae* MurA mutant, A3: Expression of empty plasmid, B1: Western blot maker, B2: Expression of *M. leprae* MurA mutant, B3: Expression of empty plasmid,. Results: Presence of histidine tagged *M. leprae* MurA detected.

SDS-PAGE analysis (Figure 5.4A: Blue rectangle) noted a large protein band equivalent to the known 46 kDa size of *M. leprae* MurA. This band was confirmed to be poly-histidine tagged based upon the Western blot x-ray (Figure 5.4B).

5.5 *M. leprae* MurC

The second *M. leprae* Mur enzyme investigated within this chapter is MurC, the first amino acid ligase which attaches N-glycine at position one of the pentapeptide stem (Mahapatra, *et al.* 2005) to only N-acetylated muramic acid due to *M. leprae* NamH being designated as a pseudogene (Mahapatra, *et al.* 2005). The 1485 bp *M. leprae murC* gene was synthesized with an N-terminal 5' NdeI enzyme restriction site and a C-terminal 3' XhoI restriction site, along with *E. coli* expression optimization of codon selection. The protein sequence similarity between other mycobacterial MurC enzymes was 71.91% (*M. smegmatis*) and 79.15% (*M. tuberculosis*) as shown in Figure 5.5.

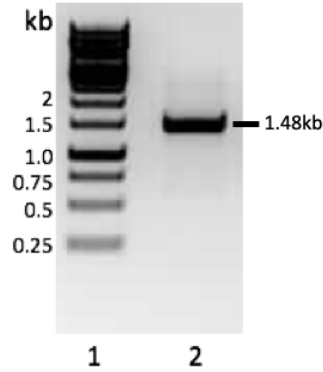


Figure 5.6 PCR amplification of *M. leprae murC*. 1% Agarose gel electrophoresis of *M. leprae murC* gene utilizing forward and reverse primers targeting the up- and downstream regions of the multiple cloning site with the vector pUC57. Lane 1. DNA marker, Lane 2. *M. leprae murC*. Result: observation of single amplified 1.48 kb DNA band corresponding to the known size of *M. leprae murC*.

Results from Figure 5.6 identified a single amplified DNA band 1.5 kb in length. The synthesized gene was evaluated by sequencing methods employing the forward and reverse pUC57 primers. Results confirmed the presence of the full length *M. leprae murC* gene sequence correctly synthesized. Similarly, to the investigation into *M. leprae MurA*, the gene was re-cloned into pCOLD vector following the established protocol, and required the addition of a poly-histidine tag sequence and a cleavable TEV region. The primers required to modify the *murC* C-terminal are shown in Table 2.2. Once the TEV and poly-histidine tag sequences were added to the *murC* gene, it was re-cloned into a pCOLD vector and identified by sequencing.

5.5.2 Expression of *M. leprae MurC*

The pCOLD-*M. leprae murC* (C-terminal poly-histidine tag) was transformed into *E. coli* tuner (DE3) cells and cultured at 37°C until early exponential phase. Cells were induced to express recombinant proteins by addition of 1 mM IPTG and further incubated at 16°C overnight. Cells were fractionated by sonication (Section 2.7.2) and centrifuged to isolate the soluble protein phase. Samples were analysed by SDS-PAGE and Western Blot as shown in Figure 5.7.

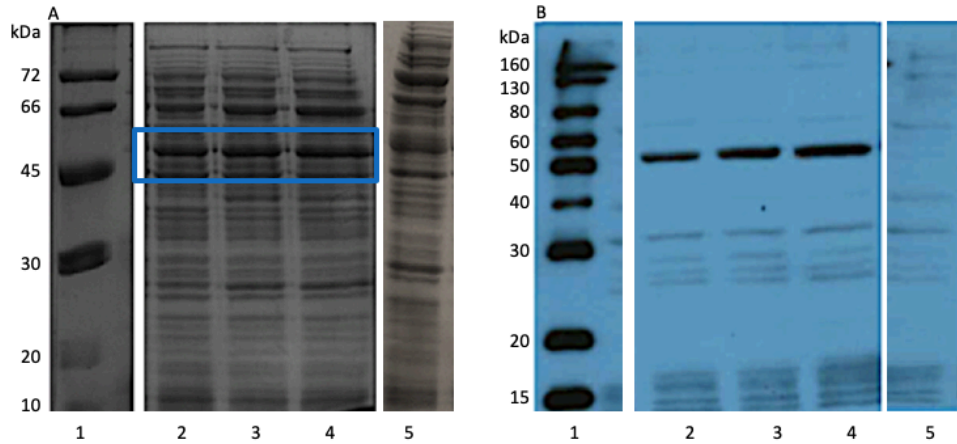


Figure 5.7. SDS-PAGE and Western blot analysis of expressed *M. leprae* MurC. Recombinant MurC protein was expressed in *E. coli* tuner (DE3) cells by the addition of 1 mM IPTG and reduction of incubation temperature from 37°C to 16°C to induced the TEE element. Cells were pelleted, resuspended and lysed by sonication and soluble fractions isolated for electrophoresis separation. Proteins were run on two SDS-PAGE gels, one (A) was Coomassie-stained and another (B) was Western blotted onto a PVDF membrane with anti-His antibodies. Lanes A1: Protein marker, A2: Expression of *M. leprae* MurC (1), A3: Expression of *M. leprae* MurC (2), A4: Expression of *M. leprae* MurC (3), A5: Expression of empty plasmid, B1: Western blot maker, B2: Expression of *M. leprae* MurC (1), B3: Expression of *M. leprae* MurC (2), B4: Expression of *M. leprae* MurC (3), B5: Expression of empty plasmid. Results: Presence of histidine tagged *M. leprae* MurC detected in each sample.

Results of Figure 5.7 demonstrated that incubation conditions and IPTG concentration were sufficient to generate the recombinant MurC protein. SDS-PAGE findings (Figure 5.7A: Blue rectangle) indicated the presence of a protein which corresponded to the known 51 kDa weight of *M. leprae* MurC. Western blotting definitively identified this protein as bound to anti-His antibodies due to the expression of the poly-histidine tag. Soluble active protein was not able to be obtained from the current protocol.

5.6 *M. smegmatis* Mur ligases

M. smegmatis is noted as the mycobacterial standard during investigations, due to its low virulence and relatively rapid growth rate (He and De Buck 2010). Collaborators in the Roper laboratory at the University of Warwick were determining the crystal structure of *M. smegmatis* MurC and MurD and permitted the enzymes binding affinities to be assessed against the two possible muramic acid substrates variants, UDP-MurNAc/UDP-MurNGlyc for MurC and UDP-MurNAc-L-ala/UDP-MurNGlyc-L-ala for MurD. Unlike *M. leprae*, *M. smegmatis* possesses a NamH hydroxylase and is therefore able to generate N-glycolylated substrates for Mur ligases. Binding

favorability of the enzymes was determined by coupled NADH-linked pyruvate kinase/lactate dehydrogenase assay to amino acid Mur ligase activity (Section 2.11.1).

5.6.1 The kinetic profile of *M. smegmatis* MurC binding affinity towards muramic acid variants

The Michaelis-menten enzymatic kinetics graph result for *M. smegmatis* MurC against UDP-MurNAc and UDP-MurNGlyc are shown in Figure 5.8 and the kinetic parameters extrapolated utilizing GraphPad Prism 6 are displayed in Table 5.1.

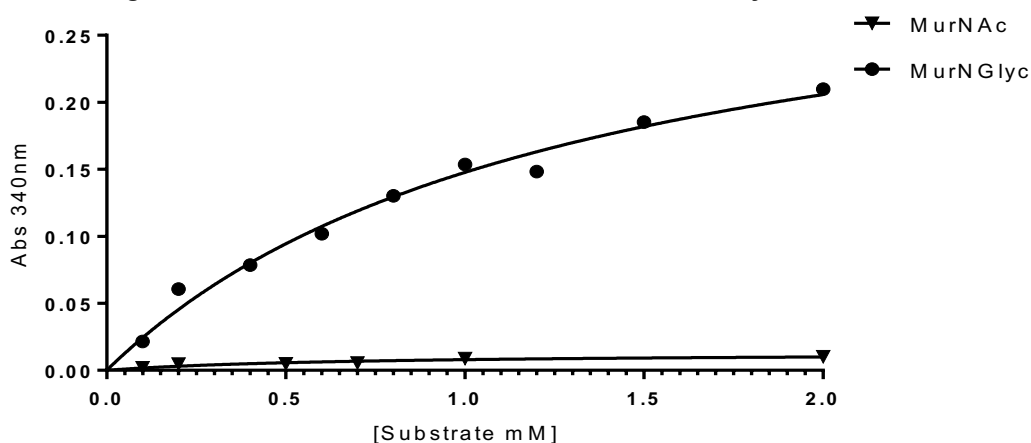


Figure 5.8. Initial rate of *M. smegmatis* MurC enzyme velocity against muramic acid variants. Michaelis-menten graphs depicting the variation in binding affinity of MurC towards UDP-MurNAc and UDP-MurNGlyc substrates at a varying range of concentrations between 0.1 and 2.0 mM. Reaction measured at 340 nm through coupling to the conversion of phosphoenolpyruvate to lactate and measuring the oxidation of NADH to NAD⁺. Graph constructed using GraphPad Prism 6.

<u>Mur Ligase</u>	<u>UDP-MurNGlyc</u>			<u>UDP-MurNAc</u>			<u>Ratio</u>
	K_m^{App} (μ M)	K_{cat}^{App} (min^{-1})	K_{cat}^{App}/K_m^{App} (min^{-1}/μ M) b	K_m^{App} (μ M)	K_{cat}^{App} (min^{-1})	K_{cat}^{App}/K_m^{App} (min^{-1}/μ M) a	b/a
MurC	1296 \pm 256	306.5 \pm 16.09	0.2364	30380 \pm 69010	165.6 \pm 333.3	0.00545	43.38

Table 5.1. *M. smegmatis* MurC kinetic activity constants comparison between binding affinity towards UDP-MurNAc and UDP-MurNGlyc substrates. K_m and K_{cat} extrapolated from the Michaelis-menten kinetic graph in Figure 5.8.

M. smegmatis MurC demonstrated a significant variation in binding affinities towards each of the two possible muramic acid substrates. The investigated concentration range of 0.1-2.0 mM permitted a hyperbolic relationship between MurC and UDP-MurNGlyc, although the binding affinity did not saturate at the concentrations investigated. The UDP-MurNAc substrate however displayed a simple linear relationship. The enzyme showed one sided favorability towards the N-glycolyl substrate with a 43 fold higher affinity and a K_m of 1.29 mM, compared to the N-acetyl substrates K_m of 30.38 mM.

5.6.2 The kinetic profile of *M. smegmatis* MurD binding affinity towards muramic acid variants

The Michaelis-menten enzymatic kinetics graph result for *M. smegmatis* MurD against UDP-MurNAc-L-ala and UDP-MurNGlyc-L-ala are shown in Figure 5.9 and the kinetic parameters extrapolated utilizing GraphPad Prism 6 are displayed in Table 5.2.

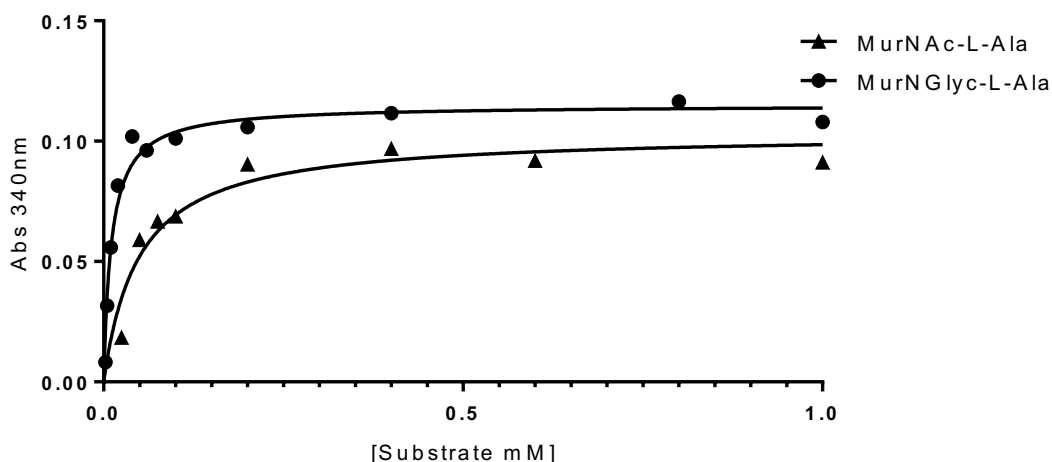


Figure 5.9 Initial rate of *M. smegmatis* MurD enzyme velocity against muramic acid variants. Michaelis-menten graphs depicting the variation in binding affinity of MurD towards UDP-MurNAc-L-ala and UDP-MurNGlyc-L-ala substrates at a varying range of concentrations between 0.01 and 1.0 mM. Reaction measured at 340 nm through coupling to the conversion of phosphoenolpyruvate to lactate and measuring the oxidation of NADH to NAD⁺. Graph constructed using GraphPad Prism 6.

<u>Mur Ligase</u>	<u>UDP-MurNGlyc-L-Ala</u>			<u>UDP-MurNAc-L-Ala</u>			<u>Ratio</u>
	K_m^{App} (μ M)	K_{cat}^{App} (min^{-1})	K_{cat}^{App}/K_m^{App} (min^{-1}/μ M) b	K_m^{App} (μ M)	K_{cat}^{App} (min^{-1})	K_{cat}^{App}/K_m^{App} (min^{-1}/μ M) a	b/a
MurD	10.83 \pm 1.71	8109 \pm 241.1	750.83	49.68 \pm 8.96	7319 \pm 237.00	147.26	5.09

Table 5.2. *M. smegmatis* MurD kinetic activity constants comparison between binding affinity towards UDP-MurNAc and UDP-MurNGlyc substrates. K_m and K_{cat} extrapolated from the Michaelis-menten kinetic graph in Figure 5.9.

The relationship between MurD and both substrate variants was hyperbolic with both interactions plateauing at concentrations greater than 0.2 mM. The noted significant catalytic preference for the N-glycolyl substrate observed in Figure 5.8 for MurC was not sustained in MurD (Figure 5.9), although MurD still demonstrated an over five-fold higher affinity for the N-glycolyl substrate. The narrower variation of substrate K_m values, 10.83 μ M in UDP-MurNGlyc-L-ala and 49.68 μ M in UDP-MurNAc-L-ala, led to a lower range of investigated substrate concentrations between 0.01 mM and 1.0 mM.

5.7 *M. tuberculosis* PonA1 and PonA2

M. tuberculosis utilizes two bifunctional PBPs, PonA1 (Rv0050) and PonA2 (Rv3682) to incorporate newly synthesized Lipid II subunits to the overall peptidoglycan architecture (Kieser, *et al.* 2015). Collaborators from the Besra laboratory at the University of Birmingham, provided both PBPs genes within pET21b expression vectors (Section A1.1.3).

5.7.1 Expression of *M. tuberculosis* PonA1 and PonA2

M. tuberculosis PonA1 and PonA2 genes were sequenced to determine the presence of the PBP, in frame with the addition of a C-terminal poly-histidine tag sequence. PonA1 was confirmed as 2460 bp and PonA2 as 2430 bp in length. Vectors were then transformed into *E. coli* BL21 (DE3) expression strains (Section 2.6.9), and successful insertion of the plasmid was observed through ampicillin resistance selection. Recombinant PBPs were expressed as described previously (Section 2.7.1).

5.7.2 Purification of *M. tuberculosis* PonA1 and PonA2

Recombinantly expressed *M. tuberculosis* PonA1 and PonA2 contained a C-terminal poly-histidine tag permitting purification by IMAC as detailed in Section 2.7.3.1 and shown in Figure 5.10 and Figure 5.11.

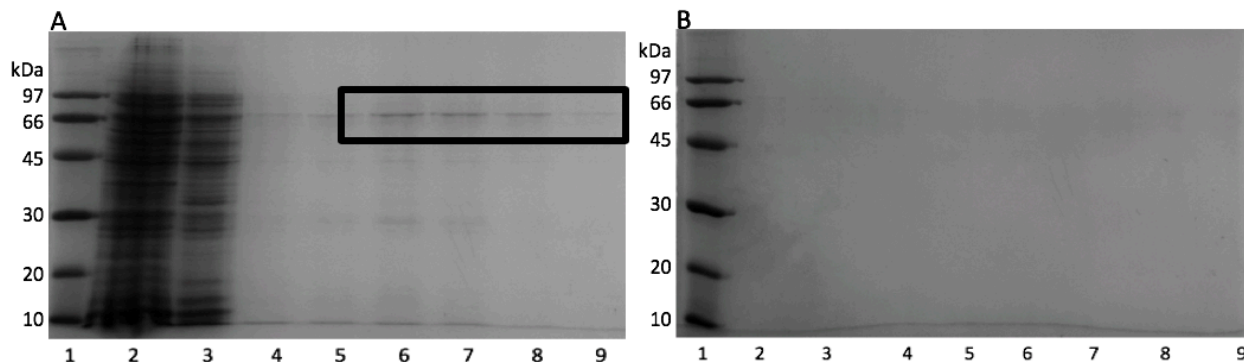


Figure 5.10 Purification of *M. tuberculosis* PonA1. 12% SDS-PAGE analysis gels of Immobilised metal affinity chromatography (5 mL Cobalt) elutions by imidazole (IM) gradient of purified recombinantly expressed PonA1 from *E. coli* BL21 (DE3) expression cell line. Bands visualized by Coomassie blue staining. Lanes A1: Protein marker, A2: Flow through, A3: Wash through, A4: 0mM IM, A5: 10mM IM, A6: 30mM IM, A7: 50mM IM, A8: 100mM IM, A9: 150mM IM, B1: Protein marker, B2: 200mM IM, B3: 250mM IM, B4: 300mM IM, B5: 350mM IM, B6: 400mM IM, B7: 450mM IM, B8: 500mM IM, B9: 500mM IM. Identification of PonA1 for further concentration noted by black rectangle.

IMAC purification of *M. tuberculosis* PonA1 led to mostly successful isolation from other cellular components. PonA1 is an 85 kDa protein present during elution with imidazole concentrations 30-150 mM in Figure 5.10 (Highlight with black rectangle). Eluted fractions corresponding to wells A6-9 were combined and dialyzed (Section 2.7.4) overnight at 4°C in PBP specific assay buffer (Section 2.10.2). The PBP was then concentrated (Section 2.7.5) below 1 mL total volume and the concentration quantified by BCA (Section 2.7.6.2). PonA1 concentration was 3.2 mM. Purification was not entirely successful with other band present in the purified sample which may impact binding.

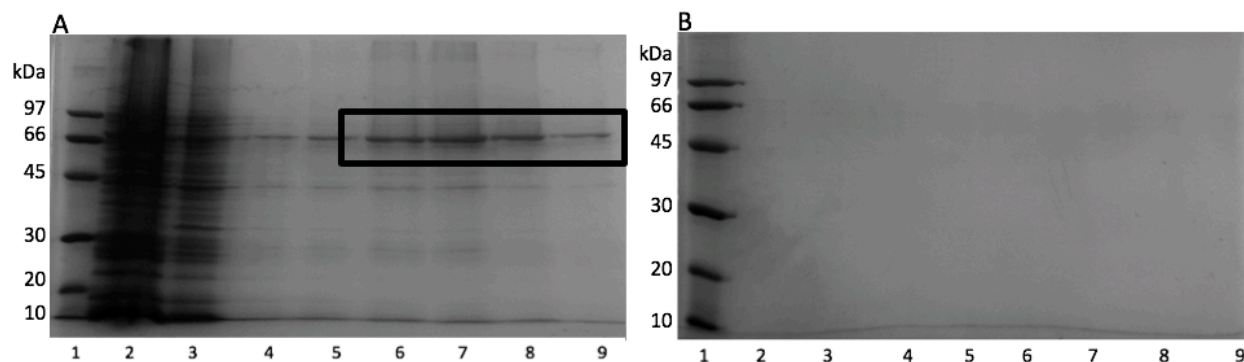


Figure 5.11 Purification of *M. tuberculosis* PonA2. 12% SDS-PAGE analysis gels of Immobilised metal affinity chromatography (5 mL Cobalt) elutions by imidazole (IM) gradient of purified recombinantly expressed PonA2 from *E. coli* BL21 (DE3) expression cell line. Bands visualized by Coomassie blue staining. Lanes A1: Protein marker, A2: Flow through, A3: Wash through, A4: 0mM IM, A5: 10mM IM, A6: 30mM IM, A7: 50mM IM, A8: 100mM IM, A9: 150mM IM, B1: Protein marker, B2: 200mM IM, B3: 250mM IM, B4: 300mM IM, B5: 350mM IM, B6: 400mM IM, B7: 450mM IM, B8: 500mM IM, B9: 500mM IM. Identification of PonA1 for further concentration noted by black rectangle.

PonA2 was eluted from the IMAC column at a similar imidazole concentration as PonA1. The 84 kDa PBP was removed from the column between 30-150 mM IM, fraction corresponding to wells A6-9 (Figure 5.11) were pooled and dialyzed overnight in PBP buffer. The recombinant protein was then concentrated and the resulting volume was quantified as containing 4.1 mM PonA2. Purification was once again not solely successful with the final elution containing more than one band.

5.7.3 Binding affinity of *M. tuberculosis* PonA1/PonA2 to Lipid II variants

PonA1 and PonA2 were assessed by BLI (2.10.2) to measure the binding affinity of the penicillin binding proteins to the two possible modified peptidoglycan subunits, N-acetylated Lipid II and N-glycolylated Lipid II. As described previously, biotinylated Lipid II variants were immobilized on streptavidin sensors and interactions between 0.2 μ M set lipid concentrations and a range of PBP concentrations between 0.03 μ M and 0.5 μ M were evaluated. The BLI buffer solution utilized was altered to specify for optimal PBP activity (Section 2.10.2). The BLI sensorgrams for each Lipid II variant against both PonA1 and PonA2 are shown in Figure 5.12 and the K_D results extrapolated for each PBP are shown in Table 5.3.

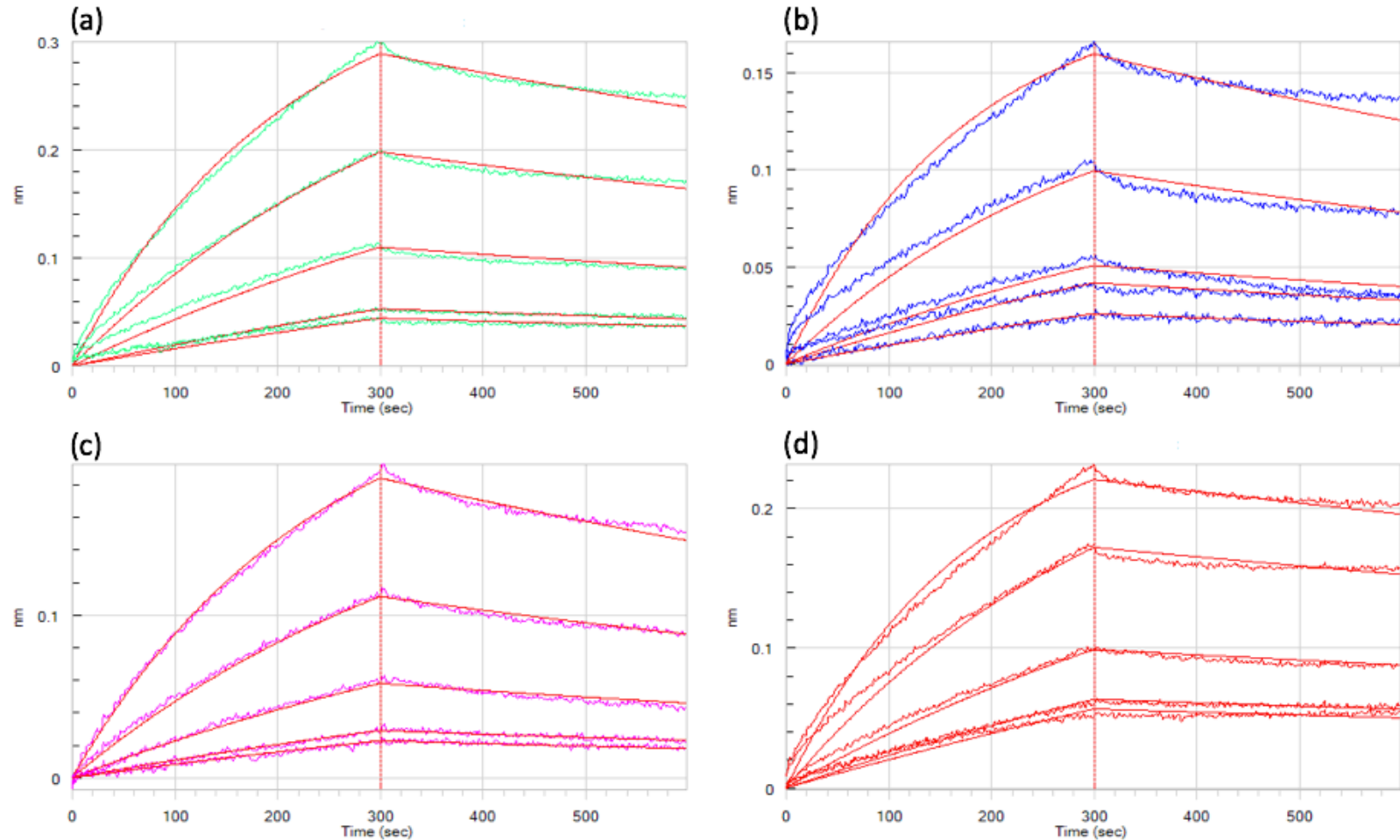


Figure 5.12. Binding affinity of biotinylated Lipid II variants against *M. tuberculosis* penicillin binding proteins PonA1 and PonA2. Sensorgrams of streptavidin coated sensors bound to N-acetylated Lipid II and N-glycolylated Lipid II were assessed by their affinity towards two-fold serial dilutions from 0.5 μM to 0.03 μM of PonA1 and PonA2. Reference sensors were used to remove any non-specific binding. (a) N-acetylated Lipid II (DAP) and PonA1, (b) N-acetylated Lipid II (DAP) and PonA2, (c) N-glycolylated Lipid II (DAP) and PonA1 and (d) N-glycolylated Lipid II (DAP) and PonA2. Binding constants were measured with the Octet Data Analysis software on an Octet Red, by global fitting the data with the 1:1 heterogenous ligand mode

Lipid II	PBP	K_D (M)	K_D Error	K_a (1/Ms)	K_a Error	K_d (1/s)	K_d Error
NAc	PonA1	$5.39 \cdot 10^{-8}$	$7.17 \cdot 10^{-10}$	$9.71 \cdot 10^{+3}$	$7.59 \cdot 10^{+1}$	$5.24 \cdot 10^{-4}$	$5.63 \cdot 10^{-6}$
NAc	PonA2	$5.50 \cdot 10^{-8}$	$8.26 \cdot 10^{-10}$	$8.81 \cdot 10^{+3}$	$7.95 \cdot 10^{+1}$	$4.84 \cdot 10^{-4}$	$5.82 \cdot 10^{-6}$
NGlyc	PonA1	$1.14 \cdot 10^{-7}$	$1.40 \cdot 10^{-9}$	$6.89 \cdot 10^{+3}$	$6.92 \cdot 10^{+1}$	$7.82 \cdot 10^{-4}$	$5.62 \cdot 10^{-6}$
NGlyc	PonA2	$8.02 \cdot 10^{-8}$	$1.93 \cdot 10^{-9}$	$1.00 \cdot 10^{+4}$	$1.77 \cdot 10^{+2}$	$8.05 \cdot 10^{-4}$	$1.32 \cdot 10^{-5}$

Table 5.3. The equilibrium dissociation constants, K_D for biotinylated Lipid II variants to *M. tuberculosis* PonA1 and PonA2. N-acetylated and N-glycolylated Lipid II (DAP) attached to streptavidin biosensors binding measured against concentrations of *M. tuberculosis* PBPs, PonA1 and PonA2 between 0.5 μ M and 0.03 μ M.

The equilibrium dissociation constants, of both PBPs in Figure 5.12 towards the N-acetylated Lipid II exhibited a similar binding affinity value of 53.9 nM for PonA1 and 55.0 nM for PonA2 (Table 5.3) respectively. The rate of association for each PBP were comparatively close with K_a values of 971 Ms^{-1} (PonA1) and 881 Ms^{-1} (PonA2). The dissociation constant for each penicillin binding protein against the N-acetylated lipid was 0.524 ms^{-1} (PonA1) and 0.484 ms^{-1} (PonA2) respectively.

The N-glycolylated Lipid II (DAP) displayed a slight preference in binding affinity towards PonA2 with a K_D of 80.2 nM compared to PonA1 with a K_D of 114.0 nM. K_a for each PBP was 689 Ms^{-1} (PonA1) and 1000 Ms^{-1} (PonA2) respectively. The dissociation constants for each PBP against the N-glycolylated lipid were 0.782 ms^{-1} (PonA1) and 0.805 ms^{-1} (PonA2) respectively.

Comparisons observed between the binding affinities of each lipid variant towards a single PBP, showed that PonA1 preferentially binds at half the K_D to the N-acetylated lipid than the N-glycolylated lipid, whereas PonA2 binds with equal affinity towards each lipid.

5.8 Discussion

5.8.1 *M. leprae* Mur enzymes

Initial investigations have been implemented with *M. leprae* Mur enzymes. Both MurA and MurC were successfully obtained and re-cloned into pCOLD expression vectors with poly-histidine tags employed to aid recombinant protein folding at lower temperatures. Both enzymes were expressed and generated soluble protein. Site directed mutagenesis was enacted to probe the sensitivity of *M. leprae* MurA to fosfomycin through the substitution of an active site aspartate residue (De Smet, *et al.* 1999). The active site mutant was also expressed and soluble. These initial experiments will be built upon to investigate the peptidoglycan regulation undertaken to control synthesis in response to external pressures such as starvation and antimicrobial therapy (Section 5.9 Further work).

5.8.2 *M. smegmatis* Mur enzymes

Previous chapters have demonstrated the importance of N-glycolylated peptidoglycan for mycobacteria to resist hydrolytic enzymes and antimicrobials. The binding affinities of *M. smegmatis* Mur ligases, MurC and MurD were probed to identify potential catalytic bias between the N-acetylated and N-glycolylated substrates. Kinetic assessments of binding affinities illustrated that the *M. smegmatis* Mur ligases displayed a higher affinity towards the N-glycolylated substrate. This impact was most significant for MurC with a 43 fold greater efficiency. The noted bias decreased significantly for MurD, demonstrating only a 5 fold preference. These findings were similar to a collaborators within the laboratory measuring the binding affinity of *M. tuberculosis* Mur ligases (Unpublished). Results showed a 30 fold preference for the N-glycolylated substrate by MurC, although each subsequent ligase, the preference was diminished until substrate affinities were equivalent for MurF. The incorporation of N-glycolylated saccharides is therefore a priority in mycobacteria, likely attributed to the organisms need to rapidly respond to host's immune responses or antimicrobial treatments.

5.8.3 *M. tuberculosis* PBPs

M. tuberculosis implements the bifunctional PBPs, PonA1 and PonA2 to construct the wider peptidoglycan sacculus and insert either N-acetylated or N-glycolylated lipids into the architecture depending upon the external conditions and challenges to maintain mycobacterial cell wall integrity. The BLI assessment of *M. tuberculosis* PBPs showed that there was little difference between PonA1 and PonA2 in their binding affinities towards each specific version of Lipid II (DAP). There was specificity observed in each PBP's own preferences. PonA1 showed twice as great affinity towards the N-acetylated lipid as the N-glycolylated, whereas PonA2 had similar affinities regardless of lipid binding partner.

Chen, *et al.* (2013) however, directly tested PonA1 activity towards lipid II analogues and found that the N-glycolylated lipid II was two-fold more efficient than its N-acetylated counterpart. The apparent discrepancy may well result from the weaker binding of N-glycolylated as opposed to the N-acetylated substrate binding seen in this project. This might be countered by a much higher maximal velocity of N-glycolylated transglycosylation as seen by Chen, *et al.* (2013).

5.9 Further work

- Characterise activity of *M. leprae* Mur enzymes

M. leprae MurA, a MurA active site mutant and MurC were successfully cloned and expressed. The Mur enzymes require an assessment of enzymatic activity characterization towards peptidoglycan intermediate synthesis of UDP-enolpyruvyl-GlcNAc (MurA and MurA mutant) and UDP-MurNAc-L-glycine (MurC) respectively compared to known Mur enzymatic activities within other organisms (Munshi, *et al.* 2013). Once standard *M. leprae* MurA activity is established, the effect of peptidoglycan synthesis can be perturbed by the MurA inhibitor, fosfomycin to determine the extent to which the active site amino acid substitution impacts

antimicrobial susceptibility of the commonly resistant enzyme. The *M. leprae* MurC implementation of L-glycine at position one of the pentapeptide stem should be re-examined to reiterate the lack of binding preference between L-glycine and L-alanine (Mahapatra, *et al.* 2000). The experiment could also be expanded to include all amino acid.

- CwIM

Recent findings (Boutte, *et al.* 2016) have identified the protein CwIM as a key factor in the regulation of MurA activity. Association of the protein with MurA once phosphorylated by the serine/threonine protein kinase, PknB increased the Mur enzymes activity by around 30 fold. Investigations should be conducted into identifying an equivalent gene in *M. leprae*, determining if the gene can be expressed or is simply a pseudogene and if so have the gene synthesized and expressed to determine the impact of *M. leprae* peptidoglycan synthesis.

- Assess *M. leprae* MurC catalytic bias towards muramic acid variants

Investigate the potential for catalytic bias of *M. leprae* MurC towards the N-glycolylated substrate compared to the N-acetylated variant as observed in *M. smegmatis*. Determine if the fact that the NamH equivalent in *M. leprae* is a pseudogene has led to no retained substrate binding preference.

- Assess PonA1 and PonA2 binding affinity towards antimicrobials

The *M. tuberculosis* PBPs were expressed with a poly-histidine tag, which permits the proteins to be bound to Ni-NTA anti-histidine antibody biosensors for BLI binding affinity assessment. Interactions between PonA1/PonA2 and PBP targeted antimicrobials such as β -lactam antibiotics and moenomycin should be investigated to decipher preferential binding of the antimicrobials.

5.10 Conclusion

Mycobacterial peptidoglycan synthesis possesses a number of unique variations to aid resistance from antimicrobial interaction. Catalytic preferences towards the N-glycosylated saccharide was shown within the Mur ligases though this effect diminished as the amino acid stem extended. Rapid implementation of peptidoglycan modification likely attributes to mycobacterial virulence.

Chapter 6. Elucidating the role of known cell wall active compounds

6.1 Inhibition screening

A collaboration between the University of Warwick and McMaster University was initiated to investigate the role of newly identified cell wall active compounds with antimicrobial activity. The compounds were identified through a new screening process described below created to avoid the issues commonly occurring in previous screens (De Pascale 2007). Previous screening methods utilised a *vanH* promoter-reporter merged to the *lacZ* gene to evaluate growth inhibition followed by targeted activity towards the bacterial cell wall. Such methods are incomplete in that they only target a specific step in peptidoglycan synthesis such as transpeptidation, although the screening process published by (Czarny, *et al.* 2014) reports on any inhibition of any step of the entire bacterial cell wall pathway.

6.1.1 Pywac compounds

The screening process performed at McMaster University by the Brown lab focused on the noted upregulation of the *ywaC* gene upon suppression of wall teichoic acid (WTA) synthesis (D'Elia, *et al.* 2009). Teichoic acids are designated as WTA due to interactions with peptidoglycan and lipoteichoic acids if anchored to lipids. Comprised from either glycerol phosphate or ribitol phosphate and attached by phosphodiester bonds, these bacterial polysaccharides are covalently bound to MurNAc subunits of the peptidoglycan sacculus (Brown, *et al.* 2014). WTA are major components of the bacterial cell wall, and in similar abundance to peptidoglycan in Gram-positive organisms, although absent from Gram-negative organisms (Swoboda, *et al.* 2010).

The vast majority of previously identified anti-bacterials which are specific for the bacterial cell wall elicit activity towards peptidoglycan synthesis (Bush 2012) although WTA synthesis is currently emerging as an encouraging new target. The screen utilises the gene *ywaC*, observed to exhibit GTP pyrophosphokinase activity (Czarny, *et al.* 2014). This

generally uncharacterised protein belongs to a class of enzymes that catalyse the production of a bacterial “alarmone”, guanosine tetra(penta)phosphate ((p)ppGpp) during cellular stresses (Hauryliuk, *et al.* 2015). In turn by binding to both β and β' subunits of RNA polymerase, the alarmone alters promoter preference, as well as upregulation and downregulation of genes, prompts precise transcriptional level gene expression (Merrikh, *et al.* 2009) and is part of the σ^w regulon, a collection of genes upregulated in the presence of cell wall antimicrobials. The screening process utilises a promoter-reporter system comprised of the promoter of *ywaC* and the lux genes from which the enzyme luciferase is expressed enabling a real-time luminescence signal. Luciferase catalyses the oxidation of a long-chain aliphatic aldehyde and reduced Flavin mononucleotide (FMNH₂) by molecular oxygen to yield H₂O, flavin mononucleotide (FMN) and a fatty acid (Baldwin, *et al.* 1975). This reaction leads to the emission of blue-green light at a wavelength of 490 nm (Wiles, *et al.* 2005).

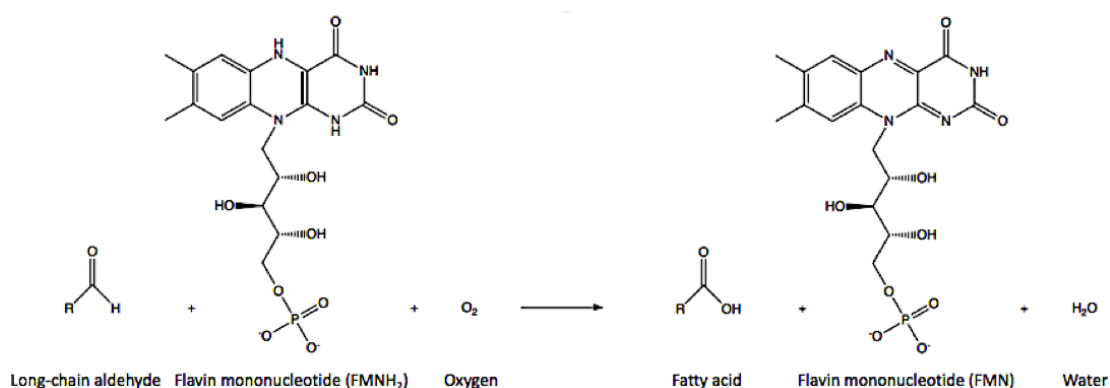


Figure 6.1 The enzymatic luminescence reaction of reduced flavin mononucleotide and a long chain aldehyde. Luciferase catalyses the oxygen dependent oxidation of FMNH₂ and a long chain aldehyde to FMN and a fatty acid with the emission of light at 490 nm.

The screen comprised wild type *B. subtilis* 168 (EB6) single colonies containing the P_{ywaC}-Lux promoter-reporter plasmids cultured LB overnight, supplemented with erythromycin. Harvested cells were subsequently diluted and spotted onto the surface of solid LB agar incorporating potential inhibitors. Assay luminescence was evaluated for 19 hours, where emission was measured at 490 nm with the isoprenoid biosynthesis inhibitor fosmidomycin (Howe, *et al.* 2013) employed as a high emission control and DMSO as a low emission control. Potential inhibitors that elicited a positive luminescence response were selected for secondary screening. Osmoprotectants such as sucrose or divalent cations like magnesium chloride have been observed to mitigate the cell wall deficiencies of compromised cells as

well as suppress P_{ywaC} activity. The secondary screen was conducted in the same manner as the first on solid agar with the addition of $MgCl_2$, sucrose and maleic acid (MSM) to the liquid LB. Nine compounds were identified (designated as pywac 1-9 from the remainder of this thesis), displaying concentration dependent prominent luminescence emissions, which were also moderately quelled by osmoprotectants and induced morphology changes in cells at sub MIC levels.

6.1.2 Pywac compound structures and MIC concentrations

The chemical formulas, structures and MIC for the pywac compounds 1-9 against *B. subtilis* as outlined in Czarny, *et al.* (2014) are recorded in table 6.1.

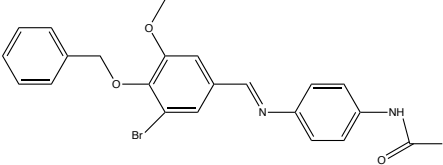
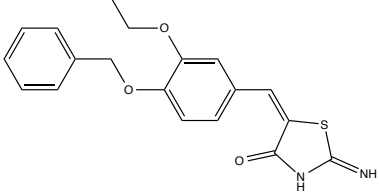
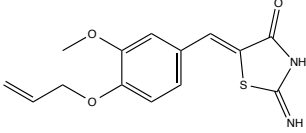
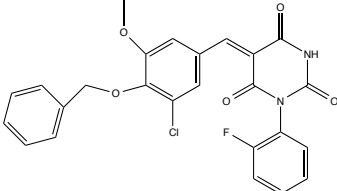
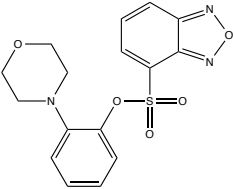
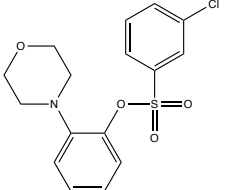
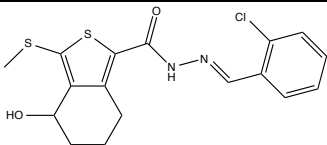
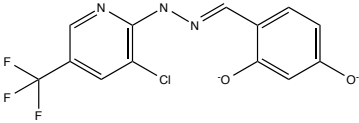
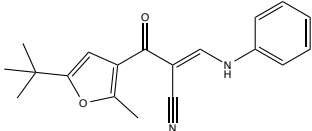
Compound Name	Chemical formula	Molecular mass (Da)	Chemical Structure	MIC
Pywac 1	C ₂₃ H ₂₁ BrN ₂ O ₃	453.34		4μM
Pywac 2	C ₁₉ H ₁₈ N ₂ O ₃ S	354.42		2μM
Pywac 3	C ₁₄ H ₁₄ N ₂ O ₃ S	290.34		32μM
Pywac 4	C ₂₅ H ₁₈ ClFN ₂ O ₅	480.88		16μM
Pywac 5	C ₁₆ H ₁₅ N ₃ O ₅ S	361.37		32μM
Pywac 6	C ₁₆ H ₁₆ ClNO ₄ S	353.82		8μM
Pywac 7	C ₁₇ H ₁₇ ClN ₂ O ₂ S ₂	380.91		16μM
Pywac 8	C ₁₄ H ₉ ClF ₃ N ₃ O ₂ ²⁻	343.69		8μM
Pywac 9	C ₁₉ H ₂₀ N ₂ O ₂	308.38		4μM

Table 6.1 The cell wall active compounds identified by P_{ywac} screening, designated pywac 1-9. Molecular weights, structures and MIC for *B. subtilis* (structures produced in ChemBio Draw 7) from (Czarny, *et al.* (2014)).

6.2 Experimental aims

To investigate the impact of the nine recently discovered cell wall active compounds on peptidoglycan synthesis as reported by evaluation of accumulated intermediates of the peptidoglycan cytosolic or membrane linked phases during incubation in excess of the MIC.

6.3 DMSO tolerance of *B. subtilis*

The nine presumptive cell wall active compounds are insoluble in aqueous solution but soluble in DMSO. Growth of cells are known to have certain tolerances for solvents, though above a certain threshold a noticeable decrease in cellular growth can be observed. Therefore it was important to identify the tolerance of *B. subtilis* wild type cells to increasing concentrations of DMSO. Throughout this chapter to minimise the impact of highly complex nutrient media preventing accumulation of cellular intermediates, minimal nutrient media (Section 2.2.4) was used. DMSO tolerance of *B. subtilis* is demonstrated in Figure 6.2.

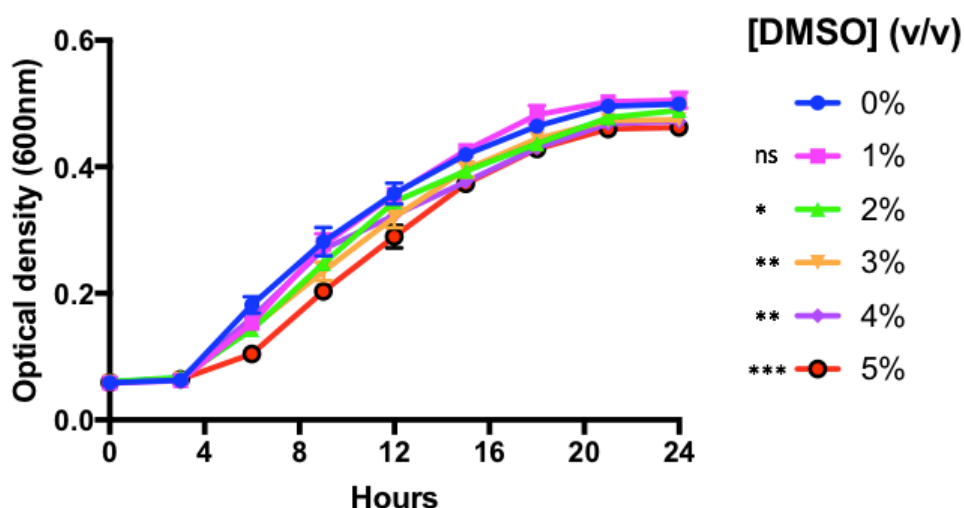


Figure 6.2 DMSO tolerance of *B. subtilis*. Cells were grown in the presence of increasing concentrations of DMSO to identify optimal tolerance for the solvent, in 96 well microtiter plates in triplicate at 37°C with intermittent shaking. Absorbance was measured at 600nm at 3 hour intervals for 24 hours. Each well contained 100 μ L minimal media. The cultured *B. subtilis* cells were standardized to an OD_{600nm} of 1 and diluted further by a factor of 10⁴ prior to incubation. Error bars represent standard deviation of triplicate measurements. DMSO concentration: 0% (v/v) Blue, 1% (v/v) Pink, 2% (v/v) Green, 3% (v/v) Orange, 4% (v/v) Purple, 5% (v/v) Red. Statistically significant results are indicated with * = p-value <0.05, ** = <0.01, *** = <0.001 and **** = <0.0001. Ns = not statistically significant. Result: DMSO percentages above 1% (v/v) slightly impacted phenotypic growth, with 5% (v/v) reducing overall growth curve area by 18%.

[DMSO] (v/v) (%)	<i>B. subtilis</i>				
	Apparent Lag Phase Duration (h)	Td (h ⁻¹)	AUC (% of 0% DMSO)	Stationary Phase OD ₆₀₀ nm attained	p-values
0	3	2.76	-	0.50	-
1	3	2.78	92.38	0.50	>0.05
2	3	3.20	92.38	0.49	<0.05
3	3	3.22	90.47	0.47	<0.01
4	3	2.94	91.13	0.47	<0.01
5	3	3.61	82.63	0.46	<0.001

Table 6.2 Statistical comparisons of *B. subtilis* growth curves in the presence of increasing concentrations of DMSO. *B. subtilis* incubated for 24 hours at 37°C with selected concentrations of DMSO (v/v) produced growth curves measured at OD_{600nm} in Figure 4.1. Variations between growth curves were measured by time taken to exit apparent lag phase (hours), the doubling time (Td) of cells during exponential phase (hours⁻¹), the area under the curve (AUC) percentage compared to the 0 % control (%), the OD_{600nm} value achieved during stationary phase and whether the growth curve variations were statistically significant compared to each 0 % control with p-values <0.05 deemed significant.

The normal growth phenotype of the wild type *B. subtilis* strain (Figure 6.2: 0% Blue) in the absence of DMSO exited apparent lag phase after 3 hours. The control data set produced a doubling time (Td) during exponential phase of 2.76 hours and reached an OD_{600nm} of 0.5 during stationary phase after 21 hours. The addition of DMSO at any concentration tested against *B. subtilis* cells did not lead to the significant impact observed in *M. smegmatis* cells cultured in 7H9 media (Figure 4.1). Any investigated concentration of DMSO did not delay the exit from apparent lag phase which remained 3 hours, however it did lead to slight variations in the Td of co-incubated cells and a gradual decrease in the area under the curve (AUC) from the 0% (v/v) control. The observed Td and AUC for each data set were 1% (v/v) DMSO: 2.78 hours, 92.38% (Figure 6.2: Pink), 2% (v/v) DMSO: 3.20 hours, 92.38% (Figure 6.2: Green), 3% (v/v) DMSO: 3.22 hours, 90.47% (Figure 6.2: Orange), 4% (v/v) DMSO: 2.94 hours, 91.13% (Figure 6.2: Purple) and 5% (v/v) DMSO: 3.61 hours, 82.63% (Figure 6.2: Red). A Student's t-test was implemented to assess the significance of growth variation in the presence of each concentration of DMSO. Each of the DMSO concentrations added produced statistically significant variation to *B. subtilis* growth curves except 1% (v/v) (p-value >0.05) with p-values of <0.05 (2% (v/v)) and <0.01 (3% and 4% (v/v)) and <0.001 (5% (v/v)) respectively.

Based upon the results obtained from Figure 6.2 the decision was taken to standardise a 2% (v/v) DMSO total concentration across all investigations within this chapter involving *B. subtilis* cells exposed to pywac compounds or just to the no compound DMSO control.

6.4 *B. subtilis* MIC of pywac compounds

To corroborate the findings of Czarny, *et al.* (2014) (Table 6.1) growth of *B. subtilis* at the reported MIC concentration of the nine compounds was monitored to validate the previous findings for subsequent MIC investigations in this chapter. Growth at the MIC for each individual pywac compound was determined in triplicate within minimal media. The phenotypic growth for *B. subtilis* cells against each pywac compound MIC is shown in Figure 6.3.

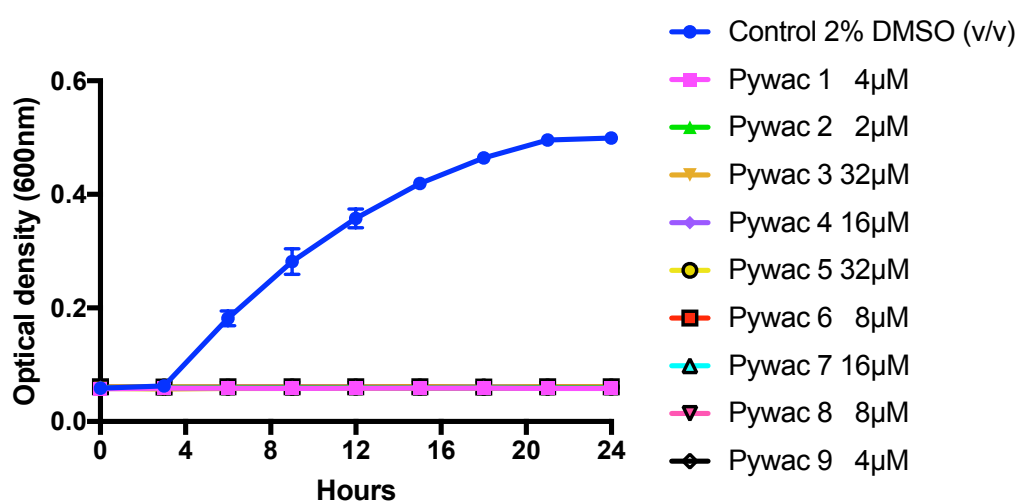


Figure 6.3 MIC of cell wall active pywac compounds against *B. subtilis*. Cells were grown in the presence of proposed MICs of pywac compounds 1-9 in 2% DMSO in 96 well microtiter plates in triplicate at 37°C with intermittent shaking. Absorbance was measured at OD_{600nm} at 3 hour intervals for 24 hours. Each well contained 100 µL minimal media. The cultured *B. subtilis* cells were standardized to an OD_{600nm} of 1 and diluted further by a factor of 10⁴ prior to incubation. Error bars represent standard deviation of triplicate measurements. Control: (Blue) *B. subtilis* cells grown in absence of compounds plus 2% (v/v) DMSO. pywac MIC: pywac 1 4µM (Pink), pywac 2 2µM (Green), pywac 3 32µM (Orange), pywac 4 16µM (Purple), pywac 5 32µM (Yellow), pywac 6 8µM (Red), pywac 7 16µM (Turquoise), pywac 8 8µM (Magenta), pywac 9 4µM (Black). Result: All proposed MIC values for each pywac compound were either correct or overstated as reported in Czarny, *et al.* (2014).

The findings show that the MICs observed by Czarny et al. (2014) were consistent with the results shown in Figure 6.3 for all nine pywac compounds. None of the concentrations of each pywac compound tested permitted observable growth of *B. subtilis* cells.

Building upon these results the main focus of this chapter was to observe the potential accumulation of cell wall intermediates during incubation with concentrations of pywac compounds exceeding their MIC values. Therefore, a positive control was required to ascertain the variation between normal cellular distribution of intermediates and compound specific causes of intermediate accumulation. For a positive control the antibiotic vancomycin was selected, which binds to the final D-alanyl-D-alanine residues of the PG precursor pentapeptide stem (Soetaerta, *et al.* 2015) inhibiting the subunit from incorporating into the peptidoglycan cell wall layer. The implementation of this control within *B. subtilis* cells would ultimately indicate that an increased concentration of vancomycin greater than the MIC would lead to an observable accumulation of UDP-MurNAc-pentapeptide DAP due to the further progress along the PG pathway being blocked by sequestration of Lipid II by vancomycin. The MIC of the *B. subtilis* wild type strain was identified as $0.03 \mu\text{g.mL}^{-1}$ by Fang, *et al.* (2014). The MIC of vancomycin against *B. subtilis* cells was assessed in Figure 6.4.

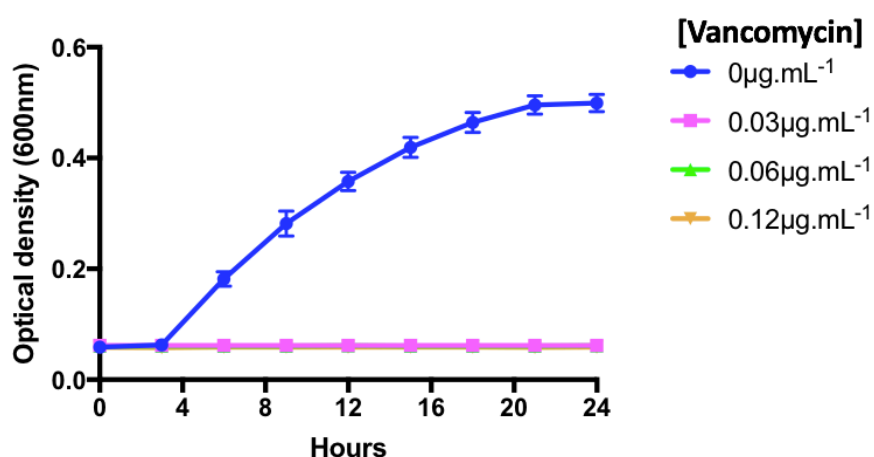


Figure 6.4 MIC of vancomycin against *B. subtilis*. Cells were grown in the presence of the proposed MIC (Pink), 2x MIC (Green) and 4x MIC (Orange) of vancomycin in 2% (v/v) DMSO in 96 well microtiter plates in triplicate at 37°C with intermittent shaking. Absorbance was measured at 600nm at 3 hour intervals for 24 hours. Each well contained 100 μL minimal media. The cultured *B. subtilis* cells were standardized diluted to an $\text{OD}_{600\text{nm}}$ of 10^{-4} prior to incubation. Error bars represent standard deviation of triplicate measurements. Control: (Blue) *B. subtilis* cells grown in absence of vancomycin plus 2% (v/v) DMSO. Result: The previously observed MIC value for vancomycin against *B. subtilis* was repeatable here.

The results found in Figure 6.4 validate the findings of Fang, *et al.* (2014). Incubation of *B. subtilis* cells with 0.03 $\mu\text{g}\cdot\text{mL}^{-1}$ vancomycin or greater (Figure 6.4) was sufficient to completely inhibit growth. The equivalent MIC of vancomycin in μM was 0.02 μM . The decision was taken to assess both 2x MIC (0.04 μM) and 5x MIC (0.1 μM) vancomycin on late exponentially growing *B. subtilis* cells to assess whether either are sufficient to obtain noticeable accumulation of the desired peptidoglycan precursor intermediates.

6.5 Analysis of *B. subtilis* peptidoglycan precursor intermediate standards

To compare and identify isolated peaks of interest from the ion exchange chromatography and mass spectrometry data of *B. subtilis* cells, known cytosolic peptidoglycan intermediates were processed individually to act as standards. The cell wall intermediates produced by *B. subtilis* are known to contain a DAP residue at position three of the pentapeptide stem (Vermeulen, *et al.* 1984). The structure of each of the seven peptidoglycan intermediates: UDP-GlcNAc, UDP-enolpyruvyl-GlcNAc, UDP-MurNAc, UDP-MurNAc-L-alanine, UDP-MurNAc-L-alanyl- γ -D-glutamate, UDP-MurNAc-L-alanyl- γ -D-glutamyl-meso-diaminopimelate and UDP-MurNAc-L-alanyl- γ -D-glutamyl-meso-diaminopimelyl-D-alanyl-D-alanine; abbreviated to UDP-MurNAc, UDP-MurNAc-L-Ala, UDP-MurNAc-L-Ala-D-Glu, UDP-MurNAc-L-Ala-D-Glu-m-DAP and UDP-MurNAc-L-Ala-D-Glu-m-DAP-D-Ala-D-Ala respectively are shown in Figure 6.5.

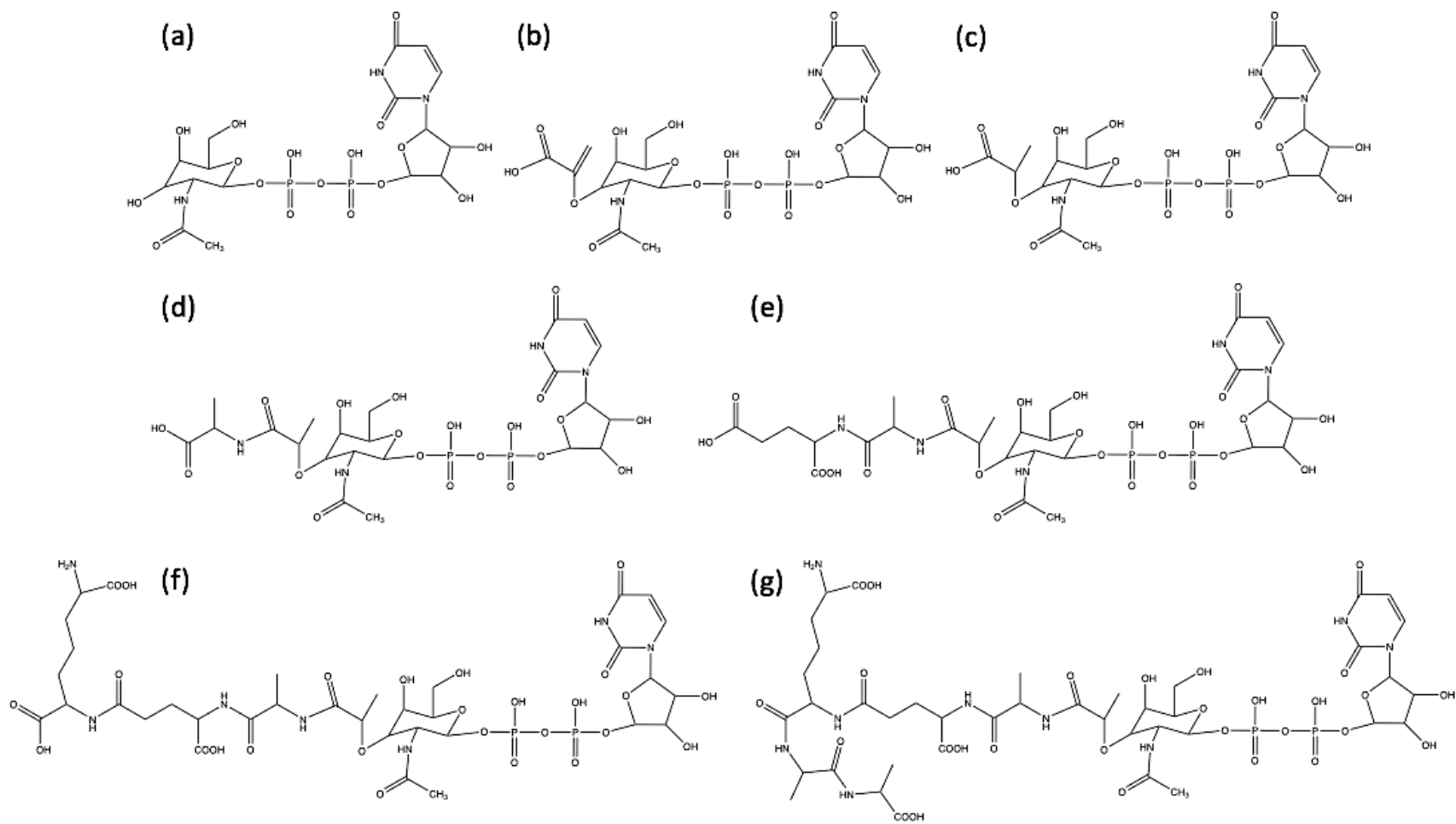


Figure 6.5: The structures of the cytosolic peptidoglycan intermediates of *B. subtilis*. (a) UDP-GlcNAc, (b) UDP- enolpyruvyl-GlcNAc, (c) UDP-MurNAc, (d) UDP-MurNAc-L-Ala, (e) UDP-MurNAc-L-Ala-D-Glu, (f) UDP-MurNAc-L-Ala-D-Glu-m-DAP and (g) UDP-MurNAc-L-Ala-D-Glu-m-DAP-D-Ala-D-Ala. The above schematic was created using ChemBioDraw.

Known peptidoglycan intermediate standards synthesised within the lab by the BaCWAN facility utilising the methods outlined in Section 2.8.1 and used to identify the elution position of each peptidoglycan intermediate on fractionation of the *B. subtilis* cytosolic metabolite pool, by anion exchange as described in Section 2.7.3.3. Samples were diluted in 10 mM ammonium acetate to 1 mM and 2 mL volumes were loaded onto the column. Notable peaks of interest were retained for subsequent characterisation by mass spectrometry. The ion exchange chromatograms for each peptidoglycan intermediate standard are shown in Figure 6.6.

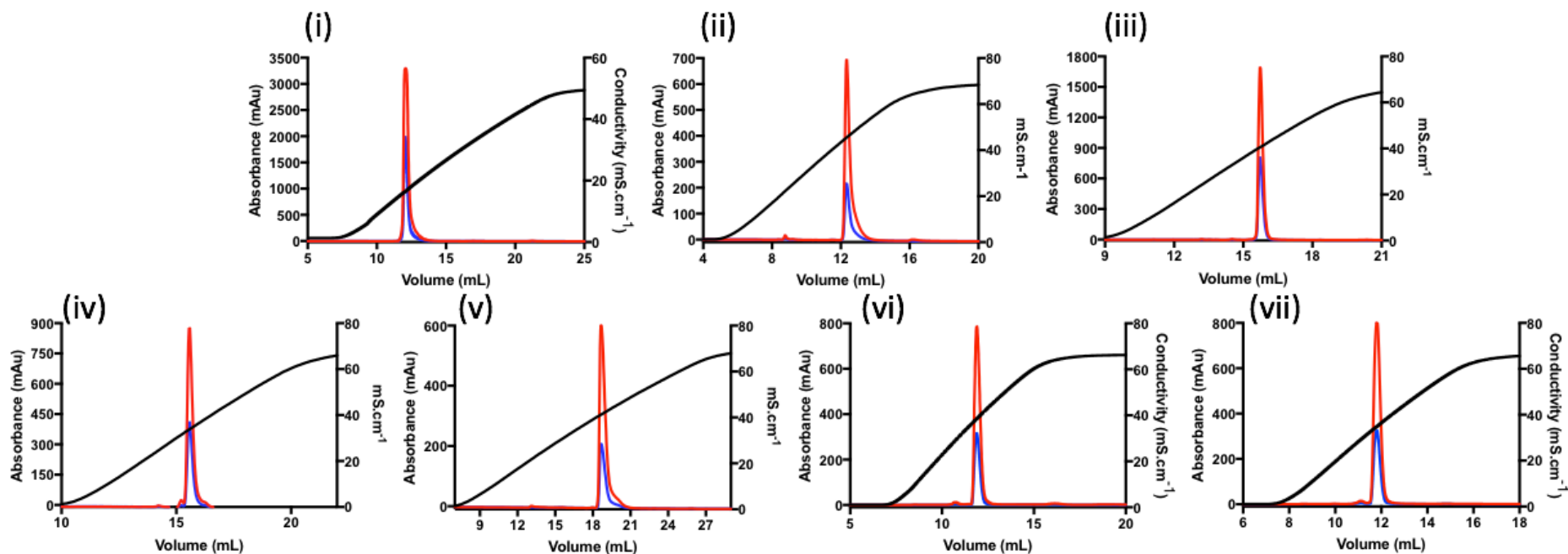


Figure 6.6: Anion exchange chromatography of peptidoglycan intermediate standards. Elution position defined by conductivity at the center of the peak of standard elution (i) UDP-GlcNAc (conductivity 16.41 mS.cm⁻¹), (ii) UDP-enolpyruvyl-GlcNAc (conductivity 45.57 mS.cm⁻¹), (iii) UDP-MurNAc (conductivity 40.61 mS.cm⁻¹), (iv) UDP-MurNAc-L-Ala (conductivity 34.68 mS.cm⁻¹), (v) UDP-MurNAc-L-Ala-D-Glu (conductivity 41.29 mS.cm⁻¹), (vi) UDP-MurNAc-L-Ala-D-Glu-m-DAP (conductivity 38.54 mS.cm⁻¹), (vii) UDP-MurNAc-L-Ala-D-Glu-m-DAP-D-Ala-D-Ala (conductivity 34.77 mS.cm⁻¹). Samples were fractionation by MonoQ 5/50 GL resin. Red trace is absorbance at 254 nm, blue trace: absorbance at 280 nm and black trace; conductivity.

The 254 nm and 280 nm absorbance measured for each peptidoglycan intermediate standard showed single distinct peaks during ion exchange chromatography purification (Figure 6.6). One common identifier of eluted intermediates is the $A_{254\text{nm}}/A_{280\text{nm}}$ ratio, which for uridine is 1:2.86 (Dawson, *et al.* 1986). The conductivity $\text{mS}\cdot\text{cm}^{-1}$ at which each of the standards eluted permitted preliminary and presumptive identification of potential peaks of interest obtained from ion exchange of metabolite pool extracted from *B. subtilis* treated with the pywac compounds. The conductivity at which each standard eluted is tabulated in table 6.3.

UDP species	Conductivity $\text{mS}\cdot\text{cm}^{-1}$
UDP-GlcNAc	16.41
UDP-enolpyruvyl-GlcNAc	45.57
UDP-MurNAc	40.61
UDP-MurNAc-L-Ala	34.68
UDP-MurNAc-L-Ala-D-Glu	41.29
UDP-MurNAc-L-Ala-D-Glu-m-DAP	35.85
UDP-MurNAc-L-Ala-D-Glu-m-DAP-D-Ala-D-Ala	34.77

Table 6.3 Conductivity of peptidoglycan precursor intermediate standards. Eluted from monoQ 5/50 column by ion exchange chromatography

To ensure that components of peaks eluted by anion exchange could be successfully characterised by mass spectrometry, the eluted peaks for each standard were subjected to three rounds of freeze drying in 50 mL H_2O to remove the ammonium acetate. Samples were resuspended in H_2O and prepared for mass spectrometry at a final concentration of 50 μM in 50% (v/v) acetonitrile, and subsequently analysed by negative ion mode mass spectrometry. The predicted mass:charge ratios (m/z) of each of the peptidoglycan intermediate standards are displayed in table 6.4, and compared to their observed value.

All mass spectrometry was carried out in this thesis were by Dr Adrian Lloyd and Mrs. Anita Catherwood. Full spectra results are shown in Figures A3.1 to Figure A3.7 in appendix 3 with embedded zoomed in m/z ranges of interest.

UDP Species	(m-1)/1		(m-2)/2		(m-3)-3	
	Observed	Expected	Observed	Expected	Observed	Expected
UDP-GlcNAc	606.07	606.07	302.53	302.53	-	201.35
UDP enol pyruvoyl GlcNAc	676.08	676.07	337.53	337.53	-	224.68
UDP-MurNAc	678.09	678.09	338.54	338.54	-	225.35
UDP-MurNAc-L-Ala	749.14	749.13	374.07	374.06	-	249.03
UDP-MurNAc-L-Ala-D-Glu	878.18	878.17	438.59	438.58	-	292.05
UDP-MurNAc-L-Ala-D-Glu-m-DAP	1050.26	1050.25	524.63	524.62	-	349.41
UDP-MurNAc-L-Ala-D-Glu-m-DAP-L-Ala-L-Ala	1192.34	1192.33	595.67	595.66	-	396.77

Table 6.4 The mass/charge ratio for the peptidoglycan cytosolic DAP intermediate standards. Singly [M-H]⁻, doubly [M-2H]²⁻ and triply [M-3H]³⁻ charged observed and expected species of the various peptidoglycan DAP intermediates.

The mass spectrometry data from Figure A3.1 to Figure A3.7 (Appendix 3) identified the peptidoglycan intermediate standards isolated from ion exchange chromatography (Figure 6.6). Singly ($[M-H]^-$) and doubly ($[M-2H]^{2-}$) charged species were located within the full spectra which related to the known m/z ratios outlined in table 6.4. The data obtained from processed cells in the absence of antimicrobials, in the presence of excess MIC of vancomycin or excess MIC of pywac compounds was then compared to the known standards to identify peaks of interest that were potentially comprised of accumulated of peptidoglycan intermediates. These monoQ conductivity comparisons were only used as an initial marker for potential identification due to differing methods of acquiring intermediates, synthesis versus accumulation. Potential intermediates were confirmed by mass spectrometry.

6.6 Normal cellular distribution of *B. subtilis* peptidoglycan intermediates

Growth of *B. subtilis* in minimal media was selected as a means of accumulating quantities of cell wall intermediates in the presence of the pywac compounds without competition from components of more complex media such as nutrient rich LB media. Pywac compounds were co-incubated at 2x MIC (Table 6.1) with *B. subtilis* cells once they had reached late exponential phase at 37°C, at this point the protocol devised by Dr. Adrian Lloyd (Section 2.9.1) was then used to isolate a crude fraction containing cytoplasmic peptidoglycan precursors which were further purified by size exclusion (Section 2.7.3.2) and ion exchange chromatography (Section 2.7.3.3) and species of interest were further characterised by mass spectrometry (Section 2.12).

Alongside the pywac compounds, two sets of control samples were also implemented. One control was a baseline examination of standard intermediate accumulation of *B. subtilis* cells in the absence of inhibitors to understand the normal cellular distribution of cell wall intermediates. The second set of controls were *B. subtilis* cells exposed to 2x and 5x MIC of vancomycin. Both sets of controls were incubated in minimal media and exposed to 2% (v/v) DMSO to accurately compare controls to investigated samples.

The inhibitor-free *B. subtilis* control sample absent of inhibitors was processed first. The chromatogram from size exclusion chromatography is displayed in Figure 6.7.

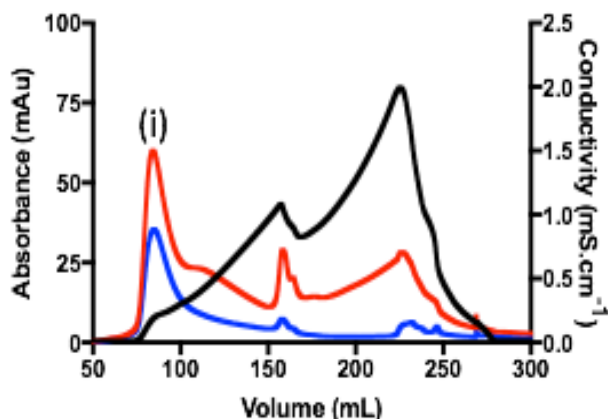


Figure 6.7: Size exclusion chromatography of *B. subtilis* control cells TCA extracted cells. Noted peak at (i) 83.29 mL. Samples were eluted by Bio-gel P2 resin. Red trace is absorbance at 254 nm, blue trace is absorbance at 280 nm and black trace; conductivity.

The gel filtration of the control *B. subtilis* sample (Figure 6.7) displayed the normal distribution of eluted peaks from control lysophilised cells separated out by size alone. Wavelengths of $A_{254\text{nm}}$ (Figure 6.7: Red) and $A_{280\text{nm}}$ (Figure 6.7: Blue) were measured along with the conductivity (Figure 6.7: Black). Size exclusion chromatography isolated three separate peaks. The most prominent peak was the first (Figure 6.7: (i)) which eluted from the column after 83.29 mL and produced the initial increase in both measured wavelengths and conductivity. Based on previous work performed in the laboratory (Dr Adrian Lloyd, personal communication) it was observed that cell wall intermediates are amongst the first species to elute from the gel filtration due to their large comparative size.

The $A_{254\text{nm}}/A_{280\text{nm}}$ ratio of the species in peak (i) was 1.72, slightly lower than expected for the presence of uridine containing components with an expected ratio of 2.86). This initial peak was isolated, freeze-dried and resuspended in water when a 2 μL aliquot was taken and added to 998 μL of H_2O . The $A_{260\text{nm}}$ of this dilution was 0.047. Subsequent samples mentioned in this chapter would also be assessed in the same way. All samples were diluted based on this measurement to

that of the most dilute sample (A260nm 0.02) prior to monoQ ion exchange to ensure that equal volume loading equated to loading of the same amount of material on a nucleotide basis. Further fractionation of peak (i) from Figure 6.9 on this basis by anion exchange on a MonoQ 5/50 GL resin column is shown in Figure 6.8.

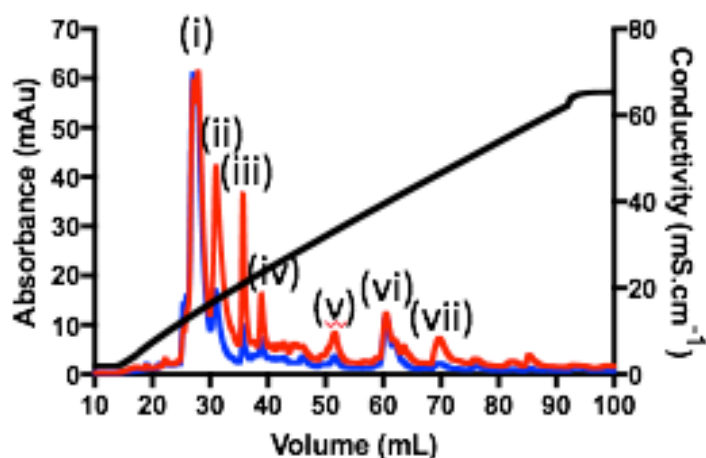


Figure 6.8: Anion exchange chromatography of isolated peptidoglycan intermediate peak of *B. subtilis* control cells. Noted peaks (i) (conductivity 13.65 mS.cm⁻¹), (ii) (conductivity 16.78 mS.cm⁻¹), (iii) (conductivity 21.27 mS.cm⁻¹), (iv) (conductivity 24.14 mS.cm⁻¹), (v) (conductivity 32.93 mS.cm⁻¹), (vi) (conductivity 38.85 mS.cm⁻¹) and (vii) (conductivity 46.13 mS.cm⁻¹). Red trace is absorbance at 254 nm, blue trace: absorbance at 280 nm and black trace; conductivity.

The monoQ elution profile of the *B. subtilis* control (Figure 6.8) indicated the presence of a number of isolated peaks, from the initial size exclusion eluted peak (Figure 6.7: (i)). Seven notable peaks were visualised. The mAu intensity of each peak decreased as the conductivity within the column increased. Based upon the comparative conductivity of peptidoglycan intermediate standards, *B. subtilis* control isolated peak (ii) (16.78 mS.cm⁻¹) eluted at a similar point to UDP-GlcNAc standard (Figure 6.6 (i): 16.41 mS.cm⁻¹), isolated peak (v) (32.93 mS.cm⁻¹) eluted at a similar point to both standards UDP-MurNAc-mono-peptide (Figure 6.6 (iv): 34.68 mS.cm⁻¹) and UDP-MurNAc-pentapeptide (DAP) (Figure 6.6 (vii): 34.77 mS.cm⁻¹), isolated peak (vi) (38.85 mS.cm⁻¹) eluted at a similar point to standard UDP-MurNAc-tripeptide (DAP) (Figure 6.6 (vi): 38.54 mS.cm⁻¹) and isolated peak (vii) (46.13 mS.cm⁻¹) eluted comparatively to standard UDP-enolpyruvyl-GlcNAc (Figure 6.6 (ii): 45.57 mS.cm⁻¹). However, elution conductivity is not sufficient to identify potential peptidoglycan intermediates, particularly because the A254/A280 ratio for the species fractionated in Figure 6.8 were not consistent with the presence of uridine

nucleotides. Therefore each of the monoQ *B. subtilis* control peaks (Figure 6.8) were collected and processed by mass spectrometry to attempt confirmation of the presence of cell wall intermediates and their relative abundance during unimpeded cellular growth. The mass spectra for each isolated peak are analysed from Figure A3.8 to Figure A3.14 in Appendix 3.

Mass spectrometric analysis of the first two eluted peaks (i) (Figure 6.8: (i) conductivity 13.65 mS.cm⁻¹) and (ii) (Figure 6.8: (ii) conductivity 16.78 mS.cm⁻¹) from the *B. subtilis* control monoQ purification shown in Figure A3.8 and Figure A3.9. Both peaks contained the initial subunit of the entire peptidoglycan biosynthesis pathway, UDP-GlcNAc, consistent with the conductivity data. Analysis of the mass spectrum of peaks (i) and (ii) identified singly charged ([M-H]⁻) species of UDP-GlcNAc: (i) expected m/z 606.07, observed m/z 606.08, (ii) expected m/z 606.07, observed m/z 606.08.

The potential accumulation of UDP-GlcNAc by the pywac compounds would suggest although not be necessarily indicative of inhibition of MurA the first enzyme in the pathway which converts UDP-GlcNAc into UDP-enolpyruvyl-GlcNAc. For each of the mass spec results it should be noted is the presence of a single peak with a m/z ratio of 237.09 (Figure A3.8) consistently found amongst all samples. The most likely cause is a contaminant found in the acetonitrile, though assumed to not interfere with the results.

Mass spectrometric analysis of the next two subsequent monoQ isolated peaks (iii) (Figure 6.8: (iii) conductivity 21.27 mS.cm⁻¹) and (iv) (Figure 6.8 (iv) conductivity 24.14 mS.cm⁻¹) from the *B. subtilis* control purification both contained UDP-MurNAc-pentapeptide DAP, the final subunit of the cytosolic peptidoglycan biosynthesis pathway. Mass spectra analysis of peaks (iii) (Figure A3.10) and (iv) (Figure A3.11) identified the doubly charged ion of UDP-MurNAc-pentapeptide in both samples. [M-2H]²⁻ (iii) expected 595.66 m/z, observed m/z 595.67, (iv) expected m/z 595.66, observed m/z 595.68 respectively. No singly charged species were identified though for either peak.

The fifth identifiable peak from the isolated monoQ fractions of the *B. subtilis* control sample was in elution (v) (Figure 6.8 (v) conductivity 32.93 mS.cm⁻¹). Mass spectra analysis (Figure A3.12)

revealed that this peak contained singly ($[M-H]^-$ observed m/z 878.19, expected m/z 878.17) and doubly ($[M-2H]^{2-}$ observed m/z 438.59, expected m/z 438.58) charged species consistent with the presence of UDP-MurNAc-dipeptide, the product of MurD and the substrate of MurE. Proposed accumulation at this stage in the peptidoglycan cell wall biosynthesis would indicate that flux through the MurD step was in excess of that through MurE.

The final two isolated peaks eluted from the control sample (vi) (Figure 6.8 (vi) conductivity $38.85 \text{ mS}\cdot\text{cm}^{-1}$ and (vii) (Figure 6.8 (vii) conductivity $46.13 \text{ mS}\cdot\text{cm}^{-1}$) on evaluation by negative ion mass spectrometry ((vi) Figure A3.13 and (vii) Figure A3.14) did not detect signals comparable to any of the known cell wall intermediates.

Overall, elutions of peptidoglycan intermediates in the *Bacillus subtilis* control experiment was similar to the elution order observed by the standards, UDP-GlcNAc, UDP-MurNAc-pentapeptide (DAP) and UDP-MurNAc dipeptide (Figure 6.6 and Figure 6.8).

The control data set established an estimation of conductivity ranges for each peptidoglycan intermediate. The inability to determine the other notable intermediates, UDP-MurNAc, UDP-MurNAc-mono-peptide and UDP-MurNAc-tri-peptide DAP from the eluted peaks is not believed to be a problem. The control sample is the observation of normal cellular growth with the peptidoglycan pathway unimpeded. During this time intermediates within the pathway should be continually turned over at normal rates so long as ATP is present. Unless the pathway was inhibited the amount of any one intermediate should be constant at steady state.

6.6.1 Intermediate accumulation of *B. subtilis* vancomycin control

Whilst the control sample illustrated that *Bacillus subtilis* demonstrated detectable concentrations of the accumulated cytosolic intermediates UDP-GlcNAc, UDP-MurNAc-dipeptide and UDP-MurNAc-pentapeptide (DAP) under normal cellular conditions the presence of the positive control vancomycin in excess MIC should specifically favour the accumulation of the peptidoglycan intermediate UDP-MurNAc-pentapeptide (DAP). Lyophilised cell contents from both the 2x and

5x MIC incubation were separated by size exclusion chromatography with a Bio-gel P2 column with a 2 mL loading volume in Figure 6.9.

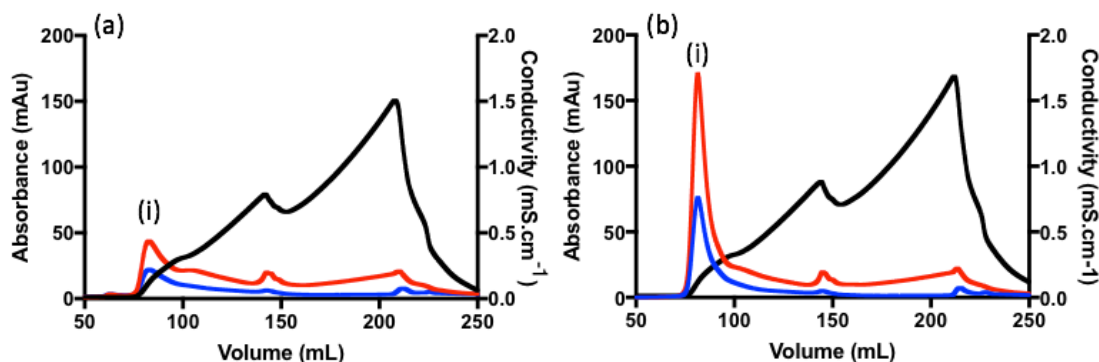


Figure 6.9: Size exclusion chromatography of *B. subtilis* TCA extracts of cells incubated with excess MIC vancomycin. (a) 2x MIC chromatogram of isolated peaks by Bio-gel P2 resin. Noted peak (i) 83.29 mL. (b) 5x MIC chromatogram of isolated peaks by Bio-gel P2 resin. Noted peak (i) 80.75 mL. 2 mL loading volume. Red trace is absorbance at 254nm, blue trace: absorbance at 280nm and black trace; conductivity.

Findings for the positive control were similar to the normal cellular control absent of antimicrobials (Figure 6.7). The primary elution peak for both concentrations (Figure 6.9: (a): (i) and (b): (i))) were at 83.29 mL and 80.75 mL respectively. The gel filtration of 2x and 5x MIC vancomycin differed solely by the intensity of the measured absorbance of the initial peaks pre 85 mL. The 2x MIC sample peak (i) plateaued at 45 mAu for $A_{254\text{nm}}$ whereas the 5x MIC control peak (i) attained a peak height of 180 mAu at $A_{254\text{nm}}$, four times the signal emitted by the potential intermediates found at 2x MIC vancomycin. The concentration of the inhibitor increased the accumulation of the primary peak and reduced the observed secondary and tertiary peaks.

Primary peak elutions of both vancomycin positive controls were isolated, measured at $A_{260\text{nm}}$, diluted to an equivalent absorbance and further separated on the monoQ column as shown in Figure 6.10.

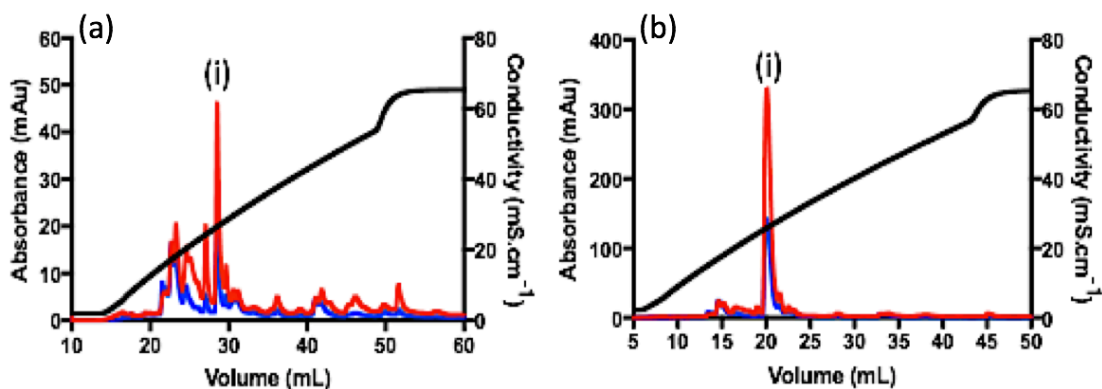


Figure 6.10: Anion exchange chromatography of gel filtration elutes (peak (i)) from *B. subtilis* treated with excess MIC vancomycin. (a) 2x MIC chromatogram of isolated peaks by MonoQ 5/50 GL resin. Noted peak (i) (conductivity 26.55 mS.cm⁻¹). (b) 5x MIC chromatogram of isolated peaks by MonoQ 5/50 GL resin. Noted peak (i) (conductivity 25.15 mS.cm⁻¹). Red trace is absorbance at 254nm, blue trace: absorbance at 280nm and black trace; conductivity.

The addition of twice the MIC of vancomycin was sufficient to alter the normal distribution of intermediates viewed in the control (Figure 6.8), culminating in the increased absorbance of a single eluted peak, which eluted from the monoQ column at a conductivity of 26.55 mS.cm⁻¹ (Figure 6.10). This peak (i) has an absorbance of 48 mAu at A_{254nm}, 2.5 times greater than the next most abundant species. Purification of the control sample showed that the initial elution peak UDP-GlcNAc (Figure 6.8 (i)) reached a maximum absorbance of 60 mAu (A_{254nm}). The corresponding UDP-GlcNAc initial elution peak in the 2x vancomycin sample amounted to only a third of that value at 20 mAu at A_{254nm}. The increased accumulation of peak (i) in the presence of 2x MIC of vancomycin reduced the relative overall abundance of the surrounding peaks. Vancomycin is known to cause UDP-MurNAc-pentapeptide accumulation. This species which eluted from the control monoQ experiment (Figure 6.8: (iv)) at a conductivity of 24.14 mS.cm⁻¹, was comparable to the conductivity at elution of peak (i) (Figure 6.10a) from the 2x MIC incubation (26.55 mS.cm⁻¹). The A₂₅₄/A₂₈₀ ratio of peak (i) at its apex was 2.78, consistent with the expected value of 2.86 for a uridine containing nucleotide.

The addition of five times the MIC of vancomycin lead to the presence of a single peak during ion exchange chromatography (Figure 6.10 (b): (i)) of greater magnitude than previously observed. The measured intensity of this peak reached 332 mAu at an absorbance of 254 nm which was 6.93 times greater than the equivalent peak noted during monoQ purification of *B. subtilis* incubated with 2x MIC of vancomycin (Figure 6.10: (a)). The A₂₅₄/A₂₈₀ ratio of peak (i) in Figure 6.10 (b)

was 2.32. The peak eluted at a conductivity of 25.15 mS.cm⁻¹, and dominated the elution profile. This observable accumulation of an intermediate diminished the absorbance of surrounding fractions as the proportion of the peak (i) material increased greatly. Each of the 2x and 5x MIC vancomycin prominent peaks from ion exchange purification were analysed by mass spectrometry to identify the potential presence of specific peptidoglycan intermediates. The data obtained from the 2x MIC vancomycin sample mass spectrometry is shown in Figure A3.15.

The mass spectral analysis in Figure A3.15 indicated the detection of a UDP-MurNAc-pentapeptide (DAP) dimeric species ($[M-2H]^{2-}$ observed m/z 595.6666, expected m/z 595.6629). The incubation of 2x MIC of the positive control is sufficient to accumulate and identify the specific intermediate targeted by antibiotic inhibition. The data obtained from the 5x MIC vancomycin sample mass spectrometry is shown in Figure A3.16.

The mass spectral analysis (Figure A3.16) identifies the fraction as containing UDP-MurNAc-pentapeptide (DAP) ($[M-2H]^{2-}$ observed m/z 595.6667, expected m/z 595.6629; $[M-3H]^{3-}$ observed m/z 396.774, expected m/z 396.7727). These observations mirrored what was observed with the 2x vancomycin MIC control (Figure A3.15). The accumulation of the intermediate was sufficient enough to be visible on the full mass spectra (Figure A3.16 (a)). The results for the positive controls indicated that this protocol is capable of investigating the potential of the pywac compounds to accumulate intermediates from the peptidoglycan pathway. The 2x MIC treatment was deemed efficient enough to measure a response and was chosen as the investigated concentration of the cell wall active pywac compounds.

6.6.2 Intermediate accumulation of *B. subtilis* against pywac compounds

Pywac compounds were incubated with a sufficient culture volume to produce a final harvested cell wet pellet weight of 1 g to provide sufficient material for further analysis. Each of the *B. subtilis* cultures incubated with pywac compounds were processed and peaks of interest further investigated. Results for pywac compounds 1-9 are combined based on similar ion exchange chromatography elution profile and mass spectrometry detect or lack thereof.

6.6.2.1 Intermediate accumulation of *B. subtilis* against pywac compounds 1, 3, 5, 6 and 7

The effects of pywac compounds 1, 3, 5, 6 and 7 on *B. subtilis* cellular contents were analysed by size exclusion and ion exchange chromatography in Figure 6.11.

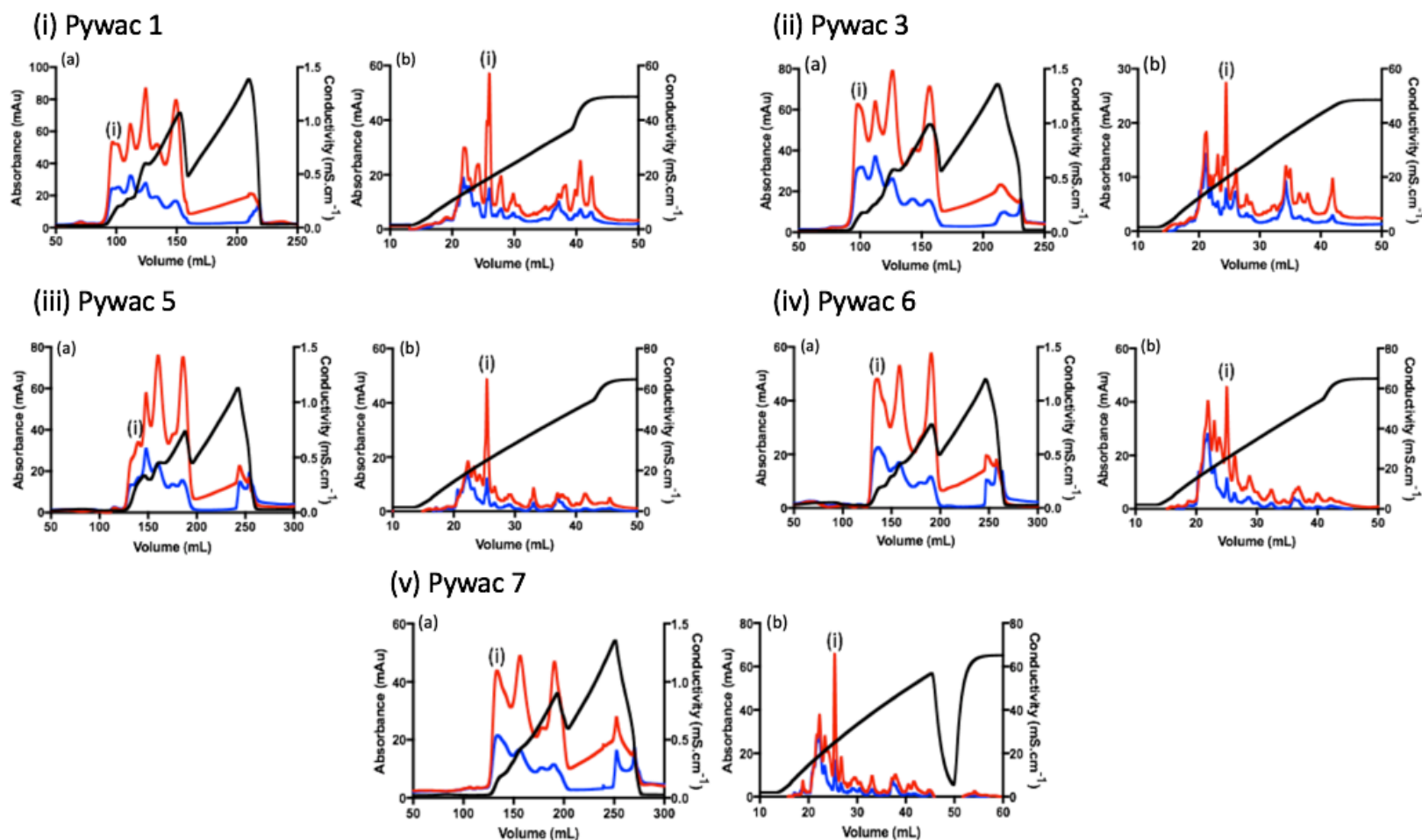


Figure 6.11: Size exclusion and ion exchange chromatography of *B. subtilis* TCA extracts of cells incubated with 2x MIC pywac 1, 3, 5, 6 and 7. (i) Pywac 1 (a) Size exclusion chromatogram of isolated peaks by Bio-gel P2 resin. Noted peak at (i) 95.51 mL. (b) ion exchange chromatogram of isolated peaks by MonoQ 5/50 GL resin. Noted peak (i) (conductivity 18.12 mS.cm⁻¹). (ii) Pywac 3 (a) Size exclusion chromatogram of isolated peaks by Bio-gel P2 resin. Noted peak at (i) 96.34 mL. (b) ion exchange chromatogram of isolated peaks by MonoQ 5/50 GL resin. Noted peak (i) (conductivity 25.47 mS.cm⁻¹). (iii) Pywac 5 (a) Size exclusion chromatogram of isolated peaks by Bio-gel P2 resin. Noted peak at (i) 133.27 mL. (b) ion exchange chromatogram of isolated peaks by MonoQ 5/50 GL resin. Noted peak (i) (conductivity 24.26 mS.cm⁻¹). (iv) Pywac 6 (a) Size exclusion chromatogram of isolated peaks by Bio-gel P2 resin. Noted peak at (i) 133.28 mL. (b) ion exchange chromatogram of isolated peaks by MonoQ 5/50 GL resin. Noted peak (i) (conductivity 25.68 mS.cm⁻¹). (v) Pywac 7 (a) Size exclusion chromatogram of isolated peaks by Bio-gel P2 resin. Noted peak at (i) 133.28 mL. (b) ion exchange chromatogram of isolated peaks by MonoQ 5/50 GL resin. Noted peak (i) (conductivity 24.17 mS.cm⁻¹). Red trace is absorbance at 254nm, blue trace: absorbance at 280nm and black trace; conductivity.

The size exclusion chromatogram (Figure 6.11: (i)-(v) (a)) of *B. subtilis* cells incubated with 2x MIC of pywac compounds 1, 3, 5, 6 and 7 differed from the *B. subtilis* control (Figure 6.7). The control chromatogram displayed isolated individual peaks whereas the pywac samples displayed a narrower elution profile with multiple peaks of similar intensities visualised. The elution of the pywac 1 and 3 samples was displaced by an extra 12 mL compared to the control, whereas pywac 5, 6 and 7 samples were displayed by an extra 49 mL. The major reason for these variations was the twice necessary repacking of P200 column with Bio-gel P2 resin, due to accidental damage. Each subsequent size exclusion chromatography in this chapter except *B. subtilis* incubation with pywac 2 (Figure 6.12) was performed with the repacked column.

As with previous experiments the initial eluted peak from size exclusion chromatography (Figure 6.11 (a): (i)) was isolated for each sample and further fractionated by ion exchange chromatography (Figure 6.11 (b)). Although the gel filtration data differed from the control, the *B. subtilis* pywac compounds chromatograms produced during MonoQ purification were reminiscent of the peak distribution observed with the control data (Figure 6.8), with one exception observed in each. A single noted variable peak of interest, greater in intensity than during the control was eluted from the MonoQ column of each sample.

The conductivity of the noted peak (i) for pywac 1 (Figure 6.11 (i) (b)) was 18.12 mS.cm⁻¹, with an absorbance three times greater than equivalent peaks found in the control. Based on the conductivity value alone, the accumulation of this peak is between conductivity results obtained for the intermediates UDP-GlcNAc (Figure 6.8 (ii) 16.78 mS.cm⁻¹) and UDP-MurNAc-pentapeptide (DAP) (Figure 6.8 (iii) 21.27 mS.cm⁻¹) identified in the control purification. The ratio between $A_{254\text{nm}}/A_{280\text{nm}}$ however was 3.82, not the expected 2.86 ratio proposed for intermediates containing a uridine ring.

The conductivity of the noted peaks (i) for pywac 3 (Figure 6.11 (ii) (b)), 5 (Figure 6.11 (iii) (b)), 6 (Figure 6.11 (iv) (b)) and 7 (Figure 6.11 (iv) (b)) were 25.47 mS.cm⁻¹, 24.26 mS.cm⁻¹, 25.68 mS.cm⁻¹ and 24.17 mS.cm⁻¹ respectively. Comparing these conductivity values to the *B. subtilis* control (Figure 6.8) suggests a similar conductivity observed in elutions containing UDP-MurNAc-pentapeptide (DAP) (Figure 6.8 (iv) conductivity 24.14 mS.cm⁻¹), although the $A_{254\text{nm}}/A_{280\text{nm}}$ ratios observed for each peak

do not demonstrate the 2.86 ratio commonly used to identify the elutions containing a uridine ring.

The mass spectrometric analysis of these peaks are shown from Figure A3.17 to Figure A3.21 in Appendix 3.

Based upon the m/z range investigated and the values attributed to known intermediates it was concluded that the incubation of *B. subtilis* with pywac compounds 1, 3 5, 6, and 7 does not lead to an accumulation of cell wall peptidoglycan intermediates. The signals analysed from the isolated elutions (Figure 6.11 (b): (i)) did not denote any of the known m/z values or spectral properties of peptidoglycan intermediates, leading to the conclusion that the observed accumulation of the sample was not a peptidoglycan precursor.

6.6.2.2 Intermediate accumulation of *B. subtilis* against pywac compound 2

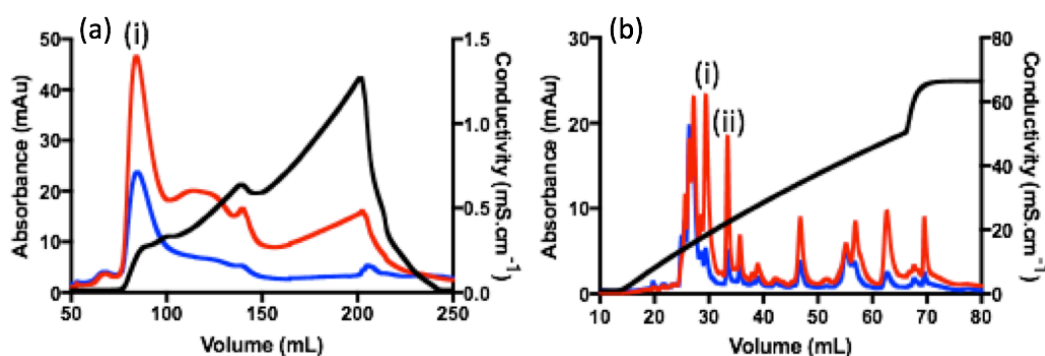


Figure 6.12: Size exclusion and ion exchange chromatography of *B. subtilis* TCA extracts of cells incubated with 2x MIC pywac 2. (a) Size exclusion chromatogram of isolated peaks by Bio-gel P2 resin. Noted peak at (i) 83.30 mL. (b) ion exchange chromatogram of isolated peaks by MonoQ 5/50 GL resin. Noted peak (i) (conductivity 18.80 mS.cm⁻¹) and (ii) (conductivity 22.11 mS.cm⁻¹). Red trace is absorbance at 254nm, blue trace: absorbance at 280nm and black trace; conductivity.

The size exclusion chromatogram of the TCA extracted sample from *B. subtilis* exposed to 2x MIC pywac 2 (Figure 6.12 (a)) was similar in elution profile to the control, with a notable initial peak (i). As cells incubated with pywac 2 were processed before the gel filtration column was repacked, leading to the elution of components of pywac 2

sample starting at 83.30 mL similar to that of the control (Figure 6.7). The monoQ purification (Figure 6.12 (b)) profile was characterised by elution of peaks (i) (Figure 6.12 conductivity 18.80 mS.cm⁻¹) and (ii) (Figure 6.12 conductivity 22.11 mS.cm⁻¹). These peaks eluted at a conductivity similar to those that in the *B. subtilis* control contained UDP-GlcNAc (Figure 6.8: (ii)) and UDP-MurNAc-pentapeptide (DAP) (Figure 6.8: (iii)) respectively. The two peaks were isolated and analysed by mass spectrometry in Figure A3.18 and Figure A3.19 in Appendix 3.

Analysis (Figure A3.18) of the first isolated peak (i) from Figure 6.12 (b) failed to identify a species with a mass to charge ratio consistent with that of any known cell wall intermediate. Therefore, this peak was not caused by accumulation of peptidoglycan precursors.

Mass spectral analysis (Figure A3.19) of the second eluted peak of note from Figure 6.12 (b) (ii) provided an immediately recognisable UDP-MurNAc-pentapeptide (DAP) doubly and triply charged signal ([M-2H]²⁻ Observed m/z 595.66 expected m/z 595.66, [M-3H]³⁻ Observed m/z 396.77, expected m/z 396.77). The increase in absorbance of the second isolated peak was slightly greater than the equivalent peak from the control sample (Figure 6.8: (iii)). Proposed accumulation of UDP-MurNAc-pentapeptide by the pywac compounds would suggest inhibition of either the enzymes involved in lipid synthesis such as MraY catalysing the formation of lipid I, recycling of undecaprenyl pyrophosphate back to undecaprenyl phosphate or that the compounds binds directly to the D-Alanyl-D-Ala subunit in a similar manner to vancomycin.

6.6.2.3 Intermediate accumulation of *B. subtilis* against pywac compounds 4 and 9

The size elution and ion exchange chromatography of *B. subtilis* cell extracts incubated with pywac compounds 4 and 9 are shown in Figure 6.13.

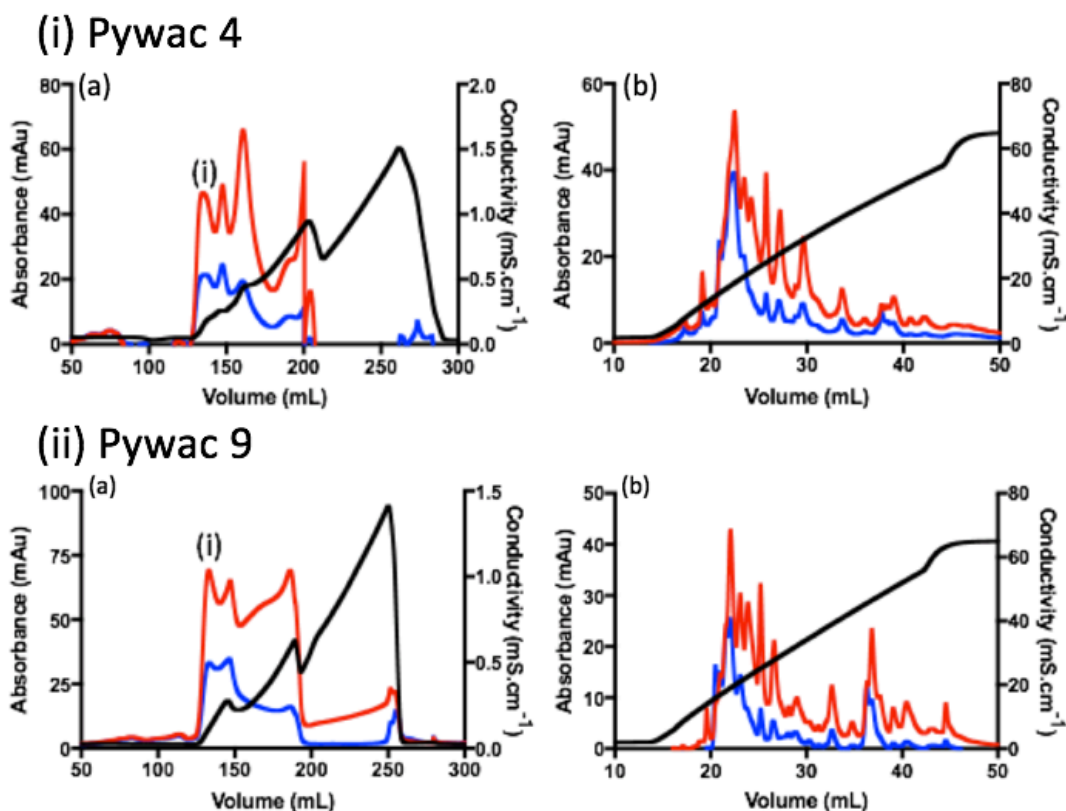


Figure 6.13: Size exclusion and ion exchange chromatography of *B. subtilis* TCA extracts of cells incubated with 2x MIC pywac compounds 4 and 9. (i) Pywac 4 (a) Size exclusion chromatogram of isolated peaks by Bio-gel P2 resin. Noted peak at (i) 133.28 mL. (b) ion exchange chromatogram of isolated peaks by MonoQ 5/50 GL resin. No noted peaks were identified. (ii) Pywac 9 (a) Size exclusion chromatogram of isolated peaks by Bio-gel P2 resin. Noted peak at (i) 133.28 mL. (b) ion exchange chromatogram of isolated peaks by MonoQ 5/50 GL resin. No noted peaks were identified. Red trace is absorbance at 254nm, blue trace: absorbance at 280nm and black trace; conductivity.

The addition of pywac compounds 4 and 9 to *B. subtilis* cells led to a similar size exclusion elution profile (Figure 6.13 (a)) observed as a result of treatment with other pywac compounds (Figure 6.11 (a)) with no obvious accumulation. The volume taken to reach the initial elution was 40 mL greater than previously observed for both compounds at 133.28 mL. The volume difference was due to further reconstruction of the Bio-gel P200 column. The initial eluted peak for both cell extracts from gel filtrations were further purified by ion exchange (Figure 6.13 (b)). The results appeared to match the control sample (Figure 6.8) leading to the conclusion that pywac compounds 4 and 9 did not alter the cell intermediate pool extracted and therefore no fractions were sent to be further analysed by mass spectrometry. Results indicated that the target of pywac compounds 4 and 9 in *B. subtilis* remains to be identified.

6.6.2.4 Intermediate accumulation of *B. subtilis* against pywac 8

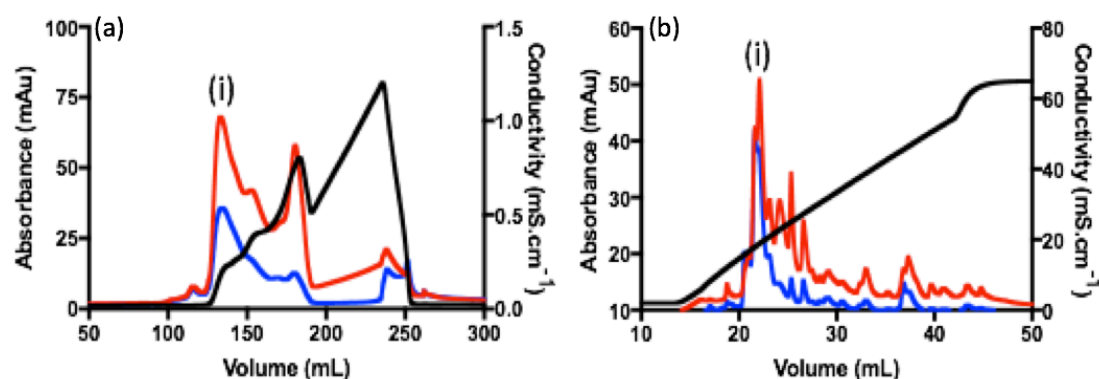


Figure 6.14: Size exclusion and ion exchange chromatography of *B. subtilis* TCA extracts of cells incubated with 2x MIC pywac 8. (a) Size exclusion chromatogram of isolated peaks by Bio-gel P2 resin. Noted peak at (i) 133.27 mL. (b) ion exchange chromatogram of isolated peaks by MonoQ 5/50 GL resin. Noted peak (i) (conductivity 18.85 mS.cm⁻¹). Red trace is absorbance at 254nm, blue trace: absorbance at 280nm and black trace; conductivity.

The penultimate compound tested, pywac 8 produced a unique size exclusion elution profile (Figure 6.14 (a)). Here pywac 8 treated cell extracts chromatographed in a similar manner reminiscent of either the control (Figure 6.7) or the vancomycin positive controls (Figure 6.9) with a significant initial peak separate from the subsequent peaks. The further purification of this fraction (Figure 6.14 (b)) led to an ion exchange chromatogram with a noted difference from the control sample (Figure 6.8). The first and major eluting peak (Figure 6.14 (b): (i)) with a conductivity of 18.85 mS.cm⁻¹ was more pronounced though not equivalent to the vancomycin positive controls, with a marked reduction in surrounding peaks. As previously observed, the initial control peak (Figure 6.8 (i)) contained the UDP-GlcNAc intermediate, which if accumulated to a degree would decrease the concentration of UDP-MurNAc-pentapeptide (DAP) previously observed in the subsequent peaks. The initial elution was analysed by mass spectrometry in Figure A3.24 in Appendix 3 to identify the presence of potential intermediates.

The mass spectrometry data in Figure A3.24 positively identified the fraction as containing the singly charged species of UDP-GlcNAc ([M-H]⁻ observed m/z 606.08, expected m/z 606.07).

6.7 Purification of non-peptidoglycan intermediate standards

A number of the ion exchange purifications identified a potential accumulation during pywac incubation not attributed to peptidoglycan intermediates. Other possible candidates for accumulation that would impact the peptidoglycan pathway include the nucleotides adenosine tri-phosphate (ATP), adenosine di-phosphate (ADP) and adenosine mono-phosphate (AMP), the structures of whom are displayed in Figure 6.15.

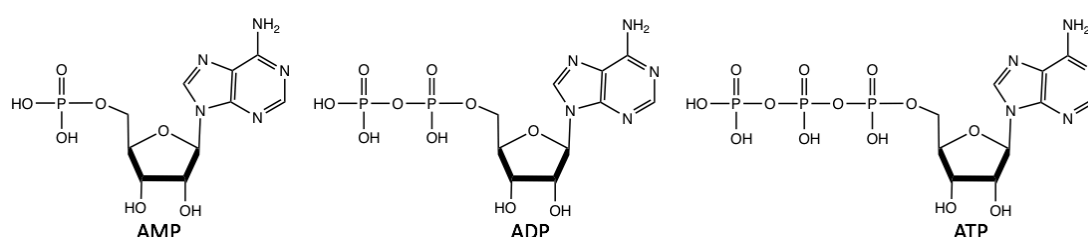


Figure 6.15: The structure of Adenosine mono-phosphate (AMP), Adenosine di-phosphate (ADP) and Adenosine tri-phosphate (ATP). Molecular weight: AMP 347.22, ADP 427.20, ATP 507.18; Chemical formula: AMP $C_{10}H_{14}N_5O_7P$, ADP $C_{10}H_{15}N_5O_{10}P_2$, ATP $C_{10}H_{16}N_5O_{13}P_3$. The above schematic was created using ChemBioDraw.

A key component of peptidoglycan pathway is the utilisation of ATP for the formation of the pentapeptide stem to UDP-MurNAc catalysed by the Mur ligases C-F (Munshi, *et al.* 2013), generating ADP. Inhibition targeted towards an ATP synthase would impact the ability of the cell to generate ATP and lead to accumulation of ADP. Samples from monoQ fractionation of gel filtration elutes of *B. subtilis* sample extracts treated with pywac compounds 1, 3, 5, 6, and 7 displayed isolated peaks of greater intensity than the control sample (Figure 6.8) but analysis of these peaks revealed that they did not contain known species of peptidoglycan intermediates. To establish whether these samples contained adenosine nucleotides initially, standards of ATP, ADP and AMP at a ratio of 3:2:1 were chromatographed by ion exchange chromatography in Figure 6.16 to observe elution conductivity and amenability to mass spectral analysis in Figure A3.25.

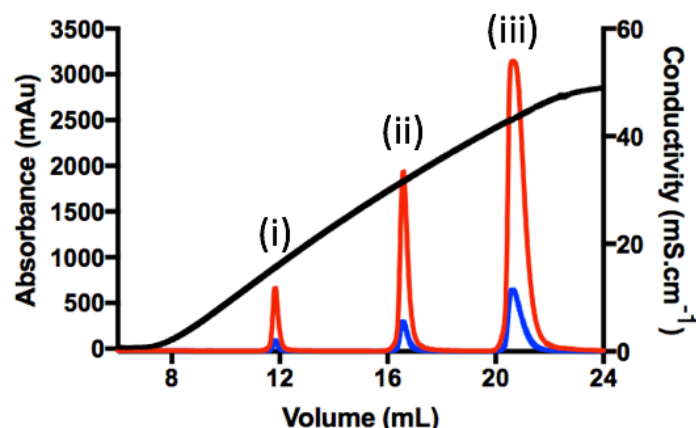


Figure 6.16: Anion exchange chromatography of AMP, ADP and ATP standards. Noted peaks (i) AMP (conductivity 15.94 mS.cm⁻¹), (ii) ADP (conductivity 31.55 mS.cm⁻¹), (iii) ATP (conductivity 43.21 mS.cm⁻¹) were isolated by MonoQ 5/50 GL resin. Red trace is absorbance at 254nm, blue trace: absorbance at 280nm and black trace; conductivity.

The three adenosine standards eluted consecutively with sufficient separation to distinguish between peaks. The standards eluted in the order of AMP (Figure 6.16 (i)), ADP (Figure 6.16 (ii)) and ATP (Figure 6.16 (iii)) with 254 nm absorbances measured at the stated ratio of 1:2:3. The conductivity of each standard was 15.94 mS.cm⁻¹ (AMP), 31.55 mS.cm⁻¹ (ADP) and 43.21 mS.cm⁻¹ (ATP). Standards were analysed by mass spectrometry in Figure A3.25 in Appendix 3. The known m/z values for each singly, doubly and triply charged species are presented in table 6.5 Comparing eluted conductivities of ATP, ADP and AMP to those peaks of interest accumulated during pywac incubation, it was clear that the pywac peaks were not adenosine nucleotides.

Adenosine nucleotide	(m-1)/1	(m-2)/2	(m-3)-3
ATP	505.98	252.49	167.99
ADP	426.02	212.51	141.34
AMP	346.05	172.52	144.68

Table 6.5 The mass/charge ratio for ATP, ADP and AMP. Singly (m-1)/1, doubly (m-2)/2 and triply (m-3)/3 charged species of the adenosine nucleotides.

The mass spectral analysis of standards showed the presence of singly charged species of each adenosine nucleotide. ATP (Figure A3.25 (i)) ([M-H]⁻ observed m/z 505.9882, expected m/z 505.9888), ADP (Figure A3.25 (ii)) ([M-H]⁻ observed m/z 426.0229, expected m/z 426.0217) and AMP (Figure A3.25 (iii)) ([M-H]⁻ observed m/z 346.0559, expected m/z 346.0554).

Another non-peptidoglycan intermediate standard to compare against the pywac accumulation was NADPH. The cofactor is utilized by MurB to reduce the enolpyruvate double bond on UDP-GlcNAc-enolpyruvate generating UDP-MurNAc. The structure is depicted in Figure 6.17.

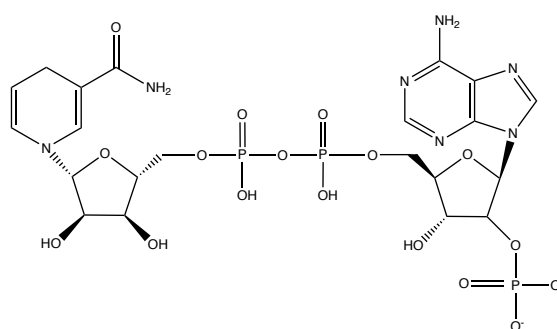


Figure 6.17: The structure of NADPH. Molecular weight: 727.41; Chemical formula: $C_{21}H_{28}N_7O_{16}P_3^{2-}$. The above schematic was created using ChemBioDraw.

A 1000 μ L aliquot 1 mM stock of NADPH was loaded onto a monoQ column to analyse the purity of the sample and identify the elution conductivity as described in Figure 6.18.

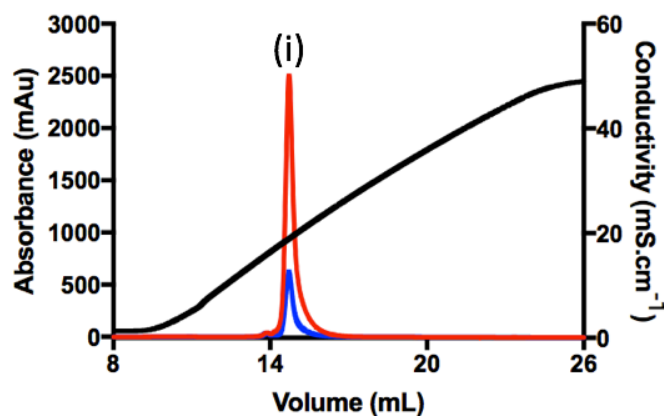


Figure 6.18: Anion exchange chromatography of NADPH standard. Noted peaks (i) (conductivity 18.93 mS.cm^{-1}) was isolated by MonoQ 5/50 GL resin. Red trace is absorbance at 254nm, blue trace: absorbance at 280nm and black trace; conductivity.

The NADPH standard eluted (Figure 6.18) at a conductivity of 18.93 mS.cm^{-1} . The conductivity of the elution of NADPH was similar to the conductivity of the first *B. subtilis* monoQ purification peak, commonly containing UDP-GlcNAc. This

conductivity was too low to equate with unknown pywac accumulations. The standard was analysed by mass spectrometry in Figure A3.26 in Appendix 3.

The mass spectra analysis of NADPH (Figure A3.26) identified the doubly ([M-2H]²⁻ observed m/z 371.54, expected m/z 371.53) charged species relating to the cofactor. Previously isolated elutions did not match NADPH.

6.8 Inhibition of Lipid II synthesis

The activity of the pywac compounds towards the bacterial cell wall likely encompasses more than just the cytosolic pathway. UDP-MurNAc-pentapeptide the product of the cytosolic pathway is converted into lipid linked intermediates by the enzymes *MraY* and *MurG* (Lloyd, Brandish et al. 2004) (Section 1.3.4). *In vitro* Lipid II is constructed through the utilisation of bacterial membranes supplemented with UDP-GlcNAc and undecaprenyl phosphate (Breukink, van Heusden et al. 2003). Extracted bacterial membranes contain native *MraY*, the standard protocol for this technique comprises of *M. flavus* membrane due to the increased abundance of the required enzymes. This method is preferred to expressing the recombinant *MraY* protein due to the difficulty of purifying this enzyme which is a ten transmembrane protein (Lloyd, Brandish et al. 2004). Small scale synthesis of Lipid II samples was prepared as outlined in Section 2.8.4 with any alterations to the protocol mentioned.

6.8.1 Lipid II synthesis utilising *B. subtilis* membranes

As the activity of the pywac compounds was tested in *B. subtilis* cells, the protocol was adapted to incorporate the membranes of this organism. Membranes were extracted from cells grown to exponential phase within minimal media and LB as detailed in Section 2.8.3. The activity of the membranes harvested from cells grown under these conditions was trialled as a small scale Lipid II synthesis (Section 2.8.4), with all reagents employed scaled down to 25% of the full lipid synthesis and samples were incubated at 37°C overnight. The resulting lipids were analysed by Silica TLC (Section

2.8.4.2) accompanied by a Lipid II (DAP) positive control. The results are shown in Figure 6.19.

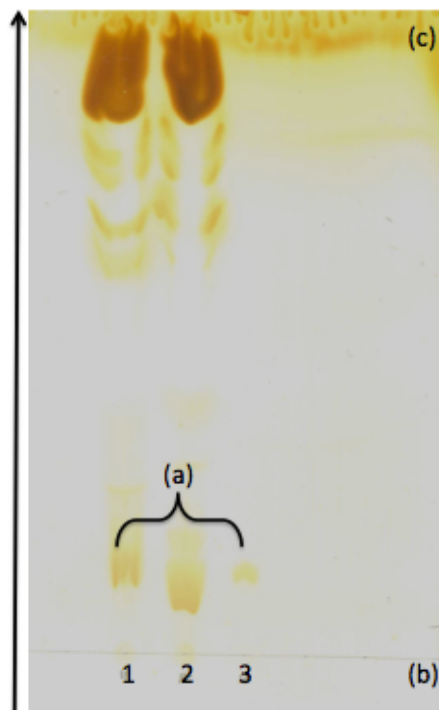


Figure 6.19: TLC of fractions from lipid synthesis of Lipid II (DAP) to assess membrane activity in selected media. *B. subtilis* membranes extracted from cells in LB (1) and minimal media (2). Lipid II (DAP) standard 50 μ M (3) identifies the migration of the lipid. Silica gel TLC plate chromatography with Chloroform/methanol/Water ammonia (88:48:10:1) solvent. TLC plate stained with iodine vapour. (a) Lipid II, (b) the origin and (c) denotes the solvent front.

The migration of the lipids was indicated by the location of the Lipid II (DAP) positive control (Figure 6.19 (3a)) Lipids (Figure 6.19 (1a) and (2a)) were synthesised from each of the small scale syntheses. The utility of minimal media for growth did not impact on the efficacy of the membranes with respect to lipid synthesis (Figure 6.19 (2)) compared to membranes prepared from cells grown in nutrient LB media (Figure 6.19 (1)). Based on this result all lipid synthesis experiments used *B. subtilis* membranes grown from minimal media to aid in determining inhibition.

6.8.2 Lipid synthesis in the presence of pywac compounds

The full scale synthesis of lipid II was performed in the presence of 50 μM of each pywac compound for 4 hours at 37°C. A control synthesis in the absence of compound was also performed as a comparison. The reduced time frame from overnight incubation to 4 hours was decided upon to maximise the sensitivity of the technique to detection of inhibition of lipid synthesis by the pywac compounds. Once the incubation was complete the lipid phase was extracted by pyridinium acetate, N-butanol and H₂O additions (Section 2.8.4). A small amount of each synthesis was separated from the main volume and all volumes were desiccated to remove liquid. The small unpurified aliquots were resuspended in a small amount of solvent A (2:3:1 Chloroform:Methanol:Water) and spotted onto warmed TLC plates to monitor lipid synthesis utilising TLC chromatography (Section 2.8.4.2). TLC plates were stained with iodine vapours and imaged as shown in Figure 6.20.

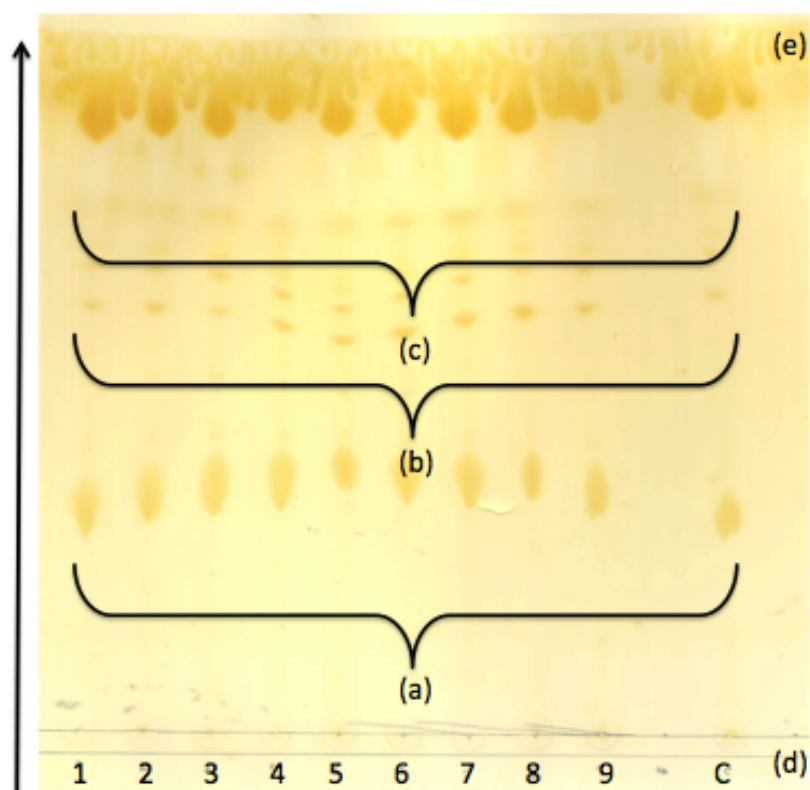


Figure 6.20: TLC of unpurified fractions from lipid synthesis of Lipid II (DAP) co-incubated with 50 μM of pywac compounds 1-9 and no compound control C. Silica gel TLC plate chromatography with Chloroform/methanol/Water ammonia (88:48:10:1) solvent. TLC plate stained with iodine vapour. (a) Synthesised lipid, (b) undecaprenyl phosphate, (c) undecaprenyl pyrophosphate, (d) the origin and (e) denotes the solvent front. 1-9 refers to pywac compounds 1-9. C refers to lipid control.

Results from Figure 6.20 indicate the presence of lipids in all synthesised samples (Figure 6.20 (a)). The variation in the migration of these lipids was caused by the uneven absorption of the TLC running buffer to the silica plate, preferentially migrating at an accelerated rate in the centre of the plate. The ability of the *B. subtilis* membranes to synthesise lipids was observed to be successful in the presence of all pywac compounds although this result alone does not identify the type of lipid produced. The absence of any form of inhibition would lead to the formation of Lipid II. Inhibition solely of MurG by the pywac compounds would lead to the creation of Lipid I, which would migrate to a similar extent as Lipid II on silica TLC. The results suggested that the nine pywac compounds do not elicit activity towards MraY, as hindrance would culminate in the absence of synthesised lipid and the presence of UDP-MurNAc-pentapeptide.

6.8.2.1 Purification of synthesised lipids co-incubated with pywac compounds

The extracted unpurified aliquots identified the synthesis of lipids when *B. subtilis* was co-incubated with pywac compounds. The remaining desiccated synthesised lipids samples were purified by anion exchange chromatography on DEAE Sephacel as described in Section 2.8.4.1. Previous investigations from other members of the laboratory (Julie Tod, personal communication) have indicated that Lipid II DAP remained bound to the column at high ammonium bicarbonate (AB) concentrations (0.2 M) and required a second 1 M wash to elute. Based upon this knowledge once all synthesised lipid samples were purified isocratically by AB concentrations ranging from 50 mM to 1 M, small aliquots were taken of the three most concentrated elutions of AB (500 mM, 1 M and 1 M repeat) for each pywac incubated sample. The three aliquots were resuspended in chloroform/methanol/water (2:3:1) (solvent A) and loaded onto Silica TLC plates. Figure 6.21 displays the TLC of purified lipids incubated with pywac compounds 1-3 as well as the compound absent control. Figure 6.22 displays the TLC of purified lipids incubated with pywac compounds 4-9.

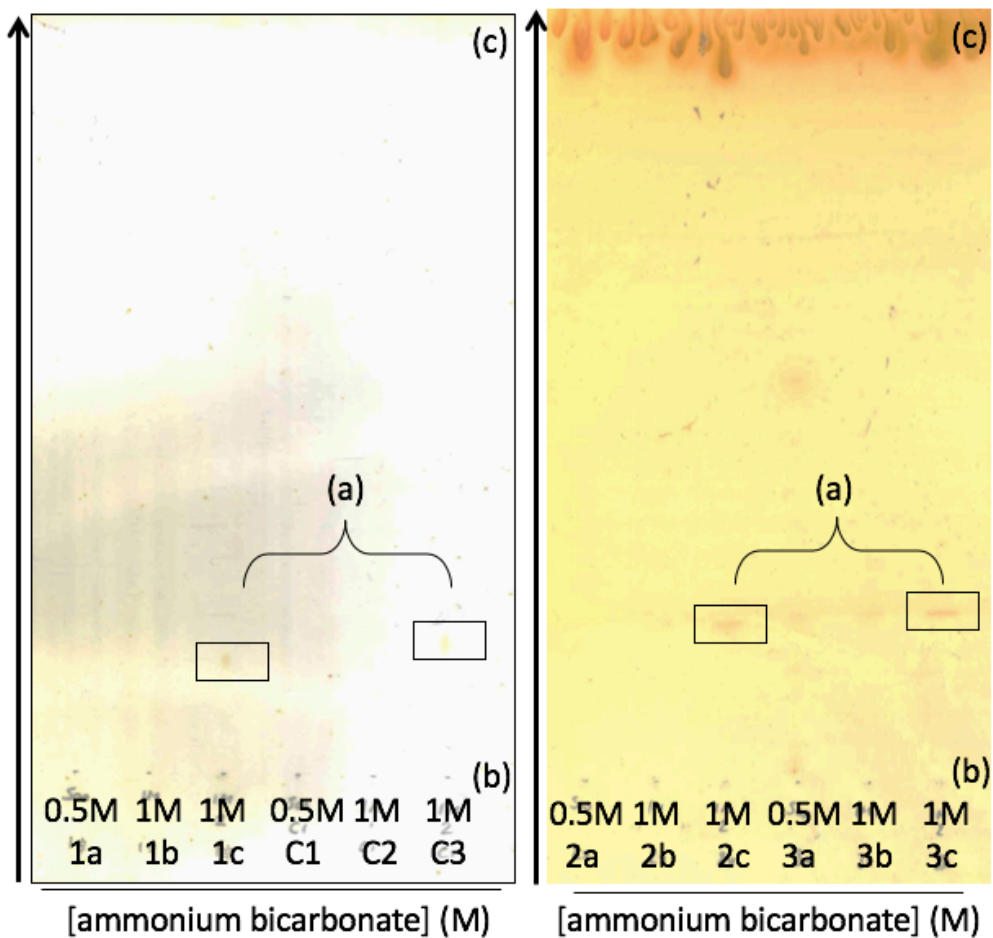


Figure 6.21: Thin-layer chromatography of purified lipid fractions co-incubated with 50 μ M pywac compounds 1, 2 3 and no compound control. Lipid synthesis utilizing *B. subtilis* membranes extracted from cells in minimal media co-incubated with compounds pywac 1 (1a-c), pywac 2 (2a-c) pywac 3 (3a-c) or without compound control (C1-3). Lipids eluted from DEAE sephacel fast flow resin column by isocratic additions of ammonium bicarbonate 50 mM to 1 M. Silica gel TLC plate chromatography with Chloroform/methanol/Water ammonia (88:48:10:1) solvent. TLC plate stained with iodine vapour. (a) Lipid II, (b) the origin and (c) denotes the solvent front. Lipids eluted during the second 1M AB wash highlighted by black squares.

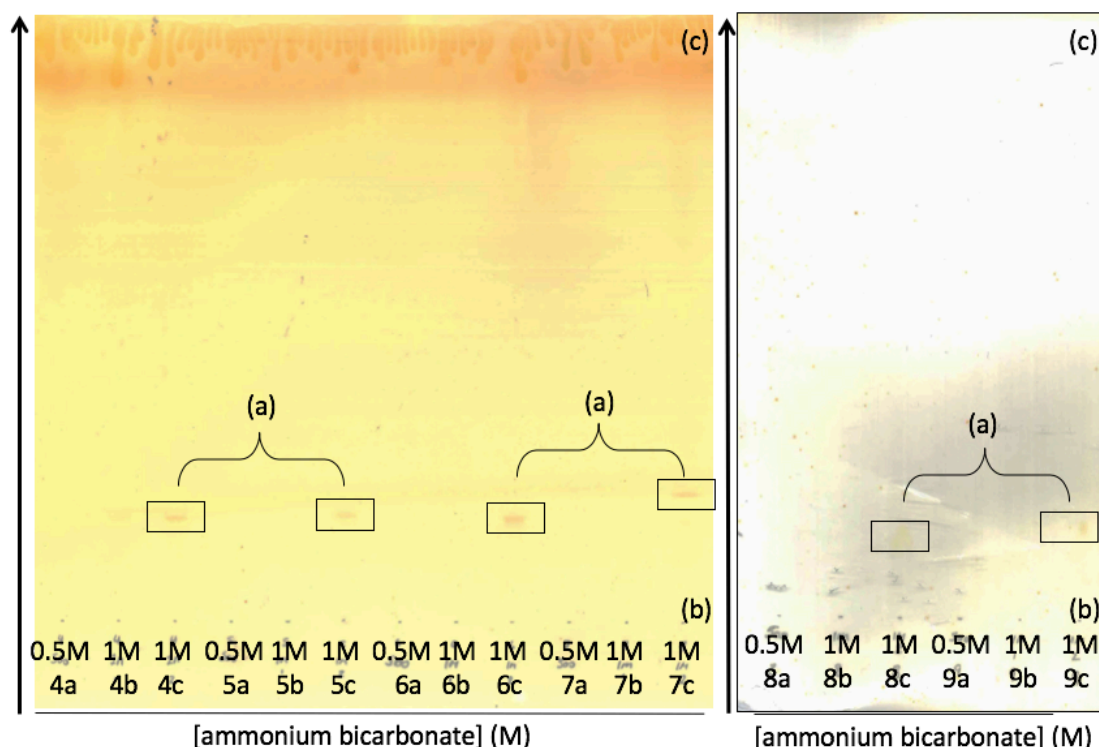


Figure 6.22: Thin-layer chromatography of purified lipid fractions co-incubated with 50 μ M pywac compounds 4, 5, 6, 7, 8 and 9. Lipid synthesis utilizing *B. subtilis* membranes extracted from cells in minimal media co-incubated with compounds pywac 4 (4a-c), pywac 5 (5a-c), pywac 6 (6a-c), pywac 7 (7a-c), pywac 8 (8a-c) and pywac 9 (9a-c). Lipids eluted from DEAE sephacel fast flow resin column by isocratic additions of ammonium bicarbonate 50 mM to 1 M. Silica gel TLC plate chromatography with Chloroform/methanol/Water ammonia (88:48:10:1) solvent. TLC plate stained with iodine vapour. (a) Lipid II, (b) the origin and (c) denotes the solvent front. Lipids eluted during the second 1M AB wash highlighted by black squares.

TLC of the purified pywac lipid samples (Figure 6.21 (a), Figure 6.22 (a)), identified the presence of purified lipids within the repeat 1 M ammonium bicarbonate elution. None of the purified lipids or any excess reagents or impurities were observed within the 500 mM and the first 1 M elution. Each of the synthesised lipids migrated to a comparable degree as the control (Figure 6.21: control (a)) with only minor variation most notably pywac sample 7. The solvents present in purified lipid samples were removed by desiccation and samples were submitted for negative ion mass spectrometry analysis.

6.8.2.2 Identification of lipids co-incubated with pywac compounds

Lipids were synthesised by the displacement of UMP from UDP-MurNAc-pentapeptide (DAP) by undecaprenyl phosphate to form Lipid I, which was subsequently glucosaminylated with UDP-GlcNAc to form Lipid II. These reactions were catalysed by MraY and MurG respectively. The expected m/z ratios for negative ion singly, doubly and triply charged species of Lipid I (DAP) and Lipid II (DAP) are recorded in table 6.6.

Lipid species	Expected m/z		
	(m-1)/1	(m-2)/2	(m-3)-3
Lipid I DAP (MurNAc)	1714.97	856.98	570.99
Lipid II DAP (MurNAc)	1918.04	958.51	638.67

Table 6.6 The mass/charge ratio for N-acetylated Lipid I DAP and N-acetylated Lipid II DAP. Singly (m-1)/1, doubly (m-2)/2 and triply (m-3)/3 charged species stated.

Each of the small scale synthesis were successful in producing lipids in the presence of all pywac compounds as observed by the TLC results (Figure 6.21 and Figure 6.22). To distinguish between the two possible variants, Lipid I and Lipid II each sample was subjected to mass spectrometric analysis beginning with the compound absent control in Figure A3.27.

The mass spectral analysis (Figure A3.27) of the control Lipid II synthesis sample detected the singly ($[M-H]^-$ observed m/z 1918.03 expected m/z 1918.04) and doubly ($[M-2H]^{2-}$ observed m/z 958.51 expected m/z 958.51) charged species of Lipid II DAP, confirming the accuracy of the protocol utilised (Section 2.8.4). The purified pywac incubated lipid samples were subsequently analysed by mass spectrometry from Figure A3.28 to Figure A3.36.

The synthesis of Lipid II (DAP) by *B. subtilis* membranes despite the presence of each pywac compound was confirmed by negative ion mass spectrometry (Figure A3.28 to Figure A3.36). The doubly (expected m/z 958.51) and triply (expected m/z 638.67) charged m/z ratios for each species agreed with the expected values for with Lipid II

(DAP). The mass spectral analysis confirmed that the activity of pywac compounds 1-9 was likely not targeted towards either MraY or MurG, with potentially one exception. Analysis of pywac 7 lipid synthesis (Figure A3.34) determined that the relative abundance of the lipid was dramatically reduced compared to the other samples. Relating the intensity of the doubly charged $[M-2H]^{2-}$ ion of Lipid II DAP to that of the constant presence of the unknown solvent contaminant (255.2346 m/z). The signal for the pywac 7 sample was negligible relative to that of other lipid samples.

Lipid II was not the sole cellular structure observed in all samples. The presence of other peptidoglycan precursors in pywac 2 and 3 samples during mass spectrometry analysis was shown in Figure A3.37 and Figure A3.38 respectively.

Two of the analysed samples incubated with pywac 2 (Figure A3.37) and pywac 3 (Figure A3.38) were also determined to contain singly ($[M-H]^-$ expected m/z 606.07) and doubly ($[M-2H]^{2-}$ expected m/z 302.53) charged species of UDP-GlcNAc. Both samples were analysed (Figure A3.29 and Figure A3.30) and as previously mentioned a significant abundance of both dimeric and trimeric species characterising Lipid II (DAP) were detected. Detection of UDP-GlcNAc in these samples is likely attributed to errors during purification and collection of separated phases, as Lipid I was not detected by mass spectrometry in either sample which would be observed during MurG inhibition.

Quantification of the purified lipid samples was undertaken to assess the comparative concentration of Lipid II once incubated with pywac compounds. The method used is described in Section 2.8.4.3. The concentration of each synthesised lipid II is stated in table 6.7

Lipid sample	Lipid concentration
Control	120 μ M
Pywac 1	110 μ M
Pywac 2	128 μ M
Pywac 3	139 μ M
Pywac 4	111 μ M
Pywac 5	121 μ M
Pywac 6	105 μ M
Pywac 7	27 μ M
Pywac 8	116 μ M
Pywac 9	123 μ M

Table 6.7 Concentrations of synthesised Lipid II co-incubated with 50 μ M of pywac compounds 1-9. Small scale lipid synthesis of 200 μ L final volume. Lipids were purified on a DEAE Sepharose Fast Flow resin column with isocratic increases in ammonium bicarbonate from 50 mM to 1 M. Quantification of lipids by measurement of phosphate release assay at A_{360nm} . Control sample is synthesised in the absence of pywac compounds.

The concentrations quantified in table 6.7 clearly demonstrate that in the presence of pywac 7 *B. subtilis* membranes produced 22% of the concentration of Lipid II DAP relative to that accumulated in the compound absent control. This disparity explains the noted variation in mass spectra analysis utilising equal final volumes from the final DEAE sepharose column elution. This data may indicate that pywac 7 is targeted towards hindrance of lipid synthesis, although further investigations are required to confirm findings.

In all other pywac incubations, Lipid II DAP was synthesised to quantities that were within 10% of the control leading to the conclusion that pywac compounds 1-6 and 8-9 did not impact Lipid II DAP synthesis significantly.

The concentrations measured for pywac compounds 2 and 3 were likely artificially inflated slightly due to the presence of UDP-GlcNAc contaminants which can also release phosphate groups, increasing the determined Lipid II concentration.

6.9 Intermediate accumulation of *S. aureus*

Preceding the initial investigation into the mode of action of the pywac compounds with respect to *B. subtilis*, the decision was taken to expand the investigation into another organism. As the peptidoglycan pentapeptide stem of *B. subtilis* contains the residue DAP at position three, the Gram-positive organism *S. aureus* was selected due to the incorporation of L-Lysine at position three.

The intension was to repeat the accumulation protocol with a Gram-positive organism in order to evaluate potential differences in peptidoglycan biosynthesis with cells that incorporate L-lysine into position 3 of the peptidoglycan peptide stem, which may aid in determining the role of each pywac compound.

Unfortunately due to health issues and time constraints a complete investigation could not be completed. The experiment data reported in this section are therefore intended as a marker for subsequent exploration. The MIC values for *S. aureus* were not established and experiments within this section utilised previously observed MIC values for *B. subtilis* (Table 6.1). Therefore these results cannot be accurately compared to equivalent *B. subtilis* experiments. Due to the high MIC values of pywac compounds 3, 4, 5 and 7 and the limited availability of these compounds, they were omitted from further investigation.

S. aureus was evaluated to determine its response to pywac compounds 1, 2, 6, 8, 9 as well as a 2x MIC vancomycin positive control.

6.9.1 DMSO tolerance of *S. aureus*

In a similar manner to *B. subtilis* (Figure 6.2) the tolerance of *S. aureus* cells towards DMSO was assessed. Increasing percentages of DMSO were added to diluted exponentially grown cells to evaluate the effect the presence of DMSO has on normal observed growth. The results are depicted in Figure 6.23.

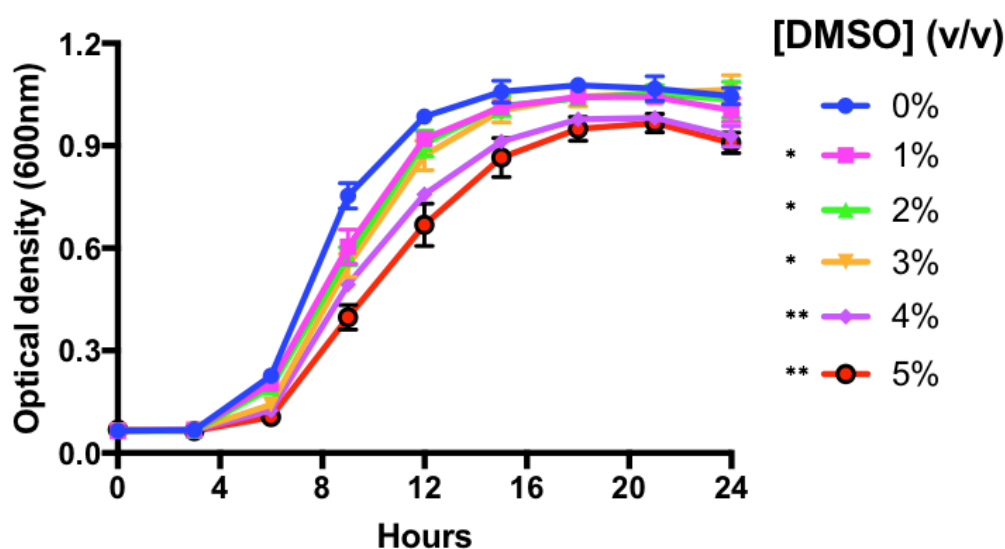


Figure 6.23 DMSO tolerance of *S. aureus*. Cells were grown in the presence of increasing concentrations of DMSO to determine the tolerance of staphylococcus proliferation for the solvent, in 96 well microtiter plates in triplicate at 37°C with intermittent shaking. Absorbance was measured at OD_{600nm} at 3 hour intervals for 24 hours. Each well contained 100 µL minimal media. *S. aureus* cells were standardized to an OD_{600nm} of 1 and diluted further by a factor of 10⁴ prior to incubation. Error bars represent standard deviation of triplicate measurements. DMSO concentration: 0% (v/v) Blue, 1% (v/v) Pink, 2% (v/v) Green, 3% (v/v) Orange, 4% (v/v) Purple, 5% (v/v) Red. Result: DMSO percentages between 1-3% (v/v) slightly impacted phenotypic growth equally, with 4-5% (v/v) reducing growth by a greater degree.

[DMSO] (%)	<i>S. aureus</i>				
	Apparent Lag Phase Duration (h)	Td (h ⁻¹)	AUC (% of 0% DMSO)	Stationary Phase OD ₆₀₀ nm attained	p-values
0	3	1.72	-	1.04	-
1	3	1.89	93.16	1.00	<0.05
2	3	1.91	92.53	1.03	<0.05
3	3	1.99	90.65	1.06	<0.05
4	3	2.07	81.49	0.927	<0.01
5	3	2.29	75.78	0.909	<0.01

Table 6.8 Statistical comparisons of *S. aureus* growth curves in the presence of increasing concentrations of DMSO. *S. aureus* incubated for 24 hours at 37°C with selected concentrations of DMSO (v/v) produced growth curves measured at OD_{600nm} in Figure 4.1. Variations between growth curves were measured by time taken to exit apparent lag phase (hours), the doubling time (Td) of cells during exponential phase (hours⁻¹), the area under the curve (AUC) percentage compared to the 0 % control (%), the OD_{600nm} value achieved during stationary phase and whether the growth curve variations were statistically significant compared to each 0 % control with p-values <0.05 deemed significant.

Results show that staphylococcal cells were less tolerant to concentrations of DMSO than *B. subtilis* (Figure 6.2). In the absence of DMSO (Figure 6.23: Blue) *S. aureus* exited apparent lag phase after 3 hours, multiplied with a Td of 1.72 hours during exponential phase and entered stationary phase after 15 hours at an OD_{600nm} of 1.0. The addition of DMSO regardless of concentration did not impede the exit from apparent lag phase which remained at 3 hours. The doubling time increased slightly with each increase in total percentage of DMSO present. The Td results were: 1% (v/v) 1.89 hours (Figure 6.23: Pink), 2% (v/v) 1.91 hours (Figure 6.23: Green), 3% (v/v) 1.99 hours (Figure 6.23: Orange), 4% (v/v) 2.07 hours (Figure 6.23: Purple), 5% (v/v) 2.29 hours (Figure 6.23: Red). Similarly, to the doubling time, the increased addition DMSO caused a gradual decrease in AUC: 1% (v/v) 93.16%, 2% (v/v) 92.53%, 3% (v/v) 90.65%, 4% (v/v) 81.49%, 5% (v/v) 75.78%. The statistical significance of each concentration was <0.05 (1%, 2% and 3% (v/v)) and <0.01 (4% and 5% (v/v)) respectively.

Based upon these results the decision was taken to continue utilising 2% (v/v) DMSO to solubilise the pywac compounds. Controls incubated in the absence of these

compounds contained the equivalent percentage of DMSO to account for the impact of DMSO alone.

6.9.2 Analysis of *S. aureus* peptidoglycan intermediate standards

The examination of *S. aureus* permitted a comparison between the implementation of the third residue of the UDP-MurNac peptide stem. The MurE ligase of most Gram positive organisms adds a L-lysine to the third position whereas *B. subtilis* MurE utilises DAP. The incorporation of L-lysine required the evaluation of new UDP-MurNac-tri and pentapeptide (Lys) standards. Previously evaluated peptidoglycan intermediate standards (Figure 6.6) minus the UDP-MurNac-tripeptide (DAP) and UDP-MurNac-pentapeptide (DAP) were still applicable to this investigation. The structures of both UDP-MurNac-tripeptide (Lys) and UDP-MurNac-pentapeptide (Lys) were presented in Figure 6.24.

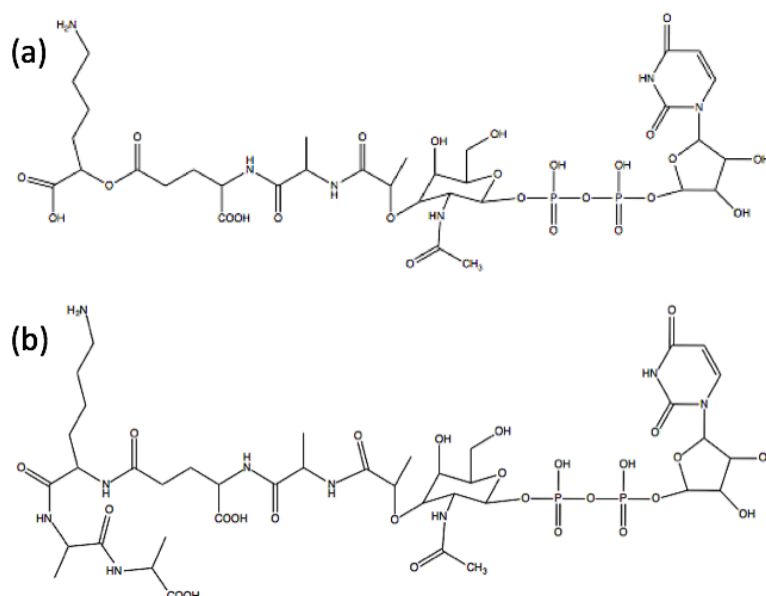


Figure 6.24: The structures of cytosolic peptidoglycan intermediates of *S. aureus*. (a) UDP-MurNac-tripeptide Lys (L-Ala-D-Glu-L-Lys) (b) UDP-MurNac-pentapeptide Lys (L-Ala-D-Glu-L-Lys-D-Ala-D-Ala). The above schematic was created using ChemBioDraw.

UDP-MurNac-tripeptide (Lys) and UDP-MurNac-pentapeptide (Lys) standards at a final concentration of 1 mM were synthesised as outlined in Section 2.8.1 and were characterised by ion exchange chromatography to establish the estimated conductivity

required for the elution of each species. The chromatogram for each standard is shown in Figure 6.25.

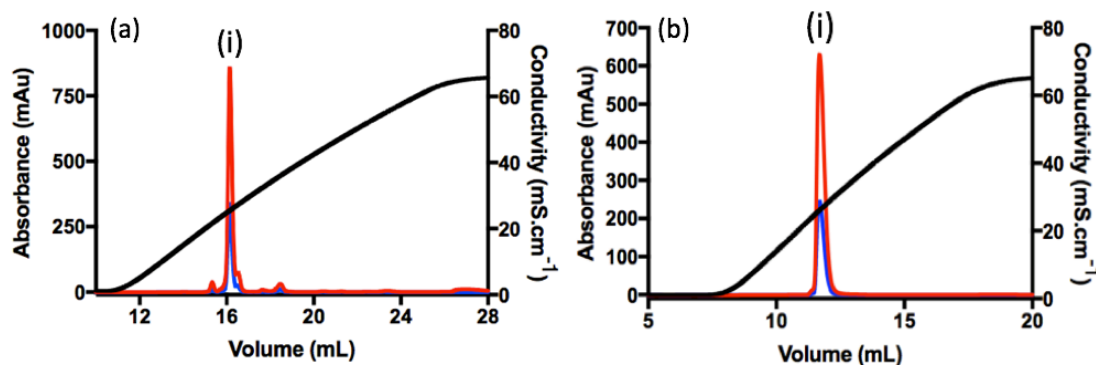


Figure 6.25: Anion exchange chromatography of *S. aureus* peptidoglycan intermediate standards. Noted peak (a) UDP-MurNAc-tripeptide (L-Ala-D-Glu-L-Lys) (conductivity 25.21 mS.cm⁻¹), (b) UDP-MurNAc-pentapeptide (L-Ala-D-Glu-L-Lys-D-Ala-D-Ala) (conductivity 26.31 mS.cm⁻¹). Samples were analysed using a MonoQ 5/50 GL resin. Red trace is absorbance at 254 nm, blue trace: absorbance at 280 nm and black trace; conductivity.

Both the tripeptide and pentapeptide standards eluted similarly from the monoQ column (Figure 6.25) with conductivities of 25.21 mS.cm⁻¹ (Figure 6.25 (a)) and 26.31 mS.cm⁻¹ (Figure 6.25 (b)) respectively. Both standards produced only a single significant peak which was analysed by mass spectrometry in Figure A3.39 (tripeptide) and Figure A3.40 (pentapeptide) in Appendix 3. The known m/z ratios for each *S. aureus* peptidoglycan intermediate are stated in table 6.9.

UDP Species	(m-1)/1	(m-2)/2	(m-3)-3
UDP-GlcNAc	606.07	302.53	201.35
UDP-GlcNAc-enolpyruvyl	676.07	337.53	224.68
UDP-MurNAc	678.09	338.54	225.35
UDP-MurNAc-L-Ala	749.13	374.06	249.03
UDP-MurNAc-L-Ala-D-Glu	878.17	438.58	292.05
UDP-MurNAc-L-Ala-D-Glu-L-Lys	1006.26	502.63	334.75
UDP-MurNAc-L-Ala-D-Glu-L-Lys-D-Ala-D-Ala	1148.34	573.66	382.10

Table 6.9 The mass/charge ratio for the peptidoglycan cytosolic gram-positive lysine intermediates. Singly (m-1)/1, doubly (m-2)/2 and triply (m-3)/3 charged species of the various peptidoglycan intermediates.

The mass spectral analysis (Figure A3.39) of the UDP-MurNAc-tripeptide (Lys) standard elution (Figure 6.25 (a)) identified the singly ($[M-H]^-$ observed m/z 1006.27, expected m/z 1006.269), doubly ($[M-2H]^{2-}$ observed m/z 502.63, expected m/z 502.630) and triply ($[M-3H]^{3-}$ observed m/z 334.75, expected m/z 334.751) charged species matching the known values attributed to the intermediate.

The mass spectral analysis (Figure A3.40) of the UDP-MurNAc-pentapeptide (Lys) standard elution (Figure 6.25 (b)) identified the singly ($[M-H]^-$ observed m/z 1148.34, expected m/z 1148.343), doubly ($[M-2H]^{2-}$ observed m/z 573.67, expected m/z 573.667) and triply ($[M-3H]^{3-}$ observed m/z 382.11, expected m/z 382.109) charged species matching the known values attributed to the intermediate.

6.9.3 Normal cellular distribution of *S. aureus* peptidoglycan intermediates

Utilising the protocol outlined in Section 2.9 *S. aureus* cells in the absence of inhibitors were grown to late exponential phase and whilst other *S. aureus* cells were then incubated with pywac compounds or vancomycin, the control sample continued incubation for the remaining three hours with the addition of equivalent DMSO percentage to that added with the pywac compound samples. Cellular extracts for chromatographic purification were prepared according to Section 2.9.2 and Section 2.9.3 and were fractionated by size exclusion chromatography followed by ion exchange chromatography. These results are shown in Figure 6.26.

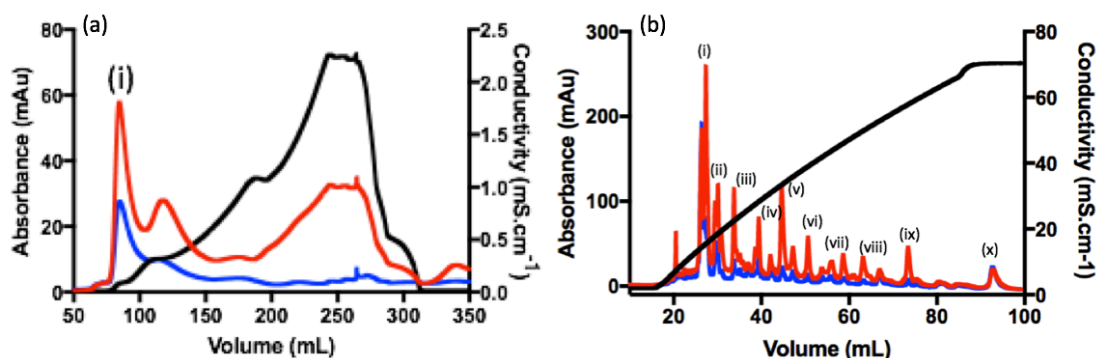


Figure 6.26: Size exclusion and ion exchange chromatography of *S. aureus* TCA extracted control cells. (a) Size exclusion chromatogram of isolated peaks by Bio-gel P2 resin. Noted peak at (i) 83.55 mL. (b) ion exchange chromatogram of isolated peaks by MonoQ 5/50 GL resin. Noted peaks (i) (conductivity 15.49 mS.cm⁻¹), (ii) (conductivity 18.63 mS.cm⁻¹), (iii) (conductivity 22.49 mS.cm⁻¹), (iv) (conductivity 28.33 mS.cm⁻¹), (v) (conductivity 33.38 mS.cm⁻¹), (vi) (conductivity 39.03 mS.cm⁻¹), (vii) (conductivity 46.05 mS.cm⁻¹), (viii) (conductivity 49.74 mS.cm⁻¹), (ix) (conductivity 57.84 mS.cm⁻¹) and (x) (conductivity 70.31 mS.cm⁻¹). Red trace is absorbance at 254nm, blue trace: absorbance at 280nm and black trace; conductivity.

The size exclusion chromatogram of the *S. aureus* control (Figure 6.26 (a)) separated lysed cell contents in a similar manner to *B. subtilis* samples. Initial conductivity increase correlated with a measurable $A_{254\text{nm}}/A_{280\text{nm}}$ increase in absorbance which eluted from the column after 83.55 mL. The significant fraction (i) was isolated and freeze-dried. The *S. aureus* control sample was resuspended in monoQ buffer A (Section 2.7.3.3), a $A_{260\text{nm}}$ reading was taken from each sample and was diluted to a standard absorbance of 0.03 before purification on an equilibrated monoQ 5/50 column. The elution profile of *S. aureus* cells shows similarity to the equivalent result in *B. subtilis* cells (Figure 6.7), with a significant initial peak and a subsequent gradual decrease in peak intensities. The initial peak reached 270 mAu at an absorbance of 254 nm. Ten noted peaks (Figure 6.26 (b): (i) - (x)) were eluted from the monoQ column of the initial *S. aureus* gel filtration peak. These elutions were isolated and analysed by negative ion mass spectrometry to identify peptidoglycan intermediates in the standard elution profile as shown from Figure A3.41 to Figure A3.50.

The first five eluted peaks from ion exchange chromatography (Figure 6.26 (b)) all contained peptidoglycan intermediates as detected by mass spectrometry (Figure A3.41 to Figure A3.45). The first eluted peak (Figure 6.26 (b): (i)) with a conductivity of 15.49 mS.cm⁻¹ contained the UDP-GlcNAc, the first precursor of the peptidoglycan pathway ([M-H]⁻ (observed m/z 606.0739, expected m/z 606.0738). The second eluted peak (Figure 6.26 (b): (ii)) with a conductivity of 18.63 mS.cm⁻¹ also contained UDP-GlcNAc ([M-H]⁻ (observed m/z 606.0738, expected m/z 606.0738). The conductivity

of the first two eluted peaks were either side of the conductivity obtained by the UDP-GlcNAc standard (Figure 6.6 (i): conductivity 16.41 mS.cm^{-1}) although this might reflect the variation in the gradient of ammonium acetate between the two runs. The remaining three eluted peaks analysed in (Figure A3.43 to Figure A3.45) were evaluated to all contain UDP-MurNAc-pentapeptide (Lys). The standard for this intermediate eluted at a conductivity of 26.31 mS.cm^{-1} (Figure 6.25 (b)). The elution conductivity of these *S. aureus* control peaks was 22.49 mS.cm^{-1} (Figure 6.26 (b): (iii)), 28.33 mS.cm^{-1} (Figure 6.26 (b): (iv)) and 33.38 mS.cm^{-1} (Figure 6.26 (b): (v)). As with the UDP-GlcNAc standard, two of these peaks fell either side of the elution value produced by the pentapeptide (Lys) standard. Mass spectra analysis identified the doubly charged UDP-MurNAc-pentapeptide (Lys) species within the three peaks, (Figure A3.43) (iii) ($[M-2H]^{2-}$ (observed m/z 573.6703, expected m/z 573.6679), (Figure A3.44) (iv) ($[M-2H]^{2-}$ (observed m/z 1148.3480, expected m/z 1148.3437) and (Figure A3.45) (v) ($[M-2H]^{2-}$ (observed m/z 1148.3492, expected m/z 1148.3437) respectively.

From the isolated *S. aureus* control peaks (vi) (conductivity 39.03 mS.cm^{-1}) to (x) (conductivity 70.31 mS.cm^{-1}) the mass spectra analysis (Figure A3.46 to Figure A3.50) produced no further evidence of peptidoglycan intermediates, therefore all eluted peaks with conductivity greater than 39.03 mS.cm^{-1} were eliminated from further consideration.

The absence of either UDP-MurNAc-mono-peptide, -di-peptide or -tri-peptide was not unexpected as similar findings were found with *B. subtilis* (Figure 6.8). This might suggest these intermediates were being consumed as fast as they were formed in the pathway under normal conditions.

6.9.4 Intermediate accumulation of *S. aureus* vancomycin control

Cell wall active pywac compounds were previously incubated with *B. subtilis* cells at twice the MIC (μM) of the positive control vancomycin (Figure 6.10). The stated vancomycin MIC for *S. aureus* strains is between $0.5\text{-}2 \mu\text{g.mL}^{-1}$ (Prakash, *et al.* 2008).

To assess the MIC of the *S. aureus* strain used here, the impact of growth of vancomycin concentrations between 0.5-2 $\mu\text{g.mL}^{-1}$ was assessed (Figure 6.27).

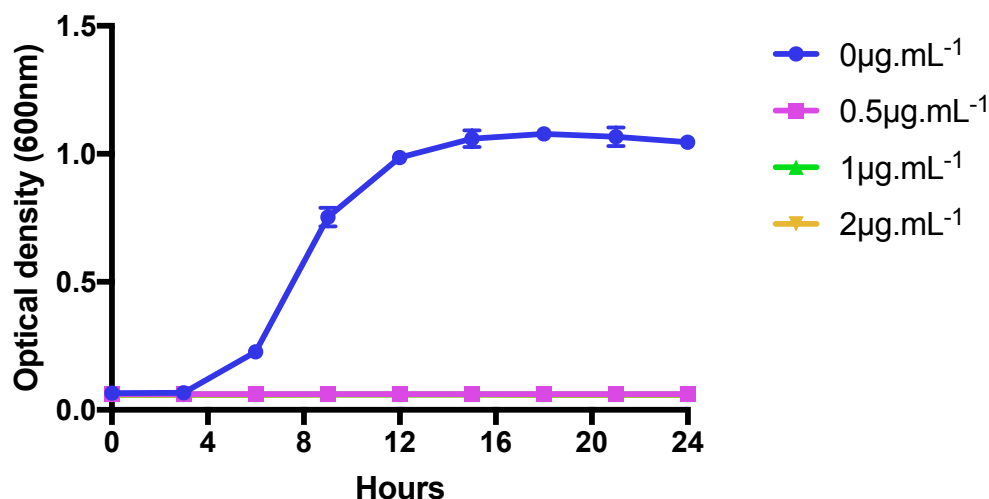


Figure 6.27 MIC of vancomycin against *S. aureus*. Cells were grown in the presence of the vancomycin 0.5 $\mu\text{g.mL}^{-1}$ (Pink), 1 $\mu\text{g.mL}^{-1}$ (Green) and 2 $\mu\text{g.mL}^{-1}$ (Orange) in 2% (v/v) DMSO in 96 well microtiter plates in triplicate at 37°C with intermittent shaking. Absorbance was measured at OD_{600nm} at 3 hour intervals for 24 hours. Each well contained 100 μL minimal media. *S. aureus* cells were standardized to an OD_{600nm} of 1 and diluted further by a factor of 10^4 prior to incubation. Error bars represent standard deviation of triplicate measurements. Control: (Blue) *S. aureus* cells grown in absence of vancomycin plus 2% (v/v) DMSO. Result: The proposed MIC values for vancomycin against *S. aureus* was correct.

Each of the vancomycin concentrations investigated (Figure 6.27) were sufficient to completely inhibit observable growth. Therefore 1 $\mu\text{g.mL}^{-1}$ was selected as $\geq 2x$ MIC against *S. aureus* cells. Following incubation and extraction by TCA/Di-ethyl ether the 2x MIC positive control sample was processed by size exclusion chromatography and ion exchange chromatography. The chromatograms for each purification step are presented in Figure 6.28.

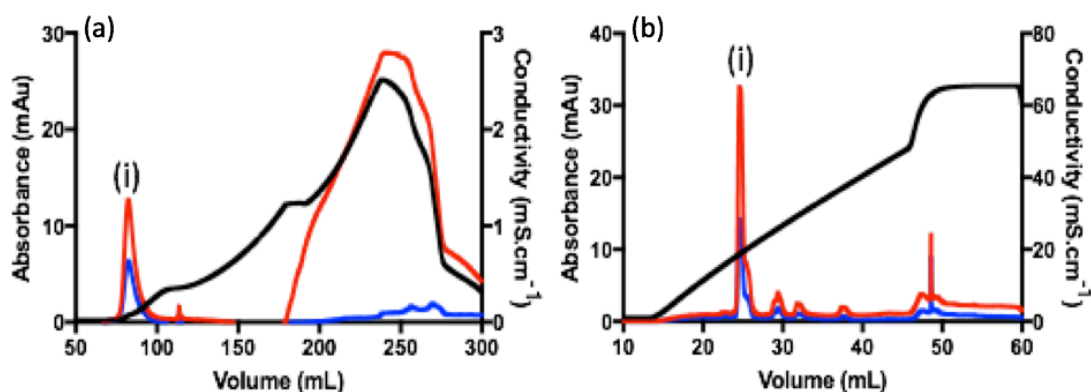


Figure 6.28: Size exclusion and ion exchange chromatography of *S. aureus* TCA extracts of cells incubated with 2x MIC vancomycin. (a) Size exclusion chromatogram of isolated peaks by Bio-gel P2 resin. Noted peak at (i) 81.47 mL. (b) ion exchange chromatogram of isolated peaks by MonoQ 5/50 GL resin. Noted peak (i) (conductivity 18.97 mS.cm⁻¹). Red trace is absorbance at 254nm, blue trace: absorbance at 280nm and black trace; conductivity.

The positive control gel filtration (Figure 6.28 (a)) lead to separation of two distinctive elution peaks. The first was the standard elution after 81.47 mL measured to coincide with the increase in conductivity and the second larger and broader peak eluting after 175 mL. As with the standard protocol the first peak was further purified by a monoQ column (Figure 6.28 (b)) which led to a very different elution profile than observed in the control sample (Figure 6.26 (b)). Instead for the distribution of a number of individual elution peaks the 2x MIC positive control displayed a single prominent peak with conductivity 18.97 mS.cm⁻¹ with the surrounding peaks severely diminished. The proposed intermediate contained within the elution should be UDP-MurNAc-pentapeptide (Lys) although the elution conductivity does not accurately match the equivalent for the standard (Figure 6.25 26.31 mS.cm⁻¹) but is closer to one of the control peaks containing the pentapeptide with a conductivity of 22.49 mS.cm⁻¹ (Figure 6.26 (b): (iii)). This variation potentially shows the difference from cellular and *in vitro* synthesis of peptidoglycan intermediates but more likely may result from the fact the ammonium acetates gradients differ in conductivity.min⁻¹. The monoQ purified peak was analysed by mass spectrometry and the data is displayed in Figure A3.51.

Mass spectra analysis (Figure A3.51) identified the 2x vancomycin MIC positive control peak as containing UDP-MurNAc-pentapeptide (Lys). The singly ([M-H]⁻ observed m/z 1148.34, expected m/z 1148.343) and doubly ([M-2H]²⁻ observed m/z 573.67, expected m/z 573.667) charged species were detected. These data indicated that

the expected accumulation of UDP-MurNAc-pentapeptide (Lys), resulting from vancomycin-challenge could be easily detected in *S. aureus*.

6.9.5 Intermediate accumulation of *S. aureus* against pywac compounds

Once again as outlined during the investigation with *B. subtilis* (Section 6.6.2), pywac compounds were incubated with a sufficient culture volume to produce a final harvested wet pellet cell weight of 1 g to aid the investigation. Each of the *S. aureus* cultures incubated with the remaining pywac compounds were processed and peaks of interest further investigated.

6.9.5.1 Intermediate accumulation of *S. aureus* against pywac 1

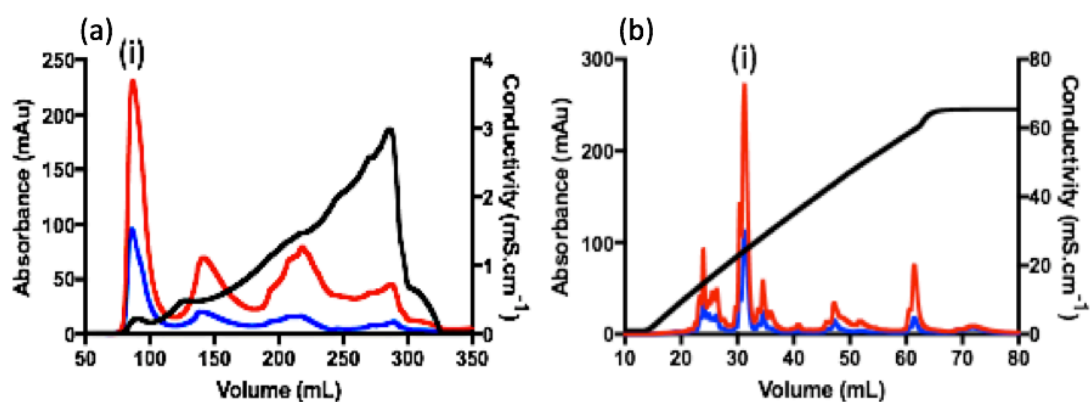


Figure 6.29: Size exclusion and ion exchange chromatography of *S. aureus* TCA extracts of cells incubated with 4 μ M pywac 1. (a) Size exclusion chromatogram of isolated peaks by Bio-gel P2 resin. Noted peak at (i) 84.99 mL. (b) ion exchange chromatogram of isolated peaks by MonoQ 5/50 GL resin. Noted peak (i) (conductivity 25.46 mS.cm⁻¹). Red trace is absorbance at 254nm, blue trace: absorbance at 280nm and black trace; conductivity.

Incubation of the gram-positive *S. aureus* cells with pywac 1 led to a size exclusion elution profile (Figure 6.29 (a)) similar in distribution to the control sample but with a significant increase in the 254 nm absorbance measured from the initial elution (Figure 6.29 (a): (i)). The peak plateaued around 240 mAu and eluted after 84.99 mL, compared to the equivalent control peak of 60 mAu after 85.55 mL (Figure 6.26 (a): (i)). The further purification by ion exchange chromatography (Figure 6.29 (b)) of this peak led

to an elution profile similar in nature to the 2x MIC vancomycin control (Figure 6.28 (b)) with a single prominent elution of over 2.5 times greater than the next greatest peak, eluting with a conductivity of 25.46 mS.cm⁻¹. Comparing this value to the standard elution peaks of the control situates the pywac 1 accumulated peak between two control peaks which both contained UDP-MurNAc-pentapeptide (Lys) (Figure 6.26 (b)) with conductivities of 22.49 mS.cm⁻¹ (Figure 6.26 (b): (iii)) and 28.33 mS.cm⁻¹ (Figure 6.26 (b): (iv)). The peak of interest was analysed by mass spectrometry in Figure A3.52.

Mass spectral analysis of the pywac 1 accumulated peak (Figure A3.52) did not identify the presence of any peptidoglycan cell wall intermediates, although an abundant signal was measured at 474.1960 m/z relating to an unknown compound.

6.9.5.2 Intermediate accumulation of *S. aureus* against pywac 2

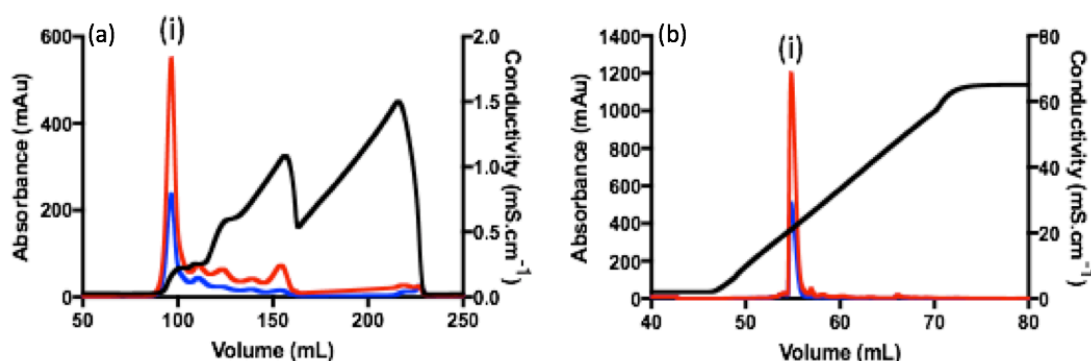


Figure 6.30: Size exclusion and ion exchange chromatography of *S. aureus* TCA extracts of cells incubated with 2 μ M pywac 2. (a) Size exclusion chromatogram of isolated peaks by Bio-gel P2 resin. Noted peak at (i) 95.93 mL. (b) ion exchange chromatogram of isolated peaks by MonoQ 5/50 GL resin. Noted peak (i) (conductivity 20.99 mS.cm⁻¹). Red trace is absorbance at 254nm, blue trace: absorbance at 280nm and black trace; conductivity.

The size exclusion chromatography (Figure 6.30 (a)) of *S. aureus* cells incubated with pywac 2 produced a similar elution profile to incubation with pywac 1 (Figure 6.29 (a)) displaying a single prominent initial peak after 95.93 mL with a 254 nm absorbance of 580 mAu. Further purification of this elution led to an ion exchange chromatogram (Figure 6.30 (b)) which contained a solitary eluted peak with a 254 nm absorbance of over 1200 mAu. There was no observed distribution of peaks surrounding the prominent elution. The conductivity of this peak was 20.99 mS.cm⁻¹, which when

compared to the control profile (Figure 6.26 (b)) falls between the second (18.63 mS.cm⁻¹) and third (22.49 mS.cm⁻¹) eluted peaks containing UDP-GlcNAc and UDP-MurNAc-pentapeptide (Lys) respectively. The peak was analysed by mass spectrometry in Figure A3.53.

Mass spectral analysis of the eluted sample (Figure A3.53) identified the singly ([M-H]⁻ observed m/z 1006.27, expected m/z 1006.26), doubly ([M-2H]²⁻ observed m/z 505.63, expected m/z 502.63) and triply ([M-3H]³⁻ observed m/z 334.75, expected m/z 334.75) charged species of UDP-MurNAc tripeptide (Lys), the substrate for amino acid ligase MurF. The tripeptide was not identified in the *S. aureus* control ion exchange chromatogram (Figure 6.26 (b)) and the tripeptide (Lys) standard (Figure 6.25 (a)) eluted with a greater conductivity of 25.21 mS.cm⁻¹.

The presence of the tripeptide moiety means that intermediate accumulation must have occurred and was solely due to the presence of the compound. As the tripeptide is accumulated it means that the compound inhibited one of three enzymes. MurF, the final Mur ligase in the addition of the pentapeptide stem to the UDP-MurNAc moiety which adheres the terminal D-alanyl-D-alanine. D-alanine racemase (Alr) which converts L-alanine to D-alanine or D-alanine-D-alanine ligase (DdlB), the enzyme that catalyses D-alanyl-D-alanine from two D-alanine residues.

6.9.5.3 Intermediate accumulation of *S. aureus* against pywac 6

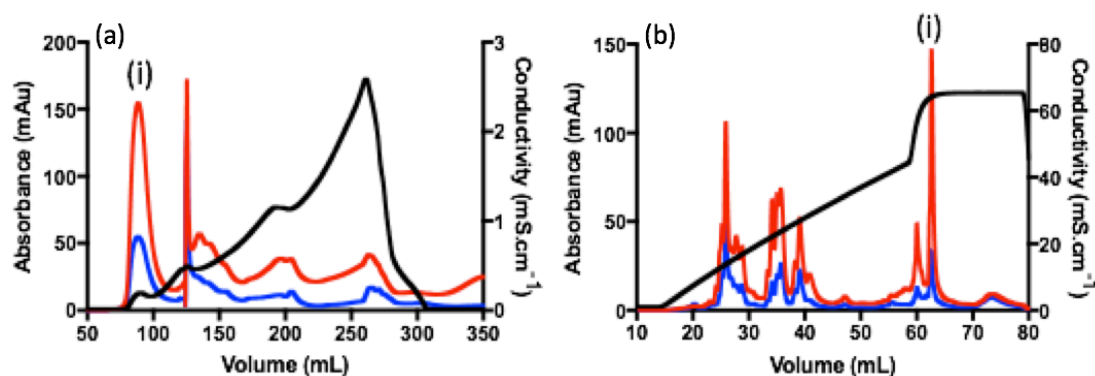


Figure 6.31: Size exclusion and ion exchange chromatography of *S. aureus* TCA extracts of cells incubated with 8 μM pywac 6. (a) Size exclusion chromatogram of isolated peaks by Bio-gel P2 resin. Noted peak at (i) 86.50 mL. (b) ion exchange chromatogram of isolated peaks by MonoQ 5/50 GL resin. Noted peak (i) (conductivity 62.04 $\text{mS}\cdot\text{cm}^{-1}$). Red trace is absorbance at 254nm, blue trace: absorbance at 280nm and black trace; conductivity.

The size exclusion chromatogram (Figure 6.31 (a)) of the pywac 6 sample displayed an initial elution peak after 86.50 mL. The sharp second peak is an artefact of pausing the AKTA during the run. Further purification of this initial peak lead to an ion exchange chromatogram (Figure 6.31 (b)) similar in distribution to the control sample (Figure 6.26 (b)) with one exception. Once the monoQ was exposed to 100% monoQ buffer B (1 M ammonium acetate) and the conductivity plateaued at 62.04 $\text{mS}\cdot\text{cm}^{-1}$, a significant eluted peak was observed. This peak had a greater conductivity value than any of the peptidoglycan cell wall intermediates or the ATP standard control (Figure 6.16). The peak was analysed by mass spectrometry to determine the presence of peptidoglycan precursors in Figure A3.54.

Mass spectral analysis in Figure A3.54, exploring the species contained within the noted peak of interest (Figure 6.31 (b)) determined as expected that the intensity of the elution was not attributed to the presence of any investigated cell wall intermediate. Based upon the m/z range investigated no known cellular metabolites were identified.

6.9.5.4 Intermediate accumulation of *S. aureus* against pywac 8

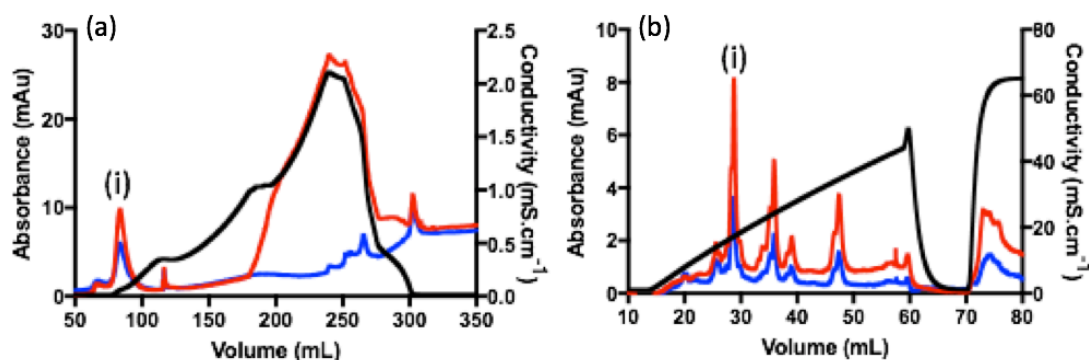


Figure 6.32: Size exclusion and ion exchange chromatography of *S. aureus* TCA extracts of cells incubated with 8 μM pywac 8. (a) Size exclusion chromatogram of isolated peaks by Bio-gel P2 resin. Noted peak at (i) 82.48 mL. (b) ion exchange chromatogram of isolated peaks by MonoQ 5/50 GL resin. Noted peak (i) (conductivity 16.02 $\text{mS}\cdot\text{cm}^{-1}$). Red trace is absorbance at 254nm, blue trace: absorbance at 280nm and black trace; conductivity.

The addition of pywac 8 to *S. aureus* cells lead to an overall similar size exclusion profile (Figure 6.32 (a)) to the control (Figure 6.26 (a)) with a smaller than average initial elution. Further purification of this isolated peak by ion exchange chromatography (Figure 6.32 (b)) demonstrated the same elution profile against pywac compound 8 exposed to *B. subtilis* cells (Figure 6.14). The similarity stems from the initial elution peak appearing more pronounced and acute that the equivalent displayed by the control peak, with fewer surrounding elution peaks. The peak eluted with a conductivity of 16.02 $\text{mS}\cdot\text{cm}^{-1}$, which falls between the conductivity of two control elutions, 15.49 $\text{mS}\cdot\text{cm}^{-1}$ and 18.63 $\text{mS}\cdot\text{cm}^{-1}$ respectively, containing UDP-GlcNAc. The intensity of the peak was not significantly different from other observed elutions in the profile so significant accumulation does not appear to be the cause of the distribution seen in the profile. The peak was analysed by mass spectrometry in Figure A3.55.

Mass spectral analysis (Figure A3.55) of the isolated peak determined the presence of UDP-GlcNAc ($[\text{M}-\text{H}]^-$ observed m/z 606.08, expected m/z 606.07). This result mirrored the equivalent result obtained in *B. subtilis* cell against 2x MIC of pywac 2 (Figure 6.14).

6.9.5.5 Intermediate accumulation of *S. aureus* against pywac 9

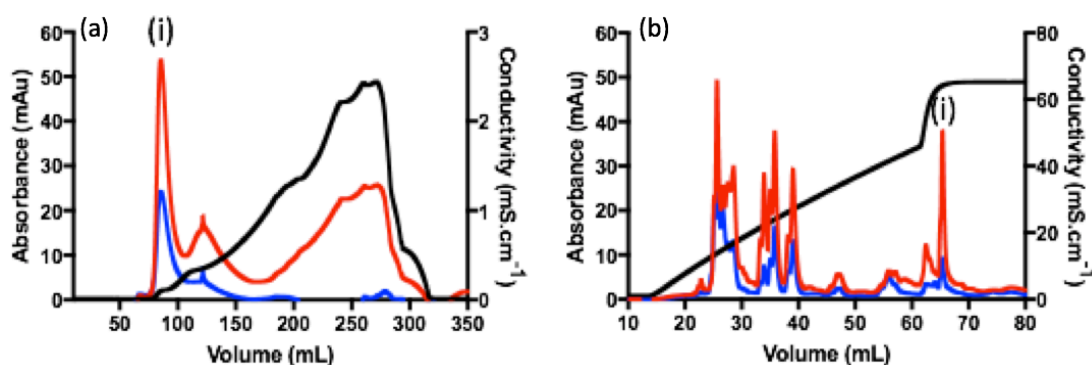


Figure 6.33: Size exclusion and ion exchange chromatography of *S. aureus* TCA extracts of cells incubated with 4 μM pywac 9. (a) Size exclusion chromatogram of isolated peaks by Bio-gel P2 resin. Noted peak at (i) 84.39 mL. (b) ion exchange chromatogram of isolated peaks by MonoQ 5/50 GL resin. Noted peak (i) (conductivity 64.74 $\text{mS}\cdot\text{cm}^{-1}$). Red trace is absorbance at 254nm, blue trace: absorbance at 280nm and black trace; conductivity.

The final compound investigated was pywac 9, which produced a similar ion exchange chromatogram (Figure 6.33 (b)) to another purification elution profile observed in cells incubated with pywac 6 (Figure 6.31 (b)). The standard distribution of elution peak followed the control chromatogram closely but once monoQ buffer B percentage was increased to 100% and the conductivity plateaued at 64.74 $\text{mS}\cdot\text{cm}^{-1}$ a noted eluted peak (Figure 6.33 (b): (i)) was measured. This level of conductivity is not attributed to any of the investigated peptidoglycan intermediates or any of the non-intermediate standards. The pywac 9 chromatogram mirrored the chromatogram observed for pywac 6 cellular extracts. The pywac 9 peak (i) was analysed by mass spectrometry in Figure A3.56.

Mass spectra analysis of pywac 9 incubated cells (Figure A3.56) could not locate charged species relating to any of the peptidoglycan intermediates, leaving the elution as currently unidentified.

6.10 Discussion

Cell wall active compounds with unknown mode of action were identified by the upregulation of the *ywac* gene based on a reduction in the measured synthesis of wall teichoic acids (D'Elia, *et al.* 2009). These nine pywac compounds were acquired to ascertain whether the peptidoglycan biosynthesis pathway contained the proposed targets. Previously stated MIC of these compounds (Czarny, *et al.* 2014) was successfully confirmed (Figure 6.3) and DMSO tolerance of the *B. subtilis* control was established because of the requirement of these compounds for DMSO as the vehicle (Figure 6.2).

6.10.1 *B. subtilis* cytosolic phase intermediate accumulation assessment

The initial probing of the *B. subtilis* cytosolic phase of peptidoglycan synthesis utilised the assessment of peptidoglycan intermediate accumulation in the presence of 2x MIC of pywac compounds compared to a control. Pywac compounds 4 and 9 produced similar anion exchange elution profiles to the control. Pywac compounds 1, 3, 5, 6 and 7 generated single isolated peaks not found within the control, although mass spectrometric analysis could not identify peptidoglycan intermediates within these elutions. Expanding the possible range of targets to include alternative metabolites such as ATP and NADH did not lead to a positive identification of these species. These six pywac compounds were therefore assumed to not elicit their mode of action within the cytosolic phase of peptidoglycan biosynthesis.

Only two of the pywac compounds (2 and 8) impacted the growth of *B. subtilis* relative to that seen in the presence of DMSO alone. Pywac 2 also caused accumulation of a species which registered as a slight increase in the intensity of one of the species detected on ion exchange fractionation of *B. subtilis* metabolites (Figure 6.12), which was identified as UDP-MurNAc-pentapeptide, the final precursor of the cytosolic phase of peptidoglycan biosynthesis. Accumulation of this intermediate was also observed during incubation with the positive control, vancomycin. Although at 2x MIC of

vancomycin accumulation of UDP-MurNAc-pentapeptide was so prominent that it dominated the ion exchange chromatogram (Figure 6.10). This was not observed with pywac compound 2. Accumulation of UDP-MurNAc-pentapeptide could therefore have arisen through the inhibition of MraY (Alderwick, *et al.* 2015) (which consumes UDP-MurNAc-pentapeptide to generate Lipid I). Alternatively, and in a similar manner to vancomycin, pywac compound 2 might have bound directly to the terminal D-alanyl-D-alanine of the pentapeptide stem impeding further enzymatic interaction (Soetaerta, *et al.* 2015). Incubation with excess concentrations of pywac 8 led to the accumulation of the first peptidoglycan intermediate of the pathway, UDP-GlcNAc (Figure 6.14). This might have arisen through inhibition of the enzyme catalysing the first committed step of the peptidoglycan pathway, MurA. This enzyme is also the target of the antimicrobial fosfomycin, which inhibits MurA through modification of a cysteine within the active site of the enzyme. (Nasiri, *et al.* 2017).

6.10.2 Pywac inhibition of *B. subtilis* lipid synthesis

Based upon the utilisation of *B. subtilis* as the test organism, the standard protocol for lipid synthesis was altered to include membranes extracted from the Gram-positive organism. The ability to generate lipids was not impeded by this deviation, permitting the investigation to probe the membrane associated enzymes required for lipid synthesis in *B. subtilis*. Co-incubation of 2x MIC of each pywac compound during lipid synthesis still led to formation of Lipid II. Lipids once purified were each identified as solely Lipid II. Quantification of lipids synthesised (Figure 6.7) demonstrated that co-incubation with each pywac compound except pywac 7 failed to modify the extent of Lipid II synthesis. These results likely indicate that these eight compounds did not inhibit either of the two enzymatic steps involving MraY and MurG in the formation of Lipid II.

The protocol for lipid synthesis involved an incubation overnight. To better evaluate synthesis, the protocol was shortened to four hours. Results showed no inhibition amongst eight of the nine compounds during this time period, though the rate of lipid synthesis before it plateaus was unknown. Further work would require reducing the

time frame of synthesis by hourly increments to ascertain when synthesis plateau occurs. The investigation will definitively show that whether there was zero inhibition in the previous experiment or whether the control rate of synthesis was rapid but the four hour time frame was sufficient for inhibited samples to generate equivalent concentrations of lipid.

Quantification of lipid synthesis co-incubated with pywac compound 7 reduced the concentration of Lipid II by almost 80%. The target of pywac 7 is likely one the two enzymes vital for lipid synthesis, *MraY* which catalyses the addition of undecaprenyl phosphate to UDP-MurNAc pentapeptide forming Lipid I or *MurG* which appends a GlcNAc subunit onto Lipid I (Bouhss, *et al.* 2008). Since based upon the TLC, Lipid II was generated but at a lesser concentration and Lipid I did not appear to be generated as assessed by mass spectrometry, the likely target is *MraY*.

6.10.3 *S. aureus* cytosolic phase intermediate accumulation assessment

Pywac active compounds were additionally exploited for initial probing of the peptidoglycan synthesis pathway of a second Gram-positive organism, *S. aureus*. The reason for the selection was to ascertain whether previously investigated cell wall active compounds which did not lead to observable accumulation of intermediates were targeted towards other cellular structures or if variations in the amino acids composition of the pentapeptide stem would increase accumulation and aid identification. *B. subtilis* cells implement m-DAP at position three of the stem whereas *S. aureus* insert L-lysine. The pywac compounds were identified as cell wall active in *B. subtilis* (Czarny, *et al.* 2014), although potential targets such as UDP-MurNAc-tripeptide (L-lys) and its synthesis may be better substrates for the compounds.

Intermediate accumulation utilising *B. subtilis* MIC values of *S. aureus* cells by pywac compounds 1 6 and 9 led to the accumulation of an individual peak not observed through the elution profile of the DMSO control. For both pywac compounds 6 and 9, this species eluted at a similar conductivity value, although neither of these nor the species detected in the presence of pywac compound 1 contained cell wall

intermediates. As previously investigated, the incubation of a Gram-positive organism with 2x MIC pywac compound 8 led to a variable elution profile within the initial eluted peaks, with mass spectrometric analysis identifying the presence of UDP-GlcNAc (Figure 6.32). Investigations into *S. aureus* with pywac compound were performed without the knowledge of the *S. aureus* MIC, therefore these results must be established before broad conclusions can be drawn and compared to the findings against *B. subtilis* cells.

The final compound initially probed against *S. aureus* was pywac 2. A significant accumulation of UDP-MurNAc-tripeptide (L-Lys) was identified with consequent and dramatic suppression of the contribution to the elution profile of other species (Figure 6.30). The accumulated elution against *B. subtilis* was measured to contain UDP-MurNAc-pentapeptide (DAP) (Figure 6.12). Comparisons between the two elution profiles demonstrates that although the pentapeptide peak of *B. subtilis* is slightly more pronounced than the equivalent in the compound absent control, the *S. aureus* accumulation attributed to pywac 2 incubation was far more significant.

Accumulation of the tripeptide would indicate an inability to attach the terminal D-alanyl-D-alanine residues, leading to the potential compound targets being either MurF, Alr or DdlB. The amino acid ligase MurC-F possess equivalent reaction mechanism attaching the specific amino acid to high-energy tetrahedral intermediates. This uniformity in function commonly equates to all four mur ligases being susceptible to the same antimicrobials, such as phosphinate inhibitors (El Zoeiby *et al.* 2003). Therefore, the target for pywac compound 2 would likely be the terminal D-alanyl-D-alanine to the peptide stem in a similar mode of action to vancomycin. The second potential target, the formation of D-alanyl-D-alanine by Alr and DdlB are known to be the cellular targets of the antimicrobial D-cycloserine (Feng, *et al.* 2003). Comparisons between pywac compound 2 and D-cycloserine in future investigation could lead to a positive identification of the cellular target.

6.10.4 Potential isolation of incomplete gel filtration intermediate pools

Once the intermediate accumulation protocol was concluded a number of potential issues arose surrounding the method used. The acquisition of the initially eluted peak from gel filtration of *B. subtilis* cell contents was isolated based upon previous purifications undertaken by Dr. Adrian Lloyd during purification of UDP-MurNAc-pentapeptide, known to elute earlier than other cellular low molecular weight components. Purification of *B. subtilis* lysed cell material commonly generated a primary broad peak corresponding to an increase in conductivity. Secondary and tertiary peaks were discarded based upon initial recommendation. Peptidoglycan intermediate standards were purified by anion exchange to establish the possible conductivity range of elution, although these initial investigations were not conducted to establish common elution volumes for the peptidoglycan intermediate standards during gel filtration. Results obtained within this chapter are valid comparisons of the initial eluted peak and there was no evidence that the intermediate pools were being split from the purified totals, although this potential oversight will be rectified in further work.

6.11 Further work

- Redesign accumulation protocol

Standardise initial gel filtration step by calibrating the Biogel P200 with UDP-MurNAc-pentapeptide, tripeptide, dipeptide, mono-peptide and UDP-MurNAc, to know that those fractions on the Biogel P200 elution will in an unbiased way contain the maximum available concentration of the precursor under consideration because it is possible that Pywac compounds that did not generate a UDP precursor response may have appeared to do so because the relevant precursor pool was missed on gel filtration.

- Establish pywac compounds MIC against *S. aureus* and repeat intermediate accumulation

Determine the MIC values for each pywac compound against *S. aureus*. Repeating the accumulation protocol with known 2x MIC of the pywac active compounds against *S. aureus* will allow a direct comparison between both investigated Gram-positive organisms. The protocol will also permit further probing into pywac compound targeting and the role of specific peptidoglycan pentapeptide stem variations on compound activity.

- Investigate PBP inhibition

One unexplored phase of peptidoglycan synthesis to investigate is the activity of the cell wall active compounds against the penicillin binding proteins (PBPs). After lipid synthesis, the final steps of peptidoglycan synthesis lead to incorporation of Lipid II precursors into the overall cell wall sacculus which involves a number of PBPs utilising transglycosylase and transpeptidase activity. The transglycosylase activity of PBPs polymerises Lipid II subunits together to increase the overall sacculi. This process has known inhibitors such as moenomycin a mimic of Lipid IV (Ostash, *et al.* 2009), the designation for the combination of two bound Lipid II molecules, which fit in the transglycosylase pocket. It is worth testing the pywac compounds on this enzymatic step to find out if they mimic moenomycin (based on structural similarities) or possibly lead to inhibition through binding to another site. The transpeptidase activity of PBPs where by the amino acid stems of the Lipid II moieties are cross-linked at the 3-4 position, releasing D-Ala residues would also be impacted by transglycosylase inhibition in the bifunctional transglycosylase/transpeptidase PBPs, however it is also possible that the transpeptidase function might itself be uniquely targeted . Assays to assess both PBP functions are vital to identifying modes of action against the currently unknown targets of half of the investigated pywac compounds.

- Assess inhibition of cytosolic Mur enzymes

A selected number of pywac compound appear to contribute to the accumulation of certain peptidoglycan intermediates. Individual Mur enzyme assays exist for synthesis of the intermediates (Section 2.8.1). Incubation with excess concentrations of pywac compounds will establish whether inhibition of individual enzymes occurs through utility of a coupled NADH-linked pyruvate kinase/lactate dehydrogenase assay for amino acid Mur ligase activity (Section 2.11.1). Once established, concentration specific investigation to probe the efficacy of each compound against the targeted enzymes will be undertaken using such an assay, taking care to ensure the coupling system was not compromised by the Pywac compounds.

- Pywac synergy with other antimicrobials

Assessing potential synergy between pywac compounds and standard antimicrobials that target peptidoglycan (Vancomycin, Fosfomycin and Clavulanic acid), protein (Chloramphenicol) and DNA (Ciprofloxacin) synthesis may aid in determining pywac mode of action towards cellular structures.

6.12 Conclusion

Newly discovered pywac compounds 1-9 are known to be active against the bacterial cell wall but their exact targets were unknown. Initial investigations against *B. subtilis* cells determined their MIC values and the range of possible targets for each pywac compound was narrowed down by probing two of the three distinct phases during the biosynthesis of peptidoglycan. Further probing of these targets is required before exact identification can be determined but these discoveries are important for identifying new interactions with new and extant targets to aid against the rise in antimicrobial resistance of standard therapies.

Chapter 7. General discussion and final conclusions

The global threat of tuberculosis affects approximately one third of the world's population (Houben and Dodd 2016). The increased prevalence of mycobacterial infection is due to insufficient drug therapy options attributed to multi-drug resistance towards standard mycobacterial antimicrobials (Zhang and Yew 2009). Mycobacteria are also inherently resistant to treatment by antimicrobials due to the expression of β -lactamases (Heesemann 1993) as well as the composition of their cell wall. The mAGP complex provides protection from external threats such as the administered antimicrobials and the secretion of host hydrolytic enzymes, through modifications made to cell wall structure. Mycobacteria and other representatives of the Actinobacteria modify the peptidoglycan layer through incorporation of N-acetylated and N-glycolylated lipids, the latter by utilisation of a NamH hydroxylase within an aerobic environment (Mahapatra, *et al.* 2008). The inclusion of the N-glycolylated lipid has previously been determined to increase mycobacterial resilience towards challenge by both lysozyme and β -lactam antibiotics (Raymond, *et al.* 2005).

The purpose of this thesis was to expand the current understanding of the function of N-glycolylation, especially with respect to mycobacterial responses to antibiotics and to external stresses during host invasion that cause lysis as well as to document the impact of N-glycolylation on peptidoglycan synthesis. The utilisation of a *M. smegmatis* $\Delta namH$ mutant which produces solely N-acetylated peptidoglycan was key in this regard.

7.1 Impact of N-glycolylation on standard mycobacterial growth

Standard mycobacterial phenotypic growth remained unaltered by the absence of N-glycolylated saccharides in typical aerobic conditions (Section 3.4). Furthermore, exposure of $\Delta NamH$ *M. smegmatis* to an extended anaerobic incubation to mimic *in vitro*, the environment created within an enclosed granuloma *in vivo*, was consistent with the view that illustrated the discovery that *namH* expression was not vital to resuscitation of the mycobacteria during re-exposure to aerobic conditions. This

conclusion was supported by the observation that wild type and Δ NamH strains exhibited equivalent propagation on both nutrient rich and deficient media on return to aerobic conditions (Section 3.5).

7.2 Impact of N-glycolylation on hydrolytic enzymes interaction

Previous investigations into the expression of solely N-acetylated mycobacterial peptidoglycan (Raymond, et al. 2005) revealed an increase in the susceptibility of *M. smegmatis* to lysozyme, a key secretion of the host immune response (Callewaert and Michiels 2010). The MIC of human lysozyme was two-fold greater in mycobacterial cells utilising N-glycolylated components, and these results were confirmed in this thesis (Section 3.6.1.1). Activity of the enzyme against mycobacterial peptidoglycan was concluded to be optimal at pH 7.0, and decline in lysis was observed when the pH was reduced to 6.0. Between pH 6.0 and 5.0 the activity of human lysozyme remained constant (Section 3.6.1.2) illustrating the efficacy of the enzyme as the pH within the phagolysosome is reduced to aid lysis. The increased susceptibility of the N-glycolyl deficient mycobacteria was noted as constant across each investigated pH.

The impact of the duration of exposure to lysozyme on mycobacterial survival was examined with a two and three-fold increase in duration (Section 3.6.1.3). Comparisons between these two time increases led to minimal variation with mycobacterial lysis plateauing at investigated concentrations and the divide between strain susceptibility remained constant. Increases to incubation time frame exacerbated mycobacterial cell lysis on both strains equally at lysozyme concentrations above 1024 μ g.ml. In conclusion, N-glycolyl deficient mycobacteria remained more susceptible to human lysozyme, with the enzymatic activity being (a) stable at phagolysosome pH conditions and (b) more effective during longer exposure.

The investigation of host-mediated challenge to mycobacterial proliferation extended to include β -hexosaminidase, a hydrolytic enzyme previously observed as being expressed specifically during mycobacterial infection in humans (Koo, *et al.* 2008). Human β -hexosaminidase (which hydrolyses the β -1,4 glycosidic bond between

peptidoglycan subunits in a similar manner to lysozyme) generated a two-fold lower MIC and MBC in the exclusively N-acetylated mycobacteria (Section 3.7.2). This result was consistent with the data of Koo, *et al.* (2008) who identified β -hexosaminidase during mycobacterial infection close to the host macrophage plasma membrane at a more neutral pH environment as well as the acidic phagolysosome. Here, the activity of the enzyme was unaltered at either condition (Section 3.7.2.1) and at both conditions the NamH deficient strain was equally susceptible to lysis.

The focus of further work should be on potential synergistic interactions between host hydrolytic enzymes, to ascertain the impact of equivalent activities of different peptidoglycan-hydrolytic enzymes encompassing the range of pH conditions present within macrophage, as well as the binding affinities of each enzyme to N-acetylated and N-glycolylated lipids to confirm preferential binding and explain increased susceptibility.

7.3 Impact of N-glycolylation on antimicrobial therapy

The generation of a *namH* and *blaS* deficient *M. smegmatis* mutant permitted the evaluation of antimicrobial mycobacterial therapies and the implementation of N-glycolylated peptidoglycan to oppose lysis. Previously published studies (Raymond, *et al.* 2005) showcased the increased susceptibility of Δ NamH to β -lactam antibiotics and the unaltered sensitivity towards non-peptidoglycan targeted antimicrobials. These findings were confirmed and extended within this thesis (Section 4.4). Both investigated mycobacterial strains lacked the BlaS β -lactamase to assess the impact of β -lactams on N-glycolylated deficient mycobacteria. The *blaS namH* double mutant was two-fold more susceptible to ampicillin than the solely *blaS* mutant, whereas both strains were equally sensitive to isoniazid. The N-glycolylated lipid may aid against β -lactam interaction due to the reduced time frame observed to synthesis the N-glycolylated version of Lipid II (Chapter 5), or through aiding substrate recognition of PBPs.

MIC and MBC susceptibility of N-glycolyl deficient mycobacteria were equivalent to the wild type during exposure to antimicrobials targeting transglycosylase activity. Although ramoplanin and mersacidin which both bind directly to Lipid II, demonstrated increased activity towards the Δ NamH strain at sub MIC values (Section 4.4). The susceptibility was explained through measuring of antimicrobial binding affinities towards modified variants of Lipid II. Both antimicrobials demonstrated a greater binding response in the presence of N-acetylated substrates than N-glycolylated at equivalent concentrations (Section 4.6). Preference towards the N-acetyl group establishes a possible *raison d'être* for maintenance by *M. smegmatis* of a 7:3 ratio of MurNGlyc to MurNAc saccharides within the peptidoglycan layer during aerobic conditions. N-glycolylation occurs prior to the lipid linked steps of peptidoglycan synthesis that occur on the inner and outer faces of the cytoplasmic membrane. However, results indicated the administration of tunicamycin, an active site inhibitor of *MraY* (*MurX*), did not lead to an alteration in antimicrobial susceptibility dependent upon the presence of the N-acetyl/N-glycolyl group (Section 4.4). Moenomycin which mimics Lipid IV and blocks binding to the TP and TG domains of bifunctional PBPs such as mycobacterial PonA1 and PonA2, displayed increased activity towards NamH deficient mycobacteria (Section 4.4). This would potentially indicate that implementation of the N-glycolyl group on Lipid II substrates may improve PBP binding to outcompete moenomycin. This hypothesis was counteracted by binding affinity assessments of *M. tuberculosis* PonA1 and PonA2 (Chapter 5) which demonstrated that the binding affinities towards Lipid II of PonA1 were two-fold greater with the N-acetylated lipid and PonA2 demonstrated equivalent affinities towards each lipid.

Due to the expansion of multidrug resistant mycobacterial strains to primary treatments, the requirement for secondary therapies such as vancomycin has increased. The N-glycolylation of peptidoglycan of the wild type strain assists in mitigating the activity of the antimicrobial, as registered by the decreased survival of the Δ NamH strain (Section 4.4). Assessment of lipid binding affinities towards vancomycin supports the hypothesis that mycobacteria include high percentages of N-glycolylated lipids to decrease recognition and reduce cell lysis (Section 4.6).

The proliferation of resistance has led to a requirement for newly antimicrobial therapies. Teixobactin has been touted as a break through, due to its unique targeting towards the prenyl-pyrophosphate-GlcNAc region of Lipid II (Ling, *et al.* 2015), and the current lack of observable resistance. MIC assessment of both investigated strains concluded that the mycobacterial composition of the peptidoglycan layer did not impact the susceptibility of *M. smegmatis* to teixobactin with equivalent MIC values (Section 4.4). Binding affinity of the antimicrobial towards the peptidoglycan lipid precursors demonstrated a five-fold preference towards the binding of N-acetylated lipid II compared to its N-glycolylated variant, although this interaction appeared to not have impact susceptibility. Due to the lack of current observable resistance, teixobactin analogues have been created by a number of collaborators to evaluate key structural components of the antimicrobial (Jad, *et al.* 2015). Arg-teixobactin displayed a four-fold reduction in MIC activity towards mycobacteria (Section 4.4), due in part to the substitution of the L-allo-endurcididine residue with L-arginine, which impacted the preferential binding affinity observed for the original teixobactin towards N-acetylated lipids.

Future experiments should focus on overcoming difficulties noted during assessment of binding affinities, especially the use of less intrusive lipid labelling and discovery into the optimal SPR chip coating concentrations to reduce the time frame of binding saturation. Expanding the range of antimicrobials investigated to examining antimicrobial synergy to circumvent resistance.

7.4 Impact of N-glycolylation on peptidoglycan synthesis

The main focus of this thesis was the impact of N-glycolylated lipids embedded with the peptidoglycan on response to external agents such as enzymatic and antimicrobial activity. A number of mycobacteria possess more unique variation in relation to peptidoglycan synthesis. Chapter 5 illustrated the initial investigations into a wide range of mycobacterial enzymes and the role of each enzymatic deviation from the common procedure.

Mycobacterial MurA species are inherently resistant to fosfomycin due to an aspartate substitution of the more common active site residue cysteine (De Smet, *et al.* 1999). One aspect of this chapter was to re-sensitise *M. leprae* MurA to fosfomycin. The mycobacterial enzyme was acquired and cloned within a pCOLD expression vector, to aid expression at decreased temperatures. The gene was modified append a C-terminal poly-histidine tag to the *murA* coding sequence. Site directed mutagenesis was implemented to alter the DNA sequence to replace an aspartate residue with a cysteine residue. Genes encoding both potentially fosfomycin sensitive and resistant MurA proteins were successfully expressed and identified through Western blotting. Further work would compare the activity of the enzymes in the presence of fosfomycin as well as the binding affinity of the antimicrobial to the enzymes. This work will be greatly facilitated by the recent discovery of a protein cofactor (CwlM, Boutte *et al.*, 2016) that when phosphorylated, activates mycobacterial MurA activity.

M. leprae MurC inserts L-glycine at position one of the pentapeptide stem instead of the commonly observed L-alanine (Mahapatra, *et al.* 2000). Previous studies have determined that there is no enzymatic preference for the amino acid, but the reason for this deviation remains unknown. Due to genomic degradation, *M. leprae* does not utilise N-glycolylated peptidoglycan, as NamH encodes only for a pseudogene (Muro, *et al.* 2011). N-glycolylation occurs on UDP-N-acetyl muramic acid product of MurB, and therefore each of the Mur ligases can utilise an N-glycolylated substrate. The purpose of this investigation was to determine whether *M. leprae* Mur ligases have a catalytic preference for muramic acid substrates as unable to generate N-glycolylation precursors. *M. leprae* MurC was cloned in a similar manner to *M. leprae* MurA, within a pCOLD expression vector with a C-terminal poly-histidine tag. Successful expression was confirmed by Western blot.

The investigation into Mur ligases and catalytic preference of substrates was expanded through acquisition of *M. smegmatis* MurC and MurD. Results demonstrated a significant substrate preference for the N-glycolylated muramic acid at a ratio of 43:1 compared to the N-acetylated variant for MurC. This ratio decreased significantly to 5:1 during assessment of MurD. This decrease in favourability as the amino acid stem was extended has also been observed in *M. tuberculosis* (Unpublished). Each

subsequent Mur ligase demonstrated a reduced catalytic preference until the ratio was almost 1:1 for *M. tuberculosis* MurF.

The reason for this catalytic bias can potentially be narrowed down based upon previous investigations within this thesis. The *M. smegmatis* wild type and Δ NamH strains displayed matching phenotypic growth during aerobic conditions (Section 3.4). Extended anaerobic incubation to replicate dormancy followed by aerobic incubation to replicate resuscitation also produced equivalent propagation in both the wild type and NamH strains. These two results indicate that implementation of N-glycolylated peptidoglycan does not appear to be to either aid standard mycobacterial growth during aerobic conditions or aid growth from dormancy. Based upon chapter 3 and 4, N-glycolylation appears to be utilised specifically against external enzymatic and antimicrobial recognition and lysis, and the catalytic bias of Mur ligases maybe to rapidly alter the peptidoglycan layer composition to resist these interactions.

The binding affinity towards both N-glycolylated and N-acetylated Lipid II was expanded to include the primary PBPs of *M. tuberculosis*, PonA1 and PonA2. A two-fold increase in affinity was noted for PonA1 towards the N-acetylated lipid over the N-glycolylated lipid, whereas binding affinity for PonA2 for either substrate was almost equal.

7.5 Cell wall active drug discovery

The pursuit of new antimicrobials to combat antimicrobial resistance has led to the generation of new screening techniques. The utilisation of *ywaC*, a gene which encoded an enzyme important in the catalysis of the bacterial alarmone (p)ppGpp were coupled with lux genes to produced real-time luminescence signals during bacterial stress (Czarny, *et al.* 2014) and screen potential antimicrobials. Nine cell wall active compounds, termed Pywac 1-9 were identified as impacting the mAGP complex in *B. subtilis*, through the exact targets were unknown.

The Pywac compounds MIC (Czarny, *et al.* 2014) values against *B. subtilis* were accurately confirmed in chapter 6, and an intermediate accumulation protocol was implemented to probe the cytosolic peptidoglycan precursor intermediates as potential targets (Section 6.6.2). Pywac 4 and 9 did not alter the intermediate elution profile produced by the compound free control. Pywac 1, 3, 5, 6 and 7 each produced a single previously unforeseen elution, though none of these peaks contained peptidoglycan precursors or co-factors. Pywac 8 increased the elution peak containing UDP-GlcNAc and Pywac 2 did the same for UDP-MurNAc-pentapeptide (DAP). With the targets of the majority of the Pywac compounds still unknown, the lipid synthesis portion of the pathway was also probed (Section 6.8.2). TLC analysis of 2x Pywac MIC incubation during lipid synthesis utilising *B. subtilis* cell membranes, identified the presence of lipids within each sample which when purified were all found to contain Lipid II. All Pywac compounds were determined to not impede lipid synthesis once equivalent lipid synthesis concentrations were established in each sample compared to the control, except Pywac 7 which reduced the lipid synthesised concentration by 80%. The presence of reduced quantities of Lipid II within the Pywac 7 sample indicate that the compound likely elicits its actions on either MraY or MurG. Further investigations are required.

Initial investigations with a secondary Gram-positive organism, *S. aureus* was used due the variation in the amino acid attached to the third position compared to *B. subtilis*. This led to a noted accumulation attributed to two Pywac compounds (Section 6.9). Once again Pywac 8 led to an increase in the elution of a peak containing UDP-GlcNAc and Pywac 2 caused a significant single eluted peak containing UDP-MurNAc-tripeptide (Lys). Inhibition of MurA by Pywac compound 2 would lead to accumulation of UDP-GlcNAc, other inhibitors with this target include fosfomycin (Bugg, 1999). Inhibition of MurF, DdlB or Alr would lead to accumulation of UDP-MurNAc-tripeptide (Lys) (Bugg, 1999). D-cycloserine is an antimicrobial which also targets DdlB and Alr whereas MurF inhibition is caused by phosphinate inhibitors (Bugg, 1999). Further investigations expanding the scope of possible targets to include the extracellular components of peptidoglycan biosynthesis such as PBPs, and investigate potential synergy and antagonism with other known antimicrobial to narrow possible targets.

7.6 Final conclusion

The purpose of this thesis was to increase current understanding of a unique structural modification within the mycobacterial genus and the impact it elicits to aid in the virulence of the organism which is a global issue. Initial findings made throughout this thesis will provide a broader platform to examine N-glycolylation and the key traits which lead to its continued prevalence with the mycobacterial cell wall.

Bibliography

Abraham, E. P., and Chain, E. (1988) An enzyme from bacteria able to destroy penicillin. 1940. *Rev Infect Dis.* **10** (4): 677-8.

Adams, L. B., Pena, M. T., Sharma, R., Hagge, D. A., Schurr E., and Truman R. W. (2012). "Insights from animal models on the immunogenetics of leprosy: a review." *Mem Inst Oswaldo Cruz* **107 Suppl 1**: 197-208.

Aguilar-Ayala, D. A., Cnockaert, M., Vandamme, P., Palomino, J. C., Martin A., and Gonzalez, Y. M. J. (2018). "Antimicrobial activity against *Mycobacterium tuberculosis* under in vitro lipid-rich dormancy conditions." *J Med Microbiol* **67** (3): 282-285.

Al-Dabbagh, B., Henry, X., El Ghachi, M., Auger, G., Blanot, D., Parquet, C., Mengin-Lecreulx, D., and Bouhss, A. (2008) Active Site Mapping of MraY, a Member of the Polyprenyl-phosphate N-Acetylhexosamine 1-Phosphate Transferase Superfamily, Catalyzing the First Membrane Step of Peptidoglycan Biosynthesis *Biochemistry.* **47** (34): 8919-8928.

Alastruey-Izquierdo, A., Gómez-López, A., Arendrup, M., Lass-Flörl, C., Hope, W., Perlin, D., Rodríguez-Tudela, J., and Cuenca-Estrella, M. (2012) Comparison of Dimethyl Sulfoxide and Water as Solvents for Echinocandin Susceptibility Testing by the EUCAST Methodology. *J Clin Microbiol.* **50** (7): 2509–2512.

Alderwick, L. J., Harrison, J., Lloyd, G. S., and Birch, H. L. (2015). "The Mycobacterial Cell Wall--Peptidoglycan and Arabinogalactan." *Cold Spring Harb Perspect Med* **5** (8): a021113.

Alekshun, M. N. and Levy, S. B. (2007). "Molecular mechanisms of antibacterial multidrug resistance." *Cell* **128** (6): 1037-1050.

Alifano, P., Palumbo, C., Pasanisi, D., and Tala, A. (2015). "Rifampicin-resistance, rpoB polymorphism and RNA polymerase genetic engineering." *J Biotechnol* **202**: 60-77.

Amaral, E., Lasunskiaia, E., and D'Imp erio-Lima, M. (2016) Innate immunity in tuberculosis: how the sensing of mycobacteria and tissue damage modulates macrophage death. *Microbes and Infection* Volume 18, Issue 1, Pages 11-20.

Appleyard, A. N., Choi, S., Read, D. M., Lightfoot, A., Boakes, S., Hoffmann, A., Chopra, I., Bierbaum, G., Rudd, B., Dawson, M. J., and Cortes, J. (2009). Dissecting Structural and Functional Diversity of the Lantibiotic Mersacidin. *Chem Biol.* **16** (5-3): 490–498.

Austrian, R. (1960). "The Gram stain and the etiology of lobar pneumonia, an historical note." *Bacteriol Rev* **24** (3): 261-265.

- Babajan, B., Chaitanya, M., and Rajsekhar, C.** (2011) Comprehensive structural and functional characterization of *Mycobacterium tuberculosis* UDP-NAG enolpyruvyl transferase (Mtb-MurA) and prediction of its accurate binding affinities with inhibitors. *Interdiscip Sci Comput Life Sci* **3**: 204.
- Bah, A., Lacarriere, C., and Vergne, I.** (2016). "Autophagy-Related Proteins Target Ubiquitin-Free Mycobacterial Compartment to Promote Killing in Macrophages." *Front Cell Infect Microbiol* **6**: 53.
- Bailey, M. A., Na, H., Duthie, M. S., Gillis, T. P., Lahiri, R., and Parish, T.** (2017). "Nitazoxanide is active against *Mycobacterium leprae*." *PLoS One* **12** (8): e0184107.
- Baldwin, T. O., Nicoli, M. Z., Becvar, J. E., and Hastings, J. W.** (1975). Bacterial luciferase. Binding of oxidized flavin mononucleotide. *J Biol Chem* **250** (8): 2763-2768.
- Banaei, N., Gaur, R. L., and Pai, M.** (2016). "Interferon Gamma Release Assays for Latent Tuberculosis: What Are the Sources of Variability?" *J Clin Microbiol* **54** (4): 845-850.
- Bennett, P. M.** (2008). "Plasmid encoded antibiotic resistance: acquisition and transfer of antibiotic resistance genes in bacteria." *Br J Pharmacol* **153 Suppl 1**: S347-357.
- Bergdoll, M. S., Borja, C. R., Robbins, R. N., and Weiss, K. F.** (1971). "Identification of enterotoxin E." *Infect Immun* **4** (5): 593-595.
- Bernard, E., Rolain, T., Courtin, P., Guillot, A., Langella, P., Hols P., and Chapot-Chartier, M. P.** (2011). "Characterization of O-acetylation of N-acetylglucosamine: a novel structural variation of bacterial peptidoglycan." *J Biol Chem* **286** (27): 23950-23958.
- Betts, J. C., Lukey, P. T., Robb, L. C., McAdam, R. A., and Duncan, K.** (2002). "Evaluation of a nutrient starvation model of *Mycobacterium tuberculosis* persistence by gene and protein expression profiling." *Mol Microbiol* **43** (3): 717-731.
- Beutler, E.** (1979). "The biochemical genetics of the hexosaminidase system in man." *Am J Hum Genet* **31** (2): 95-105.
- Beveridge, T. J.** (1999). "Structures of gram-negative cell walls and their derived membrane vesicles." *J Bacteriol* **181** (16): 4725-4733.
- Beveridge, T. J.** (2001). "Use of the gram stain in microbiology." *Biotech Histochem* **76** (3): 111-118.
- Blake, C. C., Johnson, L. N., Mair, G. A., North, A. C., Phillips, D. C., and Sarma, V. R.** (1967). "Crystallographic studies of the activity of hen egg-white lysozyme." *Proc R Soc Lond B Biol Sci* **167** (1009): 378-388.
- Bodar, E., Netea, M. G., de Jong, D. J., Kullberg, B. J., Joosten, L. A., and Van der Meer, J. W.** (2008). "NOD2 engagement induces proinflammatory cytokine

production, but not apoptosis, in leukocytes isolated from patients with Crohn's disease." *Eur Cytokine Netw* **19** (4): 185-189.

Boneca, I. G., Dussurget, O., Cabanes, D., Nahori, M. A., Sousa, S., Lecuit, M., Psylinakis, E., Bouriotis, V., Hugot, J. P., Giovannini, M., Coyle, A., Bertin, J., Namane, A., Rousselle, J. C., Cayet, N., Prevost, M. C., Balloy, V., Chignard, M., Philpott, D. J., Cossart, P., and Girardin S. E. (2007). "A critical role for peptidoglycan N-deacetylation in *Listeria* evasion from the host innate immune system." *Proc Natl Acad Sci U S A* **104** (3): 997-1002.

Borisova, M., Gaupp, R., Duckworth, A., Schneider, A., Dalügge, D., Mühleck, M., Deubel, D., Unsleber, S., Yu, W., Muth, G., Bischoff, M., Götz, F., and Mayer, C. (2006). Peptidoglycan Recycling in Gram-Positive Bacteria Is Crucial for Survival in Stationary Phase. *American society of Microbiology*. **7** (5): e0923-16.

Bosch, F. and Rosich, L. (2008). "The contributions of Paul Ehrlich to pharmacology: a tribute on the occasion of the centenary of his Nobel Prize." *Pharmacology* **82** (3): 171-179.

Bouhss, A., Trunkfield, A. E., Bugg, T. D., and Mengin-Lecreulx, D. (2008). "The biosynthesis of peptidoglycan lipid-linked intermediates." *FEMS Microbiol Rev* **32** (2): 208-233.

Boutte, C. C., Baer, C., Papavinasasundaram, K., Liu, W., Chase, M., Meniche, X., Fortune, S., Sasseti, C., Ioerger, T., and Rubin, E. (2016). A cytoplasmic peptidoglycan amidase homologue controls mycobacterial cell wall synthesis. *eLife*. **5**:e14590

Breukink, E., van Heusden, H. E., Vollmerhaus, P. J., Swiezewska, E., Brunner, L., Walker, S., Heck, A. J., and de Kruijff, B. (2003). "Lipid II is an intrinsic component of the pore induced by nisin in bacterial membranes." *J Biol Chem* **278** (22): 19898-19903.

Brown, S., Santa Maria, Jr, J., and Walker, S. (2014). Wall Teichoic Acids of Gram-Positive Bacteria. *Annu Rev Microbiol*. **67**: 10.

Buddle, B. M., Parlane, N. A., Keen, D. L., Aldwell, F. E., Pollock, J. M., Lightbody K., and Andersen, P. (1999). "Differentiation between *Mycobacterium bovis* BCG-vaccinated and *M. bovis*-infected cattle by using recombinant mycobacterial antigens." *Clin Diagn Lab Immunol* **6** (1): 1-5.

Bugg, T. D. (1999). *Bacterial Peptidoglycan Biosynthesis and Its Inhibition*. Oxford, Elsevier Science Ltd.

Bush, K. (2012). Antimicrobial agents targeting bacterial cell walls and cell membranes. *Rev Sci Tech* **31** (1): 43-56.

Cabeen, M. T. and Jacobs-Wagner, C. (2005). "Bacterial cell shape." *Nat Rev Microbiol* **3** (8): 601-610.

Callewaert, L. and Michiels, C. W. (2010). "Lysozymes in the animal kingdom." *J Biosci* **35** (1): 127-160.

Canetti, G. (1955). "[Bacteriological problems in pulmonary tuberculosis treated by excision after chemotherapy]." *Strasb Med* **6** (5): 308-309.

Canton, J., Khezri, R., Glogauer, M., and Grinstein, S. (2014). "Contrasting phagosome pH regulation and maturation in human M1 and M2 macrophages." *Mol Biol Cell* **25** (21): 3330-3341.

Chamaillard, M., Hashimoto, M., Horie, Y., Masumoto, J., Qiu, S., Saab, L., Ogura, Y., Kawasaki, A., Fukase, K., Kusumoto, S., Valvano, M. A., Foster, S. J., Mak, T. W., Nunez, G. and Inohara, N. (2003). "An essential role for NOD1 in host recognition of bacterial peptidoglycan containing diaminopimelic acid." *Nat Immunol* **4** (7): 702-707.

Chambers, H. F., Moreau, D., Yajko, D., Miick, C., Wagner, C., Hackbarth, C., Kocagoz, S., Rosenberg, E., Hadley, W. K., and Nikaido, H. (1995). "Can penicillins and other beta-lactam antibiotics be used to treat tuberculosis?" *Antimicrob Agents Chemother* **39** (12): 2620-2624.

Chan, E. D., Strand, M. J., and Iseman, M. D. (2009). "Multidrug-resistant tuberculosis (TB) resistant to fluoroquinolones and streptomycin but susceptible to second-line injection therapy has a better prognosis than extensively drug-resistant TB." *Clin Infect Dis* **48** (5): e50-52.

Chen, K., Chen P., and Cheng, C. (2016). Structural Investigation of Park's Nucleotide on Bacterial Translocase MraY: Discovery of Unexpected MraY Inhibitors *SCI Rep* **6**:31579.

Chen, K.T., Kuan, Y.C., Fu, W.C., Liang, P.H., Cheng, T.R., Wong, C.H., Cheng, W.C. (2013). Rapid preparation of mycobacterium N-glycolyl Lipid I and Lipid II derivatives: a biocatalytic approach. *Chemistry*. **19**(3): 834–838.

Chen, J., Zhang, S., Cui, P., Shi, W., Zhang, W., and Zhang, Y. (2017). Identification of novel mutations associated with cycloserine resistance in *Mycobacterium tuberculosis*. *J Antimicrob Chemother.* **72** (12): 3272-3276.

Chimara, E., Ferrazoli, L., and Leao, S. C. (2004). "Mycobacterium tuberculosis complex differentiation using gyrB-restriction fragment length polymorphism analysis." *Mem Inst Oswaldo Cruz* **99** (7): 745-748.

Chua, K., and Howden, B. P. (2009) Treating Gram-positive infections: vancomycin update and the whys, wherefores and evidence base for continuous infusion of anti-Gram-positive antibiotics. *Curr Opin Infect Dis.* **22** (6): 525–534.

Cohen-Gonsaud, M., Barthe, P., Bagneris, C., Henderson, B., Ward, J., Roumestand, C., and Keep, N. H. (2005). "The structure of a resuscitation-promoting factor domain from *Mycobacterium tuberculosis* shows homology to lysozymes." *Nat Struct Mol Biol* **12** (3): 270-273.

Cole, S. T., Eiglmeier, K., Parkhill, J., James, K. D., Thomson, N. R., Wheeler, P. R., Honore, N., Garnier, T., Churcher, C., Harris, D., Mungall, K., Basham, D., Brown, D., Chillingworth, T., Connor, R., Davies, R. M., Devlin, K., Duthoy, S., Feltwell, T., Fraser, A., Hamlin, N., Holroyd, S., Hornsby, T., Jagels, K., Lacroix, C., Maclean, J., Moule, S., Murphy, L., Oliver, K., Quail, M. A., Rajandream, M. A., Rutherford, K. M., Rutter, S., Seeger, K., Simon, S., Simmonds, M., Skelton, J., Squares, R., Squares, S., Stevens, K., Taylor, K., Whitehead, S., Woodward, J. R., and Barrell, B. G. (2001). "Massive gene decay in the leprosy bacillus." *Nature* **409** (6823): 1007-1011.

Compaan, D. M. and Ellington, W. R. (2003). "Functional consequences of a gene duplication and fusion event in an arginine kinase." *J Exp Biol* **206** (Pt 9): 1545-1556.

Consaul, S., Wright, L., Mahapatra, S., Crick, D., and Pavelka, M. (2005). An Unusual Mutation Results in the Replacement of Diaminopimelate with Lanthionine in the Peptidoglycan of a Mutant Strain of *Mycobacterium smegmatis* *JOURNAL OF BACTERIOLOGY*. p. 1612–1620.

Cordone, A., Audrain, B., Calabrese, I., Euphrasie, D., and Reyrat, J. M. (2011). "Characterization of a *Mycobacterium smegmatis* *uvrA* mutant impaired in dormancy induced by hypoxia and low carbon concentration." *BMC Microbiol* **11**: 231.

Correale, S., Ruggiero, A., Capparelli, R., Pedone, E., and Berisio, R. (2013). "Structures of free and inhibited forms of the L,D-transpeptidase LdtMt1 from *Mycobacterium tuberculosis*." *Acta Crystallogr D Biol Crystallogr* **69** (Pt 9): 1697-1706.

Coulombe, F., Divangahi, M., Veyrier, F., de Leseleuc, L., Gleason, J. L., Yang, Y., Kelliher, M. A., Pandey, A. K., Sasseti, C. M., Reed, M. B., and Behr, M. A. (2009). "Increased NOD2-mediated recognition of N-glycolyl muramyl dipeptide." *J Exp Med* **206** (8): 1709-1716.

Crick, D. C., Mahapatra, S., and Brennan, P. J. (2001). "Biosynthesis of the arabinogalactan-peptidoglycan complex of *Mycobacterium tuberculosis*." *Glycobiology* **11** (9): 107R-118R.

Czarny, T. L., Perri, A. L., French, S., and Brown, E. D. (2014). Discovery of novel cell wall-active compounds using *P ywaC*, a sensitive reporter of cell wall stress, in the model gram-positive bacterium *Bacillus subtilis*. *Antimicrob Agents Chemother* **58** (6): 3261-3269.

D'Elia, M., Millar, K., Bhavsar, A., Tomljenovic, A., Hutter, B., Schaab, C., Moreno-Hagelsieb, G., and Brown, E. (2009) Probing teichoic acid genetics with bioactive molecules reveals new interactions among diverse processes in bacterial cell wall biogenesis. *Chem Biol.* **16** (5): 548–556.

D'Ordine, R. L., Rydel, T. J., Storek, M. J., Sturman, E. J., Moshiri, F., Bartlett, R. K., Brown, G. R., Eilers, R. J., Dart, C., Qi, Y., Flasiniski, S., Franklin, S. J.

(2009) Dicamba monooxygenase: structural insights into a dynamic Rieske oxygenase that catalyzes an exocyclic monooxygenation *J Mol Biol.* **392** (2):481-97.

Davis, K. M., Nakamura, S., and Weiser, J. N. (2011). "Nod2 sensing of lysozyme-digested peptidoglycan promotes macrophage recruitment and clearance of *S. pneumoniae* colonization in mice." *J Clin Invest* **121** (9): 3666-3676.

Dawson, R. M. C., Elliott, D. C., Elliott, W. H., and Jones, K. M. (1986). *Data for Biochemical Research* (third edition): Oxford Science Publications, OUP, Oxford. ISBN 0-19-855358-7. pp 580.

de Jong, B. C., Antonio, M., and Gagneux, S. (2010). "Mycobacterium africanum--review of an important cause of human tuberculosis in West Africa." *PLoS Negl Trop Dis* **4** (9): e744.

de Keijzer, J., Mulder, A., de Beer, J., de Ru, A. H., van Veelen, P. A., and van Soolingen, D. (2016). "Mechanisms of Phenotypic Rifampicin Tolerance in Mycobacterium tuberculosis Beijing Genotype Strain B0/W148 Revealed by Proteomics." *J Proteome Res* **15** (4): 1194-1204.

De Pascale, G., Grigoriadou, C., Losi, D., Donadio, S. (2007). Validation for high-throughput screening of a VanRS-based reporter gene assay for bacterial cell wall inhibitors. *Journal of Applied Microbiology* **103**: 133-140.

de Smet, K. A., Kempell, K. E., Gallagher, A., Duncan, K., and Young, D. B. (1999) Alteration of a single amino acid residue reverses fosfomycin resistance of recombinant MurA from Mycobacterium tuberculosis. *Microbiology.* **145** (Pt 11): 3177-84.

Deb, C., Lee, C. M., Dubey, V. S., Daniel, J., Abomoelak, B., Sirakova, T. D., Pawar, S., Rogers, L. and Kolattukudy, P. E. (2009). "A novel in vitro multiple-stress dormancy model for Mycobacterium tuberculosis generates a lipid-loaded, drug-tolerant, dormant pathogen." *PLoS One* **4** (6): e6077.

Dersh, D., Iwamoto, Y., and Argon, Y. (2016). "Tay-Sachs disease mutations in HEXA target the alpha chain of hexosaminidase A to endoplasmic reticulum-associated degradation." *Mol Biol Cell* **27** (24): 3813-3827.

Desjardins, M., Huber, L. A., Parton, R. G., and Griffiths, G. (1994). "Biogenesis of phagolysosomes proceeds through a sequential series of interactions with the endocytic apparatus." *J Cell Biol* **124** (5): 677-688.

Dillon, N. A., Peterson, N. D., Feaga, H. A., Keiler, K. C., and Baughn, A. D. (2017). "Anti-tubercular Activity of Pyrazinamide is Independent of trans-Translation and RpsA." *Sci Rep* **7** (1): 6135.

Domingo-Gonzalez, R., Prince, O., Cooper, A., and Khader, S. A. (2016). "Cytokines and Chemokines in Mycobacterium tuberculosis Infection." *Microbiol Spectr* **4** (5).

Downing, K. J., Betts, J. C., Young, D. I., McAdam, R. A., Kelly, F., Young M., and Mizrahi, V. (2004). "Global expression profiling of strains harbouring null mutations reveals that the five rpf-like genes of *Mycobacterium tuberculosis* show functional redundancy." *Tuberculosis (Edinb)* **84** (3-4): 167-179.

Downing, K. J., Mischenko, V. V., Shleeva, M. O., Young, D. I., Young, M., Kaprelyants, A. S., Apt, A. S., and Mizrahi, V. (2005). "Mutants of *Mycobacterium tuberculosis* lacking three of the five rpf-like genes are defective for growth in vivo and for resuscitation in vitro." *Infect Immun* **73** (5): 3038-3043.

Doz, E., Rose, S., Court, N., Front, S., Vasseur, V., Charron, S., Gilleron, M., Puzo, G., Fremaux, I., Delneste, Y., Erard, F., Ryffel, B., Martin, O. R., and Quesniaux, V. F. (2009). "Mycobacterial phosphatidylinositol mannosides negatively regulate host Toll-like receptor 4, MyD88-dependent proinflammatory cytokines, and TRIF-dependent co-stimulatory molecule expression." *J Biol Chem* **284** (35): 23187-23196.

El Zoeiby, A., Sanschagrín, F., and Levesque, R. C. (2003). Structure and function of the Mur enzymes: development of novel inhibitors. *Mol Microbiol* **47** (1): 1-12.

Eniyan, K., Dharavath, S., Vijayan, R., Bajpai, U., and Gourina, S. (2018) Crystal structure of UDP-N-acetylglucosamine-enolpyruvate reductase (MurB) from *Mycobacterium tuberculosis*. *Biochem Biophys.* **1866** (3): 397-406.

Espinosa-Cueto, P., Magallanes-Puebla, A., Castellanos, C., and Mancilla, R. (2017) Dendritic cells that phagocytose apoptotic macrophages loaded with mycobacterial antigens activate CD8 T cells via cross-presentation. *PLoS ONE* **12** (8): e0182126.

European Committee for Antimicrobial Susceptibility Testing (EUCAST) of the European Society of Clinical Microbiology and Infectious Diseases (ESCMID) (2000). Determination of minimum inhibitory concentrations (MICs) of antibacterial agents by agar dilution. *Clin Microbiol Infect.* **6** (9): 509–515.

Eustice, D. C. and Wilhelm, J. M. (1984). "Mechanisms of action of aminoglycoside antibiotics in eucaryotic protein synthesis." *Antimicrob Agents Chemother* **26**(1): 53-60.

Falkinham, J. O., 3rd (2015). "Environmental sources of nontuberculous mycobacteria." *Clin Chest Med* **36** (1): 35-41.

Falzon, D., Gandhi, N., Migliori, G. B., Sotgiu, G., Cox, H. S., Holtz, T. H., Hollm-Delgado, M. G., Keshavjee, S., DeRiemer, K., Centis, R., D'Ambrosio, L., Lange, C. G., Bauer, M. D. (2013). Menzies and M.-T. Collaborative Group for Meta-Analysis of Individual Patient Data in 2013. "Resistance to fluoroquinolones and second-line injectable drugs: impact on multidrug-resistant TB outcomes." *Eur Respir J* **42** (1): 156-168.

Fang, C., Stiegeler, E., Cook, G. M., Mascher, T., and Gebhard, S. (2014) *Bacillus subtilis* as a Platform for Molecular Characterisation of Regulatory Mechanisms of *Enterococcus faecalis* Resistance against Cell Wall Antibiotics. *PLoS ONE* **9** (3): e93169.

Fang, X., Tiyanont, K., Zhang, Y., Wanner, J., Boger, D., and Walker, S. (2006) The mechanism of action of ramoplanin and enduracidin. *Mol Biosyst.* **2** (1): 69–76.

Fastrez, J. (1996). "Phage lysozymes." *EXS* **75**: 35-64.

Fattorini, L., Piccaro, G., Mustazzolu, A., and Giannoni, F. (2013). "Targeting dormant bacilli to fight tuberculosis." *Mediterr J Hematol Infect Dis* **5** (1): e2013072.

Fedrizzi, T., Meehan, C. J., Grottola, A., Giacobazzi, E., Fregni Serpini, G., Tagliazucchi, S., Fabio, A., Bettua, C., Bertorelli, R., De Sanctis, V., Rumpianesi, F., Pecorari, M., Jousson, O., Tortoli, E., and Segata, N. (2017). "Genomic characterization of Nontuberculous Mycobacteria." *Sci Rep* **7**: 45258.

Feng, Z., and Barletta, R. G. (2003) Roles of *Mycobacterium smegmatis* D-alanine:D-alanine ligase and D-alanine racemase in the mechanisms of action of and resistance to the peptidoglycan inhibitor D-cycloserine. *Antimicrob Agents Chemother.* **47**: 283–91.

Fernandes, M. J., Yew, S., Leclerc, D., Henrissat, B., Vorgias, C. E., Gravel, R. A., Hechtman, P., and Kaplan, F. (1997). "Identification of candidate active site residues in lysosomal beta-hexosaminidase A." *J Biol Chem* **272** (2): 814-820.

Figueiredo, T. A., Ludovice, A. M., and Sobral, R. G. (2014). "Contribution of peptidoglycan amidation to beta-lactam and lysozyme resistance in different genetic lineages of *Staphylococcus aureus*." *Microb Drug Resist* **20** (3): 238-249.

Finland, M., Garner, C., Wilcox, C., and Sabath, L. D. (1976). "Susceptibility of beta-hemolytic streptococci to 65 antibacterial agents." *Antimicrob Agents Chemother* **9** (1): 11-19.

Flannagan, R. S., Cosio, G., and Grinstein, S. (2009). "Antimicrobial mechanisms of phagocytes and bacterial evasion strategies." *Nat Rev Microbiol* **7** (5): 355-366.

Fleming, A. (1922). "Observations on a Bacteriolytic Substance ("Lysozyme") Found in Secretions and Tissues." *Br J Exp Pathol* **3** (5): 252-260.

Flores, A. R., Parsons, L. M., and Pavelka, Jr. M. S. (2005) Genetic analysis of the β -lactamases of *Mycobacterium smegmatis* and *Mycobacterium tuberculosis* and susceptibility to β -lactam antibiotics. *Microbiology.* **151** (Pt 2): 521–532.

Flores, A. R., Parsons, L. M., and Pavelka, Jr., M. S. (2005). "Characterization of novel *Mycobacterium tuberculosis* and *Mycobacterium smegmatis* mutants hypersusceptible to beta-lactam antibiotics." *J Bacteriol* **187** (6): 1892-1900.

Forster, C. and Kane, P. M. (2000). "Cytosolic Ca²⁺ homeostasis is a constitutive function of the V-ATPase in *Saccharomyces cerevisiae*." *J Biol Chem* **275** (49): 38245-38253.

Fritz, J. H., Ferrero, R. L., Philpott, D. J., and Girardin, S. E. (2006). "Nod-like proteins in immunity, inflammation and disease." *Nat Immunol* **7** (12): 1250-1257.

Galley, N. F., O'Reilly, A. M., and Roper, D. I. (2014). "Prospects for novel inhibitors of peptidoglycan transglycosylases." *Bioorg Chem* **55**: 16-26.

Garcia-Bustos, J. and Tomasz, A. (1990). A biological price of antibiotic resistance: major changes in the peptidoglycan structure of penicillin-resistant pneumococci. *Proc Natl Acad Sci U S A* **87** (14): 5415-5419.

Gaschignard, J., Grant, A. V., Thuc, N. V., Orlova, M., Cobat, A., Huong, N. T., Ba, N. N., Thai, V. H., Abel, L., Schurr, E., and Alcais, A. (2016). "Pauci- and Multibacillary Leprosy: Two Distinct, Genetically Neglected Diseases." *PLoS Negl Trop Dis* **10** (5): e0004345.

Gaynes, R. (2017). "The Discovery of Penicillin-New Insights After More Than 75 Years of Clinical Use." *Emerg Infect Dis* **23** (5): 849-853.

Ge, M., Chen, Z., Onishi, H. R., Kohler, J., Silver, L. L., Kerns, R., Fukuzawa, S., Thompson, C., and Kahne, D. (1999) Vancomycin derivatives that inhibit peptidoglycan biosynthesis without binding D-Ala-D-Ala. *Science*. **284** (5413): 507–511.

Gengenbacher, M. and Kaufmann, S. H. (2012). "Mycobacterium tuberculosis: success through dormancy." *FEMS Microbiol Rev* **36** (3): 514-532.

Glavas, S., and Tanner, M. E. (2001). Active Site Residues of Glutamate Racemase. *Biochemistry*. **40** (21), 6199-6204

Gootz, T. D. (2010). "The global problem of antibiotic resistance." *Crit Rev Immunol* **30** (1): 79-93.

Gotoh, N. (2001). "[Antibiotic resistance caused by membrane impermeability and multidrug efflux systems]." *Nihon Rinsho* **59** (4): 712-718.

Goode, R., Amin, A. G., Chatterjee, D., and Parish, T. (2009). "The arabinosyltransferase EmbC is inhibited by ethambutol in Mycobacterium tuberculosis." *Antimicrob Agents Chemother* **53** (10): 4138-4146.

Gourbatsi, E., Povey, J., Uddin, S., and Smales, C. M. (2016). "Biotherapeutic protein formulation variables influence protein integrity and can promote post-translational modifications as shown using chicken egg white lysozyme as a model system." *Biotechnol Lett* **38** (4): 589-596.

Grant, S. G., Jessee, J., Bloom, F. R. and Hanahan, D. (1990). "Differential plasmid rescue from transgenic mouse DNAs into Escherichia coli methylation-restriction mutants." *Proc Natl Acad Sci U S A* **87** (12): 4645-4649.

Guirado, E., Schlesinger, L. S., and Kaplan, G. (2013). "Macrophages in tuberculosis: friend or foe." *Semin Immunopathol* **35** (5): 563-583.

Gupta, U. D. and Katoch, V. M. (2009). "Animal models of tuberculosis for vaccine development." *Indian J Med Res* **129** (1): 11-18.

Hakenbeck, R., Brückner, R., Denapaite, D., and Maurer, P. (2012) Molecular mechanisms of β -lactam resistance in *Streptococcus pneumoniae*. *Future Microbiol.* **7** (3): 395-410.

Halder, P., Kumar, R., Jana, K., Chakraborty, S., Ghosh, Z., Kundu M., and Basu, J. (2015). "Gene expression profiling of *Mycobacterium tuberculosis* Lipoarabinomannan-treated macrophages: A role of the Bcl-2 family member A1 in inhibition of apoptosis in mycobacteria-infected macrophages." *IUBMB Life* **67** (9): 726-736.

Hammes, W. P. and Neuhaus, F. C. (1974). "On the mechanism of action of vancomycin: inhibition of peptidoglycan synthesis in *Gaffkya homari*." *Antimicrob Agents Chemother* **6** (6): 722-728.

Hansen, J.M., Golchin, S.A., Veyrier, F.J., Domenech, P., Boneca, I.G., Azad, A.K., Rajaram, M.V., Schlesinger, L.S., Divangahi, M., Reed, M.B., Behr, M.A. (2014). N-glycosylated peptidoglycan contributes to the immunogenicity but not pathogenicity of *Mycobacterium tuberculosis*. *J Infect Dis.* **209** (7):1045-54.

Hare, N. J., Lee, L. Y., Loke, I., Britton, W. J., Saunders, B. M., and Thaysen-Andersen, M. (2017). "Mycobacterium tuberculosis Infection Manipulates the Glycosylation Machinery and the N-Glycoproteome of Human Macrophages and Their Microparticles." *J Proteome Res* **16** (1): 247-263.

Harty, D. W., Mayo, J. A., Cook, S. L., and Jacques, N. A. (2000). "Environmental regulation of glycosidase and peptidase production by *Streptococcus gordonii* FSS2." *Microbiology* **146** (Pt 8): 1923-1931.

Hauryliuk, V., Atkinson, G. C., Murakami, K. S., Tenson, T., and Gerdes, K. (2015) Recent functional insights into the role of (p)ppGpp in bacterial physiology. *Nature reviews Microbiology.* **13** (5): 298-309.

He, Z. and De Buck, J. (2010). "Cell wall proteome analysis of *Mycobacterium smegmatis* strain MC2 155." *BMC Microbiol* **10**: 121.

Heesemann, J. (1993). "[Mechanisms of resistance to beta-lactam antibiotics]." *Infection* **21 Suppl 1**: S4-9.

Hett, E. C., Chao, M. C., Steyn, A. J., Fortune, S. M., Deng, L. L., and Rubin, E. J. (2007). "A partner for the resuscitation-promoting factors of *Mycobacterium tuberculosis*." *Mol Microbiol* **66** (3): 658-668.

Hett, E. C. and Rubin, E. J. (2008). "Bacterial growth and cell division: a mycobacterial perspective." *Microbiol Mol Biol Rev* **72** (1): 126-156, table of contents.

Honaker, R. W., Leistikow, R. L., Bartek, I. L., and Voskuil, M. I. (2009). "Unique roles of DosT and DosS in DosR regulon induction and Mycobacterium tuberculosis dormancy." *Infect Immun* **77** (8): 3258-3263.

Hooper, D. C. (1999). "Mode of action of fluoroquinolones." *Drugs* **58 Suppl 2**: 6-10.

Horsburgh, C. R., Jr., Caldwell, M. B., and Simonds, R. J. (1993). "Epidemiology of disseminated nontuberculous mycobacterial disease in children with acquired immunodeficiency syndrome." *Pediatr Infect Dis J* **12** (3): 219-222.

Hossain, M. A. and Roslan, H. A. (2014). "Molecular phylogeny and predicted 3D structure of plant beta-D-N-acetylhexosaminidase." *Scientific World Journal* 2014: 186029.

Houben, R. M. and Dodd, P. J. (2016). "The Global Burden of Latent Tuberculosis Infection: A Re-estimation Using Mathematical Modelling." *PLoS Med* **13** (10): e1002152.

Howe, R., Kelly, M., Jimah, J., Hodge, D., and Odom, A. (2013). Isoprenoid Biosynthesis Inhibition Disrupts Rab5 Localization and Food Vacuolar Integrity in Plasmodium falciparum Eukaryot Cell. **12** (2): 215–223.

Hu, Y., Yu, X., Zhao, D., Li, R., Liu, Y., Ge, M., and Hu, H. (2017). Isolation of nontuberculous mycobacteria from soil using Middlebrook 7H10 agar with increased malachite green concentration. *AMB Express*, 7(1), 69.

Hugonnet, J. E. and Blanchard, J. S. (2007). "Irreversible inhibition of the Mycobacterium tuberculosis beta-lactamase by clavulanate." *Biochemistry* **46** (43): 11998-12004.

Hugonnet, J., Mengin-Lecreux, D., Monton, A., den Blaauwen, T., Carbonnelle, E., Veckerlé, C., Yves, Brun, V., van Nieuwenhze, M., Bouchier, C., Tu, K., Rice, L. B., and Arthur, M. (2016). Factors essential for L,D-transpeptidase-mediated peptidoglycan cross-linking and β -lactam resistance in *Escherichia coli*. *eLife*. **5**: e19469.

Hugonnet, J. E., Tremblay, L. W., Boshoff, H. I., Barry, 3rd, C. E., and Blanchard, J. S. (2009). "Meropenem-clavulanate is effective against extensively drug-resistant Mycobacterium tuberculosis." *Science* **323** (5918): 1215-1218.

Hujer, A. M., Kania, M., and Gerken, T. (2005) Structure-Activity Relationships of Different β -Lactam Antibiotics against a Soluble Form of Enterococcus faecium PBP5, a Type II Bacterial Transpeptidase. *Antimicrobial Agents and Chemotherapy*. **49** (2): 612-618.

Inohara, N., Ogura, Y., Fontalba, A., Gutierrez, O., Pons, F., Crespo, J., Fukase, K., Inamura, S., Kusumoto, S., Hashimoto, M., Foster, S. J., Moran, A. P., Fernandez-Luna, J. L., and Nunez, G. (2003). "Host recognition of bacterial muramyl dipeptide mediated through NOD2. Implications for Crohn's disease." *J Biol Chem* **278** (8): 5509-5512.

Jad, Y. E., Acosta, G. A., Naicker, T., Ramtahal, M., El-Faham, A., Govender, T., Kruger, H., de la Torre, B., and Albericio, F. (2015) Synthesis and Biological Evaluation of a Teixobactin Analogue. *Org Lett.* **17** (24): 6182–6185.

Jenkins, R. W., Barbie, D. A., and Flaherty, K. T. (2018). "Mechanisms of resistance to immune checkpoint inhibitors." *Br J Cancer* **118** (1): 9-16.

Jesman, C., Mludzik, A., and Cybulska, M. (2011). "[History of antibiotics and sulphonamides discoveries]." *Pol Merkur Lekarski* **30** (179): 320-322.

Jolles, P. and Jolles, J. (1984). "What's new in lysozyme research? Always a model system, today as yesterday." *Mol Cell Biochem* **63** (2): 165-189.

Joshi, R. (2011). "Clues to histopathological diagnosis of treated leprosy." *Indian J Dermatol* **56** (5): 505-509.

Kana, B. D., Gordhan, B. G., Downing, K. J., Sung, N., Vostroktunova, G., Machowski, E. E., Tsenova, L., Young, M., Kaprelyants, A., Kaplan, G., and Mizrahi, V. (2007). The resuscitation-promoting factors of *Mycobacterium tuberculosis* are required for virulence and resuscitation from dormancy but are collectively dispensable for growth in vitro. *Molecular microbiology*, *67*(3), 672-84.

Kang, P. B., Azad, A. K., Torrelles, J. B., Kaufman, T. M., Beharka, A., Tibesar, E., DesJardin, L. E., and Schlesinger, L. S. (2005). "The human macrophage mannose receptor directs *Mycobacterium tuberculosis* lipoarabinomannan-mediated phagosome biogenesis." *J Exp Med* **202** (7): 987-999.

Kapil, A. (2005). "The challenge of antibiotic resistance: need to contemplate." *Indian J Med Res* **121** (2): 83-91.

Kapoor, N., Pawar, S., Sirakova, T. D., Deb, C., Warren, W. L., and Kolattukudy, P. E. (2013). "Human granuloma in vitro model, for TB dormancy and resuscitation." *PLoS One* **8** (1): e53657.

Kaprelyants, A. S., Gottschal, J. C., and Kell, D. B. (1993). "Dormancy in non-sporulating bacteria." *FEMS Microbiol Rev* **10** (3-4): 271-285.

Karakousis, P. C., Yoshimatsu, T., Lamichhane, G., Woolwine, S. C., Nuermberger, E. L., Grosset, J. and Bishai, W. R. (2004). "Dormancy phenotype displayed by extracellular *Mycobacterium tuberculosis* within artificial granulomas in mice." *J Exp Med* **200** (5): 647-657.

Keane, J. (2005). "TNF-blocking agents and tuberculosis: new drugs illuminate an old topic." *Rheumatology (Oxford)* **44** (6): 714-720.

Kendall, S. L., Movahedzadeh, F., Rison, S. C., Wernisch, L., Parish, T., Duncan, K., Betts, J. C., and Stoker, N. G. (2004). "The *Mycobacterium tuberculosis* dosRS two-component system is induced by multiple stresses." *Tuberculosis (Edinb)* **84** (3-4): 247-255.

- Kerantzas, C. A. and Jacobs, Jr., W. R.** (2017). "Origins of Combination Therapy for Tuberculosis: Lessons for Future Antimicrobial Development and Application." *MBio* **8** (2).
- Kieser, K. J., Baranowski, C., Chao, M. C., Long, J. E., Sasseti, C. M., Waldor, M. K., Sacchettini, J. C., Ioerger, T. R., and Rubin, E. J.** (2015). "Peptidoglycan synthesis in *Mycobacterium tuberculosis* is organized into networks with varying drug susceptibility." *Proc Natl Acad Sci U S A* **112** (42): 13087-13092.
- Kieser, K. J., Boutte, C. C., Kester, J. C., Baer, C. E., Barczak, A. K., and Meniche, X.** (2015) Phosphorylation of the Peptidoglycan Synthase PonA1 Governs the Rate of Polar Elongation in *Mycobacteria*. *PLoS Pathog* **11** (6): e1005010.
- Kim, C., Mwangi, M., Chung, M., Milheirico, C., de Lencastre, H., and Tomasz, A.** (2013). The mechanism of heterogeneous beta-lactam resistance in MRSA: key role of the stringent stress response. *PLoS One* **8** (12): e82814.
- Kim, S. J., Chang, J., and Singh, M.** (2015). "Peptidoglycan architecture of Gram-positive bacteria by solid-state NMR." *Biochim Biophys Acta* **1848** (1 Pt B): 350-362.
- Koch, R.** (1882). "The etiology of tuberculosis." *Berlin clinical weekly*. **15**: 221-230.
- Kohanski, M. A., Dwyer, D. J., and Collins, J. J.** (2010). "How antibiotics kill bacteria: from targets to networks." *Nat Rev Microbiol* **8** (6): 423-435.
- Kong, K. F., Schneper, L., and Mathee, K.** (2010) Beta-lactam Antibiotics: From Antibiosis to Resistance and Bacteriology. *APMIS : acta pathologica, microbiologica, et immunologica Scandinavica*. **118** (1): 1-36.
- Koo, I. C., Ohol, Y. M., Wu, P., Morisaki, J. H., Cox, J. S. and Brown, E. J.** (2008). "Role for lysosomal enzyme beta-hexosaminidase in the control of mycobacteria infection." *Proc Natl Acad Sci U S A* **105** (2): 710-715.
- Kragelund, C., Remesova, Z., Nielsen, J. L., Thomsen, T. R., Eales, K., Seviour, R., Wanner, J. and Nielsen, P. H.** (2007). "Ecophysiology of mycolic acid-containing Actinobacteria (Mycolata) in activated sludge foams." *FEMS Microbiol Ecol* **61** (1): 174-184.
- Krotoski, W. A., Mroczkowski, T. F., Rea, T. H., Almodovar, P. I., Clements, B. C., Neimes, R. E., Kahkonen, M. K., Job, C. K., and Hastings, R. C.** (1993). "Lepromin skin testing in the classification of Hansen's disease in the United States." *Am J Med Sci* **305** (1): 18-24.
- Kumar, P., Arora, K., Lloyd, J. R., Lee, I. Y., Nair, V., Fischer, E., Boshoff, H. I., Barry, C. E., 3rd.** (2012) Meropenem inhibits D,D-carboxypeptidase activity in *Mycobacterium tuberculosis*. *Mol Microbiol*. **86** (2): 367-81.

- Kumar, A., Toledo, J. C., Patel, R. P., Lancaster, Jr., J. R., and Steyn, A. J.** (2007). "Mycobacterium tuberculosis DosS is a redox sensor and DosT is a hypoxia sensor." *Proc Natl Acad Sci U S A* **104** (28): 11568-11573.
- Kumarasiri, M., Zhang, W., Shi, Q., Fisher, J., and Mobashery, S.** (2014) Protonation States of Active-Site Lysines of Penicillin-Binding Protein 6 from *Escherichia coli* and the Mechanistic Implications. *Proteins*. **82** (7): 1348–1358.
- Laemmli, U. K.** (1970). "Cleavage of structural proteins during the assembly of the head of bacteriophage T4." *Nature* **227** (5259): 680-685.
- Lambert, P. A.** (2005). "Bacterial resistance to antibiotics: modified target sites." *Adv Drug Deliv Rev* **57** (10): 1471-1485.
- Lambert, M. P. and Neuhaus, F. C.** (1972). Mechanism of D-cycloserine action: alanine racemase from *Escherichia coli* W. *J Bacteriol* **110** (3): 978-987.
- Launay, A., Ballard, S. A., Johnson, P. D., Grayson, M. L., and Lambert, T.** (2006). "Transfer of vancomycin resistance transposon Tn1549 from *Clostridium symbiosum* to *Enterococcus* spp. in the gut of gnotobiotic mice." *Antimicrob Agents Chemother* **50** (3): 1054-1062.
- Lee, A., de Lencastre, H., Garau, J., Kluytmans, J., Malhotra-Kumar, S., Peschel, A., and Harbarth, S.** (2018). Methicillin-resistant *Staphylococcus aureus* *Nature Reviews Disease Primers* volume 4, Article number: 18033.
- Lee, J., Tattoli, I., Wojtal, K. A., Vavricka, S. R., Philpott, D. J., and Girardin, S. E.** (2009). "pH-dependent internalization of muramyl peptides from early endosomes enables Nod1 and Nod2 signaling." *J Biol Chem* **284** (35): 23818-23829.
- Lee, K. S., Song, K. S., Lim, T. H., Kim, P. N., Kim, I. Y., and Lee, B. H.** (1993). "Adult-onset pulmonary tuberculosis: findings on chest radiographs and CT scans." *AJR Am J Roentgenol* **160** (4): 753-758.
- Lehrer, R. I., Lichtenstein, A. K., and Ganz, T.** (1993). "Defensins: antimicrobial and cytotoxic peptides of mammalian cells." *Annu Rev Immunol* **11**: 105-128.
- Leistikow, R. L., Morton, R. A., Bartek, I. L., Frimpong, I., Wagner, K., and Voskuil, M. I.** (2010). "The *Mycobacterium tuberculosis* DosR regulon assists in metabolic homeostasis and enables rapid recovery from nonrespiring dormancy." *J Bacteriol* **192** (6): 1662-1670.
- Levitz, S. M., Nong, S. H., Seetoo, K. F., Harrison, T. S., Speizer, R. A., and Simons, E. R.** (1999). "Cryptococcus neoformans resides in an acidic phagolysosome of human macrophages." *Infect Immun* **67** (2): 885-890.
- Lindquist, S., Weston-Hafer, K., Schmidt, H., Pul, C., Korfmann, G., Erickson, J., Sanders, C., Martin, H. H., and Normark, S.** (1993). "AmpG, a signal transducer in chromosomal beta-lactamase induction." *Mol Microbiol* **9** (4): 703-715.

- Liu, J., Chakraborty, S., Hosseinzadeh, P., Yu, Y., Tian, S., Petrik, I., Bhagi, A., and Lu, Y.** (2014). "Metalloproteins containing cytochrome, iron-sulfur, or copper redox centers." *Chem Rev* **114** (8): 4366-4469.
- Lloyd, A. J., Brandish, P. E., Gilbey, A. M., and Bugg, T. D.** (2004). Phospho-N-acetyl-muramyl-pentapeptide translocase from *Escherichia coli*: catalytic role of conserved aspartic acid residues. *J Bacteriol* **186** (6): 1747-1757.
- Lloyd, A. J., Gilbey, A. M., Blewett, A. M., De Pascale, G., El Zoeiby, A., Levesque, R. C., Catherwood, A. C., Tomasz, A., Bugg, T. D., Roper, D. I., and Dowson, C. G.** (2008). "Characterization of tRNA-dependent peptide bond formation by MurM in the synthesis of *Streptococcus pneumoniae* peptidoglycan." *J Biol Chem* **283** (10): 6402-6417.
- Lorenz, M. G. and Wackernagel, W.** (1994). "Bacterial gene transfer by natural genetic transformation in the environment." *Microbiol Rev* **58** (3): 563-602.
- Luca, S. and Mihaescu, T.** (2013). "History of BCG Vaccine." *Maedica (Buchar)* **8** (1): 53-58.
- Lund-Katz, S., Nguyen, D., and Dhanasekaran, P.** (2010) et al. Surface plasmon resonance analysis of the mechanism of binding of apoA-I to high density lipoprotein particles. *Journal of Lipid Research*. **51** (3): 606-617.
- Lyadova, I. V.** (2017). "Neutrophils in Tuberculosis: Heterogeneity Shapes the Way?" *Mediators Inflamm* **2017**: 8619307.
- Macheboeuf, P., Lemaire, D., Teller, N., Martins, A., Ados, S., Luxen, A., Dideberg, O., Jamin, M., and Dessen, A.** (2008) Trapping of an acyl-enzyme intermediate in a penicillin-binding protein (PBP)-catalyzed reaction. *J Mol Biol*. **376** (2): 405-13.
- Magnet, S., Dubost, L., Marie, A., Arthur, M., and Gutmann, L.** (2008) Identification of the L,D-Transpeptidases for Peptidoglycan Cross-Linking in *Escherichia coli* *JOURNAL OF BACTERIOLOGY*. p. 4782–4785.
- Mahapatra, S., Crick, D. C., & Brennan, P. J.** (2000). Comparison of the UDP-N-acetylmuramate:L-alanine ligase enzymes from *Mycobacterium tuberculosis* and *Mycobacterium leprae*. *Journal of bacteriology*, *182*(23), 6827-30.
- Mahapatra, S., Crick, D., McNeil, M., and Brennan, P.** (2008) Unique Structural Features of the Peptidoglycan of *Mycobacterium leprae* *JOURNAL OF BACTERIOLOGY*: 655–661.
- Mahapatra, S., Scherman, H., Brennan, P. J., and Crick, D. C.** (2005). "N-Glycosylation of the nucleotide precursors of peptidoglycan biosynthesis of *Mycobacterium* spp. is altered by drug treatment." *J Bacteriol* **187** (7): 2341-2347.
- Mahapatra, S., Yagi, T., Belisle, J., Espinosa, B., Hill, P., McNeil, M., Brennan, P., and Crick, D.** (2005). Mycobacterial Lipid II Is Composed of a Complex Mixture of

Modified Muramyl and Peptide Moieties Linked to Decaprenyl Phosphate JOURNAL OF BACTERIOLOGY. p. 2747–2757.

Malathi, M., and Thappa, D. M. (2013). "Fixed-duration therapy in leprosy: limitations and opportunities." *Indian J Dermatol* **58** (2): 93-100.

Marrakchi, H., Laneelle, G. and Quemard, A. (2000). "InhA, a target of the antituberculous drug isoniazid, is involved in a mycobacterial fatty acid elongation system, FAS-II." *Microbiology* **146** (Pt 2): 289-296.

Masson, P. L., Heremans, J. F. and Schonke, E. (1969). "Lactoferrin, an iron-binding protein in neutrophilic leukocytes." *J Exp Med* **130** (3): 643-658.

Mathews, F., Macdonald, D. W., Taylor, G. M., Gelling, M., Norman, R. A., Honess, P. E., Foster, R., Gower, C. M., Varley, S., Harris, A., Palmer, S., Hewinson, G., and Webster, J. P. (2006). "Bovine tuberculosis (*Mycobacterium bovis*) in British farmland wildlife: the importance to agriculture." *Proc Biol Sci* **273** (1584): 357-365.

Mba Medie, F., Ben Salah, I., Henrissat, B., Raoult, D., and Drancourt, M. (2011). *Mycobacterium tuberculosis* complex mycobacteria as amoeba-resistant organisms. *PloS one*, *6*(6), e20499.

McCune, R. M., Jr., McDermott, W. and Tompsett, R. (1956). "The fate of *Mycobacterium tuberculosis* in mouse tissues as determined by the microbial enumeration technique. II. The conversion of tuberculous infection to the latent state by the administration of pyrazinamide and a companion drug." *J Exp Med* **104** (5): 763-802.

McCune, R. M., Jr. and Tompsett, R. (1956). "Fate of *Mycobacterium tuberculosis* in mouse tissues as determined by the microbial enumeration technique. I. The persistence of drug-susceptible tubercle bacilli in the tissues despite prolonged antimicrobial therapy." *J Exp Med* **104** (5): 737-762.

Merrikh, H., Ferrazzoli, A. E., and Lovett, S. T. (2009). Growth Phase and (p)ppGpp Control of IraD, a Regulator of RpoS Stability, in *Escherichia coli*. *Journal of Bacteriology*. **191** (24): 7436-7446.

Metcalfe, C., Macdonald, I. K., Murphy, E. J., Brown, K. A., Raven, E. L. and Moody, P. C. (2008). "The tuberculosis prodrug isoniazid bound to activating peroxidases." *J Biol Chem* **283** (10): 6193-6200.

Miesel, L., Weisbrod, T. R., Marcinkeviciene, J. A., Bittman, R., and Jacobs, W. R. Jr. (1998). "NADH dehydrogenase defects confer isoniazid resistance and conditional lethality in *Mycobacterium smegmatis*." *J Bacteriol* **180** (9): 2459-2467.

Mihelic, M., Vlahovicek-Kahlina, K., Renko, M., Mesnage, S., Dobersek, A., Taler-Vercic, A., Jakas, A., and Turk, D. (2017). "The mechanism behind the selection of two different cleavage sites in NAG-NAM polymers." *IUCrJ* **4** (Pt 2): 185-198.

- Miller, J. H., Novak, J. T., Knocke, W. R., and Pruden, A.** (2016). "Survival of Antibiotic Resistant Bacteria and Horizontal Gene Transfer Control Antibiotic Resistance Gene Content in Anaerobic Digesters." *Front Microbiol* **7**: 263.
- Mo, J., Boyle, J. P., Howard, C. B., Monie, T. P., Davis, B. K., & Duncan, J. A.** (2012). Pathogen sensing by nucleotide-binding oligomerization domain-containing protein 2 (NOD2) is mediated by direct binding to muramyl dipeptide and ATP. *The Journal of biological chemistry*. **287** (27), 23057–23067.
- Mohammadi, T., van Dam, V., Sijbrandi, R., Vernet, T., Zapun, A., Bouhss, A., Diepeveen-de Bruin, M., Nguyen-Disteche, M., de Kruijff, B., and Breukink, E.** (2011). "Identification of FtsW as a transporter of lipid-linked cell wall precursors across the membrane." *EMBO J* **30** (8): 1425-1432.
- Mohan, V. P., Scanga, C. A., Yu, K., Scott, H. M., Tanaka, K. E., Tsang, E., Tsai, M. M., Flynn, J. L., and Chan, J.** (2001). "Effects of tumor necrosis factor alpha on host immune response in chronic persistent tuberculosis: possible role for limiting pathology." *Infect Immun* **69** (3): 1847-1855.
- Montecino-Rodriguez, E., Berent-Maoz, B., and Dorshkind, K.** (2013). "Causes, consequences, and reversal of immune system aging." *J Clin Invest* **123** (3): 958-965.
- Morita, Y., Tomida, J., and Kawamura, Y.** (2014). "Responses of *Pseudomonas aeruginosa* to antimicrobials." *Front Microbiol* **4**: 422.
- Moynihan, P. J., and Clarke, A. J.** (2010). "O-acetylation of peptidoglycan in gram-negative bacteria: identification and characterization of peptidoglycan O-acetyltransferase in *Neisseria gonorrhoeae*." *J Biol Chem* **285** (17): 13264-13273.
- Mukamolova, G. V., Turapov, O. A., Kazarian, K., Telkov, M., Kaprelyants, A. S., Kell, D. B., and Young, M.** (2002). "The *rpf* gene of *Micrococcus luteus* encodes an essential secreted growth factor." *Mol Microbiol* **46** (3): 611-621.
- Munoz-Elias, E. J., Timm, J., Botha, T., Chan, W. T., Gomez, J. E., and McKinney, J. D.** (2005). "Replication dynamics of *Mycobacterium tuberculosis* in chronically infected mice." *Infect Immun* **73** (1): 546-551.
- Munshi, T., Gupta, A., Evangelopoulos, D., Guzman, J. D., and Gibbons, S.** (2013) Characterisation of ATP-Dependent Mur Ligases Involved in the Biogenesis of Cell Wall Peptidoglycan in *Mycobacterium tuberculosis*. *PLoS ONE* **8** (3): e60143.
- Murakami, K., Ono, T., Viducic, D., Somiya, Y., Kariyama, R., Hori, K., Amoh, T., Hirota, K., Kumon, H., Parsek, M. R., and Miyake, Y.** (2017). "Role of *psl* Genes in Antibiotic Tolerance of Adherent *Pseudomonas aeruginosa*." *Antimicrob Agents Chemother* **61** (7).
- Muro, E. M., Mah, N., Moreno-Hagelsieb, G., and Andrade-Navarro, M. A.** (2011). "The pseudogenes of *Mycobacterium leprae* reveal the functional relevance of gene order within operons." *Nucleic Acids Res* **39** (5): 1732-1738.

- Myerowitz, R.** (1997). "Tay-Sachs disease-causing mutations and neutral polymorphisms in the Hex A gene." *Hum Mutat* **9** (3): 195-208.
- Nakajima, S.** (2003). "[The origin of cephalosporins]." *Yakushigaku Zasshi* **37** (2): 119-127.
- Nasiri, M., Haeili, M., Ghazi, M., Goudarzi, H., Pormohammad, A., Abbas, A., Fooladi, I., and Feizabadi, M.** (2017) New Insights in to the Intrinsic and Acquired Drug Resistance Mechanisms in Mycobacteria. *Front Microbiol.* **8**: 681.
- Nayak, S., and Acharjya, B.** (2012). "Mantoux test and its interpretation." *Indian Dermatol Online J* **3** (1): 2-6.
- Neyrolles, O., Hernandez-Pando, R., Pietri-Rouxel, F., Fornes, P., Tailleux, L., Barrios Payan, J. A., Pivert, E., Bordat, Y., Aguilar, D., Prevost, M. C., Petit, C., and Gicquel, B.** (2006). "Is adipose tissue a place for Mycobacterium tuberculosis persistence?" *PLoS One* **1**: e43.
- Ngadjeua, F., Braud, E., Saidjalolov, S., Iannazzo, L., Schnappinger, D., Ehrh, S., Hugonnet, J. E., Mengin-Lecreulx, D., Patin, D., Etheve-Quellejeu, M., Fonvielle, M., and Arthur, M.** (2018). "Critical Impact of Peptidoglycan Precursor Amidation on the Activity of L,d-Transpeptidases from Enterococcus faecium and Mycobacterium tuberculosis." *Chemistry* **24** (22): 5743-5747.
- Nigam, A., Almabruk, K. H., Saxena, A., Yang, J., Mukherjee, U., Kaur, H., Kohli, P., Kumari, R., Singh, P., Zakharov, L. N., Singh, Y., Mahmud, T., and Lal, R.** (2014). "Modification of rifamycin polyketide backbone leads to improved drug activity against rifampicin-resistant Mycobacterium tuberculosis." *J Biol Chem* **289** (30): 21142-21152.
- Nollau, P., and Wagener, C.** (1997). "Methods for detection of point mutations: performance and quality assessment. The IFCC Scientific Division, Committee on Molecular Biology Techniques." *J Int Fed Clin Chem* **9** (4): 162-170.
- Norton, B. L., and Holland, D. P.** (2012). "Current management options for latent tuberculosis: a review." *Infect Drug Resist* **5**: 163-173.
- O'Neill, J.** (2015). *Securing New Drugs for Future Generations: the Pipeline of Antibiotics. Review on Antimicrobial Resistance.*
- Ochoa, M. T., Valderrama, L., Ochoa, A., Zea, A., Escobar, C. E., Moreno L. H., and Falabella, R.** (1996). "Lepromatous and tuberculoid leprosy: clinical presentation and cytokine responses." *Int J Dermatol* **35** (11): 786-790.
- Odaka, C., and Mizuochi, T.** (1999). "Role of macrophage lysosomal enzymes in the degradation of nucleosomes of apoptotic cells." *J Immunol* **163** (10): 5346-5352.
- Ooi, W. W., and Srinivasan, J.** (2004). "Leprosy and the peripheral nervous system: basic and clinical aspects." *Muscle Nerve* **30** (4): 393-409.

- Osserman, E. F., and Lawlor, D. P.** (1966). "Serum and urinary lysozyme (muramidase) in monocytic and monomyelocytic leukemia." *J Exp Med* **124** (5): 921-952.
- Ostash, B., Makitrinsky, R., Walker, S., and Fedorenko, V.** (2009) Identification and characterization of *Streptomyces ghanaensis* ATCC14672 integration sites for three actinophage-based plasmids. *Plasmid*. **61** (3): 171-175.
- Paige, C., and Bishai, W. R.** (2010). "Penitentiary or penthouse condo: the tuberculous granuloma from the microbe's point of view." *Cell Microbiol* **12** (3): 301-309.
- Paradis-Bleau, C., Beaumont, M., Boudreault, L., Lloyd, A., Sanschagrín, F., Bugg, T. D., and Levesque, R. C.** (2006). Selection of peptide inhibitors against the *Pseudomonas aeruginosa* MurD cell wall enzyme. *Peptides* **27** (7): 1693-1700.
- Park, H. D., Guinn, K. M., Harrell, M. I., Liao, R., Voskuil, M. I., Tompa, M., Schoolnik, G. K., and Sherman, D. R.** (2003). "Rv3133c/dosR is a transcription factor that mediates the hypoxic response of *Mycobacterium tuberculosis*." *Mol Microbiol* **48** (3): 833-843.
- Park, J. T.** (1995). "Why does *Escherichia coli* recycle its cell wall peptides?" *Mol Microbiol* **17** (3): 421-426.
- Park, J. T., and Uehara, T.** (2008). "How bacteria consume their own exoskeletons (turnover and recycling of cell wall peptidoglycan)." *Microbiol Mol Biol Rev* **72** (2): 211-227, table of contents.
- Patru, M., and Pavelka, M.** (2017). A Role for the Class A Penicillin-Binding Protein PonA2 in the Survival of *Mycobacterium smegmatis* under Conditions of Nonreplication, *Mol Microbiol*. **106** (2): 304–318.
- Pauwels, A. M., Trost, M., Beyaert, R., and Hoffmann, E.** (2017). "Patterns, Receptors, and Signals: Regulation of Phagosome Maturation." *Trends Immunol* **38** (6): 407-422.
- Peddireddy, V., Doddam, S. N., and Ahmed, N.** (2017). "Mycobacterial Dormancy Systems and Host Responses in Tuberculosis." *Front Immunol* **8**: 84.
- Piddington, D. L., Kashkouli, A., and Buchmeier, N. A.** (2000). "Growth of *Mycobacterium tuberculosis* in a defined medium is very restricted by acid pH and Mg(2⁺) levels." *Infect Immun* **68** (8): 4518-4522.
- Piddock, L.** (2015) Teixobactin, the first of a new class of antibiotics discovered by iChip technology? *J Antimicrob Chemother.* **70** (10): 2679–2680.
- Pincus, M. R., Zimmerman, S. S., and Scheraga, H. A.** (1977). "Structures of enzyme-substrate complexes of lysozyme." *Proc Natl Acad Sci U S A* **74** (7): 2629-2633.

Poole, K. (2007). "Efflux pumps as antimicrobial resistance mechanisms." *Ann Med* **39** (3): 162-176.

Prakash, V., Lewis II, J. S., and Jorgensen, J. H. (2008). Vancomycin MICs for Methicillin-Resistant *Staphylococcus aureus* Isolates Differ Based upon the Susceptibility Test Method Used
Antimicrobial Agents and Chemotherapy. **52** (12) 4528.

Price, N. P., and Momany, F. A. (2005) Modeling bacterial UDP-HexNAc: polyprenol-P HexNAc-1-P transferases, *Glycobiology* **15** (9): 29-42.

Prisic, S., Dankwa, S., Schwartz, D., Chou, M. F., Locasale, J. W., and Kang, C. M. (2010) Extensive phosphorylation with overlapping specificity by *Mycobacterium tuberculosis* serine/threonine protein kinases. *Proc Natl Acad Sci USA*. **107**:7521–6. doi

Pullan, S. T., Allnut, J. C., Devine, R., Hatch, K. A., Jeeves, R. E., Hendon-Dunn, C. L., Marsh, P. D., and Bacon, J. (2016). "The effect of growth rate on pyrazinamide activity in *Mycobacterium tuberculosis* - insights for early bactericidal activity?" *BMC Infect Dis* **16**: 205.

Purdy, G., Niederweis, M. and Russell, D. (2009). Decreased outer membrane permeability protects mycobacteria from killing by ubiquitin-derived peptides. *Mol Microbiol*. **73** (5): 844–857.

Purohit, M., and Mustafa, T. (2015). "Laboratory Diagnosis of Extra-pulmonary Tuberculosis (EPTB) in Resource-constrained Setting: State of the Art, Challenges and the Need." *J Clin Diagn Res* **9** (4): EE01-06.

Quemard, A., Lacave, C., and Laneelle, G. (1991). "Isoniazid inhibition of mycolic acid synthesis by cell extracts of sensitive and resistant strains of *Mycobacterium aurum*." *Antimicrob Agents Chemother* **35** (6): 1035-1039.

Ragland, S. A., and Criss, A. K. (2017). "From bacterial killing to immune modulation: Recent insights into the functions of lysozyme." *PLoS Pathog* **13** (9): e1006512.

Ramakrishnan, L. (2012). "Revisiting the role of the granuloma in tuberculosis." *Nat Rev Immunol* **12** (5): 352-366.

Ramaswamy, S., and Musser, J. M. (1998). "Molecular genetic basis of antimicrobial agent resistance in *Mycobacterium tuberculosis*: 1998 update." *Tuber Lung Dis* **79** (1): 3-29.

Raymond, J. B., Mahapatra, S., Crick, D. C., and Pavelka, Jr., M. S. (2005). "Identification of the *namH* gene, encoding the hydroxylase responsible for the N-glycosylation of the mycobacterial peptidoglycan." *J Biol Chem* **280** (1): 326-333.

Reynolds, P. E., and Somner, E. A. (1990) Comparison of the target sites and mechanisms of action of glycopeptide and lipoglycopeptide antibiotics. *Drugs Exp Clin Res.* **16** (8): 385–389.

Riello, F. N., Brigido, R. T., Araujo, S., Moreira, T. A., Goulart, L. R., and Goulart, I. M. (2016). "Diagnosis of mycobacterial infections based on acid-fast bacilli test and bacterial growth time and implications on treatment and disease outcome." *BMC Infect Dis* **16**: 142.

Rieske, J. S., Hansen, R. E., and Zaugg, W. S. (1964). "Studies on the Electron Transfer System. 58. Properties of a New Oxidation-Reduction Component of the Respiratory Chain as Studied by Electron Paramagnetic Resonance Spectroscopy." *J Biol Chem* **239**: 3017-3022.

Roberts, D. M., Liao, R. P., Wisedchaisri, G., Hol, W. G., and Sherman, D. R. (2004). "Two sensor kinases contribute to the hypoxic response of *Mycobacterium tuberculosis*." *J Biol Chem* **279** (22): 23082-23087.

Roper, D. K. (2007) Determining Surface Plasmon Resonance Response Factors for Deposition onto Three-Dimensional Surfaces. *Chemical engineering science.* **62** (7): 1988-1996.

Rosser, A., Stover, C., Pareek, M., Mukamolova, G.V. (2017) Resuscitation-promoting factors are important determinants of the pathophysiology in *Mycobacterium tuberculosis* infection. *Crit Rev Microbiol.* **43** (5): 621-630.

Ryu, Y. J. (2015). "Diagnosis of pulmonary tuberculosis: recent advances and diagnostic algorithms." *Tuberc Respir Dis (Seoul)* **78** (2): 64-71.

Saini, D. K., Malhotra, V., and Tyagi, J. S. (2004). "Cross talk between DevS sensor kinase homologue, Rv2027c, and DevR response regulator of *Mycobacterium tuberculosis*." *FEBS Lett* **565** (1-3): 75-80.

Sales, A. M., Ponce de Leon, A., Duppre, N. C., Hacker, M. A., Nery, J. A., Sarno, E. N., and Penna, M. L. (2011). "Leprosy among patient contacts: a multilevel study of risk factors." *PLoS Negl Trop Dis* **5** (3): e1013.

Sassine, J., Xu, M., Sidiq, K., Emmins, R., Errington, J., and Daniel, R. (2017) Functional redundancy of division specific penicillin-binding proteins in *Bacillus subtilis*. *Mol Microbiol.* **106** (2): 304–318.

Saunders, B. M., and Britton, W. J. (2007). "Life and death in the granuloma: immunopathology of tuberculosis." *Immunol Cell Biol* **85** (2): 103-111.

Sauvage, E., Kerff, F., Terrak, M., Ayala, J. A., and Charlier, P. (2008). "The penicillin-binding proteins: structure and role in peptidoglycan biosynthesis." *FEMS Microbiol Rev* **32**(2): 234-258.

Sauvage, E., and Terrak, M. (2016). "Glycosyltransferases and Transpeptidases/Penicillin-Binding Proteins: Valuable Targets for New Antibacterials." *Antibiotics (Basel)* **5** (1).

Schleifer, K. H., and Kandler, O. (1972). "Peptidoglycan types of bacterial cell walls and their taxonomic implications." *Bacteriol Rev* **36** (4): 407-477.

Schmelcher, M., Donovan, D. M., and Loessner, M. J. (2012). Bacteriophage endolysins as novel antimicrobials. *Future microbiology*, *7*(10), 1147-71.

Schmitz, S., Hoffmann, A., Szekat, C., Rudd, B., and Bierbaum, G. (2006) The Lantibiotic Mersacidin Is an Autoinducing Peptide. *Applied and Environmental Microbiology*. **72** (11): 7270-7277.

Seibert, F. B. (1934). "The isolation and properties of the purified protein derivative of tuberculin." *Am Rev Tuberc* **30**: 713–720.

Shah, N. B., and Duncan, T. M. (2014) Bio-layer Interferometry for Measuring Kinetics of Protein-protein Interactions and Allosteric Ligand Effects. *Journal of Visualized Experiments : JoVE*. (84): 51383.

Shaikh, S., Fatima, J., Shakil, S., Rizvi, S. M. D., and Kamal, M. A. (2015) Antibiotic resistance and extended spectrum beta-lactamases: Types, epidemiology and treatment. *Saudi Journal of Biological Sciences*. **22** (1): 90-101.

Sham, L. T., Butler, E. K., Lebar, M. D., Kahne, D., Bernhardt, T. G., and Ruiz, N. (2014). "Bacterial cell wall. MurJ is the flippase of lipid-linked precursors for peptidoglycan biogenesis." *Science* **345**(6193): 220-222.

Sharma, S. K., Vashishtha, R., Chauhan, L. S., Sreenivas, V., and Seth, D. (2017). "Comparison of TST and IGRA in Diagnosis of Latent Tuberculosis Infection in a High TB-Burden Setting." *PLoS One* **12** (1): e0169539.

Shaw, W. V. (1983). "Chloramphenicol acetyltransferase: enzymology and molecular biology." *CRC Crit Rev Biochem* **14** (1): 1-46.

Sherpa, R. T., Reese, C. J., and Aliabadi, H. M. (2015) Application of iChip to Grow "Uncultivable" Microorganisms and its Impact on Antibiotic Discovery. *J Pharm Pharm Sci*. **18** (3): 303–315.

Shi, W., Zhang, X., Jiang, X., Yuan, H., Lee, J. S., Barry, C. E., 3rd, Wang, H., Zhang, W., and Zhang, Y. (2011). "Pyrazinamide inhibits trans-translation in *Mycobacterium tuberculosis*." *Science* **333** (6049): 1630-1632.

Shleeva, M. O., Bagramyan, K., Telkov, M. V., Mukamolova, G. V., Young, M., Kell, D. B., and Kaprelyants, A. S. (2002). "Formation and resuscitation of "non-culturable" cells of *Rhodococcus rhodochrous* and *Mycobacterium tuberculosis* in prolonged stationary phase." *Microbiology* **148** (Pt 5): 1581-1591.

- Simeone, R., Bobard, A., Lippmann, J., Bitter, W., Majlessi, L., Brosch, R., and Enninga, J.** (2012). "Phagosomal rupture by *Mycobacterium tuberculosis* results in toxicity and host cell death." *PLoS Pathog* **8** (2): e1002507.
- Simeone, R., Bottai, D., and Brosch, R.** (2009). "ESX/type VII secretion systems and their role in host-pathogen interaction." *Curr Opin Microbiol* **12** (1): 4-10.
- Singh, A., Goyal, V., and Goel, S.** (2016). "Sputum Collection and Disposal Perceptions and Practices Among Pulmonary Tuberculosis Patients from Northern India." *J Clin Diagn Res* **10** (12): LC16-LC18.
- Sivaramakrishnan, S. and de Montellano, P. R.** (2013). "The DosS-DosT/DosR *Mycobacterium* Sensor System." *Biosensors (Basel)* **3** (3): 259-282.
- Smeulders, M. J., Keer, J., Speight, R. A., and Williams, H. D.** (1999). "Adaptation of *Mycobacterium smegmatis* to stationary phase." *J Bacteriol* **181** (1): 270-283.
- Snapper, S. B., Melton, R. E., Mustafa, S., Kieser, T., and Jacobs, Jr., W. R.** (1990). "Isolation and characterization of efficient plasmid transformation mutants of *Mycobacterium smegmatis*." *Mol Microbiol* **4** (11): 1911-1919.
- Soetaerta, K., Rensb, C., Wanga X., De Bruynb, J., Lanéellec, M., Lavalc, F., Lemassuc, A., Dafféc, M., Bifanid, P., Fontaineb, V., and Lefèvre, P.** (2015) Increased Vancomycin Susceptibility in *Mycobacteria*: a New Approach To Identify Synergistic Activity against Multidrug-Resistant *Mycobacteria*. *Antimicrob. Agents Chemother.* **59** (8): 5057-5060.
- Sohaskey, C. D.** (2005). "Regulation of nitrate reductase activity in *Mycobacterium tuberculosis* by oxygen and nitric oxide." *Microbiology* **151** (Pt 11): 3803-3810.
- Somoskovi, A., Dormandy, J., Mayrer, A. R., Carter, M., Hooper, N. and Salfinger, M.** (2009). ""*Mycobacterium canettii*" isolated from a human immunodeficiency virus-positive patient: first case recognized in the United States." *J Clin Microbiol* **47** (1): 255-257.
- Sousa, E. H., Tuckerman, J. R., Gonzalez, G., and Gilles-Gonzalez, M. A.** (2007). "DosT and DevS are oxygen-switched kinases in *Mycobacterium tuberculosis*." *Protein Sci* **16** (8): 1708-1719.
- Spiro, R. G.** (1958). "The effect of N-acetylglucosamine and glucosamine on carbohydrate metabolism in rat liver slices." *J Biol Chem* **233** (3): 546-550.
- Spizizen, J.** (1958). "Transformation of Biochemically Deficient Strains of *Bacillus Subtilis* by Deoxyribonucleate." *Proc Natl Acad Sci U S A* **44** (10): 1072-1078.
- Spyropoulos, B.** (1988). "Tay-Sachs carriers and tuberculosis resistance." *Nature* **331**(6158): 666.
- Stahl, D. A. and J. W. Urbance (1990). "The division between fast- and slow-growing species corresponds to natural relationships among the *mycobacteria*." *J Bacteriol* **172** (1): 116-124.

Stenger, S. (2005). "Immunological control of tuberculosis: role of tumour necrosis factor and more." *Ann Rheum Dis* **64 Suppl 4**: iv24-28.

Strobel, W., Moll, A., Kiekebusch, D., Klein, K. E., and Thanbichler, M. (2014). "Function and localization dynamics of bifunctional penicillin-binding proteins in *Caulobacter crescentus*." *J Bacteriol* **196** (8): 1627-1639.

Studier, F. W. and Moffatt, B. A. (1986). "Use of bacteriophage T7 RNA polymerase to direct selective high-level expression of cloned genes." *J Mol Biol* **189** (1): 113-130.

Su, H. W., Zhu, J. H., Li, H., Cai, R. J., Ealand, C., Wang, X., Chen, Y. X., Kayani, M. U., Zhu, T. F., Moradigaravand, D., Huang, H., Kana, B. D., and Javid, B. (2016). "The essential mycobacterial amidotransferase GatCAB is a modulator of specific translational fidelity." *Nat Microbiol* **1** (11): 16147.

Sultana, A., and Lee, J. E. (2015). Measuring protein-protein and protein-nucleic Acid interactions by biolayer interferometry. *Curr Protoc Protein Sci.* **79**: 19.25.1–19.2526.

Swoboda, J. G., Campbell, J., Meredith, T. C., and Walker, S. (2010) Wall Teichoic Acid Function, Biosynthesis, and Inhibition. *Chembiochem: a European journal of chemical biology.* **11** (1): 35-45.

Takeda, K. and Akira, S. (2005). "Toll-like receptors in innate immunity." *Int Immunol* **17** (1): 1-14.

Tan, S. Y. and Tatsumura, Y. (2015). "Alexander Fleming (1881-1955): Discoverer of penicillin." *Singapore Med J* **56** (7): 366-367.

Tang, Y., Zeng, X., and Liang, J. (2010) Surface Plasmon Resonance: An Introduction to a Surface Spectroscopy Technique. *Journal of chemical education.* **87** (7): 742-746.

Tao, W., Lee, M. H., Wu, J., Kim, N. H., Kim, J. C., Chung, E., Hwang, E. C., and Lee, S. W. (2012). "Inactivation of chloramphenicol and florfenicol by a novel chloramphenicol hydrolase." *Appl Environ Microbiol* **78** (17): 6295-6301.

Telkov, M. V., Demina, G. R., Voloshin, S. A., Salina, E. G., Dudik, T. V., Stekhanova, T. N., Mukamolova, G. V., Kazaryan, K. A., Goncharenko, A. V., Young, M. and Kaprelyants, A. S. (2006). "Proteins of the Rpf (resuscitation promoting factor) family are peptidoglycan hydrolases." *Biochemistry (Mosc)* **71** (4): 414-422.

Teo, A. C. and Roper, D. I. (2015). "Core Steps of Membrane-Bound Peptidoglycan Biosynthesis: Recent Advances, Insight and Opportunities." *Antibiotics (Basel)* **4** (4): 495-520.

Thakur, M., Chakraborti, P. K. (2008). Ability of PknA, a mycobacterial eukaryotic-type serine/threonine kinase, to transphosphorylate MurD, a ligase involved in the process of peptidoglycan biosynthesis. *Biochem J.* **415** (1): 27-33.

Tipper, D. J. and Strominger, J. L. (1965). "Mechanism of action of penicillins: a proposal based on their structural similarity to acyl-D-alanyl-D-alanine." *Proc Natl Acad Sci U S A* **54** (4): 1133-1141.

Toke, O. (2005) Antimicrobial peptides: new candidates in the fight against bacterial infections. *Biopolymers*. **80** (6): 717–735.

Touz, E. T. and Mengin-Lecreulx, D. (2008). "Undecaprenyl Phosphate Synthesis." *EcoSal Plus* **3** (1).

Tseng, S. T., Tai, C. H., Li, C. R., Lin, C. F., and Shi, Z. Y. (2015). "The mutations of *katG* and *inhA* genes of isoniazid-resistant *Mycobacterium tuberculosis* isolates in Taiwan." *J Microbiol Immunol Infect* **48** (3): 249-255.

Tuckerman, J. R., Gonzalez, G., Dioum, E. M., and Gilles-Gonzalez, M. A. (2002). "Ligand and oxidation-state specific regulation of the heme-based oxygen sensor FixL from *Sinorhizobium meliloti*." *Biochemistry* **41** (19): 6170-6177.

Tudo, G., Laing, K., Mitchison, D. A., Butcher, P. D. and Waddell, S. J. (2010). "Examining the basis of isoniazid tolerance in nonreplicating *Mycobacterium tuberculosis* using transcriptional profiling." *Future Med Chem* **2** (8): 1371-1383.

Turapov, O., Loraine, J., Jenkins, C. H., Barthe, P., McFeely, D., Forti, F., Ghisotti, D., Heseck, D., Lee, M., Bottrill, A. R., Vollmer, W., Mobashery, S., Cohen-Gonsaud, M., and Mukamolova, G. V. (2015). "The external PASTA domain of the essential serine/threonine protein kinase PknB regulates mycobacterial growth." *Open Biol* **5** (7): 150025.

van der Wel, N., Hava, D., Houben, D., Fluitsma, D., van Zon, M., Pierson, J., Brenner, M., and Peters, P. J. (2007). "*M. tuberculosis* and *M. leprae* translocate from the phagolysosome to the cytosol in myeloid cells." *Cell* **129** (7): 1287-1298.

Vayr, F., Martin-Blondel, G., Savall, F., Soulat, J. M., Deffontaines, G., and Herin, F. (2018). "Occupational exposure to human *Mycobacterium bovis* infection: A systematic review." *PLoS Negl Trop Dis* **12** (1): e0006208.

Vera-Cabrera, L., Escalante-Fuentes, W., Ocampo-Garza, S. S., Ocampo-Candiani, J., Molina-Torres, C. A., Avanzi, C., Benjak, A., Busso, P., Singh, P., and Cole, S. T. (2015). "*Mycobacterium lepromatosis* Infections in Nuevo Leon, Mexico." *J Clin Microbiol* **53** (6): 1945-1946.

Vergne, I., Chua, J., and Deretic, V. (2003). "Tuberculosis toxin blocking phagosome maturation inhibits a novel Ca²⁺/calmodulin-PI3K hVPS34 cascade." *J Exp Med* **198** (4): 653-659.

Vermeulen, M. W., Gray, and G. R. (1984) Processing of *Bacillus subtilis* peptidoglycan by a mouse macrophage cell line. *Infection and Immunity*. **46** (2):476-483.

- Vollmer, W.** (2008). "Structural variation in the glycan strands of bacterial peptidoglycan." *FEMS Microbiol Rev* **32** (2): 287-306.
- Vollmer, W., Blanot, D., and de Pedro, M. A.** (2008). "Peptidoglycan structure and architecture." *FEMS Microbiol Rev* **32** (2): 149-167.
- Vollmer, W. and Holtje, J. V.** (2004). "The architecture of the murein (peptidoglycan) in gram-negative bacteria: vertical scaffold or horizontal layer(s)?" *J Bacteriol* **186** (18): 5978-5987.
- Vollmer, W., Joris, B., Charlier, P. and Foster, S.** (2008). "Bacterial peptidoglycan (murein) hydrolases." *FEMS Microbiol Rev* **32** (2): 259-286.
- Vollmer, W. and Tomasz, A.** (2000). "The *pgdA* gene encodes for a peptidoglycan N-acetylglucosamine deacetylase in *Streptococcus pneumoniae*." *J Biol Chem* **275** (27): 20496-20501.
- von Bargen, K., Wohlmann, J., Taylor, G. A., Utermohlen, O., and Haas, A.** (2011). "Nitric oxide-mediated intracellular growth restriction of pathogenic *Rhodococcus equi* can be prevented by iron." *Infect Immun* **79** (5): 2098-2111.
- Vong, K. and Auclair, K.** (2012). "Understanding and overcoming aminoglycoside resistance caused by N-6'-acetyltransferase." *Medchemcomm* **3** (4): 397-407.
- Voskuil, M. I., Bartek, I. L., Visconti, K., and Schoolnik, G. K.** (2011). "The response of mycobacterium tuberculosis to reactive oxygen and nitrogen species." *Front Microbiol* **2**: 105.
- Voskuil, M. I., Schnappinger, D., Visconti, K. C., Harrell, M. I., Dolganov, G. M., Sherman, D. R., and Schoolnik, G. K.** (2003). "Inhibition of respiration by nitric oxide induces a *Mycobacterium tuberculosis* dormancy program." *J Exp Med* **198** (5): 705-713.
- Walsh, C. T.** (1989). "Enzymes in the D-alanine branch of bacterial cell wall peptidoglycan assembly." *J Biol Chem* **264** (5): 2393-2396.
- Wang, F., Zhou, H., Olademehin, O. P., Kim, S. J., and Tao, P.** (2018) Insights into Key Interactions between Vancomycin and Bacterial Cell Wall Structures. *ACS Omega*. **3** (1): 37-45.
- Waxman, D. J. and Strominger, J. L.** (1983). "Penicillin-binding proteins and the mechanism of action of beta-lactam antibiotics." *Annu Rev Biochem* **52**: 825-869.
- Wayne, L. G.** (1994). "Dormancy of *Mycobacterium tuberculosis* and latency of disease." *Eur J Clin Microbiol Infect Dis* **13** (11): 908-914.
- Wayne, L. G. and Lin, K. Y.** (1982). "Glyoxylate metabolism and adaptation of *Mycobacterium tuberculosis* to survival under anaerobic conditions." *Infect Immun* **37** (3): 1042-1049.

Wayne, L. G. and Sohaskey, C. D. (2001). "Nonreplicating persistence of mycobacterium tuberculosis." *Annu Rev Microbiol* **55**: 139-163.

Weigert, C. (1875). "Staining of bacteria with aniline dyes." University of Wroclaw.

Weiss, G. and Schaible, U. E. (2015). "Macrophage defense mechanisms against intracellular bacteria." *Immunol Rev* **264** (1): 182-203.

Welin, A., Winberg, M. E., Abdalla, H., Sarndahl, E., Rasmusson, B., Stendahl, O., and Lerm, M. (2008). "Incorporation of Mycobacterium tuberculosis lipoarabinomannan into macrophage membrane rafts is a prerequisite for the phagosomal maturation block." *Infect Immun* **76** (7): 2882-2887.

Wells, C. D., Cegielski, J. P., Nelson, L. J., Laserson, K. F., Holtz, T. H., Finlay, A., Castro, K. G., and Weyer, K. (2007). "HIV infection and multidrug-resistant tuberculosis: the perfect storm." *J Infect Dis* **196 Suppl 1**: S86-107.

WHO (2011). Global Tuberculosis Report 2011.

WHO (2012). Global Tuberculosis Report 2012.

Wiest, D. B., Cochran, J. B., and Tecklenburg, F. W. (2012). "Chloramphenicol toxicity revisited: a 12-year-old patient with a brain abscess." *J Pediatr Pharmacol Ther* **17** (2): 182-188.

Wiles, S., Ferguson, K., Stefanidou, M., Young, D. B., and Robertson, B. D. (2005). Alternative luciferase for monitoring bacterial cells under adverse conditions. *Appl Environ Microbiol* **71** (7): 3427-3432.

Williams, K. J. (2009). "The introduction of 'chemotherapy' using arsphenamine - the first magic bullet." *J R Soc Med* **102** (8): 343-348.

Wohnig, S., Spork, A. P., Koppermann, S., Mieskes, G., Gisch, N., Jahn, R., and Ducho, C. (2016). "Total Synthesis of Dansylated Park's Nucleotide for High-Throughput *MraY* Assays." *Chemistry* **22** (49): 17813-17819.

Woodring, J. H., Vandiviere, H. M., Fried, A. M., Dillon, M. L., Williams T. D., and Melvin I. G. (1986). "Update: the radiographic features of pulmonary tuberculosis." *AJR Am J Roentgenol* **146** (3): 497-506.

Woods, C. M., Hooper, D. N., Ooi, E. H., Tan L. W., and Carney, A. S. (2011). "Human lysozyme has fungicidal activity against nasal fungi." *Am J Rhinol Allergy* **25** (4): 236-240.

Wu, H., Cao, D., Liu, T., Zhao, J., Hu X., and Li, N. (2015). "Purification and Characterization of Recombinant Human Lysozyme from Eggs of Transgenic Chickens." *PLoS One* **10** (12): e0146032.

Yamada, K., Takado, Y., Kato, Y. S., Yamada, Y., Ishiguro H., and Wakamatsu, N. (2013). "Characterization of the mutant beta-subunit of beta-hexosaminidase for

dimer formation responsible for the adult form of Sandhoff disease with the motor neuron disease phenotype." *J Biochem* **153** (1): 111-119.

Yang, H., Kruh-Garcia, N. A., and Dobos, K. M. (2012). "Purified protein derivatives of tuberculin--past, present, and future." *FEMS Immunol Med Microbiol* **66** (3): 273-280.

Yang, B., Wang, J., Tang, B., Liu, Y., Guo, C., Yang, P., Yu, T., Li, R., Zhao, J., Zhang, L., Dai, Y., and Li, N. (2011). "Characterization of bioactive recombinant human lysozyme expressed in milk of cloned transgenic cattle." *PLoS One* **6** (3): e17593.

Yazaki, M., Farrell, S. A., and Benson, M. D. (2003). "A novel lysozyme mutation Phe57Ile associated with hereditary renal amyloidosis." *Kidney Int* **63** (5): 1652-1657.

Yeats, C., Finn, R. D., and Bateman, A. (2002). "The PASTA domain: a beta-lactam-binding domain." *Trends Biochem Sci* **27** (9): 438.

Yount, N. Y. and Yeaman, M. R. (2013). "Peptide antimicrobials: cell wall as a bacterial target." *Ann N Y Acad Sci* **1277**: 127-138.

Zhang, X., Jiang, A., Yu, H., Xiong, Y., Zhou, G., Qin, M., Dou, J., and Wang, J. (2016). "Human Lysozyme Synergistically Enhances Bactericidal Dynamics and Lowers the Resistant Mutant Prevention Concentration for Metronidazole to *Helicobacter pylori* by Increasing Cell Permeability." *Molecules* **21** (11).

Zhang, Y., Wade, M. M., Scorpio, A., Zhang, H., and Sun, Z. (2003). "Mode of action of pyrazinamide: disruption of *Mycobacterium tuberculosis* membrane transport and energetics by pyrazinoic acid." *J Antimicrob Chemother* **52** (5): 790-795.

Zhang, Y. and Yew, W. W. (2009). "Mechanisms of drug resistance in *Mycobacterium tuberculosis*." *Int J Tuberc Lung Dis* **13** (11): 1320-1330.

Zimmerli, S., Majeed, M., Gustavsson, M., Stendahl, O., Sanan, D. A., and Ernst, J. D. (1996). "Phagosome-lysosome fusion is a calcium-independent event in macrophages." *J Cell Biol* **13** (1-2): 49-61.

Appendix 1

Plasmids and constructed vectors utilising acquired mycobacterial genes optimised for expression in *E. coli* mentioned in chapter 5.

A1.1 Plasmids

A1.1.1 pUC57

The standard plasmid utilised for synthesised gene amplification within *E. coli*. The 2710 base pair vector contained an Ampicillin resistance gene and a multiple cloning site (MCS). Restriction enzymes BsaI/NdeI and XhoI were used to insert synthesised genes. Genes synthesized by GenScript were acquired within this vector. The Vector map of pUC57 is presented in figure A1.1.

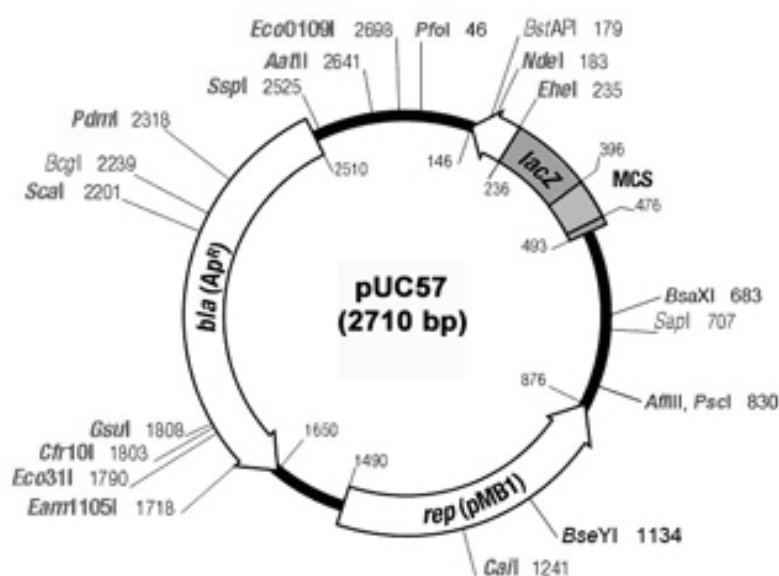


Figure A1.1 The vector map of pUC57. The plasmid contained an Ampicillin resistance gene, a lacZ operon and a multiple cloning site (MCS). Modified from www.genscript.com

A1.1.2 pCOLD

The pCOLD plasmid (4392 bp) was specifically applied to aid in expression of difficult to solubilise, low yield proteins. The vector contained an ampicillin resistance gene, a cold shock protein A (cspA) promoter, a translation enhancing element (TEE) and an N-terminal poly-histidine tag. The vector promoter cspA up-regulated downstream genes during cold-shock, which was an instant temperature decrease during incubation from 37°C to 15°C. The TEE was a five amino acid sequence (MNHKV) which enhances the translation of expressed proteins within *E. coli*. Incubation in cold conditions reduced expression of unwanted proteins, focusing expression of plasmid genes, increasing yield and solubility in comparison to standard strategies of *E. coli* expression. Restriction enzymes employed during this thesis on the pCOLD cloning/expression region were NdeI and XhoI. The vector map for pCOLD is exhibited in figure A1.2.

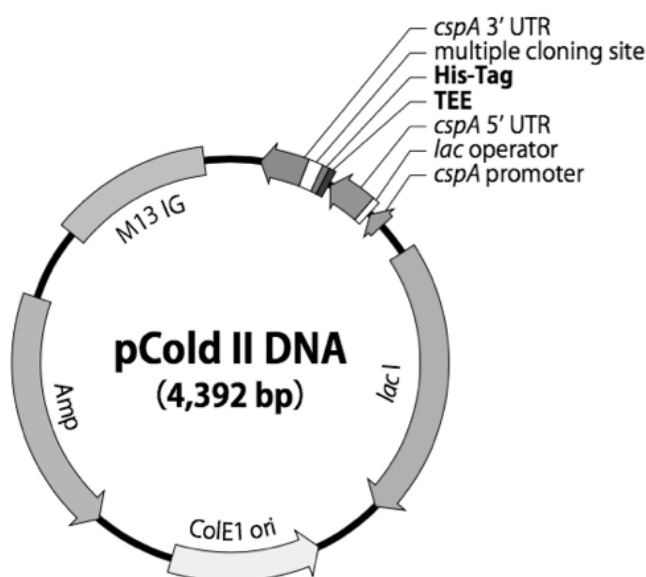


Figure A1.2 The vector map of pCOLD. The plasmid contained an Ampicillin resistance gene, a multiple cloning site, an N-terminal poly-histidine tag sequence, a lac operator, a translation enhanced element (TEE) and a cold shock cspA promoter. Modified from www.clontech.com

A1.1.3 pET21b

The T7 expression vector pET21b was 5442 bp containing a lac operator, an ampicillin resistance gene, a N-terminal T7 tag sequence and an optional C-terminal poly-histidine tag. Restriction enzymes utilised within the cloning/expression region of pET21b were NdeI and XhoI to excise the T7 tag. The vector map for pET21b is depicted in figure A1.3.

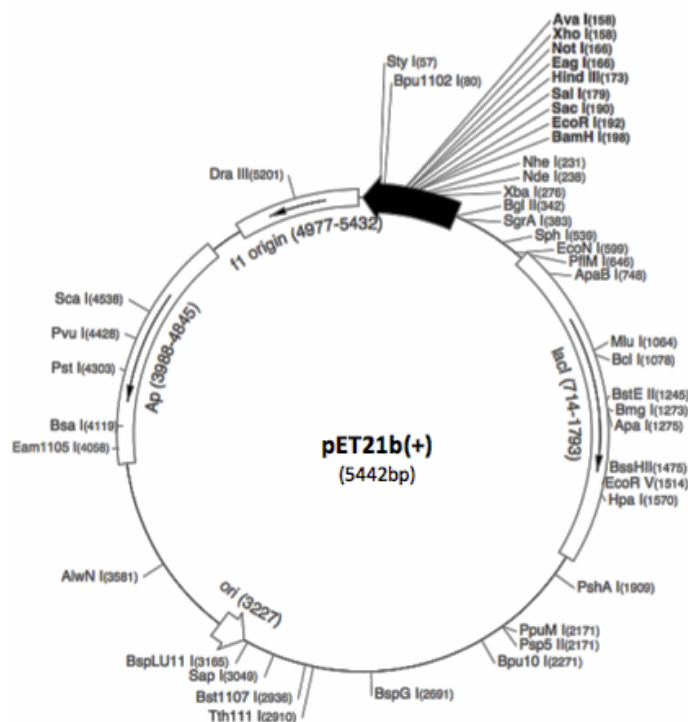


Figure A1.3 Vector map of pET21b. The expression plasmid contained an Ampicillin resistance gene, a multiple cloning site, a C-terminal poly-histidine tag sequence and a lac operator. Adapted from www.merckmillipore.com

A1.2 Gene plasmid constructs

Construct	Description	Selection	Affinity tag	Source
pUC57: <i>murA</i>	<i>M. leprae murA</i> (full length) in pUC57 vector Optimised for expression in <i>E. coli</i>	Ampicillin	Untagged	GenScript
pUC57: <i>murC</i>	<i>M. leprae murC</i> (full length) in pUC57 vector Optimised for expression in <i>E. coli</i>	Ampicillin	Untagged	GenScript

Table A1.1 Gene constructs obtained in this project

Construct	Description	Selection	Affinity tag	Source
pCOLD: <i>murA</i> N-term	<i>M. leprae murA</i> (full length) in pCOLD vector	Ampicillin	TEV-cleavable N-term 6-His	Cloned for this project
pCOLD: <i>murA</i> C-term	<i>M. leprae murA</i> (full length) in pCOLD vector	Ampicillin	TEV-cleavable C-term 6-His	Cloned for this project
pCOLD: <i>murA</i> (mutant) N-term	<i>M. leprae murA</i> D118C (full length) in pCOLD vector	Ampicillin	TEV-cleavable N-term 6-His	Cloned for this project
pCOLD: <i>murA</i> (Mutant) C-term	<i>M. leprae murA</i> D118C (full length) in pCOLD vector	Ampicillin	TEV-cleavable C-term 6-His	Cloned for this project
pCOLD: <i>murC</i> N-term	<i>M. leprae murC</i> (full length) in pCOLD vector	Ampicillin	TEV-cleavable N-term 6-His	Cloned for this project
pCOLD: <i>murC</i> C-term	<i>M. leprae murC</i> (full length) in pCOLD vector	Ampicillin	TEV-cleavable C-term 6-His	Cloned for this project
pET21b: <i>ponA1</i>	<i>M. tuberculosis ponA1</i> (full length) in pET21b vector	Ampicillin	TEV-cleavable C-term 6-His	Cloned for this project
pET21b: <i>ponA2</i>	<i>M. tuberculosis ponA2</i> (full length) in pET21b vector	Ampicillin	TEV-cleavable C-term 6-His	Cloned for this project

Table A1.2 Gene constructs created in this project

Appendix 2

Mass spectrometric analysis of synthesised peptidoglycan precursors, generated in the formation of biotinylated N-acetylated Lipid II (DAP) and biotinylated N-glycolylated Lipid II (DAP) in Chapter 4.

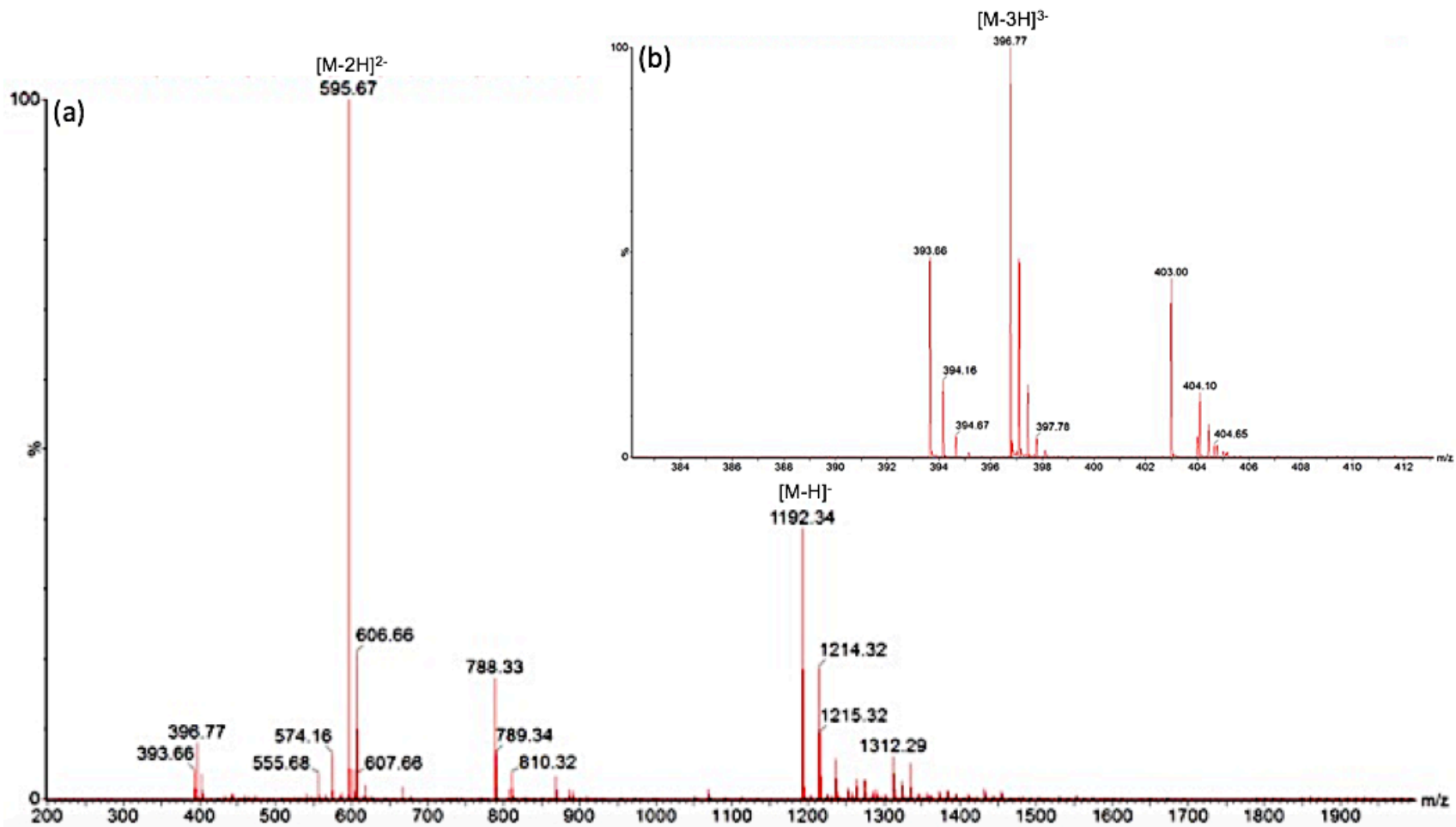


Figure A2.1: Negative ion mass spectra of synthesized UDP-MurNAc-pentapeptide DAP. (a): mass spectra with $[M-H]^{-}$ (observed 1192.34, expected 1192.33) and $[M-2H]^{2-}$ (observed 595.67, expected 595.66). (b): Zoomed in view of $[M-3H]^{3-}$ (observed 396.77, expected 396.77) (deconvoluted by MassLynx™ software (Waters, USA)).

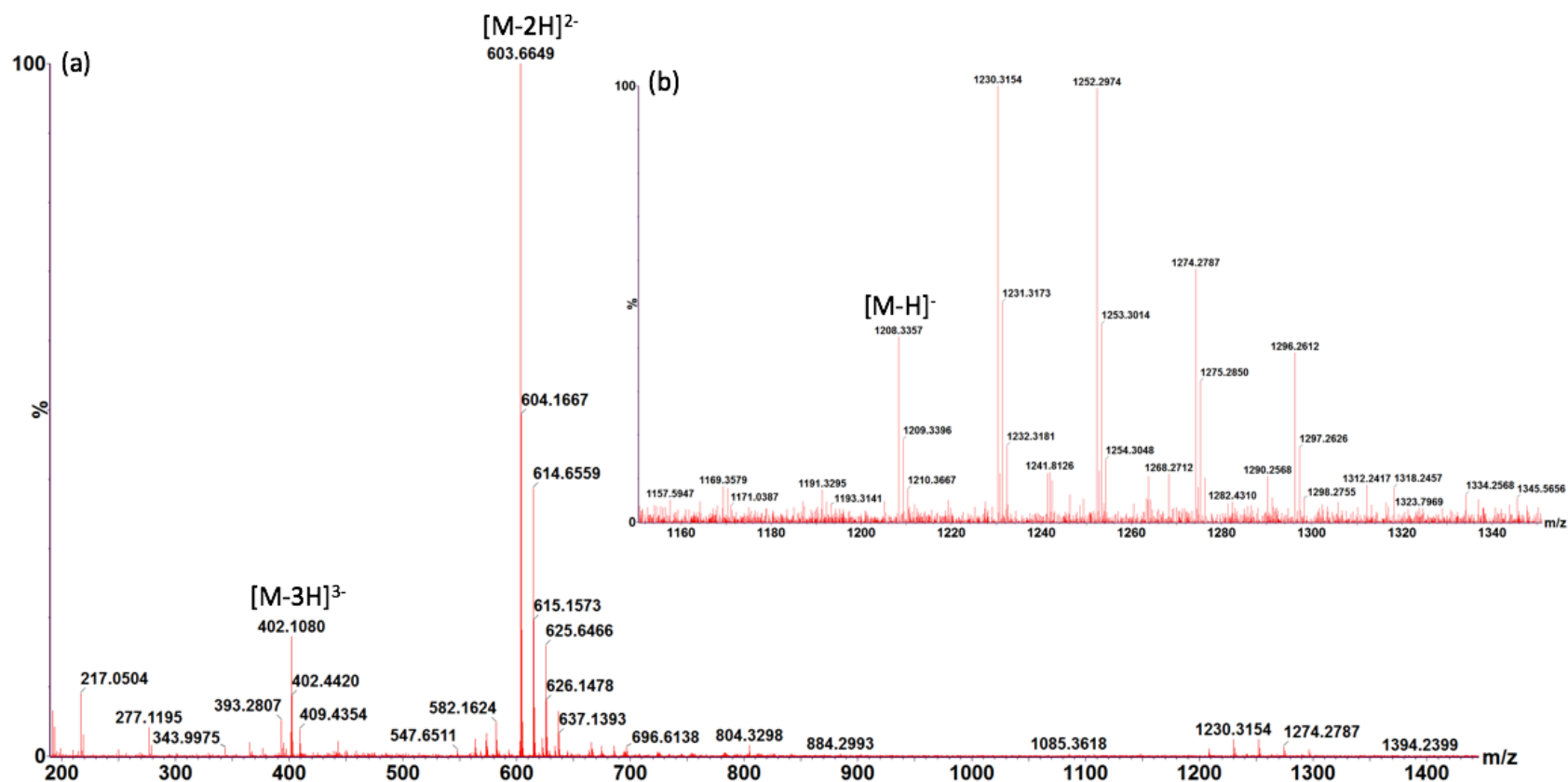


Figure A2.2: Negative ion mass spectra of synthesized UDP-MurNGlyc-pentapeptide DAP. (a): mass spectra with $[M-2H]^{2-}$ (observed 603.66, expected 603.66) and $[M-3H]^{3-}$ (observed 402.10, expected 402.10). (b): Zoomed in view of $[M-H]^{-}$ (observed 1208.33 expected 1208.32) (deconvoluted by MassLynx™ software (Waters, USA)).

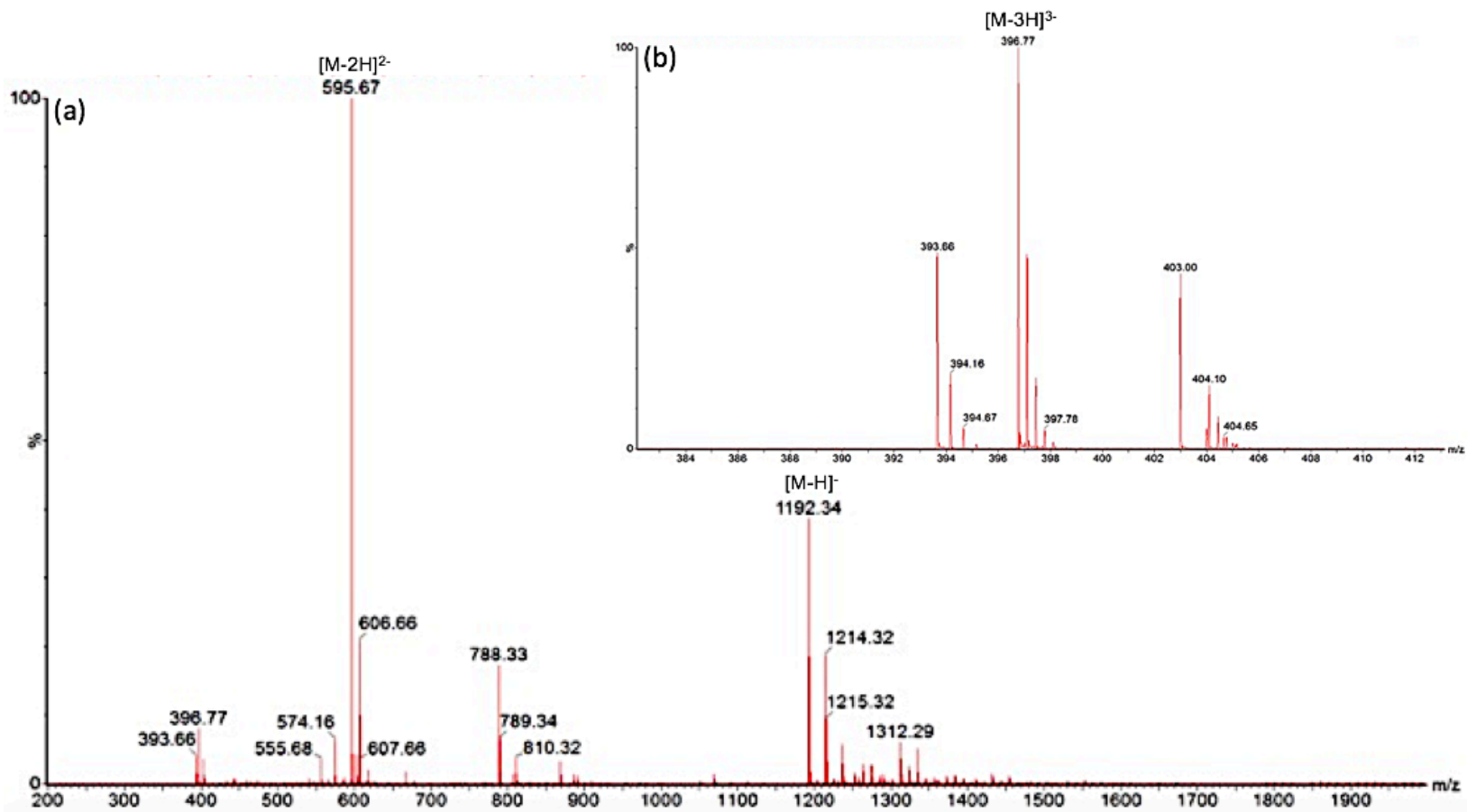


Figure A2.3: Negative ion mass spectra of unlabelled UDP-MurNAc-pentapeptide DAP. (a): mass spectra with $[M-H]^-$ (observed 1192.34, expected 1192.33) and $[M-2H]^{2-}$ (observed 595.67, expected 595.66). (b): Zoomed in view of $[M-3H]^{3-}$ (observed 396.77, expected 396.77) (deconvoluted by MassLynx™ software (Waters, USA)).

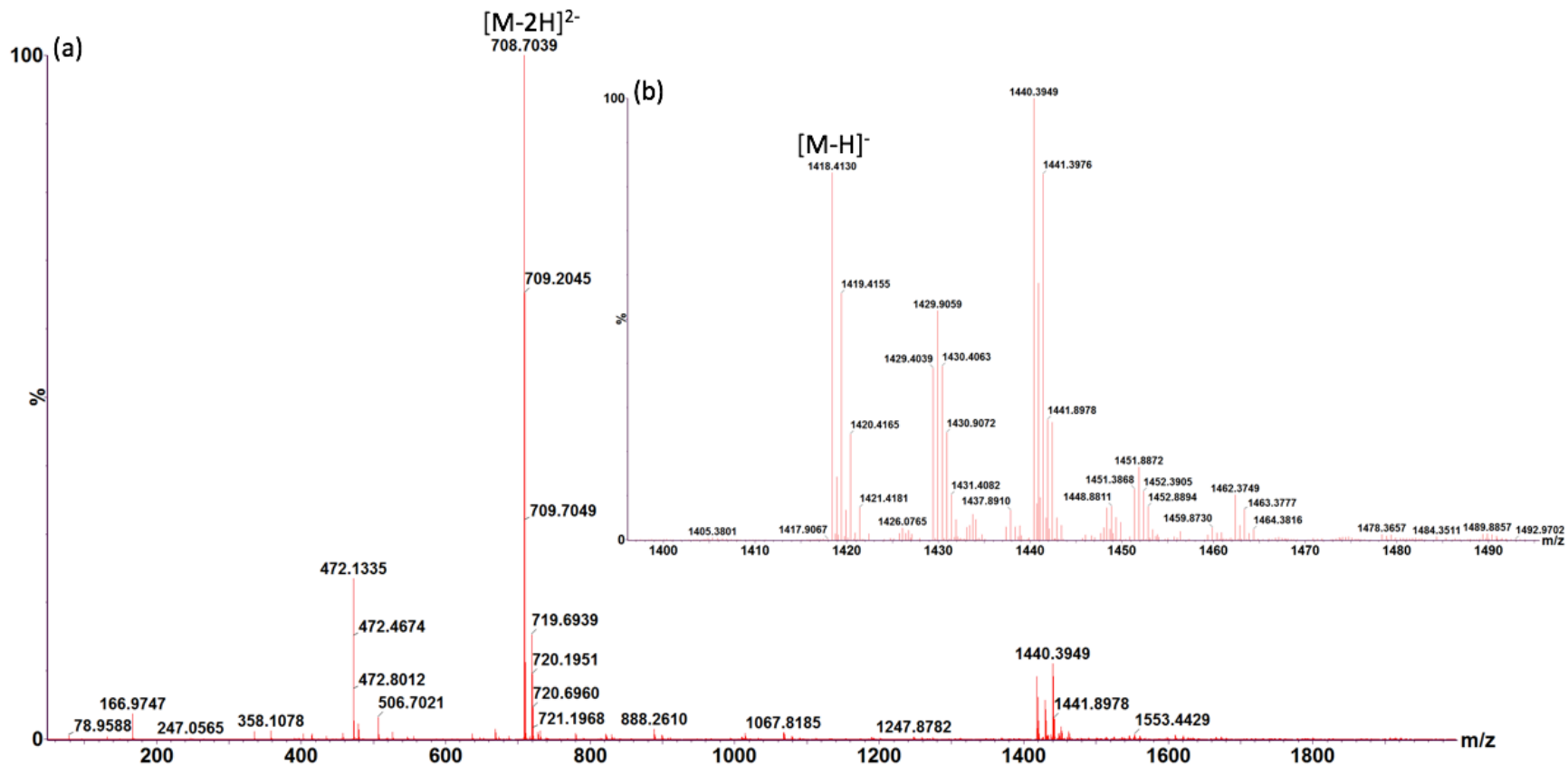


Figure A2.4: Negative ion mass spectra of biotinylated UDP-MurNAc-pentapeptide DAP. (a): mass spectra with $[M-2H]^{2-}$ (observed 708.70, expected 708.70). (b): Zoomed in view of $[M-H]^-$ (observed 1418.41, expected 1418.41) (deconvoluted by MassLynx™ software (Waters, USA)).

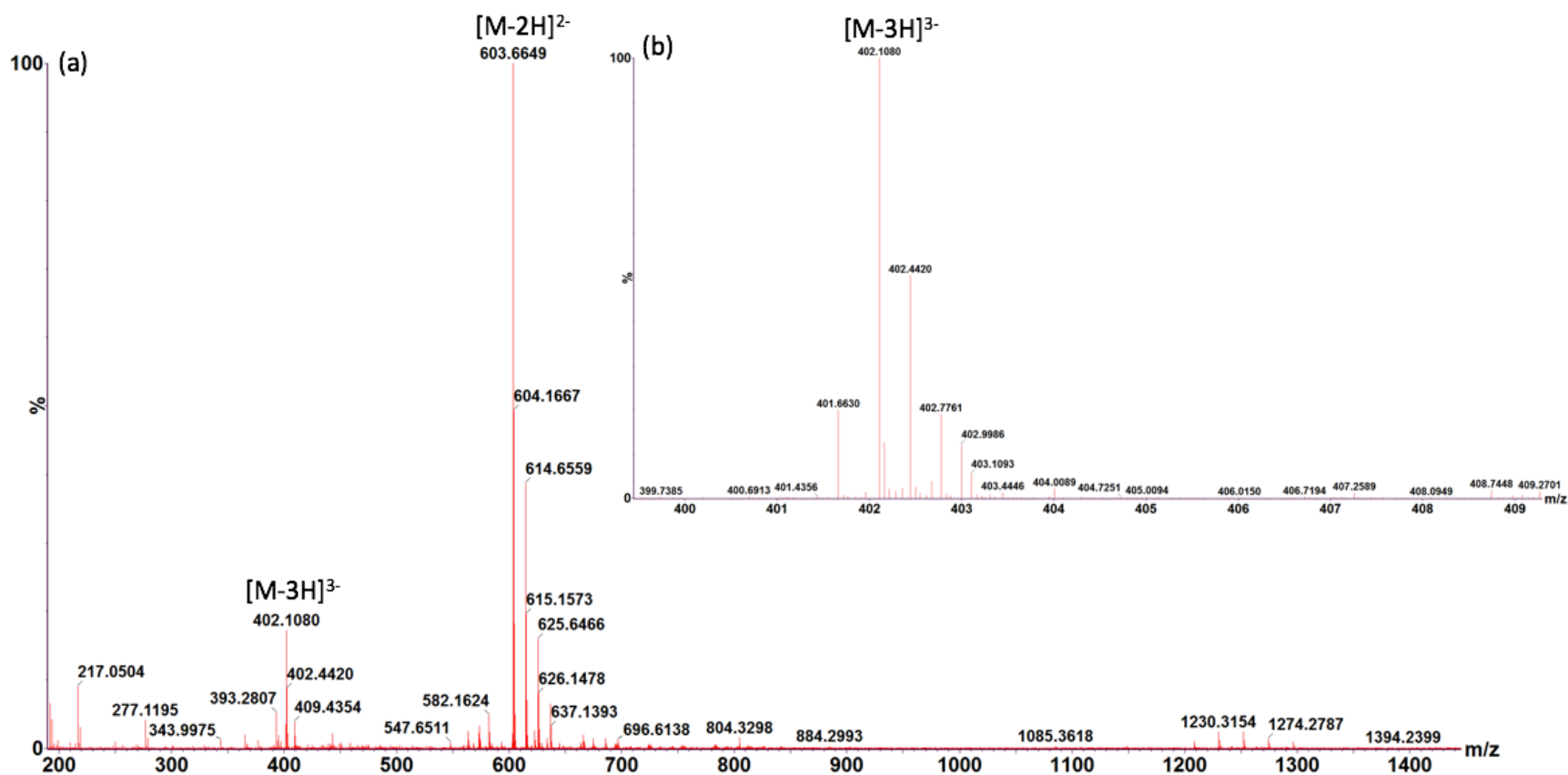


Figure A2.5: Negative ion mass spectra of unlabelled UDP-MurNGlyc-pentapeptide DAP. (a): mass spectra with $[M-2H]^{2-}$ (observed 603.66, expected 603.66) and $[M-3H]^{3-}$ (observed 402.10, expected 402.10). (b): Zoomed in view of $[M-3H]^{3-}$ (deconvoluted by MassLynx™ software (Waters, USA)).

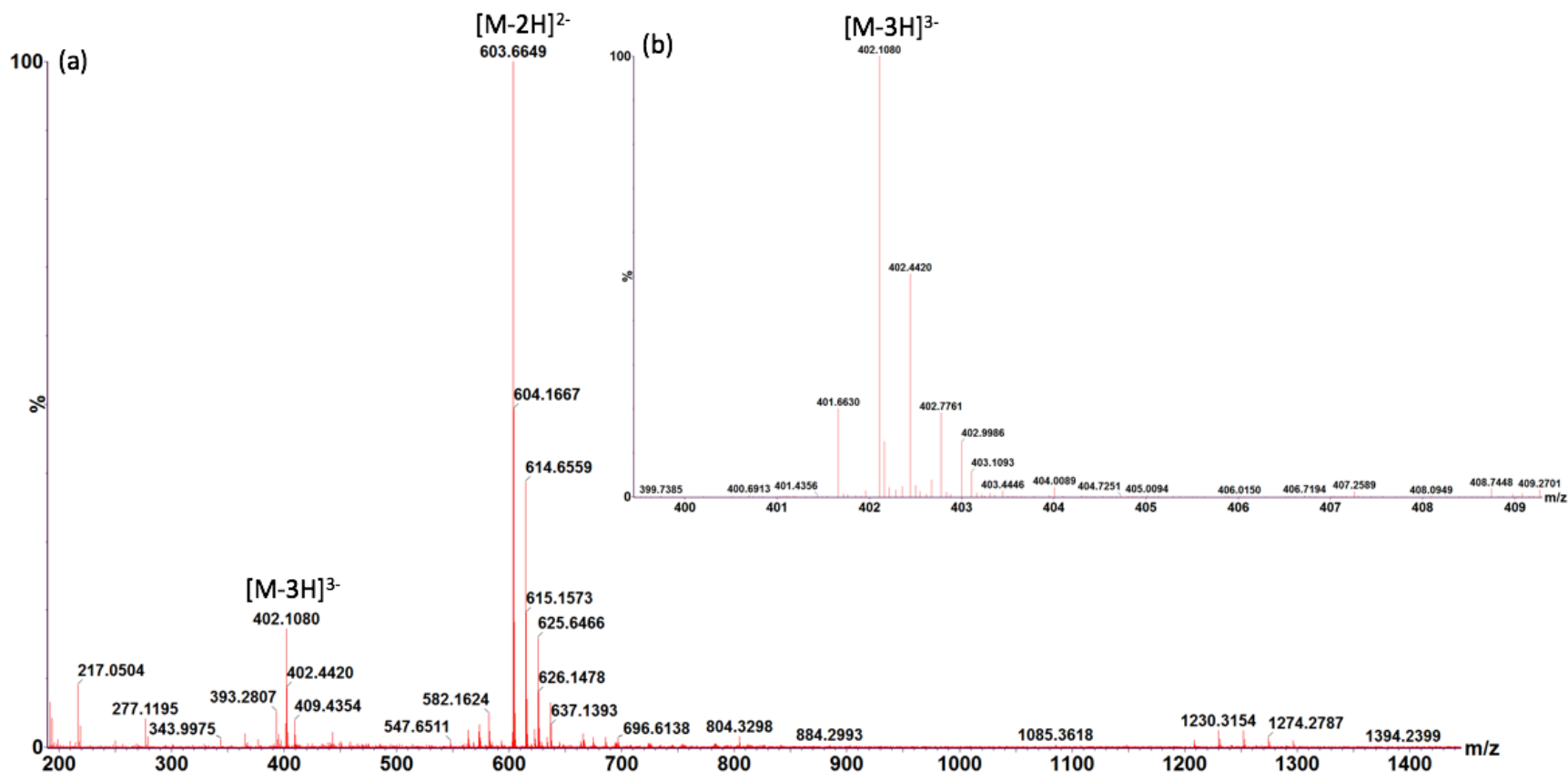


Figure A2.6: Negative ion mass spectra of biotinylated UDP-MurNGlyc-pentapeptide DAP. (a): mass spectra with $[M-2H]^{2-}$ (observed 603.66, expected 603.66) and $[M-3H]^{3-}$ (observed 402.10, expected 402.10). (b): Zoomed in view of $[M-3H]^{3-}$ (deconvoluted by MassLynx™ software (Waters, USA)).

TOF MS ES-
3.64e7

TOF MS ES-
1.02e5

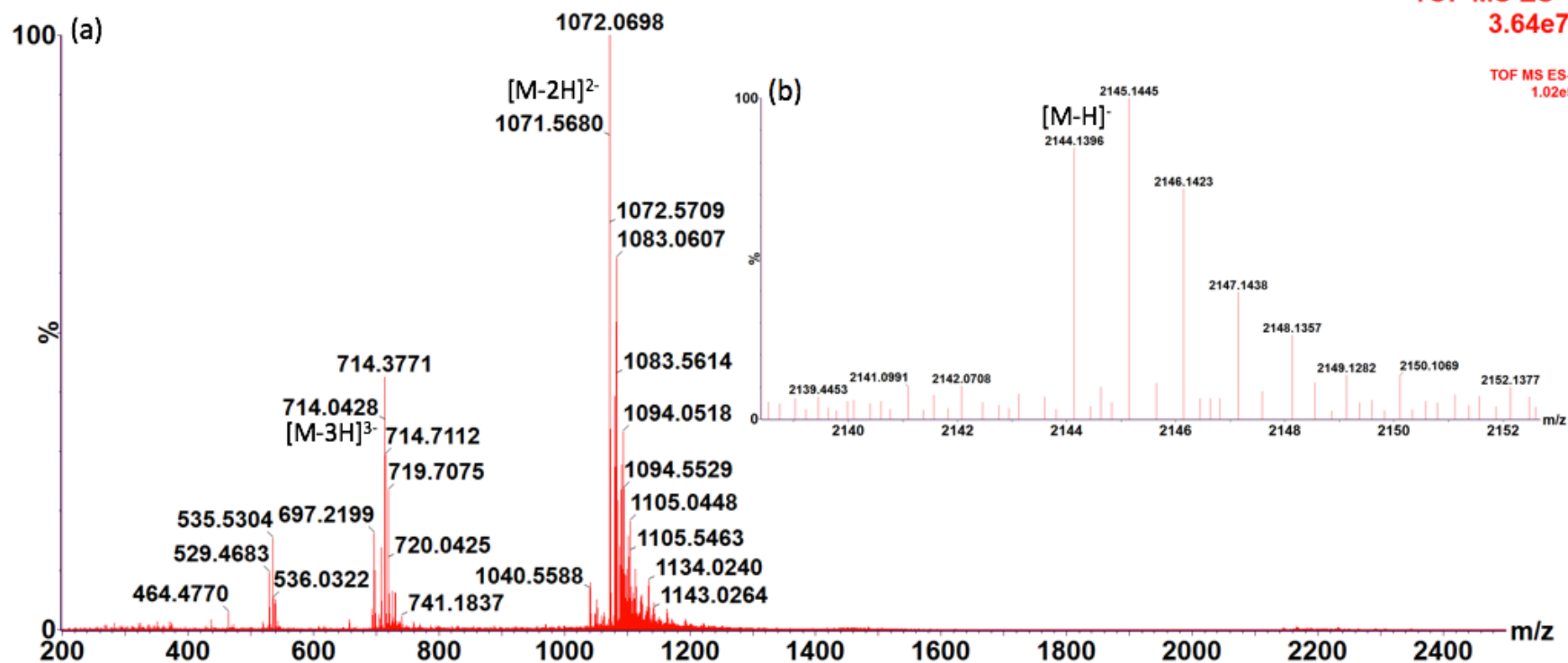


Figure A2.7: Negative ion mass spectra of biotinylated N-Acetylated Lipid II DAP. (a): mass spectra with [M-2H]²⁻ (observed 1071.56, expected 1071.56) and [M-3H]³⁻ (observed 714.04, expected 714.04). (b): Zoomed in view of [M-H]⁻ (observed 2144.13, expected 2144.13) (deconvoluted by MassLynx™ software (Waters, USA)).

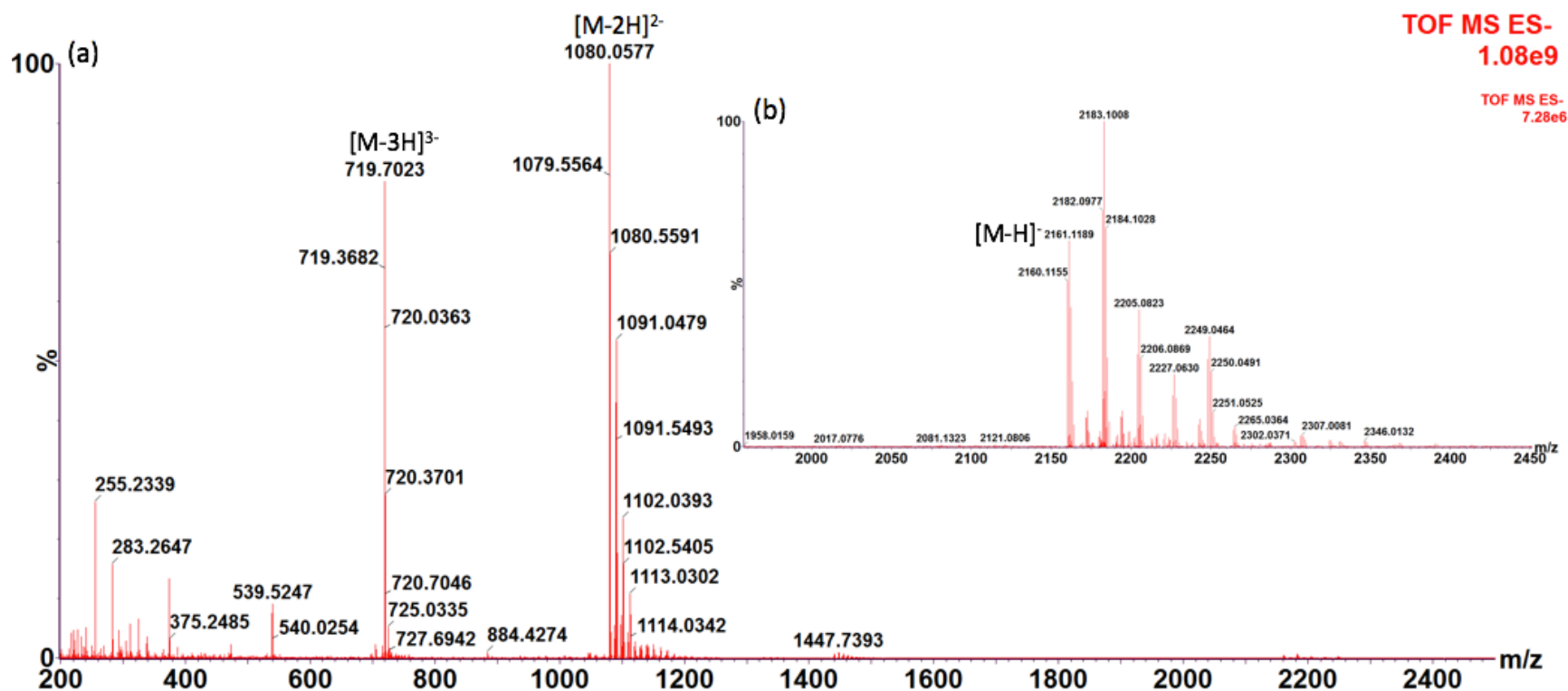


Figure A2.8: Negative ion mass spectra of biotinylated N-Glycolylated Lipid II DAP. (a): mass spectra with $[M-2H]^{2-}$ (observed 1080.05, expected 1080.05) and $[M-3H]^{3-}$ (observed 719.70, expected 719.70). (b): Zoomed in view of $[M-H]^{-}$ (observed 2161.11, expected 2161.11) (deconvoluted by MassLynx™ software (Waters, USA)).

Appendix 3

Mass spectrometric analysis of potential peptidoglycan intermediate accumulated elutions, isolated by size exclusion chromatography and ion exchange chromatography from chapter 6.

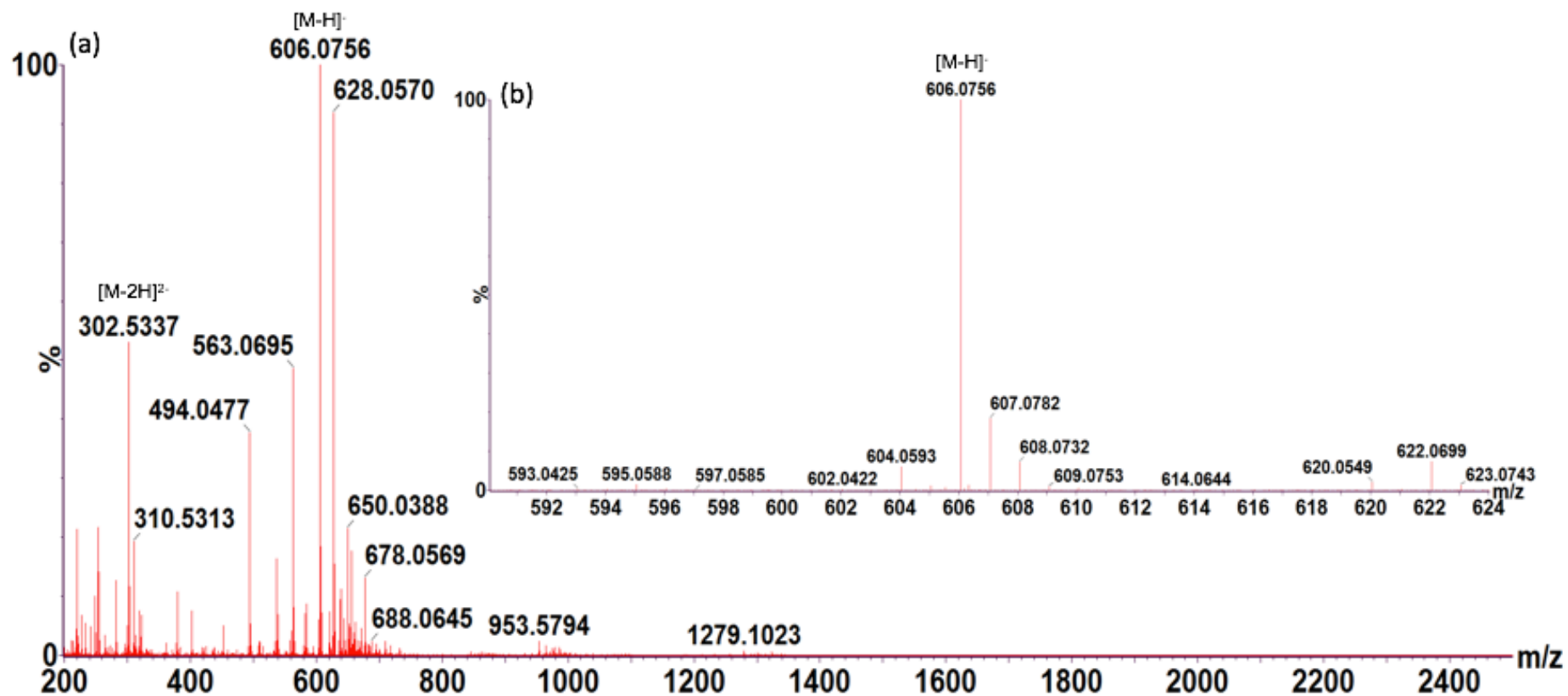


Figure A3.1: Negative ion mass spectrometry of peptidoglycan standard UDP-GlcNAc. (a): mass spectra with $[M-H]^-$ (observed 606.07, expected 606.07) and $[M-2H]^{2-}$ (observed 302.53, expected 302.53). (b): Zoomed in view of $[M-H]^-$ peak shown in (a). (deconvoluted by MassLynx™ software (Waters, USA)).

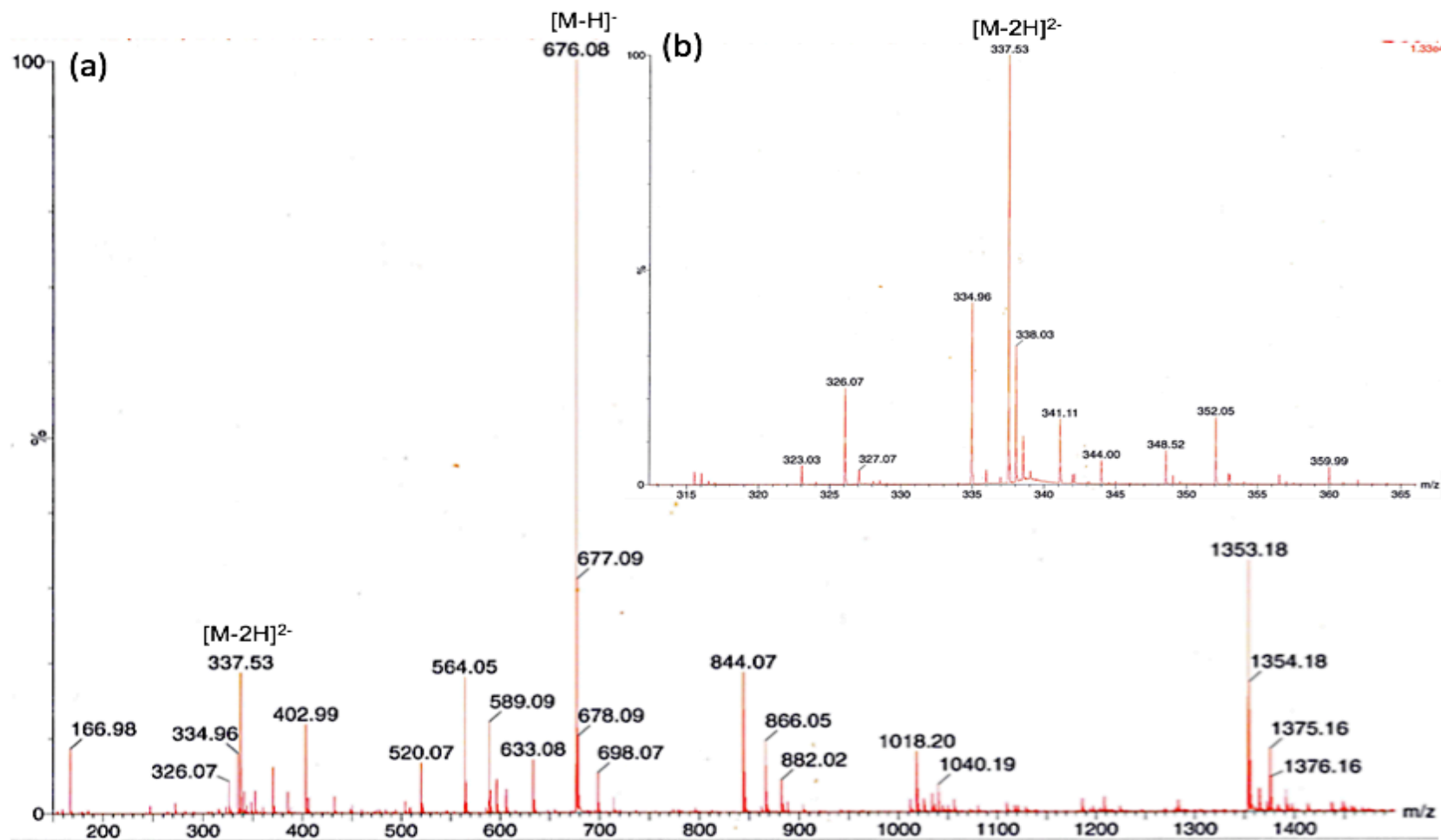


Figure A3.2: Negative ion mass spectrometry of peptidoglycan standard UDP-enolpyruvyl-GlcNAc. (a): mass spectra with $[M-H]^-$ (observed 676.08, expected 676.07) and $[M-2H]^{2-}$ (observed 337.53, expected 337.53). (b): Zoomed in view of $[M-2H]^{2-}$ peak shown in (a). (deconvoluted by MassLynx™ software (Waters, USA)).

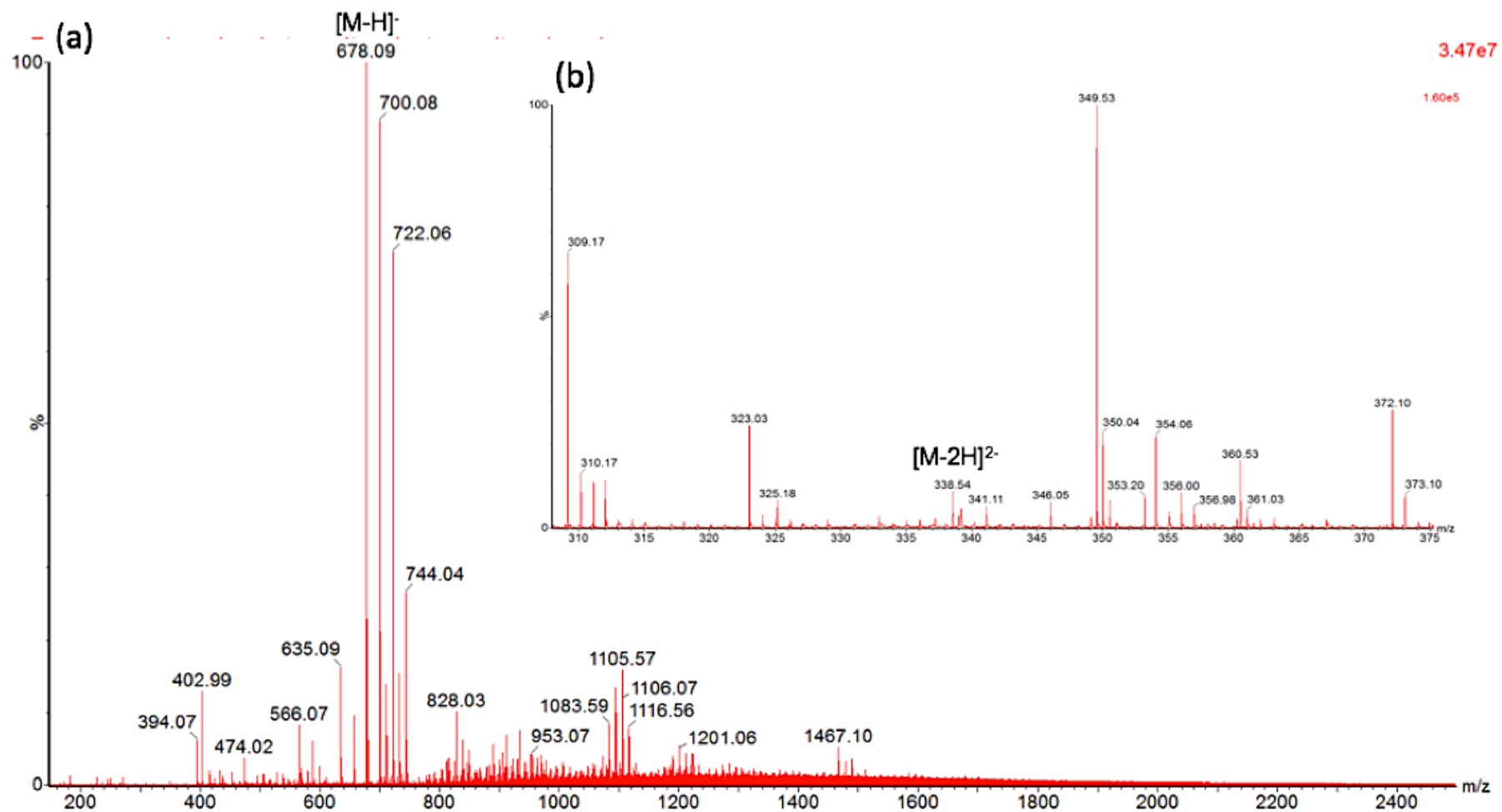


Figure A3.3: Negative ion mass spectrometry of peptidoglycan standard UDP-MurNAc. (a): mass spectra with $[M-H]^-$ (observed 678.09, expected 678.09). (b): Zoomed in view of $[M-2H]^{2-}$ (observed 338.54, expected 338.54). (deconvoluted by MassLynx™ software (Waters, USA)).

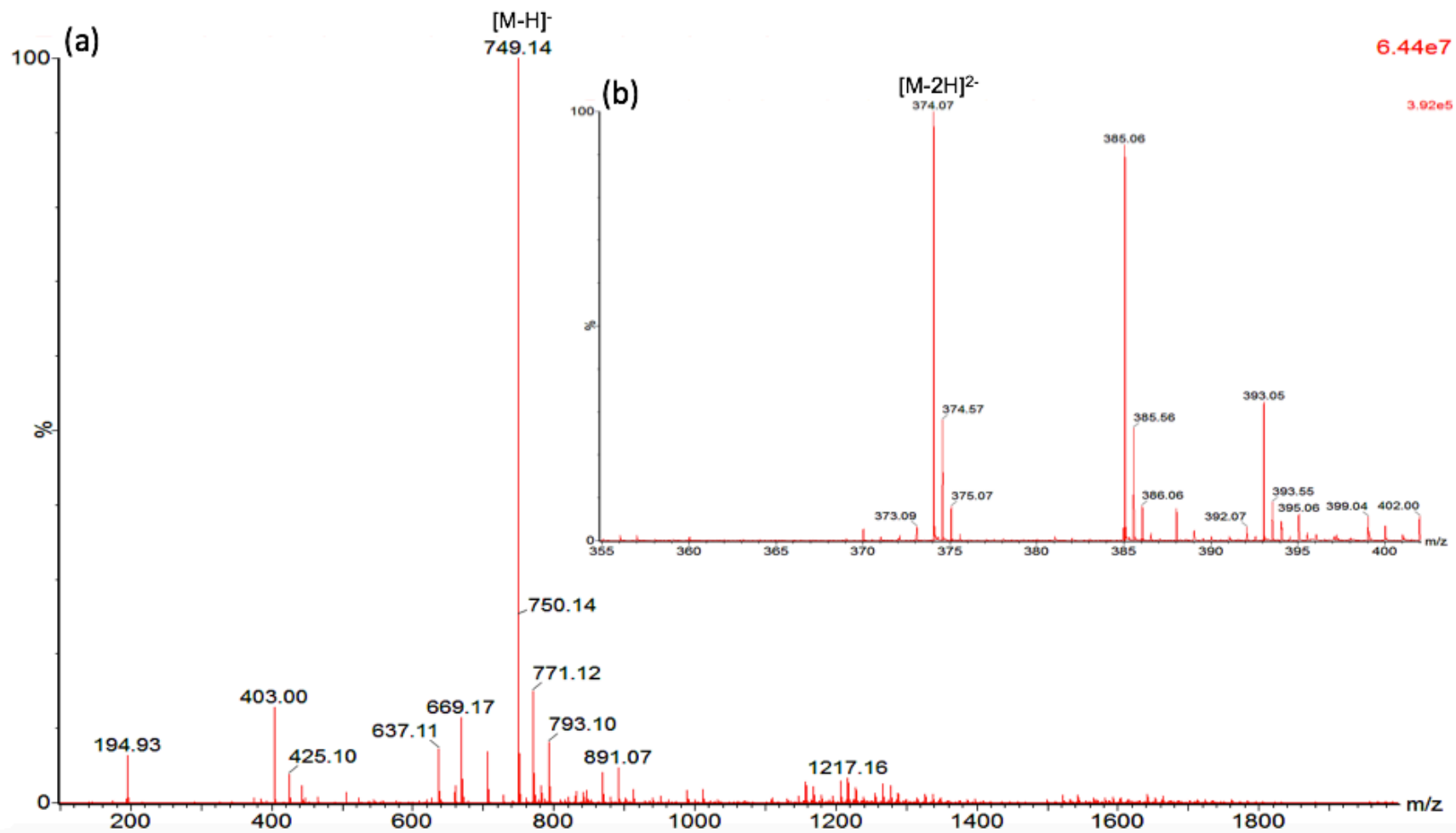


Figure A3.4: Negative ion mass spectrometry of peptidoglycan standard UDP-MurNAc-monopeptide (L-Alanine). (a): mass spectra with $[M-H]^-$ (observed 749.14, expected 749.13). (b): Zoomed in view of $[M-2H]^{2-}$ (observed 374.07, expected 374.06). (deconvoluted by MassLynx™ software (Waters, USA)).

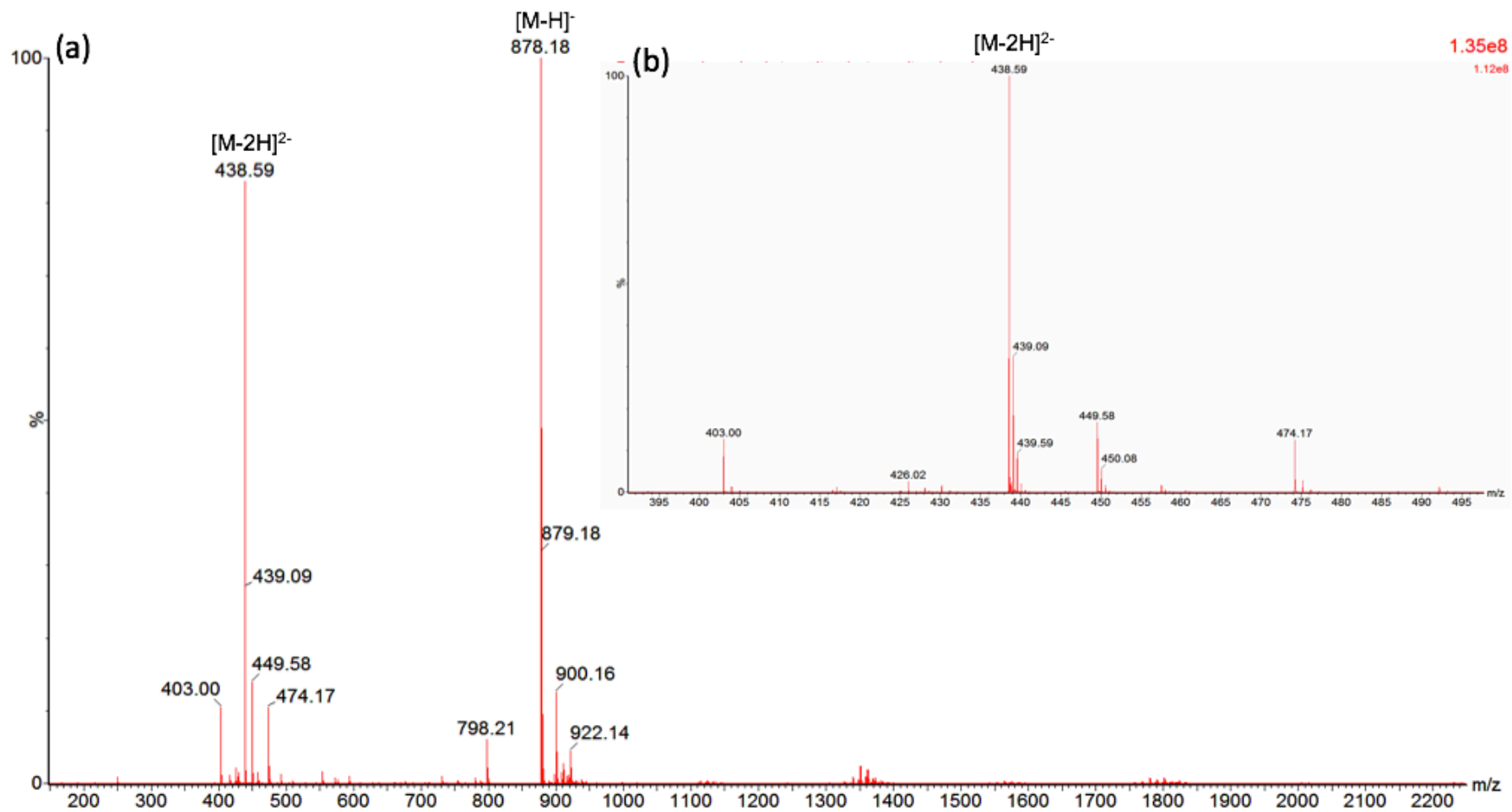


Figure A3.5: Negative ion mass spectrometry of peptidoglycan standard UDP-MurNAc-dipeptide (L-Ala-D-Glu). (a): mass spectra with $[M-H]^-$ (observed 878.18, expected 878.17) $[M-2H]^{2-}$ (observed 438.59, expected 438.58). (b): Zoomed in view of $[M-2H]^{2-}$ peak shown in (a). (deconvoluted by MassLynx™ software (Waters, USA)).

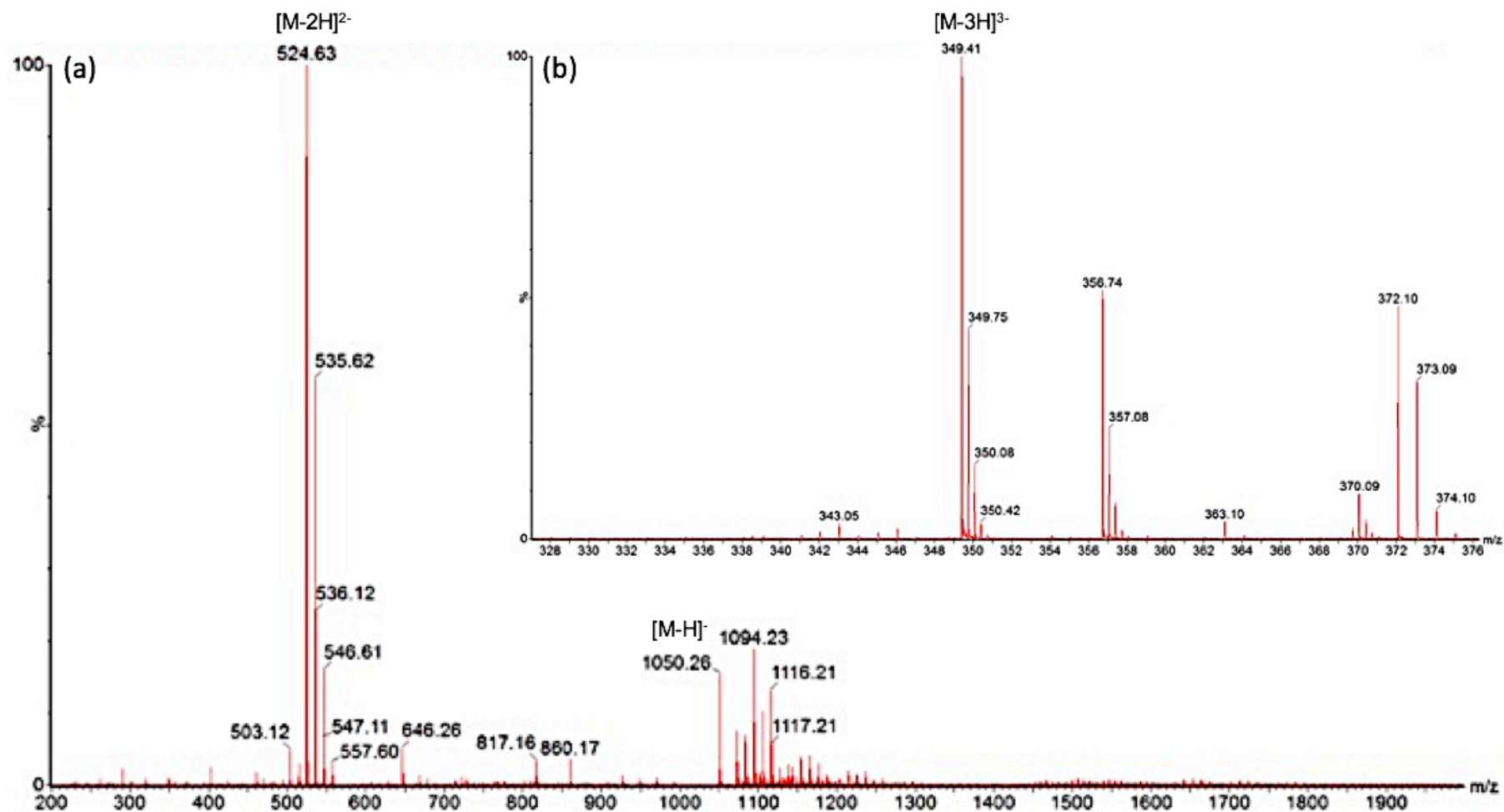


Figure A3.6: Negative ion mass spectrometry of peptidoglycan standard UDP-MurNAc-tripeptide (L-Ala-D-Glu-m-DAP). (a): mass spectra with $[M-H]^-$ (observed 1050.26, expected 1050.25) $[M-2H]^{2-}$ (observed 524.63, expected 524.62). (b): Zoomed in view of $[M-3H]^{3-}$ (observed 349.41, expected 349.41). (deconvoluted by MassLynx™ software (Waters, USA)).

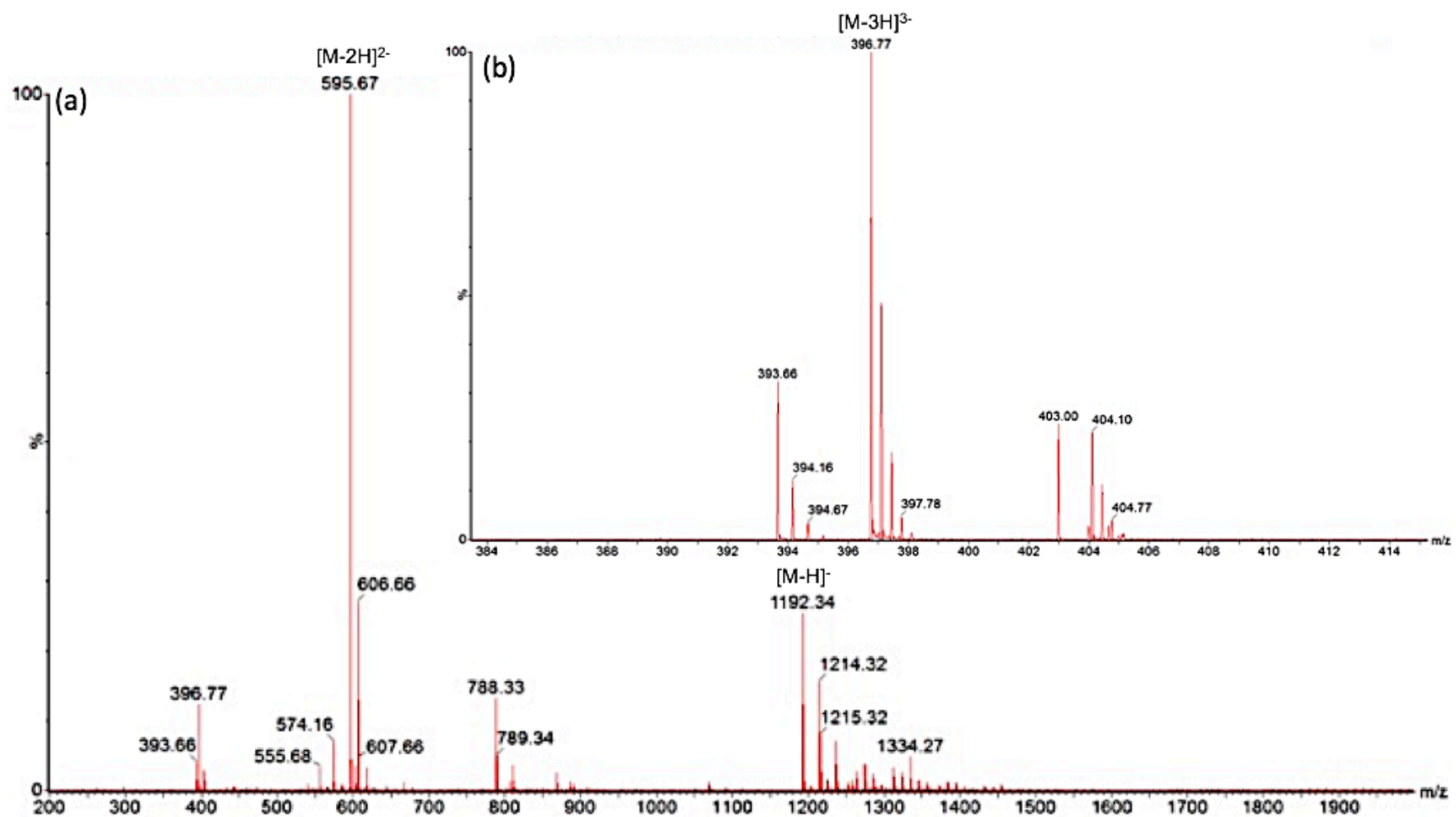


Figure A3.7: Negative ion mass spectrometry of peptidoglycan standard UDP-MurNAc-pentapeptide (L-Ala-D-Glu-m-DAP-D-Ala-D-Ala). (a): mass spectra with $[M-H]^-$ (observed 1192.34, expected 1192.33) and $[M-2H]^{2-}$ (observed 595.67, expected 595.66) (b): Zoomed in view of $[M-3H]^{3-}$ (observed 396.77, expected 396.77). (deconvoluted by MassLynx™ software (Waters, USA)).

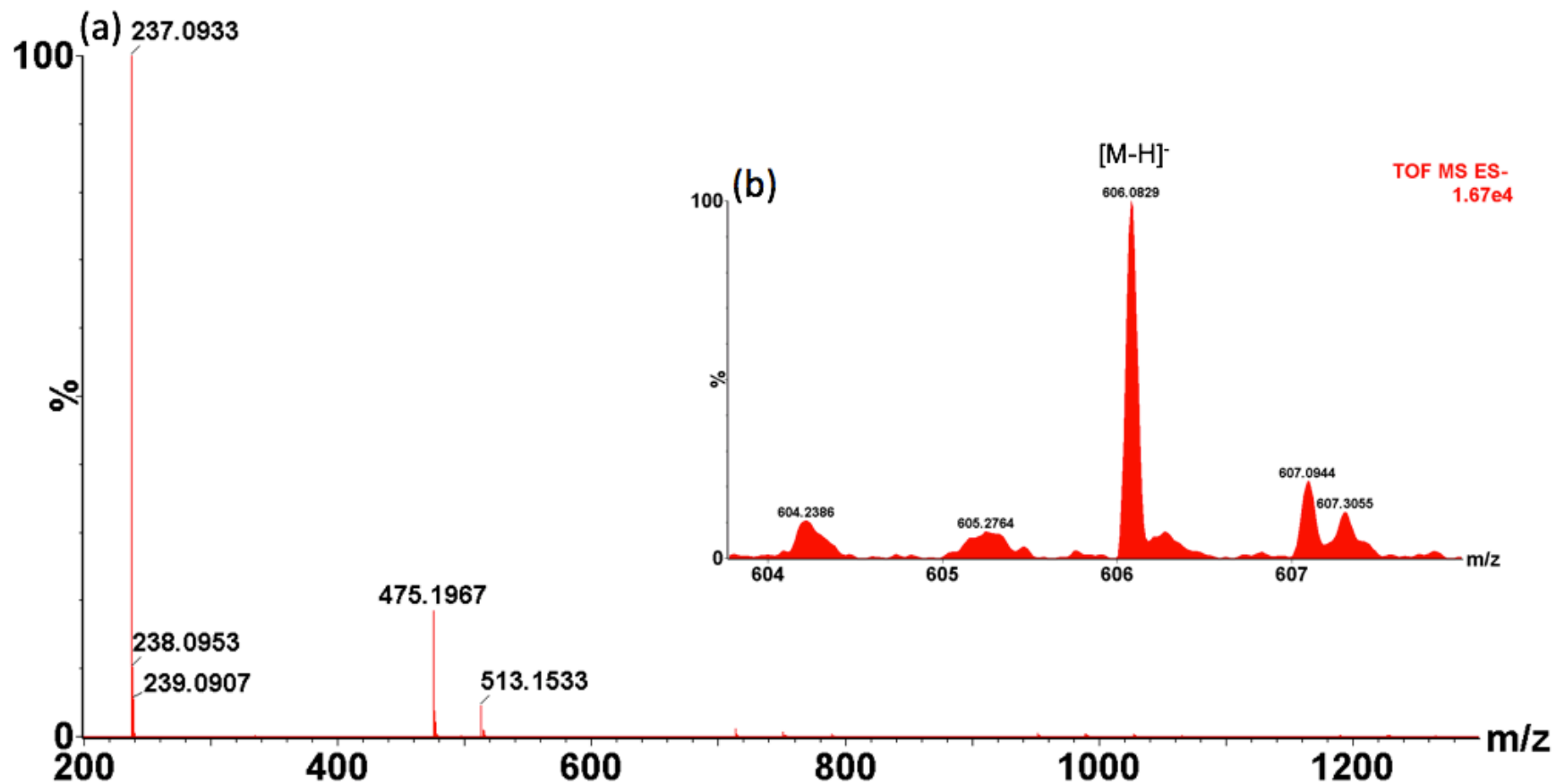


Figure A3.8: Negative ion mass spectrometry of the isolated accumulated peak (i) from *B. subtilis* control. (a): full mass spectra (no identifiable m/z). (b): mass spectra of UDP-GlcNAc [M-H]⁻ (observed 606.08, expected 606.07) (zoomed in view of (a)). (deconvoluted by MassLynx™ software (Waters, USA)).

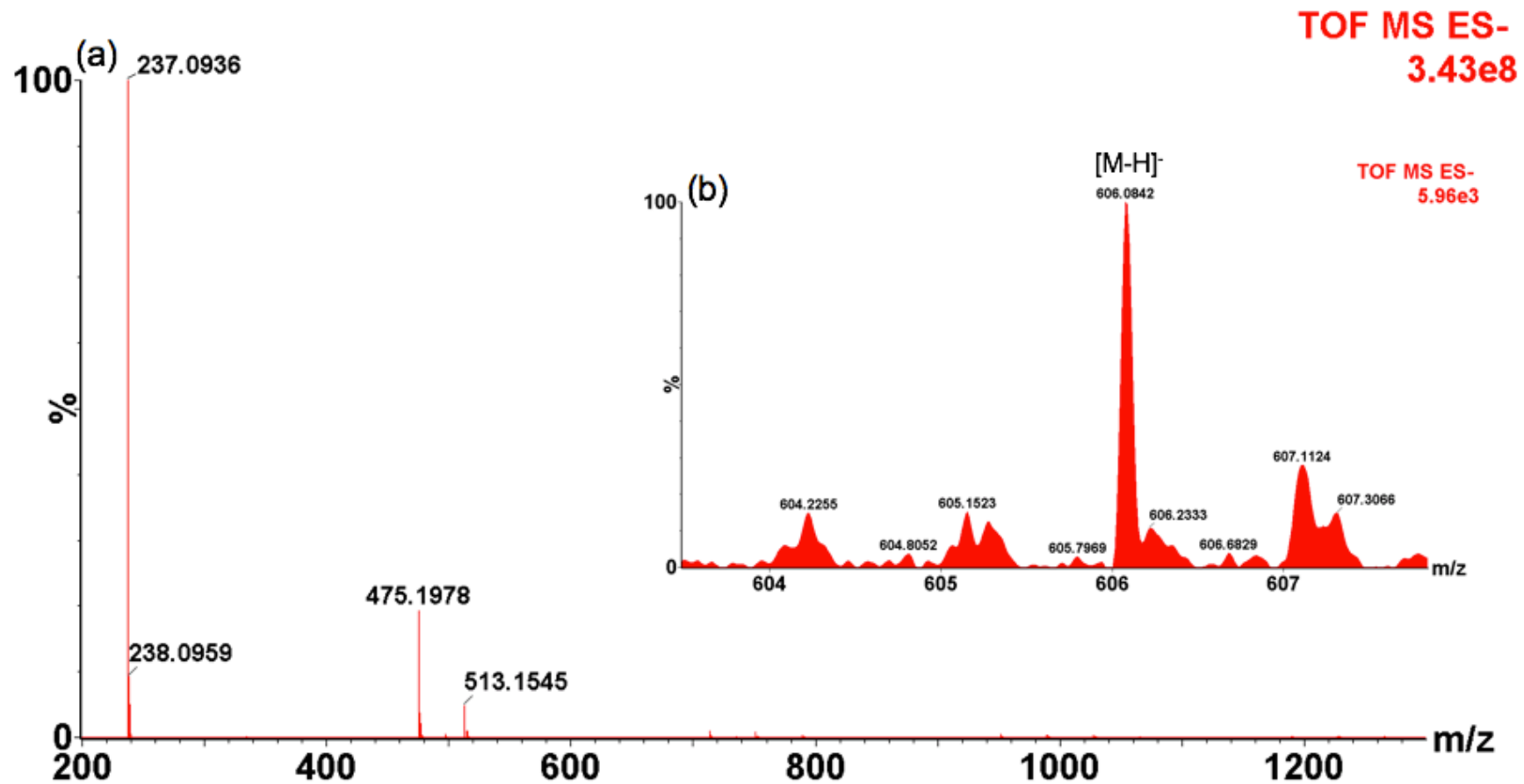


Figure A3.9: Negative ion mass spectrometry of the isolated accumulated peak (ii) from *B. subtilis* control. (a): full mass spectra (no identifiable m/z). (b): mass spectra of UDP-GlcNAc [M-H]⁻ (observed 606.08, expected 606.07) (zoomed in view of (a)). (deconvoluted by MassLynx™ software (Waters, USA)).

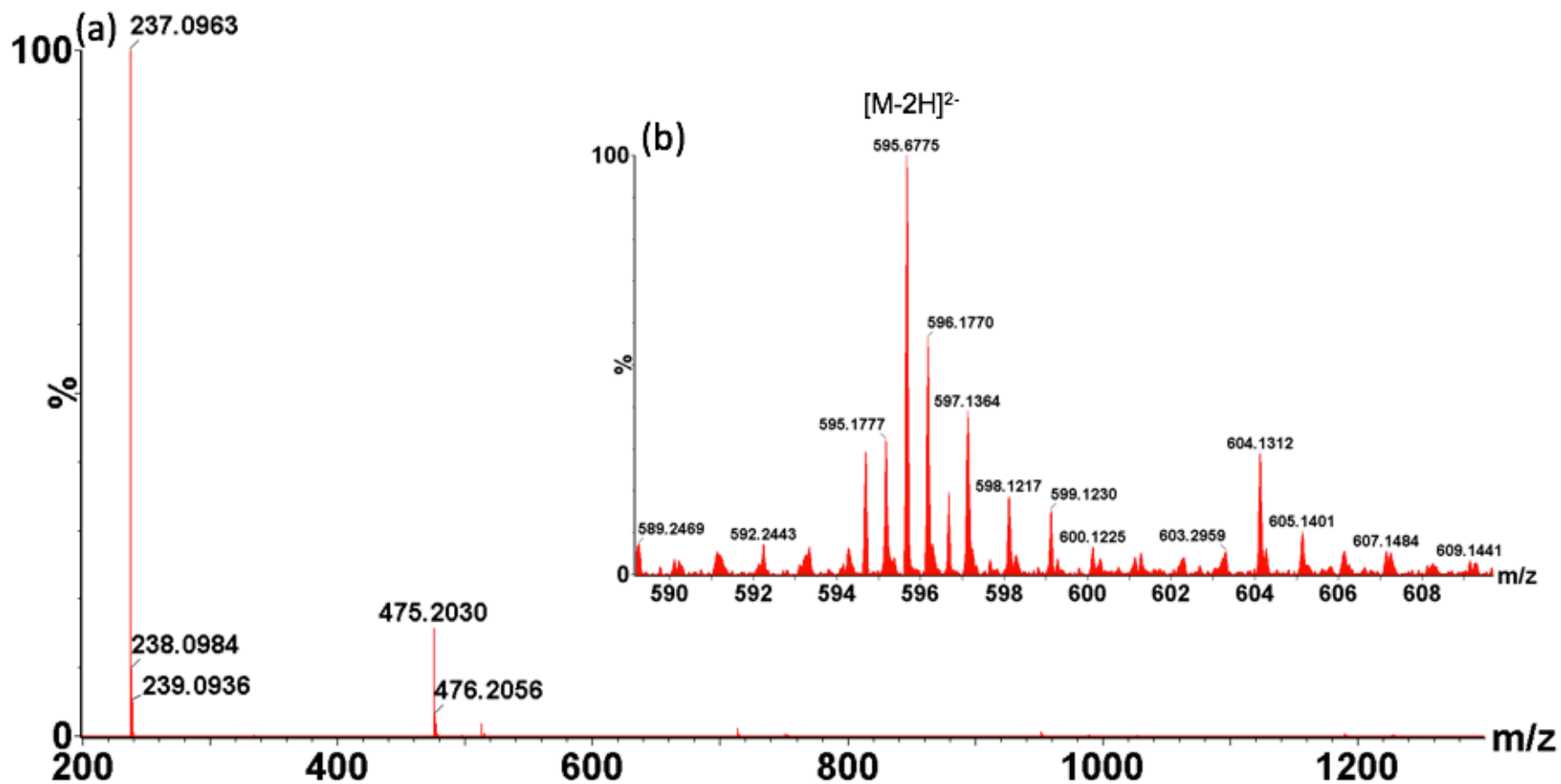


Figure A3.10: Negative ion mass spectrometry of the isolated accumulated peak (iii) from *B. subtilis* control. (a): full mass spectra (no identifiable m/z). (b): mass spectra of UDP-MurNAc-pentapeptide (DAP) $[M-2H]^{2-}$ (observed 595.67, expected 595.66) (zoomed in view of (a)). (deconvoluted by MassLynxTM software (Waters, USA)).

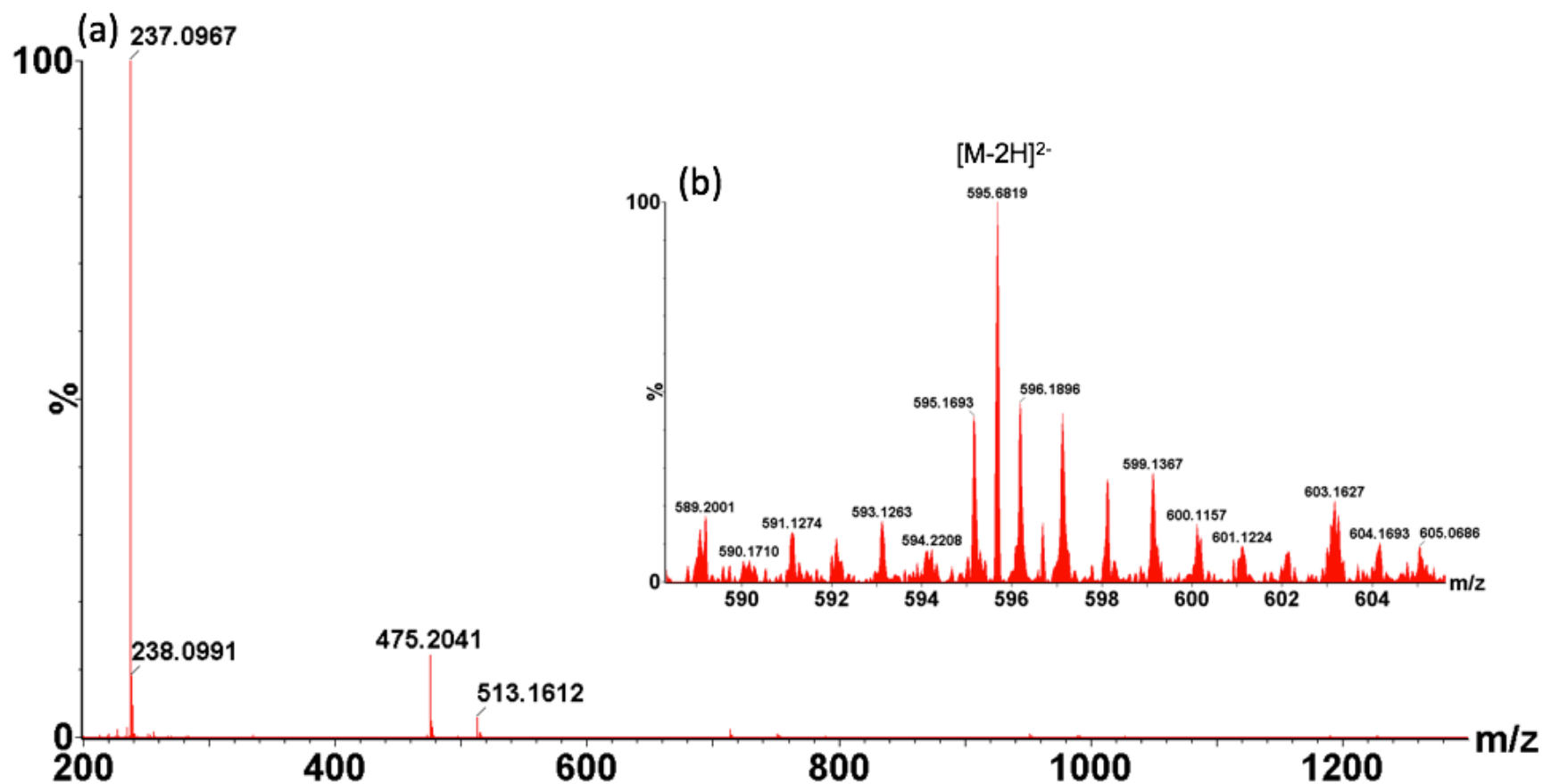


Figure A3.11: Negative ion mass spectrometry of the isolated accumulated peak (iv) from *B. subtilis* control. Peak (iv): (a): full mass spectra (no identifiable m/z). (b): mass spectra of UDP-MurNAc-pentapeptide (DAP) $[M-2H]^{2-}$ (observed 595.68, expected 595.66) (zoomed in view of (a)). (deconvoluted by MassLynx™ software (Waters, USA)).

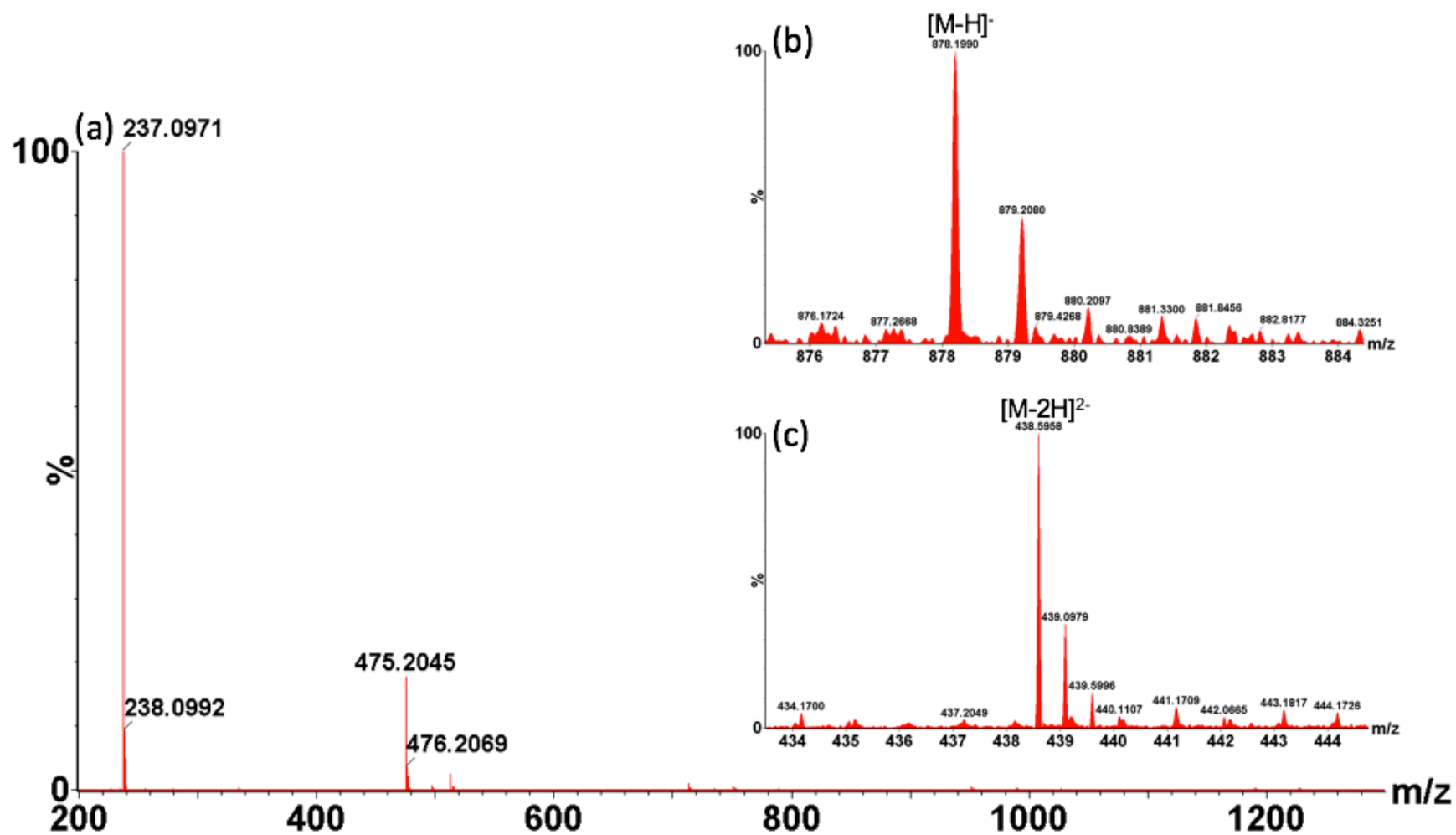


Figure A3.12: Negative ion mass spectrometry of the isolated accumulated peak (v) from *B. subtilis* control. (a): full mass spectra (no identifiable m/z). (b): mass spectra of UDP-MurNAc-dipeptide [M-H]⁻ (observed 878.19, expected 878.17) (zoomed in view of (a)). (c): Mass spectra of [M-2H]²⁻ (observed 438.59, expected 438.58). (deconvoluted by MassLynx™ software (Waters, USA)).

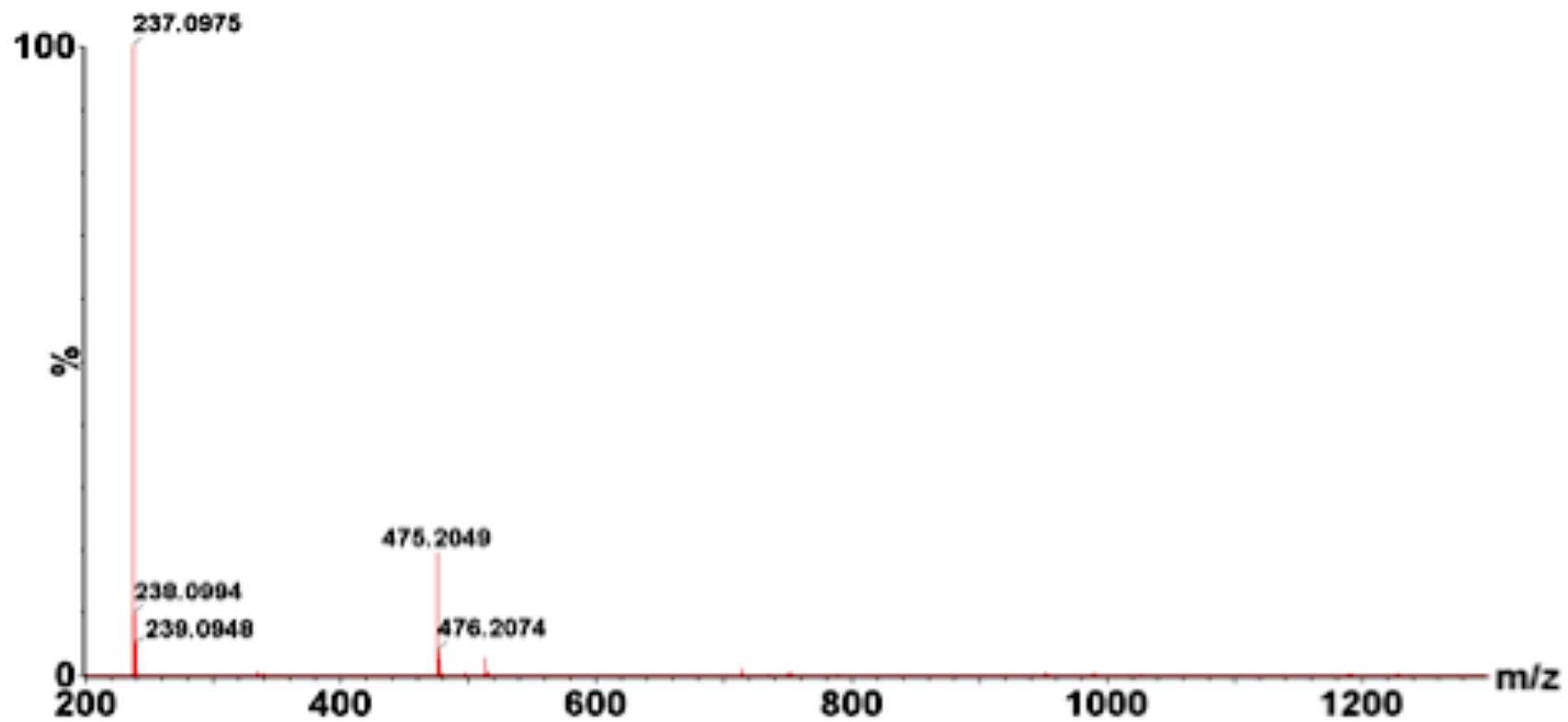


Figure A3.13: Negative ion mass spectrometry of the isolated accumulated peak (vi) from *B. subtilis* control. Full mass spectra (no identifiable m/z). (deconvoluted by MassLynx™ software (Waters, USA).

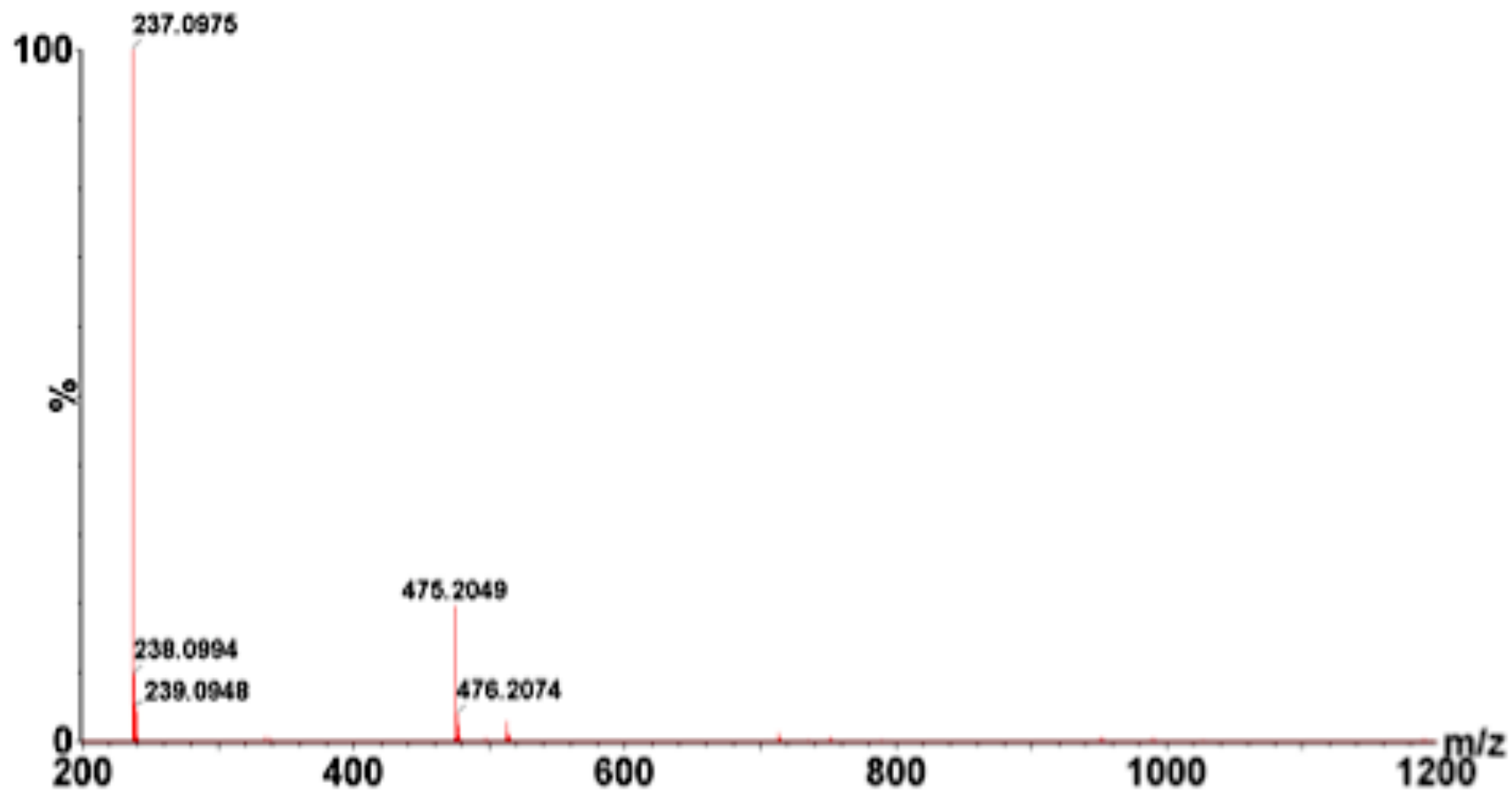


Figure A3.14: Negative ion mass spectrometry of the isolated accumulated peak (vii) from *B. subtilis* control. Full mass spectra (no identifiable m/z) (deconvoluted by MassLynx™ software (Waters, USA)).

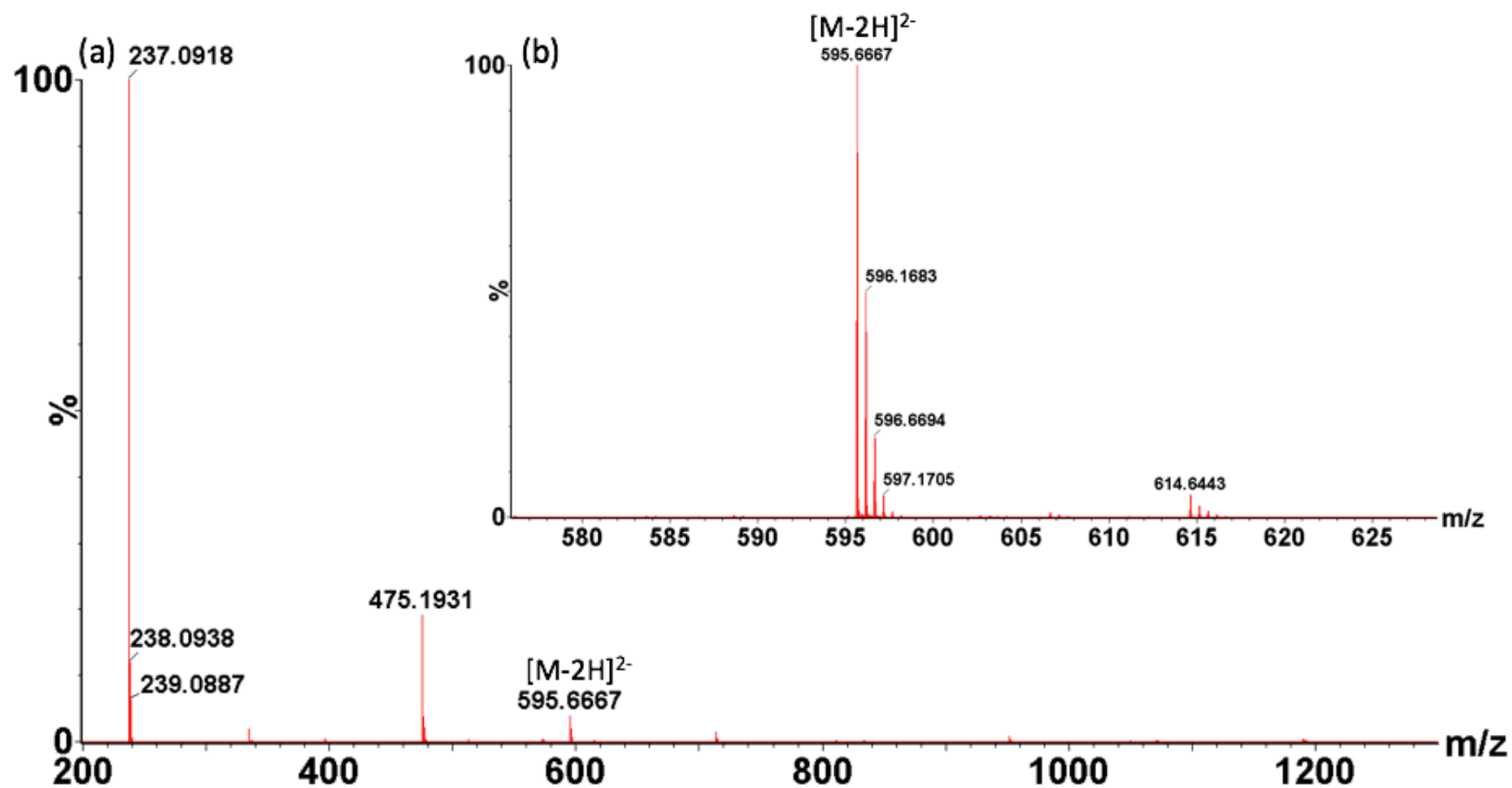


Figure A3.15: Negative ion mass spectrometry of the isolated accumulated peak of UDP-MurNAc-pentapeptide (DAP) from *B. subtilis* incubated with 2x MIC vancomycin. (a): mass spectra of $[M-2H]^{2-}$ (observed 595.66, expected 595.66). (b): Observed isotope distribution of $[M-2H]^{2-}$ (deconvoluted by MassLynxTM software (Waters, USA)).

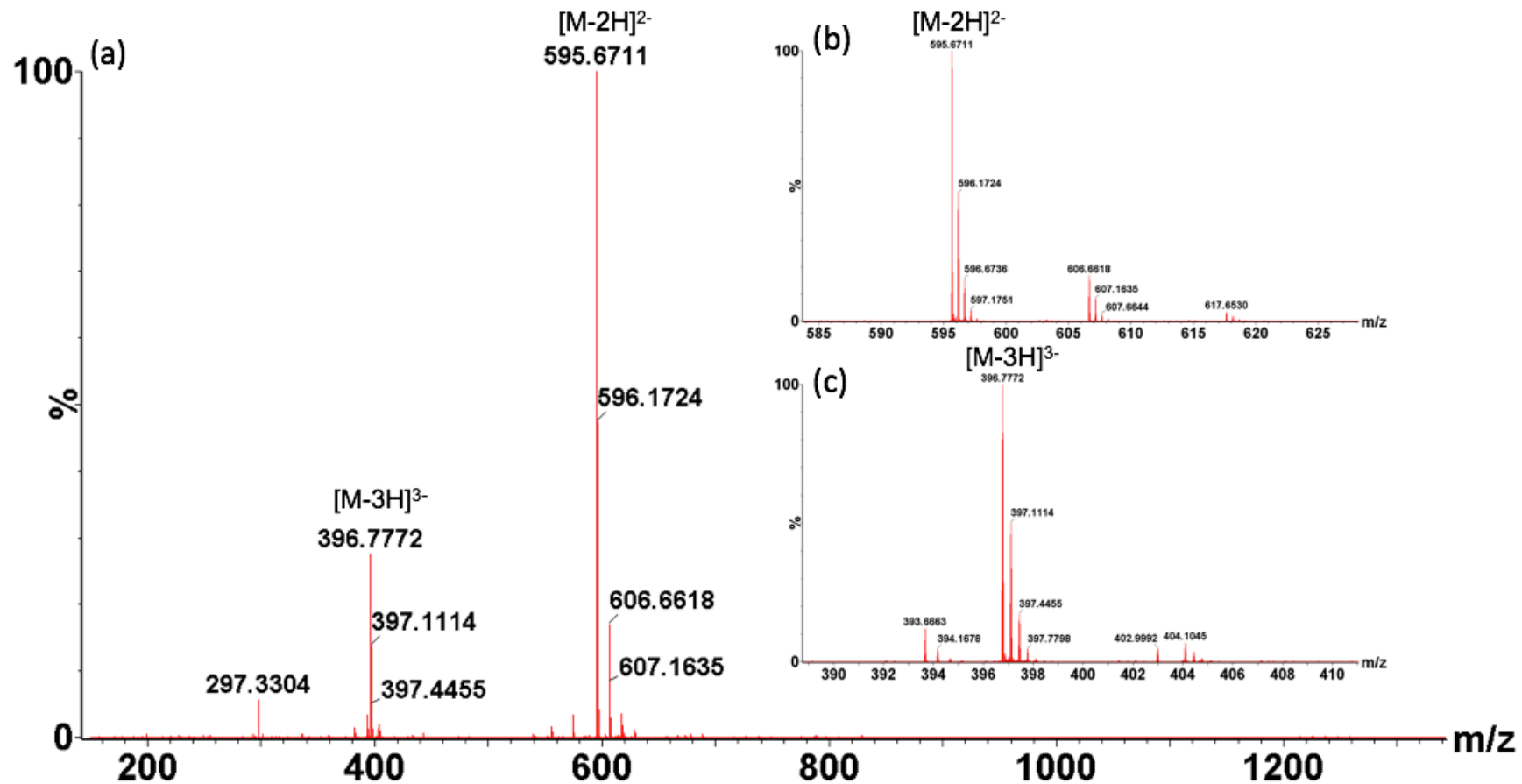


Figure A3.16: Negative ion mass spectrometry of the isolated accumulated peak of UDP-MurNAc-pentapeptide (DAP) from *B. subtilis* incubated with 5x MIC vancomycin. (a): mass spectra with $[M-2H]^{2-}$ (observed 595.67, expected 595.66) and $[M-3H]^{3-}$ (observed 396.77, expected 396.77) (deconvoluted by MassLynx™ software (Waters, USA)). (b): Observed isotope distribution of $[M-2H]^{2-}$ (zoomed in view of $[M-2H]^{2-}$ peak shown in (a)). (c): Mass spectra of $[M-3H]^{3-}$.

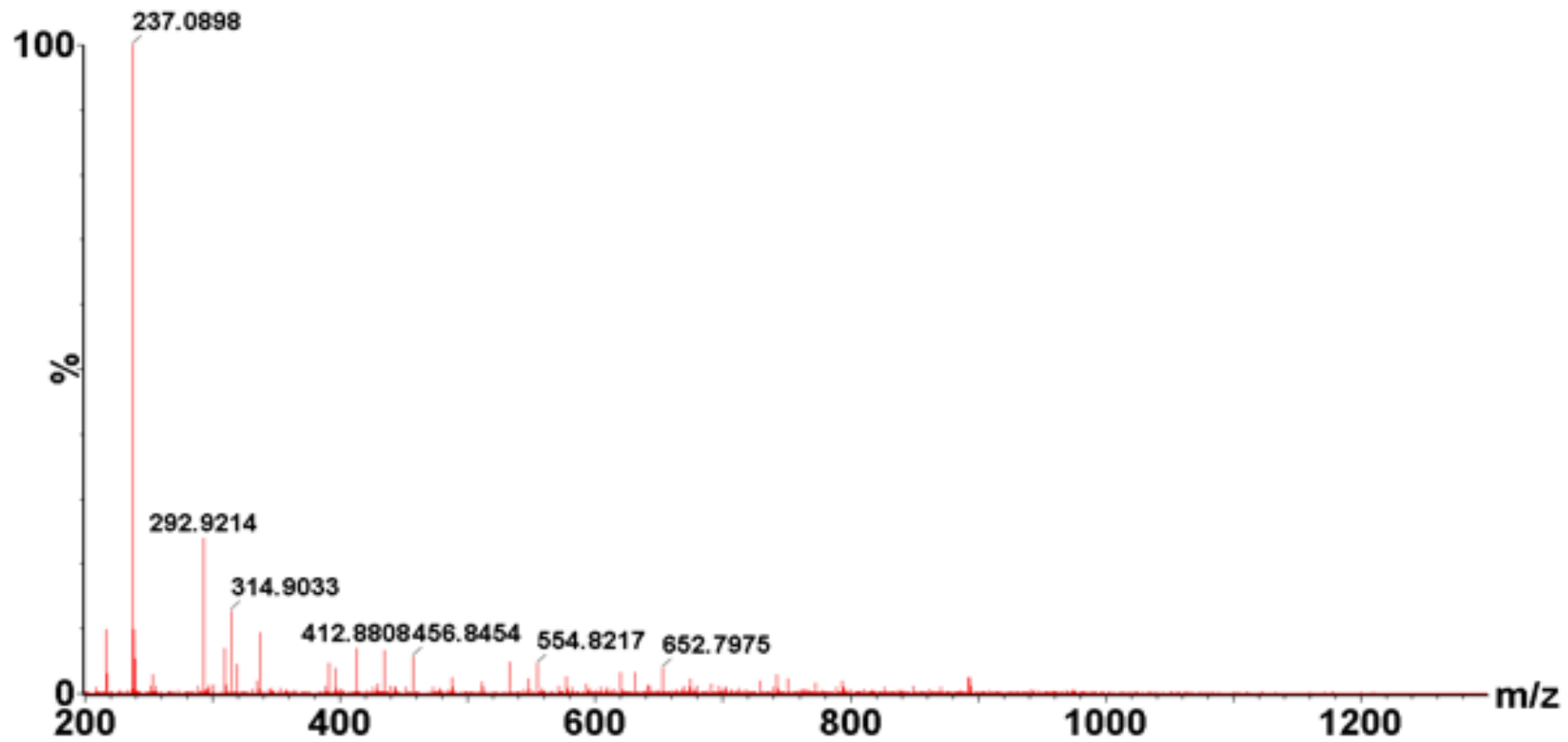


Figure A3.17: Negative ion mass spectrometry of the isolated accumulated peak (i) from *B. subtilis* cells incubated with 2x MIC pywac 1. Full mass spectra, no identifiable peptidoglycan intermediate m/z (deconvoluted by MassLynx™ software (Waters, USA)).

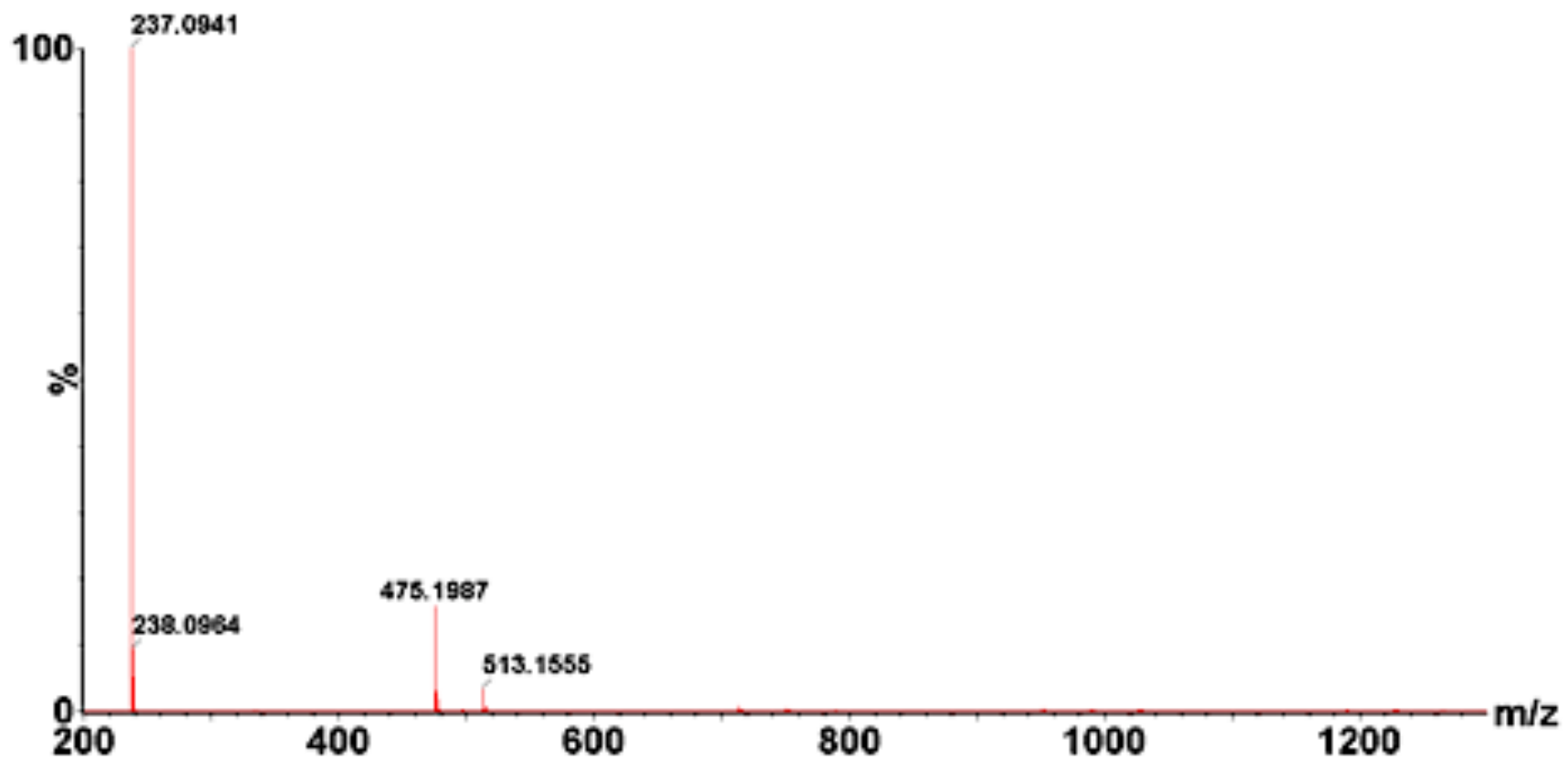


Figure A3.18: Negative ion mass spectrometry of the isolated accumulated peak from *B. subtilis* incubated with 2x MIC pywac 3. Full mass spectra, no identifiable peptidoglycan intermediate m/z (deconvoluted by MassLynx™ software (Waters, USA)).

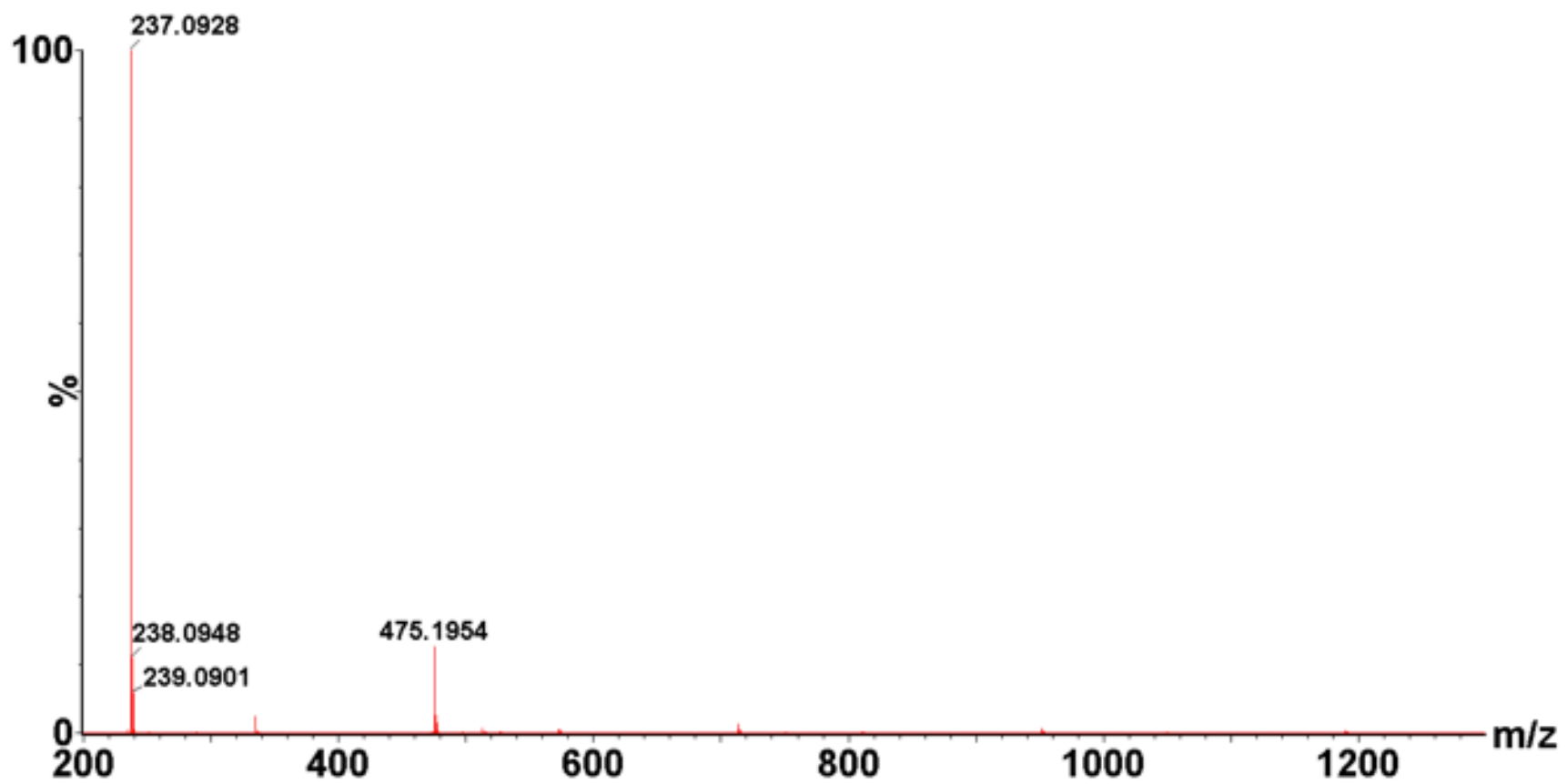


Figure A3.19: Negative ion mass spectrometry of the isolated accumulated peak from *B. subtilis* incubated with 2x MIC pywac 5. Full mass spectra (no identifiable m/z) (deconvoluted by MassLynx™ software (Waters, USA)).

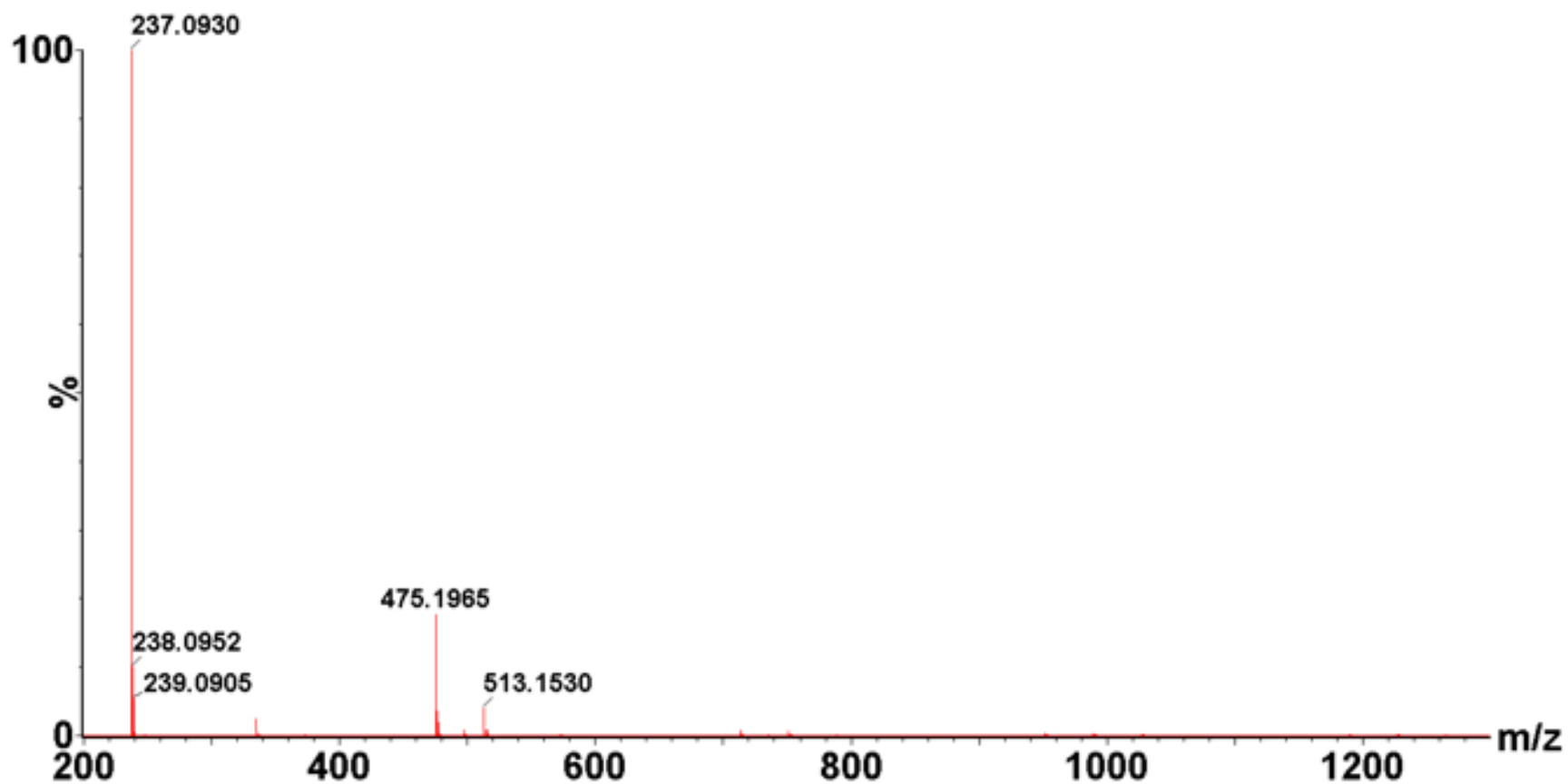


Figure A3.20: Negative ion mass spectrometry of the isolated accumulated peak from *B. subtilis* incubated with 2x MIC pywac 6. Full mass spectra (no identifiable m/z) (deconvoluted by MassLynx™ software (Waters, USA)).

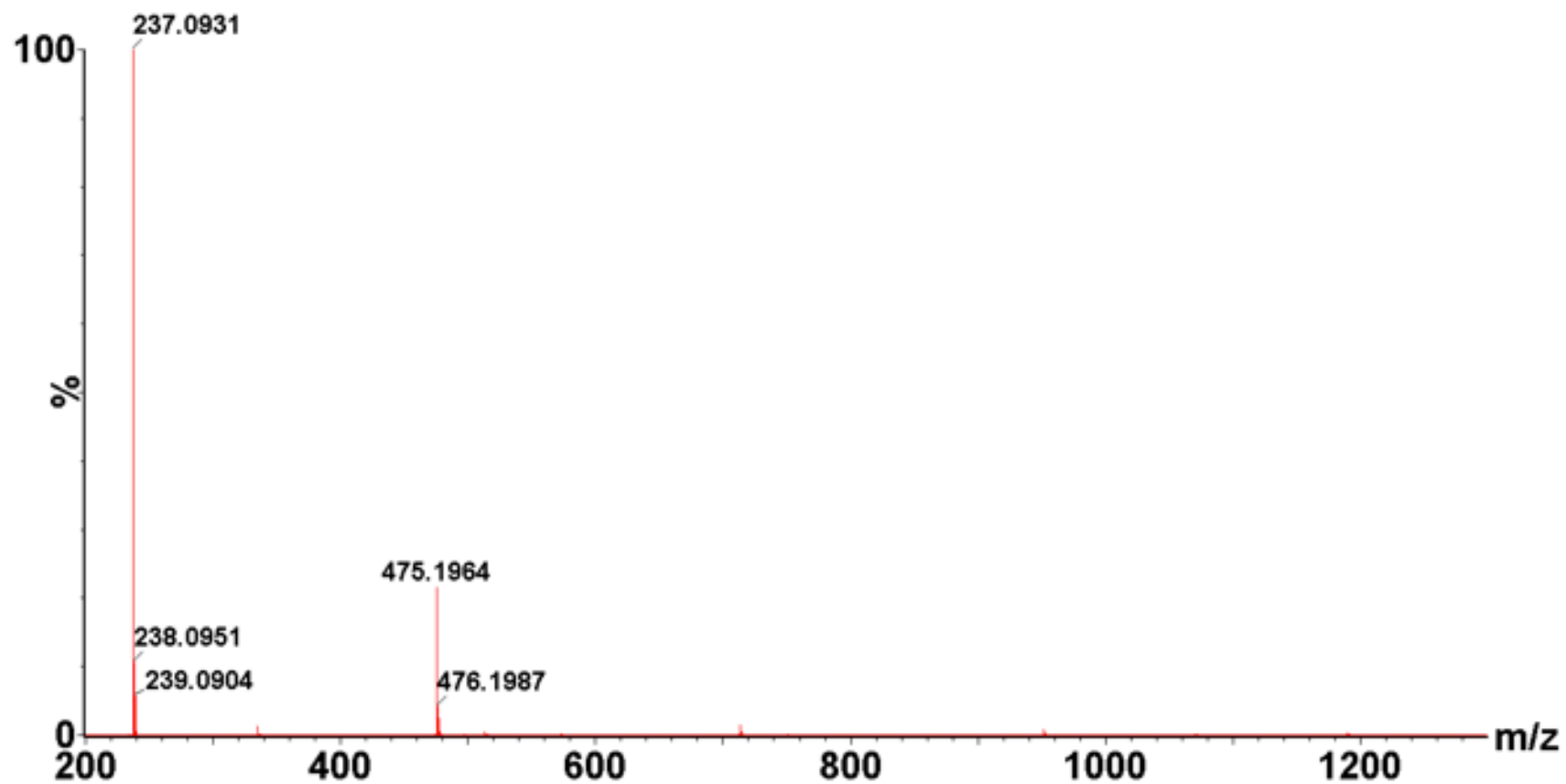


Figure A3.21: Negative ion mass spectrometry of the isolated accumulated peak from *B. subtilis* incubated with 2x MIC pywac 7. Full mass spectra (no identifiable m/z) (deconvoluted by MassLynx™ software (Waters, USA)).

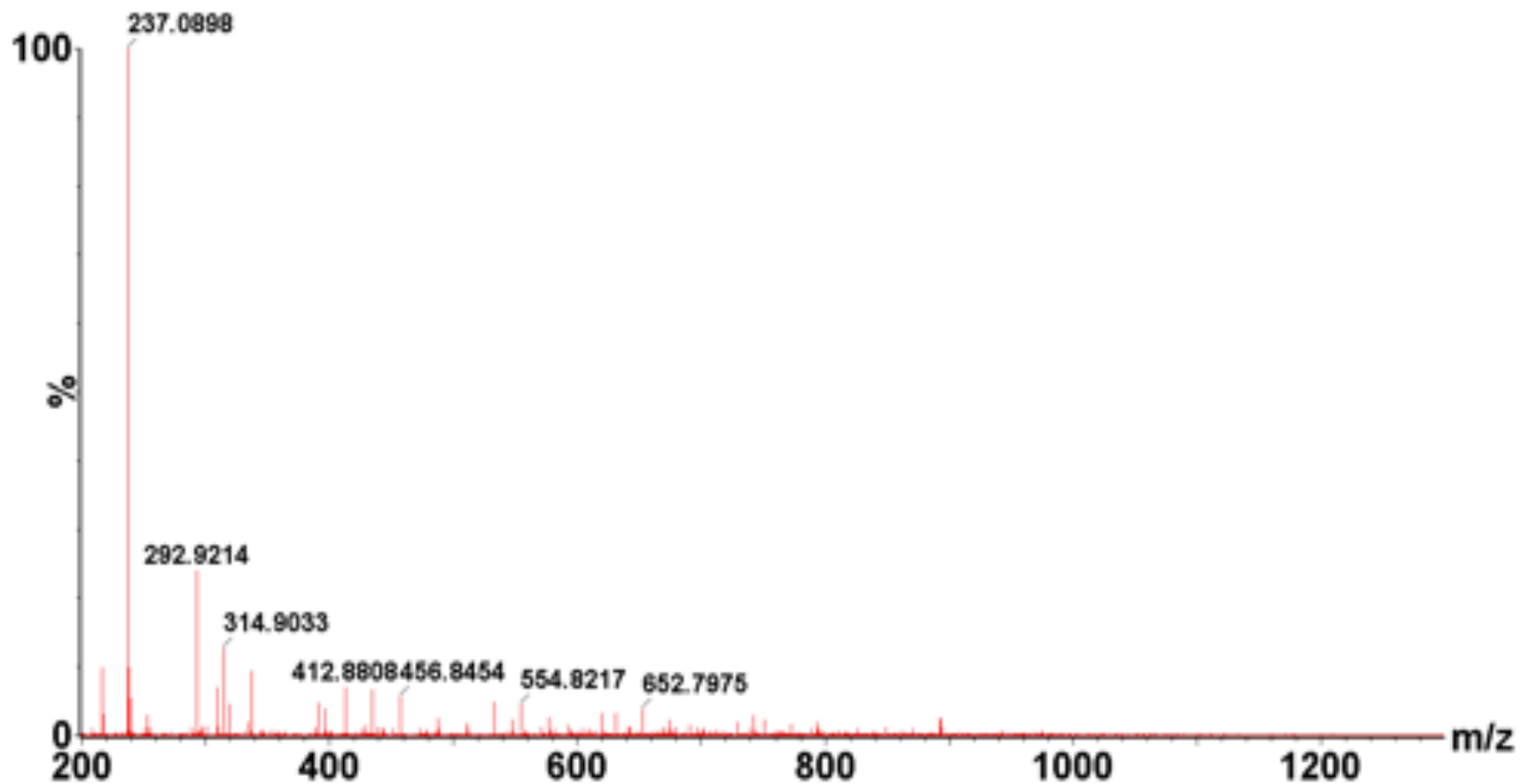


Figure A3.22: Negative ion mass spectrometry of the isolated accumulated peak (i) from *B. subtilis* incubated with 2x MIC pywac 2. Full mass spectra, (no identifiable peptidoglycan intermediate m/z) (deconvoluted by MassLynx™ software (Waters, USA)).

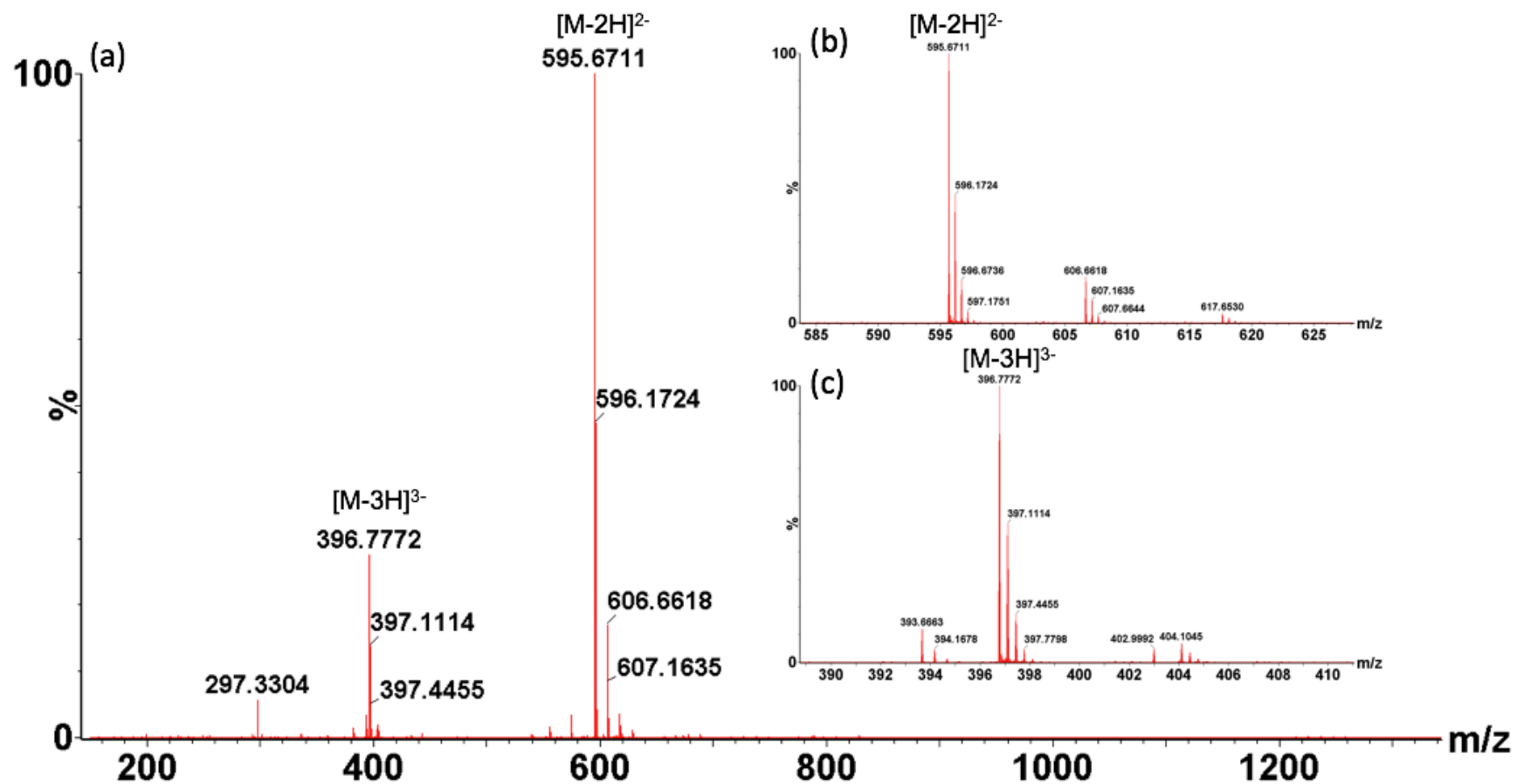


Figure A3.23: Negative ion mass spectrometry of the isolated accumulated peak (ii) from *B. subtilis* incubated with 2x MIC pywac 2. (a): full mass spectra of UDP-MurNAc-pentapeptide (DAP) with $[M-2H]^{2-}$ (observed 595.67, expected 595.66) and $[M-3H]^{3-}$ (observed 396.77, expected 396.77). (deconvoluted by MassLynx™ software (Waters, USA)). (b): Observed isotope distribution of $[M-2H]^{2-}$ (zoomed in view of $[M-2H]^{2-}$ peak shown in (a)). (c): Mass spectra of $[M-3H]^{3-}$.

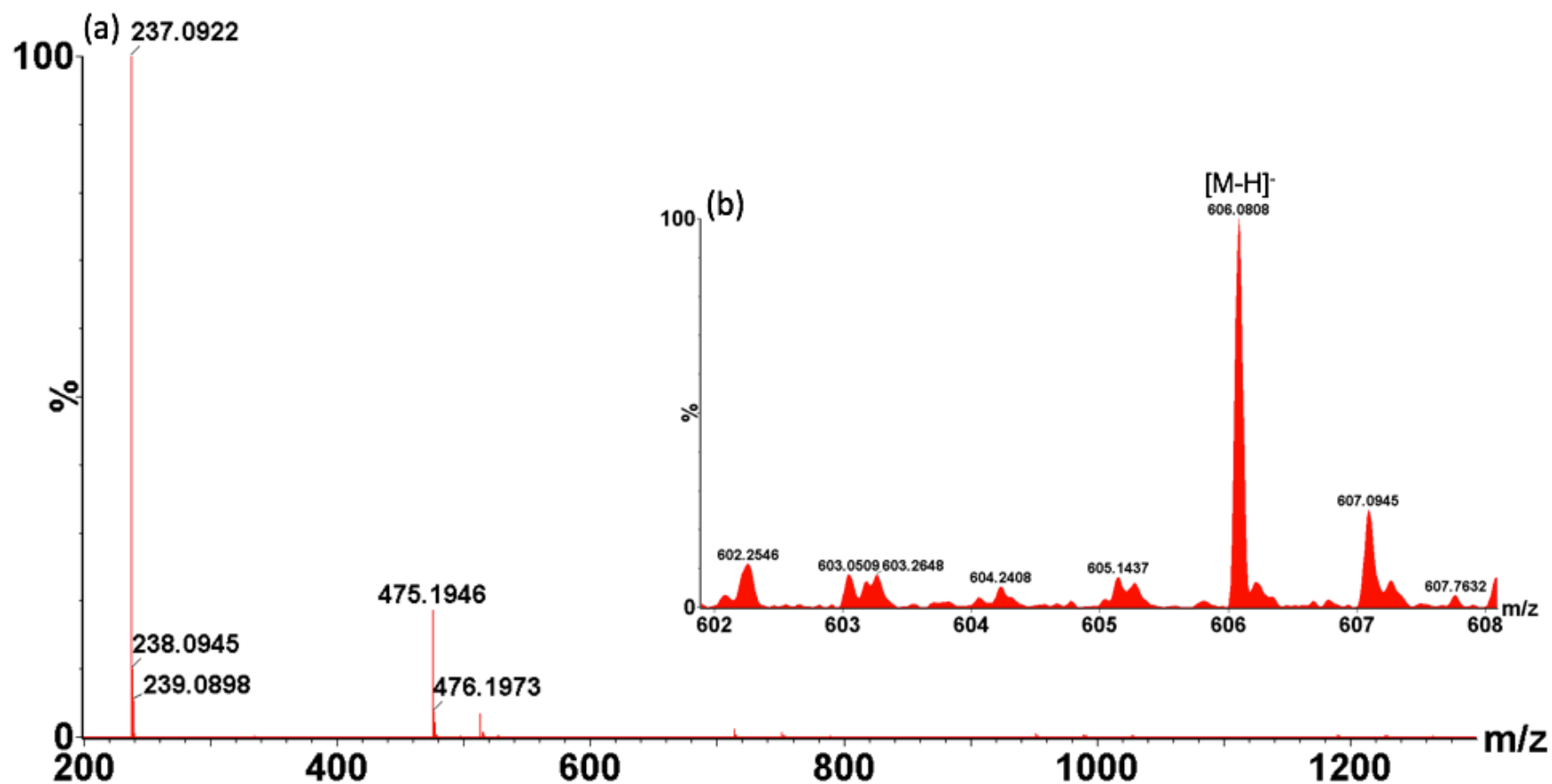


Figure A3.24: Negative ion mass spectrometry of the isolated accumulated peak of *B. subtilis* cells incubated with 2x MIC pywac 8. (a): mass spectra (no identifiable m/z). (b): Observed isotope distribution of UDP-GlcNAc [M-H]⁻ (zoomed in view of [M-H]⁻ peak shown in (a)) (observed 606.08, expected 606.07) (deconvoluted by MassLynx™ software (Waters, USA)).

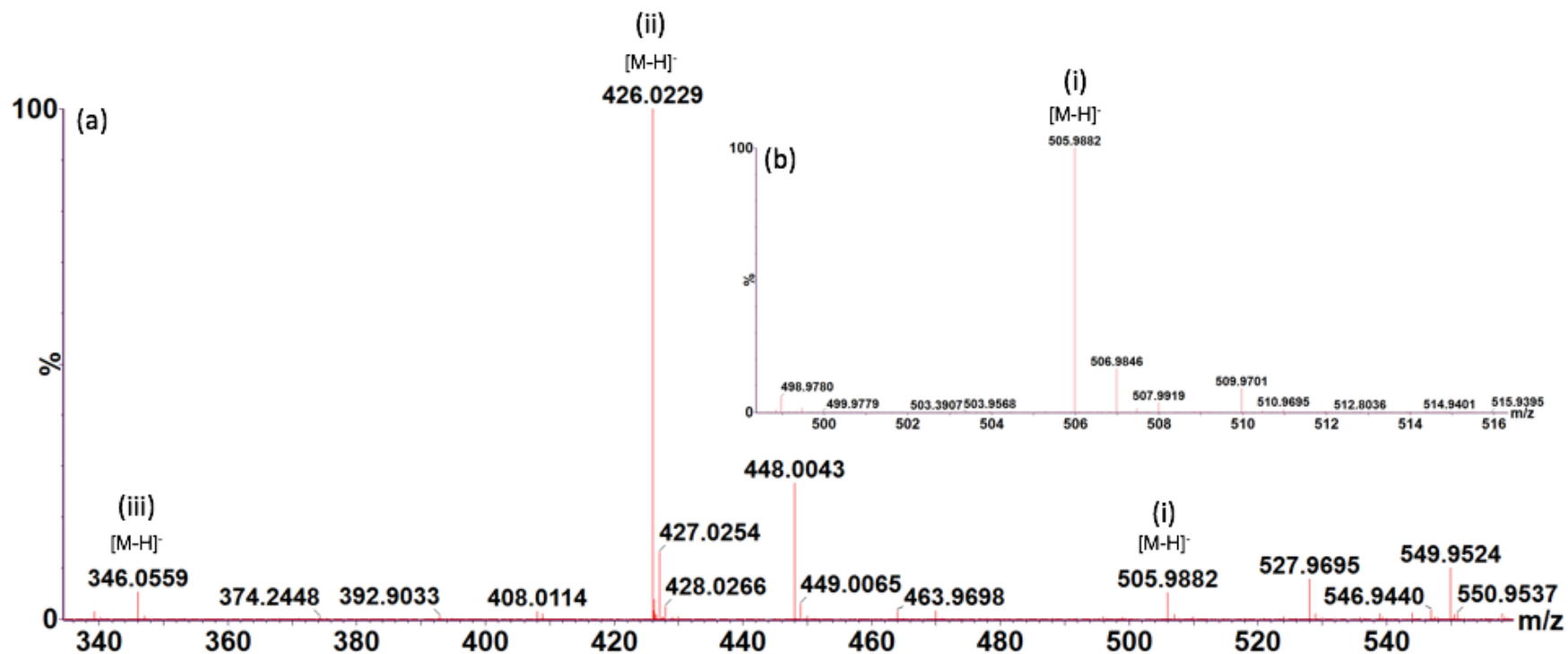


Figure A3.25: Negative ion mass spectrometry of ATP ADP and AMP standards. (a): mass spectra with (i) ATP [M-H]⁻ (observed 505.98, expected 505.98), (ii) ADP [M-H]⁻ (observed 426.02, expected 426.02) and (iii) AMP [M-H]⁻ (observed 346.05, expected 346.05). (b): Zoomed in view of ATP [M-H]⁻ peak shown in (a). (deconvoluted by MassLynx™ software (Waters, USA)).

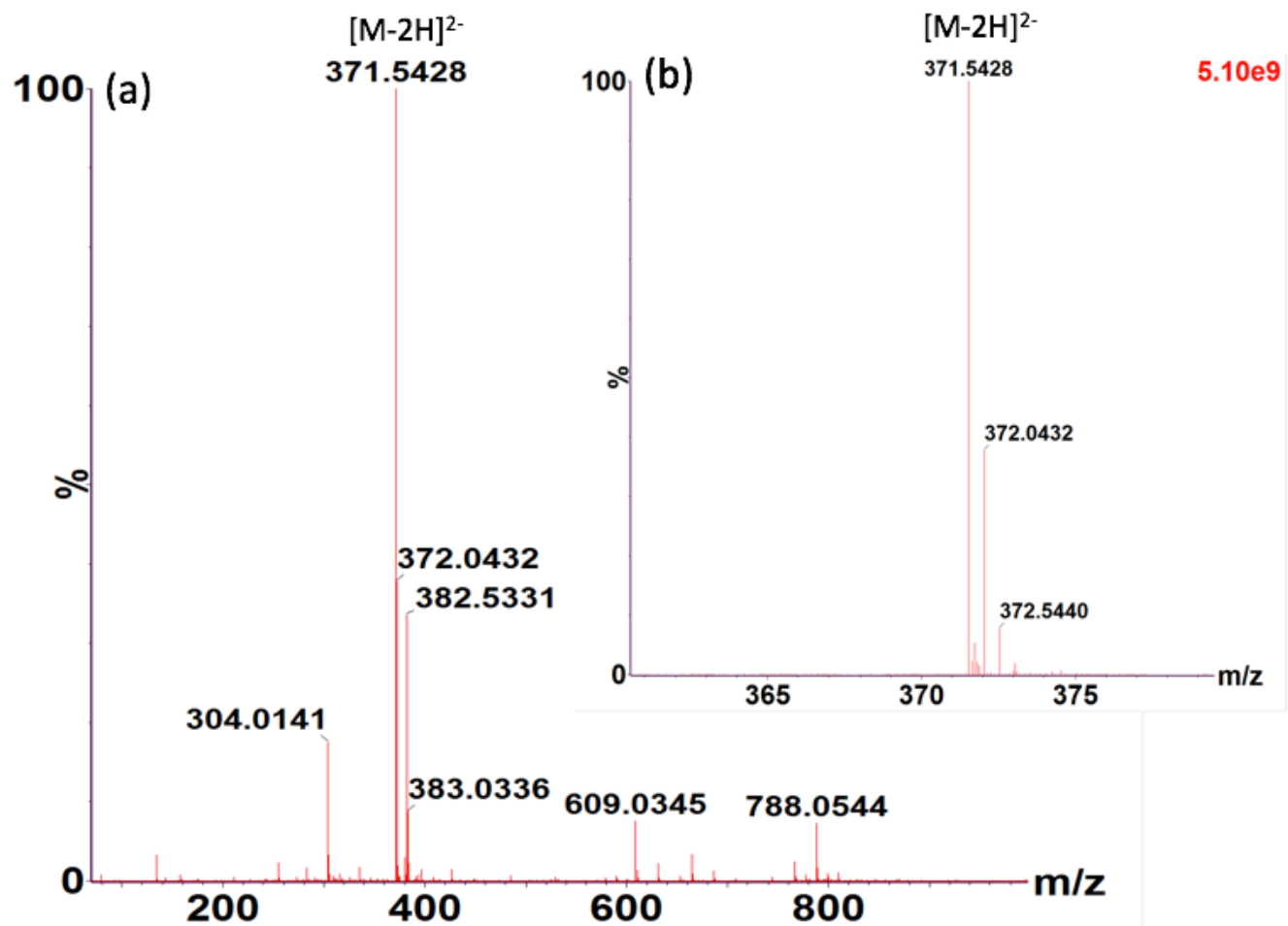


Figure A3.26: Negative ion mass spectrometry of NADPH. (a): mass spectra with $[M-2H]^{2-}$ (observed 371.54, expected 371.53) (deconvoluted by MassLynx™ software (Waters, USA)). (b): Zoomed in view of $[M-2H]^{2-}$ peak shown in (a).

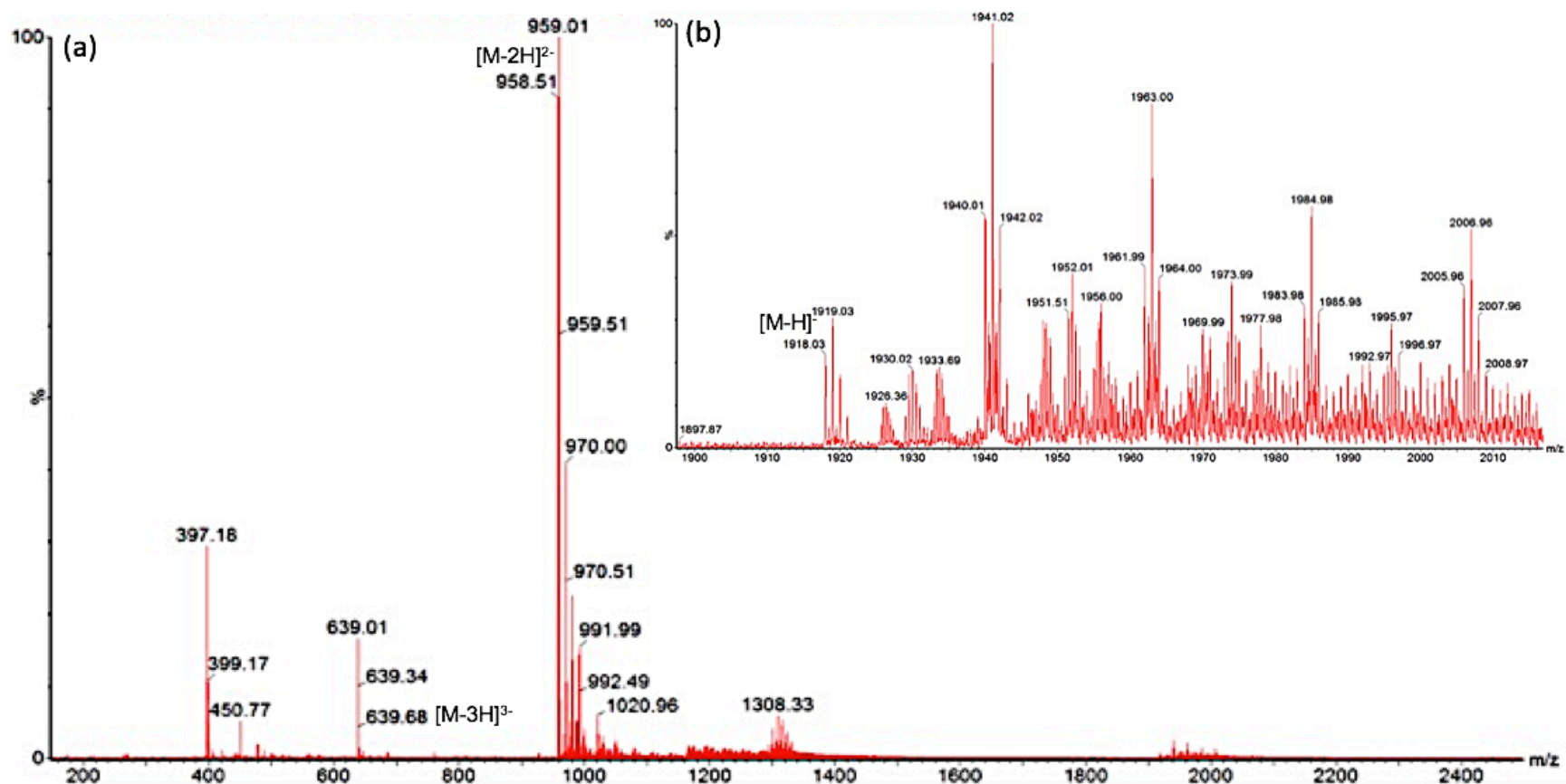


Figure A3.27: Negative ion mass spectrometry of control Lipid II DAP synthesis. (a): mass spectra with Lipid II DAP $[M-2H]^{2-}$ (observed 958.51, expected 958.51) (deconvoluted by MassLynx™ software (Waters, USA)). (b): mass spectra with $[M-H]^{-}$ (observed 1918.03, expected 1918.04).

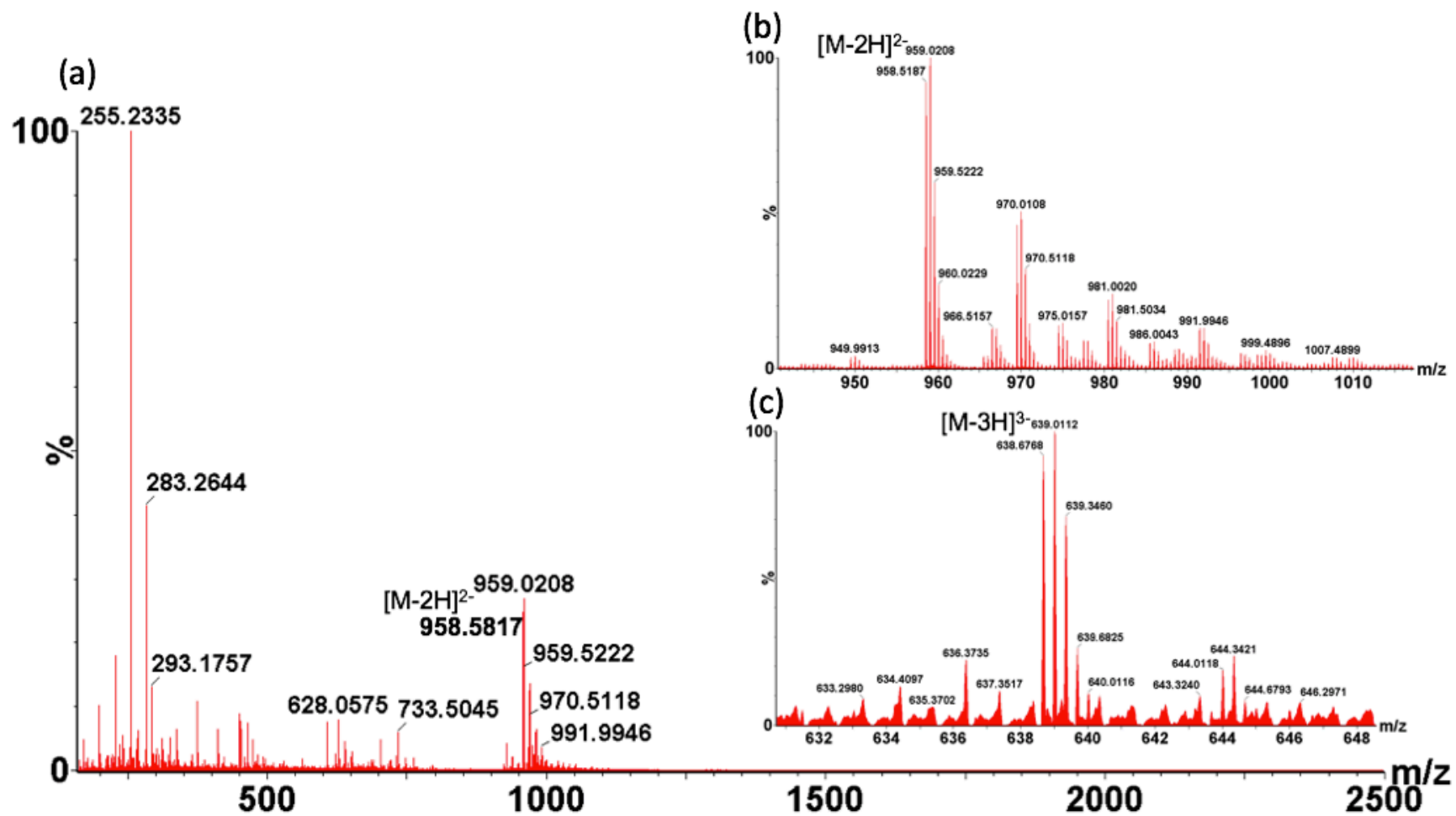


Figure A3.28: Negative ion mass spectrometry of Lipid II (DAP) synthesis sample incubated with 50 μM pywac compound 1. (a): mass spectra with $[\text{M}-2\text{H}]^{2-}$ (observed 958.51, expected 958.51). (b): Observed isotope distribution of $[\text{M}-2\text{H}]^{2-}$ (zoomed in view of $[\text{M}-2\text{H}]^{2-}$ peak shown in (a)). (c): Mass spectra of $[\text{M}-3\text{H}]^{3-}$ (observed 638.67, expected 638.67). (deconvoluted by MassLynxTM software (Waters, USA)).

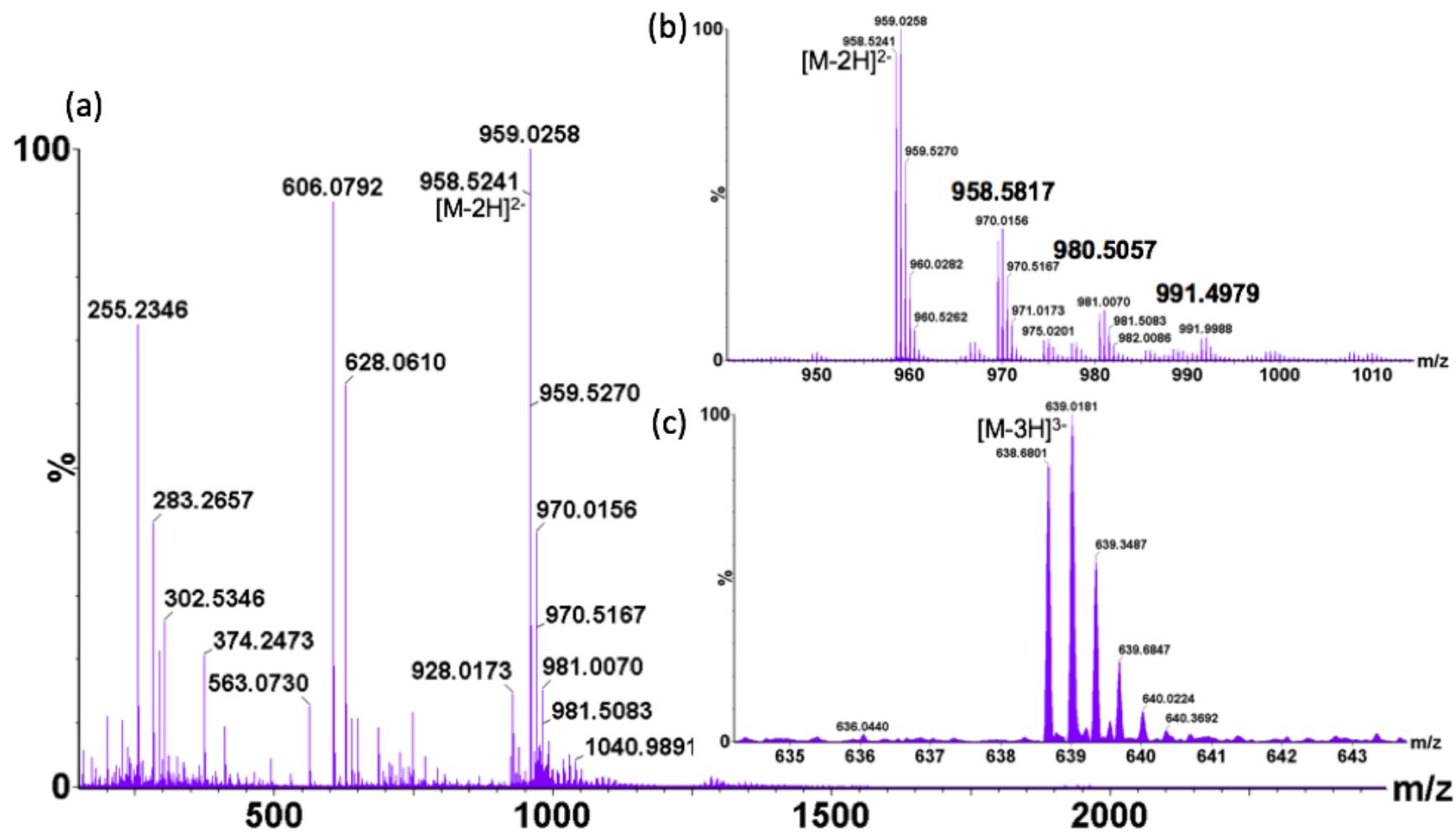


Figure A3.29: Negative ion mass spectrometry of Lipid II (DAP) synthesis sample incubated with 50 μ M pywac compound 2. (a): mass spectra with $[M-2H]^{2-}$ (observed 958.52, expected 958.51). (b): Observed isotope distribution of $[M-2H]^{2-}$ (zoomed in view of $[M-2H]^{2-}$ peak shown in (a)). (c): Mass spectra of $[M-3H]^{3-}$ (observed 638.68, expected 638.67). (deconvoluted by MassLynxTM software (Waters, USA)).

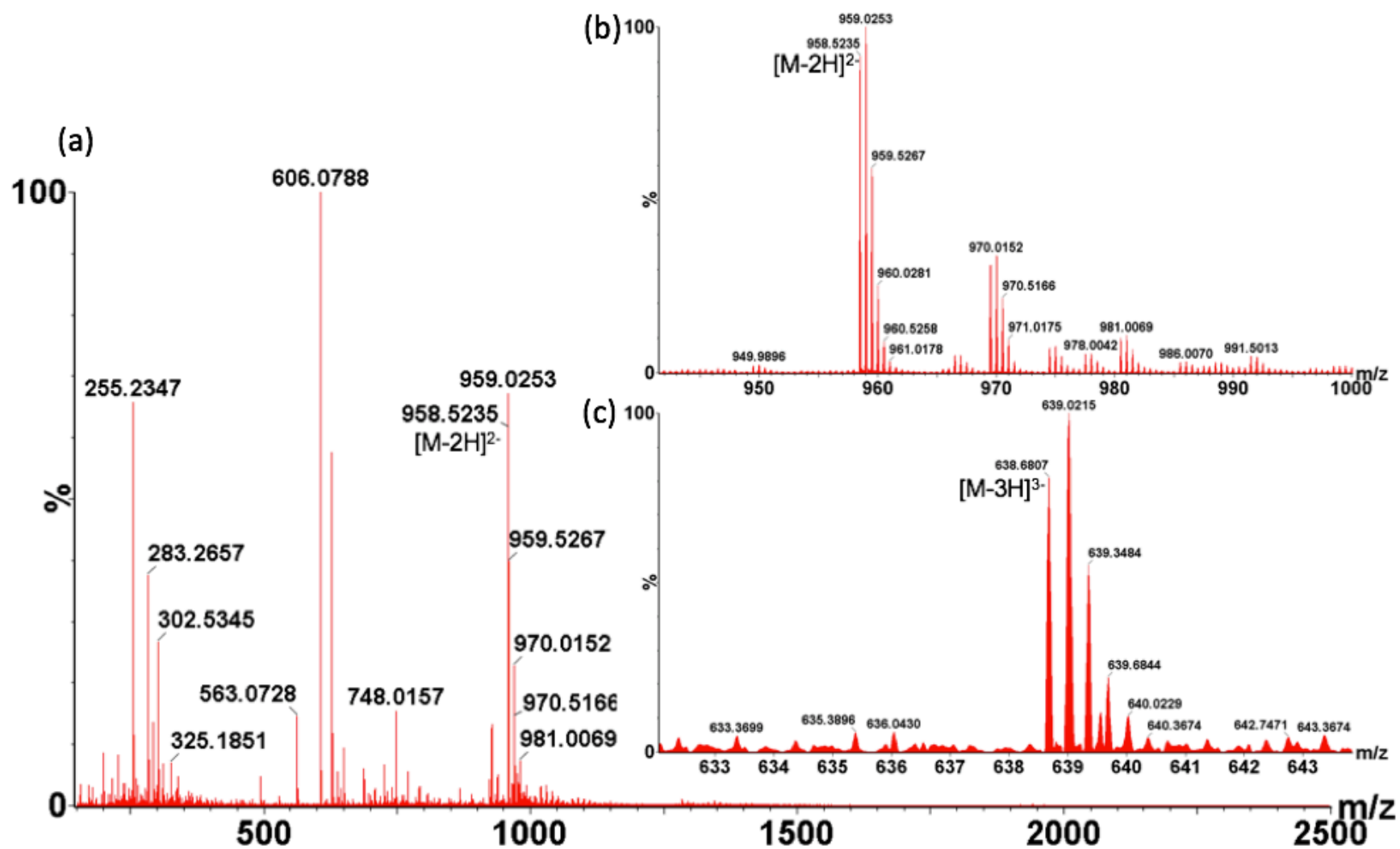


Figure A3.30: Negative ion mass spectrometry of Lipid II (DAP) synthesis sample incubated with 50 μ M pywac compound 3. (a): mass spectra with $[M-2H]^{2-}$ (observed 958.52, expected 958.51). (b): Observed isotope distribution of $[M-2H]^{2-}$ (zoomed in view of $[M-2H]^{2-}$ peak shown in (a)). (c): Mass spectra of $[M-3H]^{3-}$ (observed 638.68, expected 638.67). (deconvoluted by MassLynxTM software (Waters, USA)).

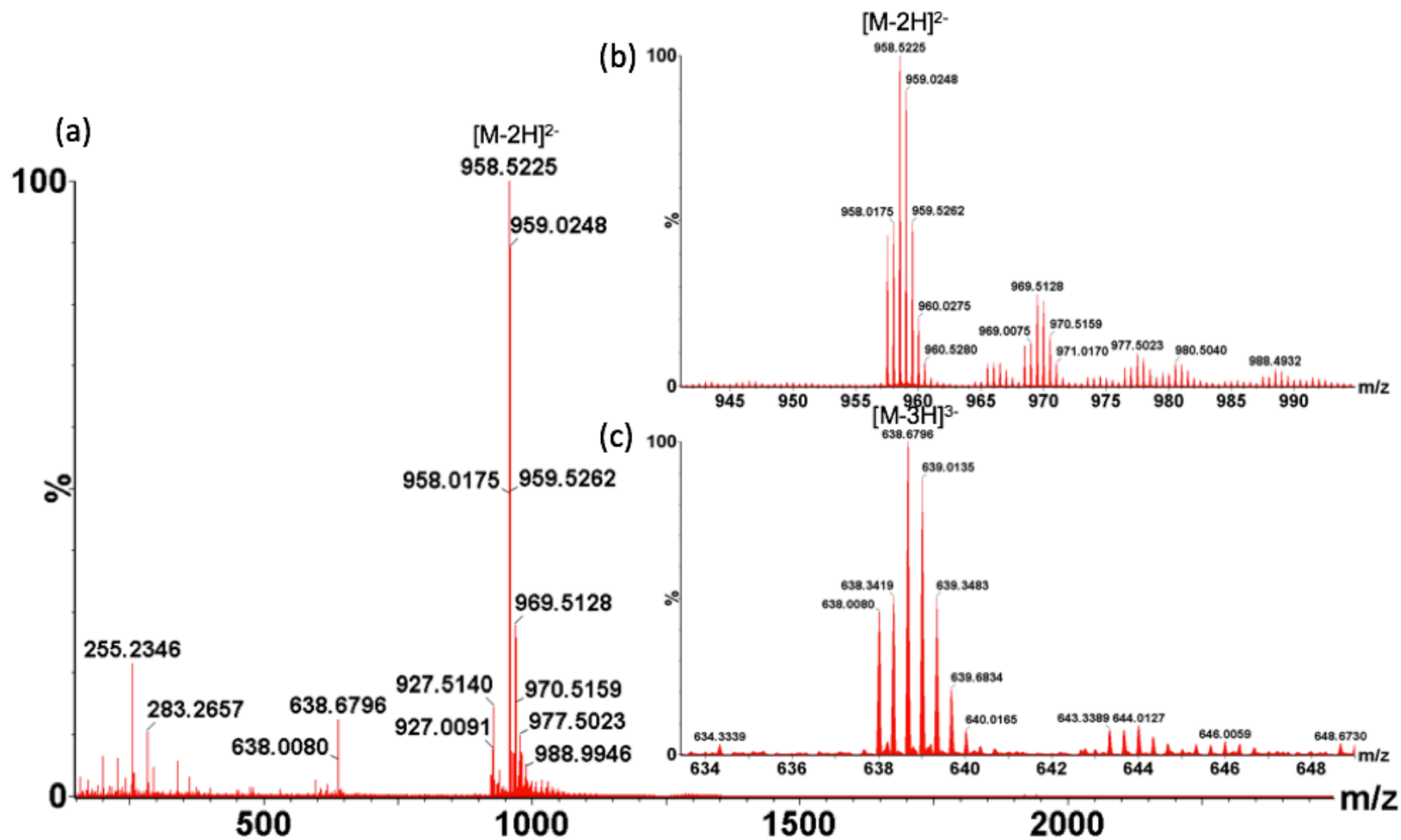


Figure A3.31: Negative ion mass spectrometry of Lipid II (DAP) synthesis sample incubated with 50 μ M pywac compound 4. (a): mass spectra with $[M-2H]^{2-}$ (observed 958.52, expected 958.51). (b): Observed isotope distribution of $[M-2H]^{2-}$ (zoomed in view of $[M-2H]^{2-}$ peak shown in (a)). (c): Mass spectra of $[M-3H]^{3-}$ (observed 638.67, expected 638.67). (deconvoluted by MassLynx™ software (Waters, USA)).

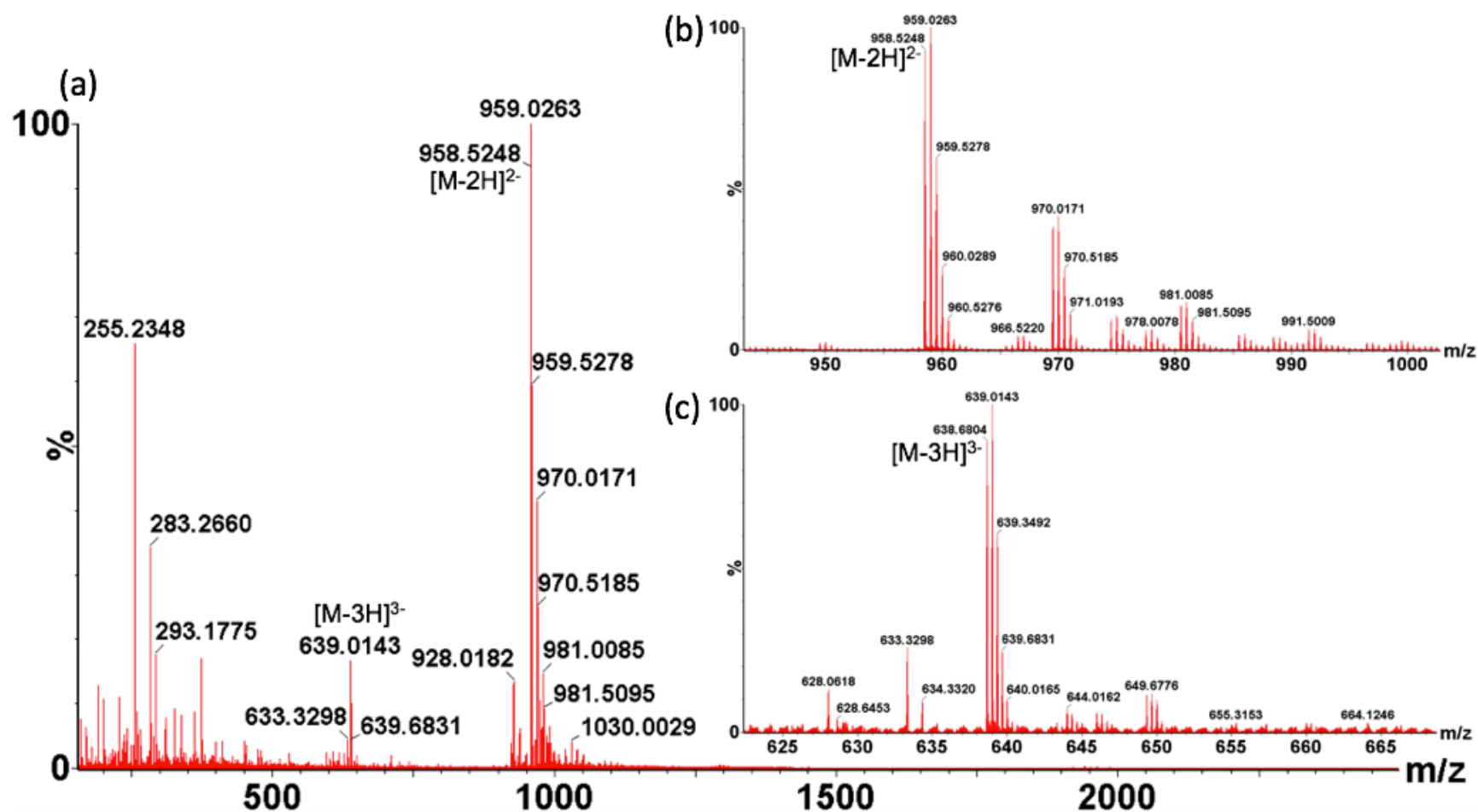


Figure A3.32: Negative ion mass spectrometry of Lipid II (DAP) synthesis sample incubated with 50 μ M pywac compound 5. (a): mass spectra with $[M-2H]^{2-}$ (observed 958.52, expected 958.51). (b): Observed isotope distribution of $[M-2H]^{2-}$ (zoomed in view of $[M-2H]^{2-}$ peak shown in (a)). (c): Mass spectra of $[M-3H]^{3-}$ (observed 638.68, expected 638.67). (deconvoluted by MassLynx™ software (Waters, USA)).

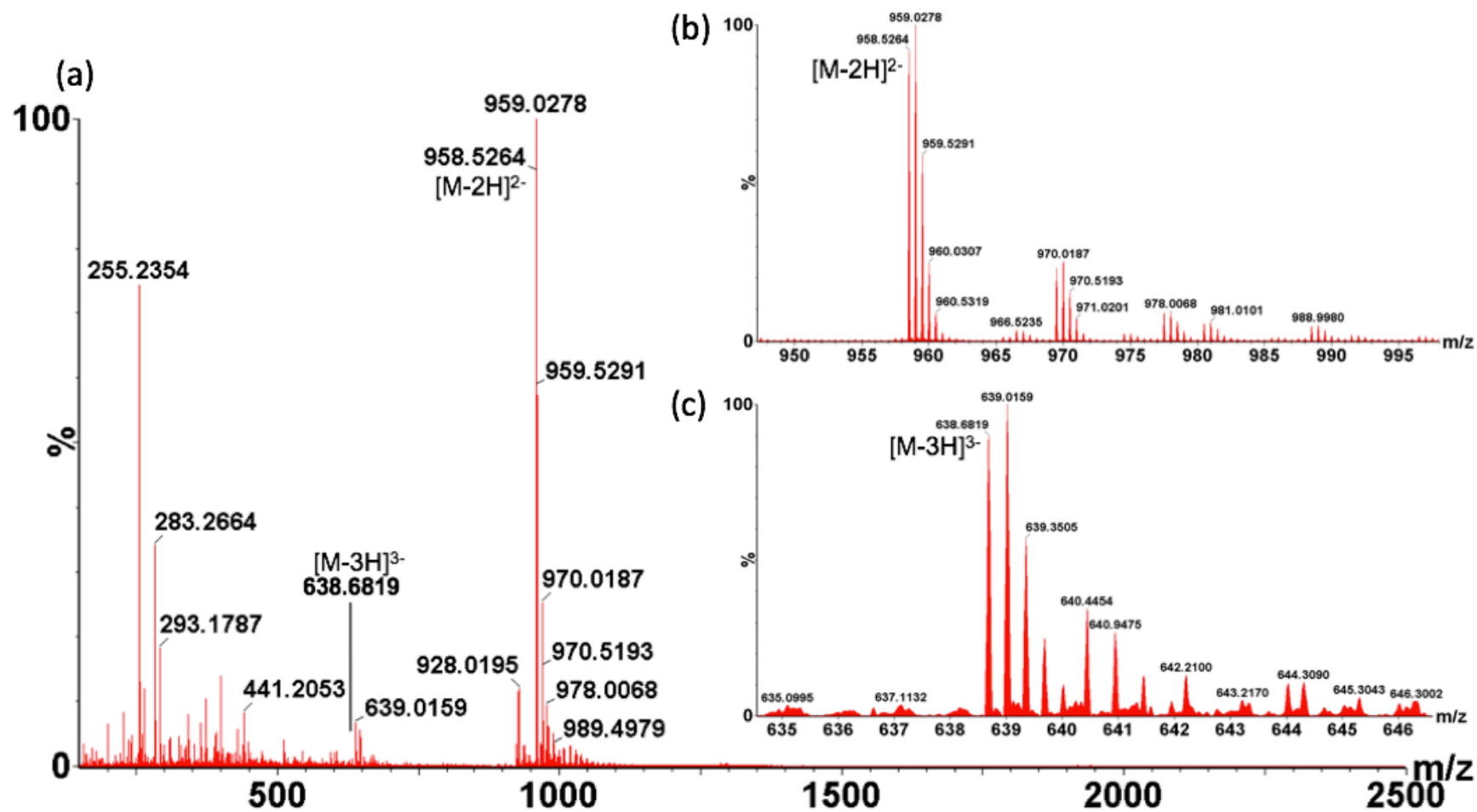


Figure A3.33: Negative ion mass spectrometry of Lipid II (DAP) synthesis sample incubated with 50 μM pywac compound 6. (a): mass spectra with $[\text{M}-2\text{H}]^{2-}$ (observed 958.52, expected 958.51). (b): Observed isotope distribution of $[\text{M}-2\text{H}]^{2-}$ (zoomed in view of $[\text{M}-2\text{H}]^{2-}$ peak shown in (a)). (c): Mass spectra of $[\text{M}-3\text{H}]^{3-}$ (observed 638.68, expected 638.67). (deconvoluted by MassLynxTM software (Waters, USA)).

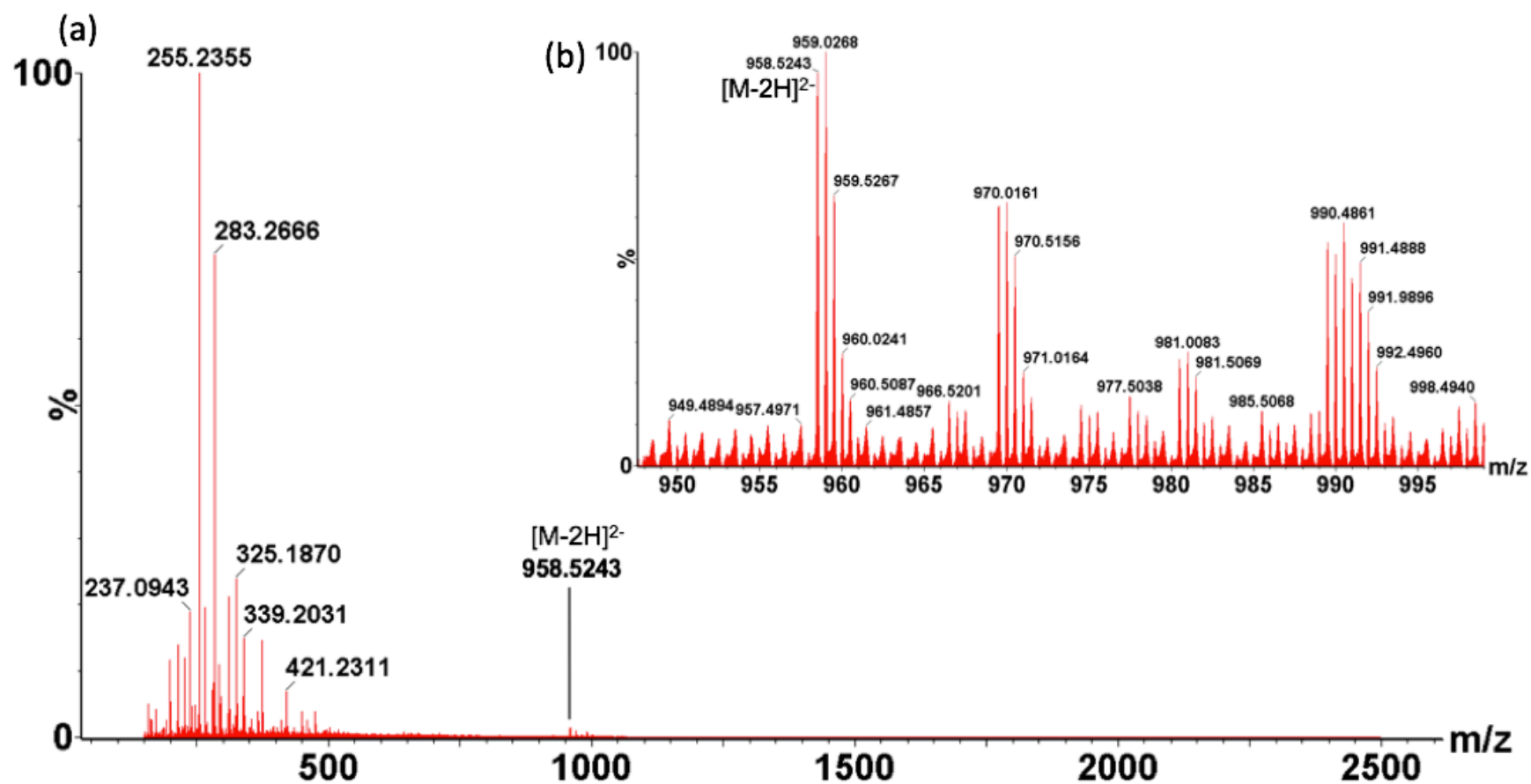


Figure A3.34: Negative ion mass spectrometry of Lipid II (DAP) synthesis sample incubated with 50 μM pywac compound 7. (a): mass spectra with $[M-2H]^{2-}$ (observed 958.52, expected 958.51). (b): Observed isotope distribution of $[M-2H]^{2-}$ (zoomed in view of $[M-2H]^{2-}$ peak shown in (a)). (deconvoluted by MassLynxTM software (Waters, USA)).

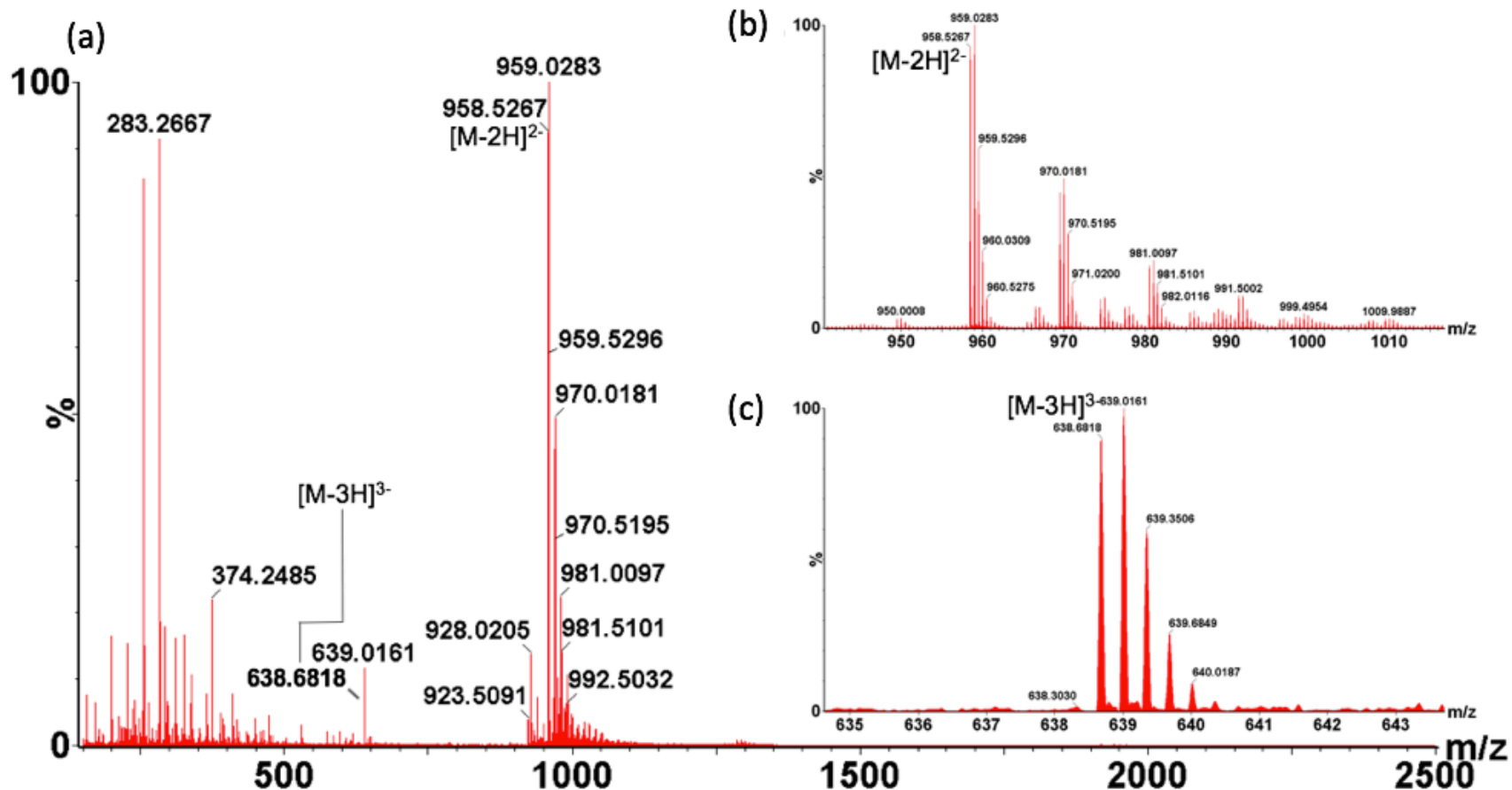


Figure A3.35: Negative ion mass spectrometry of Lipid II (DAP) synthesis sample incubated with 50 μM pywac compound 8. (a): mass spectra with $[\text{M}-2\text{H}]^{2-}$ (observed 958.52, expected 958.51). (b): Observed isotope distribution of $[\text{M}-2\text{H}]^{2-}$ (zoomed in view of $[\text{M}-2\text{H}]^{2-}$ peak shown in (a)). (c): Mass spectra of $[\text{M}-3\text{H}]^{3-}$ (observed 638.68, expected 638.67). (deconvoluted by MassLynxTM software (Waters, USA)).

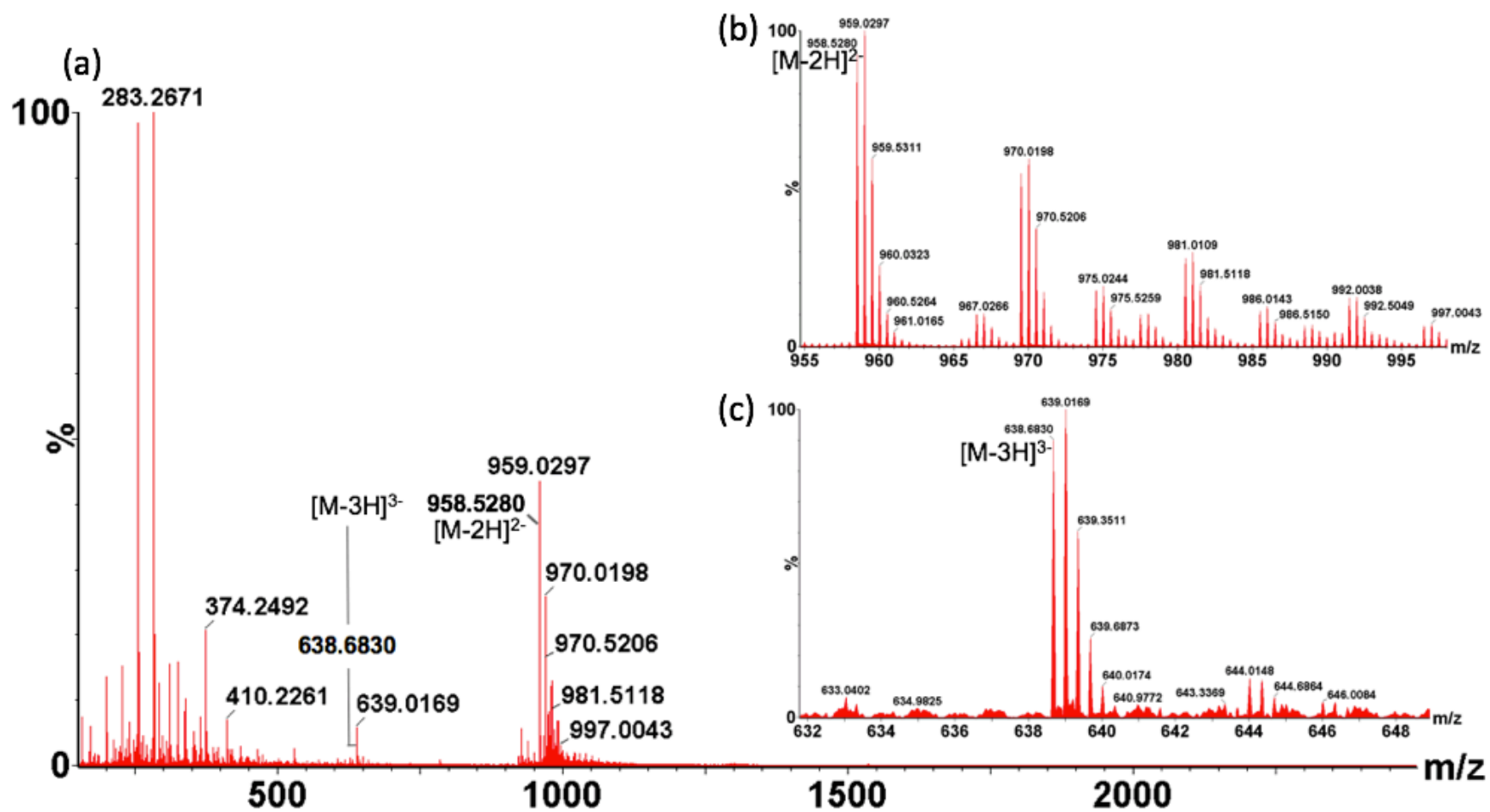


Figure A3.36: Negative ion mass spectrometry of Lipid II (DAP) synthesis sample incubated with 50 μM pywac compound 9. (a): mass spectra with $[\text{M}-2\text{H}]^{2-}$ (observed 958.52, expected 958.51) $[\text{M}-3\text{H}]^{3-}$ (observed 638.68, expected 638.67). (b): Observed isotope distribution of $[\text{M}-2\text{H}]^{2-}$ (zoomed in view of $[\text{M}-2\text{H}]^{2-}$ peak shown in (a)). (c): Mass spectra of $[\text{M}-3\text{H}]^{3-}$. (deconvoluted by MassLynx™ software (Waters, USA)).

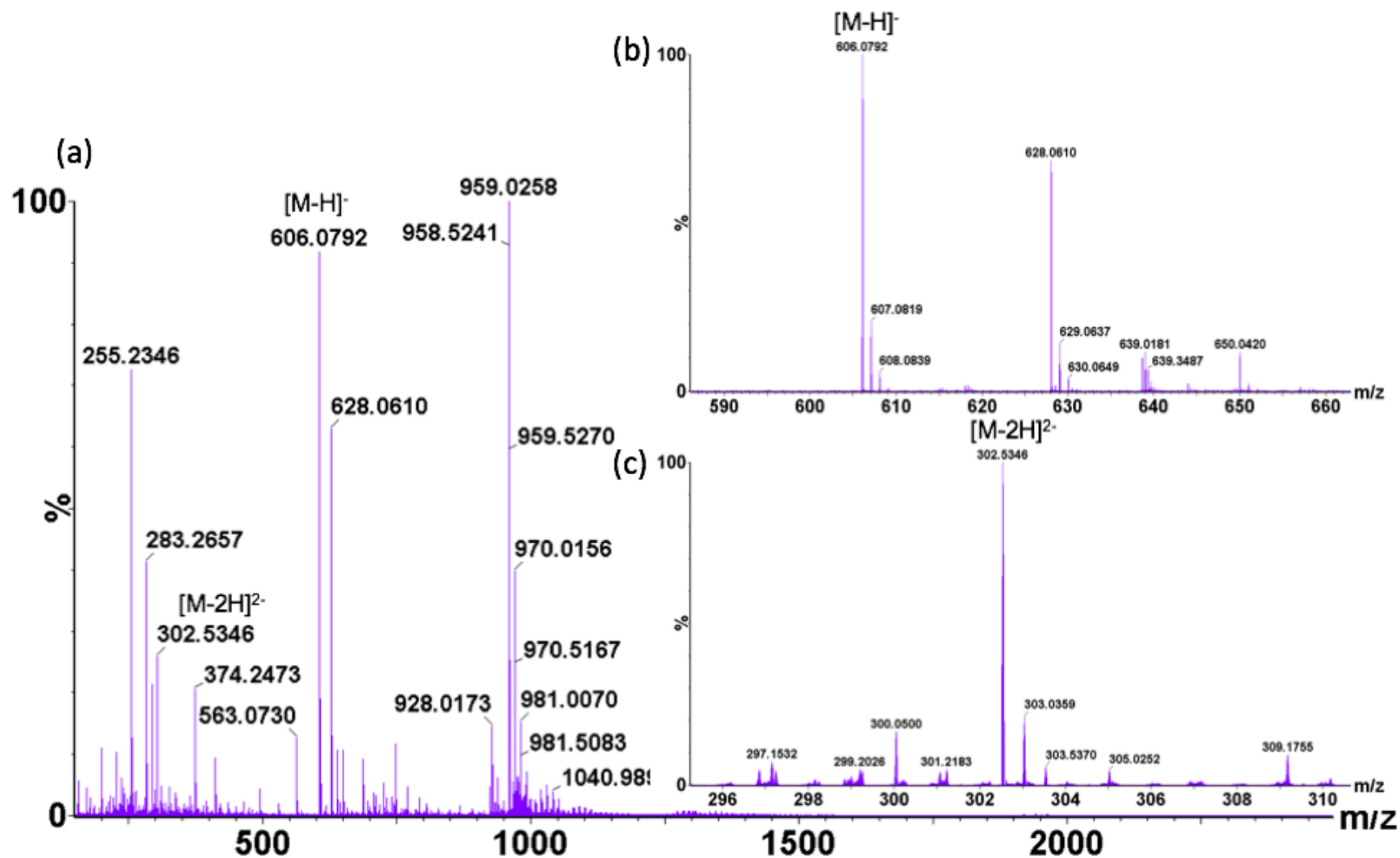


Figure A3.37: Negative ion mass spectrometry of UDP-GlcNAc present during Lipid II DAP synthesis incubated with 50 μ M pywac 2. UDP-GlcNAc (a): mass spectra with [M-H]⁻ (observed 606.07, expected 606.07) and [M-2H]²⁻ (observed 302.53, expected 302.53) (deconvoluted by MassLynx™ software (Waters, USA)). (b): Observed isotope distribution of [M-H]⁻ (zoomed in view of [M-H]⁻ peak shown in (a)). (c): Observed isotope distribution of [M-2H]²⁻ (zoomed in view of [M-2H]²⁻ peak shown in (a)).

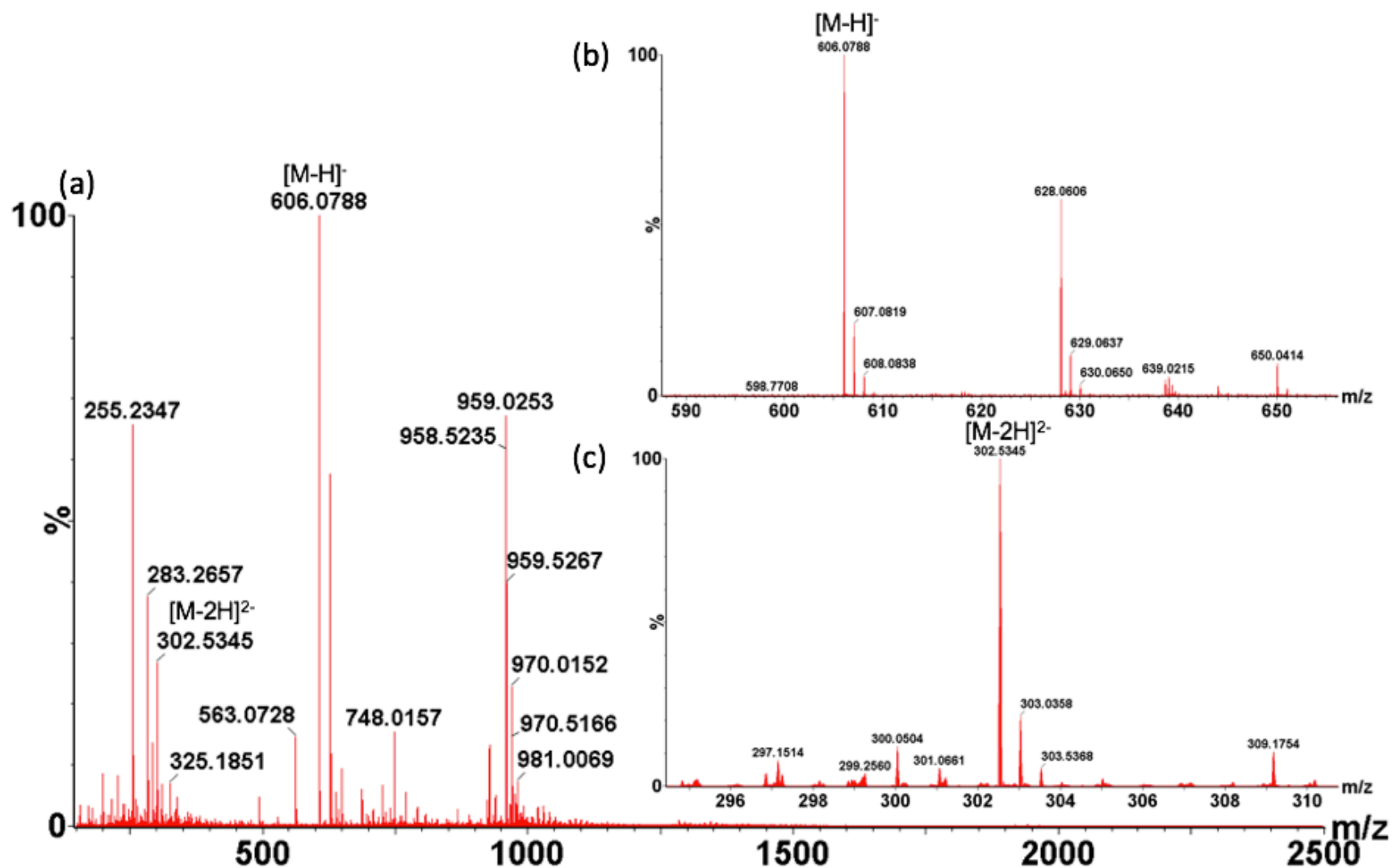


Figure A3.38: Negative ion mass spectrometry of UDP-GlcNAc present during Lipid II DAP synthesis incubated with 50 μ M pywac 3. UDP-GlcNAc (a): mass spectra with $[M-H]^-$ (observed 606.07, expected 606.07) and $[M-2H]^{2-}$ (observed 302.53, expected 302.53) (deconvoluted by MassLynxTM software (Waters, USA). (b): Observed isotope distribution of $[M-H]^-$ (zoomed in view of $[M-H]^-$ peak shown in (a)). (c): Observed isotope distribution of $[M-2H]^{2-}$ (zoomed in view of $[M-2H]^{2-}$ peak shown in (a)).

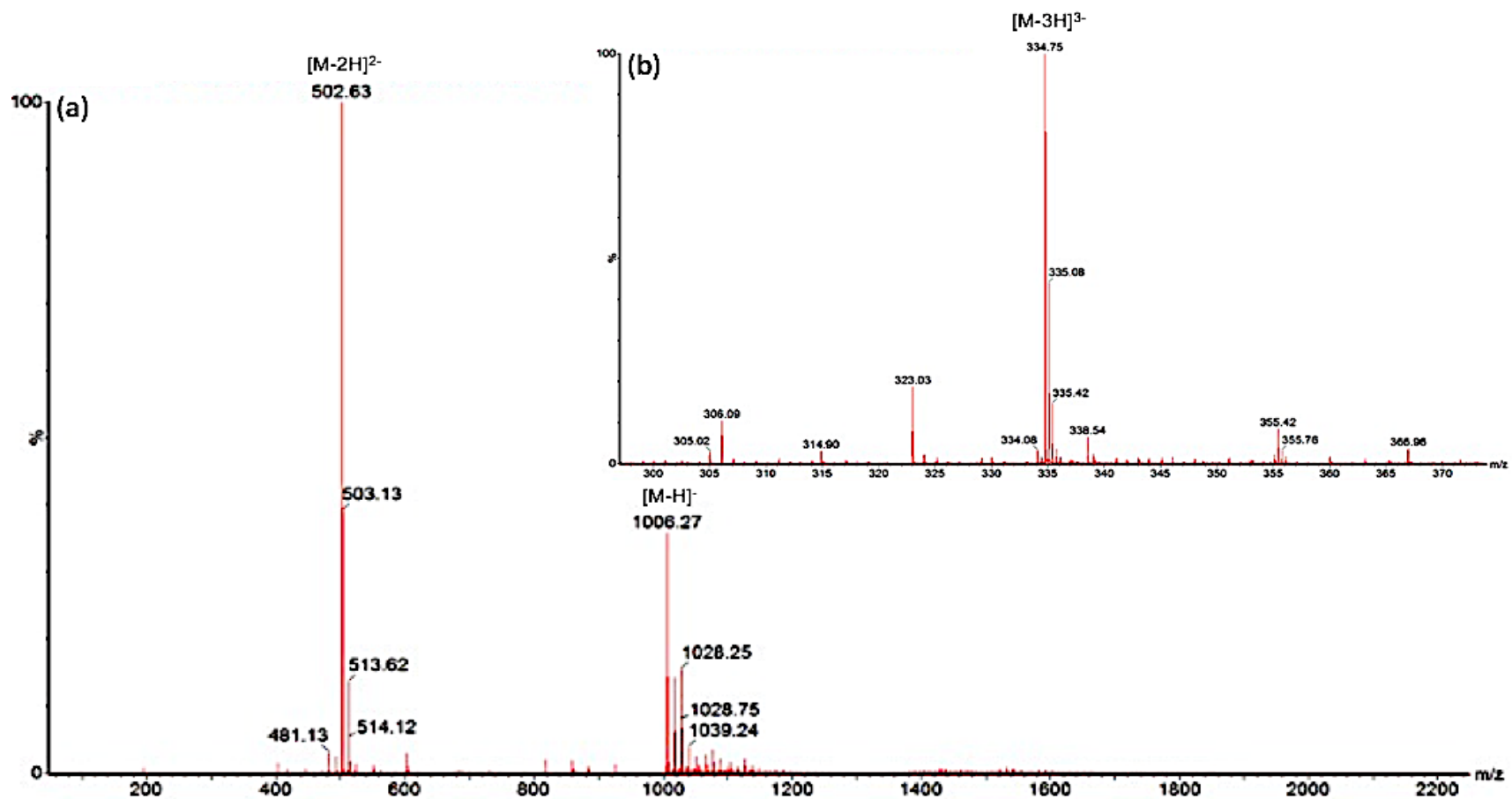


Figure A3.39: Negative ion mass spectrometry of MurNAc-tripeptide Lys standard. (a): mass spectra with $[M-H]^-$ (observed 1006.27, expected 1006.26) and $[M-2H]^{2-}$ (observed 502.63, expected 502.63) (deconvoluted) by MassLynx™ software (Waters, USA). (b): Zoomed in view of $[M-3H]^{3-}$ (observed 334.75, expected 334.75) peak shown in (a).

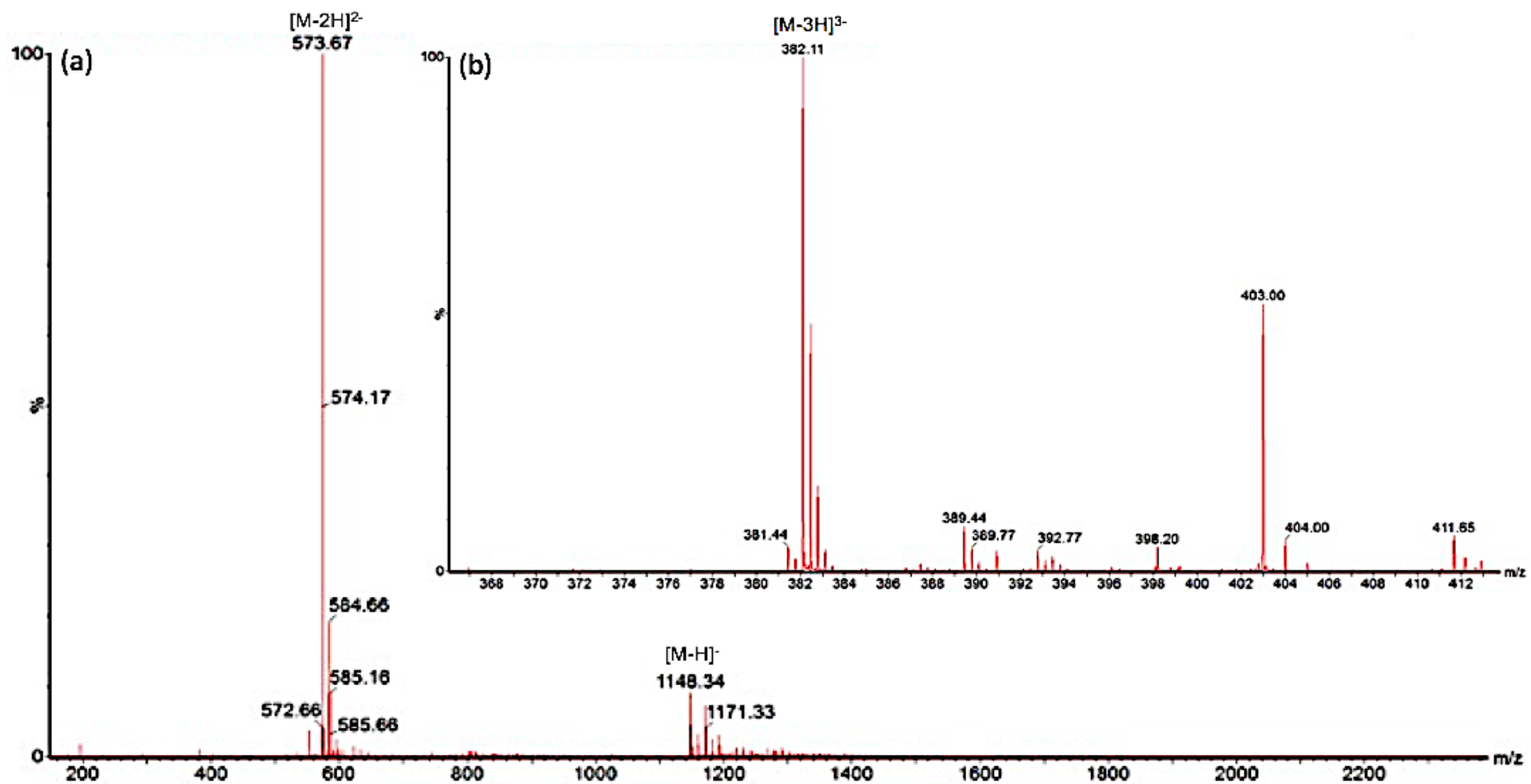


Figure A3.40: Negative ion mass spectrometry of MurNAc-pentapeptide Lys standard. (a): mass spectra with $[M-H]^{-}$ (observed 1148.34, expected 1148.34), $[M-2H]^{2-}$ (observed 573.67, expected 573.66) (deconvoluted by MassLynx™ software (Waters, USA)). (b): Zoomed in view of $[M-3H]^{3-}$ (observed 382.11, expected 382.10).

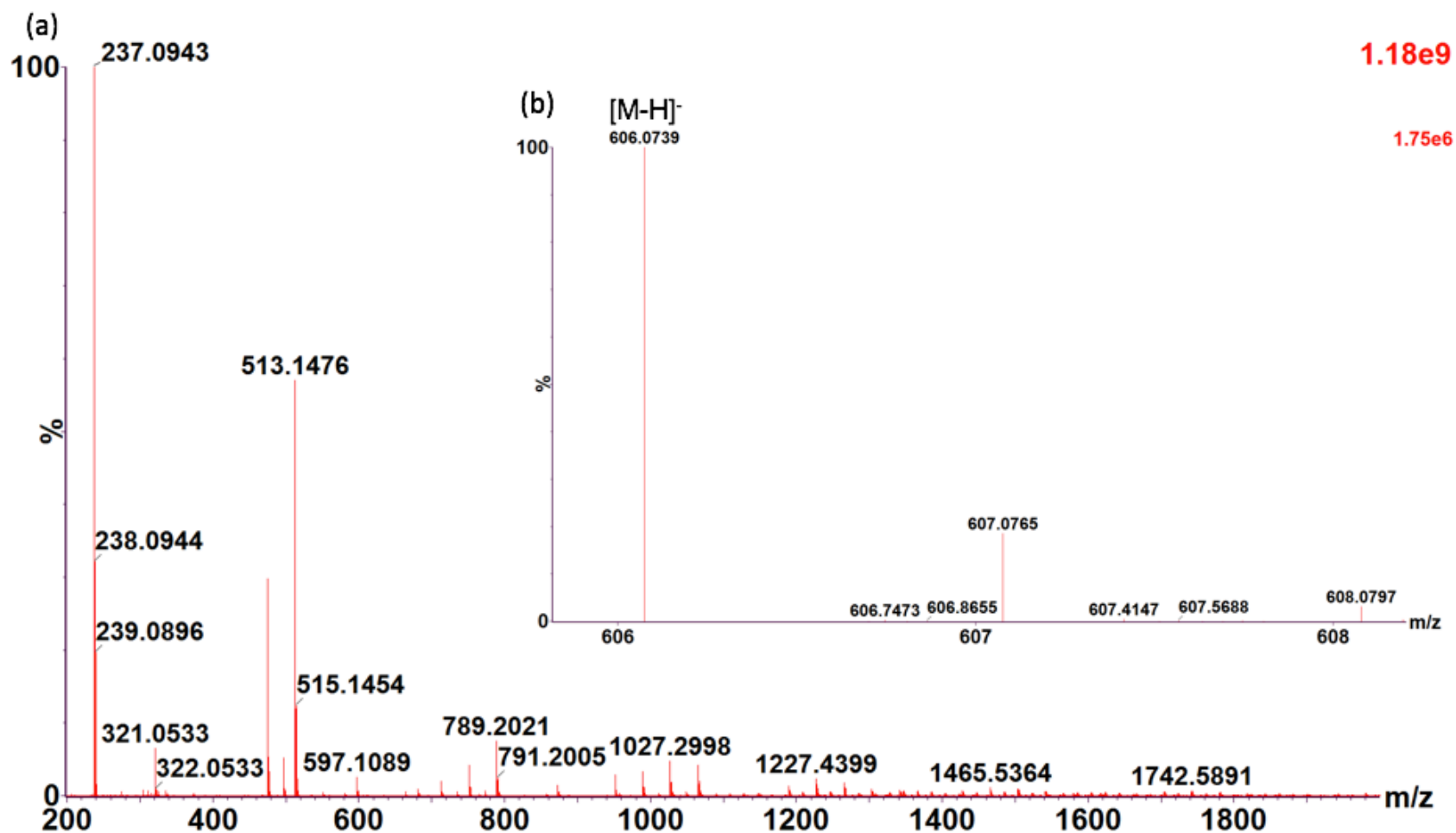


Figure A3.41: Negative ion mass spectrometry of the isolated accumulated peak (i) from *S. aureus* control. (a): full mass spectra of accumulated peak (i), no identifiable m/z. (b): mass spectra of UDP-GlcNAc [M-H]⁻ (observed 606.07, expected 606.07) (zoomed in view of (a)). (deconvoluted by MassLynx™ software (Waters, USA)).

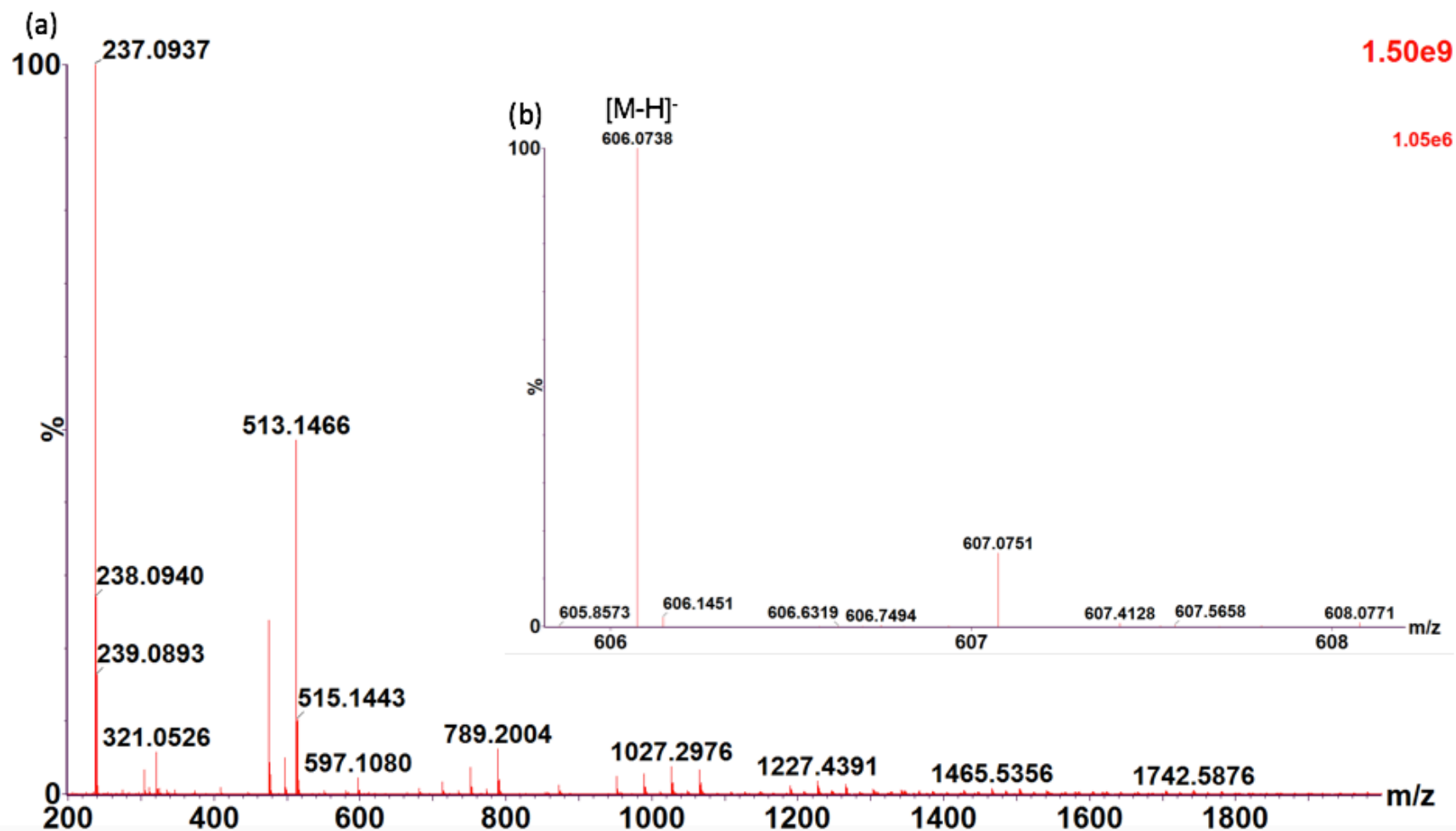


Figure A3.42: Negative ion mass spectrometry of the isolated accumulated peak (ii) from *S. aureus* control. (a): full mass spectra of accumulated peak (ii), no identifiable m/z. (b): mass spectra of UDP-GlcNAc [M-H]⁻ (observed 606.07, expected 606.07) (zoomed in view of (a)). (deconvoluted by MassLynx™ software (Waters, USA)).

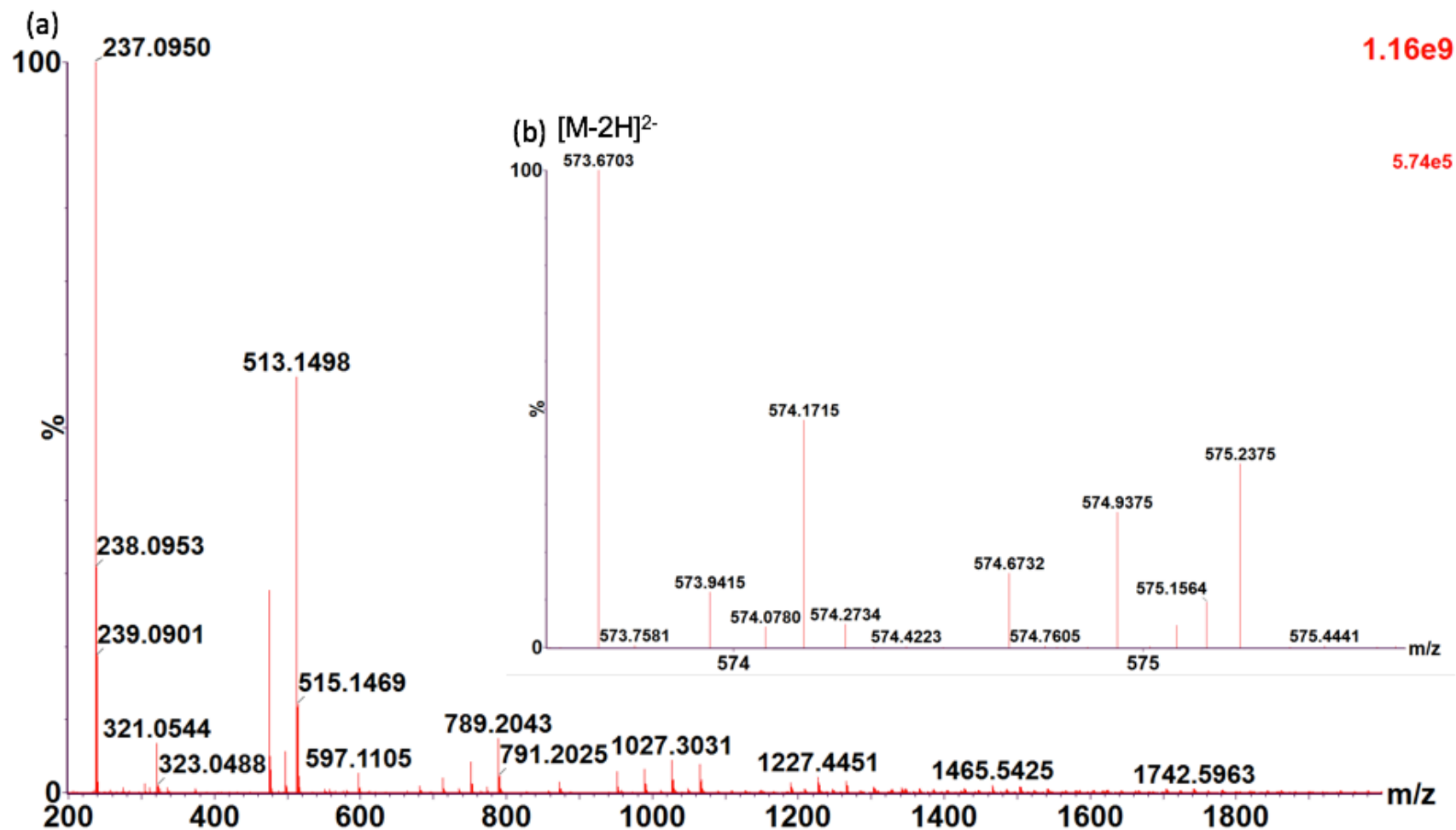


Figure A3.43: Negative ion mass spectrometry of the isolated accumulated peak (iii) from *S. aureus* control. (a): full mass spectra of accumulated peak (iii), no identifiable m/z. (b): mass spectra of UDP-MurNAc-pentapeptide Lys $[M-2H]^{2-}$ (observed 573.67, expected 573.66) (zoomed in view of (a)). (deconvoluted by MassLynxTM software (Waters, USA)).

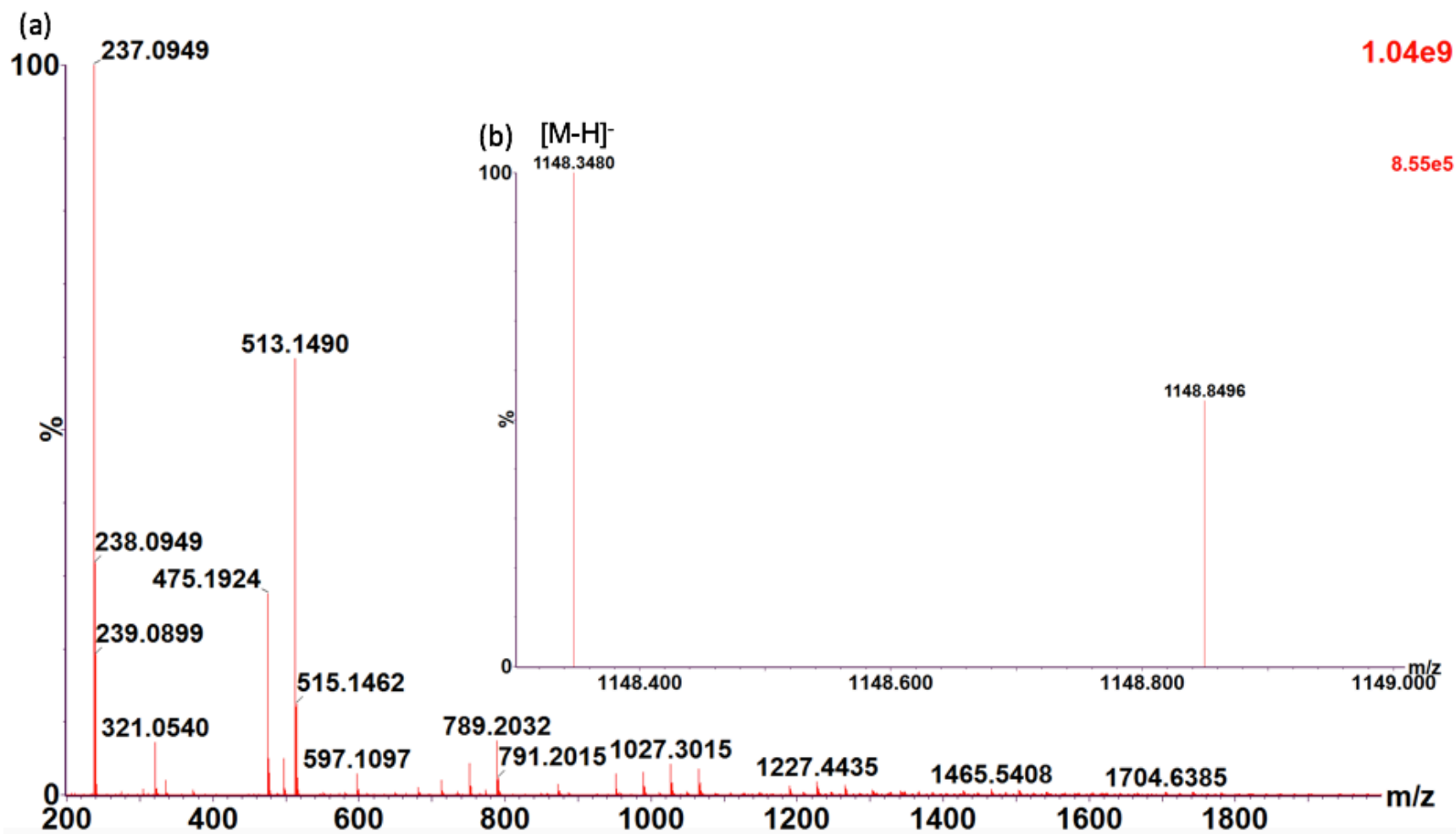


Figure A3.44: Negative ion mass spectrometry of the isolated accumulated peak (iv) from *S. aureus* control. (a): full mass spectra of accumulated peak (iv), no identifiable m/z. (b): mass spectra of UDP-MurNAc-pentapeptide Lys [M-H]⁻ (observed 1148.34, expected 1148.34) (zoomed in view of (a)). (deconvoluted by MassLynxTM software (Waters, USA)).

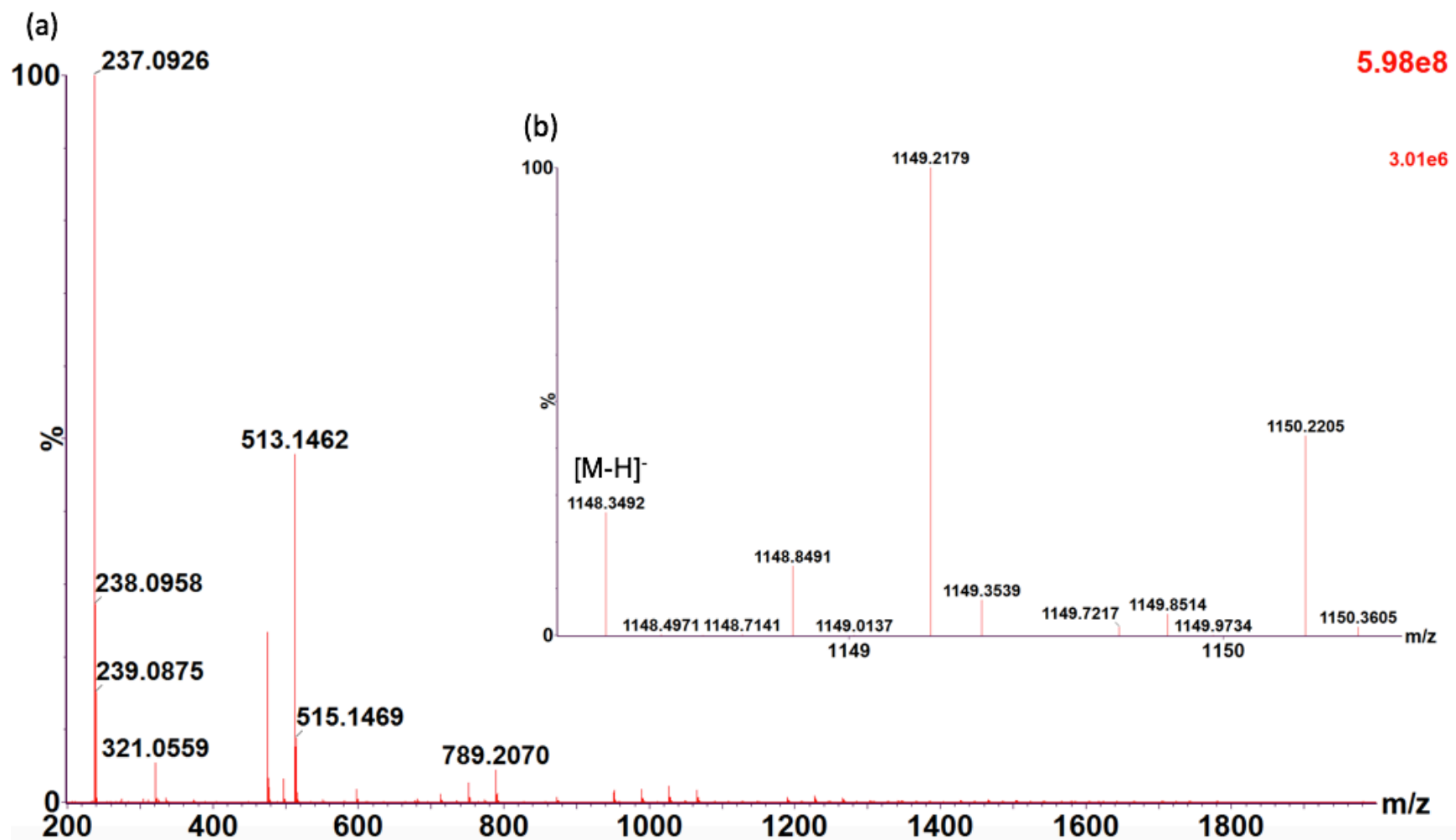


Figure A3.45: Negative ion mass spectrometry of the isolated accumulated peak (v) from *S. aureus* control. (a): full mass spectra of accumulated peak (v), no identifiable m/z. (b): mass spectra of UDP-MurNAc-pentapeptide Lys [M-H]⁻ (observed 1148.34, expected 1148.34) (zoomed in view of (a)). (deconvoluted by MassLynx™ software (Waters, USA)).

1.10e9

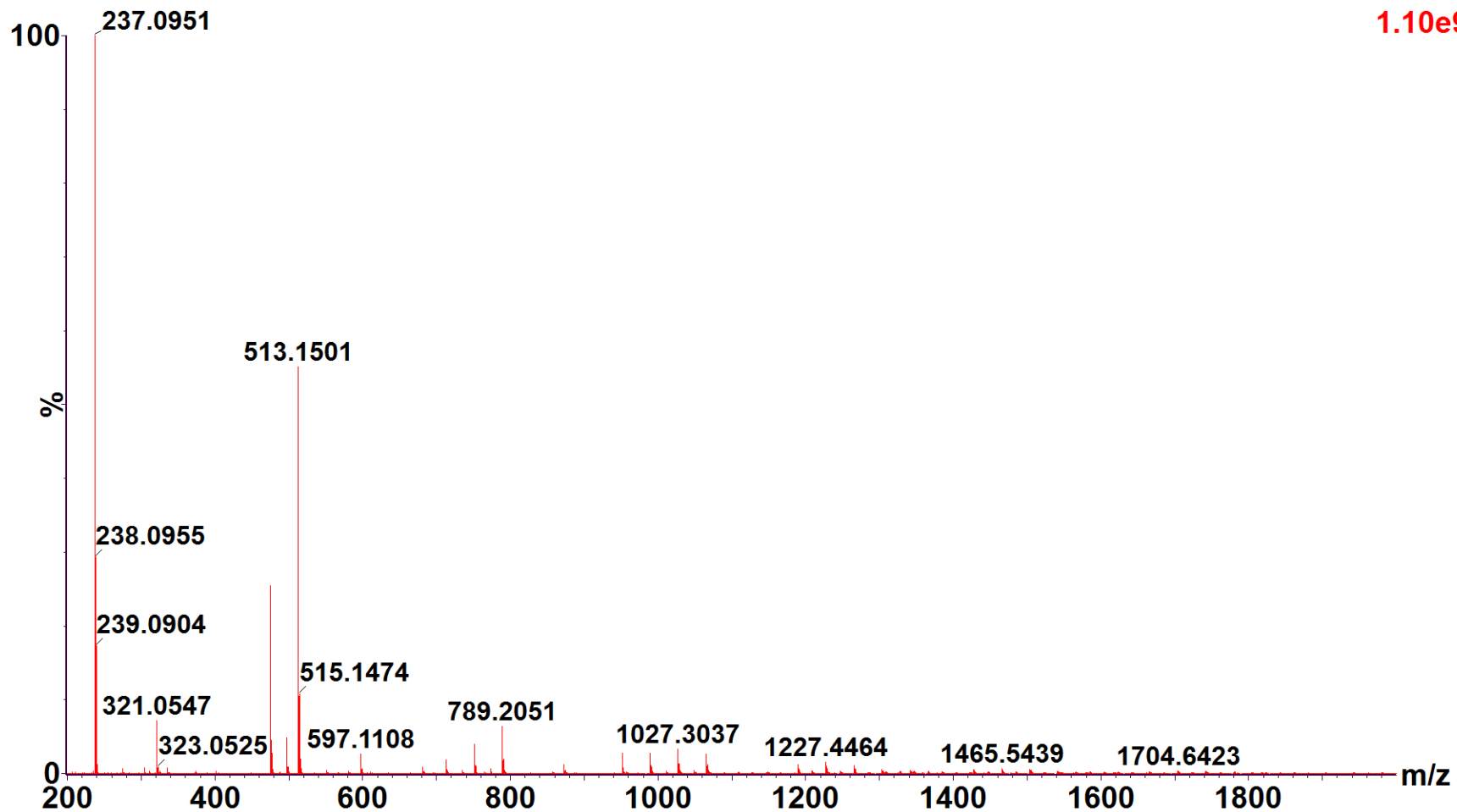


Figure A3.46: Negative ion mass spectrometry of the isolated accumulated peak (vi) from *S. aureus* control. No identifiable m/z observed. (deconvoluted by MassLynx™ software (Waters, USA)).

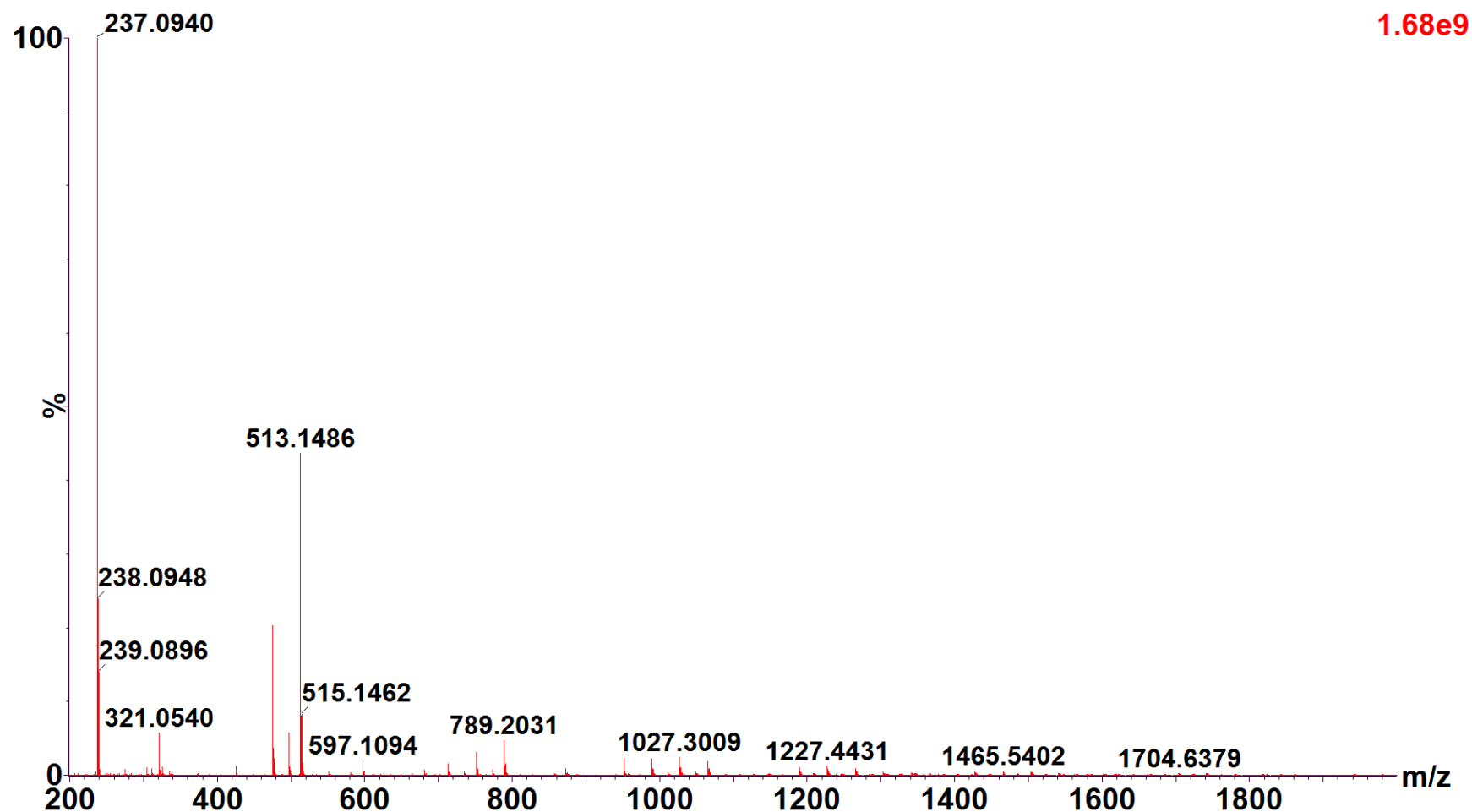


Figure A3.47 Negative ion mass spectrometry of the isolated accumulated peak (vii) from *S. aureus* control. No identifiable m/z observed. (deconvoluted by MassLynx™ software (Waters, USA)).

1.13e9

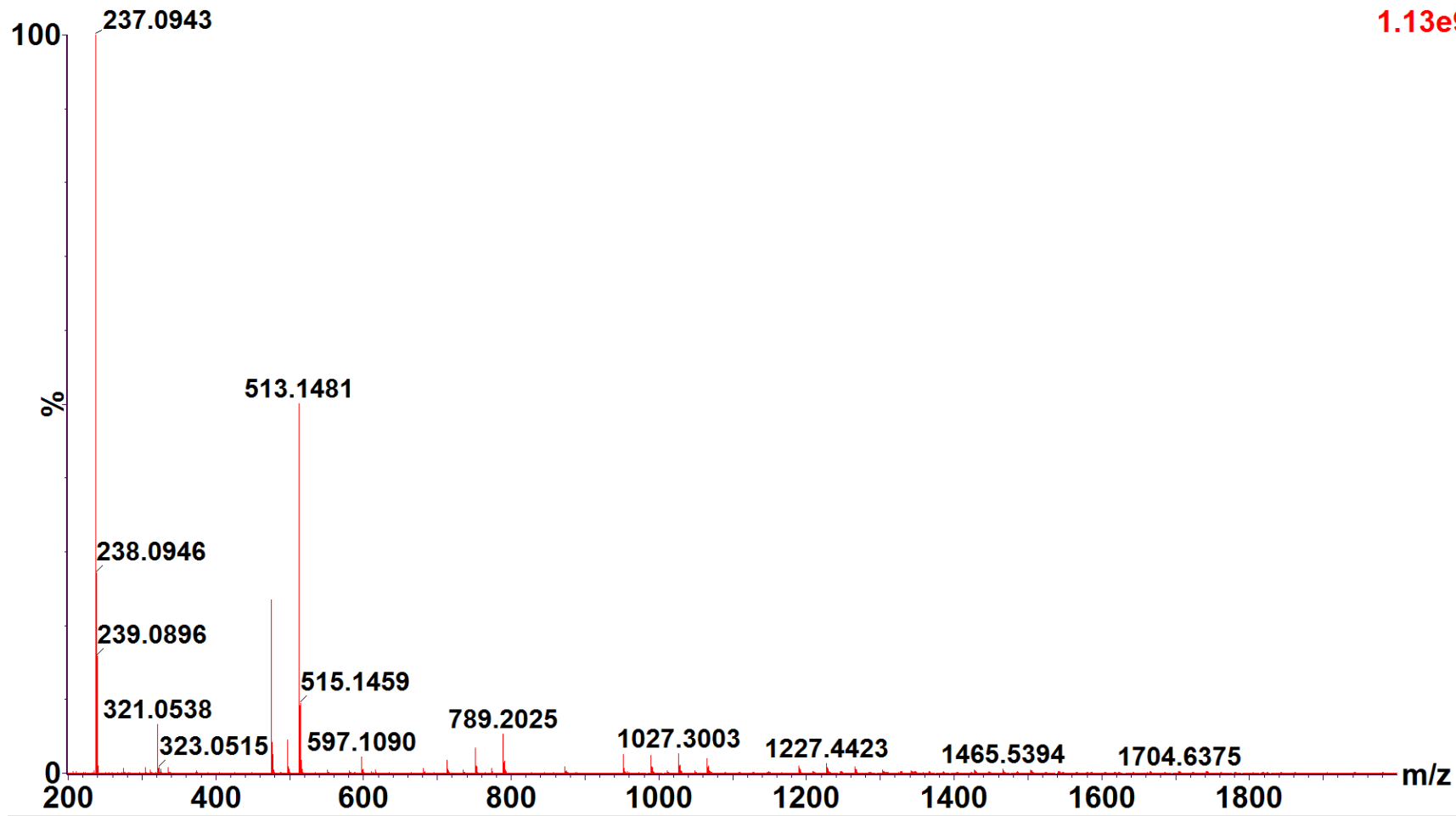


Figure A3.48: Negative ion mass spectrometry of the isolated accumulated peak (viii) from *S. aureus* control. No identifiable m/z observed. (deconvoluted by MassLynx™ software (Waters, USA).

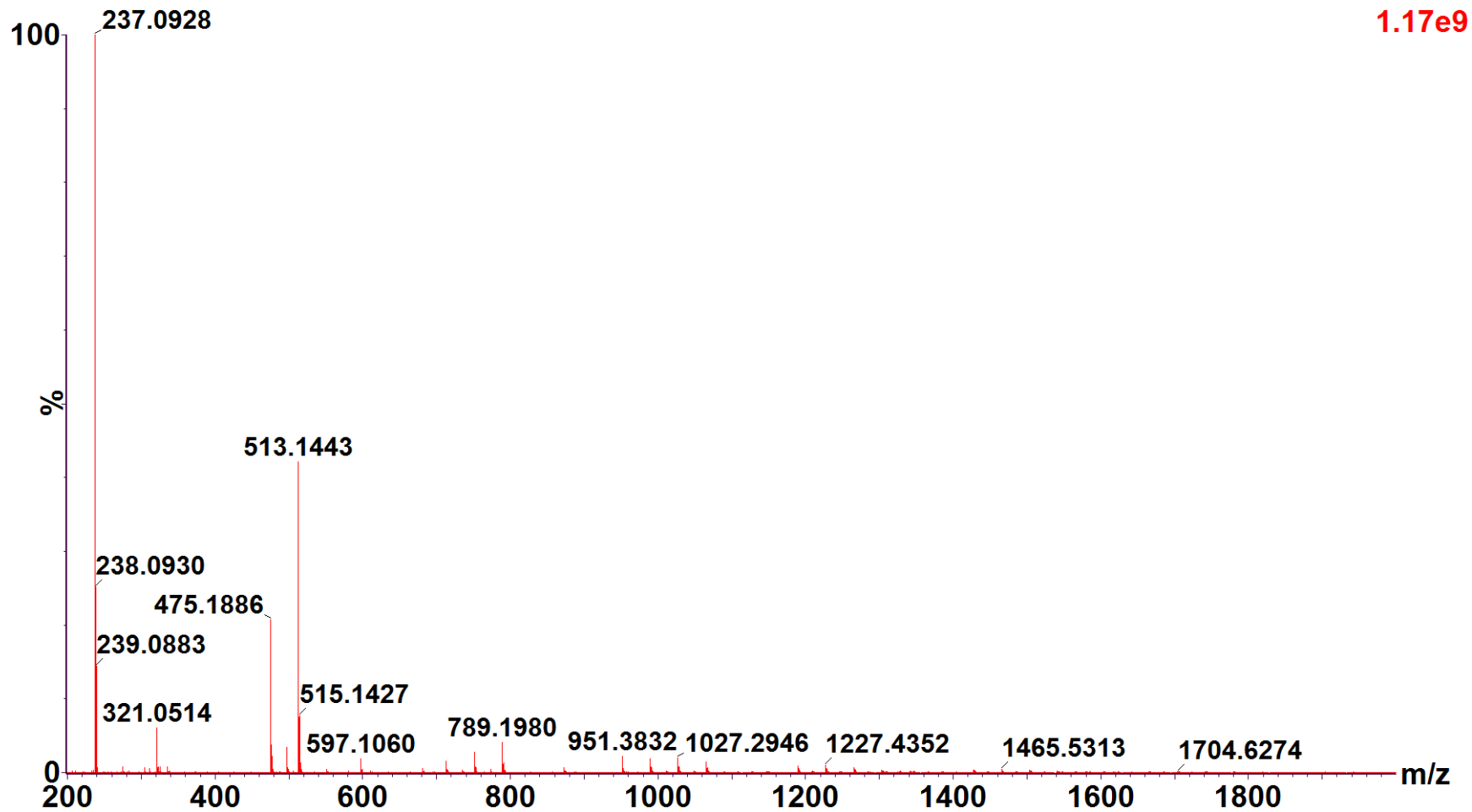


Figure A3.49: Negative ion mass spectrometry of the isolated accumulated peak (ix) from *S. aureus* control. No identifiable m/z observed. (deconvoluted by MassLynx™ software (Waters, USA)).

1.47e9

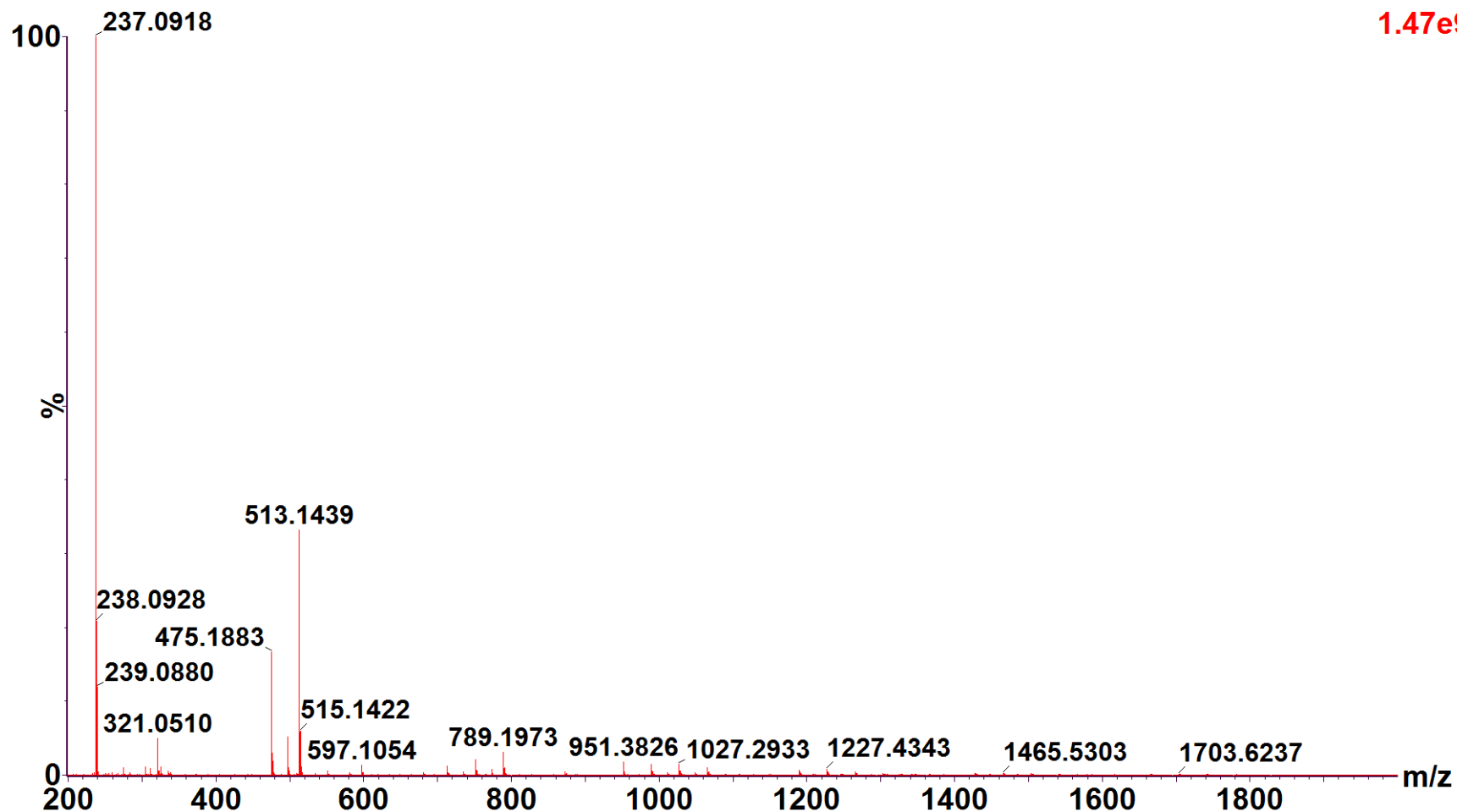


Figure A3.50: Negative ion mass spectrometry of the isolated accumulated peak (x) from *S. aureus* control. No identifiable m/z observed. (deconvoluted by MassLynx™ software (Waters, USA)).

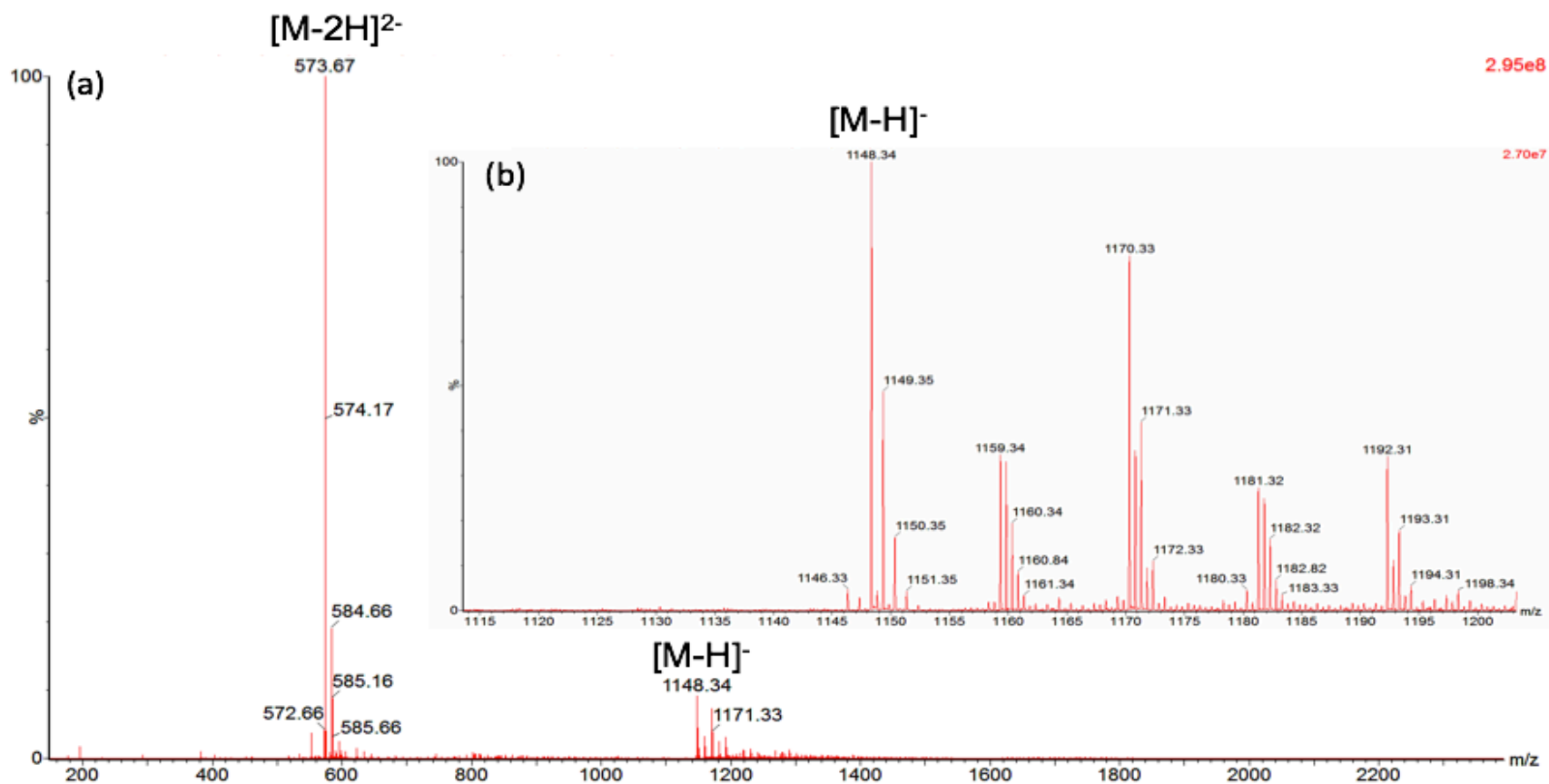


Figure A3.51: Negative ion mass spectrometry of the isolated accumulated peak of UDP-MurNAc-pentapeptide (Lys) from *S. aureus* incubated with 2x MIC vancomycin monoQ fraction. (a): mass spectra with $[M-H]^-$ (observed 1148.34, expected 1148.34), $[M-2H]^{2-}$ (observed 573.67, expected 573.66) (deconvoluted by MassLynxTM software (Waters, USA)). (b): Zoomed in view of $[M-H]^-$ peak shown in (a).

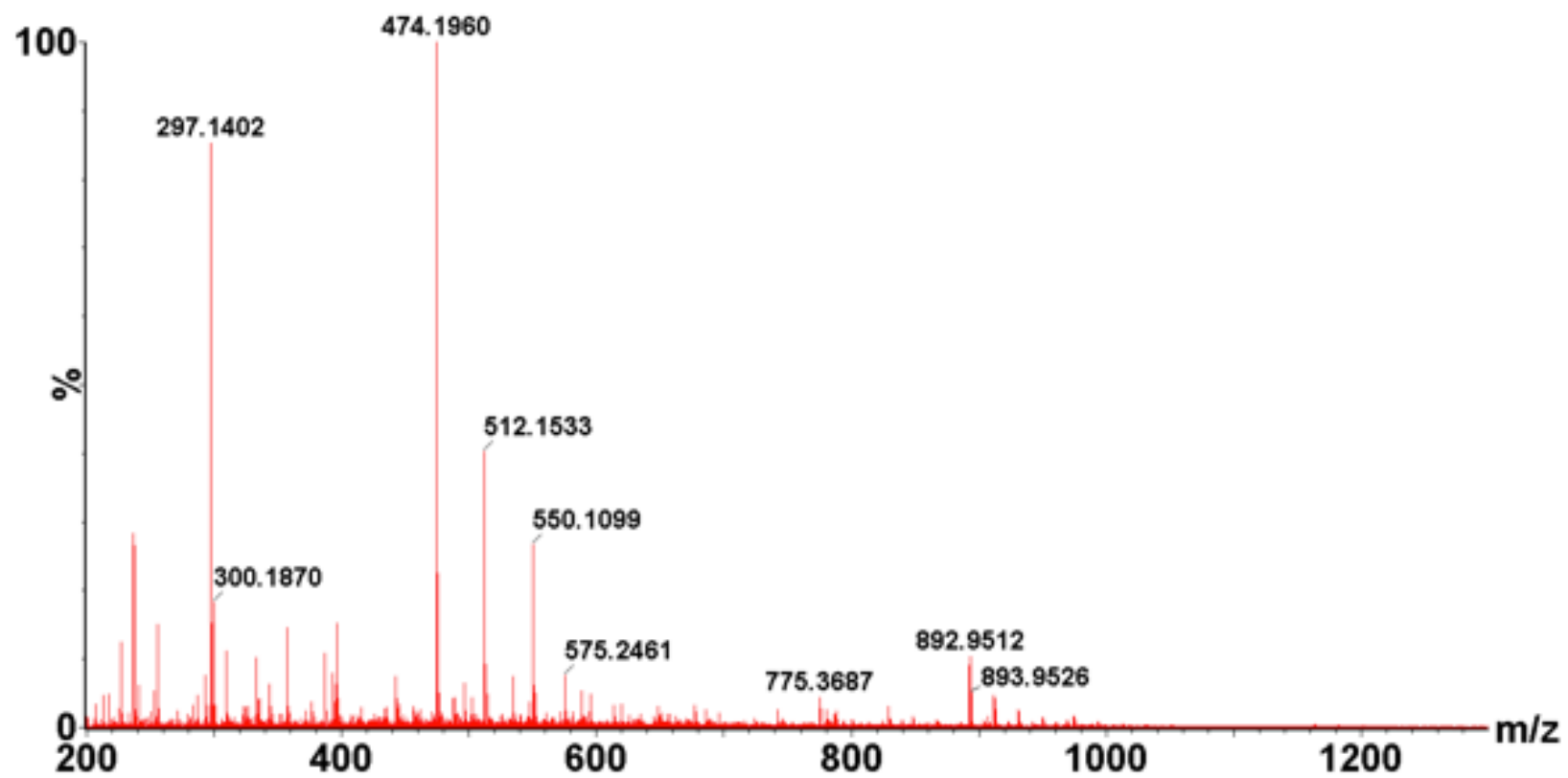


Figure A3.52: Negative ion mass spectrometry of the isolated accumulated peak from *S. aureus* incubated with 4 μ M pywac 1. Full mass spectra (no identifiable m/z) (deconvoluted by MassLynx™ software (Waters, USA)).

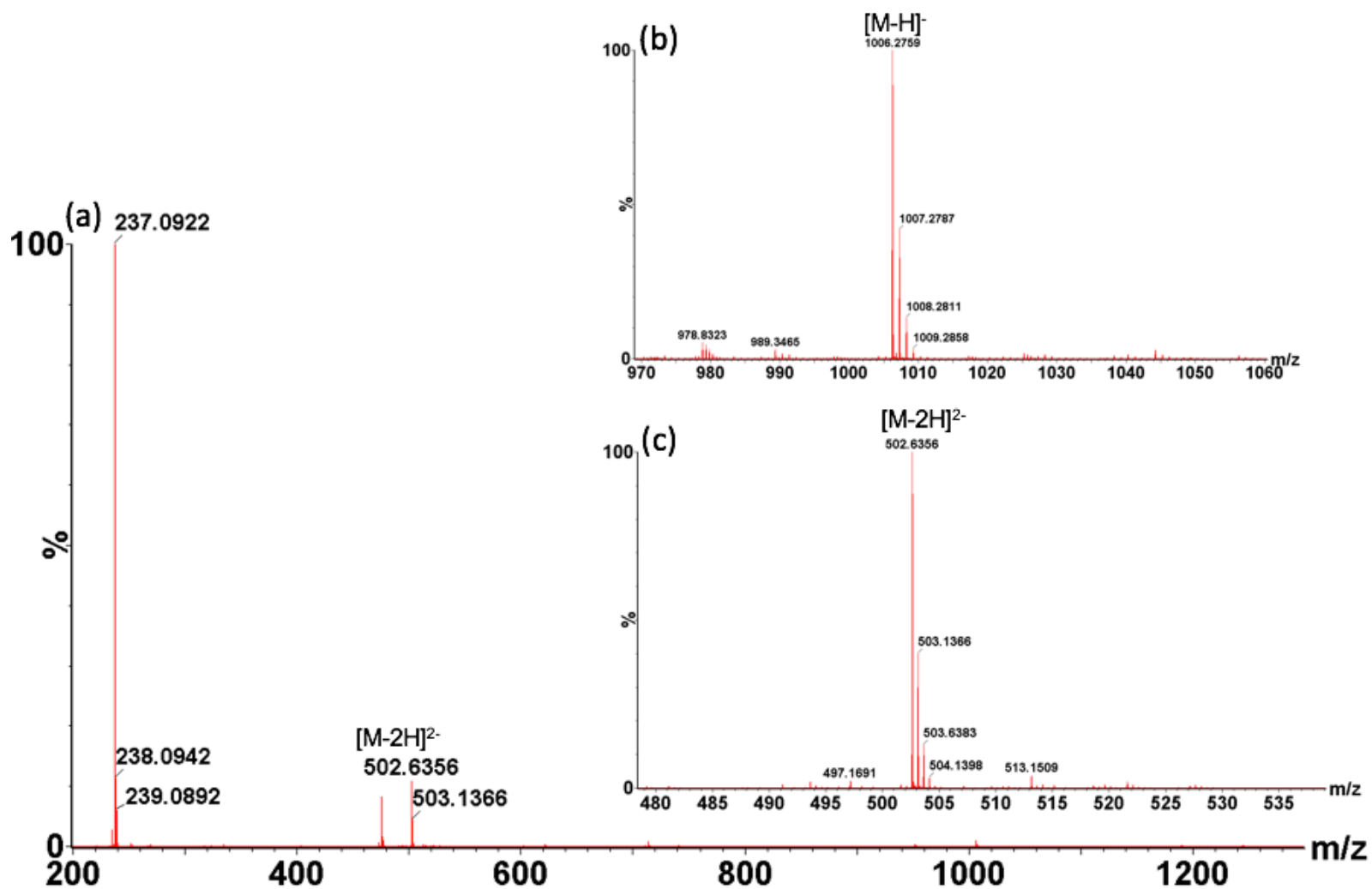


Figure A3.53: Negative ion mass spectrometry of the isolated accumulated peak of UDP-MurNAc-tripeptide (Lys) from *S. aureus* incubated with 2 μ M pywac 2. (a): mass spectra with $[M-2H]^{2-}$ (observed 502.63, expected 502.63) (deconvoluted by MassLynx™ software (Waters, USA)). (b): Mass spectra of $[M-H]^{-}$ (observed 1006.27, expected 1006.26). (c): Observed isotope distribution of $[M-2H]^{2-}$ (zoomed in view of $[M-2H]^{2-}$ peak shown in (a)).

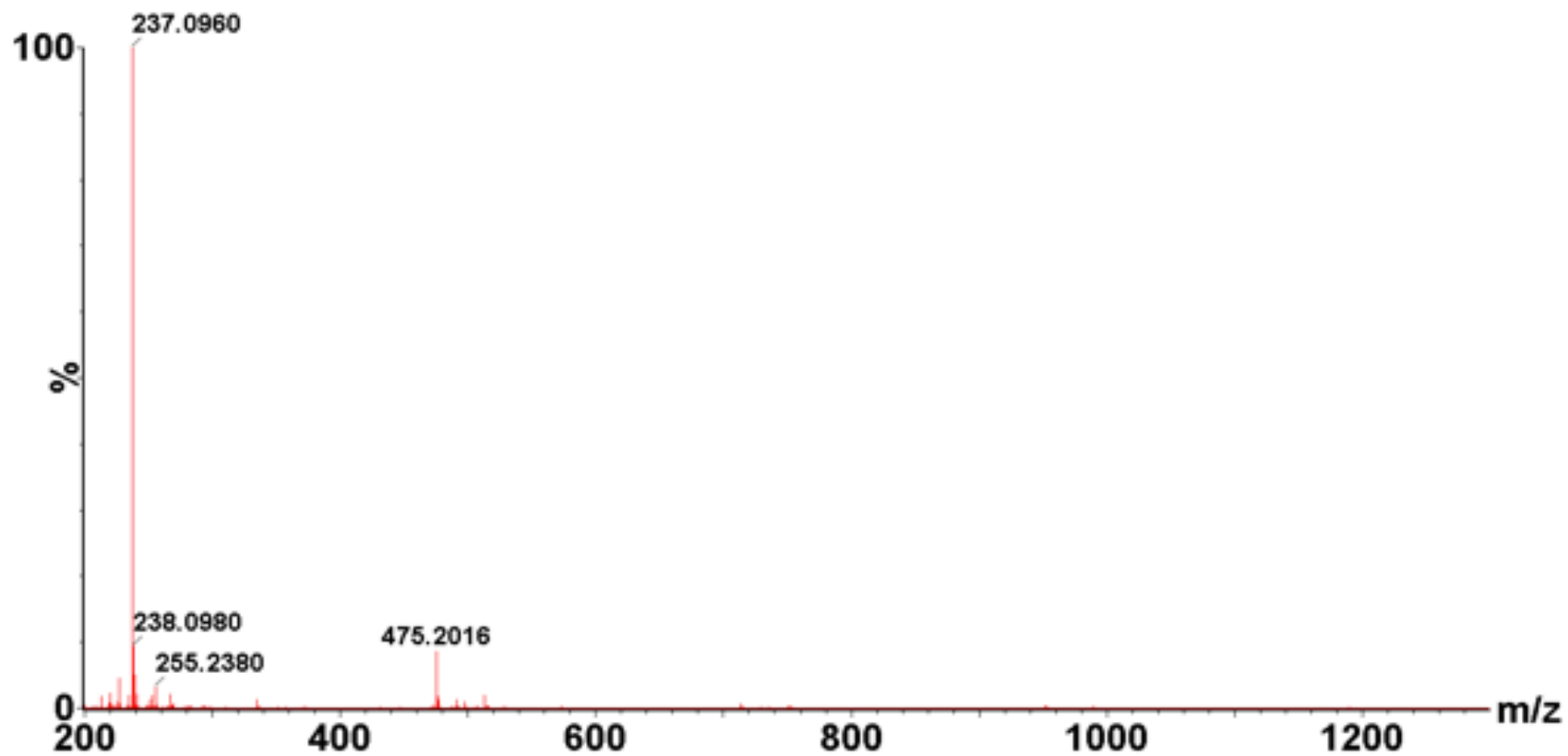


Figure A3.54: Negative ion mass spectrometry of the isolated accumulated peak from *S. aureus* incubated with 8 μ M pywac 6. Full mass spectra (no identifiable m/z) (deconvoluted by MassLynx™ software (Waters, USA)).

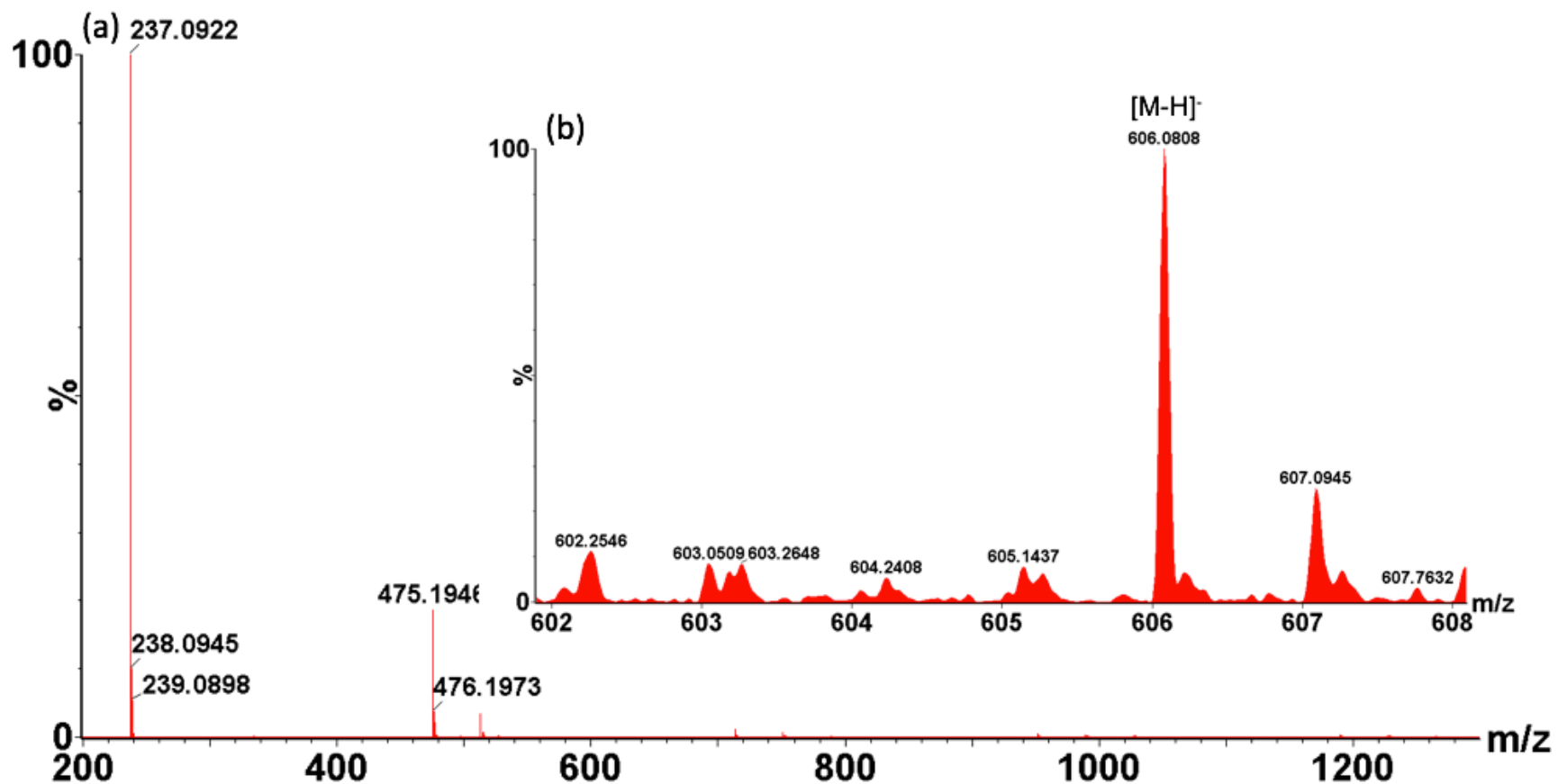


Figure A3.55: Negative ion mass spectrometry of the isolated accumulated peak of UDP-GlcNAc from *S. aureus* incubated with 8 μ M pywac 8. (a): mass spectra (no identifiable m/z). (b): Observed isotope distribution of UDP-GlcNAc [M-H]⁻ (zoomed in view of [M-H]⁻ peak shown in (a)) (observed 606.08, expected 606.07) (deconvoluted by MassLynx™ software (Waters, USA)).

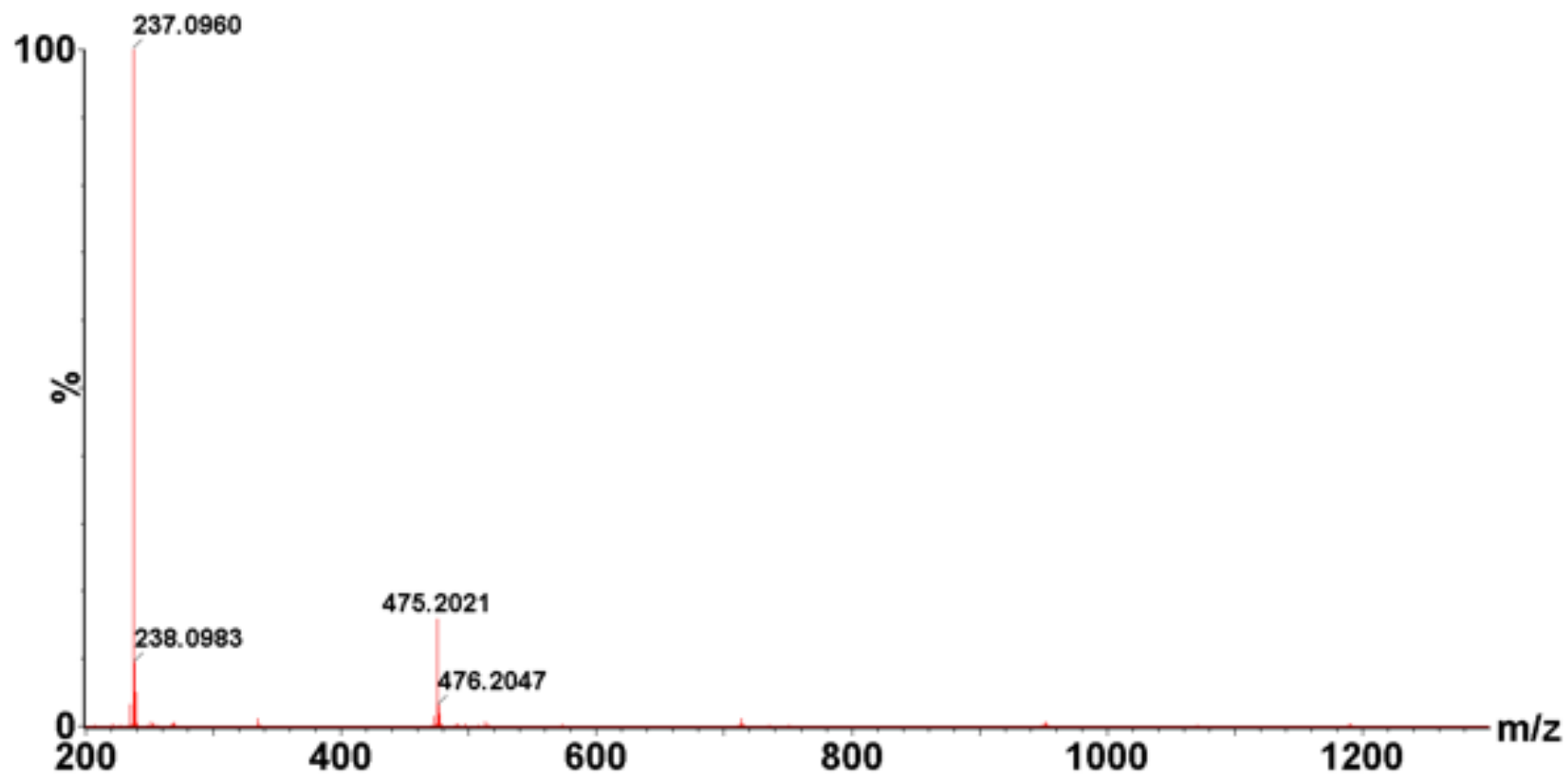


Figure A3.56: Negative ion mass spectrometry of the isolated accumulated peak from *S. aureus* incubated with 4 μ M pywac 9. Full mass spectra (no identifiable m/z) (deconvoluted by MassLynxTM software (Waters, USA)).